Olexander Kyrylenko ·
Serhii Denysiuk · Denys Derevianko ·
Ihor Blinov · Ievgen Zaitsev ·
Artur Zaporozhets *Editors*

Power Systems Research and Operation

Selected Problems II

Springer

Studies in Systems, Decision and Control

Volume 220

Series Editor

Janusz Kacprzyk, Systems Research Institute, Polish Academy of Sciences, Warsaw, Poland

The series "Studies in Systems, Decision and Control" (SSDC) covers both new developments and advances, as well as the state of the art, in the various areas of broadly perceived systems, decision making and control–quickly, up to date and with a high quality. The intent is to cover the theory, applications, and perspectives on the state of the art and future developments relevant to systems, decision making, control, complex processes and related areas, as embedded in the fields of engineering, computer science, physics, economics, social and life sciences, as well as the paradigms and methodologies behind them. The series contains monographs, textbooks, lecture notes and edited volumes in systems, decision making and control spanning the areas of Cyber-Physical Systems, Autonomous Systems, Sensor Networks, Control Systems, Energy Systems, Automotive Systems, Biological Systems, Vehicular Networking and Connected Vehicles, Aerospace Systems, Automation, Manufacturing, Smart Grids, Nonlinear Systems, Power Systems, Robotics, Social Systems, Economic Systems and other. Of particular value to both the contributors and the readership are the short publication timeframe and the world-wide distribution and exposure which enable both a wide and rapid dissemination of research output.

Indexed by SCOPUS, DBLP, WTI Frankfurt eG, zbMATH, SCImago.

All books published in the series are submitted for consideration in Web of Science.

Olexander Kyrylenko · Serhii Denysiuk ·
Denys Derevianko · Ihor Blinov · Ievgen Zaitsev ·
Artur Zaporozhets
Editors

Power Systems Research and Operation

Selected Problems II

Springer

Editors
Olexander Kyrylenko
Institute of Electrodynamics
National Academy of Sciences of Ukraine
Kyiv, Ukraine

Denys Derevianko
Power Supply Department
National Technical University of Ukraine
"Igor Sikorsky Kyiv Polytechnic Institute"
Kyiv, Ukraine

Ievgen Zaitsev
Institute of Electrodynamics
National Academy of Sciences of Ukraine
Kyiv, Ukraine

Serhii Denysiuk
Institute of Energy Saving and Energy
Management
National Technical University of Ukraine
"Igor Sikorsky Kyiv Polytechnic Institute"
Kyiv, Ukraine

Ihor Blinov
Institute of Electrodynamics
National Academy of Sciences of Ukraine
Kyiv, Ukraine

Artur Zaporozhets
Institute of General Energy
National Academy of Sciences of Ukraine
Kyiv, Ukraine

Introduction

Improving the efficiency and reliability of the functioning of electric power facilities is one of the most important problems of the unified energy system of Ukraine. This problem is multifaceted, because the correct functioning of generation, transmission and distribution systems depends on many technical, economic, social and natural factors that change the integral properties of the system. At the same time, it should take into account that for each life cycle, it is necessary to develop correct measures to compensate for disturbing influences that lead to the inoperability of the energy system or its individual components. As world practice has shown, an effective way to improve the reliability of the energy system is the improvement and construction of electric power networks and systems according to the smart grid concept. The implementation of the concept involves the modernization of the existing energy system, through the development of a fully integrated, self-regulating and self-healing electric power system, which has a network topology and includes all generating sources, main and distribution networks and all types of consumers of electrical energy, controlled by a single network of information and control devices and systems in real time. In this case, there is a need to develop new and improved existing models and methods that allow optimizing the operating modes of electrical networks, ensuring the sustainable development of the share of RES in energy production and the reliability of the operation of existing electrical equipment of power plants and networks. The research results presented in the monograph allow finding solutions to some of the problems that arise during the functioning of the integrated energy system of Ukraine in modern market conditions in the following areas:

– implementation of some problems of electrical networks operational control solving in the operational information incompleteness conditions;
– study of actual trends of electrical distribution systems automation;
– development of power systems model for various types of analysis;
– study of main methods of forecasting and optimization of energy processes by various factors for electrical networks with solar power plants, hydropower plants and other plants;

- development methods and means of diagnosing power converter technology for smart grid;
- development solutions for improving the reliability of electricity supply based on use fault indicators for smart monitoring systems of distribution networks;
- development specialized tools for mathematical and computer modeling, information technology support for automation of the preparation and decision-making process by appropriate organizational management systems of competitive electricity market participants operating in complex relationships and potential risks.

Developing these areas, the monograph covers new technologies and methods related to the management of large interconnected power systems, solving a stable and reliable problem of electricity generation, sources of electricity from renewable sources and classical energy sources. Increasingly widespread use of local sources of generation and energy storage in distribution electric networks sharply reduces the effectiveness of traditionally used methods and technical means for controlling their operating modes. The monograph considers the possibility, expediency and efficiency of the selective use of remotely controlled switching devices in distribution networks with an open loop topology. In addition, when dispersed generation sources are connected to the energy system separately, as active consumers, as part of local microgrid power systems and as separate generating facilities, a number of issues arise related to ensuring proper synchronization of the parameters of these systems, their electromagnetic compatibility, quality of electric energy, occurrence of additional losses and reliability of their work. Development of measures to ensure the quality of electricity is possible only after assessing the actual state of quality of electricity in all nodes of the electricity network. Therefore, the electricity quality assurance system should be based on a model that takes into account the load curve of the system, regulation of production, storage system, as well as the operation of renewable energy sources in the area, as well as other factors affecting the power system. These models are the basis for energy systems management and monitoring systems. Management of energy systems is not possible without optimizing the structure of the energy balance of the state, based on the requirements of energy security and ensuring the share of renewable energy, among which a significant place is occupied by solar and hydropower. Shown that, as facts, with the existing structure of production capacities in the united energy systems of Ukraine, only hydroelectric power plants and pumped storage power plants are able to balance the rapidly changing load schedule of renewable energy sources due to their high maneuverability, which requires the development of solar and wind energy storage systems. A component that allows connecting the producer and consumer of electricity is overhead and cable lines. To identify overloaded overhead lines in the power system, the use of the "H-1 principle" is proposed. The application of the method makes it possible to determine the influencing and "weak" elements of the network in order to determine measures to reduce the overload of overhead lines. To take into account damage to overhead and cable lines associated with external operating conditions, it is necessary to apply methods for detecting and locating short-term damage and limiting

them. To determine short-term damage, the use of additional damage indicators for existing monitoring systems of distribution networks is proposed.

The presented research results in monograph allow increasing the reliability and efficiency of operation of energy facilities and ensuring the stability of power systems, the introduction of effective methods and tools for forecasting electricity supply, optimize power systems and suggest road map to integrate electricity markets taking into account network constraints in modern conditions of electricity markets.

The authors of the monograph are author's team from the Institute of Electrodynamics of the National Academy of Sciences of Ukraine, Institute of Energy Saving and Energy Management of National Technical University of Ukraine «Igor Sikorsky Kyiv Polytechnic Institute» and Institute of General Energy of the National Academy of Sciences of Ukraine.

Kyiv, Ukraine   Olexander Kyrylenko
Spring 2022   Serhii Denysiuk
                                                                    Denys Derevianko
                                                                          Ihor Blinov
                                                                      Ievgen Zaitsev
                                                                  Artur Zaporozhets

Contents

Simulation of the Load–Frequency Control of the Power System with Renewables

Vsevolod Pavlovskyi , **Anton Steliuk** , **Lukian Lukianenko** ,
Viacheslav Hrechko , **and Pavlo Horoshko**

Abstract Load–frequency control is one of the principal tasks of providing the reliability of power system operation considering the increasing share of renewable energy sources. This chapter covers the various aspects of providing the power system operation with renewables. The chapter consists of three parts. In the first part, the identification methodology of the overloaded elements in the power system is presented. The proposed methodology is based on the "N-1 principle" allowing identifying weak elements in the network. The second part covers the issue of the participation of windfarms in the secondary frequency control. In the third part of the chapter, the simulation results of the windfarm controller and energy storage system to improve primary frequency control are provided.

Keywords Load–frequency control · Power flow · Renewable energy sources · Overloading · Automatic generation control · Energy storage system · Power system

1 Introduction

Load–frequency control is one of the important tasks of reliable power system operation. At present, the development of power systems is characterized by the increased share of renewable energy sources (RES) in the generation structure that affects on power system's steady-state and dynamic properties. The first factor is decreasing the system inertia and corresponding to increasing the rate of change of frequency and frequency deviation in the power system. Besides, the additional RES generation results in the redistribution of the active power flows in the transmission and distribution networks. As a result, some elements of the power system may be overloaded (especially in "N-1" cases) which requires the development of the identification method of such elements based on the "N-1 principle".

V. Pavlovskyi (✉) · A. Steliuk · L. Lukianenko · V. Hrechko · P. Horoshko
Institute of Electrodynamics of National Academy of Sciences of Ukraine, Kyiv, Ukraine
e-mail: vsevolod_pavlovsky@yahoo.com

Another factor, defining the importance of the load–frequency control in power systems with RES is their participation in the load–frequency control. For example, the generation power of the windfarm can be regulated by changing the blade angle of the wind turbines under the action of the local windfarm controller at the power plant level. The principal task of this controller is generating a control action considering a setpoint from the automatic generation control regulator as well as the current generation power of the windfarm. It should be noted the energy storage systems (ESS) can also be used to improve a load–frequency control in the power system with RES. One of the advantages of such systems is to provide a quick active power response that allows for improving the primary frequency control. Considering the mentioned above, providing a load–frequency control in the power system with a significant RES share is an important issue.

2   Identification and Classification of the "Critical Overhead Lines" Using the "N-1 Principle"

One of the factors determining the normal operating conditions of the interconnected power system (IPS) of Ukraine is the provision of permissible active power flows through internal and interstate transmission lines. Thus, by [1], the value of allowable power flow (maximum allowable—for normal modes and emergency allowable—for forced ones) is determined by the relevant active power safety factor during the power systems steasy-state stability analysis. The allowable flow calculation is carried out by determining the stability limit. The operation mode of the controlled nodes of the power system is also controlled by the allowable voltage values during the calculation. In particular, the admissibility of the voltage mode in the load nodes is determined by the voltage safety factor [1]. The method of PV-curves, which allows the analysis of voltage levels on certain bus systems with the increasing active power flow in the intersection [2, 3], has become widespread to analyze the boundary modes of intersections in the practice of power systems of European countries. As can be seen from the above-mentioned, the main attention is paid to maintaining acceptable voltage levels while increasing the power flow across the interface. At the same time, the analysis of interface operation in such modes necessitates the loading check of each overhead line (OHL), which is part of this interface. Appropriate identification of such OHLs will prevent their overloading, disconnection under the action of current protection, and consequently—further overloading of other OHLs remaining in operation. Thus, the development of a method for identifying transmission lines with "critical" loading for normal as well as emergency power system schemes is an important issue.

This work aims to improve the well-known "N-1 principle" and extend it to the problem of OHLs identification with "critical" loading, forming a clear criterion and classification of such overloaded OHLs.

The main aspects of the "N-1 principle" are presented in [4]. It should be noted that the contingencies (emergencies) corresponding to the standard type in the classification of [5, 6] are analyzed.

The basis for the identification of "critical OHLs" are the results of the load flow calculations associated with the failure of one element: transmission line, transformer, generator, etc. Thus, for each considered situation, the loading of each transmission line is determined and compared with an allowable value:

$$loading_i = \frac{I_i}{I_{allow\,i}}, \%　\; i = 1, \ldots, n, \tag{1}$$

where $loading_i$ is a loading of i-th OHL, I_i is an actual current of the line, $I_{allow\,i}$ is an allowable current value for i-th line considering the permissible currents of individual elements: substation busbar arrangements, current transformers, high-frequency barriers, etc.

When determining "critical transmission lines", a permissible loading value of 100% or the method of expert assessments may be used. Then, as mentioned above, the excess of the transmission line permissible loading value in the simulated post-emergency mode should be considered as the criterion for assigning this line to the critical overloaded element.

To identify "critical transmission lines" let us introduce a vector column of "influential" elements M_{elem}:

$$M_{elem} = \begin{bmatrix} elem_1 \\ elem_2 \\ \ldots \\ elem_i \\ \ldots \\ elem_n \end{bmatrix}, \quad i = 1, \ldots, n, \tag{2}$$

where $elem_i$ is an i-th power system element, which disconnection from the network leads to exceeding the transmission line allowable loading; n is the number of such "influential" elements.

In addition, let us also form a vector-string of "weak" transmission lines M_{OHL}:

$$M_{OHL} = \begin{bmatrix} OHL_1 \; OHL_2 \; \ldots \; OHL_j \; \ldots \; OHL_m \end{bmatrix}, \quad j = 1, \ldots, m, \tag{3}$$

where OHL_j is a j-th transmission line, which loading exceeds the allowable value in the event of a standard type of emergency (disconnection of one element of the vector-column M_{elem}); m is the number of such "weak" transmission lines.

Let's form a loading matrix M_{ldg} defining the relation between "weak" transmission lines with the "influential" elements:

$$M_{ldg} = \begin{bmatrix} loading_{11} & loading_{12} & \ldots & loading_{1j} & \ldots & loading_{1m} \\ loading_{21} & loading_{22} & \ldots & loading_{2j} & \ldots & loading_{2m} \\ \ldots & \ldots & \ldots & \ldots & \ldots & \ldots \\ loading_{i1} & loading_{i2} & \ldots & loading_{ij} & \ldots & loading_{im} \\ \ldots & \ldots & \ldots & \ldots & \ldots & \ldots \\ loading_{n1} & loading_{n2} & \ldots & loading_{nj} & \ldots & loading_{nm} \end{bmatrix}, \qquad (4)$$

where $loading_{ij}$ is the value of the OHL_j transmission line loading (M_{OHL} vector) when the $elem_i$ element (M_{elem} vector) is disconnected.

Then, based on M_{elem} and M_{ldg} it is possible to form a matrix $M_{aff.elem}$, characterizing "weak" elements:

$$M_{aff.elem} = \begin{bmatrix} n_{\max 1} & loading_{\max 1} \\ n_{\max 2} & loading_{\max 1} \\ \ldots & \ldots \\ n_{\max i} & loading_{\max i} \\ \ldots & \ldots \\ n_{\max n} & loading_{\max n} \end{bmatrix}, \qquad (5)$$

where $n_{\max i}$ is the number of exceedances of the allowable value of transmission line loading in the event of an i-th dangerous emergency (i.e., under disconnection of the $elem_i$ element in M_{elem} vector):

$$n_{\max i} = \sum_{j=1}^{m} P_{ij},$$

$$P_{ij} = \begin{cases} 1, & \text{if } loading_{ij} \geq loading_{allow} \\ 0, & \text{if } loading_{ij} < loading_{allow} \end{cases}, \quad i = 1, \ldots, n; \; j = 1, \ldots, m, \qquad (6)$$

where $loading_{allow}$ is an allowable loading.

The maximum value of the loading observed in the event of an i-th dangerous emergency is determined as follows:

$$loading_{\max i} = \max(loading_{ij}), \quad i = 1, \ldots, n. \qquad (7)$$

Similarly, but based on M_{OHL} and M_{ldg}, let us create a matrix $M_{weak.OHL}$, which characterizes the "weak" transmission lines:

$$M_{weak.OHL} = \begin{bmatrix} n_{OHL.\max 1} & n_{OHL.\max 2} & \cdots & n_{OHL.\max j} & \cdots & n_{OHL.\max m} \\ loading_{\max 1} & loading_{\max 2} & \cdots & loading_{\max j} & \cdots & loading_{\max m} \end{bmatrix}, \qquad (8)$$

where $n_{OHL.\max j}$ is the number of exceedances of the allowable loading for j-th transmission line in the event of all dangerous emergencies (i.e., under disconnection of each element of the M_{elem} vector):

$$n_{OHL.\max j} = \sum_{i=1}^{n} P_{ij},$$

$$P_{ij} = \begin{cases} 1, \text{if } loading_{ij} \geq loading_{allow} \\ 0, \text{if } loading_{ij} < loading_{allow} \end{cases}, \quad i = 1, \ldots, n; \ j = 1, \ldots, m. \quad (9)$$

The maximum value of the loading for the j-th transmission line in the event of all dangerous emergencies is defined as

$$loading_{OHL.\max j} = \max(loading_{ij}), \quad j = 1, \ldots, m. \quad (10)$$

The matrix $M_{weak.OHL}$, in fact, defines two classes of "weak" transmission lines:

- "weak" transmission lines at the maximum value of loading in one of the most severe post-emergency mode—$loading_{OHL.\max j}$;
- "weak" transmission lines in the incidence of exceeding the allowable loading value for all post-emergency modes: $n_{OHL.\max j}$.

At the same time, the matrix $M_{aff.elem}$ determines the class of "influential" elements, which disconnection leads to the largest number $n_{\max i}$ of loading excess on the transmission line in the power system.

Thus, the definition of "critical transmission lines" for any power system obtained using the "N-1 principle" can be compactly represented by the composition of three matrices: M_{OHL}, $M_{aff.elem}$ and $M_{weak.OHL}$. In its turn, this allows for the classification of critical transmission lines by the following factors (Fig. 1).
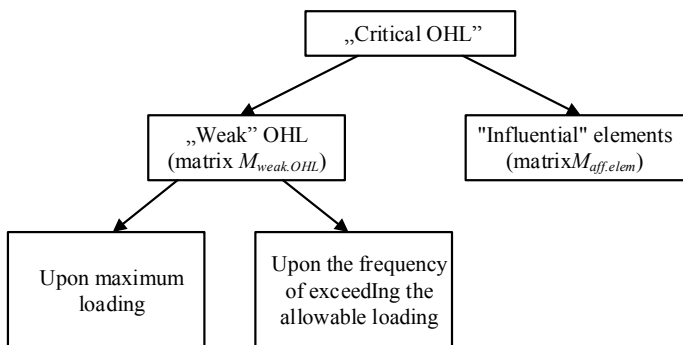
Fig. 1 Classification of "critical transmission lines"
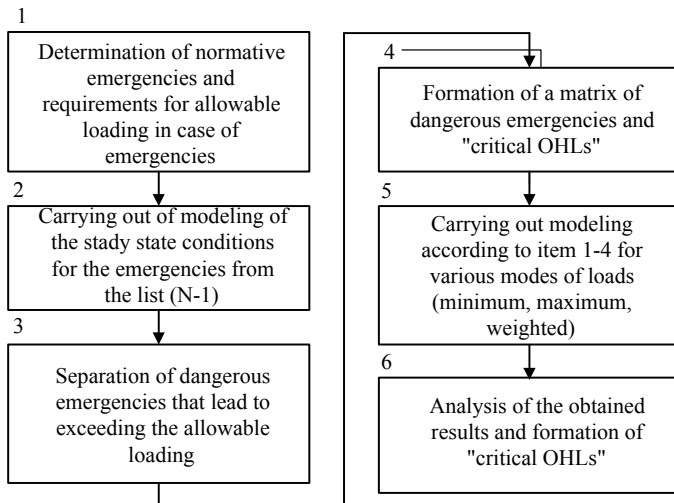
Fig. 2 Algorithm for identifying "critical transmission lines"

The implementation of the proposed matrix approach to the identification of "critical transmission lines" is presented in the form of an algorithm flowchart (Fig. 2).

Let us illustrate the use of the proposed approach on the example of the Institute of Electrical and Electronics Engineers (IEEE) test scheme is presented in Fig. 3.

The simulation of the considered power system is performed using DIgSILENT PowerFactory software. The calculation of post-emergency steady-state condition is performed in case of the disconnection of synchronous generators, transformers, and transmission lines (Fig. 3). Meanwhile, the transmission lines' allowable loading value $loading_{allow}$, exceeding which transmission lines are "critical", was assumed to be 100%.

Vector column of "dangerous" elements M_{elem}:

$$M_{elem} = \begin{bmatrix} L1-2/1 \\ L1-2/2 \\ L6-12 \\ T-1 \end{bmatrix}. \tag{11}$$

Vector line of "critical transmission lines" M_{OHL}:

$$M_{OHL} = \begin{bmatrix} L1-2/1 & L1-2/2 & L6-13 & L9-10 & L9-10 \end{bmatrix}. \tag{12}$$

Loading matrix M_{ldg}:
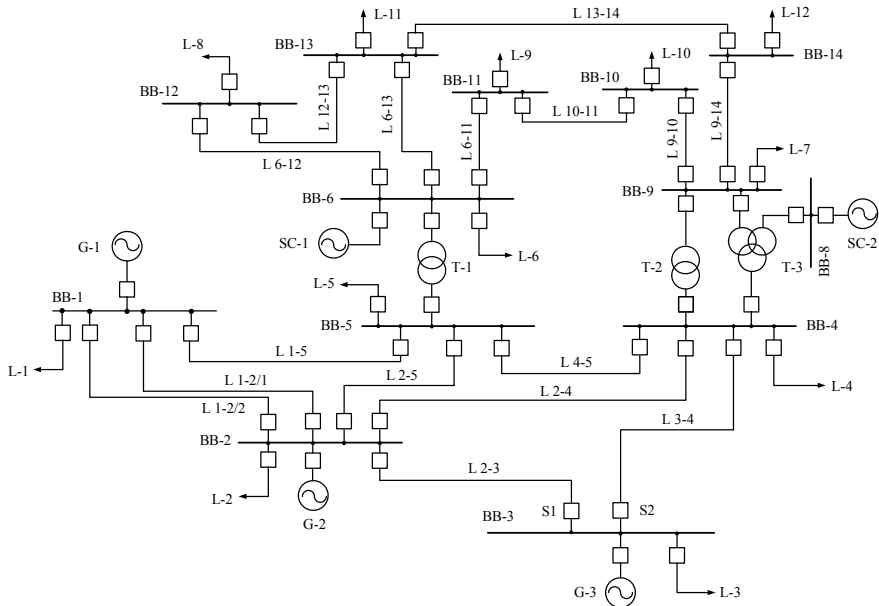
Fig. 3 The institute of electrical and electronics engineers test scheme

$$M_{ldg} = \begin{bmatrix} & 154.1 & & 104.9 \\ 154.4 & & & \\ & & 129.4 & \\ & & & 113.6 \end{bmatrix}. \tag{13}$$

As a result of M_{OHL} matrix processing $M_{aff.elem}$ "influential elements" matrix was obtained:

$$M_{aff.elem} = \begin{bmatrix} 2 & 154.1 \\ 1 & 154.4 \\ 1 & 129.4 \\ 1 & 113.6 \end{bmatrix}. \tag{14}$$

as well as $M_{weak.OHL}$ "weak transmission lines" matrix

$$M_{weak.OHL} = \begin{bmatrix} 1 & 1 & 1 & 1 & 1 \\ 154.4 & 151.1 & 129.4 & 113.6 & 104.9 \end{bmatrix}. \tag{15}$$

As can be seen from the obtained results, the most "influential element" in the power system (Fig. 3) is the overhead line L 1-2/1. In case of this OHL disconnection, the critical overloading of OHLs L 1-2/2 and L 1-5 is observed. At the same time, the

results of the analysis of the obtained $M_{weak.OHL}$ matrix show that for all transmission lines under consideration, there is one case of allowable overloading.

It should be noted that the use of the proposed approach to perform the analysis of "N-1 principle" in the IPS of Ukraine requires some modification of the calculation model. Under 750 kV transmission line disconnection, it is necessary to provide for the simultaneous shunt reactors switching-off at its ends, as well as to present ("expand") an equivalent circuit with a higher voltage level of detail.

Thus, the "N-1 principle" has been extended to the problem of "critical" OHLs identification. The classification of "critical transmission lines" was offered as well as the algorithm for their identification based on allowable loading was developed and tested. The proposed approach allows to automate calculations of the power systems' emergency operation regimes.

3   Development of the Windfarm Local Controller Model

Increasing the installed capacity of power plants based on the renewable energy sources (RES) strengthens the requirements for ensuring the controllability of power systems in such conditions. This primarily concerns the quality of regulation of frequency and active power, voltage, and reactive power and, accordingly, the organization of dispatch control of power systems. It should be noted that in power systems with significant installed RES capacity, in particular, wind farms (in power systems of Germany, Denmark, etc.) there is a fundamental possibility of involving these power plants in load–frequency control depending on the power system's actual operation conditions [5–10]. Let us estimate the features of the local regulator model on the example of a wind power plant (WPP). For example, the following approaches to active power regulation are used in the Danish power system [7, 8]:

1. Maximum power limit—if the wind farm generation power exceeds the set value P_{max}, the wind farm generation is limited to this level. Thus, the station "loses" power $\Delta P_{weak} = P_{g.WPP} - P_{max}$, provided that $P_{g.WPP} > P_{max}$;
2. Regulation under the power balance ensuring condition—power regulation is carried out by the generation schedule, which is set in the system operator's dispatcher center. If the actual power generation of the wind farm exceeds the set one, the share of set power exceeding is also lost;
3. Limitation on the rate of change of generation power—if the generation power change rate exceeds the set speed, then the wind power generation output is carried out by the generation set speed;
4. Delta-regulation—wind farms generation is carried out with the provision of a given power reserve $\Delta P_{g.WPP} = P_{g.max} - P_{g.nom}$, where $P_{g.max}$—the generation maximum power that can be issued by wind farms; $P_{g.nom}$—actual WPP generation capacity, based on the need to provide a power reserve $\Delta P_{g.WPP}$.

Thus, the latter approach can be used to implement the primary (with given droop and dead-band) and secondary frequency control [7, 8]. Considering the mentioned
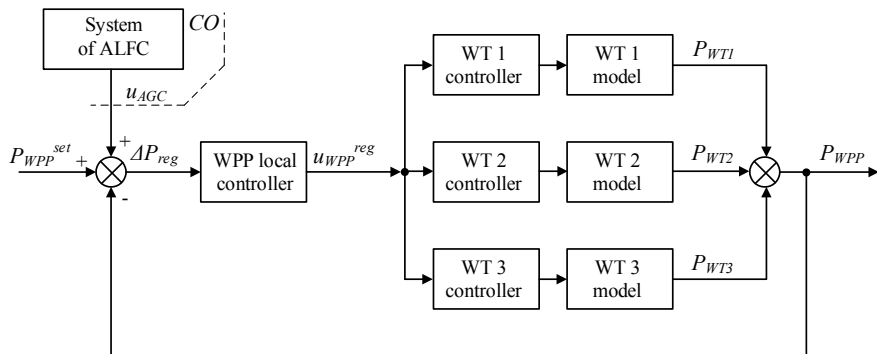
Fig. 4 Organization of automatic frequency and power control considering wind farms

above, the structure and model of the wind farms local regulator in the DIgSILENT PowerFactory software are offered in this paper. The organization of automatic load–frequency control (ALFC) involving wind farms is shown in Fig. 4.

As can be seen in Fig. 4, the input signals of the local wind farm controller are the control action u_{AGC} from the automatic load–frequency control system (ALFCS) located in the control center of the transmission system operator, as well as the set power P_{WPP}^{set} to be produced by the station. At the same time, the actual generation power P_{WPP} developed by the WPP is also transmitted via feedback. Given the above, the deviation in active power at the input of the local wind farm controller can be determined as follows:

$$\Delta P_{reg} = u_{reg} + P_{WPP}^{set} - P_{WPP}. \tag{16}$$

Accordingly, the control action u_{WPP}^{reg} generated at the output of the local wind farm controller is determined as follows:

$$u_{WPP}^{reg} = K_p \Delta P_{reg} + K_i \int_{t_1}^{t_2} \Delta P_{reg} dt, \tag{17}$$

where K_p, and K_i are the transmission rates of the proportional and integral parts of the regulator, t_1, t_2 define integration range.

At the next step, a separate control action is determined u_{WTi}^{reg}, which is transmitted to the input of the controller model of an individual wind turbine (WT):

$$u_{WTi}^{reg} = \gamma_i u_{WPP}^{reg}, \tag{18}$$

where γ_i is the ratio of WT individual participation in the automatic load–frequency control.
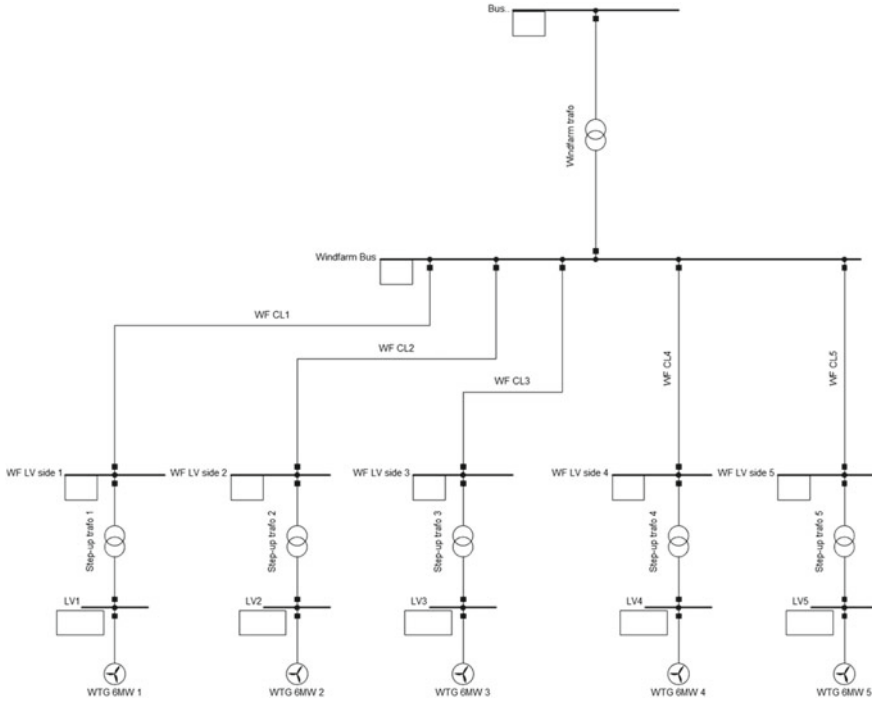
Fig. 5 Diagram of a wind farm

The block diagram of a wind power plant considered in the study is shown in Fig. 5.

As seen in Fig. 5, five wind turbines with a fully rated converter are used. The nominal capacity of each wind turbine is 6 MW. The total generation capacity of the windfarm is 30 MW. The Block diagram of the composite model of the local wind farm controller developed in DIgSILENT PowerFactory software is depicted in Fig. 6.

As can be seen in Fig. 6, the model input signals are the actual generation power of the wind turbines, as well as the actual frequency in the power system. The output signals of the local controller (in Fig. 6 are not shown) are active power setpoints transmitted to the individual wind turbine. The parameters of the composite model of the local wind farm controller are shown in Fig. 7.

Let us consider a more detailed diagram of the local regulator of wind farms depicted in Fig. 8. As mentioned above, the input signals of the controller are the actual frequency at the point of the common coupling of the wind farm to the power system, as well as the actual power generation of wind turbines of the wind farm. In addition, the input signal of the local controller is a control action from the system part of ALFCS. Based on these signals, the deviation signal for active power is determined, which is transmitted to the input of the proportional-integrated regulator
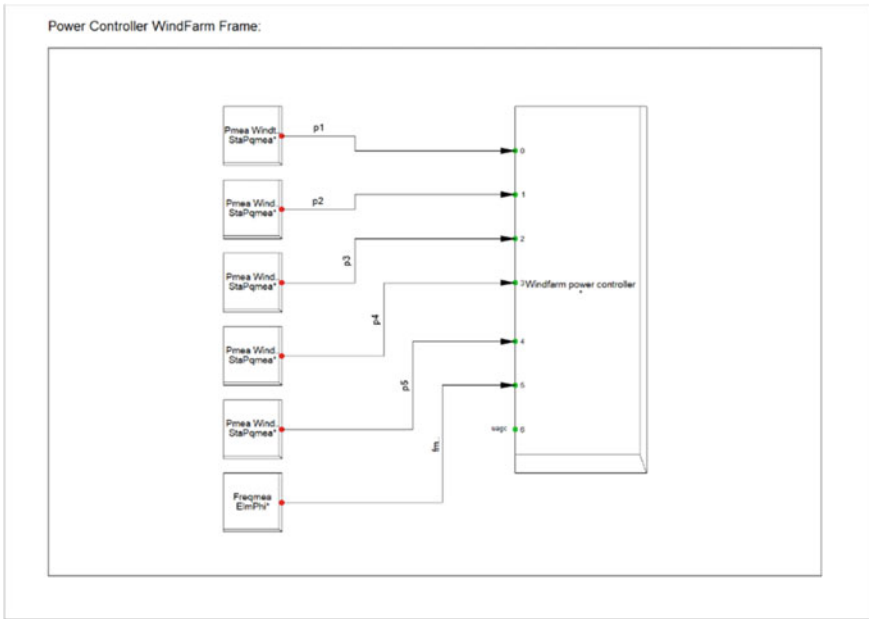
Fig. 6 Block diagram of the local wind farm controller developed in DIgSILENT PowerFactory software
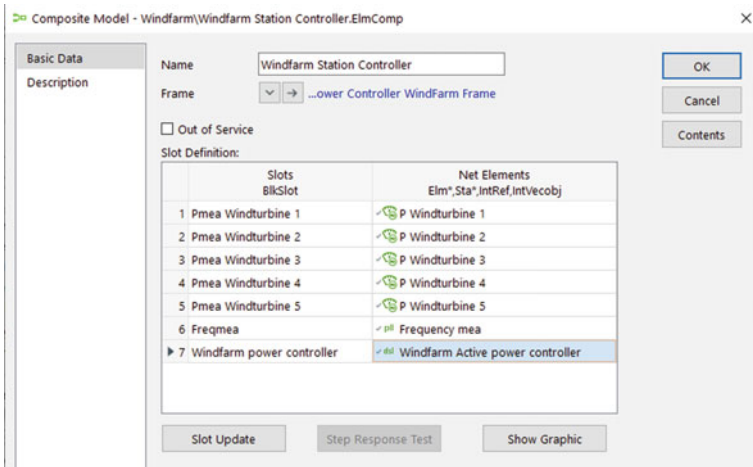
Fig. 7 The dialog box of the composite model of the local wind farm controller
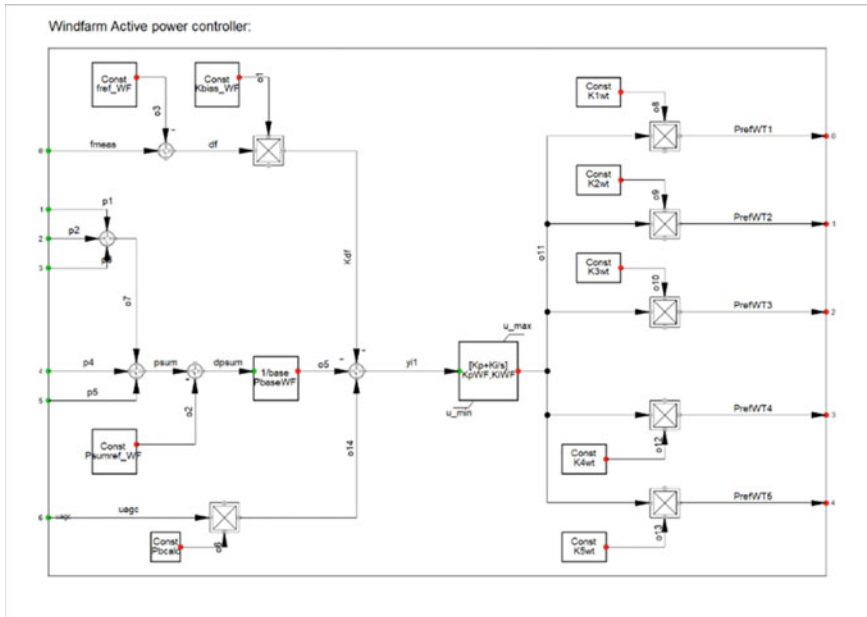
Fig. 8 Block diagram of the model of the local regulator of the windfarm

of the wind farm controller, which generates active power settings for the wind turbines.

The settings of the parameters of the local regulator of the wind farm are shown in Fig. 9.

Thus, the created model of the regulator allows studying load–frequency control considering the windfarm operation under ALFCS.

4 Load–Frequency Control Structure in Power Systems with Renewable Energy Sources

The study of the ALFCS operation considering the local regulator of wind farms was performed on the example of an improved IEEE test scheme depicted in Fig. 10.

The simulated power pool consists of two power systems. As shown in Fig. 10, this is Power system 1 and Power system 2. In the first power system, the generator G-1 of the first power plant participates in the secondary frequency control. The ALFCS1 operates in automatic frequency control mode (control criterion is $\Delta f = 0$). In the second power system, the system part of the ALFCS regulates the net interchange power flow with the frequency adjustment. In the second power system, the system, power plant, and aggregate levels of the ALFCS are used (Fig. 11). The participation factors of the second and third power plants, as well as the wind power
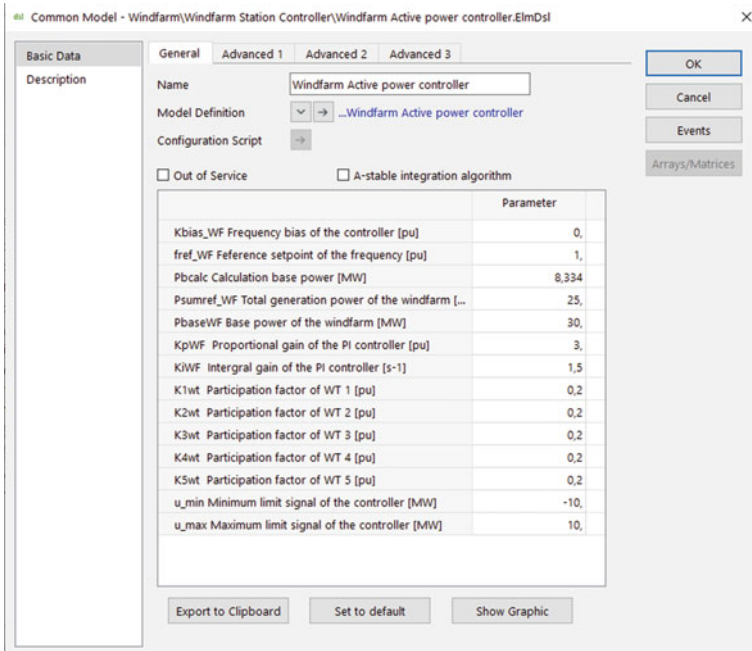
Fig. 9 The dialog box with the parameter settings of the local wind farm controller
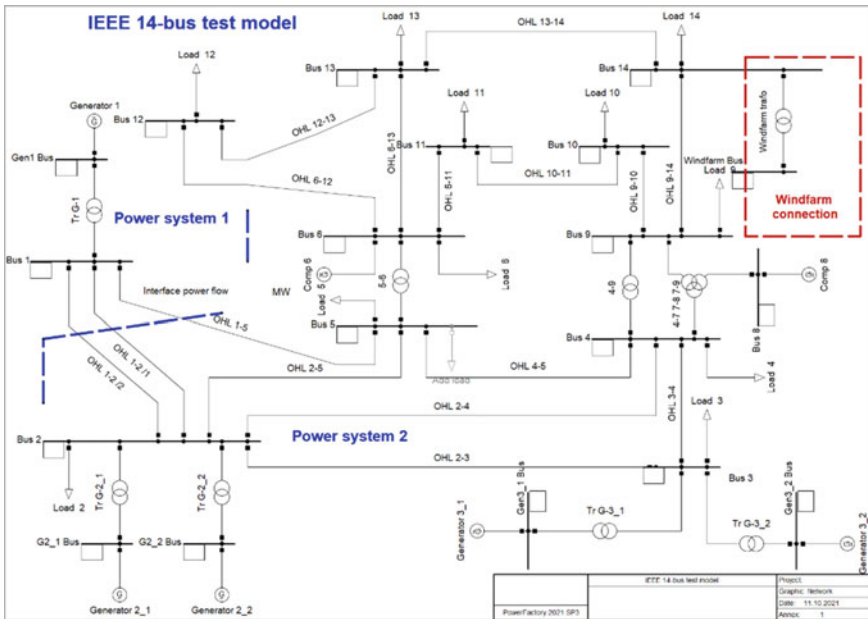
Fig. 10 IEEE test scheme to study load–frequency control considering RES
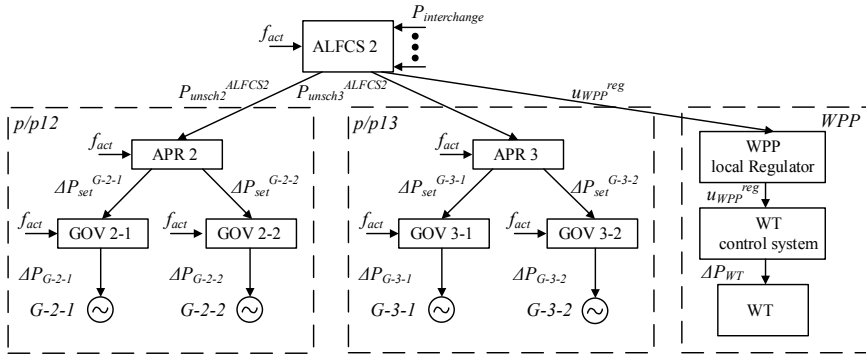
Fig. 11 The organization of automatic frequency control in IPS2

plant in the secondary frequency control equal 0.6, 0.35, and 0.05 p.u., respectively. At the station level, the shares of the G-2-1 and G-2-2 generators of the second power plant in the secondary frequency control are 0.65 and 0.35 p.u., and the G-3-1 and G-3-2 generators of the third power plants—0.45 and 0.55 p.u. respectively.

At the upper (system) level there is a system part of ALFCS2. The input signals of this controller are an actual frequency f_{act} in IPS2 and a net interchange power $P_{interch}$ through interface including transmission lines L-1-2/1, L-1-2/2, and L-1-5 (Fig. 11). Based on the actual frequency f_{act} and the calculated net interchange power of the controlled lines P_{bal}, the *area control error* (*ACE*) [11, 12] is calculated:

$$ACE = (P_{bal} - P_{bal.set}) + K_{freq}(f_{act} - f_{set}), \qquad (19)$$

or

$$ACE = \Delta P_{set} + K_{freq}\Delta f, \qquad (20)$$

where $P_{bal.set}$ is the setpoint of the net interchange power; f_{set} is the frequency setpoint; K_{freq} is the frequency bias factor; ΔP_{set} is a deviation of the net interchange power; Δf is a frequency deviation.

The calculated value of *ACE* is transmitted to the input of the proportional-integral controller generating an unscheduled component of active power P_{unsch}^{ALFCS2}:

$$P_{unsch}^{ALFCS2} = K_p ACE + K_I \int_{t_1}^{t_2} ACE \, dt, \qquad (21)$$

where K_p, K_I are proportional and integral gains of the regulator; t_1, t_2 are integration limits. The use of a PI-controller provides the corresponding control quality. For example, a proportional link provides the desired control speed and the integral

one—the control accuracy. Due to the integral link, the secondary frequency control is astatic, i.e. ACE equals zero in the steady-state condition.

The distribution of the unscheduled component of active power $P_{unsch}{}^{ALFCS2}$ at the system level of the ALFCS in Power system 2 among the second and third power plants, as well as for the wind power plant is provided according to their participation factors in the secondary frequency control:

$$P_{unsch2}^{ALFCS2} = \alpha_2 P_{unsch}^{ALFCS2}, \tag{22}$$

and

$$P_{unsch3}^{ALFCS2} = \alpha_3 P_{unsch}^{ALFCS2}, \tag{23}$$

and

$$u_{WPP}^{reg} = \alpha_{WPP} P_{unsch}^{ALFCS2}, \tag{24}$$

where $P_{unsch2}{}^{ALFCS2}$, $P_{unsch3}{}^{ALFCS2}$ are unscheduled components of active power setpoints at the second and third control power plants; $u_{WPP}{}^{reg}$ is an unscheduled component from the system controller at the wind farm; α_2, α_3 are the participation factors of these power plants in the secondary frequency control; α_{WPP} is a participation factor of the wind farm in the secondary frequency control.

The station level of ALFCS is represented by automatic power regulators (APR), used to adjust the relevant unscheduled component of the active power from ALFCS2 considering the actual frequency f_{act}.

Unscheduled component of the active power $P_{unsch}{}^{e/sti}$ of i-th control station generated at the output of the APR, is defined as follows:

$$P_{unsch}^{p/pli} = K_P^{APR} \left(K_{fc}\Delta f + P_{unschi}^{ALFCS2} - \sum_{j=1}^{m} \Delta P_{m.j} \right)$$
$$+ K_I^{APR} \int_{t_1}^{t_2} \left(K_{fc}\Delta f + P_{unschi}^{ALFCS2} - \sum_{j=1}^{m} \Delta P_{tot.j} \right) dt, \tag{25}$$

where $K_P{}^{APR}$, $K_I{}^{APR}$ are gains of the proportional and integral links of the APR; K_{fc} is frequency bias; $P_{unschi}{}^{ALFCS2}$ is an unscheduled component of active power from the system-wide part of ALFCS2 to i-th power station; $\sum_{j=1}^{m} \Delta P_{tot.j}$ is a change in total turbine power (number of m) of generators participating in the secondary frequency control, $j = 1, …, m$; t_1, t_2 are integration limits.

The distribution of the unscheduled component of active power $P_{unsch}{}^{p/pli}$ at the station level between the control units is carried out by their participation factors β_{ij} in the secondary frequency control:

$$P_{set}^{G-i-j} = \beta_{ij} P_{unsch}^{e/sti},\tag{26}$$

with

$$P_{unsch}^{e/sti} = \sum_{j=1}^{m} \Delta P_{set}^{G-i-j},\tag{27}$$

where $\Delta P_{set}{}^{G-i-j}$ is a setpoint for active power on the *j-th* control unit ($j = 1, \ldots,$ *m*) of the *i-th* station; β_{ij} is a participation factor of the *j*-unit *i*-power plant in the secondary frequency control.

Further calculation of the setpoints $\Delta P_{set}{}^{G-i-j}$ from the APR is carried out based on the governor characteristics of the turbine.

At the aggregate level, the governors provide the turbine power change according to the APR control action.

5 Simulation of the Load–Frequency Control in Power System with Renewables

5.1 Simulation of ALFCS Operation in Case of the Setpoint Change of the Net Interchange Power

The obtained simulation results correspond to the setpoint change of the net interchange power in the ALFCS2 controller from 222 MW in initial load flow to 200 MW.

The simulation results of the initial load flow and after the secondary frequency control are given in Table 1.

As seen, ALFCS2 provides the requirements of the secondary frequency control (the net interchange power changes to 200 MW). The total generation change of the power plants in IPS2 after the secondary frequency control is 23.1 MW. The generation change of the second power plant equals 14.3 MW, the third power plant is 7.3 MW, while the wind farm generation change is 1.5 MW.

The simulation results in the time domain considering the developed ALFCS model are depicted in Figs. 12, 13, and 14. It should be noted that the negative values of active power flow through the controlled interface correspond to the receiving side of the transmission line (in Power system 2).

As seen in Figs. 13 and 14, after the secondary frequency control, the setpoints of the net interchange power flow (200 MW) and nominal frequency are provided due to the generation change of the regulating power plants.

The simulation results, given in Table 1 and Figs. 12, 13 and 14, indicate the correct operation of the ALFCS2 controller (at the system level) in the case of the

Table 1 The simulation results of the initial load flow and after the secondary frequency control

Element	Active power, MW		Active power change, MW
	Initial load flow	Load flow after the secondary frequency control	
Power plant № 1	231	207.3	23.7
Generator G-1	231	207.3	23.7
Power plant № 2	200	214.3	14.3
Generator G-2-1	100	110.7	10.7
Generator G-2-2	100	103.6	3.6
Power plant № 3	200	207.3	7.3
Generator G-3-1	100	104	4
Generator G-3-2	100	103.3	3.3
Windfarm	27.5	29	1.5
OHL 1-2/1	71.6	61.1	−9.1
OHL 1-2/2	71.6	61.1	−9.1
OHL-1-5	86.9	78.1	−5.1
Total generation	658.3	657.7	−0.6
Total consumption	640.9	641.6	0.7
Total losses	17.4	16.1	−1.3
Net interchange power flow	222.3	200.3	22

setpoint change of the net interchange power plow. The transient time is 150 s, which also satisfies the requirements of the secondary frequency control.

5.2 Load–Frequency Control in Case of the Active Power Imbalance

The connection of the additional load which equals 50 MW is considered an imbalance of active power. The results of the RMS simulation for this case are presented in Figs. 15, 16, 17, 18 and 19.

As seen, the additional load power leads to changes in the frequency and net interchange power (Figs. 15 and 19). It should be noted that after the secondary frequency control, the normal frequency and scheduled net interchange power flow are maintained. As seen in Figs. 16 and 17, the control action from ALFCS2 leads to the generation change of the synchronous generators and wind turbines of the wind farm. It should be noted that the power generation of wind farms changes much more slowly compared to synchronous generators. This is because the control system of the wind turbine with a fully rated converter acts to change the angle of rotation of the
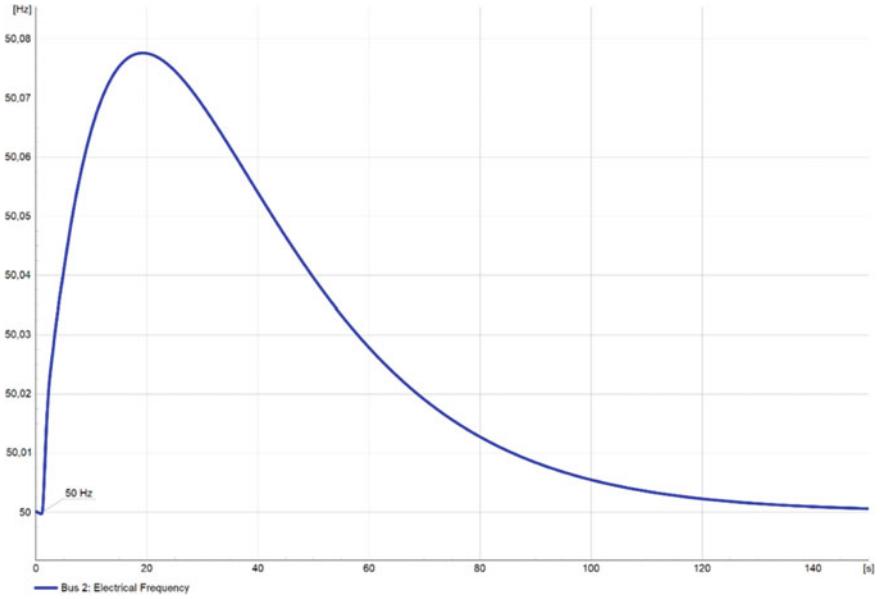
Fig. 12 Frequency change in Power system 2
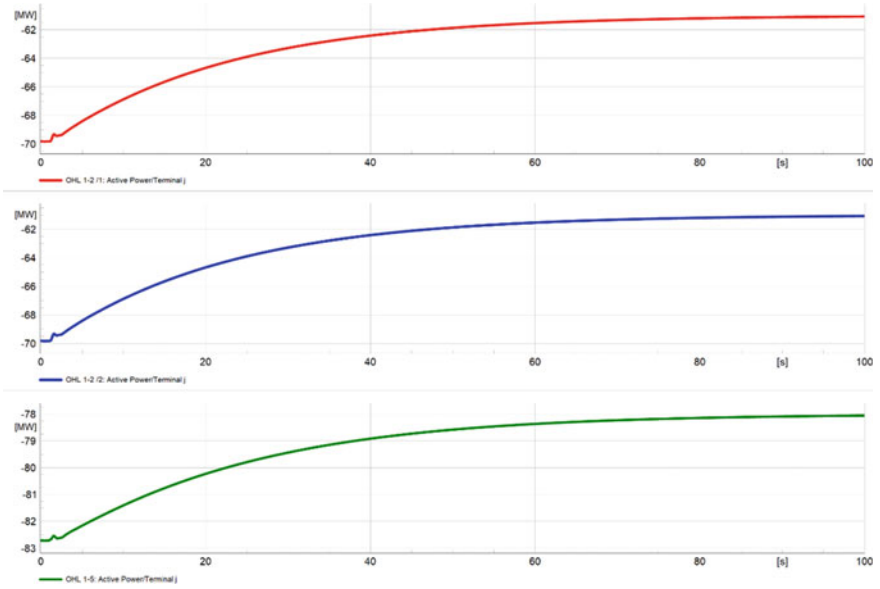
Fig. 13 Power flows at overhead lines of the controlled interface
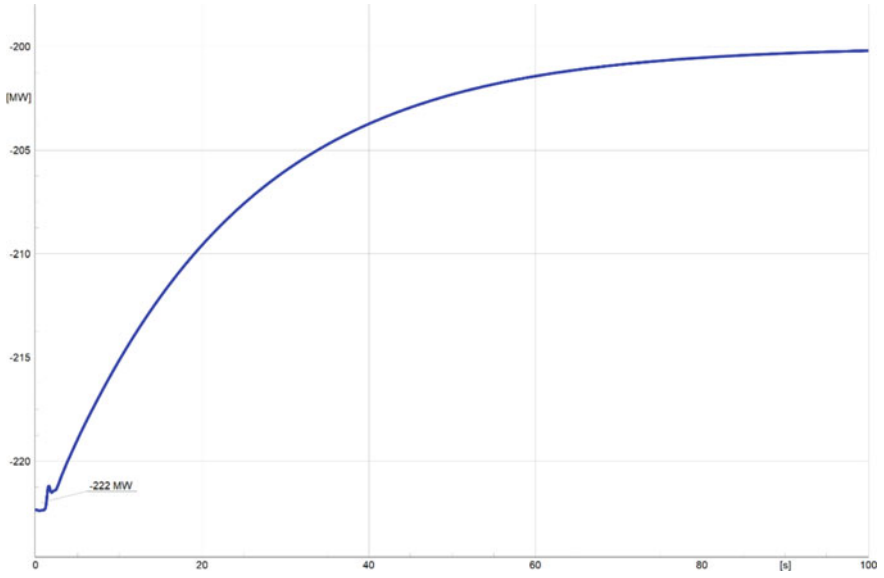
Fig. 14 The net interchange power change between Power systems 1 and 2
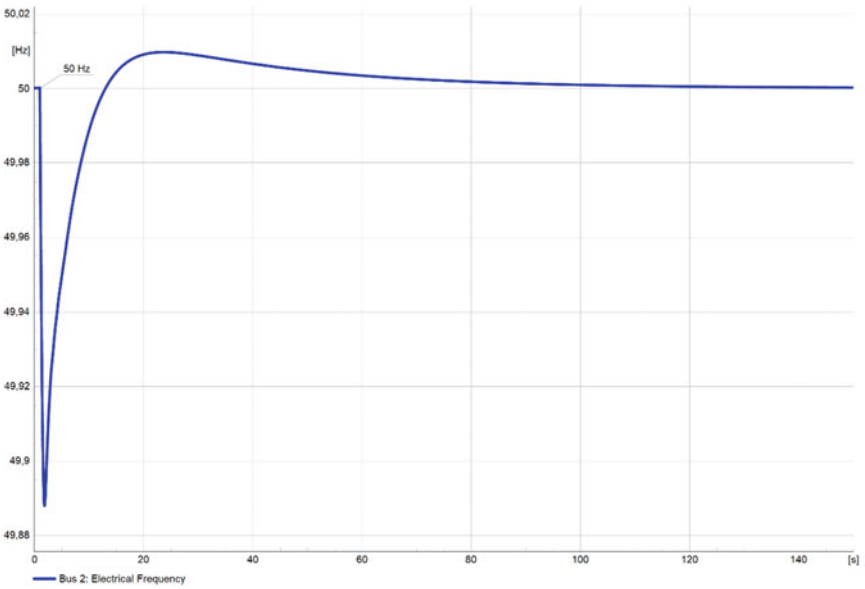
Fig. 15 Frequency change in case of the active power imbalance
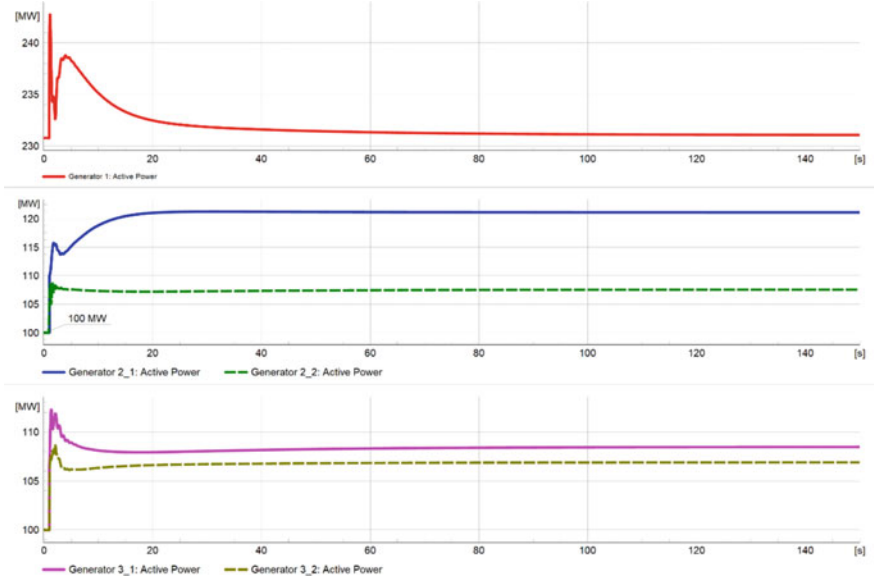
Fig. 16 Generation of the second and third control power plants in IPS2
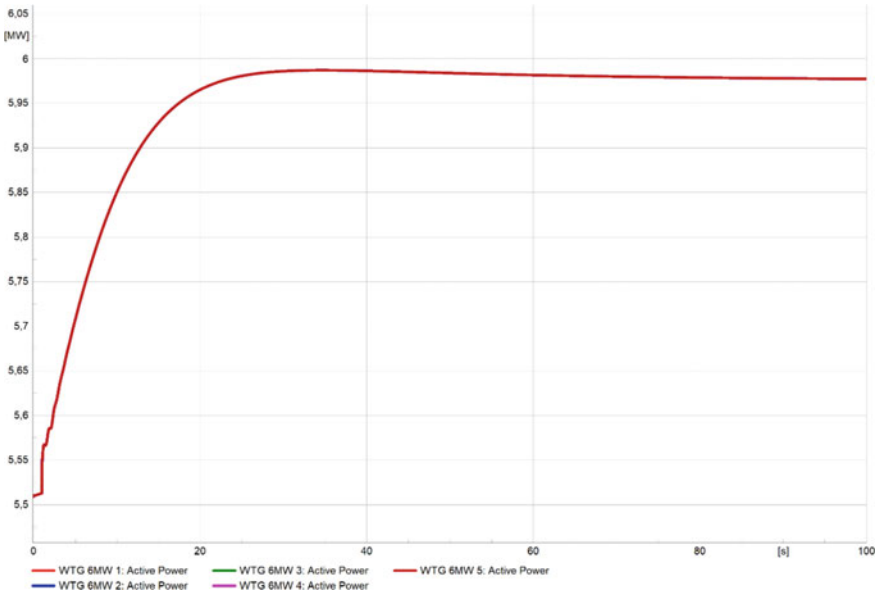
Fig. 17 Wind turbines' power change
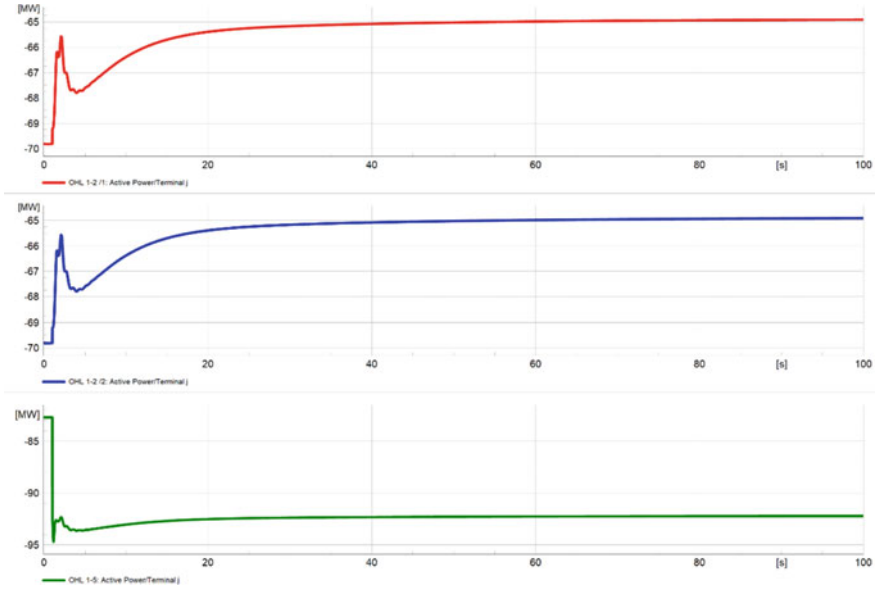
Fig. 18 Power flows change of the controlled overhead lines
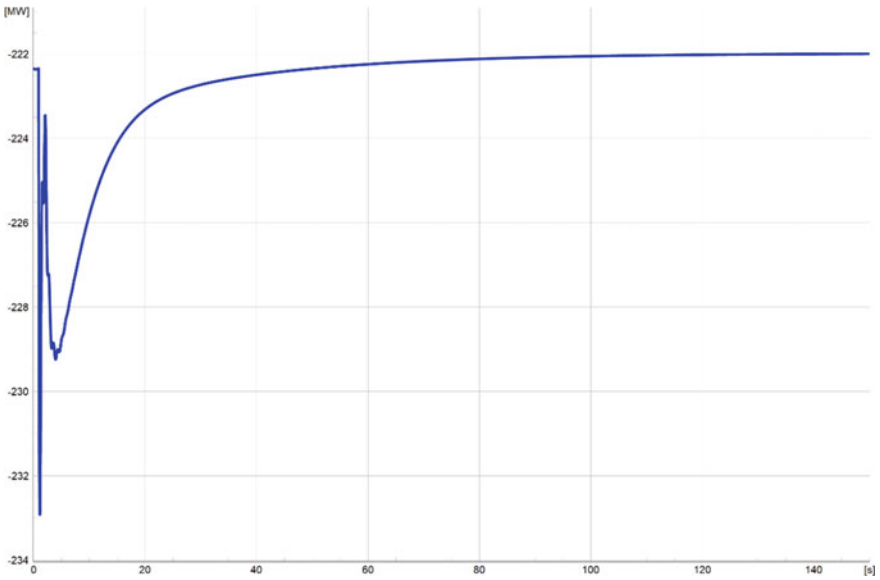
Fig. 19 Net interchange power flow change at the controlled interface

blades of wind turbines, which is a long process. However, the duration of changes in the power generation of wind farms is 50–60 s, which satisfies the requirements for the duration of secondary frequency control (up to 900 s).

5.3 Load–Frequency Control in Case of the Generation Setpoint Change in the Windfarm Controller

The results of the RMS simulation for this case are depicted in Figs. 20, 21, 22, 23 and 24.

As seen, the correct operation of the wind farm local controller is provided. At the same time, the change in the setpoint of the total capacity of the wind farm encourages a slight change in the frequency and the net interchange power at the controlled interface (Figs. 20 and 23, respectively).

Thus, as simulation results indicate, there is a possibility of participation of wind farms in the load–frequency control.
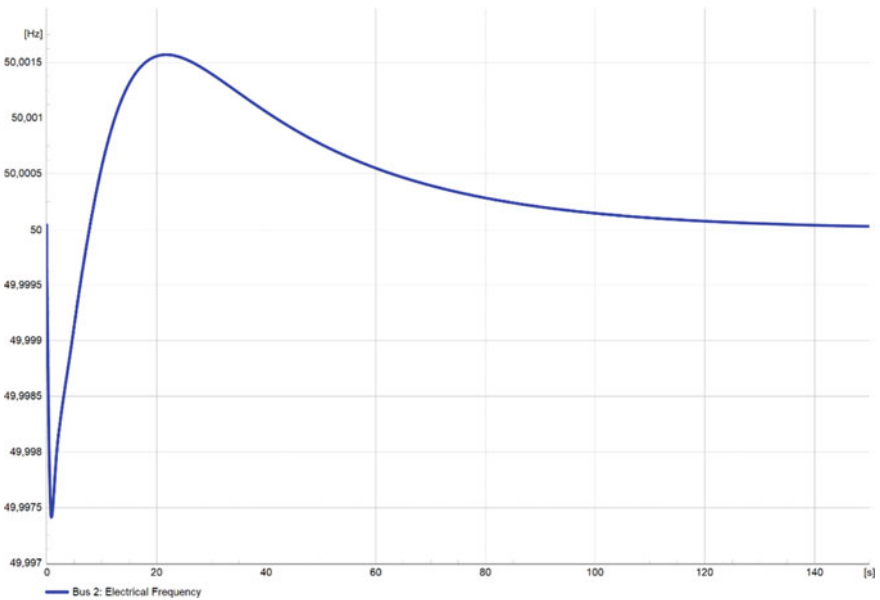
Fig. 20 Frequency change in the power system
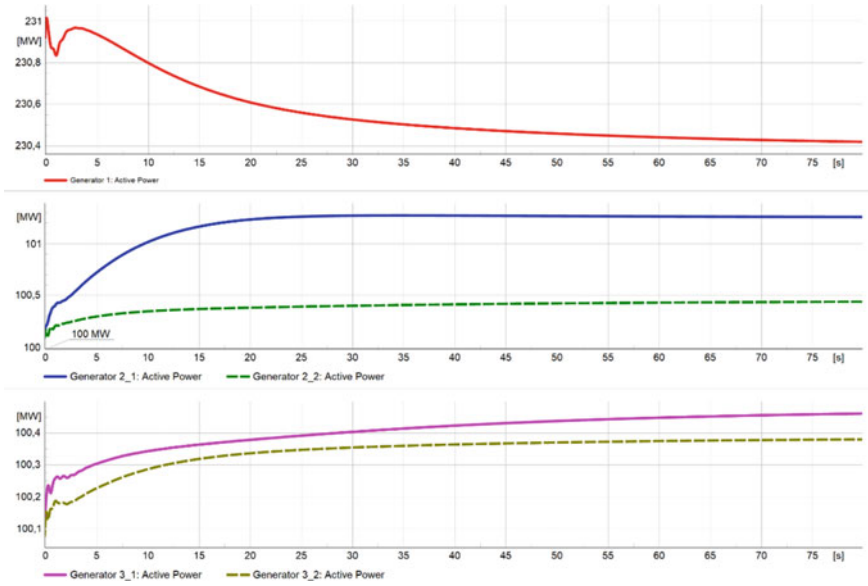
Fig. 21 Generation of the regulated power plants
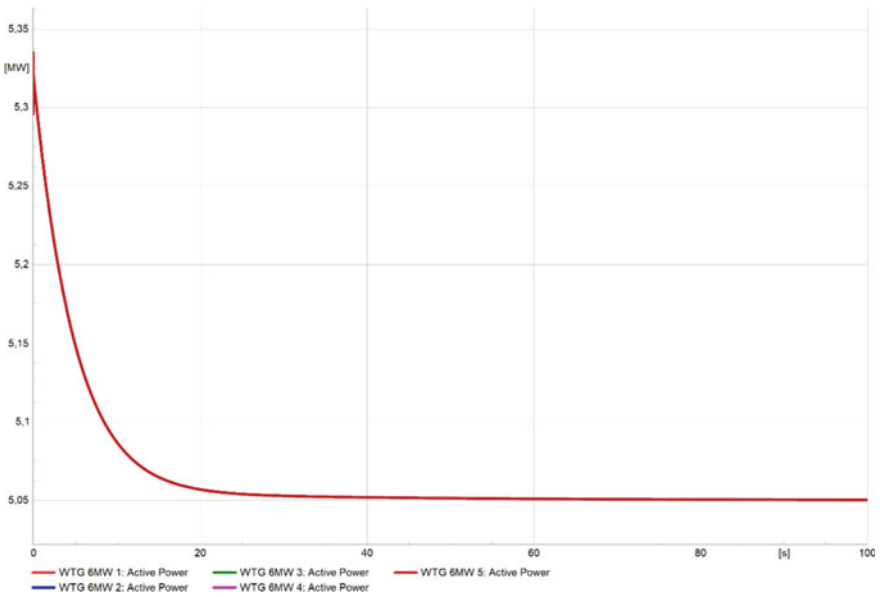
Fig. 22 The change of the wind turbines' power
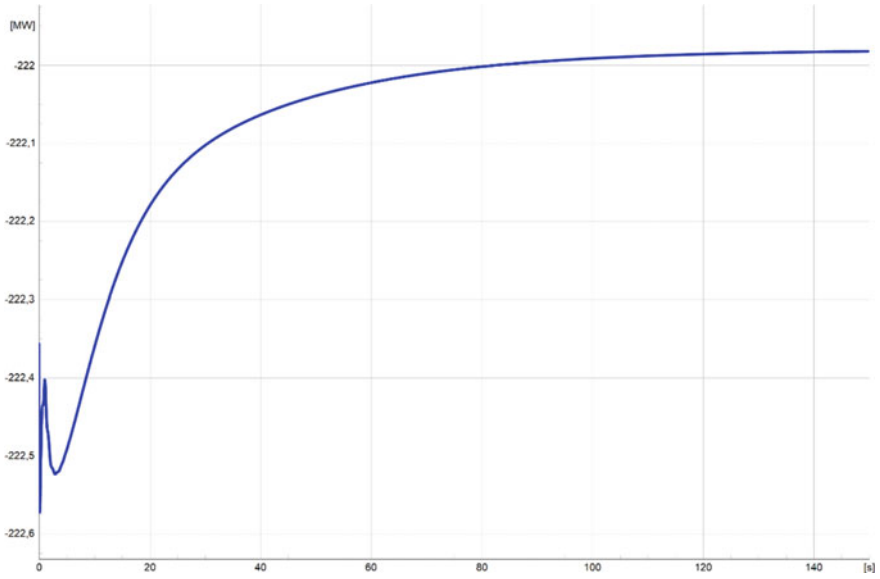
Fig. 23 Net interchange power flow at the controlled interface
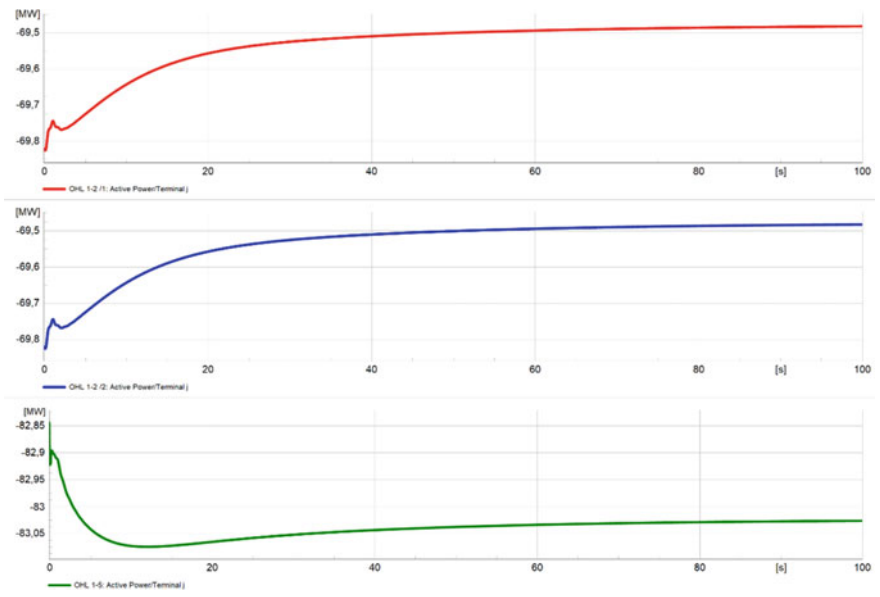
Fig. 24 Active power flows change of the controlled overhead lines

6 Load–Frequency Control Study with the Energy Storage Systems

According to the obtained research results, the wind farm units allow ensuring the participation of these stations in the automatic secondary frequency control within their control range. It should be noted that the change in wind turbine power is carried out by the change of the rotation angle of the turbine blades to a certain angle. In addition, the angle change is relatively slow, which somewhat limits the participation of wind farms in the primary frequency control. At present, the use of energy storage systems (ESS) is becoming widespread, especially in the power system with a significant share of RES.

To assess the quality of the load–frequency control including ESS, the load–frequency control study is performed using the test power system model depicted in Fig. 25.

As seen in Fig. 25, ESS with an installed capacity of 20 MW is used in the load–frequency control. The ESS characteristics are presented in Fig. 26 and indicate that the storage system can operate both in the generation and consumption mode of the active power. In the case of the frequency decreasing in the power system, ESS increases the generated active power and vice versa. Such an approach to frequency
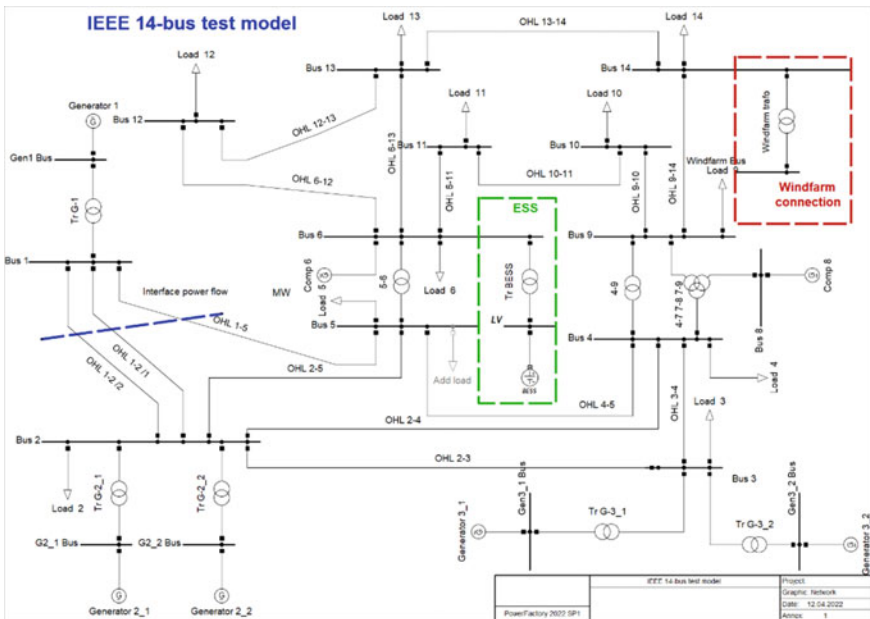
Fig. 25 Block diagram of the test power system considering the ESS

control corresponds to the principles of primary frequency control. To study the influence of ESS on load–frequency control, it is assumed that the initial ESS generation equals zero.

Let us consider the ESS control system block diagram in detail, which is depicted in Fig. 27.

In the model, there are units used for measuring AC voltage, active and reactive power, as well as frequency. Based on the measured value of the frequency f_{rq}, considering the specified droop, the deviation of the active power dp_{ref} is calculated, which is proportional to the deviation of the frequency f_{rq}. This signal, along with the above signals (AC voltage, active and reactive power), as well as changes in the
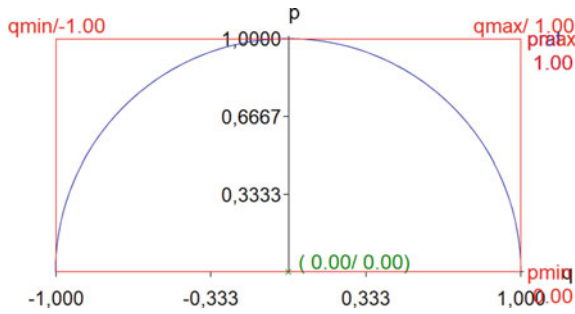
Fig. 26 Generation characteristics of the ESS system
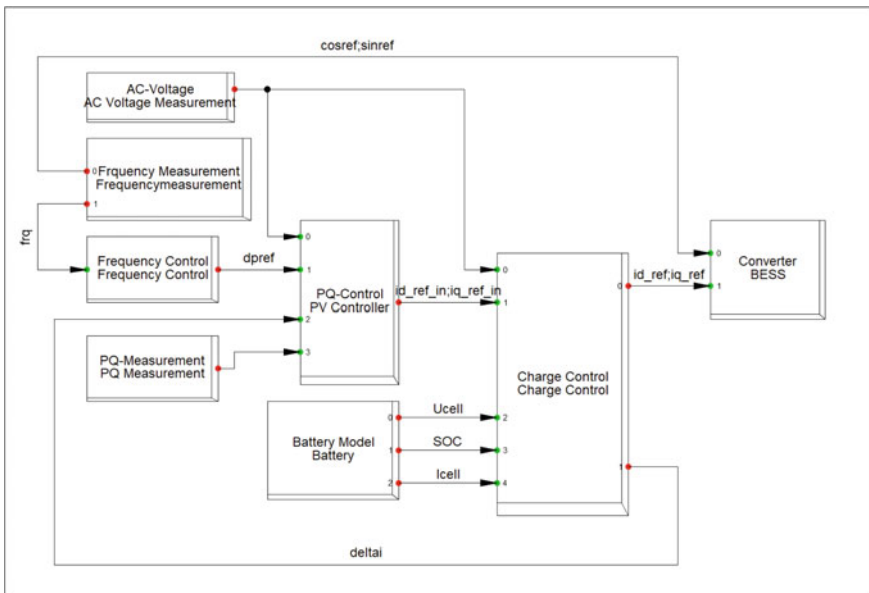
Fig. 27 Block diagram of the ESS control system

deltai charge current are transmitted to the input of the active and reactive power control unit. At the output of the specified unit, the reference currents *id_ref _in* and *iq_ref _in* are produced in *dq*-coordinates that are proportional to the setpoints for active and reactive power. These signals are transmitted to the input of the storage charge control unit, which, from the battery model unit, also supplies the U_{cell} *voltage* and I_{cell} *current* of the battery cell, as well as the signal of the actual state of its charge *SOC* (State of Charge). Accordingly, at the output of the charge control unit of the setpoint accumulation system for currents in *dq*-coordinates: *id_ref* and *iq_ref*, which, along with the actual frequency in the power system, are input signals of the ESS controller.

The simulation results of the load–frequency control in case of the additional load connection at SS-6 are shown in Figs. 28, 29, 30, 31 and 32. It should be noted that curves with a solid line correspond to the case of the use of ESS, while the curves with a dotted line correspond to the case of the absence of ESS in the power system.

As seen, the use of ESS leads to load–frequency control improvement, especially at the stage of the primary frequency control. Thus, ESS generates an additional power during 20 s (Fig. 32) that corresponds to the stage of the primary frequency control. As a result, this leads to a decrease in the dynamic frequency deviation (Fig. 28) and the deviation of the net interchange power flow at the controlled interface between the first and second power systems (Fig. 31). Thus, ESS can be used to provide the primary frequency control in the power systems with renewables.
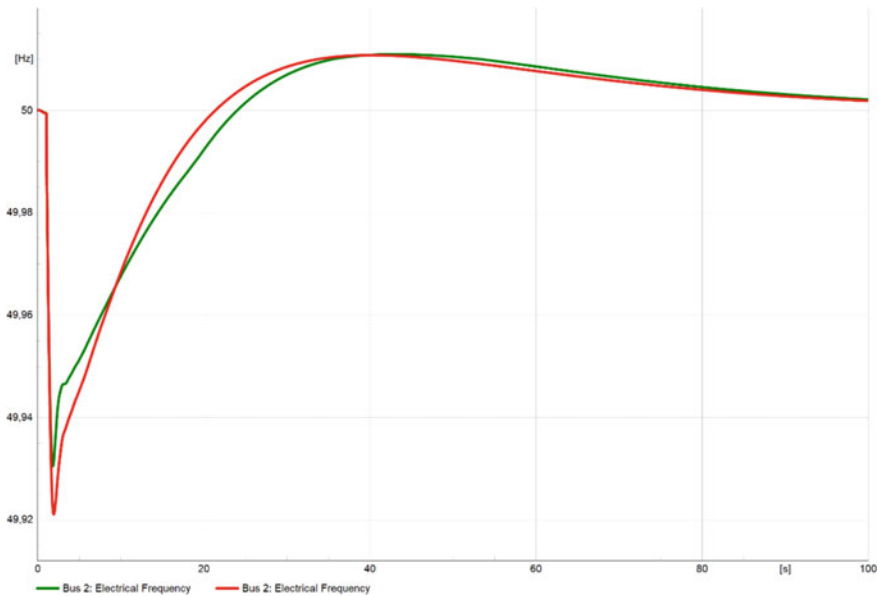
Fig. 28 Frequency change in the power system (green curve—including ESS, red curve—without ESS)
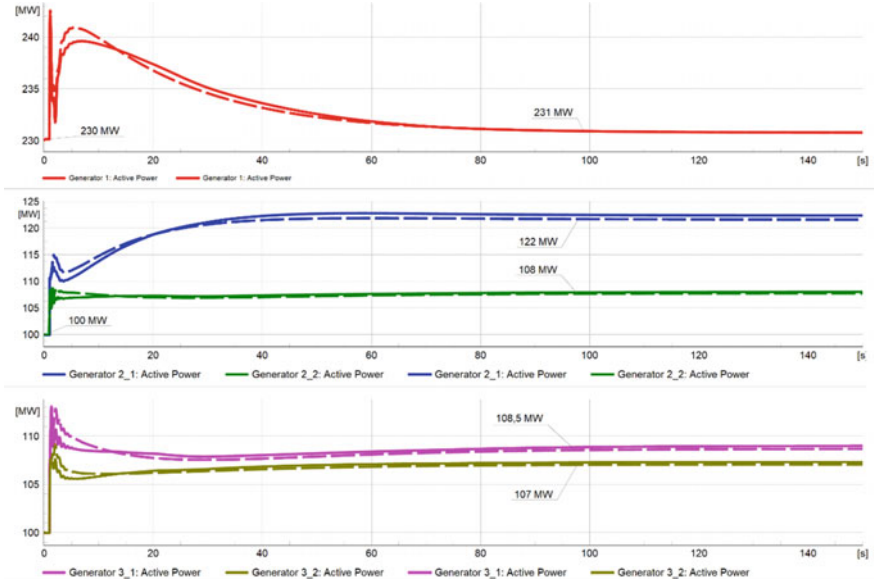
Fig. 29 Generation of the power plants in the first and second power systems
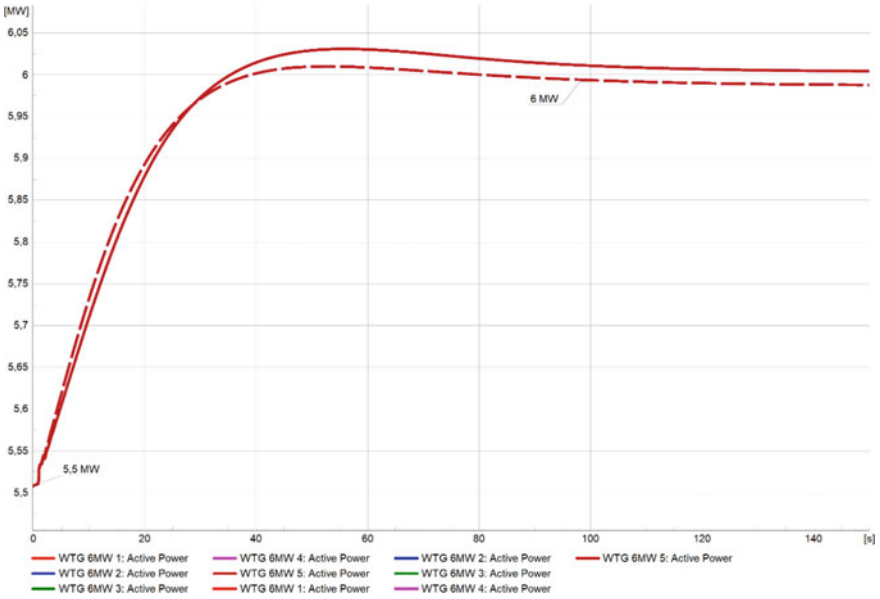
Fig. 30 Generation of wind turbines
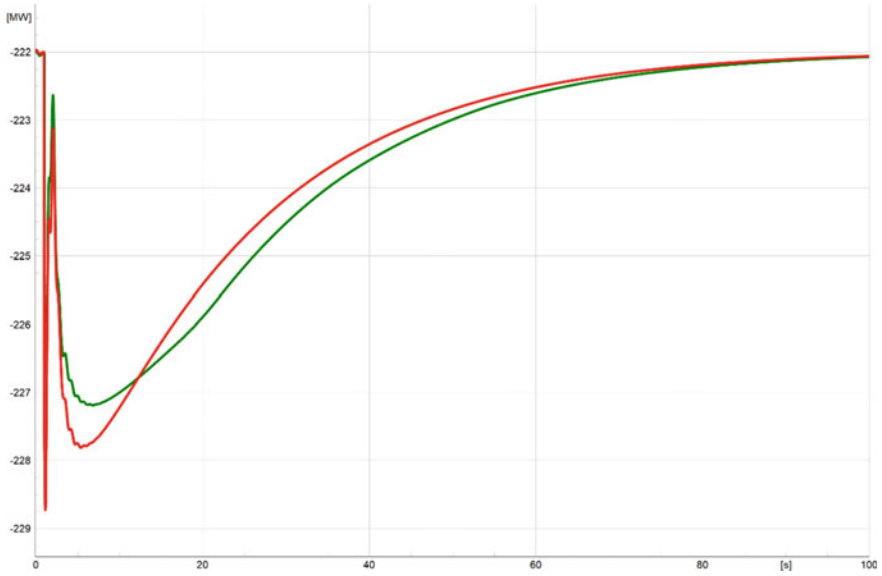
Fig. 31 Change of the net interchange power flow at the controlled interface
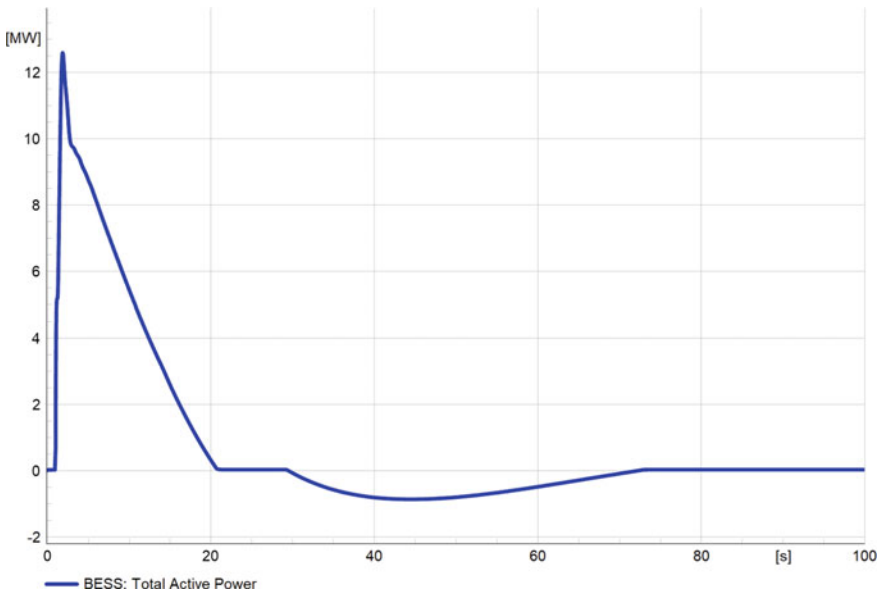
Fig. 32 ESS generation change

References

1. ENTSOE Operation Handbook. P5—Policy 5: Emergency Operations
2. Kundur, P.: Power System Stability and Control. McGraw-Hill (1994)
3. Machowski, J., Bialek, J., Bumby J.: Power System Dynamics. Stability and Control, 2nd ed. Wiley (2008)
4. Stelyuk, A.O., Zaichenko, V.B., Pavlovsky, V.V., Lukyanenko, L.M., Makogonchuk, V.S.: Identification and classification of "critical voltage points" in power systems based on modeling of modes on "N-1 principle." Energ. Electr. **6**, 10–13 (2010)
5. ENTSO-e Operation Handbook—Policy 3: Operational Security—Final Version, p. 21
6. ENTSO-e Operation Handbook—Appendix 3: Operational Security—Final Version, p. 41
7. Tarnowski, G.C.: Coordinated frequency control of wind turbines in power systems with high wind power penetration, p. 288. Ph.D. Thesis, Technical University of Denmark, November 2011
8. Sørensen, P., Hansen, A.D., Thomsen, K., Buhl, T., et al.: Operation and control of large wind turbines and wind farms—Final report, RISO Laboratory, p. 44
9. McCalley, J.D.: Frequency control (MW-Hz) with wind, PSERC Seminar, p. 32
10. Aho, J., Buckspan, A., Laks, J., Jeong, Y., et al.: Tutorial of wind turbine control for supporting grid frequency through active power control, p. 14. Preprint, National Renewable Energy Laboratory
11. Kyrylenko, O., Pavlovsky, V., Steliuk, A., Vyshnevskyi, M.: Simulation of the normal and emergency operation of the interconnected power system of Ukraine for frequency stability study. Techn. Electrodyn. **2**, 57–60 (2017)
12. Pavlovsky, V.V., Stelyuk, A.O., Lukyanenko, L.M., Lenga, O.V.: Analysis of frequency change in the IPS of Ukraine under conditions of disconnection of the power unit of a nuclear power plant. Tech. Electrodyn. **4**, 89–94 (2018)
13. Pavlovsky, V.V., Stelyuk, A.O., Lenga, O.V., Grechko, V.V., Zaichenko, V.B., Vorobey, V.V., Tkachuk, T.V.: Ensuring sustainable operation of the IPS of Ukraine in frequency under conditions of active power imbalances. Energ. Electr. **4**, 9–15 (2019)
14. Pavlovsky, V., Steliuk, A., Lenga, O., Hrechko, V.: Frequency stability of the bulk isolated power system with high share of renewables and nuclear generation. In: Power Systems Research and Operation. Selected problems, p. 180. Springer (2021). https://doi.org/10.1007/978-3-030-82926-1_8

On One Approach to Distribution Electrical Networks' State Estimation Under Information Incompleteness Conditions

Oleksandr Butkevych ⓘ

Abstract In this chapter one approach to the problem's solving of distribution electrical networks' (ENs) state estimation under telemetered information incompleteness conditions is presented. This approach is focused on the use in the dispatching system and in addition to telemetered EN operational condition parameters involves also using of the results of seasonal control measurements processing and expert fuzzy estimates on the possible boundary values of the loads' active power of the so-called unobservable nodes. Such expert information is formalized in the form of corresponding trapezoidal membership functions. Problem solving results are expert-calculation estimates of EN operational condition parameters. An example of EN scheme's fragment with the rated voltage of 110 kV and corresponding results illustrating the proposed approach application are presented.

Keywords Distribution electrical network · Electrical network dispatching · Observability · State estimation problem · Information incompleteness · Fuzzy expert information

1 Introduction

Some problems of the electrical networks (ENs) dispatching are carried out under operational information incompleteness conditions. That information incompleteness takes place to a greater extent in distribution ENs (with nominal voltage of 110, 35, 20, 10, and 6 kV, such nominal voltage row for distribution ENs is used in Ukraine). Sometimes the factor of operational information incompleteness affects the quality of solving dispatching problems and, accordingly, the adequacy of the results obtained and the efficiency of EN dispatching as a whole. The state of the

O. Butkevych (✉)

The Institute of Electrodynamics of the National Academy of Sciences of Ukraine, Peremohy Avenue, 56, Kyiv 03057, Ukraine
e-mail: o.butkevych@gmail.com

National Technical University of Ukraine "Igor Sikorsky Kyiv Polytechnic Institute", Peremohy Avenue, 37, Kyiv 03056, Ukraine

controlled system is determined by the state variables which form its state vector, the classical interpretation of that requires the equality of the number of coordinates of the system's complete mathematical model to the number of independent variables. That is why to determine the EN's state vector operational telemetry information (TI) is required (in general case a lot of TI consists of signals' groups which indicate equipment status, protections relay and EN operational condition parameters' values) which gives possibility to form a corresponding equations to solve the EN state estimation problem. Such system must be at least definite (but it is better to have an excess TI amount to form an overridden system of the equations and to use a TI redundancy to verify information authenticity). In the case of some overridden equations system (provided that there are no gross errors in TI or if such errors already have been eliminated) the problem of EN operational condition parameters estimation can be reduced, as is known, to the problem of so-called EN's operational condition balancing.

A distribution EN is traditionally unobservable (partially observable) due to the large number of connection points and corresponding high costs associated with EN's equipping with telemetry devices. In the case due to the TI deficiency the equations' system turns out to be underdetermined (having a lot of solutions), then without using other available information that compensates TI deficiency it is impossible to correctly estimate EN operational condition parameters. It must be noted that with TI deficiency various methods and means to estimate EN operational condition parameters can be used.

A lot of publications are devoted to the problem of power systems state estimation but, obviously, ones of the fundamental and first ones should be attributed [1–3], although the statement of the problem itself appeared a little earlier (1966) and it was associated with the dispatching creation in the French power system (Electricité de France). Even if we proceed from a lot of number of recent publications devoted to solving this problem, taking into account the different level of technical equipment of ENs with different measuring devices and techniques, for example, [4–6] we can conclude that despite the long period of its existence this problem remains relevant.

2 The Features of Problem's Setting, Formalizing, and Solving

First, let us consider general provisions of the proposed solving approach to the problem of EN state estimation using all available information, including expert one to make up for the TI deficiency. All consumers which are supplied by the lines extending from the buses of electrical substations can be taken into account in the form of *equivalent bus loads* (Fig. 1) or as *equivalent substation loads* (as the sum of such *equivalent bus loads*)—differently for different substations.

That form of loads' accounting also corresponds to the extent of generalization of information obtaining in the ENs during seasonal control measurements. Taking
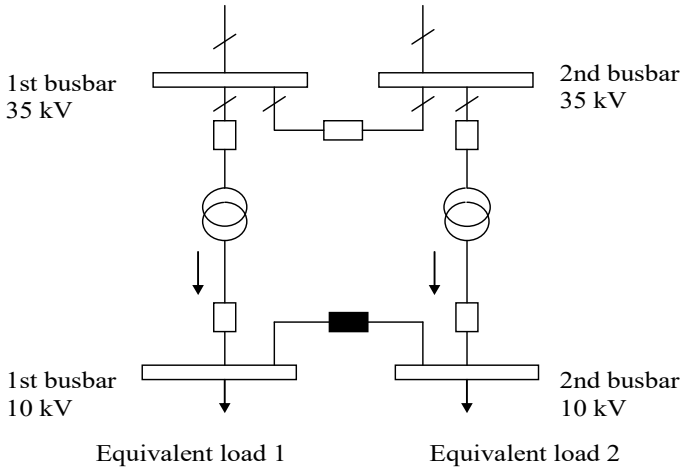
Fig. 1 Electrical substation 35/10 kV scheme's example

into account the information composition that is available in the EN load dispatch centers as a result of EN state estimation the following should be provided:

- a compliance of the *balance* part of EN operational condition parameters' measurements with the estimates (that is, the operational balance of the active power of the EN is taken as given, although, there is certainly some error in its determination);
- the estimates should be of a good quality, in particular, the differences of obtained estimates of EN operational condition parameters and corresponding measurements of the same parameters should be minimal;
- in the case of using the values of the EN operational condition parameters obtained as a result of the EN state estimation the restrictions in the form of EN steady-state condition equations must be satisfied

$$W = W(X, Y) = 0, \tag{1}$$

where X and Y are the vectors of independent and dependent variables (mode parameters) respectively.

In addition, independent variables and some functions of them $F(X)$ to which $Y(X)$ also belong always have the restrictions due to circumstances of both a physical property (for example, the restrictions due to the thermal resistance limit of electrical lines' wires) and a technological nature (for example, the need to ensure regulated voltage levels on substation buses)

$$X_{\min} \leq X \leq X_{\max}; \tag{2}$$

$$F(X) \leq 0. \tag{3}$$

It should be noted that obtained EN operational condition parameters' estimates can be within wider limits when compared with the limits set on the basis of technological requirements because in the real EN operational condition the latter are not always fulfilled if corresponding parameters are not controlled.

A mathematical formulation of the EN state estimation problem can be presented as a mathematical programming problem. At the same time the differences' function (Φ) of the EN operational condition parameters' values (V) those are obtaining during process of problem solving and corresponding measurements of the same parameters

$$\Phi(\Delta V) \rightarrow \min.$$

If we neglect the measurement errors' correlation then, as is known, the indicated function $\Phi(\Delta V)$ will be represented by the sum of m scalar functions (φ_i) of scalar variables

$$\Phi(\Delta V) = \sum_{i=1}^{i=m} \rho_i \varphi_i(\Delta v_i),$$

where $\varphi_i(\Delta v_i)$) is a scalar function of the deviation some EN operational condition parameter v_i from its measured value v_{iT}.

In this case a quadratic function is used, that is $\Phi(\Delta V)$ is a function of the least weighted squares method

$$\Phi(\Delta V) = \sum_{i=1}^{i=m} \rho_i \varphi_i(\Delta v_i) = \sum_{i=1}^{i=m} \rho_i (v_i - v_{iT})^2, \tag{4}$$

where ρ_i is the weight coefficient depending on measurement accuracy of corresponding parameters.

Since in the EN under consideration TI incompleteness presents, then, as already noted, the system of independent equations, which contain TI parameters and establish the dependencies between EN operational condition parameters will be under-determined. With the appearance of the *information pseudo-completeness defect* and corresponding restrictions on the pseudo-TI use in the case of inability to use statistical historical data [7] TI incompleteness can only be filled by using information on the loads obtained on the basis of processing seasonal control measurements and information in the form of expert estimates of unobserved loads consumers (see *equivalent loads* in Fig. 1). Moreover, the experts can judge the values of these loads' active power at different time points of the daily power consumption schedule only in terms of possibility of one or another value with varying degrees of confidence.

Let us give a typical example of the form in which information about the load's active power of some electrical substation can be received from an expert,

"At the indicated time of day a load active power value of the electrical substation will most likely be in the interval from 3 to 4 MW."

It is obvious that such information is subjective and fuzzy (the information provided by a more experienced expert, as a rule, is also more certain). If for the above expert judgment we use the method of the membership function constructing based on expert estimates described, then the membership function of the fuzzy set of load's active power values of the electrical substation (μ_P) "The value of the load's active power will most likely be in the interval from 3 to 4 MW" we obtain based on the membership functions' construction for two point expert estimates (for 3 and 4 MW in this example) each of which is represented by the expressions:

$$\mu_3(P) = e^{-\alpha_3(3-P)^2}; \quad \mu_4(P) = e^{-\alpha_4(4-P)^2},$$

where $\mu_3(P)$ and $\mu_4(P)$ are the membership functions of fuzzy set of loads' active power values which approximately equal to 3 MW and 4 MW respectively, and $\alpha_3 = -4 \ln 0.5 / \beta_3^2$, $\alpha_4 = -4 \ln 0.5 / \beta_4^2$ where β_3, β_4 are the distances between transition points for $\mu_3(P)$ and $\mu_4(P)$ respectively, that is the points at which the functions $\mu_3(P)$ and $\mu_4(P)$ take the value 0.5.

Thus, in the case under consideration, the task of constructing $\mu_{P_{L2}}$ is reduced to β_3, α_3, β_4, α_4 determining and $\mu_3(P)$ and $\mu_4(P)$ constructing; their left and right halves together with the upper segment connecting their vertices form μ_{P_L} (it is shown in Fig. 2 by a solid line).

The membership function μ_P can be interpreted as "expert's confidence distribution that the load's active power will take an appropriate value in the indicated interval of possible values."

It should be noted that both normal and logarithmically normal distribution of expert estimations are possible (this allows use quartile characteristics for expert survey results' processing, because their calculation and use does not require knowledge of the law of expert estimates distribution [8]).

In the most practical cases trapezoidal membership functions are used. The form of such membership function is shown in Fig. 3 where P^b (bottom) and P^u (upper) are the boundaries of the interval (point estimates) to which in the considered example the values of 3 and 4 MW correspond.
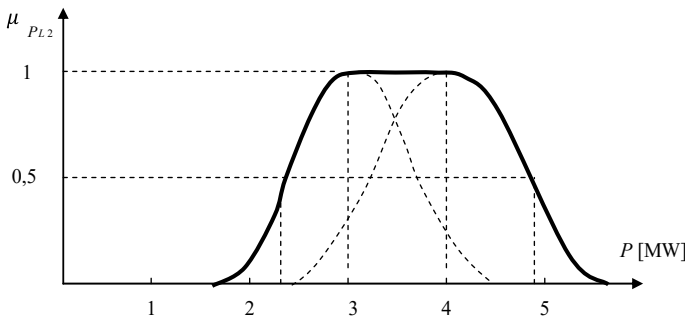
Fig. 2 $\mu_{P_{L2}}$-construction taking into account some expert estimation
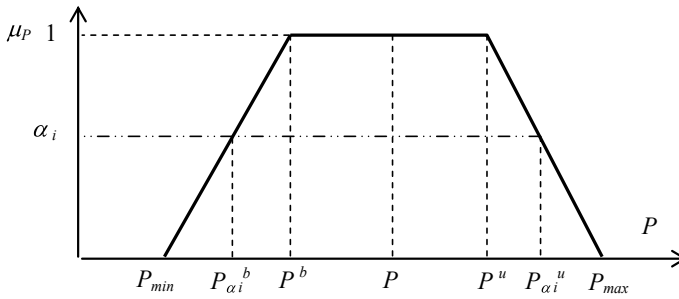
Fig. 3 Trapezoidal membership function

Such representation is acceptable if we take into account the nature of available information and a need to take into account clear boundary values (P_{min} and P_{max} in Fig. 3) beyond which the considered value cannot (physically or technologically) go. In support of such representation the circumstance can also be used that in the presence of information only about the range of variation of a random variable the hypothesis on the law of uniform probability distribution density is always accepted as the most cautious hypothesis.

Since the direct consideration of the *clear* boundary values of the loads' active power of unobserved EN nodes when using membership functions of such form as in Fig. 2 is problematic, it is quite natural to take into account indicated boundary values by constructing the combined membership function, the upper part of which (corresponding to the values $0.5 \leq \mu \leq 1$) has the same form as in Fig. 2, and the lower one consists on the linear sections allowing to take into account the boundary values of the load's active power.

Figure 4 shows the combined membership function of the fuzzy set of load's active power values corresponding to the interval estimate "most likely to be in the values' interval from 3 to 4 MW" where dotted lines 1 and 2 are drawn from points *c* and *d*, as well the dashed line 3 that is drawn from point *a* correspond to the examples of different clear restrictions.

However, to solve the state estimation problem of considered ENs it is necessary to take into account practical aspects of constructing and using membership functions of a fuzzy set of active power values of the loads. Even in the case of taken into account consumers' loads in the form of equivalent loads their number can be significant. It must be noted that combined membership functions construction (such function is shown in Fig. 4) is too laborious process. In addition, unjustified computational costs also arise when calculating the boundary interval values of the active power of such loads ($P_{\alpha i}^{b}$ and $P_{\alpha i}^{u}$ in Fig. 4), corresponding to certain given values of the membership function (α_i in Fig. 4), which will be discussed below. The construction of trapezoidal membership functions analytically represented by expressions (5) is a very real task for the practical implementation.
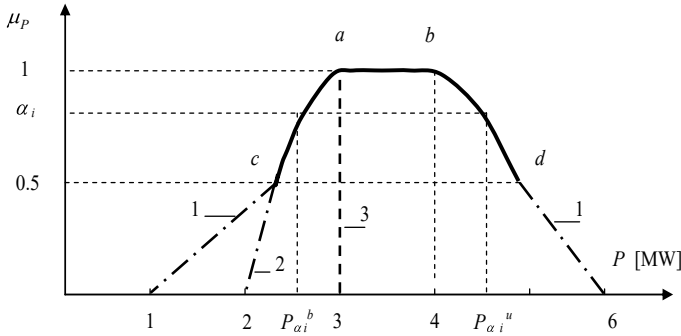
Fig. 4 Combined membership function

$$\mu(P) = \begin{cases} \frac{P - P_{\min}}{P^b - P_{\min}} & \text{if } P_{\min} < P < P^b; \\ 1 & \text{if } P^b \leq P \leq P^u; \\ \frac{P_{\max} - P}{P_{\max} - P^u} & \text{if } P^u < P < P_{\max}; \\ 0 & \text{if } P \leq P_{\min} \text{ or } P \geq P_{\max}. \end{cases} \tag{5}$$

In addition, boundary interval values of the loads' active powers ($P_{\alpha i}^b$ and $P_{\alpha i}^u$ in Fig. 3) corresponding to certain values of membership functions (α_i in Fig. 3) are easily determined by using the first and third equalities-conditions (5): first, the values of P are determined and then using the obtained values of P (respectively, we denote P_1 and P_3) $P_{\alpha i}^b = P_1$ and $P_{\alpha i}^u = P_3$ are taken.

Let us now consider the issue of information using on the loads determined on the basis of processing data obtained during seasonal control measurements, when power system operational condition parameters are measured every hour on the appointed day by all available means. In the absence of other (more accurate) information about the loads of unobservable nodes (except the information obtained from the data of seasonal control measurements) as the most cautious hypothesis about the load's power graphs in such nodes may be accepted the hypothesis about maintaining their similarity to the corresponding graphs obtained from seasonal control measurements. Then in accordance with this assumption the current value of the load's active power of the unobserved i-th node is determined as follows:

$$P_i = \left(P_\Sigma - P_{c\Sigma} - \Delta P\right) P_i^{sm} / P_\Sigma^{sm}, \tag{6}$$

where P_Σ is the current (determined based on telemetry data) total value of active power entering to the NE; $P_{c\Sigma}$ is the current total value of active power in the observed load nodes (these include both nodes, the load power value of which can be determined by telemetering using, and the nodes the load graphs of which are a priori known); ΔP is the average (for corresponding EN operational conditions) value of total active power losses in the EN (more precisely the value ΔP can be determined using polynomial dependence ΔP from P_Σ and several observed

EN operational condition parameters (such polynomial dependence can be obtained based on a series of EN steady state operational conditions calculations); P_i^{sm} is the value of the load active power in the i-th unobserved node at the hour of the day of the control measurements, corresponding to the current hour (in the EN load dispatch centers there are corresponding load graphs based on the data of the day of control measurements); P_Σ^{sm} is the total value of the loads' active power of unobserved nodes at the hour of the day of control measurements corresponding to the current hour.

Such simplified approach to distribution the part of total active power entering to the EN among unobserved nodes, of course, does not allow to take into account many factors' influence and is very approximate, but it allows to determine initial approximations of active power of unobserved nodes (these approximations are subject to clarification about which will be discussed below), because more accurate methods and meaningful mathematical loads' models use (decomposition into characteristic components, decomposition into harmonic components etc.) requires information which is very problematic to obtain under existing conditions. It should be noted that initial approximations of the loads' active power values of unobserved nodes obtained in this way in most cases fall into trapezoidal membership function cores $\left[P^b, P^u\right]$; trapezoidal membership functions previously are constructed for the corresponding time points. However, the cases are not excluded when the values of the loads' active powers of some unobserved nodes are outside of corresponding intervals $\left[P^b, P^u\right]$ which is not consistent with expert estimates. For preliminary coordination of obtained values with expert estimates, the procedures of *pulling up* the loads' active powers of unobserved nodes to the expert estimates and *compensating* the resulting power imbalances are performed. The implementation of the *pull-up* and *compensation* procedures is an attempt to find a certain compromise between the values of the loads' active power obtained with a rough distribution in accordance with the expression (6) and the experts' knowledge about these loads. Moreover, one can try to perform the *pull-up* either in full (until the membership degree of the value of the load's active power of each node obtained as a result of the *pull-up* becomes equal to one) or limit oneself to an attempt to *pull up* active powers to the boundaries of corresponding intervals (membership function cores) $\left[P^b, P^u\right]$.

In the first case a clear preference is given to expert estimates and there is a greater difference between obtained values and the values determined using expression (6). The second approach which provides for *pulling-up* expert estimates (values) to the boundaries of the intervals (membership function cores) $\left[P^b, P^u\right]$) seems to be more balanced, although it is also aimed at achieving a compromise between expert estimates and the values of active power which are determined using expression (6). Each of the approaches is based on the same type of procedures. To clarify the features of these procedures, let consider the second approach using the same Fig. 3.

Let for a certain unobservable k-th node using (6) the power value was obtained which turned out to be equal to $P_{\alpha i}^b$ or $P_{\alpha i}^u$ (see Fig. 3), that is, it went beyond the boundaries of the interval $\left[P^b, P^u\right]$. To *pull- up* the obtained value of the k-th node's active power to the expert estimate it is necessary to bring it to the boundary of the interval $\left[P^b, P^u\right]$.

There are two possible options to do this:

- if the power value turned out to be less than P^b then obtained active power value should be changed by the value $\Delta P_{Uk} = P^b - P^b_{\alpha i}$,
- if the power value turned out to be more than P^u then obtained active power value should be changed by the value $\Delta P_{Uk} = P^u - P^u_{\alpha i}$.

In the general case there can be n_L such nodes, and the total value of the active power imbalance of unobserved nodes $(\Delta P_{U\sum})$ which will arise as a result of the considered *pulling up* the power of all n_L nodes is calculated by algebraic summation of ΔP_{Uk} over all such k-th nodes.

To eliminate the emerging imbalance the value of $\Delta P_{U\sum}$ must be compensated by changing the power of remaining unobserved nodes by the same value $\Delta P_{U\sum}$ but of the opposite sign. For this purpose the nodes are used the values of the active power of the loads of which obtained according to the expression (6) turn out to be in their intervals $\left[P^b, P^u \right]$ as for example, P_i in Fig. 3.

Some remoteness of the active power value of such j-th node from the boundaries of the specified interval (a kind of adjustment range) in the direction of increasing and decreasing is $\Delta P_{Uj} = P^u - P_j$ and $\Delta P_{Dj} = P_j - P^b$ respectively.

The number of such j-th nodes is equal to the total number of unobserved nodes minus n_L, therefore their total *compensation* powers (in each of the $\Delta P_{U\Sigma}$ and $\Delta P_{D\Sigma}$ directions) are determined by the corresponding summation of the values ΔP_{Uj} and ΔP_{Dj} for all such j-th nodes. If it turns out that the value of $\Delta P_{U\Sigma}$ can be compensated by $\Delta P_{U\Sigma}$ or $\Delta P_{U\Sigma}$ (depending on $\Delta P_{U\Sigma}$ sign), then a full *compensation* procedure is performed, otherwise, it is performed only to the extent that corresponds to available *compensation* possibilities ($\Delta P_{U\Sigma}$ or $\Delta P_{D\Sigma}$ choice depends on $\Delta P_{U\Sigma}$ sign).

It should be noted, if the *compensation* powers are sufficient to perform full *compensation*, then the sequence in which the selection and *pull-up* of the power of unobserved nodes is performed does not matter, otherwise, the *pull-up* should be performed in such way as to increase the degree certainty of active power values of unobserved nodes. In this case different approaches are possible both to the implementation of the *compensation* procedure and to the implementation of the *pull-up* procedure.

When the *compensation* procedure is carried out at least two main approaches to changing the power of *compensation* nodes (the nodes by certain changes of load powers of which the indicated *compensation* is carried out) are practically applicable. At the first of two indicated approaches the weighted distribution of the total value of the *compensation* power is carry out (depending on the power and the available adjustment range of each *compensation* node). At the second approach an attempt to ensure (as a result of the implementation of the *compensation* procedure) a shift of power values of *compensation* nodes to the centers of their power intervals $\left[P^b, P^u \right]$ is carry out.

The first approach is quite simple and universal while the second one is limited in use and explicitly applicable when the *compensation* powers significantly exceed $\Delta P_{U\Sigma}$ (so much so that they can provide *compensation* $\Delta P_{U\Sigma}$ limiting themselves practically only to those nodes whose power values will be shifted to the centers of their intervals $\left[P^b, P^u \right]$ and then will not go far from them).

The first of these approaches is focused on the maximum preservation of the proportions of the power distribution obtained in accordance with (6) while the second one leads to more their change because expert estimates are preferred (when implementing the second approach the first one can be used as its component-procedure). Note that as a result of performing the *compensation* procedure in the first approach the values of *compensated* powers also do not leave their intervals $\left[P^b, P^u\right]$, therefore, given its greater universality and weightedness this approach is used as the main one in determining initial approximations of the load powers of unobserved nodes.

Let us consider **main stages of the implementation of the *compensation* procedure** in accordance with this approach.

STAGE 1. Determining the amount of *compensated* power $\Delta P_{C\Sigma}$. It is determined by the value $\Delta P_{U\Sigma}$ (with full *compensation*), or (if the *compensation* possibilities are limited) by one of the values $\Delta P_{U\Sigma}$ or $\Delta P_{D\Sigma}$ (depending on the sign of $\Delta P_{U\Sigma}$).

STAGE 2. The coefficients (K_{P_j}) of active power ($\Delta P_{C\Sigma}$) distribution determination between *compensation* (*j*-th) nodes:

$$K_{P_j} = \beta_j \gamma_j \Big/ \sum \beta_j \gamma_j,$$

where $\beta_j = P_j \big/ \sum P_j$; P_j is the value of the *j*-th *compensation* node's active power obtained in accordance with expression (6); $\gamma_j = \Delta P_{adjj} \big/ \Delta P_{C\Sigma}$; ΔP_{adjj} is an adjustment range of the *j*-th *compensation* node's active power (in the direction determined by the sign $\Delta P_{U\Sigma}$).

STAGE 3. The power changing of each *j*-th *compensation* node by the value $\Delta P_{C\Sigma} K_{P_j}$.

Let us consider **the features of the *pull-up* procedure implementation** in accordance with this approach.

Two cases are of our interest:

1. when the value $\Delta P_{U\Sigma}$ cannot be *compensated* completely;
2. when compensatory capabilities of the nodes are generally absent.

In implementation terms both of above cases come down to the same procedure. The purpose of *pulling up* is to achieve the maximum possible value (the same for all) of membership functions of fuzzy sets of active power values of the loads of all or part of unobserved nodes of the EN (in the latter case, this applies to those nodes where the values of the indicated membership functions are less than a certain value) without decreasing original values of membership functions. To achieve this goal the condition of partial *self-compensation* must be met: active powers of some nodes can be *pulled up* in the direction of their increase, and others—in the direction of decrease.

For further explanations we will use Fig. 5 that shows membership functions of fuzzy sets of the values loads' active power of the nodes *A*, *B*, and *C*.

Let after the distribution according to (6) the values of the loads' active power of indicated nodes *A*, *B*, *C* amounted to 3 MW, 3 MW, and 16 MW respectively (all of
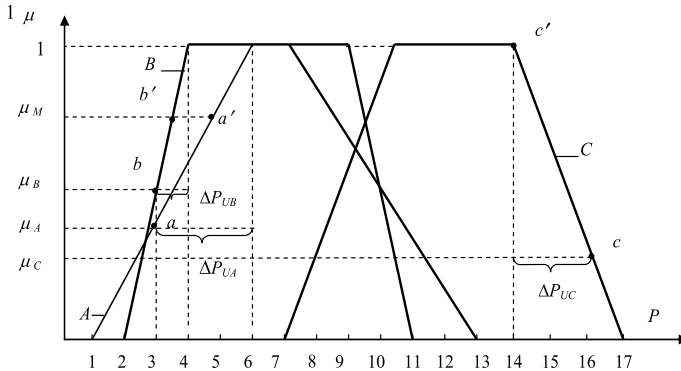
Fig. 5 Membership functions of fuzzy sets of loads' active power of the nodes *A*, *B*, and *C*

them are outside their intervals $\left[P^b, P^u\right]$ cores of membership functions and they correspond to the degrees of the membership μ_A, μ_B, μ_C.

To *pull up* the active powers of these loads to the boundaries of their intervals $\left[P^b, P^u\right]$ it is necessary to change their values to ΔP_{UA}, ΔP_{UB}, and ΔP_{UC} respectively, which will require 2 MW of *compensatory* unloading power (ΔP_C), because at *pull-up* 2 MW *self-compensate* (as a result of algebraic summation ΔP_{UA}, ΔP_{UB}, and ΔP_{UC}).

Let us consider the case when there is no possibility of *compensation*, that is the possibility of *self-compensation* must be determined (further it will become clear that the procedure considered below is also applicable to the case of partial *compensation*). Based on the condition for ensuring *compromise proximity* of the loads' active power values of unobserved nodes obtained using expression (6), and expert estimates for which the membership functions are presented by expressions of the form (5) and constructed, the loads' active power values of EN nodes and the degree belonging of these values to corresponding fuzzy sets should be determined.

It is obvious that if we limit ourselves to *pulling-up*-decreasing the load power of the node *C* only to the corresponding core's boundary of the trapezoidal membership function equal to 14 MW (see Fig. 5—due to such *pulling-up*-decreasing the new load's active power value in the node *C* will correspond to the point *c'* instead of the point *c* on the lateral side of the trapezoidal membership function) then load active powers in the nodes *A* and *B* can't be fully *pulled-up*-increased to the cores' boundaries of their trapezoidal membership functions due to the shortage of 2 MW of the *compensation* power.

To determine new values of load active powers of the nodes *A* and *B* and corresponding them membership degrees (equal to each other) to fuzzy sets of loads' active power values we will compose the balance equation of the remaining *unpulled-up* active power of the loads and the equality condition of the membership functions' values for the loads power of these nodes.

Note that the equation of the indicated balance is writing already taking into account *self-compensation*. Using (5) and introducing an additional lower subscript

indicating belonging to node *A* or *B* we write for the example under consideration
(see Fig. 5) the equation of the indicated balance and the equality condition of the
membership functions' values

$$(P_A^b - P_A) + (P_B^b - P_B) = P_C; \qquad (7)$$

$$(P_A - P_{A\,min}) / (P_A^b - P_{A\,min}) = (P_B - P_{B\,min}) / (P_B^b - P_{B\,min}) \qquad (8)$$

Substituting the specific values presented in Fig. 5 we get

$$(6 - P_A) + (4 - P_B) = 2;$$

$$(P_A - 1)/(6 - 1) = (P_B - 2)/(4 - 2),$$

whence we find $P_A = 4.571$ MW and $P_B = 3.429$ MW.

New values of the loads' active powers of the nodes *A* and *B* will be characterized
by new values of the membership functions corresponding to points *a'* and *b'* on the
trapezoids of the membership functions (see Fig. 5), which, taking into account (8),
are equal to each other and equal to $\mu_M = 0.7143$.

Note that in the general case the equalities number of the form (8) is one less than
the number of *pulled-up* load powers of the nodes.

Obviously, when implementing the *pull-up* procedure in the case of partial
compensation, as was mentioned above, it is sufficient to take into account the corre-
sponding value of the *compensation* power in the expression (7). The same *pull-up*
procedure is applicable if not all values of active powers of the loads are subject
to *pull-up*, but only which are characterized by the values of membership functions
less than a certain value. In this case the expressions (7) and (8) are written for the
conditions of *pulling up* only the indicated powers (rest powers are not subject to
pulling-up). It should be noted that in the considered example it is possible to *pull-
up* the powers of nodes *A* and *B* to the boundaries of their intervals (6 and 4 MW,
respectively), but this purpose will require an additional unloading of 2 MW in the
node *C* which already indicates a greater leaving from the values of loads' powers
obtained according to the expression (6), towards expert estimates.

After initial values (approximations) determination of the loads' active power of
unobserved nodes is completed, the initial values of the reactive power are deter-
mined. If there is relevant information that makes it possible to determine initial
approximations of the reactive power of the loads of individual nodes, then it is
used, otherwise indicated values are determined based on the equality assumption
the tangents of the load power angles in each *i*-th node at the current time and at the
corresponding hour of seasonal control measurements' day

$$Q_i = P_i \cdot Q_i^{sm} / P_i^{sm}, \qquad (9)$$

where P_i already takes into account the results of the implementation of the considered preliminary *pull-up* and *compensation* procedures.

At the next stage the minimization problem of the function $\Phi(\Delta V)$ (4) is carried out taking into account the restrictions (1)–(3) while fixing power balance components defined as the measurements of power flows through external electrical connections (set by the power constancy in corresponding boundary nodes).

A refinement of the load power values of unobserved nodes is directly related to the minimization of the function $\Phi(\Delta V)$ (4). Obviously, due to the action of various factors [7], in the process of $\Phi(\Delta V)$ minimizing only a certain (non-zero) minimum value can be achieved, depending on the restrictions on changing the load powers in the nodes: the absence of these restrictions with unreliable measurements can lead to unrealistic power estimates in individual nodes, and the severe restrictions presence of can hinder the $\Phi(\Delta V)$ minimization. If more accurate information is not available, then expert-defined minimum and maximum power values in particular nodes are accepted. If we use Fig. 3, then P^b and P^u or $P_{\min}$ and $P_{\max}$ can be taken as these restrictions.

Obviously, in the first case the restrictions may turn out to be too strict, while in the second case the opposite is true: a too wide range of possible power values is allowed. These restrictions are fuzzy in fact. The considered problem of the function $\Phi(\Delta V)$ (4) minimizing provided that some of the constraints are fuzzy is a problem of mathematical programming with fuzzy constraints. Therefore a slightly different approach to determining the restrictions on changing the loads power seems to be more reasonable.

In this case it is convenient to use the concept of a level set α of a fuzzy set [9]. Formally, the level set α of the fuzzy set P_L in P will be the set ($P_{L\alpha}$) composed of elements $p \in P$ whose membership degrees in the fuzzy set P_L is not less than the number α, i.e.

$$P_{L\alpha} = \big\{ p | p \in P, \ \mu_{P_L}(p) \geq \alpha \big\}.$$

Decomposition of the P_L fuzzy set by its sets of level α makes it possible to move although to subjective (expert) but more differentiated and clear restrictions if we introduce the *degree of subjective tolerance* to do it possible to change the load power (here and below for brevity we will use the *degree of subjective tolerance*) defined as $(1 - \alpha)$. The greater is the *degree of subjective tolerance*, the greater is the interval of possible values of the load power of the unobserved node (zero value of the *degree of subjective tolerance* corresponds to $\alpha = 1$).

For example, the level α_i of the fuzzy set (see Fig. 4) corresponds to the *degree of subjective tolerance* equal to $(1 - \alpha_i)$ while the range of possible values of the active power of the node is limited by the values $P^b_{\alpha i}$ and $P^u_{\alpha i}$ (with zero *degree of subjective tolerance* the specified interval is limited by the values of P^b and P^u). It should be emphasized that the *degree of subjective tolerance* does not have a probabilistic interpretation and reflects only the expert (subjective) knowledge about the load power changing possibility.

   This approach to the restrictions determining imposed on the possible values of
nodes' load powers allows to minimize the function $\Phi(\Delta V)$ (4) with different *degrees
of subjective tolerance.*

   If in this minimization process it turns out that established power limitations
in a number of the nodes prevent to decrease in individual terms of the function
$\Phi(\Delta V)$ then this is due either to measurements unreliability of the corresponding
EN operational condition parameters which are used in (4) or with expert's knowledge
discrepancy (representations) about real possibilities of the load power changes in
above nodes.

   If the second case occurs then by increasing the *degree of subjective tolerance* for
indicated nodes (by increasing respectively and the interval of the possible change
in the load power) and continuing the process of $\Phi(\Delta V)$ minimizing it is possible to
achieve a decrease in the values of the corresponding terms $\varphi_i(\Delta v_i)$ of the function
$\Phi(\Delta V)$.

   Load power values of indicated unobserved nodes obtained as a result of the EN
state estimation do it possible also to correct subjective expert ideas on possible
values of these nodes load power.

3   Illustrative Example

As an illustration of the above approach use to replenishment in the missing infor-
mation and obtaining *expert-calculation* estimates of the EN operational condition
parameters the EN fragment with the rated voltage of 110 kV was used (see Fig. 6),
and EN lines' parameters are given in Table 1. Let us first give a brief description
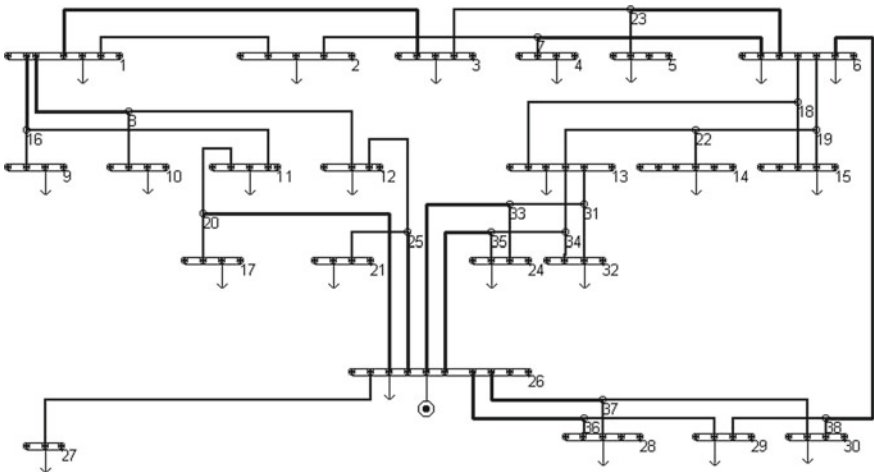
Fig. 6 EN fragment (nodes connection diagram)

Table 1 EN lines parameters' values

The node numbers to which line's poles are attached		Line's resistance, Ohm	Line's reactance, Ohm	Line's capacitive conductivity, Siemens $\times 10^{-6}$
Pole 1	Pole 2			
1	2	1.93	6.52	48.1
1	3	1.93	6.52	89.2
1	8	2.28	7.89	62.2
1	16	2.28	7.89	68.5
2	7	1.62	2.78	37.1
3	23	2.02	3.46	81.3
5	23	0.42	0.73	39.3
6	19	0.065	0.17	14.2
6	18	0.3	0.67	19.2
7	4	0.75	1.28	62.4
7	6	1.65	3.05	42.7
8	10	0.65	0.99	35.2
8	12	0.14	0.49	70.6
11	20	0.69	1.23	79.4
12	25	0.74	1.14	81.7
13	31	0.16	0.28	6.20
13	34	0.16	0.28	5.35
16	9	0.65	0.99	62.1
16	11	0.14	0.49	18.1
18	13	2.07	3.5	4.69
18	15	0.47	0.81	5.49
19	15	0.22	0.38	79.2
19	22	0.26	0.58	43.4
20	17	0.75	1.28	68.3
20	26	1.81	4.63	60.4
22	13	1.39	2.39	59.9
22	14	0.43	2.42	7.21
23	6	0.75	1.28	0.749
25	21	0.75	1.28	86.6
25	26	1.81	4.63	60.7
26	27	1.48	2	8.35
26	36	1.02	2.6	42.3
26	37	1.02	2.6	22.9
29	38	0.05	0.09	88.7

Table 1 (continued)

The node numbers to which line's poles are attached		Line's resistance, Ohm	Line's reactance, Ohm	Line's capacitive conductivity, Siemens $\times 10^{-6}$
Pole 1	Pole 2			
31	32	0.023	0.043	96.3
31	33	0.023	0.043	27.4
33	24	0.72	1.24	22.7
33	26	0.56	1.9	30.6
34	32	0.023	0.043	94.4
34	35	0.69	1.19	84.5
35	24	0.72	1.24	46.3
35	26	0.56	1.9	94.7
36	28	0.32	0.56	95.3
36	29	0.82	1.41	75.7
37	28	0.32	0.56	31.0
37	30	0.82	1.41	69.3
38	6	4.08	8.65	74.2
38	30	0.1	0.1	42.6

of this EN fragment in terms of available information on measured EN operational condition parameters which are used in EN state estimation.

The node (busbar) number 26 is the node of the input to the EN of the generated power. On this busbar a constant voltage value is ensured (according to telemetering information this value is 115 kV). The power flows telemetering from this node is characterized as a higher reliability compared to other telemetering information.

It is known that at the busbar with number 1 the load is absent and the loads at the busbars with numbers 2 and 13 are the power flows through observed external electrical connections which are taken into account in this way as the loads (these power flows along with power flows from tires 26 are used to determine the balance of power supplied to the EN).

When the problem is solving the values of power flows through external EN connections are taking fixed and they are represented by constant power load model taking account corresponding signs ($P = $ const, $Q = $ const) with telemetered data use ($P_2 = 4.02$; $Q_2 = 1.96$; $P_{13} = -9.0$; $Q_{13} = 0.0$).

When initial approximations of unobserved nodes (busbars) loads' power were determining in the nodes with 5, 24, and 32 numbers the procedures of *pull-up* and *compensation* considered above were performed. Before minimizing the objective function $\Phi(\Delta V)$ (4) its value was equal to 401.1663 and after minimizing became equal to 34.8496.

State estimation results and measured values of active and reactive power flows (respectively in MW and MVAr) through EN lines are given in Table 2 where in the

columns marked P_{T1}, Q_{T1}, P_{T2}, and Q_{T2} telemetry data measured at the side of the first (index T1) and second (index T2) ends of the lines (such ends we'll call poles) are presented, and in the columns marked P_1, Q_1, P_2, and Q_2 the values of active and reactive power flows obtained at the sides of respective poles as the EN state estimation results are given.

Shaded rows in Table 2 contain telemetering values of EN operational condition parameters which should be fixed (remain unchanged) during the EN state estimation procedure execution (the results of the EN state estimation should practically coincide with them). This requirement is satisfied with satisfactory accuracy when setting values of corresponding weight coefficients ρ_i in the expression (4) will be an order of magnitude larger in comparison with weight coefficients relating to others telemetered EN operational condition parameters.

Table 3 contains for EN nodes estimated EN operational condition parameters. Shaded rows indicate the values which were fixed (remained unchanged) during state estimation procedure's execution. According to obtained estimates the total active

Table 2 State estimation results and TI values of active and reactive power flows

The node numbers to which line's poles are attached		P_1	Q_1	P_{T1}	Q_{T1}	P_2	Q_2	P_{T2}	Q_{T2}
Pole 1	Pole 2								
1	2	−1.84	0.23	–	–	1.84	−0.24	–	–
1	3	−4.37	−1.48	–	–	4.36	1.47	–	–
1	8	3.67	1.20	4.07	1.59	−3.67	−1.21	–	–
1	16	2.55	0.05	2.79	1.37	−2.55	−0.05	–	–
2	7	2.176	2.20	–	–	−2.18	−2.20	–	–
3	23	6.78	4.21	6.75	4.01	−6.79	−4.22	–	–
5	23	1.87	0.92	–	–	−1.87	−0.92	–	–
6	18	10.25	2.75	8.99	3.61	−10.25	−2.76	–	–
6	19	8.94	8.24	8.03	8.01	−8.94	−8.25	–	–
7	4	−1.64	−0.89	–	–	1.64	0.89	1.59	0.78
7	6	3.82	3.09	–	–	−3.82	−3.09	–	–
8	10	−4.37	−2.83	–	–	4.37	2.83	4.5	–
8	12	8.03	4.04	–	–	−8.04	−4.04	−7.91	−4.04
11	20	12.28	5.23	12.8	5.37	−12.29	−5.24	–	–
12	25	14.24	6.22	14.57	–	−14.26	−6.24	–	–
13	34	14.24	2.22	–	–	−14.24	−2.22	–	–
13	31	16.05	2.61	–	–	−16.05	−2.61	–	–

(continued)

Table 2 (continued)

The node numbers to which line's poles are attached		P_1	Q_1	P_{T1}	Q_{T1}	P_2	Q_2	P_{T2}	Q_{T2}
Pole 1	Pole 2								
16	9	−5.51	−4.59	–	–	5.51	4.59	5.5	–
16	11	8.06	4.64	–	–	−8.06	−4.65	−8.08	−4.7
18	13	15.77	2.45	–	–	−15.81	−2.51	–	–
18	15	−5.52	0.31	–	–	5.51	−0.32	4.55	0
19	15	1.56	0.68	–	–	−1.56	−0.69	−2.56	−0.68
19	22	7.38	7.56	–	–	−7.38	−7.56	–	–
20	17	−5.16	−3.94	–	–	5.15	3.93	5.62	–
20	26	17.45	9.18	–	–	−17.50	−9.32	−17.5	−9.32
22	13	23.42	2.21	–	–	−23.48	−2.31	–	–
22	14	−16.04	5.35	–	–	16.03	−5.41	15.1	–
23	6	8.66	5.14	–	–	−8.67	−5.15	−8.5	−5.03
25	21	−0.97	−0.78	–	–	0.97	0.78	1.28	0.79
25	26	15.23	7.02	–	–	−15.27	−7.12	−15.27	−7.12
26	27	−11.70	−10.50	−11.7	−10.5	11.67	10.46	–	–
26	36	−20.51	−8.45	−20.51	−9.07	20.47	8.35	–	–
26	37	−20.53	−8.42	−20.53	−7.8	20.49	8.33	–	–
29	38	−3.43	1.50	−4.4	−1.9	3.43	−1.50	–	–
31	33	23.51	4.66	–	–	−23.51	−4.66	–	–
31	32	−7.46	−2.05	–	–	7.46	2.05	–	–
33	24	−0.24	−1.61	–	–	0.24	1.61	–	–
33	26	23.75	6.27	–	–	−23.78	−6.36	−23.7	−6.67
34	32	4.46	0.85	–	–	−4.46	−0.85	–	–
34	35	9.79	1.38	–	–	−9.79	−1.39	–	–
35	24	−8.41	−2.72	–	–	8.41	2.71	–	–
35	26	18.20	4.11	–	–	−18.22	−4.16	−18.3	−3.74
36	28	−5.16	−2.12	–	–	5.156	2.12	4.35	–
36	29	−15.31	−6.23	–	–	15.29	6.20	14.5	6.25
37	28	−5.07	−2.24	–	–	5.07	2.24	5.0	2.1
37	30	−15.43	−6.09	–	–	15.41	6.06	–	–
38	6	−4.40	0.73	–	–	4.39	−0.74	4.05	–
38	30	0.96	0.77	–	–	−0.96	−0.77	−0.5	0.92

and reactive power input into the EN is 127.5034 MW and 54.3208 MVAr respectively, and the consumed active and reactive power is 127.0343 MW and 53.2609 MVAr respectively.

From preliminary analysis of obtained results it can be concluded that overall "picture" is relatively satisfactory but the question regarding the differences between individual calculated values and corresponding telemetering values of reactive power flows needs some explanation. For example (see Table 2), such reactive power values are shown from first poles side for the lines (*i-j*): 1-16, 6-18, 29-38 and from the second pole side for the line 38-30. One of the reasons for these differences may be telemetering errors because in the EN operation practice the dispatchers, as a rule, pay less attention to telemetering values of reactive power flows then others EN operational condition parameters.

Table 3 State estimation results of EN operational condition parameters (shaded rows indicate the values which remained unchanged during state estimation procedure's execution)

Node's number	P_L, MW	Q_L, MVAr	U, kV	φ_u, degrees	I, A
1	0.0	0.0	114.14	−0.432	0.0
2	4.0200	1.9600	114.12	−0.487	22.6
3	11.1475	5.6778	113.98	−0.545	63.4
4	1.6390	0.8911	114.18	−0.483	9.4
5	1.8700	0.9200	114.21	−0.484	10.5
6	11.0918	2.0060	114.34	−0.448	56.9
9	5.5110	4.5878	114.12	−0.355	36.3
10	4.3657	2.8289	114.24	−0.328	26.3
11	4.2187	0.5818	114.22	−0.330	21.5
12	6.2088	2.1807	114.32	−0.303	33.2
13	−9.0	0.0	114.74	−0.202	45.3
14	16.0319	−5.4065	114.47	−0.613	85.3
15	3.9536	−1.0019	114.36	−0.441	20.6
17	5.1540	3.9328	114.27	−0.296	32.8
21	0.9727	0.7755	114.46	−0.255	6.3
24	8.6500	4.3200	114.76	−0.177	48.6
27	11.6723	10.463	114.67	−0.034	78.9
28	10.2226	4.3583	114.60	−0.204	56.0
29	11.8595	7.6947	114.44	−0.266	71.3
30	14.4451	5.2913	114.44	−0.268	77.6
32	3.0000	1.2000	114.77	−0.186	16.3

4   Conclusions

Distribution ENs traditionally are unobservable (partially observable only). That is why in order to ensure EN expert-computational observability and to obtain corresponding EN state estimation results this approach is focused on the use, additionally to telemetered EN operational condition parameters, also the results of seasonal control measurements processing and experts' estimates of active power loads of unobservable EN's nodes. Performed calculations' results including the given illustrative example of the EN's fragment with the rated voltage of 110 kV confirm operability and suitability of the proposed approach for practical application in the dispatching system of distribution ENs' load dispatch centers.

References

1. Schweppe, F.C., Wildes, J.: Power system static-state estimation, Part I: Exact model. IEEE Trans. Power Apparatus Syst. **PAS-89**(1), 120–125 (1970). https://doi.org/10.1109/TPAS.1970. 292678
2. Schweppe, F.C., Room, D.B.: Power system static-state estimation, Part II: Approximate model. IEEE Trans. Power Apparatus Syst. **PAS-89**(1), 125–130 (1970). https://doi.org/10.1109/TPAS. 1970.292679
3. Schweppe, F.C.: Power system static-state estimation, Part III: Approximate model. IEEE Trans. Power Apparatus Syst. **PAS-89**(1), 130–135 (1970). https://doi.org/10.1109/TPAS.1970.292680
4. Azimian, B., Sen Biswas, R., Pal, A., Tong, L.: Time Synchronized State Estimation for Incompletely Observed Distribution Systems Using Deep Learning Considering Realistic Measurement Noise. Nov 2020. https://www.researchgate.net/publication/345653670_Time_S ynchronized_State_Estimation_for_Incompletely_Observed_Distribution_Systems_Using_D eep_Learning_Considering_Realistic_Measurement_Noise
5. Comden, J., Colombino, M., Bernstein, A., Liu Z.: Sample complexity of power system state estimation using matrix completion. In: IEEE International Conference on Communications, Control, and Computing Technologies for Smart Grids, Beijing, China, Oct 21–24, Conference Paper NREL/CP-5D00-74580 Nov 2019 (2019)
6. Táczi, I., Sinkovics, B., Vokony, I., Hartmann, B.: The challenges of low voltage distribution system state estimation—an application oriented review. Energies **14**, 5363 (2021). https://doi. org/10.3390/en14175363
7. Butkevych, O.F.: About one of the aspects of the problem setting of electrical networks state estimation under information incompleteness conditions. Tekhnichna Elektrodynamika. **2**, 60–66 (1998)
8. Vartazarov, I.S., Gorlov, I.G., Minaev, E.V., Hvastunov, R.M.: Expert assessments and their application in the energy sector, Hvastunov, R.M. (ed.), p. 188. Energoizdat, Moscow (1981)
9. Kyrylenko, O.V., Seheda, M.S., Butkevych, O.F., Mazur, T.A.: Mathematical modeling in power engineering, p. 608. Lvivska politekhnika, Lviv, ISBN 978-966-553-938-4 (2010)

Improving the Efficiency of HPP and PSHPP Participation in the Electricity Market of Ukraine

Ihor Blinov , **Dmytro Olefir** , **Euvgen Parus** , **and Olexander Kyrylenko**

Abstract The main requirements for the volume of ancillary services in the IPS of Ukraine, in particular, the frequency containment reserve and frequency restoration reserves are considered. The influence of renewable energy sources (RESs) on the balance of production and consumption of electricity is shown. The place of hydro-electric power plants in the modern conditions of functioning of the IPS of Ukraine and the structure of the market of ancillary services is considered. It is shown that with the existing structure of production capacities in the IPS of Ukraine, in fact, only HPP and PSHPP units are able to balance the fast-changing load schedule of renewable energy sources due to their high maneuverability. Features of operation of HPP units in normal and emergency modes are provided. The plan of HPPs/PSHPPs operation in the electricity market is provided, which takes into account the indicators of the forecast balance of the IPS of Ukraine (monthly electricity production volumes of each HPP), water management constraints, current marks of the levels of HPP reservoirs, specific consumption of hydro resources, etc. Prospects for the development of ancillary services in the IPS of Ukraine are identified. According to the results of the operation feature analysis of the IPS of Ukraine, the need for updating the regulatory framework is set out, in particular as for updating the requirements for the minimum required reserves volumes to adjust frequency and active capacities in the IPS of Ukraine given the growing share of unregulated RESs in the production capacity structure. Certain measures are provided to increase the level of operational security of modes in the conditions of further development of RES and plans for synchronization of the IPS of Ukraine with ENTSO-E energy systems. Measures are provided to correct the situations related to the imbalance of HPP hydro modes. The model of optimal distribution of production capacities of the HPP cascade by

I. Blinov (✉) · E. Parus · O. Kyrylenko
Institute of Electrodynamics of the NAS of Ukraine, Kyiv, Ukraine
e-mail: blinovihor@gmail.com

D. Olefir
"Ukrhydroenergo" PJSC, Kyiv, Ukraine

I. Blinov
National Technical University of Ukraine "Igor Sikorsky Kyiv Polytechnic Institute", Kiev, Ukraine

segments of the electricity market under the conditions of observance of the prede-termined balance of hydro resources is provided. Using the provided model allows to maximize the economic effect of HPPs/PSHPPs operation in the electricity market.

1 Introduction

Since 2019, a liberalized electricity market has been operating in Ukraine [1, 2]. While the launch of organized segments of the electricity market [3–6] of Ukraine took place in July 2019, the start of the ancillary services market [7–9] was delayed due to the long-term procedure of certification of power plant units to provide certain types of ancillary services. Therefore, the first trading in this market segment took place in March 2020. At the same time, the Transmission System Operator (TSO) in Ukraine ("Ukrenergo" NPC) has repeatedly introduced technological constraints on both generation volumes (in particular, for renewable energy stations—RES) and in terms of electricity import/export. However, according to retrospective information published on the official website of "Ukrenergo" NPC, the share of trading in the balancing market not often exceeds 5%, which indicates a sufficiently high level of forecasting the balance of production and consumption of electricity. Therefore, the essence of the problems of balancing modes of the IPS of Ukraine is primarily in the mismatch of available resources of ancillary services with the actual needs of maintaining the operational security of modes of the IPS of Ukraine.

The Transmission System Code (hereinafter referred to as the TSC) [9] approved by the Regulator (the National Commission for State Regulation of Energy and Util-ities—NCSREU) defines the volumes of frequency containment reserves, frequency restoration reserves and replacement reserves for different modes of operation of the integrated power system (IPS) of Ukraine, in particular, for isolated operation mode, synchronously with the ENTSO-E [10, 11] energy union or synchronously with the CIS and Baltic countries. The requirements of the TSC for defining the volume of frequency restoration reserves (for secondary regulation) were formed based on the normative document SOU-N E NEC 04.156:2009 "Basic Requirements for Frequency and Power Regulation in the IPS of Ukraine" (see Table 1), and did not take into account significant increase in the balance of capacity of the power system of Ukraine of the share of power plants operating on renewable energy sources (see Fig. 1). Thus, in accordance with the requirements of Chap. 8 of Sect. 5 of the TSC, the frequency containment reserve (FCR) should be ±1000 MW for the mode of operation of the IPS of Ukraine separated from other power systems. At the same time, the TSC assumes that in the isolated mode of operation of the power system of Ukraine, the value of 1000 MW may be the total volume of FCR and frequency restoration reserves (FRR). This requirement is due to the economic feasibility of

Table 1 Requirements for the volumes of reserves in accordance with SOU-N E NEC 04.156:2009

Type of reserve		Required volume of reserve, MW	
		IPS of Ukraine	"Burshtyn TPP Island"
Frequency containment reserve	Loading	119 ÷ 190*	8
	Unloading	119 ÷ 190*	8
Frequency restoration reserve	Loading	1000	200
	Unloading	500	100
Replacement reserve	Loading	1000	200
	Unloading	500	100

Note *—depends on the mode of operation of the IPS of Ukraine with neighboring energy associations

maintaining the FCR. Subject to synchronous work with the CIS and Baltic Energy Union or ENTSO-E, the volume of FCR is accordingly calculated and approved by the TSO. For the IPS of Ukraine, this volume may be about ±140–190 MW. Therefore, it is not feasible to keep larger volumes of FCR for the isolated mode. With regard to the requirements for the volume of FRR and replacement reserves (RR), the TSC regulates 1000 MW of reserves for loading and 500 MW for unloading.

Calculations carried out at the request of the Transmission System Operator in 2012 demonstrated that the volume of renewable generation should not exceed 2500–3000 MW. However, the capacity of RES power plants has increased almost 9 times within 3 years. Therefore, at the time of approval of the TSC, the volumes of frequency restoration reserves were no longer sufficient to meet the needs of the energy system of Ukraine.

According to the register of ancillary service units published on the official website of "Ukrenergo" NPC on September 22, 2021, 18 power plants may participate in auctions for purchasing ancillary services in the IPS of Ukraine [12]. These include eight HPPs, eight TPPs, one TPS and one NPP. As of September 22, 2021, the
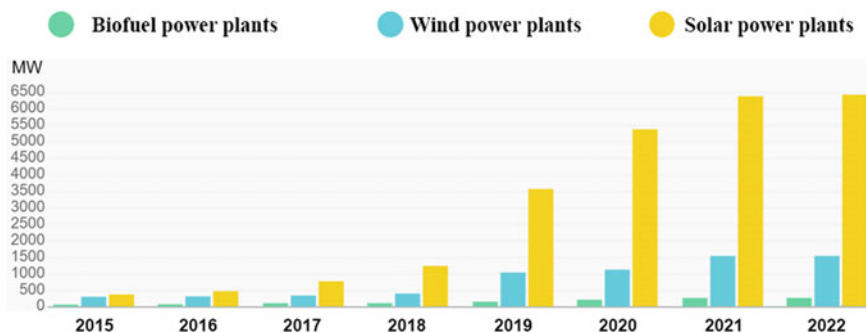
Fig. 1 The growth of RES in the IPS of Ukraine during 2015–2022

total volume of certified FCRs was ±270 MW, automatic FRRs (aFRRs) 1714 MW (±978 MW), manual FRRs (mFRRs) 4091 MW (−4040 MW) and RR 4840 MW.

These requirements do not take into account changes in the structure of production capacities of the IPS of Ukraine, especially the increase in the share of RES and their impact on imbalances in the IPS of Ukraine [13, 14].

2 Influence of RES on Electricity Production/Consumption Balances

In the period of 2018–2021, the determined capacity of solar plants (SPP) and wind plants (WPP) increased from 1100 to 8250 MW [15] (Fig. 1). Over the last three years, there has been a significant imbalance in the IPS of Ukraine due to the fast and uncontrolled commissioning of RES, especially SPP and WPP.

A significant increase in the determined capacity of RES results in an increase of fluctuations in unregulated electricity supply in the IPS of Ukraine [16–19]. Already in 2018, according to "Ukrenergo" NPC, the deviation of actual capacity values from the planned ones for solar and wind power plants was about 450 MW (Fig. 2).

Not sufficient attention was paid to the development and increase of quick-acting power reserves in the power system.

This is confirmed by the fact that the Report on Compliance Assessment (sufficiency) of the Generating Facilities to meet projected electricity demand and provide for the required reserve in 2020 [20] states that in order to increase electricity production by RES power plants without applying constraints by the dispatcher of "Ukrenergo" NPC (decreasing the load of RES power plants), the IPS of Ukraine should include at least 2 GW of highly maneuverable facilities. Thus, the TSC needs to be
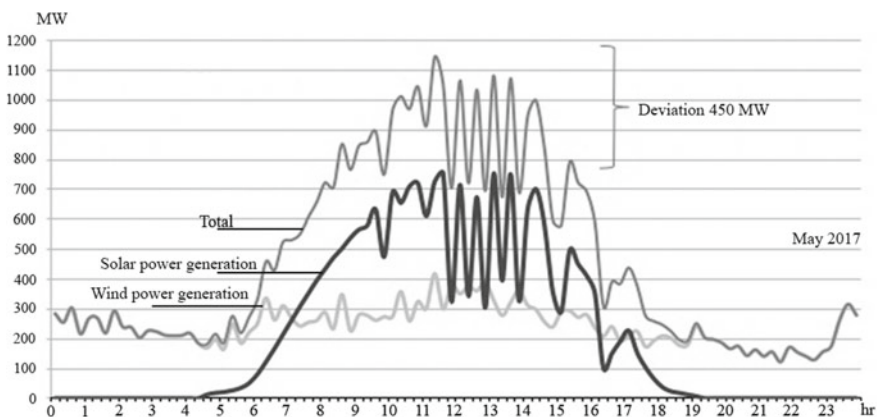
Fig. 2 Fluctuations in the volumes of generation from RES in 2017
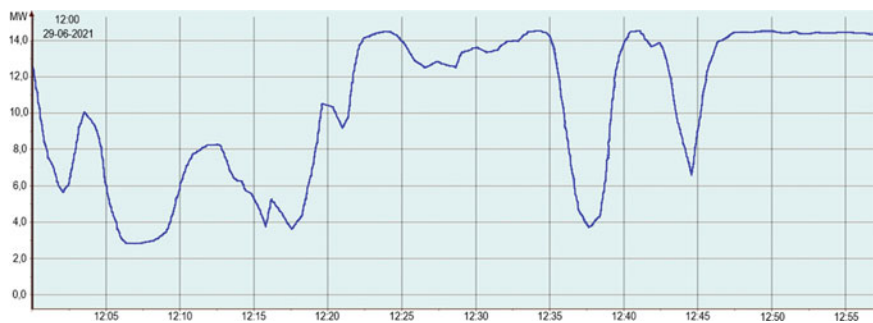
Fig. 3 An example of the actual operation of the SPP

revised in terms of determining the minimum required reserve volumes for frequency and power regulation in the IPS of Ukraine.

An example of the actual operation of a solar power plant with a determined power of 18 MW in the period 1200 ÷ 1300 06/29/2021 is shown in Fig. 3. As seen from the diagram, the change in power within 2–3 min is almost 60% of the determined power of the SPP [21], the minimum load value of this SPP was 3 MW, and the maximum was 14.5 MW. Within 2–3 min, the change in power was 10.5 MW.

According to the retrospective information on daily schedules of electricity production/consumption in the IPS of Ukraine published by "Ukrenergo" NPC (see Fig. 4), in the period from 12:00 (pm) to 13:00 (pm) on 06/29/2021, the total RES capacity was 3149 MW, of which the dominant share in this hour of the day belongs to the SPPs themselves. Even taking into account the mutual compensation of power fluctuations of individual SPPs in different parts of the IPS of Ukraine, the change in RES power in adjacent intervals of real-time units can reach 1000 MW. Appropriate in-depth studies are needed to more accurately estimate RES generation fluctuations in the IPS of Ukraine.

It should be noted that fluctuations in RES power occur at intervals of several minutes. Thus, the problem of compensation for fluctuations is solved by the services of the FRR, which leads to a corresponding increase in the requirements for the FRR volumes.

It should also be noted that the requirements of the TSC on the volumes of frequency containment reserves (for primary regulation) are not adequate for different modes of operation of the IPS of Ukraine. Thus, the TSC states that "the value of the required total normalized primary reserve for the regulation area of the IPS of Ukraine for operation as part of ENTSO-E is ±3000 MW, and for operation as part of the energy union of the CIS, Baltic countries and Georgia is ±1200 MW." In fact, such volumes of frequency containment reserves should be provided for in total by all energy systems that are part of the respective energy union.

Analysis of the requirements of the Report on Compliance Assessment (sufficiency) of the Generating Facilities to cover the projected demand for electricity and provide for the required reserve in 2020 shows that:
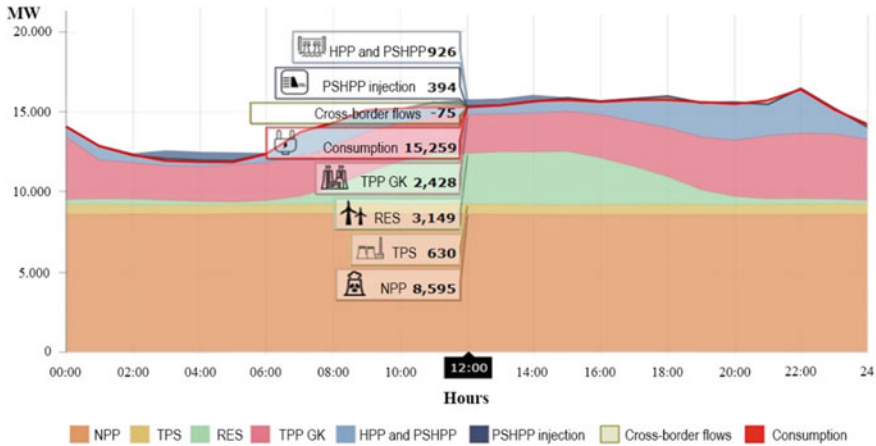
Fig. 4 Production of electricity by power plants of Ukraine on June 29, 2021

- "to maximize the production of electricity by power plants using RES by minimizing their involvement in the provision of services to reduce the load, high-maneuvering facilities should be at least 2 GW";
- "without the involvement of RES in the regulation or forced constraint of NPP capacities, the need for electricity storage systems may increase to 2 GW."

The above data suggest that the requirements of the TSC in terms of determining the volumes of frequency containment and restoration reserves should be adjusted, especially taking into account the planned synchronization of the IPS of Ukraine with the energy union ENTSO-E.

3 The Importance of Hydropower Plants in the Structure of Ancillary Services

The actual volumes of power reserves certified by the Transmission System Operator located at TPP, NPP power units, and HPP units are listed in Table 2. Lack of auctions for replacement reserves in the presence of significant delays in paying balancing services in the balancing market can result in disruptions in the operation of TPPs, especially in the conditions of global crisis in the coal market.

The data in Table 2 may indicate that the IPS of Ukraine has sufficient power reserves.

Another important issue that needs careful study is the allocation of power reserves at different types of power plants.

Some experts argue that HPPs and PSHPPs should be involved in providing ancillary services to provide for frequency containment reserves [22, 23]. However, dependence on hydro resources, change of available power depending on pressure,

Table 2 Actual power reserves in the IPS of Ukraine

PSE	Type and volume of reserve (MW)			
	Frequency containment reserve (FMR)	Automatic frequency restoration reserve (aFRR)	Manual frequency restoration reserve (mFRR)	Replacement reserve (RR)
"Ukrhydroenergo" PJSC	0	1219 (±608)	3193	3340
"DTEK SKHIDENERGO" LLC	±130	250 (±125)	250	420
"Kharkiv TPS-5" PJSC	±27	180 (±90)	90	180
"DTEK DNIPROENERGO" JSC	±63	310 (±155)	307	551
"DTEK ZACHIDENERGO" JSC	±10	0	251	349
"Energoatom" NNPC SE	±40	0	0	0
"Burshtyn TPP" Island	±20	290	290	450
Total on the IPS of Ukraine	±270	1956 (±978)	4091 (−4040)	4840

presence of inertia of directing devices, etc. do not allow to ensure compliance with the requirements of the TSC for frequency containment reserves by HPP and PSHPP units. It is feasible to use HPP and PSHPP units for secondary and tertiary regulation (for frequency restoration reserves and replacement reserves, accordingly).

NPPs operate in the around-the-clock mode, so it is feasible to involve NPP units in the provision of frequency containment reserves. In fact, after the completion of the certification of NPP power units, their reserves will be sufficient to cover the required volumes of FCR in the IPS of Ukraine.

As for TPPs and TRSs, it is feasible to involve them in providing all types of reserves. At the same time, it is feasible to provide frequency containment reserves only by means of those power units that will operate in the around-the-clock mode. TPS power units will be able to provide ancillary services for frequency and power regulation only during the autumn-winter period (in the heating period), as their operation on gas is very expensive [24–26].

Regarding the participation of energy storage systems (except for PSHPPs), their participation in tertiary regulation is infeasible due to technical constraints and high cost of such systems [27–30] (Table 3).

As NPPs cover the base load and RES power plants do not have balancing mechanisms, the main load to maintain the balance between electricity production and

Table 3 The feasibility of placing power reserves on different types of generation

Type of power plant	Frequency containment reserve (FCR)	Automatic frequency restoration reserve (aFRR)	Manual frequency restoration reserve (mFRR)	Replacement reserve (RR)
NPP	YES	NO	NO	NO
TPP	YES	YES	YES	YES
TPS	YES	YES	YES	YES
HPP	NO	YES	YES	NO
PSHPP	NO	YES	YES	YES
Other CHEs	YES	YES	YES	NO

consumption in the event of sudden changes in RES capacity rests with TPPs and HPPs (PSHPPs). It should be noted that the change in load on TPP units is carried out at a rate of 3–5 MW per minute and to compensate for fluctuations in RES power and to reliably compensate for fluctuations in RES capacity in the IPS of Ukraine must hold up to 3000 MW of FCR capacities, which is currently physically impossible. The problem of significant shortage of FCR in the IPS of Ukraine is currently solved mainly by significant volumes of FCR service, which is provided primarily by HPPs and PSHPPs. Therefore, with the existing structure of production facilities in the IPS of Ukraine, only HPP and PSHPP units are able to balance the fast-changing schedule of SPP loads due to their high maneuverability (change of power at HPP and PSHPP units lasts from several tens of seconds to several minutes).

In recent decades, the company has been carrying out large-scale modernization and reconstruction of existing equipment at HPPs and PSHPPs, as well as building new facilities, in particular, at the Dniester PSHPP.

The main tasks of the company include:

- at the request of the Integrated Power System of Ukraine, providing for coverage of peak loads, providing mobile reserves for frequency regulation and power balancing in the power system;
- maintaining optimal hydrological modes of water reservoirs in order to provide water to all water users (urban water supply, recreation, flood passages, water saving in summer time, sanitary water passages, etc.).

The availability of mobile power reserves allows "Ukrhydroenergo" PJSC to take an active part in the balancing market and the market of ancillary services.

As of January 1, 2021, the company has certified units of Kyiv, Kaniv, Kremenchuk, Middle Dnipro, Dnipro and Kakhovka HPPs. The number of certified units and regulating ranges for each HPP are provided in Table 4.

Units of HPPs and PSHPPs provide participation in automatic and manual secondary regulation of frequency and power and, with sufficient hydro resources present, in tertiary regulation.

Table 4 Certified HPP equipment of "Ukrhydroenergo" PJSC

Series No.	SE provision unit	Pmax, Pmin of the certified GUs	MW	Number of the certified GUs	Total number of GUs
1	Kyiv HPP	Pmax	336	16	20
		Pmin	160		
		Regulating range	176		
2	Kaniv HPP	Pmax	264	12	24
		Pmin	120		
		Regulating range	144		
3	Kremenchuk HPP	Pmax	234	4	12
		Pmin	92		
		Regulating range	142		
4	Middle Dnipro HPP	Pmax	300	6	8
		Pmin	135		
		Regulating range	165		
5	Dnipro HPP1	Pmax	495	7	10
		Pmin	390		
		Regulating range	105		
6	Dnipro HPP2	Pmax	479	4	8
		Pmin	280		
		Regulating range	199		
7	Kakhovka HPP	Pmax	312	6	6
		Pmin	120		
		Regulating range	192		

The difficulty of planning the operation of HPPs and PSHPPs in the balancing market and ancillary services [7, 31] market is that HPP water reservoirs are cascaded on rivers (see Fig. 5), and their hydro modes depend on weather conditions, rainfall, accuracy of water resources forecasting, a certain water reservoir functioning, water management constraints (water reservoirs marks, sanitary and ecological water passages, flood passages, etc.). The operation of each water reservoir depends on the condition of other reservoirs.

A peculiarity of HPPs operation is the fact that each of them has different types of hydraulic units (horizontal capsule, rotary blade, radial axial ones, etc.) with different determined power, different restricted areas, and as a result, different specific water consumption and different power ranges for regulation (see Tables 5 and 6).

Table 5 shows that the specific water consumption at the Kyiv HPP is 3.3 times higher than at Dnipro HPP. At the same time, the data in Table 6 shows that during the operation of four units at Kyiv HPP and Dnipro HPP-1, their determined capacities differ by 3.5 times, and power ranges for automatic control differ by 2 times.
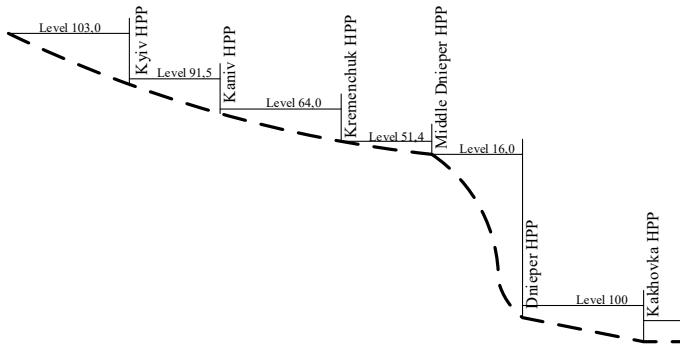
Fig. 5 Cascade of water reservoirs on the Dnipro River

Table 5 Hydropower indicators of hydropower plants

Power plant	Daily water consumption plan, m^3/s	Specific water consumption $m^3/kW*h$	HPP energy, plan per day, MW*h
Kyiv HPP	250	38.4	563
Kaniv HPP	320	38.0	728
Kremenchuk HPP	335	26.2	1105
Middle Dnipro HPP	405	32.4	1080
Dnipro HPP1	400	11.6	439
Dnipro HPP2		11.5	2562
Kakhovka HPP	500	26.2	1649
Dniester HPP	110	8.7	1092

Table 6 Regulating ranges of individual HPP units

Name of HPP	GU power, MW	Number of GU	Total power, MW	Regulating range, MW
Kyiv	22	4	88	$12 \cdot 4 = 48$
Dnipro	72	4	288	$24 \cdot 4 = 96$

This means that when planning the operation of HPP units in different segments of the ancillary services market, it is necessary to take into account a significant amount of output data: current water reservoir bief marks, sanitary water passage volumes, unit specific costs, determined powers and regulation ranges, etc.

4 Planning of HPP/PSHPP Operation in the Electricity Market

Planning of work in the electricity market consists of several steps. On the first step, the indicators of the forecast balance of the IPS of Ukraine (monthly volumes of electricity production by each HPP), water management constraints, current level marks of HPP waters reservoirs, specific costs of hydro resources, etc. are taken into account.

Based on this data, in the month preceding the month of delivery, volumes are planned for the sale of electricity on the market of bilateral agreements (usually these volumes include water volumes of HPPs which operate in the around-the-clock mode), and contracted volumes are included in the daily schedule of electricity production of each HPP. Based on monthly volumes of water discharges and volumes of electricity production, daily volumes of water discharges and volumes of electricity production are formed.

The planned volumes of water discharges through HPP turbines and daily volumes of electricity production at HPPs determine the volumes of electricity for trading on the day ahead market (DAM) and intraday market (IDM) [32, 33], volumes for trade of ancillary services (reserves for frequency and power regulation) on the auction platform, and, as a consequence, forming the daily schedule of loads of HPPs and PSHPPs.

However, the actual operation of HPPs and PSHPPs in the electricity market may differ significantly from the planned operation due to electricity production in the balancing market according to the commands by a dispatcher of "Ukrenergo" and the automatic testing of commands by the central regulator of the System of Automatic Regulation of Frequency and Power (SARFP) in the IPS of Ukraine.

Simplified activities of "Ukrhydroenergo" PJSC in the electricity market is shown in Fig. 6.

Under normal operating conditions of the IPS of Ukraine, the actual daily volumes of electricity production are equal to the planned ones, and, accordingly, the actual daily water discharges are equal to the planned ones. At the same time, there may be a slight imbalance of the hydro modes of HPPs water reservoirs due to testing the commands by the central regulator in the IPS of Ukraine and executing the commands by the dispatcher "on operational safety" when the actual daily volumes of water discharges by the company are equal to the planned ones, and there is an unintentional redistribution of volumes of hydro resources between different water reservoirs of HPPs.

In case of an emergency situation in the IPS of Ukraine due to a power imbalance (both toward shortage and toward surplus), the actual daily electricity production volumes differ significantly from the planned ones, and, accordingly, the actual daily water discharges differ significantly from the planned ones. Under such conditions, there is a significant imbalance in the hydro modes of HPPs water reservoirs, which can lead to violations of water management constraints (bief level marks, mandatory discharges of water, etc.).
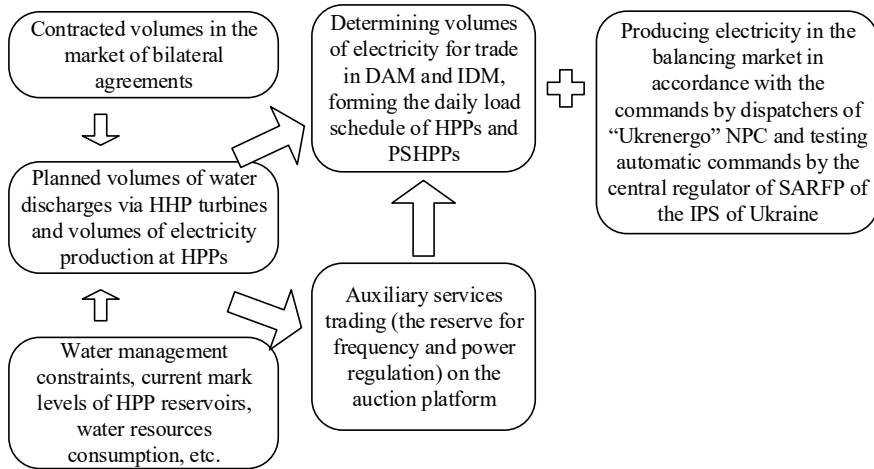
Fig. 6 Simplified block diagram of activities of "Ukrhydroenergo" PJSC in the electricity market

Especially negative emergency situations in the IPS of Ukraine are noted in the periods of floods or other limited periods.

For example, in the first decade of December 2020 (Fig. 7), because of a power shortage associated with the emergency shutdown of a number of thermal and nuclear power units, there was a significant unplanned initiation of HPP resources, which resulted in violations of the upper bief marks of HPP water reservoirs established by the Interdepartmental Commission on coordinating modes of operation of the Dnipro and Dniester water reservoirs. Thus, starting from December 11, 2021, at Kyiv and Kremenchuk HPPs, the lower set limits have been violated, while at Kaniv and Kakhovka HPPs, the upper set limits have been violated, i.e., there was an imbalance of the agreed mode of operation of the water reservoirs cascade.

Prior to the start of operation of the liberalized model of the electricity market in Ukraine in the spring, HPPs usually operated in a basic mode in order to prevent overflow of water reservoirs, further boost water discharges and prevent "idle" water discharges. However, in May 2021, a different situation was observed. During the flood occurring on the Dnipro River, there was a gradual filling of water reservoirs. The significant increase in electricity production by RES power plants in the spring of 2021 necessitated the unloading of HHPs to zero based on the commands by a dispatcher of "Ukrenergo" NPC. In order to prevent damaging to hydraulic engineering structures, hydromechanical equipment of the dam, to reduce the forcing of water reservoirs and other negative consequences, 47 emergency applications were submitted to "Ukrenergo" NPC in April–May 2021 (11 applications in April and 36 applications in May). Table 7 shows the data on the violation of water management constraints by HPPs water reservoirs in May 2021.

In August 2021, the opposite situation was observed, when in the low-water period there was an unplanned initiation of hydro resources at the HPPs. Table 8 includes

Table 7 Violation of water management constraints at HPPs water reservoirs

Number of the day of the month name of HPP	1	2	3	4	5	6	7	8	9	10	11	12	13	14	15
Kyiv HPP	102	102	102	103	103	102	102	102	102	102	102	102	102	102	102
Kaniv HPP	91	91	91	91	91	91	**91**	**91**	**91**	**91**	**91**	**91**	**91**	**91**	**91**
Kremenchuk HPP	80	80	80	80	80	80	80	81	81	81	81	81	81	81	81
Middle Dnipro HPP	63	63	**63**	**63**	**63**	**63**	63	63	63	63	63	63	63	64	64
Dnipro HPP1, HPP2	51	51	51	51	51	51	51	51	51	51	51	51	51	51	51
Kakhovka HPP	15	15	15	15	15	15	15	15	15	15	15	15	15	15	15
Dniester HPP	119	119	119	119	119	119	119	119	119	119	119	119	119	119	119

Number of the day of the month name of HPP	16	17	18	19	20	21	22	23	24	25	26	27	28	29	30
Kyiv HPP	103	103	103	103	103	103	103	103	103	103	103	102	**103**	**103**	**103**
Kaniv HPP	**91**	**91**	**91**	**91**	**91**	**91**	**91**	**91**	**91**	**91**	**91**	**91**	**91**	**91**	**91**
Kremenchuk HPP	81	81	81	81	81	81	81	81	81	81	81	81	81	81	**81**
Middle Dnipro HPP	64	64	63	63	64	64	64	63	63	63	63	63	**63**	64	64
Dnipro HPP1, HPP2	51	51	51	51	51	51	51	51	**51**	51	51	51	51	51	51
Kakhovka HPP	15	15	15	15	15	15	15	15	15	15	15	15	15	15	15
Dniester HPP	119	119	119	119	119	119	119	119	119	119	119	119	119	119	119

Fig. 7 Violation of hydro modes of HPP water reservoirs in December 2020

the data which shows that, for example, on August 2, the planned discharges of water through the Kremenchuk hydro unit should have been equal to 470 m³/s.

According to the results of bidding in all segments of the electricity market, the planned water discharges had to be 486 m³/s. However, according to the results of work on the balancing market, the actual discharges of water through the Kremenchuk HPP amounted to 1098 m³/s, which was 2.37 times higher than planned.

Table 8 Operation of hydro resources in August 2021

Date	Power plant	Updated plan D-1 (hydro resource), m³/s	Trading schedule (sales of PSO, BC, DAM, IDM), m³/s	The fact of el. production, m³/s
08/02/2021	Kyiv HPP	300	300	398
08/02/2021	Kaniv HPP	350	348	461
08/02/2021	Kremenchuk HPP	470	486	1098
08/02/2021	Middle Dnipro HPP	417	408	973
08/02/2021	Dnipro HPP	400	409	965
08/02/2021	Kakhovka HPP	500	476	894
08/02/2021	Dniester HPP	125	125	230
08/02/2021	Total:	2562	2552	5019
08/03/2021	Kyiv HPP	300	241	364
08/03/2021	Kaniv HPP	400	310	454
08/03/2021	Kremenchuk HPP	500	562	913
08/03/2021	Middle Dnipro HPP	408	470	830
08/03/2021	Dnipro HPP	400	462	806
08/03/2021	Kakhovka HPP	500	318	643
08/03/2021	Dniester HPP	120	110	182
08/03/2021	Total:	2628	2473	4192
08/04/2021	Kyiv HPP	300	265	340
08/04/2021	Kaniv HPP	400	334	437
08/04/2021	Kremenchuk HPP	500	535	989
08/04/2021	Middle Dnipro HPP	408	443	810
08/04/2021	Dnipro HPP	400	435	864
08/04/2021	Kakhovka HPP	500	410	696
08/04/2021	Dniester HPP	120	120	204
08/04/2021	Total	2628	2542	340

In order to correct the situations related to the imbalance of HPPs hydro modes, specialists are currently taking the following measures:

- decreasing/increasing in sales of aFFR and mFFR at auctions (decreasing/increasing in the number of units involved in automatic and manual secondary regulation), or redistributing reserves volumes between HPPs;
- changing in sales volume of the reserve type: symmetric, asymmetric (for loading/unloading) depending on the need to fill or initiate the water reservoir;
- certifying additional power reserves in the volume of 525 MW (including at PSHPPs), as well as implementing the project to introduce hybrid systems for electricity production with a total volume of 250 MW;
- diversifying sales at the expense of other segments of the electricity market: selling electricity at bilateral contracts market (BCM), DAM or IDM.
- improving the accuracy of forecasting hydro resources (by building mathematical models, timely receipt of forecasts of hydrometeorological conditions and actual bief marks of water reservoirs, analysis of the IPS of Ukraine and the electricity market operations, etc.). In the future, it is planned to introduce an automated system, Water Management System;
- putting constraints on the operation of HPPs and PSHPPs in case of violation of water management constraints or technological capacities of PSHPPs.

5 Modeling of HPP/PSHPP Operation in the Electricity Market

The main goal of the HPP cascade functioning is to maximize the profit from the sale of electricity and services in market segments:

$$\sum_i (Prof_i - Cost_i) \rightarrow \max,$$

where $Prof_i$ is profit from the sale of electricity or services in the i-th market segment; $Cost_i$ is costs related to the production of electricity or provision of related services.

The main activities of "Ukrhydroenergo" in market segments are shown in Table 9.

Detailed balance of production capacities in the target function for a separate calculation period of time, h:

$$\sum C_h^{XX} \cdot V_h^{HPP(XX)} \rightarrow \max,$$

where XX is a segment of the electricity market of Ukraine from the list given in Table 9, under the contracts, in which the corresponding volumes of generation $V_h^{HPP(XX)}$ are allocated at the price, C_h^{XX}, formed in the segment.

The target function is complemented by a system of equality and inequality constraints, which determine the technical and economic characteristics [34], as

Table 9 Activities of	BCM	Sale of mandatory volumes of electricity under PSO
"Ukrhydroenergo" PJSC in market segments		Commercial sale of electricity
	DAM	Commercial sale of electricity
	IDM	Buying/selling electricity to reduce imbalances
		Commercial sale of electricity
	BM	Sale of services of loading/unloading of power units
	ASM	Reservation of capacities for the provision of ancillary services
		Actual provision of ancillary services

well as the equation of the balance of hydro resources consumption, from water consumption for a single generator to water flow for the entire HPP cascade. The structure of the mathematical model of optimization of hydro resources of the HPP cascade is shown in Fig. 8. Consider components of the mathematical model shown in more detail in Fig. 8.

Models of market segments are used to derive the values of prices of electricity or services, C_h^{XX}, in certain market segments, *XX*. In most simulation problems, it is permissible to assume without compromising the accuracy of calculations that there is no impact of the volumes of electricity proposed by the HPP cascade on the prices in the relevant market segments. In this case, it is possible to use retrospective data on prices and tariffs in the electricity market for calculations. If necessary, the impact of the supply volumes of electricity or services on market prices shall be modeled by relative means of simulating pricing processes in the relevant market segments.
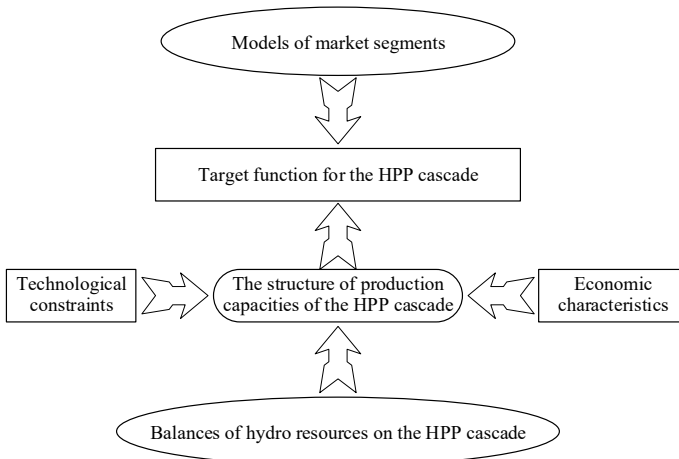
Fig. 8 The structure of the model of optimal resource allocation of the HPP cascade

The system of technological constraints determines the possibilities of actual operation of individual hydro generators and power plants in terms of electricity generation for the calculation period. Thus, for an individual hydrogenerator, the constraint of the minimum and maximum load levels at any time, t, shall be determined:

$$P_{\min}^{HG} \leq P_t^{HG} \leq P_{\max}^{HG},$$

where $P_{\min}^{HG}$, $P_{\max}^{HG}$ is, accordingly, the minimum and maximum levels of the hydrogenerator loading.

The above constraint applies only to the technological characteristics of the hydrogenerator and does not depend on the time of day or the peculiarities of the modes of Ukrainian power systems.

For a power plant, the technological constraint of the maximum load level, P_h^{HPP}, for a particular calculation period, h, shall be determined as follows:

$$P_h^{HPP} \leq P_{\max,h}^{HPP},$$

where $P_{\max,h}^{HPP}$ is a maximum allowable level of the HPP loading during the calculation period, h.

In the general case, the technological maximum of the HPP loading shall be calculated as the sum of technological maxima available for operation during the calculation period, h, of hydrogenerators:

$$P_{\max,h}^{HPP} = \sum_i P_{\max}^{HG(i)},$$

where $P_{\max}^{HG(i)}$ is a technological maximum of the i-th hydrogenerator available for operation.

The value of the maximum level of the HPP loading for the calculation period, h, may be further limited by the maximum level of electricity supply, $P_{\max,h}^{EM}$, given the mode constraints of the power systems of Ukraine:

$$P_{\max,h}^{HPP} \leq P_{\max,h}^{EM}.$$

The most important component of the model of optimal participation of the HPP cascade in the electricity market is the system of equations of the hydro resources balance. The system of equations of the hydro resources balance connects technical and economic characteristics of technological equipment at levels from an individual hydrogenerator to the HPP cascade.

The volume of electrical energy for the calculation period, h, for the i-th hydrogenerator is provided for by water consumption in accordance with technical characteristics of the respective generator:

$$V_{h,i}^{HG} = \frac{\Psi_{h,i}^{HG}}{\Upsilon_{h,i}^{HG}} (MW \cdot h),$$

where $\Psi_{h,i}^{HG}$ is a given water inflow for the HPP (m^3) for the calculation period, t; $\Upsilon_{h,i}^{HG}$ is technological water consumption for the production of electricity for the i-th hydrogenerator (m^3/(MW·h)).

The planned balance of water consumption for the i-th hydrogenerator for the calculation period, h, shall be defined in the following way.

The planned water balance in the target function for the calculation period, h, for one hydrogenerator is as follows:

$$\Psi_{h,i}^{HG} = \sum_{i} V_{h,i}^{(XX)} \cdot \Upsilon_{h,i}^{HG},$$

where $V_{h,i}^{(XX)}$ is volumes of electricity produced by the i-th hydrogenerator for the calculation period, h, which are put up for auction in the market segment, XX, in accordance with the list provided in Table 9.

The volumes, $V_{h,i}^{(XX)}$, presented in the market segments, XX, are free variables of the optimization problem, which shall be taken into account directly in the target function.

At the level of the j-th HPP, the water balance shall take into account the total water consumption of all involved hydrogenerators:

$$\Psi_{h,j}^{HPP} = \sum_{i} \Psi_{h,i}^{HG}$$

The water balance at the level of the j-th HPP shall be formed based on the overall balance of the "HPP—water reservoir" system:

$$\begin{cases} \Psi_{\min,j}^{WR} \leq \Psi_{h,j}^{WR} + \Psi_{h,j}^{WI} + \Delta\Psi_{h,j}^{WRF} - \Psi_{h,j}^{HPP} \leq \Psi_{\max,j}^{WR} \\ \Psi_{h,j}^{san} \leq \Psi_{h,j}^{HPP} \end{cases},$$

where $\Psi_{h,j}^{WI}$ is given water inflow for the j-th HPP (m^3) for the calculation period, h; $\Psi_{h,j}^{WR}$ is the initial water volume in the water reservoir of the j-th HPP (m^3) for the calculation period, h; $\Psi_{\min,j}^{WR}$ is the minimum allowable volume of filling of the water reservoir of the j-th HPP (m^3); $\Psi_{\max,j}^{WR}$ is the maximum allowable volume of filling of the water reservoir of the j-th HPP (m^3); $\Psi_{h,j}^{san}$ is sanitary water runoff for the calculation period, h, for the j-th HPP (m^3); $\Psi_{h,j}^{HPP}$ is estimated water consumption for the j-th HPP (m^3) for the period, h; $\Delta\Psi_{h,j}^{WRF}$ is the volume of increase/decrease of the water reservoir filling level for the j-th HPP (m^3) planned for the end of the calculation period, h.

Optimization of the operation of an individual HPP for the calculation period, h, shall be performed in compliance with the volume of filling of the water reservoir for the j-th HPP planned at the end of the calculation period. However, HPPs actively provide significant volumes of ancillary services. At the same time, the volumes of actual activation of services may differ significantly from those previously reserved. As a result of the discrepancy between the planned and actually provided volumes of ancillary services, as well as due to the active participation of HPPs in the Balancing Market segment, the difference between the planned and actual volumes of filling of the HPP water reservoir increases over time. As a result, there is a need to solve an additional problem of optimizing the operation of the HPP cascade in terms of compensating for the difference between the planned and actual volumes of filling of the water reservoir, which arose when providing the services on operational security support of Ukrainian power systems. Then the formulation of the optimization problem shall be carried out by determining the corrective volume of changes in the filling of the water reservoir, $\Delta \Psi_{h,j}^{WRF}$:

$$\Psi_{h,j}^{WR} - \Psi_{h,j}^{HPP} = \Delta \Psi_{h,j}^{WRF}.$$

In the considered problem for i generators of the j-th HPP, the planned water balance of water consumption in the target function for the calculation period, h, shall be defined as:

$$\Psi_{h,j}^{HPP} = \Delta \Psi_{h,j}^{WRF} + \sum_i V_{h,i}^{(XX)} \cdot \Upsilon_{h,i}^{HG}.$$

The water balance at the level of the HPP cascade reflects a sequential chain, the nodes of which are "water reservoir + HPP" systems. For each node of the "water reservoir + HPP" system, intermediate water extraction for the economic needs of the surrounding areas and additional inflow of water from smaller rivers are additionally taken into account, as shown in Fig. 9.

The system of water balance equations for the cascade with J HPP for the calculation period, h, has the following form:
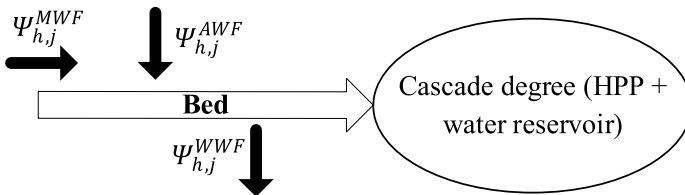

Fig. 9 Water balance of an individual stage of the HPP cascade

$$
\begin{cases}
\Psi_{h,j}^{WF} = \Psi_{h,j}^{MWF} + \Psi_{h,j}^{AWF} - \Psi_{h,j}^{WWF} \forall j \in J \\
\Psi_{h,j}^{MWF} = \begin{cases} 0 : j = 1 \\ \Psi_{h,j-1}^{HPP} : \forall j > 1 \end{cases}
\end{cases},
$$

where $\Psi_{h,j}^{MWF}$ is the main water flow for the j-th HPP (m^3) set for the calculation period, h; $\Psi_{h,j}^{AWF}$ is the additional water flow for the j-th HPP (m^3) set for the calculation period, h; $\Psi_{h,j}^{WWF}$ is intermediate withdrawal of water flow for the j-th HPP (m^3) set for the calculation period, h; $\Delta\Psi_{h,j}^{WRF}$ is the volume of increase/decrease of the water reservoir filling level for the j-th HPP (m^3) planned for the end of the calculation period, h.

The system of water balance equations for the HPP cascade is formed based on the following principle. The volume of water flow along the riverbed for the j-th HPP shall be made equal to the water consumption of the HPP of the previous $j-1$ degree: $\Psi_{h,j}^{MWF} = \Psi_{h,j-1}^{HPP}$. According to this concept, the volume of water flow along the riverbed for HPPs of the initial (zero) degree in the cascade shall be made equal to zero: $\Psi_{h,0}^{MWF} = 0$.

The main tasks solved using the written model include:

- planning of economic operation of the HPP cascade in compliance with the projected balance of hydro resources for the calculation period of time (day, week, decade, month, etc.);
- adjusting economic operation of the HPP cascade to eliminate water balance deviations from the planned indicators.

The main reasons for the water balance deviations from the planned indicators include:

- inaccuracy of the forecast of water flows along the main and additional beds;
- inaccuracy of forecasts of water use by settlements and commercial enterprises;
- discrepancy between the reserved and actually activated volumes of ancillary services (inaccuracy of the forecast of the use of operational security resources of the IPS of Ukraine);
- inaccuracy of the forecast of volumes of demand for resources of balancing of electricity in the Balancing Market.

In addition, the deviations of the actual results of economic operation of the HPP cascade due to the inaccuracy of the forecast of prices and tariffs in the segments of the electricity market of Ukraine should be taken into account.

Thus, the adequacy of the calculations performed using the model described is determined primarily by the adequacy of the solution of the relevant forecasting problems. Accordingly, improving the accuracy of planning the economic operation of the HPP cascade is achieved primarily by improving the quality of forecasting the above factors.

6   Conclusions

According to the results of the analysis of the IPS of Ukraine, the need is determined for updating the Transmission System Code in terms of updating the requirements for the minimum required reserves volumes to regulate the frequency and active power in the IPS of Ukraine given the increasing share of unregulated RESs in the production capacities structure, which results in the need to increase the resources volumes of the modes regulation. It is noted that HPPs and PSHPPs actually dominate in the segment of ancillary services of Ukraine, as the only source of highly maneuverable (peak) capacities in the IPS of Ukraine and, in particular, PSHPPs provide for smoothing of electricity consumption schedule, and, recently, compensation for electricity supply by RESs. Reconstruction of existing HPP and PSHPP facilities and construction of new ones is a necessary condition for maintaining the operational safety of the modes, as well as increasing the opportunities for synchronization of the IPS of Ukraine with the ENTSO-E energy union. Given the uncontrolled volumes of water resources of rivers, it is also feasible to introduce additional resources to regulate the modes for increasing the reliability of functioning of the IPS of Ukraine. Said measures will help increase the level of operational security of the modes in the conditions of further development of RESs and plans for synchronization of the IPS of Ukraine with ENTSO-E.

A model of optimal distribution of production capacities of the HPP cascade is provided. The model is designed to solve problems of planning and adjusting the balance of hydro resources in water reservoirs along the riverbed. The condition of adjusting the balance of the hydro resources in the water reservoirs allows to determine the volume of production capacities required for the implementation of this balance for each HPP. The calculated volumes of production capacities are distributed among the segments of the electricity market in order to maximize the profit obtained from the sale of electricity and/or services of regulation of the modes of the IPS of Ukraine. The use of the provided model allows to maximize the economic effect of the HPP cascade operation with the containment within the allowable levels of filling of the water reservoirs.

References

1. On Electricity Market: The Law of Ukraine. No. 2019-VIII of 13.04.2017
2. NEURC's Resolution "On Approval of Market Rules" No. 307 dd 14.03.2018
3. NEURC's Resolution "On Approval of Day Ahead Market and Intraday market" No. 308 dd 14.03.2018
4. Blinov, I.V., Parus, Y.V.: Congestion management and minimization of price difference between coupled electricity markets. Tekhnichna elektrodynamika **4**, 81–88 (2015)
5. Blinov, I., Kyrylenko, O., Parus, E., Rybina, O.: Decentralized market coupling with taking account power systems transmission network constraints. In: Power Systems Research and Operation. Studies in Systems, Decision and Control, vol. 388. Springer, Cham (2022). https://doi.org/10.1007/978-3-030-82926-1_1

6. Kyrylenko, O.V., Blinov, I.V., Parus, Y.V., Ivanov, H.A.: Simulation model of day ahead market with implicit consideration of power systems network constraints. Tekhnichna elektrodynamika (5), 60–67 (2019). https://doi.org/10.15407/techned2019.05.060

7. Kyrylenko, O.V., Blinov, I.V., Parus, Y.V.: Operation evaluation of power plants in the provision of ancillary services of primary and secondary frequency control in the Ukrainian power system. Tekhnichna elektrodynamika **5**, 55–60 (2013)

8. Blinov, I.V., Parus, Y.V., Ivanov, H.A.: Imitation modeling of the balancing electricity market functioning taking into account system constraints on the parameters of the IPS of Ukraine mode. Tekhnichna elektrodynamika **6**, 72–79 (2017). https://doi.org/10.15407/techned2017.06.072

9. NEURC Resolution "On Approval of Transmission Network Code" No. 309 of 14.03.2018

10. Pavlovskyi, V., Steliuk, A., Lenga, O. and Hrechko, V.: Frequency stability of the bulk isolated power system with high share of renewables and nuclear generation. In: Power Systems Research and Operation. Selected problems, p. 180. Springer (2021). https://doi.org/10.1007/978-3-030-82926-1_8

11. Pavlovsky, V.V., Stelyuk, A.O., Lukyanenko, L.M., Lenga, O.V.: Analysis of frequency change in the IPS of Ukraine under conditions of disconnection of the power unit of a nuclear power plant. Tech. Electrodyn. 2018(4), 89–94 (2018)

12. Register of ancillary service units for IPS of Ukraine // NEC «Ukrenergo». 2021. https://ua.energy/wp-content/uploads/2021/09/Reyestr-vid-22.09.2021.pdf

13. Grid integration of large-capacity Renewable Energy sources and use of large-capacity Electrical Energy Storage, White paper. IEC., p. 102 (2020)

14. Kyrylenko, O.V., Basok, B.I., Baseyev, Y.T., Blinov, I.V.: Power industry of Ukraine and realities of the global warming. Tekhnichna elektrodynamika (3), 52–61 (2020). https://doi.org/10.15407/techned2020.03.052

15. Analytical report on the development of wind power and solar power plants within the IPS of Ukraine. NEC «Ukrenergo», p. 11 (2020)

16. Basok, B.I., Butkevych, O.F., Dubovskyi, S.V.: Technical and economic aspects of decarbonisation prospects assessing of the interconnected power system of Ukraine. Tech. Electrodyn. **5**, 55–62 (2021). https://doi.org/10.15407/techned2021.05.055

17. Butkevich, O.F., Yuneeva, N.T., Gureeva, T.M.: On the issue of placement of energy storage in the Ukrainian UES. Tekhnichna elektrodynamika **6**, 59–64 (2019) (Ukr). https://doi.org/10.15407/techned2019.06.059

18. Ivanov, H.A., Blinov, I.V., Parus, Y.V., Miroshnyk, V.O.: Components of model for analysis of influence of renewables on the electricity market price in Ukraine. Tekhnichna elektrodynamika (4), 72–75 (2020). https://doi.org/10.15407/techned2020.04.072

19. Kulyk, M., Zgurovets, O.: Modeling of power systems with wind, solar power plants and energy storage. In: Systems, Decision and Control book series, SSDC, vol. 298, pp. 231–245. Springer (2020). https://doi.org/10.1007/978-3-030-48583-2_15

20. Zaporozhets, A.: Photovoltaic technologies: problems, technical and economic losses, prospects. In: Zaporozhets, A., Sverdlova, A. The 1st International Workshop on Information Technologies: Theoretical and Applied Problems 2021. CEUR Workshop Proceedings. vol. 3039. p. 166–1811. http://ceur-ws.org/Vol-3039/paper19.pdf

21. Report on compliance assessment (sufficiency) of the generating facilities. NEC «Ukrenergo». p. 122 (2020)

22. Kulyk, M.M., Kyrylenko, O.V.: The state and prospects of hydroenergy of Ukraine. Tech. Electrodyn **4**, 56–64 (2019). https://doi.org/10.15407/techned2019.04.056

23. Intelligent power systems: elements and modes: under the total ed. of acad. of NASU AV Kyrylenko. The Institute of Electrodynamics of the NASU, p. 408 (2014)

24. Popov, O., Iatsyshyn, A., Kovach, V., Artemchuk, V., Kameneva, I., Radchenko, O., Nikolaiev, K., Stanytsina, V., Iatsyshyn, A., Romanenko, Y.: Effect of power plant ash and slag disposal on the environment and population health in Ukraine. J. Health Pollut. **11**(31), 210910 (2021). https://doi.org/10.5696/2156-9614-11.31.210910

25. Iatsyshyn, A., Artemchuk, V., Zaporozhets, A., Popov, O., Kovach, V.: Mathematical approaches for determining the level of impact of ash-slag dumps of energy facilities on the environment. In: Babak, V., Isaienko, V., Zaporozhets, A. (eds.) Systems, Decision and Control in Energy I. Studies in Systems, Decision and Control, vol. 298, pp. 1–13 (2020). https://doi.org/10.1007/978-3-030-48583-2_1

26. Zaporozhets, A.O.: Correlation analysis between the components of energy balance and pollutant emissions. Water Air Soil Pollut. **232**(3), 114 (2021). https://doi.org/10.1007/s11270-021-05048-9

27. Electrical Energy Storage. White paper. IEC, pp. 79 (2019)

28. Kyrylenko, O.V., Blinov, I.V., Tankevych, S.E.: Smart grid and organization of information exchange in electric power systems. Tekhnichna elektrodynamika **3**, 44–54 (2012)

29. Kyrylenko, O.V., Blinov, I.V., Parus, E.V., Trach I.V.: Evaluation of efficiency of use of energy storadge system in electric networks. Tech. Electrodyn. **4**, 44–54 (2021). https://doi.org/10.15407/techned2021.04.044

30. Blinov, I., Trach, I., Parus, Y., Khomenko, V., Kuchanskyy, V., Shkarupylo, V.: Evaluation of the efficiency of the use of electricity storage systems in the balancing group and the small distribution system. In: 2021 IEEE 2nd KhPI Week on Advanced Technology (KhPIWeek), pp. 262–265 (2021) https://doi.org/10.1109/KhPIWeek53812.2021.9569981

31. Blinov, I., Parus, E.: Approach of reactive power pricing for ancillary service of voltage control in Ukraine. In: 2014 IEEE International Conference on Intelligent Energy and Power Systems (IEPS), pp. 145–148 (2014). https://doi.org/10.1109/IEPS.2014.6874167

32. Saukh, S.; Borysenko, A.: (2019) Representation of transmission and distribution networks in the mathematical model of the electricity market equilibrium. In: 2019 IEEE 20th International Conference on Computational Problems of Electrical Engineering (CPEE) (2019). https://doi.org/10.1109/CPEE47179.2019.8949116

33. Lin, J., Magnago, F.: (2017) Electricity markets: theories and applications. IEEE Press Series on Power, pp. 352 (2017)

34. Momoh, J., Mili, L.: Economic market design and planning for electric power systems. Institute of Electrical and Electronics Engineers, pp. 277 (2009). https://doi.org/10.1002/9780470529164

Application of Energy Storage for Automatic Load and Frequency Control

Oleksandr Zgurovets and **Mykhailo Kulyk**

Abstract The study is devoted to the issue of creating an effective automatic load and frequency control system using modern electric energy storage systems based on high-capacity batteries. As part of the study, different types of regulators are considered. The authors proposed an approach to the implementation of a control system using battery energy storage systems. Comparative calculations of different control systems are performed and the advantage of the proposed approach is demonstrated. The study was carried out by numerical simulation of an automatic load and frequency control system with emergency disturbance. The efficiency of regulation was determined on the basis of the analysis of the accepted indicators of the regulation quality, namely, the maximum frequency deviation and the duration of the transient process. It was found that the use of high-speed battery energy storage systems in the automatic load and frequency control system shows the best performance in frequency stabilization, satisfying the regulatory requirements established in the power system.

Keywords Frequency · Regulation · Power · Speed · Power system · Battery energy storage systems

1 Introduction

Parallel operation of multiple high-capacity power plants as part of an integrated power system is possible only if there are system means of ensuring their functioning. The main such means are dispatch control and fast-acting automatic control systems, in particular, the system of automatic load and frequency control (ALFC). If one of the main tasks of the dispatch control of the integrated power system is to ensure effective coverage of its electrical load schedules during the day, the tasks of the ALFC include maintaining the frequency in the power system at a given set point in time, even in the events of significant (emergency) disturbances. This is why the

O. Zgurovets (✉) · M. Kulyk
Institute of General Energy of NAS of Ukraine, Kyiv, Ukraine
e-mail: zgurovets_ov@nas.gov.ua

ALFC system has more stringent requirements for the speed of the regulators that can be used in its control loop.

Historically, Ukraine's power system had mostly basic generating capacities and did not have sufficient capacities of maneuvering regulators. This situation was caused by the fact that the Ukrainian energy system was created as part of the Soviet energy system and was primarily intended to cover the consumers of the highly developed industrial sector, as well as due to its western location it was seen as export-oriented for the former Warsaw Pact countries. Furthermore, the territory it covered lacked sufficient hydro resources to construct significant capacities of hydro-electric power plants (HPPs), which are typically used as power generator-regulators in the ALFC system. For these reasons, at the time of separation the Ukrainian power system consisted mainly of high-capacity units of thermal (TPP) and nuclear (NPP) power plants, which were not devoted for the needs of load and frequency control.

Due to the lower requirements for the regulators speed to cover the load schedules, the lack of the available HPP capacity was compensated by using units of thermal power plants. This solution was not the best in efficiency terms of thermal power generation use, but it allowed the dispatching control system to function quite reliably while covering the load schedules. The ALFC system required more high-speed capacity reserves, so they were provided through imports from Russia's higher-capacity power system, first and foremost, through the Volzhsky-Kamskiy cascade of HPP.

Increased requirements to the quality of electric power and transition to carbon-neutral energy with the development of technologies of using wind and solar energy are the main characteristic tendencies of the current electric power industry development [1]. In recent years, the development of the Integrated Power System (IPS) of Ukraine has been carried out through the introduction of large volumes of renewable energy sources with insufficient introduction of regulating capacities. This makes it much more difficult both to cover the schedules of electric loads of the power system as well as ensuring the requirements for frequency and voltage stability in the nodes of the power system with use of the existing means of dispatching control.

Unlike traditional sources of energy, wind (WPP) and solar (SPP) power plants cannot independently meet the requirements for frequency, power and voltage stability, which are required in the energy system. Moreover, WPP and SPP generate unstable energy, which is characterized by very high rates of change in its power output. The unstable nature of power supply by these power plants to the grid affects on the frequency regulation processes in the power system, making them significantly more difficult. Balancing additional unpredicted generation in the power system leads to increased costs for its functioning and the cost of energy for the end user [2].

In today's realities with the disconnection from the Russian and Belarusian power systems and the need to meet the requirements imposed by the European Union power system on the stability of the IPS and the quality of electrical energy, the issue of creating a reliable ALFC system becomes very important. On the one hand, it is necessary to substitute missing regulating capacities, and on the other hand—to respond to modern challenges associated with the growing share of unpredictable generation in the balance of the power system.

Almost all power systems around the world use the traditional approach in building automatic load and frequency control systems, when additional (regulating) capacities are put into operation when a capacity deficit appears in the integrated power system for one reason or another. Along with this, Ukraine has an opportunity to build ALFC system based on powerful BESSs. Operating modes of BESSs involve not only the possibility of power output during peak hours and accumulation during the hours of minimum consumption in order to equalize the load schedules, but also allow participation in the processes of secondary control (in the ALFC system). This is caused, first of all, by development of technologies for creation storage units with necessary parameters of power, capacity and speed [3].

The main disadvantages for the implementation of fully traditional ALFC system in Ukraine, which meets the ENTSO-E requirements, are the lack of sufficient hydro resources [4], as well as the high cost of the traditional regulating generators. The use of BESSs in the role of load and frequency regulators would allow to reduce the amount of required costs, compensating the expenses by the additional effect from the providing of secondary services to the energy system [5].

2   Mathematical Model

To determine the possibility of using BESSs as regulators of the ALFC system, it is necessary to simulate their operation. Since the processes occurring in frequency control are transient, the corresponding models that describe them can be written both in the form of differential equations and in the form of Laplace transforms.

An analysis of existing publications [6–24], which deal with both modeling of system elements and the power system as a whole, has shown that the most widespread approach to modeling is the use of transfer functions. With all the convenience of recording the system in the form of transfer functions, their main disadvantage is that this apparatus can be used only for linear (well linearized) systems of differential equations.

As a result, the method of transfer functions for investigation of transient processes in the energy system in the process of frequency stabilization can be used only in cases when the changes in the system are insignificant and well linearized. The described processes of frequency stabilization are accompanied by disturbances, which can cause nonlinear behavior of the elements included in the energy system. Primarily, it is related to technological limitations typical for regulators-generators. Therefore, modeling of such systems should be carried out by means of systems of differential equations with nonlinear constraints and numerical methods of their solution.

For this reason, we chose our own model, which would include both a complete description of the power system and its elements, taking into account the existing nonlinear constraints of regulators. This allowed to ensure the necessary accuracy and adequacy of the model and practical calculations.

The basis for the new model was the model developed earlier by the authors, which was used in the study of the ALFC system with consumer-regulators, and

was further developed in the studies of frequency stabilization processes in power systems with renewable energy sources [25, 26]. The difference from the previous model is that the equation describing the operation of BESSs is used as the regulator of the ALFC system instead of the consumer-regulator. The obtained model has the form of a system of nonlinear differential and algebraic Eqs. (1)–(6) shown below.

$$\frac{d\omega(t)}{dt} = \frac{\sum_{i=1}^{I} P_{pi}(t) + P_{BESS}(t) + P_r(t) - P_l(t) - P_g(t)}{T_g P_{\Sigma p0} \omega(t)} \omega_0^2; \tag{1}$$

$$\frac{dP_{pi}(t)}{dt} = \frac{B_{pi}(\omega(t) - \omega_0) - P_{pi}(t) + P_{p0i}}{\tau_{pi}}, \quad i = \overline{1, I}; \tag{2}$$

$$\frac{dP_l(t)}{dt} = \frac{C_l(\omega(t) - \omega_0) - P_l(t) + P_{l0}}{\tau_l}; \tag{3}$$

$$\frac{dP_r(t)}{dt} = \frac{B_r(\omega(t) - \omega_0) + F_r(t) - P_r(t)}{\tau_r}; \tag{4}$$

$$P_{BESS}(t) = P_{BESS}(t_0) + F_{BESS}(t); \tag{5}$$

$$F_r(t) = A_r(\omega(t) - \omega_0) + Q_r \frac{d\omega}{dt} + S_r \int_{t_0}^{t_1} (\omega(\tau) - \omega_0)d\tau; \tag{6}$$

$$F_{BESS}(t) = A_{BESS}(\omega(t) - \omega_0) + Q_{BESS} \frac{d\omega}{dt} + S_{BESS} \int_{t_0}^{t_1} (\omega(\tau) - \omega_0)d\tau, \tag{7}$$

where T_g is time constant of the grid; $P_{\Sigma p0}$ is the total capacity of the generators at the initial moment of time; $P_{pi}(t)$, $P_l(t)$, $P_r(t)$, $P_{BESS}(t)$, $P_g(t)$ are required variables-functions that correspond to the generators, load, generator-regulator, BESS and losses in the network respectively; τ_{pi}, τ_l, τ_r are generator, load and generator-regulator time constants respectively; B_{pi}, B_r, C_l are steepness of frequency characteristics of generators, generator-regulator and load respectively; A_r, A_{BESS}, Q_r, Q_{BESS}, S_r, S_{BESS} are coefficients of gain of the proportional, differential and integral components of the law of regulation for generator-regulator and BESS respectively; t is time variable.

Moreover, in the system (1)–(7) there are constraints (8)–(13) given below:

- constraints on power change rate

$$L_{rlg} \leq \left| \frac{dP_r(t)}{dt} \right| \leq L_{rhg}, \quad t \in [t_0, T], \quad P_r \in [P_{rg1}, P_{rg2}]; \tag{8}$$

$$L_{BESSlg} \leq \left| \frac{d P_{BESS}(t)}{dt} \right| \leq L_{BESShg}, \ t \in [t_0, T], \ P_{BESS} \in [P_{BESSg1}, P_{BESSg2}],$$

(9)

- power level limits

$$P_{r\,min} \leq P_r(t) \leq P_{r\,max};$$

(10)

$$P_{BESS\,min} \leq P_{BESS}(t) \leq P_{BESS\,max},$$

(11)

- dead band

$$\frac{d P_r(t)}{dt} = const, \ \omega(t) - \omega_0 \in [\omega_{rs1}, \omega_{rs2}];$$

(12)

$$\frac{d P_{BESS}(t)}{dt} = const, \ \omega(t) - \omega_0 \in [\omega_{BESSs1}, \omega_{BESSs2}],$$

(13)

where $[t_0, T]$ is interval of time at which the processes in the power system are investigated; g is index indicating the generator-regulator and BESS power intervals in which the speed limit applies; $P_{r\,min}$, $P_{BESS\,min}$, $P_{r\,max}$, $P_{BESS\,max}$ are limits of minimum and maximum power of the generator-regulator and BESS; $[\omega_{rs1}, \omega_{rs2}]$, $[\omega_{BESSs1}, \omega_{BESSs2}]$ is dead band of generator-regulator and BESS.

The model also contains the following initial conditions:

$$\begin{cases} \omega(t_0) = \omega_0; \\ P_{pi}(t_0) = P_{pi0}; \\ P_l(t_0) = P_{l0}; \\ P_r(t_0) = P_{r0}; \\ P_{BESS}(t_0) = P_{BESS0}. \end{cases}$$

(14)

At the given mathematical model (1)–(14) Eq. (1) represents in canonical form the total power balance in power system; Eq. (2) models the process of power change at all generators in dependence on circular frequency $\omega(t)$; Eq. (3)—the same for the load; Eqs. (4) and (5) reflect the regulating power of the generator-regulator $P_r(t)$ and BESS $P_{BESS}(t)$. Control functions $F_r(t)$ and $F_{BESS}(t)$ are used as proportional-differential-integral (PID) law of regulation depending on frequency deviation (Eqs. (6) and (7)).

The mathematical model (1)–(14) was solved using the modified Runge-Kutta 4th order method. This method was implemented in the software "Chastota-M" developed by the authors at the Institute of General Energy of the National Academy of Sciences of Ukraine. Peculiarities of implementation of the numerical calculation method allow to control the values of all variables on each calculation step to comply

with the nonlinear limitations specified in the model, ensuring high accuracy and adequacy of calculation of transient processes in the power system.

3 Modelling Example

Study of the processes of load and frequency stabilization by means of regulators based on HPP (generator-regulator, HPP_r) and BESS was carried out using the method of equivalent generators on the design scheme of the power system, with the parameters listed in Table 1.

Apart from the regulator of the specified type, the calculated power system included equivalent thermal, nuclear and hydroelectric power plants of high capacity, as well as the load and losses in the grid. During modeling, the optimum values of the PID coefficients of the regulation law were determined. The coefficients at proportional and differential components were selected the same for the generator-regulator (HPP_r) and BESS, and were equal to 10,000 and 20,000 respectively, the values of coefficients at integral part varied depending on the type of the regulator and were equal to 25 and 1000 respectively. The values of power change rates, as one of the most important properties of the regulators, which characterizes the speed of change in the output (regulating) power, are also different for HPP_r and BESS. In the research, the values of 2.5 and 714 percentage points of the nominal capacity of the regulator per second for HPP_r and BESS, respectively, was used.

According to the requirement of stability, which is specified by the European Union power system ENTSO-E, the power system must withstand the loss of its largest power unit. Moreover, frequency in the power system should return to the range of 50 ± 0.02 Hz for 15 min after the occurrence of power imbalance. For the Integrated Power System of Ukraine such power capacity corresponds to the capacity of WWER-1000 unit, i.e. 1000 MW. This power capacity was taken in the research as the initial disturbance at the moment of time $t_0 = 0$ s. Thus, at the initial

Table 1 Parameters of the power system model

System element	Steepness of frequency characteristic, MW/Hz	Time constant, s	Rated capacity, MW	Initial power, MW
HPP	0.37	5	2870	2870
TPP	0.73	5	6592	6592
NPP	1.81	5	12,415	12,415
Load	153	0.5	20,877	20,877
HPP_r	5	0.5	1000	0
BESS	–	–	1000	0
Loses	–	–	2000	2000
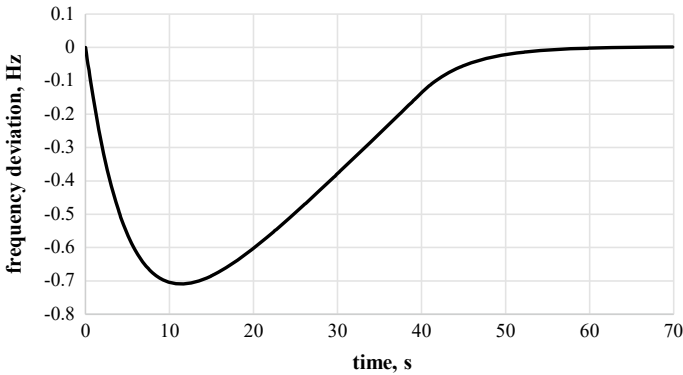
Fig. 1 Frequency deviation in the power system during load and frequency regulation by means of HPP$_r$

moment of time the system starts to operate with a significant power deficit. The control system should compensate the received power imbalance by available means as quickly as possible, returning the frequency to normal values. That is why it is important for the ALFC system, that the generators used in the control circuit have high maneuverability and can quickly gain the set power.

Among the available traditional generators, HPP units have the highest speed, therefore for the presence of the necessary power they are used for the solving of such tasks. For this reason, in the first study as a generator-regulator of the ALFC system, a large HPP was used with the installed capacity, corresponding to the initial imbalance.

Simulation of frequency stabilization processes was performed for 70 s, which was enough to return the frequency to its normal value. Figure 1 shows the graph of frequency deviation in the studied power system.

In accordance with initial conditions (14) at the moment t_0 the frequency deviation is not observed, but at each successive moment of time, due to lack of power, the frequency deviation grows rapidly, reaching its maximum -0.709 Hz at the moment $t = 11.35$ s. After the regulation law is applied, the frequency begins to return to normal values and within a minute from the beginning of the accident the deviation of the frequency becomes -0.002 Hz.

Figure 2 shows the power of the HPP$_r$ regulator, which enables the regulation process by compensating for the lost power. As shown in Fig. 2, the regulator's power begins to increase immediately at a constant speed, which corresponds to the limitation on the rate of HPP$_r$ power change, and reaches its maximum at the time $t = 40$ s, after that it remains unchanged and corresponds to the lost capacity unit in the power system.

Apart from the maximum frequency deviation in the transient process and its duration, the indicators of the quality of frequency control also include such characteristics as the nature of the transient process (oscillation or aperiodic), as well as the absence or presence of constant-error behavior after the end of the transient process.
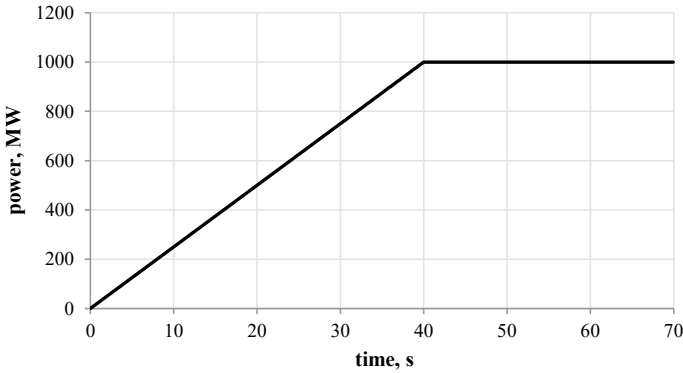
Fig. 2 Graph of HPP$_r$ power output during regulation

The application of the PID-law of regulation in the research allowed to avoid constant-error behavior and to achieve the aperiodic character of the transient process. This was achieved due to the integral and differential components of the law.

The next stage of the research was to determine the feasibility of using a battery-operated energy storage unit as an ALFC system regulator. In the simulation was used the same scheme of the power system with the appropriate initial disturbance. The graph of the resulting frequency deviation in the power system is shown in Fig. 3.

The obtained results of ALFC system operation with BESS in comparison with the previous study show better indicators of regulation efficiency. The maximum frequency deviation in the power system and the time of the transient decreased significantly.

Due to the fast response of the regulator on BESS basis the maximum frequency deviation is reduced to − 0.013 Hz at the time $t = 1.8$ s, after that the frequency is returned to its initial level. The control system needs 19 s of time to return frequency

Fig. 3 Frequency deviation in the power system during load and frequency regulation by means of BESS
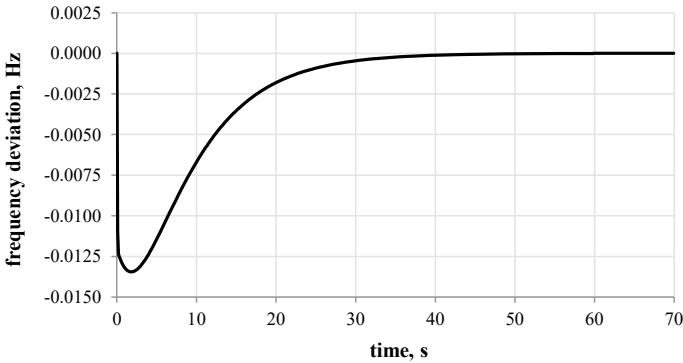
Fig. 4 Graph of BESS power output during regulation

Table 2 Frequency regulation process in the power system with BESS for the first 0.5 s

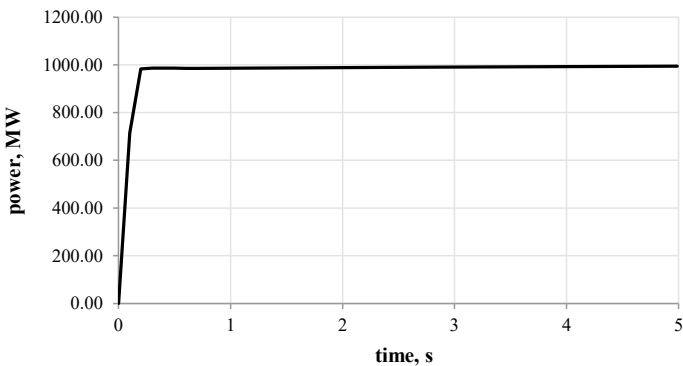| Time, s	Frequency deviation, Hz	Power, MW				
		Load	HPP	TPP	NPP	BESS
0.0	0.0000	20,877.00	2870.00	6592.00	12,415.00	0.00
0.1	− 0.0110	20,875.83	2870.00	6592.00	12,415.00	714.00
0.2	− 0.0123	20,873.95	2870.00	6592.00	12,415.00	983.64
0.3	− 0.0125	20,872.34	2870.00	6592.00	12,414.99	986.79
0.4	− 0.0126	20,871.00	2870.00	6592.00	12,414.99	986.26
0.5	− 0.0127	20,869.88	2870.00	6592.00	12,414.99	985.86

deviation to 0.002 Hz. For a better understanding of the regulation process, we can refer to the BESS power graph shown in Fig. 4.

The high speed of the regulator allows it to reach its maximum power of 984 MW in 0.2 s (Table 2). This is achieved by absence of mechanical elements of design, which could negatively influence the permissible rate of power change. Unlike traditional generators, storage batteries and their power electronics of voltage and frequency inverter allow just a fraction of a second to reach the maximum power. Regulation process by means of BESS also has an aperiodic character and does not contain constant-error behavior due to the use of PID regulation law.

4   Conclusions

According to the results of the conducted research, we can conclude that the use of high-power BESSs in the role of ALFC regulators not only has an advantage over classical generator-regulator HPPs, but also will allow to create an ALFC system, which meets the requirements of the European Union ENTSO-E energy system.

The important advantage of the ALFC system based on BESS is that with a standard disturbance of 1000 MW, it does not allow the frequency deviation to exceed the limits allowed even for the ENTSO-E system (Fig. 3), as ALFC on the basis of HPP cannot do (Fig. 1). This important feature ensures the situation in IPS, when during such a severe accident the power system does not detect it on its critical indicators.

The high speed of the BESS power output change reduces the time required to compensate for imbalances in the power system. This allows a more efficient use of the regulator's power, improves the quality of frequency regulation and reliability of power system operation. Considering the rapid development of technologies of electric energy storage and reducing the price of such systems, they have the prospects for implementation as competitive alternatives to regulators based on traditional generators in the load and frequency control systems of the integrated power systems. Given the insufficient amount of hydro resources available in Ukraine, related environmental issues and significant financial costs for the construction of new HPPs, the use of BESS in the loop of ALFC system becomes very relevant and reasonable.

References

1. Kyrylenko, O.V., Basok, B.I., Baseyev, Y., Blinov, I.V.: Power industry of Ukraine and realities of the global warming. Tech. Electrodyn. **3**, 52–61 (2020). https://doi.org/10.15407/techned2020.03.052
2. Ivanov, H.A., Blinov, I.V., Parus, E.V., Miroshnyk, V.O.: Components of model for analysis of influence of renewables on the electricity market price in Ukraine. Tech. Electrodyn. **4.c.**, 72–75 (2020). https://doi.org/10.15407/techned2020.04.072
3. Electricity and Energy Storage (updated Jan 2020). World Nuclear Assotiation. Access mode: http://www.world-nuclear.org/information-library/current-and-future-generation/electricity-and-energy-storage.aspx
4. Kulyk, M.M., Kyrylenko, O.V.: The state and prospects of hydroenergy of Ukraine. Tech. Electrodyn. **4**, 56–64 (2019). https://doi.org/10.15407/techned2019.04.056
5. Kyrylenko, O.V., Blinov, I.V., Parus, E.V., Trach, I.V.: Evaluation of efficiency of use of energy storadge system in electric networks. Tech. Electrodyn. **4**, 44–54 (2021). https://doi.org/10.15407/techned2021.04.044
6. Asghar, F., Talha, M., Kim, S.H.: Fuzzy logic-based intelligent frequency and voltage stability control system for standalone microgrid. Int. Trans. Electr. Energy Syst. **28**(4) (2018). https://doi.org/10.1002/etep.2510
7. Bahloul, M., Khadem, S.K.: Design and control of energy storage system for enhanced frequency response grid service. Paper presented at the Proceedings of the IEEE International Conference on Industrial Technology, Feb 2018, pp. 1189–1194 (2018). https://doi.org/10.1109/ICIT.2018.8352347
8. Indu, P.S., Jayan, M.V.: Frequency regulation of an isolated hybrid power system with superconducting magnetic energy storage. Paper presented at the Proceedings of 2015 IEEE International Conference on Power, Instrumentation, Control and Computing, PICC 2015 (2016). https://doi.org/10.1109/PICC.2015.7455752
9. Jamroen, C., Dechanupapritta, S.: Coordinated control of battery energy storage system and plug-in electric vehicles for frequency regulation in smart grid. Paper presented at the 2019 IEEE PES GTD Grand International Conference and Exposition Asia, GTD Asia 2019, pp. 286–291 (2019). https://doi.org/10.1109/GTDAsia.2019.8715962

10. Melo, S.P., Brand, U., Vogt, T., Telle, J.S., Schuldt, F., Maydell, K.V.: Primary frequency control provided by hybrid battery storage and power-to-heat system. Appl. Energy **233–234**, 220–231 (2019). https://doi.org/10.1016/j.apenergy.2018.09.177

11. Yan, S., Wang, M., Yang, T., Hui, S.Y.R.: Instantaneous frequency regulation of microgrids via power shedding of smart load and power limiting of renewable generation. Paper presented at the ECCE 2016—IEEE Energy Conversion Congress and Exposition, Proceedings (2016). https://doi.org/10.1109/ECCE.2016.7855207

12. Arul, P.G., Ramachandaramurthy, V.K.: Mitigating techniques for the operational challenges of a standalone hybrid system integrating renewable energy sources. Sustain. Energy Technol. Assess. **22**, 18–24 (2017). https://doi.org/10.1016/j.seta.2017.05.004

13. Cho, S., Jang, B., Yoon, Y., Jeon, W., Kim, C.: Operation of battery energy, storage system for governor free and its effect. Trans. Korean Inst. Electr. Eng. **64**(1), 16–22 (2015). https://doi.org/10.5370/KIEE.2015.64.1.016

14. Habib, M., Ladjici, A.A., Harrag, A.: Microgrid management using hybrid inverter fuzzy-based control. Neural Comput. Appl. (2019). https://doi.org/10.1007/s00521-019-04420-5

15. Guney, M.S., Tepe, Y.: Classification and assessment of energy storage systems. Renew. Sustain. Energy Rev. **75**, 1187–1197 (2017). https://doi.org/10.1016/j.rser.2016.11.102

16. Naranjo Palacio, S., Kircher, K.J., Zhang, K.M.: On the feasibility of providing power system spinning reserves from thermal storage. Energy Build. **104**, 131–138 (2015). https://doi.org/10.1016/j.enbuild.2015.06.065

17. Orihara, D., Saitoh, H.: Evaluation of battery energy storage capacity required for battery-assisted load frequency control contributing frequency regulation in power system with wind power penetration. IEEJ Trans. Power Energy **138**(7), 571–581 (2018). https://doi.org/10.1541/ieejpes.138.571

18. Wen, Y., Dai, Y., Zhou, X., Qian, F.: Multiple roles coordinated control of battery storage units in a large-scale island microgrid application. IEEJ Trans. Electr. Electron. Eng. **12**(4), 527–535 (2017). https://doi.org/10.1002/tee.22408

19. Lytvynchuk, V.A., Kaplin, M.I., Bolotnyi, N. P.: The method of design an optimal under-frequency load shedding scheme. In: IEEE 6th International Conference on Energy Smart Systems, pp. 14–17 (2019). https://doi.org/10.1109/ESS.2019.8764241

20. Xie, P., Li, Y., Zhu, L., Shi, D., Duan, X.: Supplementary automatic generation control using controllable energy storage in electric vehicle battery swapping stations. IET Gener. Transm. Distrib. **10**(4), 1107–1116 (2016). https://doi.org/10.1049/iet-gtd.2015.0167

21. Biroon, R.A., Pisu, P., Schoenwald, D.: Large-scale battery energy storage system dynamic model for power system stability analysis. In: 2020 IEEE Texas Power and Energy Conference (TPEC) (2020). https://doi.org/10.1109/TPEC48276.2020.9042536

22. Akram, U., Nadarajah, M., Shah, R., Milano, F.: A review on rapid responsive energy storage technologies for frequency regulation in modern power systems. Renew. Sustain. Energy Rev. **120**, 109626 (2020). https://doi.org/10.1016/j.rser.2019.109626

23. Chang, C.S., Fu, W.: Area load frequency control using fuzzy gain scheduling of PI controllers. Electr. Power Syst. Res. **42**(2), 145–152 (1997). https://doi.org/10.1016/s0378-7796(96)01199-6

24. Anderson, P.M.: In: Anderson, P.M., Fouad, A.A. (eds.) Power Systems Control and Stability, 678 p. IEEE Press Power Engineering Series, United States of America (2003)

25. Kulyk, M., Zgurovets, O.: Modeling of power systems with wind, solar power plants and energy storage. In: Babak, V., Isaienko, V., Zaporozhets, A. (eds.) Systems, Decision and Control in Energy I. Studies in Systems, Decision and Control, vol. 298. Springer, Cham (2020). https://doi.org/10.1007/978-3-030-48583-2_15

26. Zgurovets, O., Kulyk, M.: Comparative analysis and recommendations for the use of frequency regulation technologies in integrated power systems with a large share of wind power plants. In: Zaporozhets, A., Artemchuk, V. (eds.) Systems, Decision and Control in Energy II. Studies in Systems, Decision and Control, vol. 346. Springer, Cham (2021). https://doi.org/10.1007/978-3-030-69189-9_5

Short-Term Load Forecasting in Electrical Networks and Systems with Artificial Neural Networks and Taking into Account Additional Factors

Volodymyr Miroshnyk [ID]**, Pavlo Shymaniuk** [ID]**, Viktoriia Sychova** [ID]**, and Stepan Loskutov** [ID]

Abstract The reliability of electrical networks and systems largely depends on the accuracy of load forecasts used to calculate losses, imbalances, and modes of operation of power systems. The use of modern forecasting methods allows us to obtain more accurate results, faster calculations, flexible enough to solve a wide range of problems. Artificial neural networks today are one of the most common tools for building complex mathematical models depending on the tasks. This spread of artificial neural networks is due to the significant development of computer technology. Depending on the characteristics of electrical networks and their loads, the accuracy of different forecasting methods may vary. Additional factors also have a significant impact on forecasting accuracy. Therefore, accurate load forecasts for different load levels require modern and effective methods that could take into account the relationship of additional factors. Among the factors that have a significant impact on changes in the electrical load of the power system are meteorological factors, namely temperature. To determine the exact relationship between load and external factors, the method of decomposition of graphs using the Hilbert-Huang method is considered. This chapter discusses the possibilities and prospects for the application of modern forecasting methods based on artificial neural networks, respectively, for forecasting electrical networks of different hierarchies with the possibility of taking into account temperature.

Keywords Short-term forecasting · Total electrical load · Nodal electrical load · Neural network · Deep learning · Integrated power system · Hierarchical levels of the energy system · Decomposition of graphs

V. Miroshnyk (✉) · P. Shymaniuk · V. Sychova · S. Loskutov
Institute of Electrodynamics, National Academy of Sciences of Ukraine, Kyiv, Ukraine
e-mail: miroshnyk.volodymyr@gmail.com

1   Introduction

Many studies in Ukraine are aimed at solving current problems of energy markets [1–4] and electricity systems [5–9]. The transition in Ukraine to a newly liberalized electricity market has led to the functioning of such segments as the market of bilateral agreements, the market for the "day ahead", the intraday market, and the balancing market [10, 11]. The emergence of new market segments has strengthened the urgency of improving the accuracy and stability of the results of short-term forecasting of both total electrical load (TEL) [12] and nodal load. In particular, the accuracy of forecasts determines the level of imbalances in electricity in the electricity system, which are created by different market participants [13, 14]. Accordingly, different approaches can be used for short-term forecasting tasks of both TEL and short-term forecasting of nodal electric load.

One of the approaches is the idea of short-term forecasting of the Integrated Power System (IPS) of Ukraine at each of the three hierarchical levels independently. Research in this direction is given in [15, 16], modern methods of hierarchical forecasting are divided into two groups: "bottom-up" and "top-down". The first approach combines lower-level forecasts for forecasting for each higher level, and the second approach uses only historical data from all levels for forecasting. Based on this, it can be argued that to increase the accuracy of forecasting at the upper level of the hierarchical system, it is necessary to increase the accuracy of forecasting at lower levels.

Another approach to solving the problems of short-term forecasting of TEL is the solution by building a multifactor mathematical model, which takes into account the structure and nature of electricity consumption taking into account the factors of influence. Improving the methods of short-term forecasting of TEL allows to increase in the efficiency of market participants [13] and distribution system operators(DSO) [14] in organized segments of the electricity market, as well as transmission system operator (TSO) during the organization of the balancing electricity market of Ukraine [17].

The development of multifactor models is also effective for predicting nodal loads. Determining the relationship between load nodes and between additional influencing factors also indicates the need to consider additional factors when predicting load.

The accuracy of forecasts of both total and nodal loads affects the cost-effectiveness of generating equipment and, accordingly, the cost of electricity. In particular, the forecast of nodal loads [18, 19] is needed to optimize future and adjust current regimes, accept operational dispatch requests, as well as to submit applications for the purchase and sale of electricity to distribution system operators, which necessitates obtaining forecast data for electricity purchases. different market segments.

2 Application of Artificial Neural Networks for Forecasting Electrical Load at Different Levels of Power Systems

2.1 Forecasting of Hierarchical Levels of the Power System

Using artificial neural networks for energy problems demonstrates advantages over classical statistical forecasting methods. For example, in [20], some methods of statistical and artificial intelligence are used to predict the electric load considered as well as the factors influencing the accuracy of forecasts are analyzed. The transition to hybrid models combines two or more models. In [21], was shown that neural network models are gradually becoming more accurate for load prediction compared, to multiple linear regression, the reference vector method, the Random Forest, and others. Data from the Irish energy system were used to test the effectiveness of short-term forecasting methods for different types of workloads (residential, small, and medium-sized enterprises). The obtained results demonstrate the high accuracy of neural networks compared to other methods, especially for short-term forecasting with a prediction of 1–7 days, where they have a better advantage.

To test the effectiveness of forecasting different hierarchical levels, a model was built for each hierarchical level of the IPS of Ukraine based on artificial neural networks, namely:

- for the distribution system operator (DSO) level;
- for the level of the regional power system of the transmission system operator (TSO);
- for the IPS level of Ukraine.

The model is evaluated based on Kyivenerho, the Central Electric Power System of National Power Company (NPC) Ukrenergo, and the IPS of Ukraine for the period 2015–2016.

The data of the total electric load are time series. These are indicators that are collected over a period and correspond to some samples. Within the framework of this publication, the hourly values of TEL in MW at each of the given hierarchical levels of the IPS of Ukraine were used. A recurrent artificial neural network, which is widely used for time series prediction problems, was chosen for modeling.

A recurrent neural network is an improved version of a conventional artificial neural network (multilayer perceptron) that contains feedback to store information. One of the types of architecture of recurrent networks is LSTM (long-short time memory) [22], a network that is capable of learning on long-term dependencies.

For this task, a single-layer recurrent neural network of the LSTM type was used, to which a two-layer fully connected network was added. Data for two weeks with hourly discreteness is submitted to the network input. The input layer has 24 neurons, ie for each neuron of the LSTM layer values are given every hour for the previous two weeks. Thus, we obtain the sequence in which the input data for a particular hour enters the input of a particular neuron, which in turn transmits the output data to the next neuron both horizontally and vertically. This neural network is implemented in
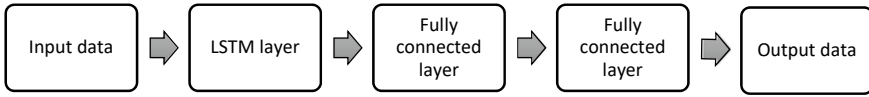
Fig. 1 Neural network architecture

the Python programming language. In Fig. 1 shows the general architecture of the proposed neural network.

Before submitting the data to the network input, the data of the training sample was normalized to the form from 0 to 1 according to formula (1). Test sample data were normalized in the same way, but using the minimum and maximum values from the training sample.

$$x_{i,j} = \frac{x_{i,j} - \min(x_j)}{\max(x_j) - \min(x_j)}, \tag{1}$$

where i—is the row number and, j—is the column number.

The LSTM expects the input to match some structure of the 3D array. Therefore, the best option is to use the previous time steps in our time series as input data to predict the output data in the next step. That is, for each neuron of data of separate time intervals is given, and through feedback, the information from the previous steps is transferred to the following. Thus, the network receives data not only for a specific hour but also information from previous time steps.

2.2 Retrospective Data and Results of Forecasting Different Hierarchical Levels of the Power System

Prediction of each of the hierarchical levels is performed on the model of the artificial neural network described above, for each hierarchical level training was conducted separately on the corresponding data samples. Approbation of the forecasting results was performed on the data of DTEK Kyiv Electric Networks and the Central Electric Power System of NPC Ukrenergo for the period from 2015 to 2017 with hourly discreteness. Training samples of the same dimension for the period from January 2, 2015, to August 22, 2016, were used to train the models. Test samples were divided into summer and winter. The summer sample contained data for the period from August 22 to September 1, and the winter—from 22 to 31 December 2016. The RELU function was used as the activation function of the fully connected layers. The RMSE function was used as an evaluation parameter.

Table 1 shows the RMSE forecast errors (square root of the root mean square error) as a percentage and in absolute values for the test samples.

Table 1 Forecast errors

Hierarchical levels	Summer period (MW)	Summer period (%)	Winter period (MW)	Winter period (%)
Distribution system level	57.58	5.9	60.52	4.5
The level of the regional energy system	98.3	3.8	75.1	2
IES level of Ukraine	395	2.6	308.65	1.5

RMSE graphs for summer and winter testing periods are presented in Figs. 2 and 3 for the DSO level, the regional TSO power system and the IES level of Ukraine, respectively.

The results of the calculations show that the accuracy of forecasting increases with each higher hierarchical level. That is due to factors that affect them. In particular, the lower levels are affected by several factors. The forecast for the winter period shows a smaller error. The graphs show that at each higher hierarchical level the error is more uniform without obvious bevels.

The analysis of forecasting results showed that the forecast error is smallest in the winter period for all hierarchical levels, which is in the range of 1.5 … 4.5%, while for the summer period the error is in the range of 2.6 … 5.9%. With each higher level, the error decreases in both testing periods, this is since the lower levels
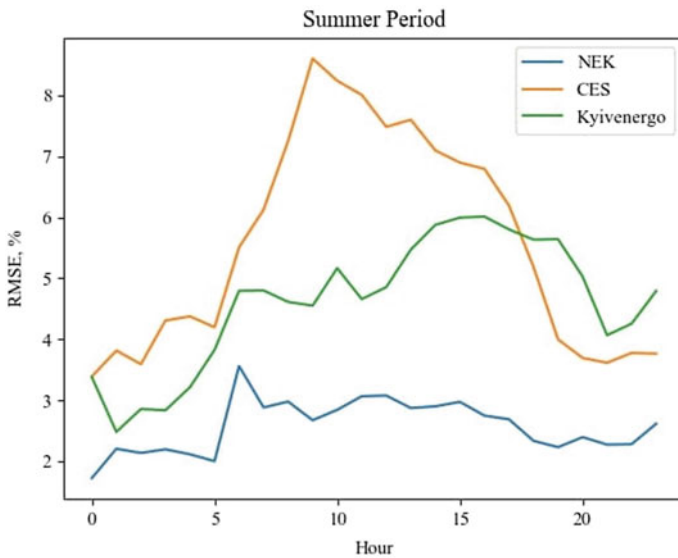
Fig. 2 RMSE errors for summer period for all power system levels
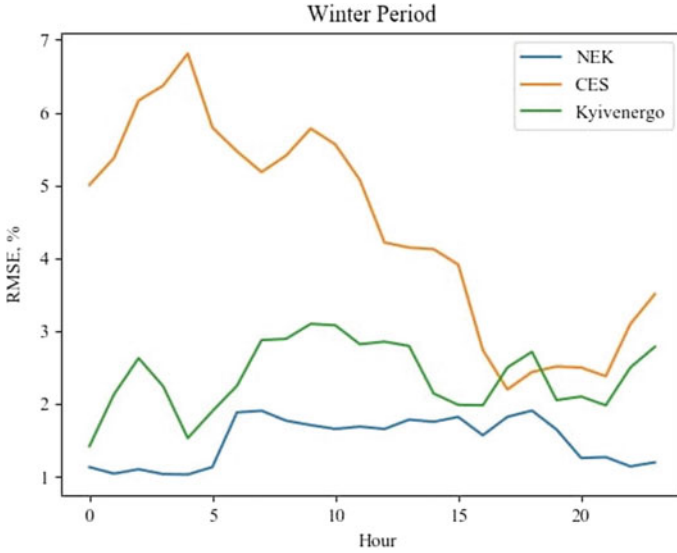
Fig. 3 RMSE errors for winter period for all power system levels

are affected by more external factors, so it is more dispersion. To test the impact of external factors on the lower levels of the power system, a study was conducted to predict the total load of the DSO, taking into account air temperature. This study is described in Sects. 2.3 and 2.4.

2.3 Decomposition of Schedules of Total Electric Load and Forecasting of Total Electric Load Taking into Account Temperature

Since at the lower levels the TEL values are influenced by both internal (technological) and external (meteorological, astronomical, etc.) factors, to determine the degree of influence of a factor, it is advisable to decompose graphs of TEL hour sections and predict each component separately depending on the factor.

In this model, the Hilbert-Huang method is used to decompose TEL schedules into temperature and base components [23]. This method is promising for the study of nonlinear and nonstationary processes. The classical algorithm of the Hilbert-Huang method looks like this:

1. Search in the TEL curve of the hour section $P(x)$ of local extrema, grouping separately local minima and maxima of TEL.

2. Construction of curved curves by interpolation of curves of local minima *ub(xb)* and maxima *ut(xt)*. Since the number of points in the curves can differ significantly, it is necessary to interpolate (using cubic splines) and extrapolate (using the first-order Brown method) their functions over the entire sample size *ub(x)* and *ut(x),* respectively, where *x* varies from 1 to *n*-sample size.
3. Then the first component m is found as the mean value between the functions *ub(x)* and *ut(x)* (2):

$$m_i = \frac{ub_i + ut_i}{2}.$$ (2)

4. The second component c_k (*k*—iterations number) is the difference between the values of full load and the first component.
5. In the following iterations, y(x) takes the value mk-1 and algorithm 1–4 continues until the number of local minima or maxima is less than 2.

Thus, in [24] described method is used for pre-processing of data in one-factor forecasting using neural networks.

In the developed model, this algorithm is adapted to match the decomposition results to the real process of the effect of temperature change on the TEL. In particular, the following changes were made:

1. Only the curve of the local minima of the TEL schedule is used in the calculations, so for the most part the base and temperature components are positive, in addition, the limit of the "insensitivity zone" is determined, at temperatures below which the temperature component is zero.
2. After each iteration, the selected components ck are added, and the correlation coefficient between the sum of the selected components Σc_k and the air temperature is calculated, it is an additional condition for stopping the decomposition cycle.

To predict the temperature component, polynomial regression is used with the selection of the optimal degree and model (3):

$$P = \sum_{i=0}^{m} a_i t^i,$$ (3)

where *u* varies from 0 to the optimal degree of *m*; *a*—coefficients of the polynomial equation.

These coefficients are determined in the following sequence: a system of algebraic Eq. (4) is formed using the matrix method. Since the matrix of input parameters (air temperature values) $t\{[1], [t_i], [t_i^2]... [t_i^m]\}$ is often rectangular, it is necessary to apply the matrix transformations of Eq. (4), then the required coefficients are determined by Eq. (5):

$$t A = P;$$ (4)

$$t^T t A = \left(t^T P\right). \tag{5}$$

To increase the universality of the method of calculating the system of Eq. (4), namely to avoid cases where the matrix $t^T t$ has no inverse, the resulting system of algebraic equations is solved using the Gaussian method. The analysis of preliminary calculations showed that the selection of the degree from 2 to 10 is sufficient. At the same time, the optimal model is selected for each degree. The criterion of minimum means absolute percentage error (MAPE) is accepted as a target function for selecting the optimal model.

Pugachev's method of canonical decomposition of random processes was used to predict the base component of TEL [25]. The method of canonical decomposition is a representation of the function $Pb(t)$ in the form:

$$Pb(t) = m_{Pb}(t) + \sum_V V_V \varphi_V(t), \tag{6}$$

where $m_{Pb}(t)$—mathematical expectation of the base component of TEL, Vv—some random variables whose mathematical expectation is 0, $\varphi_v(t)$—coordinate function calculated by the following formula:

$$\varphi_V(t) = \frac{1}{D_v} M(Pb(t) V_v), \tag{7}$$

where D_v—variance of an array of random numbers; $Pb(t)$—values of the base component of TEL, centered on the average value (deviation of the original function from the average value).

An array of random numbers must satisfy the following conditions:

$$M[V_v] = 0; \ M[V_v V_m] = 0 (m \neq v). \tag{8}$$

Numbers were obtained using a white noise generator.

Prediction of the base component of TEL is performed by the formula:

$$Pb(t + 1) = m_{Pb}(t) + \varphi v(t) V_v. \tag{9}$$

The synthesis of the forecast graph is performed as the algebraic sum of the temperature and base components in each hour of the daily schedule.

2.4 Analysis of the Results of Total Forecasting Taking into Account the Temperature

The study was conducted according to Kyivenerho for the winter period from 01/11/2015 to 31/03/2016 and the summer period from 01/06/2015 to 31/08/2015. Both samples are hourly and contain only working days from Tuesday to Thursday. Data on air temperature were obtained from open sources for the city of Kyiv with the discreteness of 3 h, so these data were interpolated to obtain hourly values.

Figure 4 shows the graphs of the temperature component and the temperature for the 12-h cross-section of both samples, where the inverse (for winter) and direct (for summer) correlations are observed. Testing of the mathematical model was performed for several days, for the summer period—for four days, for the winter period—for three days. The MAPE value is used to estimate the forecast error. The forecasting results are given in Table 2.
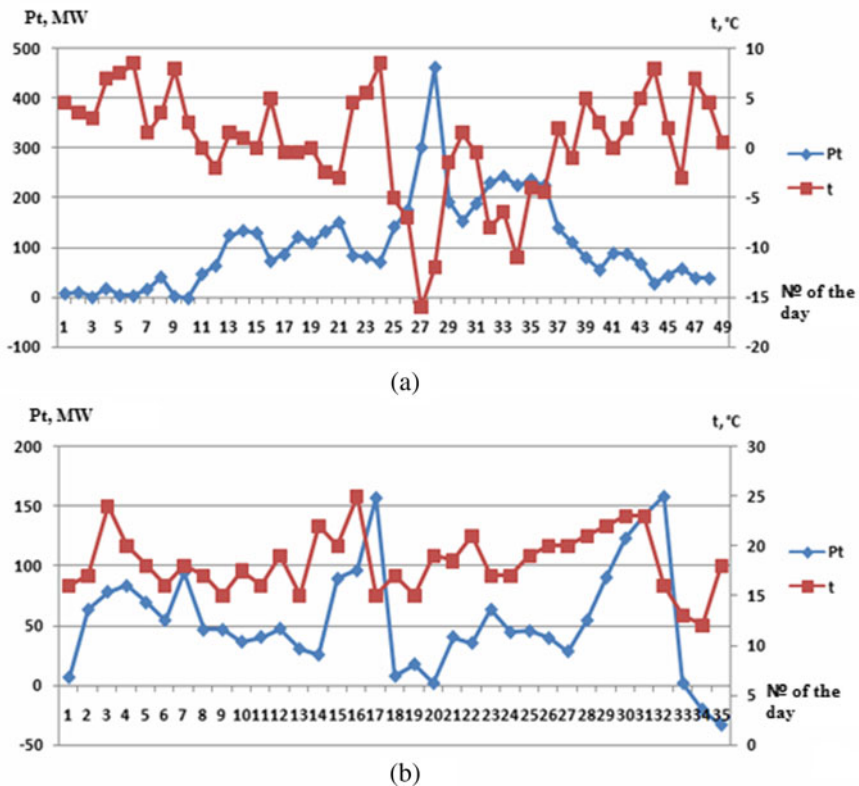

Fig. 4 Schedules of the temperature component and air temperature

Table 2 Errors of the total forecast taking into account the temperature

Forecast days	Summer period				Winter period		
	1	2	3	4	1	2	3
MAPE (%)	1.95	1.46	1.65	1.89	1.98	1.88	3.15

3 Short-Term Nodal Load Forecasting Taking into Account Temperature

Based on the results of short-term forecasting of nodal loads in the services of power system modes, most of the technical tasks of mode planning are solved, which are aimed at improving the efficiency and reliability of power systems. At this time, this problem is solved very simply: the node loads are determined using the coefficients of distribution of the total load according to the degree of their relationship with the node loads. However, there are works in which more advanced forecasting methods are used to determine the nodal loads. Thus, in [26], inversion of a neural network based on a multilayer perceptron is used to predict nodal loads. In [14], an algorithm based on an artificial neural network of the multilayer perceptron type, combined with a mathematical apparatus of autoregression, was considered to predict nodal loads. Using the autoregression method, the data is pre-processed and the parameters of the mathematical model (MM) are estimated. The error of forecasting results for working days is in the range of 2.4–6.2%. In addition, methods based on artificial neural networks can be used for problems of renewable energy sources and their forecasting [27, 28]. In some published works on short-term forecasting of total electrical load, the influence of meteorological factors (temperature, clouds, etc.) is taken into account [12]. Preliminary studies have also shown that to increase the accuracy and reliability of short-term forecasting results, it is necessary to take into account additional technological factors, in particular, the mode of operation of energy-intensive enterprises.

LSTM deep learning neural network, the architecture of which is present in [18], was used to predict nodal loads. Such a neural network is a combined architecture based on a multilayer perceptron hidden layer which contains a recurrent LSTM memory module [22], as well as two fully connected layers, and one bypass connection that provides input to the output, which is summed to improve the neural network learning process. The data on the input of the neural network happens in increments of 24 values. The SELU (scaled exponential linear unit) function is used as an activation function of hidden layers [29]. Training is carried out using the ADAM optimizer (adaptive moment estimation) [30]. A period of 100 epochs was chosen for study. Ambient temperature data was used as a virtual node and concatenated with the input load vector of the nodes.

To study the influence of air temperature on the accuracy of forecasting of nodal loads used to load data obtained from the automated system of control and accounting of electricity (ASCAE) "Vinnytsiaoblenergo" for the period from 10.01.2017 to

06.10.2019, monthly loading of 15 universities with hourly discreteness. Air temperature data were obtained from the meteorological station of Vinnytsia (according to the index of the International Meteorological Organization 33,562). The temperature data used have a discreteness of one hour.

To determine the relationship between the load nodes, the correlation of data for working days and weekends was performed.

As can be seen from the above data, when the nodal correlation of working day data was found, several nodes that have no connection with the nodes are nodes 4, 11, and 13 (correlation coefficient of which is in the range of $0.2 - (-0.2)$). Whereas for weekends only 4 nodes have no connection with other nodes. You can select the nodes with the highest correlation coefficients, these are 3.5, 6, 7, 8, and 12. (correlation is in the range from 0.7 to 1). You can also group nodes 9–10 to 14–15 with a correlation coefficient of 0.7–0.6, and nodes 1–2 with a correlation coefficient of 0.5–0.4 (Tables 3 and 4).

The correlation of data between nodes load and temperature was also investigated. According to the results of which (Table 5), it is seen that the relationship between working days and weekends with the temperature is identical. Almost all nodes have a negative correlation with temperature.

To determine the optimal scope of training samples for winter and summer periods, a comparative analysis of the average daily load and temperature graphs for all nodes for the entire period was conducted. After analyzing the graphs of load and air temperature, we can identify the following common features:

- All nodes are dependent on temperature in winter, with some having a linear relationship (ie the form of load graphs and similar temperatures), while others have a negative correlation.
- The winter period can be conditionally allocated starting from the period 25/09–10/10/2017 to 04–05/04/2018. During this period there is a decrease in temperature and an increase in the magnitude of the load on the nodes.

Table 3 Correlation between nodal of working days

Nodes	1	2	3	4	5	6	7	8	9	10	11	12	13	14	15
1	1	0.58	0.43	−0.22	0.45	0.49	0.54	0.66	0.27	0.49	0.54	0.59	0.22	0.59	0.43
2		1	0.57	−0.18	0.60	0.66	0.59	0.85	0.53	0.68	0.67	0.74	0.26	0.64	0.55
3			1	0.04	0.70	0.77	0.74	0.67	0.69	0.68	0.74	0.79	0.52	0.69	0.66
4				1	−0.05	−0.11	0.04	−0.23	0.20	−0.07	0.06	−0.08	0.21	−0.01	0.00
5					1	0.81	0.79	0.73	0.74	0.74	0.81	0.87	0.54	0.75	0.68
6						1	0.85	0.80	0.74	0.79	0.83	0.91	0.56	0.75	0.74
7							1	0.71	0.74	0.71	0.86	0.89	0.71	0.82	0.72
8								1	0.59	0.79	0.76	0.88	0.32	0.73	0.67
9									1	0.72	0.79	0.75	0.59	0.67	0.71
10										1	0.80	0.81	0.41	0.69	0.72
11											1	0.89	0.60	0.82	0.74
12												1	0.58	0.87	0.75
13													1	0.61	0.47
14														1	0.66
15															1

Table 4 Correlation between nodal of weekends

Nodes	1	2	3	4	5	6	7	8	9	10	11	12	13	14	15
1	1	0.58	0.43	−0.22	0.45	0.49	0.54	0.66	0.27	0.49	0.54	0.59	0.22	0.59	0.43
2		1	0.57	−0.18	0.60	0.66	0.59	0.85	0.53	0.68	0.67	0.74	0.26	0.64	0.55
3			1	0.04	0.70	0.77	0.74	0.67	0.69	0.68	0.74	0.79	0.52	0.69	0.66
4				1	−0.05	−0.11	0.04	0.23	0.20	−0.07	0.06	−0.08	0.21	−0.01	0.00
5					1	0.81	0.79	0.73	0.74	0.74	0.81	0.87	0.54	0.75	0.68
6						1	0.85	0.80	0.74	0.79	0.83	0.91	0.56	0.75	0.74
7							1	0.71	0.74	0.71	0.86	0.89	0.71	0.82	0.72
8								1	0.59	0.79	0.76	0.88	0.32	0.73	0.67
9									1	0.72	0.79	0.75	0.59	0.67	0.71
10										1	0.80	0.81	0.41	0.69	0.72
11											1	0.89	0.60	0.82	0.74
12												1	0.58	0.87	0.75
13													1	0.61	0.47
14														1	0.66
15															1

Table 5 Correlation of load nodes with temperature

Correlation of nodes with temperature	1	2	3	4	5	6	7	8	9	10	11	12	13	14	15
Weekdays	−0.66	−0.76	−0.34	0.33	−0.42	−0.47	−0.48	−0.79	−0.25	−0.57	−0.58	−0.63	0.13	−0.53	−0.40
Weekend	−0.66	−0.76	−0.34	0.33	−0.42	−0.47	−0.48	−0.79	−0.25	−0.57	−0.58	−0.63	0.13	−0.53	−0.40

- Then in the period from 4 to 9 April, there is a sharp decline in load and conditionally begins the summer period during which the load is almost independent of temperature. This period ends on September 20–25, 2018.
- In some nodes there is a significant number of load failures (in some cases it is characterized by the presence of holidays and in others—the emergence of probable emergencies), in node 10 there is an abnormal increase in load in November 2018, exceeding normal values by 4 times.

Thus, for training samples, it is possible to allocate conditionally winter from 10/01/2017 to 04/04/2018 and conditionally summer from 04/09/2018 to 09/20/2018 periods with the allocation of the last 7 days to assess the forecast. Figures 5, 6 and 7 show examples of load-temperature ratio charts for the selected period.

Also, to check the effectiveness of forecasting nodal loads, data analysis was performed to identify anomalous values and omissions (hereinafter referred to as data analysis). To do this, a two-stage validation algorithm was developed, which includes the stage of data clustering to select anomalous values and replace them, after which the seasonal decomposition method selects residual data, which is used for re-verification by the clustering method.

Detailed analysis of the node load data revealed a significant number of anomalous values that need to be replaced.

Table 6 shows the statistical load characteristics of nodes 1 and 11, before and after the authentication procedure.
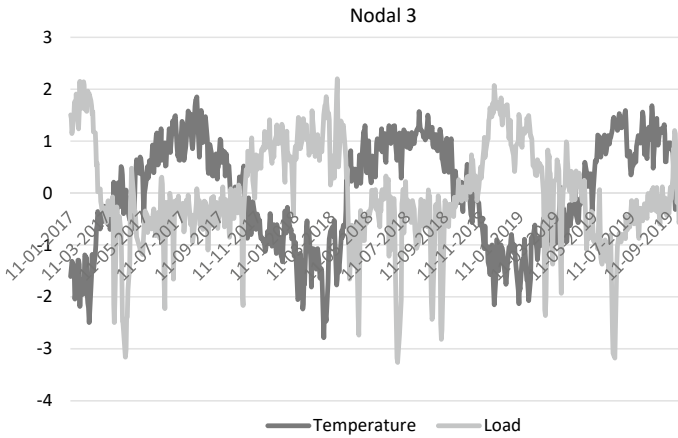
Fig. 5 Graphs of the ratio of load and temperature of the node 3
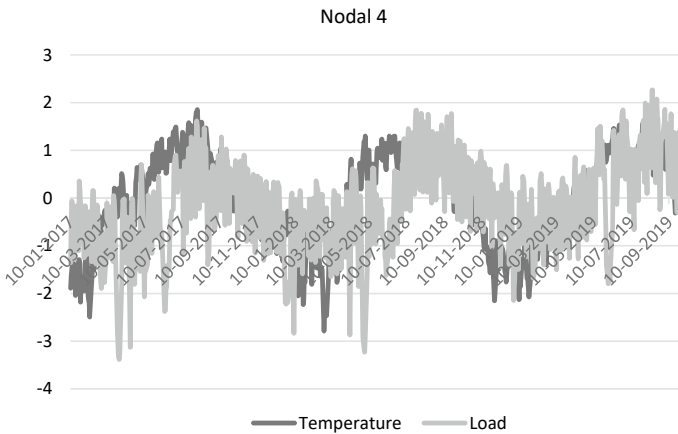
Fig. 6 Graphs of the ratio of load and temperature of the node 4

The schedule of loading of the corresponding knots before and after authentication is shown in Fig. 8 (Table 7).

As can be seen from the above data, the verification algorithm as a whole successfully detected and recovered single emissions, but the quality of identification and recovery of group emissions is much lower.

Tables 8 and 9 show the forecast results. The MAPE was used to assess error. The calculation of the error was performed on the data for the period from 01/01/2019 to 06/10/2019, which was not used for neural network training.

Thus, it is shown that the use of the confidence method for nodal load data can reduce the average forecast error from 13.74 to 11.52%. The use of air temperature data as additional forecasting factors can further reduce forecast errors in the range
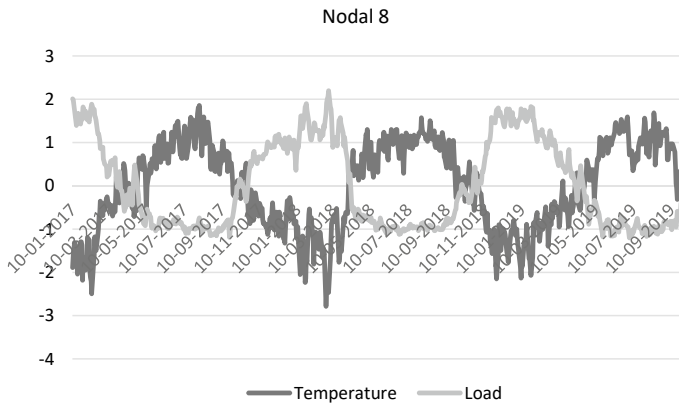
Fig. 7 Graphs of the ratio of load and temperature of the node 8

Table 6 Statistical load characteristics of nodes 1 and 11 before and after the authentication procedure

Node	Node 1		Node11	
	To authentication	After authentication	To authentication	After authentication
Average, kW h	2365	2393	15,684	13,058
Standard deviation, kW h	444	372	13,787	3315
Coefficient of variation, relative unitsacting	0.19	0.16	0.88	0.25
The minimum value of kW h	0	1284	0	4777
25 percentile kW h	2136	2148	10,760	10,609
Median, kW h	2387	2394	12,939	12,765
75 percentile kW h	2638	2641	15,797	15,318
Maximum value, kW h	3814	3814	181,949	24,773

from 14.22 to 11.17%. The accuracy of the prediction also depends on the data samples. When using samples for the conditionally winter or summer period, in some cases this reduces the forecast errors, but the accuracy depends primarily on the sample size.
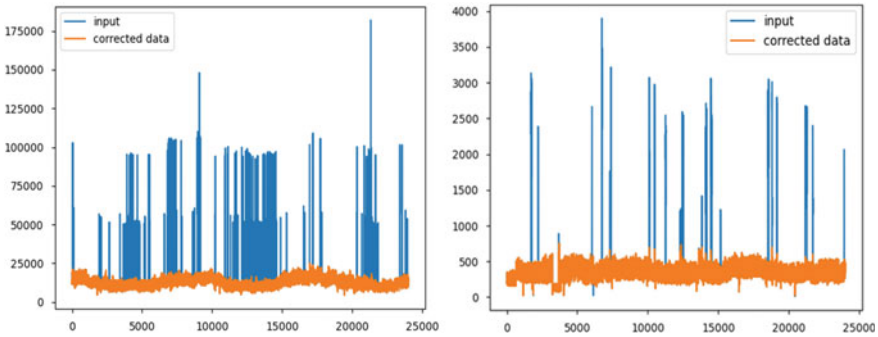
Fig. 8 Schedule of loading of knots before authentication and after authentication

Table 7 Samples of training and test data samples for forecasting

Sample	Additional factors		Data analysis	Training sample size	Test sample size
The whole period	With temperature		Unverified data	10/01/2017–06/09/2019	06/09/2019–06/10/2019
			Authenticated data	10/01/2017–06.09.2019	06/09/2019–06/10/2019
	Without temperature		Unverified data	10/01/2017–06/09/2019	06/09/2019–06/10/2019
			Authenticated data	10/01/2017–06/09/2019	06/09/2019–06/10/2019
Working days	With temperature	Winter period	Authenticated data	01/11/2017–20/03/2018	21/03/2018–29/03/2018
	With temperature	Summer period	Authenticated data	01/05/2018–20/08/2018	21/08/2018–29/08/2018
Weekend	With temperature	Winter period	Authenticated data	04/11/2017–18/03/2018	24/03/2018–04/04/2018
	With temperature	Summer period	Authenticated data	05/05/2018–19/08/2018	25/08/2018–15/09/2018

4   Conclusion

The results of complex studies are aimed at improving the accuracy of forecasting electrical loads through the use of artificial neural networks and taking into account additional factors, including air temperature. Prediction of the total load using the decomposition of TEL graphs (separately for each slice) using the Hilbert-Huang method with the proposed and made changes to solve the problem obtained temperature component that has a close correlation with air temperature, which helps to build more exact regression dependence for its prediction. The use of the proposed method allows ensuring the error of the results of short-term forecasting of TEL within 1.5 ÷ 3.15%.

Table 8 Forecast errors for different configuration

Data type	Unverified data		Authenticated data	
Type of forecast	One-factor	Multi-factor	One-factor	Multi-factor
1	7.60	8.33	6.80	5.86
2	24.49	23.31	23.48	24.17
3	16.76	16.87	16.28	15.73
4	13.92	10.52	9.78	8.34
5	8.74	8.57	8.28	8.66
6	10.60	10.48	10.51	10.04
7	13.40	14.10	13.95	13.24
8	7.18	6.93	6.68	6.83
9	12.01	12.18	11.44	11.65
10	20.91	20.55	20.27	19.74
11	22.57	26.96	9.30	8.38
12	6.87	7.01	7.01	6.62
13	16.32	23.42	9.31	9.31
14	17.69	16.63	11.68	11.00
15	7.12	7.40	7.96	7.95
Mean	13.74	14.22	11.52	11.17
Minimal	6.87	6.93	6.68	5.86
Maximum	24.49	26.96	23.48	24.17

The use of a recurrent neural network is effective when forecasting data with different dimensions and provides high accuracy of forecasting at the level of the IPS of Ukraine, namely within 1.5 … 2.6%. For other hierarchical levels, forecasting accuracy is reduced to 6%. To increase the accuracy at the regional level and the IPS level of Ukraine, it is advisable to take into account the results of forecasts at lower hierarchical levels, taking into account the listed external factors.

The use of air temperature as an additional factor for short-term forecasting of nodal load can reduce the forecast error from 11.52 to 11.17%. Based on the analysis of load and temperature data, it was determined that the data have the opposite correlation. Also, depending on the type of data sample, the effect of temperature changes and thus changes the accuracy of forecasting results. It is established that the choice of the training sample and its volume for neural network training depends on the accuracy of forecasting results. The use of the developed method of verification allows the detection of significant anomalous values and omissions of data, thereby improving the accuracy of forecasting. Careful analysis of the results of forecasting node loads showed that reducing the error for nodes with sharply variable loads requires a more advanced method of data validation.

Table 9 Forecast errors for diferent day types

Data type	Winter period (01.11.2017–04.04.2018)		Summer period (01.05.2018–15.09.2018)	
Type of forecast	Working days	Weekend	Working days	Weekend
1	10.13	8.34	8.79	11.05
2	10.01	19.18	16.47	7.29
3	12.36	39.12	19.62	17.1
4	19.06	20.65	21.02	19.37
5	6.88	5.3	7.7	10.6
6	8.44	4.96	12.87	10.82
7	8.46	9.68	10.24	9.77
8	9.24	4.6	4.79	4.82
9	11.37	6.8	5.44	4.76
10	11.78	39.03	17.95	22.39
11	6.61	7.12	8.42	8.78
12	7.59	3.88	4.4	4.84
13	5.97	11.78	18.84	13.42
14	6.58	6.68	13.91	20.91
15	28.3	13.46	25.86	19.98
Mean	10.85	13.37	13.09	12.39
Minimal	5.97	3.88	4.4	4.76
Maximum	28.3	39.12	25.86	22.39

References

1. Blinov, I., Tankevych, S.: The harmonized role model of electricity market in Ukraine. In: 2016 2nd International Conference on Intelligent Energy and Power Systems, IEPS 2016 Conference Proceedings (2016). https://doi.org/10.1109/IEPS.2016.7521861
2. Blinov, I.V., Parus, Y.V.: Congestion management and minimization of price difference between coupled electricity markets. Tekhnichna Elektrodynamika **4**, 81–88 (2015)
3. Blinov, I., Kyrylenko, O., Parus, E., Rybina, O.: Decentralized market coupling with taking account power systems transmission network constraints. In: Power Systems Research and Operation. Studies in Systems, Decision and Control, vol. 388. Springer, Cham (2022). https://doi.org/10.1007/978-3-030-82926-1_1
4. Ivanov, H.A., Blinov, I.V., Parus, Y.V., Miroshnyk, V.O.: Components of model for analysis of influence of renewables on the electricity market price in Ukraine. Tekhnichna Elektrodynamika **4**, 72–75 (2020). https://doi.org/10.15407/techned2020.04.072
5. Kyrylenko, O.V., Blinov, I.V., Parus, Y.V.: Operation evaluation of power plants in the provision of ancillary services of primary and secondary frequency control in the Ukrainian power system. Tekhnichna Elektrodynamika **5**, 55–60 (2013)
6. Basok, B.I., Butkevych, O.F., Dubovskyi, S.V.: Technical and economic aspects of decarbonisation prospects assessing of the interconnected power system of Ukraine. Technical Electrodynamics **5**, 55–62 (2021). https://doi.org/10.15407/techned2021.05.055

7. Kyrylenko, O.V., Blinov, I.V., Parus, E.V. Trach, I.V.: Evaluation of efficiency of use of energy storage system in electric networks. Technical Electrodynamics **4**, 44–54 (2021).https://doi.org/10.15407/techned2021.04.044

8. Kyrylenko, O.V., Basok, B.I., Baseyev, Ye.T., Blinov, I.V.: Power industry of Ukraine and realities of the global warming. Tekhnichna Elektrodynamika **3**, 52–61 (2020). https://doi.org/10.15407/techned2020.03.052

9. Butkevich, O.F., Yuneeva, N.T., Gureeva, T.M.: On the issue of placement of energy storage in the Ukrainian UES. Tekhnichna Elektrodynamika **6**, 59–64 (2019). https://doi.org/10.15407/techned2019.06.059

10. On Electricyty Market: The Law of Ukraine. No. 2019-VIII of 13.04.2017

11. Ivanov, H., Blinov, I., Parus, Y.: Simulation model of new electricity market in Ukraine. In: IEEE 6th International Conference on Energy Smart Systems (2019). https://doi.org/10.1109/ESS.2019.8764184

12. Chernenko, P., Sychova, V.: Improving the algorithm for determining the effect of air temperature on the overall electrical load of the power system to improve the accuracy of short-term forecasting. Tekhnichna Elektrodynamika **2**, 77–83 (2021)

13. Blinov, I.V., Miroshnyk, V.O., Shymaniuk, P.V.: Short-term interval forecast of total electricity generation by renewable energy sources producers. In: Pratsi Instytutu elektrodynamiky NAN Ukrainy **54**, 5−12. (2019). https://doi.org/10.15407/publishing2021.59.068

14. Blinov, I., Miroshnyk, V., Shymaniuk, P.: The cost of error of day ahead forecast of technological losses of electrical energy. Tech. Electrodynam. **5**, 70–73 (2020). https://doi.org/10.15407/techned2020.05.070

15. Chernenko, P.O.: Multilevel interdependent forecasting of electrical loads of the power association. Enerhoefektyvnist 99–104 (2000)

16. Fallah, S.N., Ganjkhani, M., Shamshirband, S.: Computational intelligence on short-term load forecasting: a methodological overview. MDPI

17. NEURC's Resolution "On Approval of Market Rules" No. 307 dd 14. 03.2018

18. Chernenko, P., Miroshnyk, V., Shymaniuk, P.: Univariable short-term forecast of nodal electrical loads of energy systems. Tekhnichna Elektrodynamika **2**, 67–73. (2020). https://doi.org/10.15407/techned2020.02.067

19. Han, A., Zhang, B., Sun, Z., Niu, Z., Wang, J.: Nodal load forecast model considering network topology constraints. In: IEEE PES Asia-Pacific Power and Energy Conference. Xi'an. China, pp. 939–943 (2016)

20. Peng, Y., Wang, Y., Lu, X., Li, H.. Shi, D., Wang, Z.: Jie Li Short-term load forecasting at different aggregation levels with predictability analysis. IEEE Innovative Smart Grid Technologies—Asia (ISGT Asia), China (2019). https://doi.org/10.1109/ISGT-Asia.2019.8881343

21. Zhao, T., Wang, J., Zhang, Y.: Day-ahead hierarchical probabilistic load forecasting with linear quantile regression and empirical copulas

22. Hochreiter, S., Schmidhuber, J.: Long short-term memory. Neural Comput. **9**, 1735–1780 (1997)

23. Huang, N.E., Shen, Z., Long, S.R., Wu, M.C., Shih, H.H., Zheng, Q., Yen, N.-C., Tung, C.C., Liu, H.H.: The empirical mode decomposition and the Hilbert spectrum for nonlinear and non-stationary time series analysis. Proc. R. Soc. Lond. A. **454**, 903–995 (1998)

24. Kurbatskyi, V.H., Sydorov, D.N., Spyriaev, V.A., Tomyn, N.V.: On a neural network approach to forecasting non-stationary time series based on the Hilbert-Huang transform. Avtomat. y telemekh. **7**, 58–68 (2011)

25. Puhachev, V.S.: The theory of random functions and its application to problems of automatic equations. M. : Hos. yzd-vo fyz.-mat. lyt., 883 (1962)

26. Shumilova, G.P., Gotman, J.N., Starceva, T.B.: Prediction of the active and reactive load of EPS units using inversion of an artificial neural network. Elektrichestvo. **6**, 7–13 (2007)

27. Hou, G., Xu, K., Yin, S., Wang, Y., Han, Y.**,** Wang, Z., Mao, Y., Lei, Z.: A novel algorithm for multi-node load forecasting based on big data of distribution network. In: International conference on advanced electronic science and technology (AEST 2016), Shenzhen, pp. 655–667 (2016)

28. Miroshnyk, V., Shymaniuk, P., Sychova, V.: Short term renewable energy forecasting with deep learning neural networks. Power Syst. Res. Operat. 121–142 (2022). https://doi.org/10.1007/978-3-030-82926-1_6
29. Klambauer, G., Unterthiner, T., Mayr, A., Hochreiter, S.: Self-normalizing neural networks. Adv. Neural Inf. Proc. Syst. **30**, 971–980 (2017)
30. Kingma, D.P., Ba Adam, J.: A method for stochastic optimization. In: Proceeding of the 3rd international conference on learning representations (ICLR)

Synthesis of Models of the Complex Electric Power Systems

Serhii Denysiuk [iD], **Denys Derevianko** [iD]**, and Halyna Bielokha** [iD]

Abstract The chapter is devoted to the development of theoretical and methodological bases for the synthesis of models of the complex electric power systems with distributed generation and renewable energy sources. When distributed generation (DG) sources are connected to the united power system (UPS) of Ukraine separately, as active consumers (prosumers), as part of microgrids and as separate generating facilities, a number of issues arise related to ensuring proper synchronization of the parameters of aforementioned systems, their electromagnetic compatibility, quality of electricity, occurrence of additional losses and reliability of their work. This chapter of the monograph discusses the technical means (and their parameters) and economic models and methods that should be used in the process of synthesis of the complex power systems with DG to ensure their optimal functioning. The chapter provides a game-theoretic approach of addressing a hard task of synthesis of complex power systems with DG and renewable energy sources. Game theory attempts to mathematically simulate strategic behavior in game situations. Various mathematical formulations of cooperative game theory have been applied for loss and cost allocation. Shapley, Aumann-Shapley, and Nucleolus-Based are the most common. The proposed game allows not only to combine both technical and economic models for power systems with DG sources and RES, but also to find an optimal solution in the process of synthesis of complex power systems. This optimal solution is found as Nash equilibrium for the proposed game.

S. Denysiuk (✉)
Institute of Energy Saving and Energy Management, National Technical University of Ukraine "Igor Sikorsky Kyiv Polytechnic Institute", Kyiv, Ukraine
e-mail: spdens@ukr.net

D. Derevianko
Power Supply Department, National Technical University of Ukraine "Igor Sikorsky Kyiv Polytechnic Institute", Kyiv, Ukraine

Institute of Engineering, Thermophysics of NAS of Ukraine, Kyiv, Ukraine

H. Bielokha
National Technical University of Ukraine "Igor Sikorsky Kyiv Polytechnic Institute", Kyiv, Ukraine

1 Introduction

Global climate changes at the end of XX century highly influenced the policies of many countries in the stream of reorganization of highly emitting economic sectors [1]. The economy sectors with highest level of emissions are: energy sector (about 40%), transport (about 22%) and industry (about 18%) as shown in Fig. 1 [1].

Intergovernmental Panel on Climate Change presented the estimated limits which will imply an atmospheric CO_2 concentration of no more than 450 parts per million (for 2°) or 430 ppm (for 1.5°). On current trends, these limits are estimated to be reached sometime between the late 2020s and the late 2030s, which leaves less than 10 or 20 years to make profound changes to the energy system and the global economy.
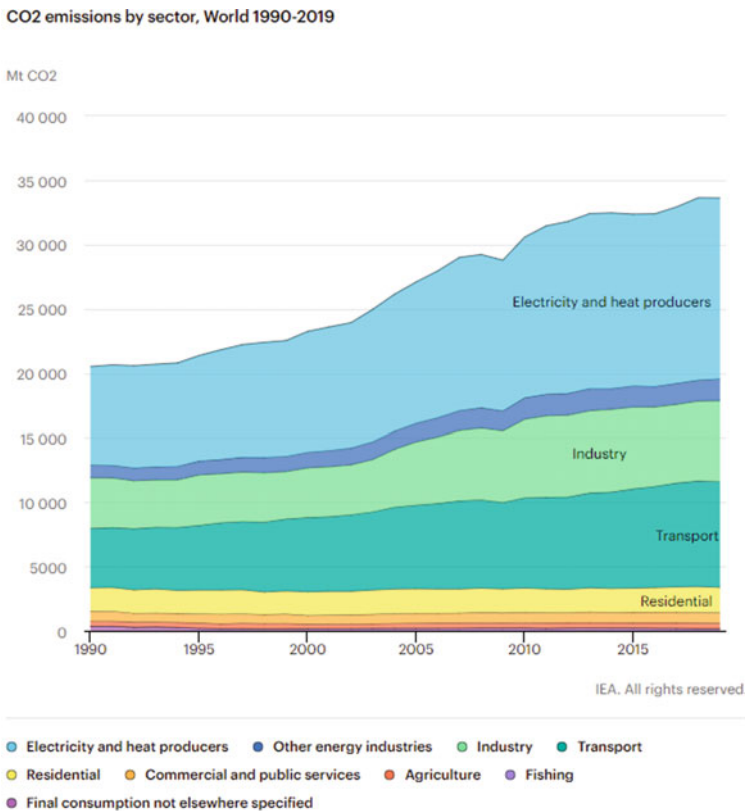
Fig. 1 CO_2 emissions by sector, World 1990–2019

As shown in [1, 2], the major methods of lowering the emissions in energy sector are: energy efficiency and substitution of fossil consuming generators with low-emitting renewable energy sources (RES). The implemented policies already influenced the growth of share of RES in the world and in Ukraine (Figs. 2 and 3). Due to this fact global CO_2 emissions declined by 5.8% in 2020 in comparison to 2019, or almost 2 Gt CO_2—the largest ever decline and almost five times greater than the 2009 decline that followed the global financial crisis. Despite the decline in 2020, global energy-related CO_2 emissions remained at 31.5 Gt, which contributed to CO_2 reaching its highest ever average annual concentration in the atmosphere of 412.5 parts per million in 2020—around 50% higher than when the industrial revolution began [1].

Still the implementation of RES is not as fast as the Demand growth [3]. This is due issues with power quality and system reliability which are caused by various RES types [4, 5]. In the other hand the evolution of RES brought a new type of power

- ○ Share of renewables in power generation
- ○ Share of coal in power generation
- ○ Share of gas in power generation
- ● Share of low carbon sources in power generation
- ● Share of oil in power generation
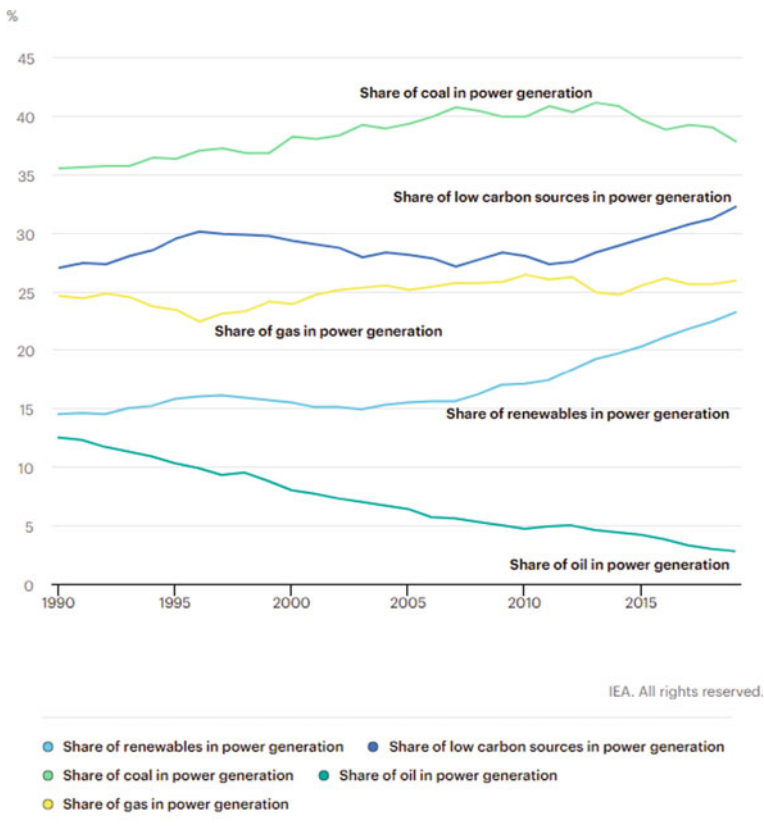
Fig. 2 Share of renewables, low-carbon sources and fossil fuels in power generation, World 1990–2019
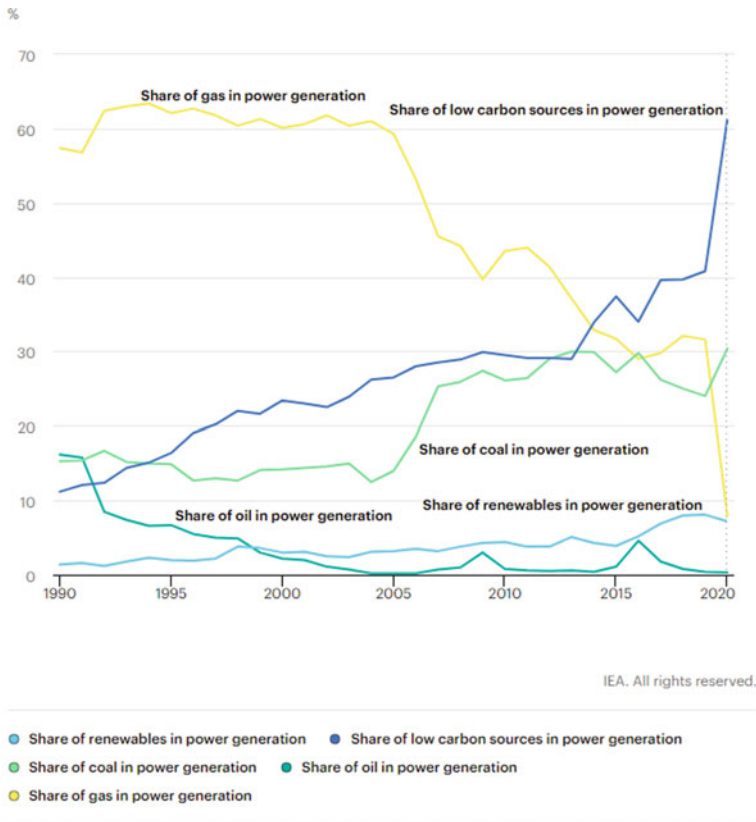
Fig. 3 Share of renewables, low-carbon sources and fossil fuels in power generation, Ukraine 1990–2019

systems known as Microgrids to reality [4]. Microgrids and RES are often distributed and are considered as distributed generation (DG) sources.

According to mentioned above, the major task of energy sector today is to raise the overall systems efficiency and decarbonization. To solve this tasks, it is important to find the optimal methods of joint operation of DG systems with centralized energy system maintaining the power quality, reliability and financial issues.

2 Mechanisms and Constrains of Synthesis of the Complex Power Systems with RES

2.1 Power Quality Issues of RES Integration to the Power Systems

The modern set of distributed technologies includes natural gas and diesel engines, gas turbines, fuel cells, solar panels, small hydropower plants and wind turbines (Table 1). Distributed technologies are usually less than 100 MW in total capacity [6–9]. They are very flexible and suitable for a large number of final consumers, including electricity and mechanical energy consumption [10].

The advantages of RES compared to traditional power sources are [4, 5]:

- practical inexhaustibility of primary fuel;
- low environmental pollution;
- there is no need for extraction, processing and delivery of fuel;
- no need to use water for cooling purposes, remove waste or decomposition products;
- there is no need for scarce high-temperature materials, except for solar heat concentrators;
- DG sources can work without maintenance;
- no need to transport primary fuel to energy source.
- The main disadvantage of most renewable energy sources is the instability of their energy potential which may lead to systems frequency deviations, voltage deviations and as a result to additional outages which influence the systems reliability [5, 11].

The implementation of DG sources affects the distribution networks in Microgrids and turns them into active elements. This leads to the need for changes (or revision and modernization) in the management, operation and mode planning strategy in Microgrids [7, 12, 13]. At the same time, their impact can be both positive and negative, so it is advisable to carefully analyze the issue of connecting DG sources to the Microgrids.

Most DG sources are connected to the grid via different converters. When connected, these converters must provide the required power quality. However, the high switching frequency of the valve elements in the converters can cause additional harmonics of voltage and current in the Microgrids and reduce the quality of electricity [7, 12, 13].

Installation of DG sources in Microgrids near the load can change the direction of power flow [14]. Installation of DG sources can both increase and decrease power losses in Microgrids, which mainly depends on the location and of DG sources in Microgrids, their $\cos\varphi$, as well as on the topology (configuration) of Microgrids and so on. There are two types of influence of the DG on the voltage in the Microgrids: the impact on the voltage level in the steady state operation of the Microgrids and

Table 1 Characteristics of DG sources based on RES

Characteristic	PV	WPP	SHPP	Fuel cell	Gas turbines	Steam turbines	Diesel generator
Primary fuel presence	Depending on the geographical location	Depending on the geographical location	Depending on the geographical location	Always	Always	Always	Always
Output signal	DC	DC/AC	AC	DC	AC	AC	AC
Management	Unmanageable	Unmanageable	Unmanageable	Controlled	Controlled	Controlled	Controlled
Type of converter	DC–DC–AC	AC–DC–AC	Synchronous or asynchronous generator	DC–AC	–	–	–
Primary fuel	Solar energy	Wind energy	Energy of rivers	Energy of chemical reactions	Natural and biogas	Natural and biogas	Refined products
Efficiency (%)	6–20	1–35	92–94	up to 85	30–45	20–40	30–45
Installed capacity	Up to 1 MW	0.1–2.5 MW	Up to 10 MW	5 кВт – 5 MW	0.1–30 MW	30 kW–10 MW	Up to 6 MW
Ability to work on schedule	Restricted	Restricted	Possibly	Possibly	Possibly	Possibly	Possibly
GHG level	–	–	–	–	High	High	High

Table 2 Types of distortions for different DG sources

Distortion type	Wind turbines	Solar PV	SHPP
Voltage sag	+		+
Voltage dip	+		
Voltage imbalance		+	
Voltage fluctuations	+		
Harmonics of voltage	+	+	+
Flicker	+	+	
Harmonics of current	+	+	+
Interruptable generation mode	+	+	

the influence of the DG on the voltage fluctuations in the Microgrids [4, 12, 15]. Installation of DG sources has a very significant impact on the power quality [13, 16, 17] as well as on the stability and reliability of Microgrids. DG sources increase the dose of flicker, can generate higher-order harmonics, and also affect voltage dips, which are mostly related to the type of generator [17, 18] (see Tables 1 and 2).
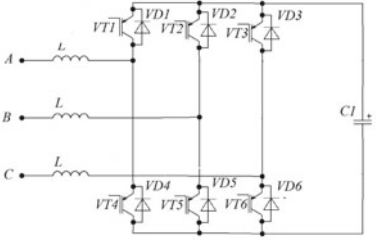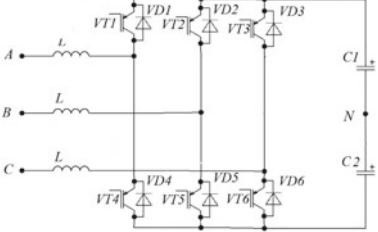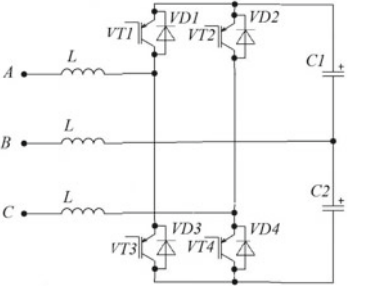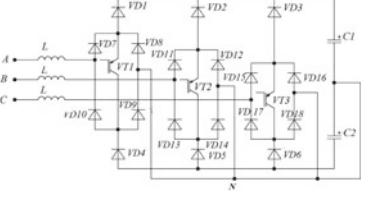
Summarizing the above mentioned facts, we can highlight the list of mandatory measures in systems with DG sources: ensuring a constant level of frequency; provision of reserve capacities (increase of reliability); reactive power compensation (caused by DG sources with power electronics (PE) devices).

At the same time, the following advantages can be distinguished for the general network: provision of additional reserve capacities of the power system during electricity generation to the network; improving the quality of power supply (possibility of autonomous operation in case of emergency shutdowns in the power system); maintenance of voltage and power levels in limited areas of the general network during generation from DG sources.

If the DG sources are used only as backup power sources, it can be stated that the reliability of the power supply system is increased. However, when DG sources operate in parallel with the system, the reliability of power supply to consumers in some cases may decrease [5]. For example, a decrease in the level of reliability may occur at high concentrations of DG sources of the same type (at the concentration of photovoltaic cells, the power of which depends on the intensity of solar radiation).
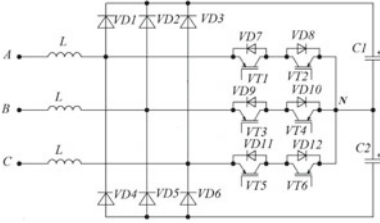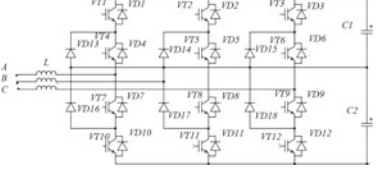
Therefore, the optimal in terms of the integration (synthesis) of Microgrids with DG sources to UPS of Ukraine is the construction of market-oriented strategy which will allow to handle both technical and financial issues of synthesis of a complex power system of Ukraine with Microgrids including DG sources and RES. The result should represent a complex power system with a balanced power supply from diverse RES and DG sources working in parallel to UPS of Ukraine ensuring its reliable and stable operation. Another issue which should be taken into account is the provision of needed level of power supply quality indicators in accordance with EN 50,160 standard which is mandatory in Ukraine. The issue of reliability assessment of systems with DG sources is discussed in [19] and this chapter is mainly focused

Table 3 Converter circuits

Converters	Parameters Advantages, disadvantages
Two level converter	
1	*Inverter or rectifier* *AC voltage:* three phase three wire *DC-link voltage*: $U_{dc} > 1.1\sqrt{3}\,U_m$ *Advantages:* • Simple design • Low switching frequency • Bidirectional power transmission • Availability of modules for assembly *Disadvantages:* • Phase interference • Presence of "dead time"
2	*Inverter or rectifier* *AC voltage:* three phase four-wire *DC-link voltage*: $U_{dc} > 2.2\,U_m$ *Advantages:* • Simple design • Low switching frequency • Bidirectional power transmission *Disadvantages:* • Phase interference • Presence of "dead time
3	*Inverter or rectifier* *AC voltage:* three phase three wire *DC voltage* $U_{dc} > 2.2\sqrt{3}\,U_m$ *Advantages:* • The simplest design and system control • Highest DC-voltage • Current control in two phases • Bidirectional power transmission *Disadvantages:* • High switching frequency (three times more than in other schemes)
Three level converter	
4	*Rectifier* *AC voltage:* three phase four wire or three wire *DC voltage* $U_{dc} > 2.2U_m$ *Advantages:* • Low switching frequency *Disadvantages:* • One-way power transmission • Complex design • Conduction losses when diodes are connected in series

(continued)

Table 3 (continued)

Converters	Parameters Advantages, disadvantages
5	*Rectifier* *AC voltage:* three phase four wire or three wire *DC voltage:* $U_{dc} > 2.2U_m$ *Advantages:* • Low switching frequency • Low losses in transistors *Disadvantages:* • Complex design • One-way power transmission
6	*Inverter or rectifier* *AC voltage:* three phase four wire or three wire *DC voltage:* $U_{dc} > 2.2U_m$ *Advantages:* • Low switching frequency • Bidirectional power transmission *Disadvantages:* • Complex design • High price

on the technical and financial methods of synthesis of models of the aforementioned systems combined by the game-theoretic approach.

2.2 Technical Means of Synthesis of the Complex Power Sytems with DG and RES

The use of power electronics is a high-performance solution for converting energy from renewable sources when transferring it to the network, to the consumer or to storage elements with further transfer to the consumer [10].

In DG systems the reliability of the power electronic converters is a major concern in obtaining cost effective solutions.

The introduction of power converters affects the reliability of the entire system. Most power converters do not have power and voltage capacities, as well as backup circuits. Any malfunction of components or subsystems will lead to the shutdown of the whole system. These unexpected shutdowns increase the cost of operating the system. For example, in the case of a photovoltaic power generation system, the cost of failure consists of the cost of energy that will be generated to the consumer from the network while the system is not working, as well as the cost of repair and replacement of components [20].

One shall select the power converter in such a way that its cost and losses are minimal. That is, its power rating must be equal to the power of the sources in order to ensure high efficiency of conversion in normal operation.

In order to reduce cost, one shall often choose the converter with less power than the power rating. It operates at maximum parameters, resulting in a higher failure frequency. Additional inverter protection devices are also required when the power rating is exceeded. In case of a choice of a converter with a power higher than the power of the wind turbines or solar modules used, then there is no need for the use of additional protection circuits. Though, this increases its cost.

The issue of power quality is closely related to reliability. According to the requirements for power quality, all quality indicators shall comply with the standards [21].

In the presence of higher harmonics, the active resistance of the cable increases. Additional losses occur as well due to an increase in losses in the dielectric of the cable insulation.

Voltage and current harmonics in systems with wind turbines result in additional power losses in the rotor windings, in the stator circuits, as well as in the steel of the stator and rotor, which leads to an increase in the overall temperature of the generator and local overheating. All this affects the reliability and durability of the generator.

In transformers, voltage harmonics cause an increase in losses to hysteresis, steel eddy current losses, and winding losses. In addition, the service life of the insulation is reduced.

The main indicators of power quality include the harmonic component THD and the power factor. The permissible value of THD, as well as the coefficients of separate harmonics, depends on the ratio of system power and load [21]. The power factor shall be close to 1. This can be achieved by reducing the reactive power to zero.

The study [22] features research on the effect of reactive power on the reliability of photovoltaic inverters. Inverter service life will be reduced by 7.6% at a power factor of 0.8 if compared to 1.

An inverter, which operates at 96% efficiency at a power factor of 1, has a 91.3% efficiency at a power factor of 0.55. These energy losses will significantly reduce the service life of the inverter components [23].

There are the following reactive power compensation methods for microgrid with renewable sources:

- passive filters,
- active harmonic filter,
- converter with special control system.

Passive LCL filters are used for reducing the harmonics of the switching frequency of transistors. This solution reduces cost as well as filter size and load if compared to a regular L-filter [24].

The operating principle of active filters is based on the analysis of the current harmonics of a non-linear load and the generation of the same current harmonics into the distribution network but in antiphase. As a result, the higher harmonic components of the current are neutralized at the active filter connection point. This means that they

do not extend from the non-linear load into the network. An active filter is capable of simultaneously compensating reactive power and current harmonics. In case there is no power from the source, the active filter can still work to improve the quality of power from the network [25].

The use of active filters is seriously limited due to the fact that the installed capacity must be commensurate with the load power. Therefore, filters will be of a high cost.

The use of passive filters in combination with active filters, but of lower power, is a more economical way to solve the problem. Hybrid filters are a compromise technical solution. They combine the advantages of traditional passive and active filters of relatively low power.

The use of converters with the active formation of network currents and power factor correction can be another option for improving electromagnetic compatibility [26]. This option is preferred because the power part of the system is simplified.

Converter for renewable systems consists of two converters with a DC link. Such circuit design allows for separate and independent control of the processes of generation of current (voltage) of a renewable source and the quality of the output power.

The converter includes an inverter regardless of the type of renewable source [27, 28].

The circuit design of modern inverters is shown in Table 1.

The schemes consist A capacitive filter C1, C2, (or C1-scheme 1) which provides a constant voltage Udc, is installed at the output of the inverter. L–phase inductance. Table 1 shows two-level inverters and three-level ones. The two-level converter is 27% cheaper than the three-level. The difference is due to the cost of diodes, which are not needed in two-level converter [29].

DC/DC converters are the first link of energy conversion for microgrid with solar panels. Different types of converters are used depending on the voltage levels that shall be matched.

Converters that are used for wind-power engineering are frequency converters. They consist of a rectifier and an inverter. The complexity of the converter depends on the type of generator used, power, voltage level, and the requirement for electromagnetic compatibility with the network.

Converters of two types are used, namely: frequency converters with DC link (consist of an input rectifier, both controlled and not, and an output inverter, the output frequency of which can be any) and direct frequency converters (a cycle converter, which converts AC power into AC power with an output frequency less than the input frequency; or a matrix converter, which can control the RMS value of the load voltage and can produce any output frequency) [24].

Rectification can be performed using a three-phase diode or thyristor rectifiers. The current harmonic coefficient of such rectifiers is equal to THD = 20–30%.

The circuit design of rectifiers for wind-power engineering and their comparative characteristics are shown in Table 1 (some circuits can be both rectifiers and inverters).

For the sake of reliability and electromagnetic compatibility, the converter control system provides the following:

- sinusoidal network current in the modes of energy consumption and output due to hysteresis or pulse-width control methods using closed-loop automatic control systems with feedback sensors for voltage and current of the network.
- reduction of losses during energy conversion due to optimization of control algorithms.
- the possibility to control not only the current distortion factor of the network, but also the shear coefficient, which provides full control over a wide range of power factor at the input of a semiconductor converter with the implementation of its unit, inductive or capacitive values.

Recognizing the potential benefits of photovoltaic and other inverter-based power sources as distributed reactive power sources, the IEEE 1547a standard allowed smart inverters to provide reactive power compensation beyond their previously accepted contributions [30, 31].

The inverter can supply inductive or capacitive power, which is limited by its rated apparent power S. The reactive power Q, which can be supplied by the inverter, is given by the formula [32]:

$$|Q| \leq \sqrt{(kS)^2 - P^2},\tag{1}$$

where k indicates the excess value, which is initially set to 1.

If the available power is greater than the required power, the inverter can supply the exact required power. Otherwise, the inverter generates reactive power according to its power reserve, resulting in partial compensation.

However, it is necessary to take into account the additional costs for such an inverter due to the use of components with a higher current carrying capacity. The service life of the inverter is directly related to the amount of power being processed since this increases the operating temperature for each component of the inverter, reducing the overall service life.

The results obtained in [31] reflect the importance of using a more powerful photovoltaic inverter (to increase reactive power) in "voltage-reactive power" control for consumers that are located far from the distribution transformer in order to successfully solve overvoltage problems. In the case of this control, the value of the power factor decreased as the consumer moved further away from the starting point.

When compensating for reactive power, the inverter must process a higher level of current, which shortens its life and increases power losses. Industry-specific total reactive power compensation reduces system service life by 24.1% if compared to traditional use. However, system reliability can be maintained by increasing the capacity of the photovoltaic inverter. The cost increase of 14% due to the use of the inverter in multifunctional mode was offset by the benefit [32].

A comprehensive study was carried out on digital models of the suggested converters. A control system with relay controllers that provide maximum speed and implement a tracking system for the mains current was developed. The control of the transfer of energy from a renewable source to the network and load can be arranged using the control system.

Efficiency was studied for different values of the power factor. The efficiency had the highest value at cos = 1. A 40% decrease in power factor resulted in a 6% reduction in efficiency (92%).

The harmonic composition of currents was studied as well. THD values were within the normal range for all circuits studied (Table 2).

The reliability of the inverter system depends on the number of components. In a system with n components, the system cannot work if one of the *n* components fails.

According to the components counting method for a structure with n subsystems, each *i*-th subsystem has a failure rate λ_i.

Total unreliability can be determined by the following formula [10]:

$$\lambda_{sys} = \sum_{i=1}^{n} \lambda_1. \tag{2}$$

MTTF (mean time to failure-the average time during which the system (converter) successfully operates before it fails) can be calculated:

$$MTTF = \frac{1}{\lambda_{sys}}. \tag{3}$$

For assessing the reliability, the number of each element (transistor, diode, capacitor, inductance) in the scheme must be determined and λ of each element must be attained of its special military handbook or datasheet. Failure rates provided by the MIL-HDBK-217 F (Military Handbook for Reliability Prediction of Electronic Equipment), are used for the reliability calculation [33].

Data for calculation: $\lambda_{IGBT} = 0.06$, $\lambda_{diode} = 0.22$, $\lambda_{capasitor} = 0.0004 \lambda_{induc\tan ce} = 0.00003 (Failures/10^6 \text{h})$[33].

$$\lambda_{sys} = \sum_{i=1}^{n} \lambda_{IGBT} + \sum_{j=1}^{m} \lambda_{diode} + \sum_{k=1}^{h} \lambda_{capacitor} + \sum_{k=1}^{l} \lambda_{inducance}, \tag{4}$$

where λ_{IGBT}—transistor failure rate, λ_{diode}—diode failure rate, $\lambda_{capaitor}$—capacitor failure rate, $\lambda_{inducance}$—inductance failure rate, *n, m, h, l*—amount of elements.

The simplicity of this method is its main advantage. It provides an adequate reliability assessment for small systems. It is also effective at the initial design stage. The disadvantage of this method is that, when considering, it is assumed that any malfunction leads to the failure of the entire system. Though, in some cases, these malfunctions can be easily replaced at minimal cost.

MTTF was estimated for the suggested converters (Table 4). Circuit 3 has the highest reliability.

It should be mentioned that in addition to circuit element failures, reliability is affected by external factors (thermal circulation due to exceeding the rated power) and weather conditions: humidity, ambient temperature. In contrast to thermal circulation,

Table 4 Calculation results

№ converter	1	2	3	4	5	6
THD, %	3.7	2.8	1.38	2.05	2.38	1.54
λ, F/10^6 h	1.68049	1.68089	1.12	4.14	3	4.68
MPPT,10^6 h	0.595	0.594	0.89	0.241	0.333	0.21

which leads to the de-rating of power devices and the occurrence of single failures, humidity causes corrosion due to diffusion through sealing and ion migration.

The conducted study shows that the overall reliability and service life, as well as the cost of a system with power converters and renewable energy sources, depend on many factors, namely: converter circuit design, full compensation of reactive power with the ability to control reactive power, compensation of higher harmonics, and the availability of emergency and backup circuits.

2.3   Demand Side Management Mechanisms of Synthesis of the Comples Power Sytems with DG and RES

The increasing integration of RES in a Microgrid leads to difficulty in balancing its power supply and demand. Although this can be achieved using spinning reserves or the energy storage systems (ESS), it incurs a significant investment cost [34]. Therefore, energy operators emphasize a demand response that balances the power supply and demand based on customers' participation. This is because of its involvement in generation-following strategies that respond to the availability of power generation rather than load-following ones, as shown in Fig. 4.

As, traditionally, energy providers do not provide incentives for consumers to change their load patterns, clients are unaware of ways to efficiently use energy [35]. However, those who exhibit a demand response by changing their power consumption in relation to the market's electricity prices are currently encouraged by the provision of different types of programs, such as direct load control, the emergency demand response program (EDRP), demand bidding, capacity market programs, interruptible rates, time-of-use (TOU), real-time pricing (RTP) and critical peak pricing (CPP) (Fig. 5) [36–41].

These programs have their own unique features that determine their suitability for a particular community and basically offer financial incentives or impose penalties to encourage customers to use their loads flexibly. Some loads that a customer can reschedule according to the response of a program are those of air conditioning systems, water heaters, EVs, washing machines and pumps. A demand response can help to achieve peak-load shaving, improve energy efficiency, decrease generation capacity, manage electricity costs, ensure network security, save energy and increase grid reliability. Also, it can maximize the capacity of a network by deferring the need
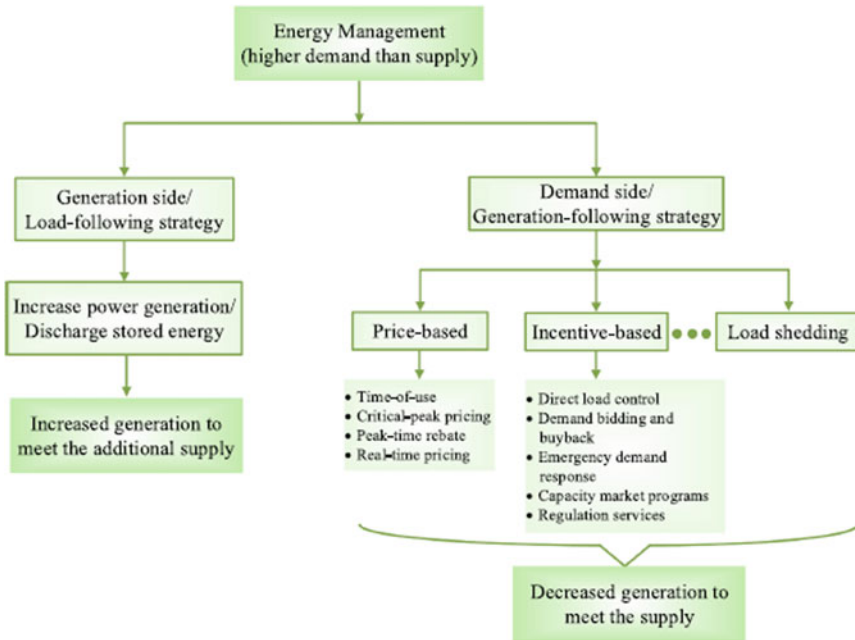
Fig. 4 Energy management of Microgrid including DSM

for new investment in constructing the lines required by increased power demand [42, 43].

Figure 5 describes the potential impact of DR measures on customer service levels in Microgrids. Economic operations based on the demand responses of a Microgrid are investigated in [44–46] and various price-based offers aimed at encouraging customers to participate in programs discussed in [44]. In [45], interruptible load-based programs available for a variety of consumers are demonstrated while a real-time load-scheduling algorithm for the short-term power management of RESs at a minimum reserve cost is presented in [46]. An optimal economic dispatch of grid-connected microgrids considering the demand response which aims to minimize the effect of intermittent RESs and provide incentives to consumers is discussed in [37]. In [40], the effects of irrational incentive values and consumers' participation in an EDRP in the presence of various uncertainties are analyzed, and it is concluded that the optimum operational cost is related to the accurate selection of incentive values.

A financial-based demand response still suffers from promoting its rapid acceptance by electricity clients [47] while the demand response to a real-time price requires modifying the hardware on both the utility and consumer sides. As a result, both ageing utility workers and customers are unwilling to accept any quick changes in terms of technological infrastructures, e.g., the installation of communication lines and smart meters, purchasing energy storage systems, installation of Smart converters to address the power quality issues of the grid which are perceived as intrusive [2].
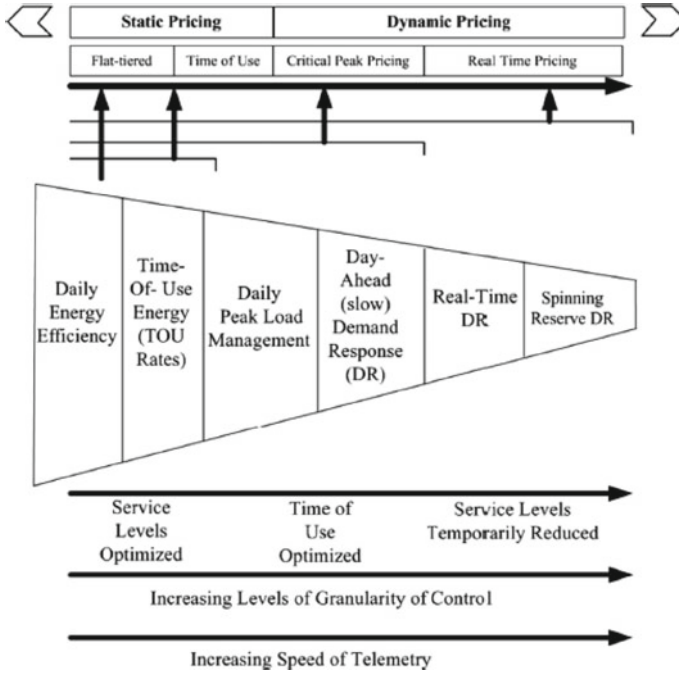
Fig. 5 DSM pricing strategies for microgrids

Therefore, the development of cost-based effective cooperative mechanism is essential to realize a large scale implementation of the infrastructure technologies for synthesis of complex power systems such as Microgrids with DG and UP S of Ukraine with involvement of demand response, otherwise it may take longer than expected to observe its widespread effectiveness.

3 Game-Theoretic Approach to Optimization of Synthesis of the Complex Power Systems with DG and RES

Game theory attempts to mathematically simulate strategic behavior in game situations [48]. In different literatures, various mathematical formulations of cooperative game theory have been applied for loss and cost allocation. Shapley, Aumann-Shapley, and Nucleolus-Based are the most common. In [48], Aumann-Shapley method has been employed for loss allocation in transmission systems. The authors of this paper have claimed that this method is superior to Shapley Method due to considering each participant as a set of infinitesimal parts. However, the accuracy of the result directly depends on the methods for determining the participation of each

agent in lines current. In [49], cost allocation has been defined as a cooperative game which solved by employing Shapley Value and Nucleous-Based Methods.

In this paper, we propose to formulate a game-theoretic approach which would allow players to get profit by DG players which take part in reduced amount of losses, reliability improvement and cost minimization.

3.1 Cost Effective Parameter Optimization Methods for Complex Power Systems with RES

Nowadays, distributed generations (DGs) have become an economic solution for electrical generation in distribution networks. Integration of Microgrids with DG units in distribution networks of UPS of Ukraine provides many potential benefits to distribution companies. These benefits include loss reduction, reliability improvement, voltage support, power quality improvement, capacity release, as well as deferment of upgrading distribution infrastructures. Consequently, Microgrids with DGs could enhance the competitiveness power of distribution companies in a competitive environment.

Since the methods of reliability improvement and loss reduction in electricity grids are various and may require implementation of various technologies our aim is to provide a cost-based approach which will be most efficient for Microgrids and distribution networks with DG and ESS.

One of such approaches establishes the parameters for the allocation of financial incentives in line with incremental prices in DGs. The objective function of the proposed method is introduced by Eqs. (5)–(8) [19].

$$\min(f_1), \ f_1 = CoR \quad \min(f_2), \ f_2 = CoL; \tag{5}$$

$$CoL = \pi \sum_{br=1}^{N_{br}} R_{br} |I_{br}|^2; \tag{6}$$

$$CoR = \sum_{br=1}^{N_{br}} E_{COST_{br}} = \sum_{br=1}^{N_{br}} L_{br} C_{br} \lambda_{br}; \tag{7}$$

$$E_{COST_{br}} = L_b C_b \lambda_b, \tag{8}$$

where CoR and CoL are the expenses the network would pay to consumers in the event of a power outage and monetary charge for loss, respectively.

As a result, a different function for examining reliability is regarded in comparison with current studies [50]. This method is different from other conventional studies [19]. Since the proposed method focuses on the pricing procedure in microgrids, reliability is characterized in the form of a factor that signifies the provision of
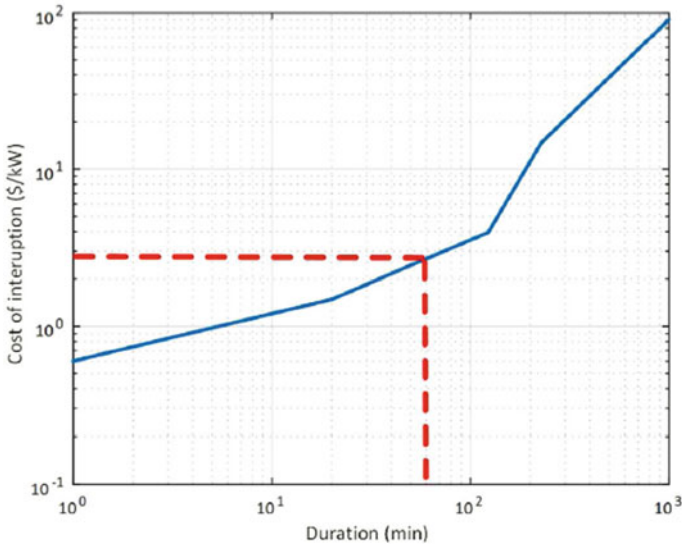
Fig. 6 Calculation of a one-hour interruption tariff [52]

demands at each bus individually through power failures. These forms of load-point indices are widely utilized to assess the reliability of microgrids [51–53].

However, since the cost of sustaining load supply during outages should eventually be expressed in the cost, a new solution from [50] has been investigated, which proposes that in the event of an interruption, convert the consumer's loss of load into the corresponding cost utilizing the Complementary Cumulative Distribution Function (CCDF) curve (Fig. 6).

Therefore, the objective is calculated using the ECOSTbr index, which is dependent on the reliability level. This index, which is obtained by Eq. (7), is utilized to determine the objective represent to the reliability level. where Lb is the load of each bus (kW) and Cb is the interruption tariff ($/kW), which is nonlinear with respect to time and is obtained from the CCDF curve. In this way, the feeder's failure rate (failures per year) with the largest impedance is equal to 0.4 per year and, the feeder's failure rate with the smallest impedance is considered to be 0.1 per year. It should be noted that for other feeders, the failure rate is measured using linear interpolation and is directly proportionate to these two rates as well as the related impedance. Equation (6) would be used to measure the expense of preserving the loads in contingencies and possible interruption using ECOST [19].

To calculate the economic burden that loss inflicts to the system (active power loss), Eq. (6) is presented regarding the energy price (πc), where Rbr and Ibr are the resistance and current of birth branch, respectively.

Location and size of energy storage are a design criterion with a relevant impact on distribution network reliability. These parameters are considered during the planning of distribution networks as well as the reliability assessment.
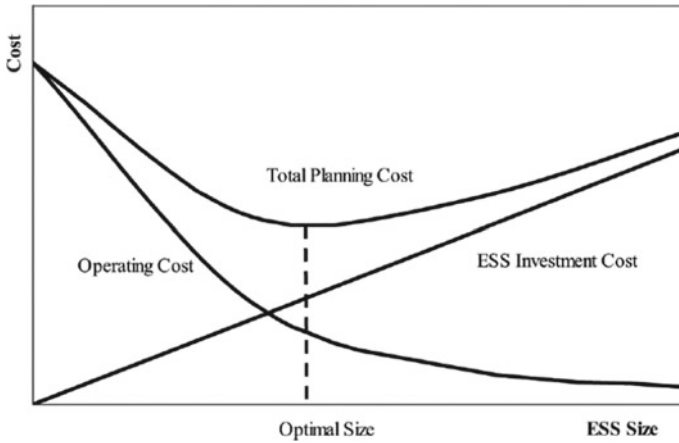
Fig. 7 Optimal ESS sizing [28]

The ESS size includes power rating and energy rating. The proposed optimal ESS sizing problem in [54] minimizes the total microgrid cost, which includes ESS investment cost and microgrid operating cost. A stochastic approach was used in [54] to generate power system operation scenarios.

The expected load curtailment in each reduced scenario is determined and consequently a reliability index, i.e., loss of load expectation (LOLE), was calculated. Figure 7 depicts the total microgrid cost as a function of ESS size. As the ESS size is increased the investment cost added to the microgrid is increased in a linear fashion while the microgrid operating cost is reduced. The optimal ESS size would minimize the total microgrid cost [54, 55].

In accordance to the mentioned above the optimal formulation for ESS sizing in microgrids and distribution networks with DG can be formulated as follows (Eqs. (1)–(3) [54]):

$$\min(f_3), \ f_3 = CoESS, \tag{9}$$

where CoESS are the expenses for the energy storage system.

The cost function for the Microgrid system depends on the mode of its operation as shown in Fig. 8. When connected to the network, the difference between the load consumption and the output power of microgenerators is balanced dynamically [56]. That is, if necessary, Microgrid buys electricity in the general network or sells the surplus to get income.

The target function of operating costs of a microgrid with DG is determined as:

$$\min(f_4), \ f_4 = CoOMG; \tag{10}$$

Fig. 8 Contribution of energy storage and demand response to improve the reliability of power supply
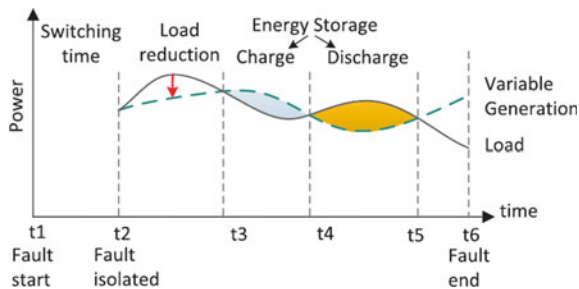
$$CoOMG = \sum_{k=1}^{T} \Delta t_k \left[\sum_{i=1}^{N} (CF_i + COM_i) + CB_{i,k} - CS_{i,k} \right], \qquad (11)$$

where CoOMG—costs of operation of the microgrid, T—total operating time of the microgrid; N is the total number of generating blocks; Δt_k—duration of the time interval k; CF_i—cost of fuel of the microgeneration unit i; COM_i—cost of operation and maintenance of the microgeneration unit i; $CB_{i,k}$—purchased electricity of the microgeneration unit i for Δt_k, if the load requirement exceeds the generated power; $CS_{i,k}$—income from sold electricity of the microgeneration unit i for Δt_k, if the generated power exceeds the load [3, 57].

To address the reliability and losses issue the proposed financial mechanism should be implemented:

$$opt(F), F = \begin{cases} \min(f_1), f_1 = CoR \\ \min(f_2), f_2 = CoL \\ \min(f_3), f_3 = CoESS \\ \min(f_4), f_4 = CoOMG \\ \max(f_5), f_5 = CoPR \\ \min(f_6), f_6 = LCOE_{MG} \end{cases}, \qquad (12)$$

where CoPR are profit for reliability improvement while supplying energy to distribution grids during the outage period (see Fig. 6 [52]), LCOE_MG is as follows [3]:

$$LCOE_{MG} = \frac{\sum_{t=1}^{n} \frac{I_t + O\&M_t + F_t + T_t + Ext_t + L_t}{(1+r)^t}}{\sum_{t=1}^{n} \frac{E_t}{(1+r)^t}}, \qquad (13)$$

where LCOE—cost of electricity, averaged over the period n; I_t—investment costs per year; $O\&M_t$—operating costs and maintenance costs per year; F_t—fuel component costs per year; T_t—tax payments per year; E_t—volume of electricity production per year, kWh/year; r—discount rate, n—duration of the project, t—year of the project, Ext_t—external costs per year; L_t—liquidation costs per year.

3.2 Game-Theoretic Approach to Complex Power System Synthesis Optimization

The optimal scheduling of flexible demand-side resources can be classified as a multi-decision-maker problem, which is not amenable to business-as-usual, centralized, non-behavior-aware treatments if the behavioral risk factors affecting the supply of DR services are to be characterized to improve the reliability and validity of DSM business models.

The Stackelberg, strategic (non-cooperative) game concept can provide a systematic framework to unveil the hidden relationships between the targeted incentive-driven load reductions and what would be achieved in practice provided that there are no penalties for noncompliance with the grid operator orders—in an attempt to make explicit the assumptions underlying the core concepts of the discipline. Non-cooperative game theory centers on the study of independent, rational decision-making in circumstances of strategic interaction (conflict) to achieve the Nash equilibrium.

The game $G = <I, S, u>$ is played with two distinct sets of players, namely: RES operators and distribution system operators (DSO). The set of players is presented as follows:

$$I = \{RES_1, \ RES_2...RES_N, \ DSO_1, \ DSO_2...DSO_M\}.$$

The RES operator is assumed to be an entity belonging to the utility providing electricity service to the considered case study area, which has full ownership of the RES assets. DSO seeks to alleviate the load in the distribution networks in predicted periods of peak energy use and to involve less expensive electricity suppliers to cover the peak demand.

For this game each set of players will have different strategies. Strategies of DSO's will be:

$$S_{DSOi} = \{"NR"," RES", "CHP", "BAU"\},$$

where NR—network reconfiguration, RES—RES and DG sources involvement for DSM programs, CHP–CHP involvement to cover peak demand and for reliability improvement, BAU—business as usual operation without additional generation involvement.

Strategies of RES operators will be:

$$S_{RESi} = \{''BAU'','' DSM'' \},$$

where BAU—business as usual operation without DSM programs involvement, DSM—involvement into various DSM programs.

The profit of each set of plates taking into account Chap. 3.1 will be as follows:

$$u_{RESi} = \{0, 1, 2 \},$$

where 0—self supply, 1—profit from RE sold in the electricity market, 2—additional profit from involvement into various DSM programs;

$$u_{DSOi} = \{0, 1, 2 \},$$

where 0—BAU operation, 1—loss reduction and reliability improvement, 2—loss reduction and reliability improvement with less expenses due to various DSM programs.

The game matrix will be:

		DSO			
		NR	RES	CHP	BAU
RES	BAU	(1;1)	(1;0)	(1;1)	(1;0)
	DSM	(1;0)	(2;2)	(1;0)	(1;0)

As one may see with such formulation of the game the optimal mechanism of operation of complex power system with DG sources and RES according to Nash equilibrium will be: $S_i = \{DSM_{RES}, RES_{DSO}'' \}$.

4   Conclusions

The chapter provides a game-theoretic approach of addressing a hard task of synthesis of complex power systems with DG and RES. While the process of synthesis, tasks of technical parameters harmonization and feasibility of operation should be solved. Various methods and technical solutions are presented in this chapter show that separate technical tasks concerning power supply quality and loss reduction in the complex power systems with DG sources and RES can be solved by implementation of certain technologies that address each specific task. DSM and feasibility optimization functions concerning cost reduction in power systems with RES show that technical tasks can be solved in economically viable manner.

The proposed game allows not only to combine both technical and economic models for power systems with DG sources and RES, but also to find an optimal

solution in the process of synthesis of complex power systems. This optimal solution is found as Nash equilibrium for the proposed game.

References

1. https://www.iea.org/
2. Robert, F.C., Sisodia, G.S., Gopalan, S.: A critical review on the utilization of storage and demand response for the implementation of renewable energy microgrids. Sustain Cities Soc **40**, 735–745 (2018)
3. Denysiuk, S., Derevianko, D.: The cost based DSM methods in microgrids with DG sources. In: 2021 IEEE 2nd KhPI Week on Advanced Technology (KhPIWeek), vol. 1, pp. 544–548, September 2021.
4. Ackerman T.: Interaction between distributed generation and the distribution network. In: Ackerman, T., Knyazkin, V. (eds.) Transmission and Distribution Conference and Exhibition: Asia Pacific IEEE/PES, vol. 2, pp. 1357–1362 (2000)
5. Denysiuk, S., Derevianko, D., Horenko, D.: Reliability analyses in local power systems with DG sources based on the exchange processes assessment. In: 2020 IEEE KhPI Week on Advanced Technology, KhPI Week 2020—Conference Proceedings, pp. 232–235 (2020)
6. Bossi, C., Degner, T. Tselepis, S.: Distributed generation with high penetration of renewable energy sources. In: Dispower, Final Public Report, Laboratory Tests Case Studies and Field Experience, Kessel. Germany (2006)
7. Dondi, P., Bayoumi, D., Haederli, C., Julian, D., Suter, M.: integration of distributed power generation Network. J. Power Sources **106**, 1–9 (2002)
8. DTI (2005) Micro-generation strategy and low carbon buildings programme-consultation
9. Hatziargyriou, N. (ed.): Microgrids: Architectures and Control. IEEE Press, Wiley (2014)
10. Yang, Y., Kim, K., Blaabjerg, F., Sangwongwanich, A.: Advances in grid-connected photovoltaic power conversion systems (2018)
11. Derevianko, D., Hilevych, K.: Reliability assessment in local power systems with renewables. In: 2020 IEEE 7th International Conference on Energy Smart Systems, ESS 2020, Proceedings, pp. 243–246 (2020)
12. Cutsem, V., Vournas, T., Kluwer, C.: Voltage Stability of Electric Power Systems . Kluwer Academic Publishers Group, Boston, 379p. (1998)
13. Dolezal, J., Sautarius, P., Tlusty, J.: The effect of dispersed generation on power quality in distribution system. In: Quality and security of electric power delivery systems. CIGRE/IEEE PES International Symposium, pp. 204–207 (2003)
14. Denysiuk, S.P., Derevianko, D.H., Iu, K.: Sumenko Osoblyvosti otsinky yakosti elektropostachannia lokalnykh elektrotekhnichnykh system z rozoseredzhenoiu heneratsiieiu [Tekst]. Hirnytstvo **27,** 90–97 (2015)
15. Blinov I.V., Trach I.V., Parus Ye. V., Derevianko D.G., Khomenko V.M.: Voltage and reactive power regulation in distribution networks by the means of distributed renewable energy sources. Tekhnichna elektrodynamika **2**, 60–69 (2022). https://doi.org/10.15407/techned2022.02.060
16. Engineering Recommendation G59/1 Recommendations for the connection of embedded generation plant to the regional electricity companies' distribution systems. Electricity Assoc (1991)
17. Esposito, G., Golovanov, N., Lazaroiu, C., Zaninelli, D.: Impact of embedded generation on the voltage quality of distribution networks. Electrical Power Quality and Utilisation, EPQU **3**(1). - Режим доступу: http://www.leonardo-energy.org/webfm_send/1079
18. Flatabo, N., Ognedal, R., Carlsen, T.: Voltage stability condition in a power transmission system calculated by sensitivity methods. IEEE Trans. 5(4):1286–1293 (1990)
19. Nazari, M.H., Bagheri Sanjareh, M., Khodadadi, A., Torkashvand, M., Hosseinian, S.H.: An economy-oriented DG-based scheme for reliability improvement and loss reduction of active

distribution network based on game-theoretic sharing strategy. Sustainable Energy, Grids and Networksthis link is disabled, vol. 27, 100514 (2021)

20. Ristow, M.B., Pregelj, A., Rohatgi, A.: Development of a methodology for improving photovoltaic inverter reliability. IEEE Trans. Ind. Electron., **55**(7), 2581–2592

21. IEEE Recommended Practice and Requirements for Harmonic Control in Electric Power Systems. In: IEEE Std 519–2014 (Revision of IEEE Std 519–1992), pp.1–29, 11 June 2014. https://doi.org/10.1109/IEEESTD.2014.6826459

22. Nagarajan, A., Thiagarajan, R., Repins, I., Hacke, P.: 2019. Photovoltaic inverter reliability assessment. Golden, CO: National Renewable Energy Laboratory. NREL/TP-5D00–74462. https://www.nrel.gov/docs/fy20osti/74462.pdf

23. Flicker, J., Gonzalez, S.: Performance and reliability of PV inverter component and systems due to advanced inverter functionality. In: 2015 IEEE 42nd Photovoltaic Specialist Conference (PVSC), pp. 1–5. https://doi.org/10.1109/PVSC.2015.7355978

24. Arifujjaman, Md., Iqbal, M.T., Quaicoe, J.E.: Power Electronics reliability comparison of grid connected small wind energy conversion systems. Wind Eng. **35**(1), 93–110. (2011). https://doi.org/10.1260/0309-524X.35.1.93

25. Tuyen, N.D., Fujita, G.: PV-active power filter combination supplies power to nonlinear load and compensates utility current. IEEE Power and Energy Technol. Syst. J. **2**(1), 32–42 (2015). https://doi.org/10.1109/JPETS.2015.2404355

26. Kolar, J.W., Friedli, T.: The essence of three-phase PFC rectifier systems—Part I. IEEE Trans. Power Electron. **28,** 176–198 (2013)

27. Bielokha, H., Shevchenko, I.: Active rectifiers in the electrical system of aircraft. In: 2021 IEEE International Conference on Modern Electrical and Energy Systems (MEES), pp. 1–4. https://doi.org/10.1109/MEES52427.2021.9598724

28. Bielokha, H., Samcheleev, Y.: Electromagnetic compliant of voltage source with relay control. Int. Conf. Mod. Electr. Energy Syst. (MEES) **2017**, 32–35 (2017). https://doi.org/10.1109/MEES.2017.8248921

29. Ikonen, M., Laakkonen, O., Kettunen, M.: Two-level and three-level converter comparison in wind power application (2005)

30. IEEE Standard for Interconnection and Interoperability of Distributed Energy Resources with Associated Electric Power Systems Interfaces. In: IEEE Std 1547–2018 (Revision of IEEE Std 1547–2003), pp. 1–138, 6 April 2018. https://doi.org/10.1109/IEEESTD.2018.8332112

31. Almeida, D., Pasupuleti, J., Ekanayake, J.: Comparison of reactive power control techniques for solar PV inverters to mitigate voltage rise in low-voltage grids. Electronics **10**, 1569 (2021). https://doi.org/10.3390/electronics10131569

32. Design for Reliability of Multifunctional PV Inverters used in Industrial Power Factor Regulation/Lucas Soares Gusman. Belo Horizonte, MG, pp. 2020–2083

33. MIL-HDBK-217F. Reliability Prediction of Electronic Equipment. Available online: https://snebulos.mit.edu/projects/reference/MIL-STD/MIL-HDBK-217F-Notice2.pdf (Accessed on 9 December 2020).

34. Kyrylenko, O.V., Blinov, I.V., Parus, E.V., Trach, I.V.: Evaluation of efficiency of use of energy storadge system in electric networks. Tekhnichna elektrodynamika **4**, 44–54 (2021) (Ukr) https://doi.org/10.15407/techned2021.04.044

35. Kirschen, D.S., Strbac, G.: Fundamentals of Power System Economics. Wiley (2004)

36. da Silva, H.B., Santiago, L.P.: On the trade-off between real-time pricing and the social acceptability costs of demand response. Renew Sustain Energy Rev. **81**, 1513–1521 (2018)

37. Imani, M.H., Niknejad, P., Barzegaran, M.: The impact of customers' participation level and various incentive values on implementing emergency demand response program in microgrid operation. Int. J. Electr. Power Energy Syst. **96**, 114–125 (2018)

38. Jin, M., Feng, W., Marnay, C., Spanos, C.: Microgrid to enable optimal distributed energy retail and end-user demand response. Appl Energy **210**, 1321–1335 (2018)

39. Mehdizadeh, A., Taghizadeghan, N.: Robust optimization approach for bidding strategy of renewable generation-based microgrid under demand side management. IET Renew Power Gener **11**(11), 1446–1455 (2017)

40. Nwulu, N.I., Xia, X.: Optimal dispatch for a microgrid incorporating renewables and demand response. Renew Energy **101**, 16 (2017)
41. Palensky, P., Dietrich, D.: Demand side management: demand response, intelligent energy systems, and smart loads. IEEE Trans. Industr Informat **7**(3), 381–388 (2011)
42. Hussain, M., Gao, Y.: A review of demand response in an efficient smart grid environment. Electricity J. **31**, 55–63 (2018)
43. Strbac, G.: Demand side management: benefits and challenges. Energy Policy **36**(12), 4419–4426 (2008)
44. Aghajani, G., Shayanfar, H., Shayeghi, H.: Presenting a multi-objective generation scheduling model for pricing demand response rate in micro-grid energy management. Energy Convers Manage **106**, 308–321 (2015)
45. Alharbi, W., Raahemifar, K.: Probabilistic coordination of microgrid energy resources operation considering uncertainties. Electr. Power Syst. Res. **128**, 1–10 (2015)
46. Subramanian, A., Garcia, M.J., Callaway, D.S., Poolla, K., Varaiya, P.: Real-time scheduling of distributed resources. IEEE Trans. Smart Grid **4**(4), 2122–2130 (2013)
47. Feuerriegel, S., Neumann, D.: Integration scenarios of demand response into electricity markets: load shifting, financial savings and policy implications. Energy Policy **96**, 231–240 (2016)
48. Molina, Y.P., et al.: Complex losses allocation to generators and loads based on circuit theory and Aumann-Shapley method. IEEE Trans. Power Syst. **25**(4), 1928–1936 (2010)
49. Bhakar, R., et al.: Probabilistic game approaches for network cost allocation. IEEE Trans. Power Syst. **25**(1), 51–58 (2010)
50. Etemadi, A.H., Fotuhi-Firuzabad, M.: Distribution system reliability enhancement using optimal capacitor placement. IET Gener. Transm. Distrib. **2**(5), 621 (2008). https://doi.org/10.1049/iet-gtd:20070515
51. Kavousi-Fard, M.-R. Akbari-Zadeh: Reliability enhancement using optimal distribution feeder reconfiguration. Neurocomputing **106**, 1–11 (2013). https://doi.org/10.1016/j.neucom.2012.08.033
52. Kavousi-Fard, T.N.: Optimal distribution feeder reconfiguration for reliability improvement considering uncertainty. IEEE Trans. Power Deliv. **29**(3), 1344–1353 (2014).https://doi.org/10.1109/TPWRD.2013.2292951
53. Niknam, T., Kavousi Fard, A., Baziar, A.: Multi-objective stochastic distribution feeder reconfiguration problem considering hydrogen and thermal energy production by fuel cell power plants. Energy **42**(1), 563–573. https://doi.org/10.1016/j.energy.2012.02.023
54. Bahramirad, S., Reder, W., Khodaei, A.: Reliability-constrained optimal sizing of energy storage system in a microgrid. IEEE Trans. Smart Grid **3**(4), 2056–2062 (2012). https://doi.org/10.1109/TSG.2012.2217991
55. Blinov, I., Trach, I., Parus, Y., Khomenko, V., Kuchanskyy, V., Shkarupylo, V.: Evaluation of the efficiency of the use of electricity storage systems in the balancing group and the small distribution system. In: 2021 IEEE 2nd KhPI Week on Advanced Technology (KhPIWeek). pp. 262–265 (2021). https://doi.org/10.1109/KhPIWeek53812.2021.9569981
56. Denysiuk, S., Derevianko, D.: Optimisation features of energy processes in energy systems with Distributed Generation. In: 2020 IEEE 7th International Conference on Energy Smart Systems, ESS 2020—Proceedings, pp. 211–214 (2020)
57. Ren, G., Juebo, W., Wen, H.: Dynamic economic dispatch solution for a microgrid using improved ant colony optimization. Int. J. Grid Distrib. Comput. **9**(8), 345–356 (2016)

Optimization of Energy Processes in Local Power Supply Systems with Variable Operating Modes

Serhii Denysiuk [iD] **, Borys Basok** [iD] **, and Vitalii Opryshko** [iD]

Abstract The chapter shows that for the analysis of the optimality of processes in local power supply systems (LPSS) are crucial for improvement and further additional development of methods for demand response effectiveness assessment in systems with active consumers. The main differences between the existing LPSS and next generation, based on the Smart Grid concept, mechanisms of influence and effects from implementation of Demand Side Management (DSM) were assessed, what allowed to choose the minimisation of Frieze reactive power Q_F as a criterion for cost reduction. Proposed method for estimating the impact of uneven electricity consumption on the level of losses in LPSS in contrast to the existing ones, uses modified Frieze Q_F power decomposition indicators and common determinations of Frieze Q_F power for an arbitrary time interval, which considers the influence of uneven power levels on electricity consumption, as well as $k_{\Delta opt}$, which characterizes the efficiency of regulation and determines the level of suboptimal energy transfer in terms of eliminating its losses. The system of energy efficiency indicators has been expanded by Frieze Q_F power loss criterion, which assess the influence of uneven electricity consumption factors and operation modes of LPSS for a certain time interval. The obtained values for the calculation of losses from the uneven generation modes and consumption of electricity are used in the case of retrospective, prospective and real-time analysis, changes in $\cos\varphi$, voltage deviations, the influence of higher harmonic components. A methodology for optimizing power consumption schedules using Q_F power decomposition in the case of targeted power consumption mode management and implementation of electricity demand management programs is proposed. Methodology is implemented as an algorithms and suitable software for detailed transmission, accumulation, and consumption time period T analysis for management improvement by the distribution system operator (DSO). The LPSS daily electricity consumption schedule optimisation method was improved on the example of residential complex an optimisation problem was formed for prosumers:

S. Denysiuk (✉)
Institute of Energy Saving and Energy Management, National Technical University of Ukraine "Igor Sikorsky Kyiv Polytechnic Institute", Kyiv, Ukraine
e-mail: spdens@ukr.net

B. Basok · V. Opryshko
Institute of Engineering Thermophysics, National Academy of Sciences of Ukraine, Kyiv, Ukraine

energy costs reduction and daily consumption schedule optimisation, considering it consumption modes and values of equipment flexibility index k_{flex}.

Keywords Local power supply · Energy process · Frieze power · Power losses · Demand side management

1 Introduction

The key trend in the development of power supply systems (PSS) at the beginning of the XXI century is the modernization of existing systems and the introduction of their new architectures based on the concept of Smart Grid [1, 2]. The necessity of the Smart Grid concept implementation caused by factors of technological development, consumer requirements for quality and reliability of energy supply, factors of the liberalized market and growing requirements in the field of environmental safety and energy efficiency.

Taking into account the European experience and reforms in the energy sector in Ukraine, it is important to implement modern requirements for PSS, which are determined by the principles of Smart Grid and provide, above all, achieving reliability and cost-effectiveness [3]. Prosumers have their own generation, including renewable energy sources (RES) and energy storage systems, and can manage their own schedule and influence on overall schedule of the power system. The growth of their number is closely related to the liberalization of the electricity market, the introduction of customer-oriented business processes of electricity supply companies, creation of favourable conditions for mutually beneficial operation of PSS elements [4].

The key problems of EPS are the problems of energy efficiency, uneven consumption and generation schedules, quality of electricity supply (reliability, stability, etc.), the need to modernize systems component taking into account the growing trend of RES. This is especially evident at the level of local PSS (LPSS), which are a group of interconnected consumers and generators with clearly defined electrical boundaries, which in relation to the general network act as a single controlled and monitored object [4, 5].

It is established that to ensure coordination of work and increase the efficiency of electricity generation, transmission and consumption in LPSS it is necessary to create control mechanisms that include integration of RES and data accumulation, including assessment and analysis of technical, technological and organizational control mechanisms in the process of liberalization of the electricity market.

In order to effectively implement new market mechanisms and ensure a systematic approach in the case of integration of RES into PSS, energy processes should be considered not at the level of Ukraine's energy system as a whole, but at the lower hierarchical level—at the level of LPSS The development and dissemination of Smart Grid-based LPSS allows to integrate Demand Side Management (DSM) programs

to address a number of issues related to covering the uneven energy generation and consumption schedule [5].

2 Features of Local Power Supply Systems Development According to the Smart Grid Concept

To create and ensure the effective functioning of LPSS, there is a need to assess the performance of energy supply processes and the impact of generators and consumers on the functioning of modern LPSS [3]. The transition to new structures (architectures) of LPSS in the form of integrated intelligent energy supply systems is relevant and provide integration of self-organizing electricity and heat supply systems, built on the multi-agent principle on an intellectual basis [6].

Conditionally, the levels of connection of LPSS to the general network can be divided into 3 levels (Fig. 1) [7]:

(1) Micro-sources including storage systems;
(2) Sources—medium and high power generation units;
(3) Micro-networks that have a common connection point to the public network.

The main differences between LPSS and the traditional power system are:

(1) RES are much smaller than the main generators;
(2) Generation sources can be connected directly to the consumer;
(3) Sources of distributed generation are installed close to the consumer, providing efficient power supply with the necessary parameters of voltage and frequency without significant losses of electricity that occur in conventional power grids.
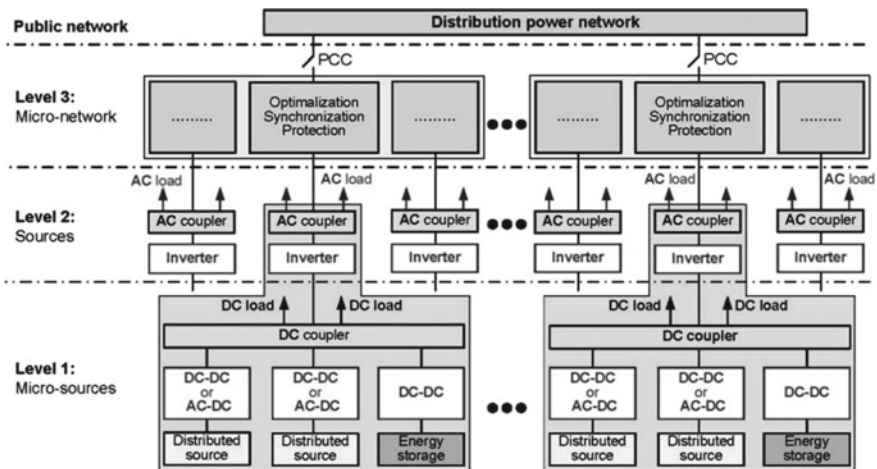

Fig. 1 Three levels structure of LPSS connection to the network

The efficiency and reliability of LPSS is based on the search for its optimal architecture for the distribution of electricity flows and complete information about its condition [8].

Implementation of the principle of decentralization leads to greater diversity and development of local networks. Thus, within the LPSS there are Microgrid—innovative systems of small energy, which also are local network energy structures [7, 9]. The unified structure of the Microgrid system includes batteries, power electronics devices, charge/discharge controllers, various types of distributed generation.

The main stage of LPSS development should be the evolution of the consumer to smart consumer, with the subsequent transition to the class of smart prosumer. At the same time, smart prosumer can not only manage its own consumption, but also involve generation and storage systems within the energy management system [3, 10].

The operating conditions of LPSS are determined by the modes of operation of generators and consumers and are characterized by appropriate load schedules. The main load schedule—daily—is characterised by significant uneven consumption with characteristic areas. Electricity consumption during the day varies sharply over relatively short periods of time, which can be represented by hourly or even minute time intervals. The operation of the power system according to the uneven load schedule is associated with additional costs such as overconsumption of fuel and the presence of surplus generating equipment with associated resources, which are included in the electricity tariff to maintain cost-effectiveness LESP as a whole, which increases consumer costs.

It is important for LPSS to evaluate (monitor) the schedules of generation and consumption of electricity in LPSS with further optimisation of electricity generation and consumption schedules, in particular the processes of energy exchange and transmission of active energy [7, 11].

Ensuring the balance of generated and consumed electricity is quite a difficult task, to solve which it is advisable to use energy storage systems, relevant control laws based on current monitoring and optimisation of generation and consumption of electricity [6–8]. Consumer potential is used in the management of LPSS modes to reduce schedule irregularities, and DSM programs are widely used to reduce peak consumption as a means of reconciling generation and consumption modes.

Today, the primary task of optimizing the operation of LPSS is to continuously ensure the balance of load and generation schedules by quickly covering the load schedule with the appropriate level of generated power [12]. Failure to meet the balance condition in the system changes frequency, rated voltage levels and other indicators, which can lead to mass outages of consumers or damage to generating, transmitting and distributing equipment and consumer equipment. In the case of electricity losses in the elements of LPSS analysis, the necessary and additional losses are identified, as well as indicators that identify their presence. Since distortions in LPSS are caused by the work of consumer's electrical installations, the joint influence of which determines the total level of distortion at the point of connection to the system, there is a need to determine the individual contribution of each element in the suboptimal generation and consumption schedules. Economic losses due to

the influence of various factors of suboptimality have two components: electromagnetic and technological. As an integral characteristic for estimating electricity losses should be considered reactive power Frieze [13]:

$$Q_F = \sqrt{S^2 - P^2}. \tag{1}$$

In estimating the current level of power consumption, the expression for the reactive power of the Frieze Q_F is actually a quadratic measure of the discrepancy between the total S and active P power. Even in the absence of reactive elements, the ratio Q_F > 0 will occur in the case of uneven processes.

3 Features of LPSS Modes Optimisation with Demand Side Management Programs

Energy Demand Management (DSM) is divided into Demand Response and energy efficiency and aims to change the demand of energy consumers through various methods, such as financial incentives or energy efficiency initiatives, including new business processes, generation aggregation and optimal energy consumption [14]. In LPSS, DSM-related measures are aimed at long-term operation and include reducing overall energy consumption by implementing energy efficiency and energy saving measures. The effect of the application is estimated in most cases as a reduction in peak electricity consumption [15]. By reducing the total load on the electrical network, DSM allows you to reduce total energy losses, reduce the number of accidents by reducing the number of outages, as well as increase system reliability. The use of DSM programs helps to overcome barriers that prevent the adoption of many related energy efficiency programs and to raise funds for the development of LESP from the economic benefits of rational use of electricity and savings from off-peak consumption.

The main mechanism of DSM programs includes organizational, technical and economic tools for changing peak and off-peak consumption [9, 16]. Thus, the types and mechanisms of consumption management (Demand Response) are divided into direct (Direct load control, Demand Buyback, Interruptible load, Voluntary curtailment) and indirect (Time of use pricing, Real time pricing, Veriable peak pricing, Critical peak pricing, Critical peak rebates) methods.

In the case of managing LPSS modes to reduce schedule irregularities, the potential of consumers is used and DSM programs related to reducing peak consumption are widely used as a means of reconciling generation and consumption modes [17]. As an example of the existing estimate, we can use the value of the actual voltage and current ratio λ_T as the ratio of the minimum possible power losses to their actual value in the interval of the technological process of T [18]:

$$\lambda_T = \sqrt{\frac{\Delta P_{\min}}{\Delta P}}. \tag{2}$$

To solve the problem of suboptimal consumption and generation of electricity in LPSS, it is necessary to assess the impact of uneven consumption and to propose a mathematical assessment apparatus in financial and energy terms. The problem of efficient electricity consumption can be solved by comparing the modes of different combinations of power management systems and electricity demand management. Despite global trends, the issue of managing electricity demand in Ukraine remains open.

For LPSS, DSM tools should be represented not only by algorithms of regulatory actions in the case of regulating the "behaviour" of the load, but also by mechanisms of direct access to load management at the level of technological processes [1]. This determines the need for precise regulation of energy processes, taking into account the requirements for electricity quality, reliability and stability of electricity supply.

Management in LPSS has to implement a number of DSM programs by providing various services according to the situation and requirements of the concluded contracts, in particular, cooperation of electric transport management systems, power consumption management systems of stationary industrial and commercial facilities, household electricity management systems and advanced consumption and demand forecasting.

Traditionally, DSM for LPSS is divided into two classes of subtasks: energy efficiency methods and demand response (DR) or Load management (LM) [11]. It is important for LPSS to provide two types of demand management programs—based on price signals and technical and economic requirements. Today, within the Smart Grid concept, it is important to combine optimisation procedures for electricity generation and consumption, in particular, to build appropriate criteria for optimizing the schedules of electricity generation and consumption.

In general, it is advisable to use power modifications Frieze Q_F [19, 20]. In particular, in the case of active power P power P_1 (first harmonic) and ΔP (active power) for higher harmonics can determine the Frieze power with the solution of the influence on the optimum transmission of active power on the first harmonic (main) P and active power transmission on higher harmonics ΔP [19].

4 Application of Frieze Reactive Power Q_F to Assess the Optimality of LPSS Operation Modes

For a more detailed analysis of LPSS energy processes, we use a macromodel: generator, converter, load with network connections and cross-sections generator-converter and load-converter (Fig. 2) [12].

In the following we will analyse the regimes that occur at the intersections "2" and "4" (see Fig. 2).
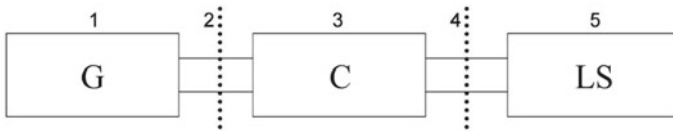
Fig. 2 Macromodel (G—generator, C—converter, LS—load system)

Consider and analyse the operation of the system should be on the time interval T_T and distinguish 4 groups of modes of the equation between the graphs of the instantaneous values of the generation power $p_g(t)$ and consumption $p_c(t)$:

(1) $pg(t) = pc(t), \forall t, t \in [0, T_T]$; $Pg = Pc$; full coordination of generation and load (consumers) operation modes;
(2) $pg(t) \neq pc(t)$; $\frac{1}{T} \int_0^T p_g(t)dt = \frac{1}{T} \int_0^T p_c(t)dt$; $Pg = Pc$; should be provided by the use of technical means, first of all systems of energy storage, reactive power compensation, compensation of non-sinusoidality and asymmetry;
(3) $pg(t) \neq pc(t)$; $Pg < Pc$; should be implemented not only through technical means, in particular, given for the second group of modes, but also primarily through the implementation of DSM programs;
(4) $pg(t) \neq pc(t)$; $Pg > Pc$; should provide not only to increase the levels of electricity consumption of the existing load, but also the ability to connect additional loads.

If the Frieze power concept Q_F extends to an arbitrary time interval $\tau = T_T$, the power $Q_{F\tau}$ determines the root mean square discrepancy between suboptimal ($S > P$) and optimal ($S = P$) levels of active power load consumption at time interval $\tau = T_T$.

The reactive current $i_{P\tau}(t)$ in the interval $\tau = T_T$, which characterizes the suboptimal transmission of electricity is determined from the relation [13, 19]:

$$i_{p\tau}(t) = i(t) - \frac{\left(\int_0^\tau u(t)i(t)dt\right)u(t)}{\int_0^\tau u(t)dt}. \tag{3}$$

In fact, the power $Q_{F\tau}$ from a mathematical point of view is the root mean square discrepancy between two functions in the interval τ [13, 20].

The concept of "non-optimality characteristic" can be used when one of the functions we will consider as optimal (in this case it is the function of active power consumption). The power $Q_{F\tau}$ according to relation (3) can be used for retrospective, perspective and real-time analysis with identification of the effects of suboptimal components: voltage deviation ΔU, current deviation ΔI, components of voltage harmonics k_{pu}, current k_{pi}, reactive component ($\cos\varphi \neq 1$).

The methodology of using $Q_{F\tau}$ (hereinafter we will omit the index "τ") to assess the non-optimality of processes will be extended to functions that are based on the integrated characteristics of instantaneous processes in the j-th period T of the generator. Note that the integral characteristics may change over time in the interval T_T. We will assume that there is a condition $T_T/T = nT, n_t \in N. (T_T \gg T)$.

Then the functions of average $U_{av}(t)$ and active voltage $U_D(t)$, active $P(t)$ and reactive $Q_1(t)$ according to the first harmonic, active values of total $I(t)$, active $I_A(t)$ and reactive IP (t) currents are defined as follows:

(1) $U_{av}(t) = U_{av}$; $j = $ const; $U_D(t) = U_{D,j} = $ const;
(2) $P(t) = P_j = $ const; $Q_1(t) = Q_{1,j} = $ const;
(3) $I(t) = I_j = $ const; $I_A(t) = I_{A,j} = $ const; $I_p(t) = I_{p,j} = $ const;
(4) $t \in [jT, (j+1)T]$; $j = [0, n_T - 1]$; $n_T = T_T/T$.

To simplify the further presentation of the material, we will assume that the functions $U_{av}(t)$, $U_D(t)$, $P(t)$, $Q_1(t)$, $I(t)$, $I_A(t)$, $I_R(t)$ on interval T_T approximated by piecewise linear functions. The accuracy of such an approximation (type of approximation) and the operating conditions of the system. We can distinguish the following modes of operation of the system:

(1) $u(t) = U_{1M}\sin\omega t$; $i(t) = \sum_j i_j(t)$; $Q_1(t) = 0$; $p(t) \neq 0$, there is no reactive power consumption;
(2) $u(t) = U_{1M}\sin\omega t$; $i(t) = \sum_j i_j(t)$; $Q_1(t) \neq 0$; $p(t) \neq 0$; reactive power is consumed;
(3) $u(t) = U_{1M}\sin\omega t$; $i(t) = \sum_j i_j(t)$; higher harmonics are present in the generators current;
(4) $u(t) = \sum_j u_j(t)$ t; $i(t) = \sum_j i_j(t)$; presence of higher harmonics of voltage and current.

Thus, to determine Q_F on the T_T interval, we can use formula (1), calculating the values of S and P on for certain functions on the T_T time interval.

First, consider the mode of LPSS operation, for which the normalized schedule of voltage and current is shown in Fig. 3, the voltage and current on the selected normalized consumption interval changed on ΔU and ΔI, respectively [12].

In the case of proportional increase in voltage and current, ie under the conditions of increments $\Delta U/U = \Delta I/I = \Delta$, the value for the square of active power takes the form:

$$P^2 = \left(U_1 I_1 \delta + U_1 I_1 \Delta^2 (1-\delta)\right)^2$$
$$= U_1^2 I_1^2 \delta^2 + 2U_1^2 I_1^2 \Delta^2 (1-\delta)\delta + U_1^2 I_1^2 \Delta^4 (1-\delta); \tag{4}$$

$$P^2 = U_1^2 I_1^2 \left(\delta^2 + 2\Delta^2(1-\delta)\delta + \Delta^4(1-\delta)\right) = U_1^2 I_1^2 \left(\delta + \Delta^2(1-\delta)\right)^2. \tag{5}$$
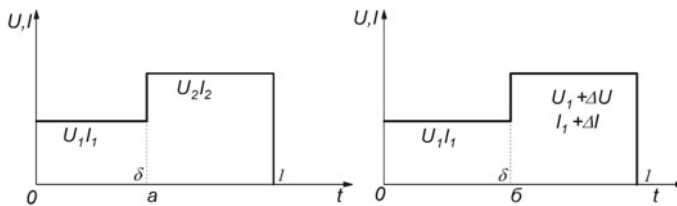
Fig. 3 Voltage and current change at two normalized intervals

The value of square total power:

$$S^2 = U_1^2 I_1^2 \big(\delta + \Delta^2(1-\delta)\big)^2. \tag{6}$$

Analysing the mode of proportional increase of voltage and current, we can conclude that the process is relatively optimal. This is due to the $R = \text{const}$. As a result, $Q_F = 0$. In case of disproportionate U, I change [12], P can be expressed as:

$$P = U_1 I_1 \delta + (U_1 + \Delta U)(I_1 + \Delta I)(1-\delta); \tag{7}$$

$$P = U_1 I_1 + (\Delta U I_1 + \Delta I U_1 + \Delta U \Delta I)(1-\delta). \tag{8}$$

Accordingly, the total power S can be expressed as:

$$S^2 = \big(U_1^2 \delta + (U_1 + \Delta U^2)(1-\delta)\big)\big(I_1^2 \delta + (I_1 + \Delta I)^2(1-\delta)\big); \tag{9}$$

$$S^2 = \big(U_1^2 + (2U_1\Delta U + \Delta U^2)(1-\delta)\big)\big(I_1^2 + (2I_1\Delta I + \Delta I^2)(1-\delta)\big). \tag{10}$$

Substitute the values of total and active power in relation (1), we obtain:

$$Q_F = \sqrt{\big(U_1^2 \delta + U_2^2(1-\delta)\big)\big(I_1^2 \delta + I_2^2(1-\delta)\big) - (U_1 I_1 \delta + U_2 I_2(1-\delta))^2}. \tag{11}$$

In general case of LPSS mode analysis, there are three main options that will further determine the impact of suboptimal factors on the magnitude of electricity losses:

Option 1. No increase in current and the presence of voltage increase $\Delta I = 0$, $\Delta U \neq 0$, $I_1 = I_2$ can be expressed as:

$$Q_F = \sqrt{\big(U_1^2 \delta + (U_1 + \Delta U)^2 \delta_2\big)\big(I_1^2 \delta + I_1^2 \delta_2\big) - \big(U_1 I_1 \delta + (U_1 + \Delta U)I_1 \delta_2\big)^2}; \tag{12}$$

$$Q_F = \sqrt{\big(U_1^2 \delta + U_1^2 \delta_2 + 2U_1 \Delta U \delta_2 + \Delta U^2 \delta_2\big)I_1^2 - (U_1 \delta_1 + U_1 + \delta_2 + \Delta U \delta_2)^2 I_1^2}$$
$$= I_1 \sqrt{\big(U_1^2 + 2U_1 \Delta U \delta_2 + \Delta U^2 \delta_2\big) - \big(U_1^2 + 2U_1 \Delta U \delta_2 + \Delta U^2 \delta_2^2\big)}; \tag{13}$$

$$Q_F = I_1 \Delta U \sqrt{\delta_2 - \delta_2^2}. \tag{14}$$

Option 2. No voltage gain $\Delta U = 0$, the presence of current gain $\Delta I \neq 0$ (12) can be rewritten similarly (14) taking into account $\delta_2 = 1 - \delta$ as:

$$Q_F = U_1 \Delta I \sqrt{\delta_2 - \delta_2^2}. \tag{15}$$

Option 3. When there are voltage deviations $\Delta U = \text{var}$, current $I = I_{\text{var}} = I_D$ in case of change of time interval by increment δ_2^*, namely: $\Delta t \neq 0$, $\Delta t \neq 0$, $\delta_2 = \delta_2 + \delta_2^*$;

$$Q_F = I_1 \sqrt{U_1^2 \delta_1 + (U_1 + \Delta U)^2 (\delta_2 + \delta_2^*) - (U_1 \delta_1 + (U_1 + \Delta U)(\delta_2 + \delta_2^*))^2}. \tag{16}$$

The expression can be written as $Q_F = I_1 \sqrt{a}$:

$$a = U_1^2 \delta_1 + U_1^2 \delta_2 + 2U_1 \Delta U \delta_2 + \Delta U^2 \delta_2 + U_1^2 \delta_2^* + 2U_1 \Delta U \delta_2^* + \Delta U^2 \delta_2^*$$
$$- (U_1 \delta_1 + U_1 \delta_2 + U_1 \delta_2^* + \Delta U \delta_2 + \Delta U \delta_2^*)^2. \tag{17}$$

As a result of algebraic transformations of expression (17) we obtain relations for the analysis of the influence of growth δ_2^* on Q_F value:

$$Q_F = I_1 \sqrt{\Delta U^2 (\delta_2 + \delta_2^*) - 2U_1^2 \delta_2^* - \left(U_1 \delta_2^* + \Delta U (\delta_2 + \delta_2^*)^2\right)}. \tag{18}$$

Analysis of the obtained ratios shows that with deviations of voltage or current, the value of the Frieze increases in proportion. In the case of changes in ΔI and ΔU, with a negative deviation, there is a decrease in the value of the Frieze power, compared with the positive deviation. This leads to a deterioration in the quality of electricity, an increase in networks reactive energy, the equipment operates in an abnormal mode, which leads to additional losses [12].

Consider LES operation mode in the case of different intervals of current and voltage $t_u \neq t_i$. change. To analyse the change of the Frieze reactive power Q_F at $t_u \neq t_i$ we determine the conditionally optimal values of voltage and current (Fig. 4).

As a conditional optimal value of voltage, we use the average value of voltage. Therefore, U_0 is expressed as follows [12, 20]:
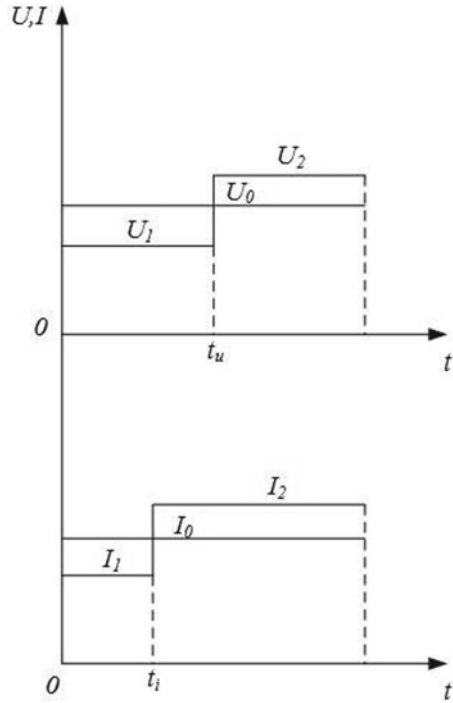
$$U_0 = \frac{U_1 t_u + U_2 (T - t_u)}{T}. \tag{19}$$

Similarly to (19) we can write the conditionally optimal value of the current I_0:

$$I_0 = \frac{I_1 t_i + I_2 (T - t_i)}{T}. \tag{20}$$

Substituting the value $P_0 = U_0 I_0$ in the power formula, we obtain values for voltage U and current I:

Fig. 4 Voltage and current consumption at different intervals

$$\begin{cases} U^2 = U_1^2 \delta_u + U_2^2 (1 - \delta_u); \\ I^2 = I_1^2 \delta_i + I_2^2 (1 - \delta_i); \\ \delta_u = t_u/T, \ \delta_i = t_i/T. \end{cases} \tag{21}$$

Taking into account (19−21) for the Frieze power Q_F we get:

$$Q_F^2 = U^2 I^2 - P^2 = (U_1^2 \delta_u + U_2^2 (1 - \delta_u))(I_1^2 \delta_i + I_2^2 (1 - \delta_i)) \\ - ((U_1^2 \delta_u + U_2^2 (1 - \delta_u))((I_1^2 \delta_i + I_2^2 (1 - \delta_i)))^2. \tag{22}$$

There is a following trend of deviations: the greater they are, the greater the value of the Frieze reactive power. This approach to Q_F estimation is important for determining the degree of non-optimality of LPSS regimes in relation to the generated and consumed active power [12].

5 Analysis of the Influence of Cosφ Change and Non-sinusoidality on the Change on Q_F Value

Consider the features of Q_F in the case of time intervals approximation and analysis of the following factors effects to assess the non-uniformity of processes will be shown on the example of a mode characterized by the voltage and current values U_i and I_i, $i = 1, \ldots, n$, T_i—the duration of the i-th interval, and $P = U_0 I_0$ where, U_0, I_0—the average values. If $\cos \varphi = 1$ for the interval $T_T > T_\Gamma$, one can write an expression for the power of the Frieze Q_F in the form:

$$Q_F = \sqrt{\left(\sum_{i=1}^{n} U_i^2 \frac{T_i}{T}\right)\left(\sum_{j=1}^{n} I_j^2 \frac{T_i}{T}\right) - U_0^2 I_0^2}, \tag{23}$$

which with $\delta_i = T_i/T$; $\sum_{i=1}^{n} \delta_i = 1$ can be written as:

$$Q_F = \sqrt{\sum_{i=1}^{n} U_i^2 \delta_i \cdot \sum_{i=1}^{n} I_i^2 \delta_i - \sum_{i=1}^{n} (U_i I_i \delta_i)^2}. \tag{24}$$

Analysis of the non-uniformity process influence taking into account reactive power ($\cos\varphi < 1$) is performed for two intervals, where the moments of voltage change t_u and current t_i may coincide ($t_u = t_i$) or not coincide ($t_u \neq t_i$), and voltage increments ΔU and current ΔI on the second interval (index "2") can both increase and decrease in relation to their values on the first interval (index "1"). The active power P is determined from the ratio:

$$P = \sum_{i=1}^{n} U_i I_i \delta_i \cos \varphi_i.$$

When analysing the impact of non-uniformity of processes taking into account the reactive power ($\cos\varphi < 1$) we can identify 12 possible LPSS configuration options (modes):

(1) $t_i = t_u$, $U_2 = U_1 + \Delta U \infty$, $I_2 = I_1 + \Delta I$
(2) $t_i = t_u$, $U_2 = U_1 - \Delta U$, $I_2 = I_1 - \Delta I$
(3) $t_i = t_u$, $U_2 = U_1 - \Delta U$, $I_2 = I_1 + \Delta I$
(4) $t_i = t_u$, $U_2 = U_1 + \Delta U$, $I_2 = I_1 - \Delta I$
(5) $t_i > t_u$, $U_2 = U_1 + \Delta U$, $I_2 = I_1 + \Delta I$
(6) $t_i > t_u$, $U_2 = U_1 - \Delta U$, $I_2 = I_1 - \Delta I$
(7) $t_i > t_u$, $U_2 = U_1 - \Delta U$, $I_2 = I_1 + \Delta I$
(8) $t_i > t_u$, $U_2 = U_1 + \Delta U$, $I_2 = I_1 - \Delta I$
(9) $t_i < t_u$, $U_2 = U_1 + \Delta U$, $I_2 = I_1 + \Delta I$
(10) $t_i < t_u$, $U_2 = U_1 - \Delta U$, $I_2 = I_1 - \Delta I$

(11) $t_i < t_u, \ U_2 = U_1 - \Delta U \ \ I_2 = I_1 + \Delta I$
(12) $t_i < t_u, \ U_2 = U_1 + \Delta U \ \ I_2 = I_1 - \Delta I$

The ratio for the reactive power Q_F for the 1st variant ($t_i = t_u$, $U_2 = U_1 + \Delta U$, $I_2 = I_1 + \Delta I$) when normalizing the interval T_T has the form:

$$Q_F^2 = \left(U_1^2 \delta_t + (U_1 + \Delta U)^2 (1 - \delta_t)\right)\left(I_1^2 \delta_t + (I_1 + \Delta I)^2 (1 - \delta_t)\right)$$
$$- (U_1 I_1 \delta_t \cos \varphi_t + (U_1 + \Delta U)(I_1 + \Delta I)(1 - \delta_t) \cos \varphi_{T-t})^2;$$

Consider the non-uniformity of processes with deviation of voltage ΔU, current ΔI, voltage ripple k_{pu} and current k_{pi}, taking into account reactive power ($\cos\varphi < 1$).

In the general case, the active power is the sum of the active power on the first P_1 and higher harmonics: $P_\infty : P_\Sigma = P_1 + P_\infty$. Assuming $P_\infty \approx 0$, we obtain:

$$Q_F^* = \sqrt{S^2 - P_1^2} \qquad (25)$$

$$P_1 = (U_1 + \Delta U_1)(I_1 + \Delta I_1) \cos \varphi, \qquad (26)$$

where ΔU та ΔI—deviation of the current values of voltage and current on the first harmonic.

Taking into account (19) and (20) we can write $t_u \neq t_i$:

$$Q_F^2 = (U_0^2 + \frac{\Delta U_1^2 \Delta t_u + \Delta U_2^2 (T_T - \Delta t_u)}{T_T}) \cdot (I_0^2 + \frac{\Delta I_1^2 \Delta t_i + \Delta I_2^2 (T_T - \Delta t_i)}{T_T})$$
$$- U_0^2 I_0^2. \qquad (27)$$

We can write the ratio:

$$\begin{cases} U_2^2 = U_1^2 (1 + \Delta U)^2 (1 + k_{pu}^2); \\ U_1^2 = U_1^2 (1 + k_{pu}^2); \\ I_1^2 = I_1^2 (1 + k_{pi}^2); \\ I_2^2 = U_1^2 (1 + \Delta I)^2 (1 + k_{pi}^2). \end{cases} \qquad (28)$$

In the case of entering relative values for two time intervals $\delta 1$, $\delta 2$, the value $k_{\Delta opt} = Q_F / P$ characterizes the regulation efficiency and determines the level of suboptimal energy transfer in terms of eliminating its losses [11] and is calculated as the change in values relative to the first time interval t_1.

Taking into account the relation $P_0 = U_0 I_0$, we simplify Eq. (27) to the form:

$$Q_F = U_1^2 (1 + \Delta_u)^2 (1 + k_{\Pi u}^2) \cdot I_1^2 (1 + k_{\Pi i}^2)(1 + \Delta_i)^2 \delta_2^2 \sin^2 \varphi_2$$
$$+ 2\delta_1 \delta_2 U_1^2 I_1^2 (1 + k_{pu}^2)(1 + k_{pi}^2)(1 + \Delta u_u)(1 + \Delta u_i)(1 - \cos \varphi_1 \cos \varphi_2). \qquad (29)$$

Then we can calculate the value $k_{\Delta\,opt} = Q_\Phi/P$

$$
\begin{aligned}
k_{\Delta opt} = {} & (1 + \Delta_u)^2(1 + k_{pu}^2) \cdot (1 + k_{pi}^2)(1 + \Delta_i)^2\delta_2^2\sin^2\varphi_2 \\
& + 2\delta_1\delta_2(1 + k_{pu}^2)(1 + k_{pi}^2)(1 + \Delta_u)(1 + \Delta_i)(1 - \cos\varphi_1\cos\varphi_2).
\end{aligned} \quad (30)
$$

As in the previous case, we can also identify 12 possible options (modes) LPSS calculation Q_F with a similar change in values t_u, t_i, δ_u and δ_i. The ratio for Q_F for the one of them ($\Delta t_i = \Delta t_u$, $U_2 = U_1(1 + \delta_u)$, $I_2 = I_1(1 + \delta_i)$) has the form:

$$
\begin{aligned}
Q_F^2 = {} & \left(U_1^2\delta_t + U_1^2(1 + \delta_u)^2(1 - \delta_t)\right)\left(I_1^2\delta_t + I_1^2(1 + \delta_i)^2(1 - \delta_t)\right) \\
& - (U_1I_1\delta_t + U_1I_1(1 + \delta_i)(1 + \delta_u)(1 - \delta_t))^2.
\end{aligned}
$$

Consider in more detail the effect of harmonic components on the value of current $i(t)$ and voltage $u(t)$ as:

$$
u(t) = \sum_{j=1}^{n} u_j(t) = \sum_{j=1}^{n} U_{M,j}\sin\left(j\omega t + \varphi_j^u\right); \quad (31)
$$

$$
i(t) = \sum_{j=1}^{n} i_j(t) = \sum_{j=1}^{n} I_{M,j}\sin\left(j\omega t + \varphi_j^i\right); \quad (32)
$$

$$
U^2 = U_1^2 + U_3^2; \quad I^2 = I_1^2 + I_3^2; \quad (33)
$$

$$
k_{pu,3} = \frac{U_3}{U_1}; \quad k_{pi,3} = \frac{I_3}{I_1}. \quad (34)
$$

The total power taking into account the ripple coefficients is calculated as

$$
S^2 = U_1^2 I_1^2\left(1 + k_{pu}^2\right)\left(1 + k_{pi}^2\right). \quad (35)
$$

To determine the influence of harmonic components of the 1st and 3rd harmonics:

$$
\begin{aligned}
U_3 &= U_1\left(1 + k_{pu,3}\right); \quad I_3 = I_1\left(1 + k_{pi,3}^2\right); \\
S_{1,3}^2 &= U_1^2 I_1^2\left(1 + k_{pu,3}^2\right)\left(1 + k_{pi,3}^2\right).
\end{aligned} \quad (36)
$$

To determine the influence of harmonic components of the 1st, 3rd and 5th harmonics:

$$
S_5^2 = U_1^2 I_1^2\left(1 + k_{pu,3}^2 + k_{pu,5}^2\right)\left(1 + k_{pi,3}^2 + k_{pi,5}^2\right). \quad (37)
$$

The active power in this case is defined as:

$$P = \sum_{j=1}^{n} U_j I_j \cos(\varphi_j^u - \varphi_j^i). \tag{38}$$

To determine the effect of harmonious components 1 and 3 harmonics:

$$P = U_1 I_1 \cos(\varphi_1^u - \varphi_1^i) + U_3 I_3 \cos(\varphi_3^u - \varphi_3^i); \tag{39}$$

$$Q_{F,1-3}^2 = U_1^2 I_1^2 (1 + k_{pu,3}^2)(1 + k_{pi,3}^2)$$
$$-(U_1 I_1 \cos(\varphi_1^u - \varphi_1^i) + U_3 I_3 \cos(\varphi_3^u - \varphi_3^i))^2. \tag{40}$$

In the analysis of the higher harmonics of voltage and current influence, when the signals are represented by Fourier series, the calculation of the Frieze power Q_F can be modified taking into account the amplitude values of voltage U_M and current I_M when we can write current values as: $U_D = U_M/\sqrt{2}$, $I_D = I_M/\sqrt{2}$,

$$u(t) = \sum_{j=1}^{n} u_j(t) = \sum_{j=1}^{n} U_{M,j} \sin(j\omega t + \varphi_j^u); \tag{41}$$

$$i(t) = \sum_{j=1}^{n} i_j(t) = \sum_{j=1}^{n} I_{M,j} \sin(j\omega t + \varphi_j^i); \tag{42}$$

$$P = \sum_{j=1}^{n} \frac{U_{M,j} I_{M,j}}{\sqrt{2}} \cos(|\varphi_j^u - \varphi_j^i|); \tag{43}$$

$$S^2 = U_D^2 (1 + k_{pu}^2) I_D^2 (1 + k_{pi}^2); \tag{44}$$

$$S^2 = \sum_{j=1}^{n} \frac{U_{M,j}^2 (1 + k_{pu,j}^2)}{2} \sum_{j=1}^{n} \frac{I_{M,j}^2 (1 + k_{pi,j}^2)}{2}. \tag{45}$$

Substituting the values for the square of full S^2 and active P^2 power, we get:

$$Q_F^2 = \frac{\sum_{j=1}^{n} U_{M,j}^2 (1 + k_{pu,j}^2) \sum_{j=1}^{n} I_{M,j}^2 (1 + k_{pi,j}^2) - \sum_{j=1}^{n} U_{M,j}^2 I_{M,j}^2 \cos^2(|\varphi_j^u - \varphi_j^i|)}{2}. \tag{46}$$

When considering electricity processes during the day, the ratio should be approximated by four components Fig. 5 that reflect the average levels of voltage and current. This approach formally reflects electricity consumption in the evening and morning highs and night and day lows [20].

For the daily schedule of consumption relative to the conditionally optimal level $U_0 I_0$ we can write:
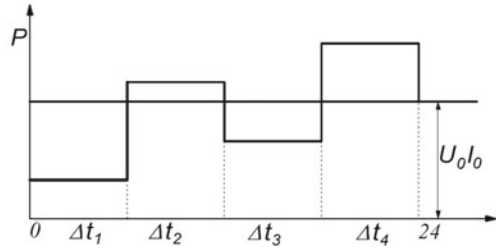
$$Q_{F,24}^2 = (U_0^2 + \sum_{j=1}^{4} \Delta U_j^2 \delta_j)(I_0^2 + \sum_{j=1}^{4} \Delta I_j^2 \delta_j) - U_0^2 I_0^2. \tag{47}$$

The obtained indicator Q_F allows to estimate the level of uneven consumption of electricity during the day on the basis of optimal or average values in the case of four time intervals Δt_i and the theoretical assumption of $\cos\varphi = 1$ [12]:

$$U_0 = \frac{U_1 \Delta t_1 + U_2 \Delta t_2 + U_3 \Delta t_3 + U_4 \Delta t_4}{T};$$

$$I_0 = \frac{I_1 \Delta t_1 + I_2 \Delta t_2 + I_3 \Delta t_3 + I_4 \Delta t_4}{T}.$$

Considering the values of the current values for voltages and currents, taking into account the deviation of the value of ΔU and ΔI, respectively, we obtain the following equations: $U_i = U_0 + \Delta U$ та $I_i = I_0 + \Delta I_i$, де $i = 1,\dots,4$; $\Delta t/T = \delta_i$ [12, 20].

$$S^2 = \left[(U_0 - \Delta U_1)^2 \delta_1 + (U_0 + \Delta U_2)^2 \delta_2 + (U_0 - \Delta U_3)^2 \delta_3 + (U_0 + \Delta U_4)^2 \delta_4\right]$$
$$\times \left[(I_0 - \Delta I_1)^2 \delta_1 + (U_0 + \Delta I_2)^2 \delta_2 + (U_0 - \Delta I_3)^2 \delta_3 + (U_0 + \Delta I_4)^2 \delta_4\right];$$

$$S^2 = \left(U_0^2 + \sum_{j=1}^{4} \Delta U_j^2 \delta_j\right)\left(I_0^2 + \sum_{j=1}^{4} \Delta I_j^2 \delta_j\right). \tag{48}$$

Substituting the value of the square of total power S^2 from (48) taking into account (47), we obtain:

$$Q_{F,24}^2 = U_0^2 \sum_{j=1}^{4} \Delta I_j^2 \delta_j + I_0^2 \sum_{j=1}^{4} \Delta U_j^2 \delta_j + \left(\sum_{j=1}^{4} \Delta I_j^2 \delta_j\right)\left(\sum_{j=1}^{4} \Delta U_j^2 \delta_j\right). \tag{49}$$

The obtained integrated characteristics allow to estimate the level of non-uniformity of electric energy consumption in LPSS during the day on the basis of optimal or average values.

6 Optimisation of Power Supply System Operation Modes Based on Minimisation of Frieze Reactive Power Q_F Components

Optimisation of certain types of equipment is based on the consideration of the function and involves the use of the criterion $k\Delta_{opt} = Q_F/P \to$ min, simultaneously with the implementation of the DSM program.

Value of $k\Delta_{opt}$ characterizes the efficiency of regulation and determines the level of losses from the unevenness of processes.

The generalized optimisation function is:

$$Q_F = F_Q(U, I, \cos\varphi, \Delta U, \Delta I, k_{pu}, k_{pi}). \tag{50}$$

In the general case, the optimisation of equipment involves the following steps:

(1) factors of influence are determined and relations are formed (30);
(2) change of QF value from changes in absolute values of influencing factors, such as changes in function $Q_F = F_Q(U, I, \Delta I)$;
(3) the number of zones nΔI of QF values changes and QF,j is calculated in case of changes in ΔI, j; j =1,..., nΔI;
(4) for the j-th zone for certain types of equipment control influences are determined on the basis of functional dependences of each equipment type operation control mode according to DSM programs which provide $k\Delta_{opt} = Q_F/P \to$ min condition.

The problem of optimal electricity consumption can be solved by comparing the modes in the case of different combinations of power management systems and electricity demand management. Consider the optimisation of the current level of electricity consumption in power supply systems.

In the general case, the objective function for the organization of the process of solving the mathematical expression of the goal of optimal control of the system is formalized in the form of a function of control quality [12, 20]

$$F(X) \to opt; \tag{51}$$

$$
\begin{aligned}
&F(X) = \big(F_{\text{gen}}(X), \quad F_{\text{tran}}(X), \quad F_{\text{cons}}(X)\big); \\
&X \in \Omega; \ X = (X_1; X_2; \ldots; X_n); \\
&\Omega = \{X : a_i \le X_i \le b_i, i = 1...n\},
\end{aligned} \tag{52}
$$

where $F(X)$ is the objective function; X is the vector of optimized parameters; a_i, b_i are the limits of change of optimized parameters.

For a particular case, the objective function of the optimisation problem can be written as:

$$F_{\text{gen}} = (\Delta U_{\text{gen}}, \ \Delta I_{\text{gen}}, \ \Delta f_{\text{gen}}, \ \Delta \varphi_{\text{gen}}, \ \Delta P_{\text{gen}}, \ g_{\text{gen}});$$

$$F_{\substack{\text{transfer} \\ \text{transformation}}} = (\Delta U_{\text{transfer}}, \ \Delta I_{\text{transfer}}, \ \Delta f_{\text{transfer}}, \ \Delta \varphi_{\text{transfer}}, \ \Delta P_{\text{transfer}}, g_{\text{transfer}}); \quad (53)$$

$$F_{\text{cons}} = (\Delta U_{\text{cons}}, \Delta I_{\text{cons}}, \Delta f_{\text{cons}}, \Delta \varphi_{\text{cons}}, \Delta P_{\text{cons}}, g_{\text{cons}}),$$

where ΔU—voltage deviation; ΔI—current deviation; Δf—frequency deviation; $\Delta \varphi$—power factor changes; ΔP—power loss; g—other factors, which arise as a result of uneven processes, and which must be considered when optimizing LPSS modes.

The general objective function (51) is vector, in some cases scalarisation is necessary, i.e., knowing initial conditions and restrictions, to define such mode of work which maximizes or minimizes the uniform set criterion indicator [21].

Having identified the indicator of suboptimality, which characterizes the efficiency of regulation and determines the level of suboptimality of energy transfer, we analyse the available load profiles, in which there are three main options: retrospective with decreasing time interval δ, perspective within the analysis of processes with increasing time interval δ, real-time analysis at δ = 0.

We present a system of indicators of the current LPSS optimality operation level based on the Frieze reactive power index Q_F. Considering the possible variants of current and voltage changes, it is necessary to identify the following variants of change in the case of deviations, it is necessary to take into account the shape of the curves.

The analysis showed that the value depends most on the change of ΔI than ΔU, but ΔU affects the shape of the curve and the presence of extrema. An important step in the calculation is to establish the optimal values for voltage U_0 and current U_0. In the absence of data, averages should be used.

The optimisation methodology envisages initial data at the first stage, and using the appropriate Frieze power Q_F calculation option, we can analyse the potential of change in daily schedule to reduce consumption inequality by using DSM programs.

Consider the closest to real conditions mode of LPSS operation with three options [12]: the level of suboptimality is set manually or calculated on the basis of average values; assessment of the general level of suboptimality; assessment of suboptimality at a given interval.

1. In the case of estimating of energy processes in LPSS non-optimality level, which has different optimal values for voltage and current at each interval, the values for the optimal generation level are variable, but have fixed values, where changes ΔU_j and ΔI_j can be both positive and capacious, we can write

$$Q_{F,24}^2 = \sum_{j=1}^{4} \left(U_{0,j}^2 + \Delta U_j^2 \right)\left(I_{0,j}^2 + \Delta I_j^2 \right)\delta_j^2 - \sum_{j=1}^{4} \left(U_{0,j}^2 I_{0,j}^2 \delta_j^2 \right)^2. \quad (54)$$

Here, the average values of voltage and current according to (19) and (20) are one of the possible variants of optimal values.

2. In the absence of values for the optimal mode, the calculation is performed to assess the overall suboptimal consumption:

$$S_{24}^2 = \left(\sum_{j=1}^{4} U_j^2 \delta_j \right) \left(\sum_{j=1}^{4} I_j^2 \delta_j \right); \ P_{24}^2 = \sum_{j=1}^{4} \left(U_j I_j \delta_j \right)^2;$$

$$Q_{F,24}^2 = \left(\sum_{j=1}^{4} U_j^2 \delta_j \right) \left(\sum_{j=1}^{4} I_j^2 \delta_j \right) - \sum_{j=1}^{4} \left(U_j I_j \delta_j \right)^2. \tag{55}$$

3. For a detailed analysis of the LPSS operation mode for a certain period of time, it is necessary to calculate for a larger number of intervals. The given expression for the calculation of the Frieze power can be represented as $Q_{F, Treg}^2$ [12]:

$$Q_{F,Treg}^2 = \left(\sum_{j=1}^{n} U_j^2 \delta_j \right) \left(\sum_{j=1}^{n} I_j^2 \delta_j \right) - \sum_{j=1}^{n} \left(U_j I_j \delta_j \right)^2. \tag{56}$$

In the future, it may be appropriate to form quasi-optimal profiles of energy consumption in LPSS.

7 Optimisation of Electricity Demand Management Processes by Optimizing Consumers Operation Modes

Obviously, when DSM mechanisms are implemented, it is necessary to evaluate the demand management performance, which is usually performed on indicators such as [7, 21]:

– the factor of filling the load schedule k_L;
– the total cost of consumed electricity C_e.

Accordingly, it is necessary to apply two criteria, which are presented in the form of objective functions (OF) [21–23].

The first OF corresponds to the maximisation of the load factor of the load schedule k_L [17].

$$k_3 = \frac{\sum_{i=1}^{N} \sum_{j=1}^{J} P_{(i,j)} t_j}{\sum_{j=1}^{J} t_j \sum_{j=1}^{J} P_{(i,j)}} \rightarrow \max, \tag{57}$$

where optimisation variables are selected by the power consumption values $P_{(i,j)}$ at time interval t_j (usually the time interval is 1–2 h) by consumer groups i. Accordingly, the numerator of the objective function represents the amount of consumed power. The OF is linear with respect to the optimisation variables. The dimension of the problem is $N \times J$, where N—number of consumer groups; J—the number of time intervals [17].

The second OF is to minimize the cost C [17]:

$$C = \left[\sum_{i=1}^{N} \sum_{j=1}^{J} P_{(i,j)} \cdot t_{(j)} \cdot ce_{(i,j)} \right] + \left[\sum_{i=1}^{N} \sum_{j=1}^{J} P_{(i,j)} \cdot t_{(j)} \cdot cd_{(i,j)} \right] \rightarrow \min, \quad (58)$$

where the OF by criterion Ce—cost of consumed electricity is also linear and represents a minimisation of consumed electricity cost. Optimisation variables are selected: power consumption over time interval t_j by consumer groups i, electricity tariff Ce, charge for installed capacity cd. The first addition is the charge for the amount of consumed energy, the second addition is the payment for the power.

Optimized schedules of daily electricity consumption are constructed with restrictions in mind [17, 21, 23]:

$$P_{new}(i) = P_{old}(i)_{\forall} t_o \rightarrow t_k, t_h \rightarrow T_D. \quad (59)$$

That is, the total amount of power consumed Pt the T_D time interval remains unchanged and must be constrained at every interval:

$$P_{new}(i) \leq P_{(value\ 1)} \forall t_k \rightarrow t_h; \quad (60)$$

$$P_{new}(i) \geq P_{(value\ 2)} \forall t_k \rightarrow t_h. \quad (61)$$

However, peak consumption from the time interval $(t_k; t_h)$ is evenly transferred to time intervals $(t_o; t_k) \cup (t_h; T_D)$:

$$P_{(value\ 2)} \leq P_{(value\ 1)}. \quad (62)$$

The constraints of the problem relate to the need to save the total power consumption over the billing period: $P_{new,i} = P_{old}$, and limiting the maximum values of the maximum power consumption: $P_{new,i} < P_{max}$, arising from network and power system boundary capabilities, such as limited power generation of power system equipment, restrictions on the capacity of the distribution network, transformers, etc.

The above description of the optimisation problem $(57{-}62)$ problem is somewhat simplified and does not take into account the ability of the consumer to change consumption profiles in automatic mode for different types of equipment. To consider the ability of consumers to change the level of their equipment consumption, it is necessary to enter the third criterion and formulate an appropriate optimisation

problem. Idea is minimisation of the initial load schedule irregularity degree after DSM application—min F_g.

The peculiarities of consumers are taken into account by the flexibility coefficient of demand k_g, which can take a value from 0 to 1. Value of 0 corresponds to the least flexibility of the equipment, 1 to the maximum flexibility. This coefficient represent the willingness of the consumer to change the consumption profile of specific equipment by shifting consumption to other time intervals [17]. Nonlinear multicriteria optimisation problem for OF F_g:

$$\min \ F_{\Gamma\text{pa}\Phi} = \sum_{i=1}^{N} \sum_{j=1}^{T} (P_{new} - P_{old})^2 \cdot \frac{1}{k_{\Gamma}}; \tag{63}$$

$$\min y = \begin{cases} C(P_{new}) - w_1 \cdot y_1 \leq g_1 \\ Cur(P_{new}) - w_2 \cdot y_2 \leq g_2 \\ E_{new} = E_{old} \\ P_{new,i} \leq P_{\max} \end{cases}. \tag{64}$$

It is proposed to consider separately the pairs of criteria as being appropriate to the objectives of the consumer and the electricity supply organization:

(1) the load factor and the coefficient of irregularity of the graph;
(2) reduction of consumed electricity cost and the coefficient of consumption schedule irregularity.

To illustrate the results of the optimisation model, a group of one thousand households was selected, with the basic equipment: dishwashers, heating and air conditioning, refrigerators, lighting, cooking equipment and multimedia systems. In the following, the average power values for typical equipment in this class are discussed. It should be noted that the current two-zone tariff was chosen as the criterion for reducing the consumption of electricity, and the equipment flexibility coefficients were selected from the experience of a number of experts on the use of household appliances. Optimisation of the daily schedule was carried out in MatLab.

In case of optimisation taking into account the current tariffs and the coefficients of flexibility of consumption between 7:00 and 23:00 is transferred to the night zone. It is suggested to consider results 5 and 7 as being achievable in the case of demand management programs.

Optimisation of the fill factor, which in this case is ideal example of reducing peak consumption, is in practice unattainable, since an important requirement for DSM programs is to balance the benefits gained and the deterioration of consumer comfort (Fig. 6). Unlike optimisation of the consumption schedule in case of maximisation of the fill factor without maintaining the balance (Fig. 7), minimizing costs while maintaining the balance of consumed electricity (Fig. 8) is the most attractive for consumers of electricity, since they directly benefit from changing their own mode of operation electricity consumption.
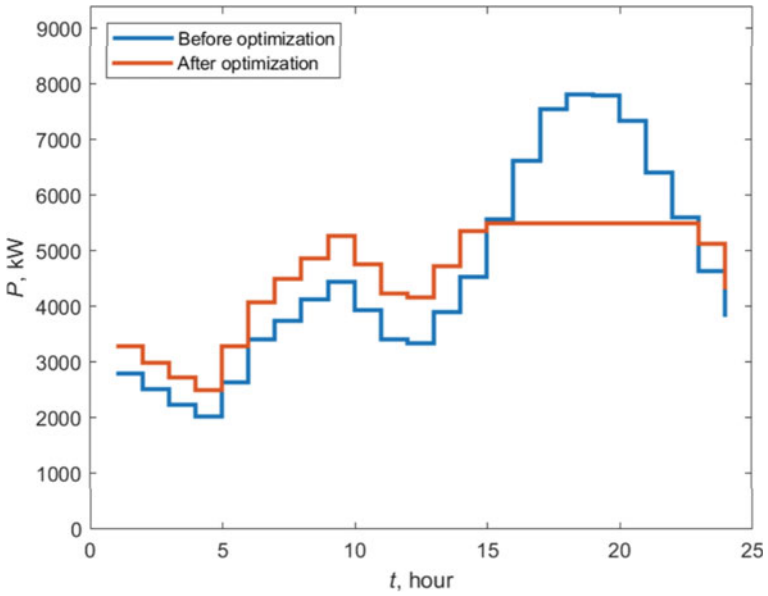
Fig. 6 Results of households daily schedule optimisation in case of maximisation of the fill factor for maintaining the balance of consumed electricity
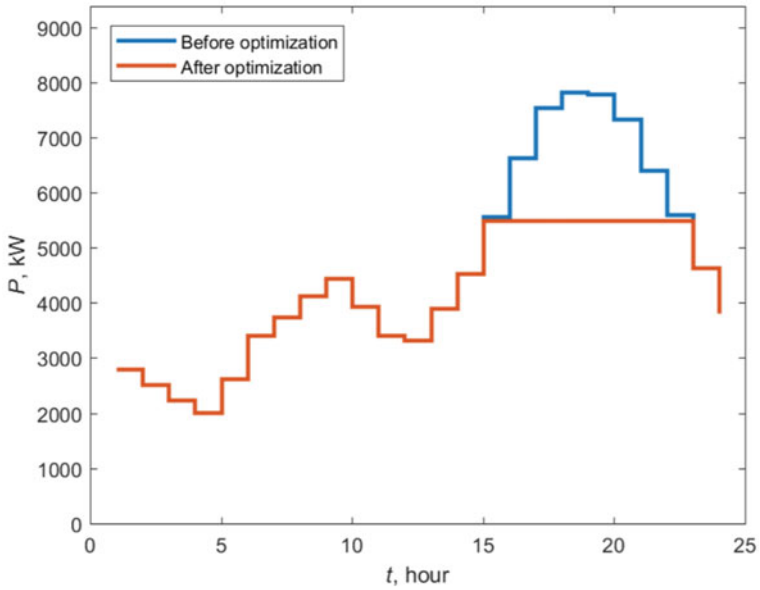
Fig. 7 Maximizing the fill factor without maintaining the balance of electricity consumed
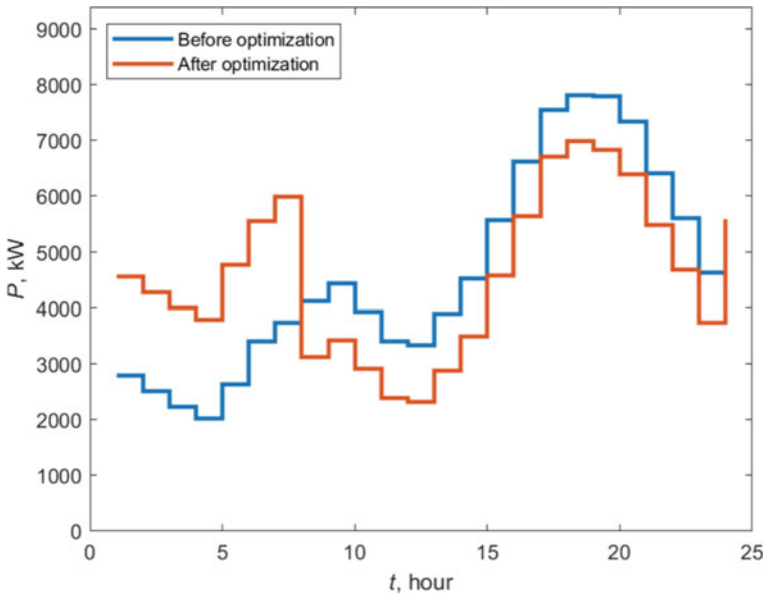
Fig. 8 Minimizing costs while maintaining the balance of consumed electricity

Table 1 shows the numerical values of the received OFs on funds and the coefficient of the graph fill before and after optimisation, also shows the change in the value of their numerical values.

It is suggested not only to use metrics to evaluate optimisation results C and k_g, as well as an indicator of loss reduction based on Frieze reactive power $Q_F^2 = S^2 - P^2$ [19] extended to the daily time interval is calculated as (47) [17].

In this case, the calculation can be simplified in the case of fully active consumption $\cos\varphi = 1$ and the calculation of voltage loss as (Table 2).

Table 1 Obtained values before and after optimisation

The value of OF	Before optimisation	After	Indicator change, %
Costs C_e	189.6	174.8	7.8
Fill factor k_g	0.587	0.835	29.63

Table 2 Change of Q_F power index for each optimisation model

Change of QF in case of optimisation	QF kvar, before	QF kvar, after	ΔQF(%)
Costs C_e	1817.2	1412.9	22.25
Fill factor kg	1817.2	980.2	46.1

$$\Delta U_{\%} = \frac{P \cdot R - Q \cdot X}{10U_{\mathrm{H}}^2} = \frac{P \cdot R}{10U_{\mathrm{H}}^2},$$

The optimisation of operation modes on both indicators led to a decrease in the value of the reactive power of the Frieze Q_F, which is a characteristic reflection of the decrease in the irregularity of the daily schedule of power consumption.

In conclusion, while constructing the power supply systems with DG sources and Prosumers, one should consider the generation source types and the variety of their modes of operation.

8   Conclusions

The section shows that in order to assess the optimality of energy processes in LPSS, it is important to improve and further develop methods for assessing the efficiency of energy processes in the cross sections of the system. As a criterion for optimizing power losses selected minimisation of Q_F in the interval of technological process T_T. This allowed to expand the system of indicators for estimating the components of electricity losses, taking into account the influence of uneven electricity consumption factors in LPSS based on Frieze power Q_F, as well as to develop a methodology for optimizing power consumption graphs using Q_F decomposition in case of DSM programs.

References

1. Jenkins, N., Long, C., Wu, J.: An overview of the smart grid in Great Britain. Engineering **1**(4), 413–421 (2016)
2. Bazyuk, T., Blinov, I., Butkevich, O., et al.: Intelligent electrical networks: elements and modes. In: Under the general. ed. acad. NAS of Ukraine O Kirilenko. K .: Institute of Electrodynamics of the National Academy of Sciences of Ukraine, vol. 400, pp. 3. (2016)
3. Zafar, R., Mahmood, A., Razzaq, S., Ali, W., Naeem, U., Shehzad, K.: Prosumer based energy management and sharing in smart grid. Renew. Sustain. Energy Rev. **82**, 1675–1684 (2018) August 2016
4. Ritzer, G., Dean, P., Jurgenson, N.: In: Behavioral Scientist The Coming of Age of the Prosumer (2012)
5. Mariam, L., Basu, M., Conlon, M.F.: A review of existing microgrid architectures. J. Eng. (United States) (2013)
6. Ren, Y., Fan, D., Feng, Q., Wang, Z., Sun, B., Yang, D.: Agent-based restoration approach for reliability with load balancing on smart grids. Appl. Energy **249**(April), 46–57 (2019)
7. Denysiuk, S., Opryshko, V., Strzelecki, R.: The smart grid concept implementation by expanding the use of demand side managment and modern power electronic installations. Energy: Econ. Technol. Ecol. **4**, 7–16 (2016)
8. de Wildt, T.E., Chappin, E.J. L., van de Kaa, G., Herder, P.M., van de Poel, I.R.: Conflicting values in the smart electricity grid a comprehensive overview. Renew. Sustain. Energy Rev. **111**, 184–196 (2019) December 2018

9. Siano, P.: Demand response and smart grids—a survey. Renew. Sustain. Energy Rev. **30**, 461–478 (2014)
10. Carvallo, A., Cooper, J.: In: The Advanced Smart Grid. pp. 6. (2011)
11. Denysiuk, S., Opryshko, V.: Research on demand side management programs and analysis of their usage efficiency. Technol. Audit Prod. Reserv. **3**, 1(29), 69 (2016)
12. Denisyuk, S., Opryshko, V.: Estimation of electric energy consumption and generation non-uniformity in local electric power systems. Works of Institute Electrodynamics of NAS of Ukraine **48**, 43–51 (2017)
13. Tonkal, V., Novoseltsev, A., Denisyuk, S. et al.: Energy balance in electrical circuits. Nukova Dumka, Kyiv, vol. 310. pp.199–214. (2021)
14. Chiu, W., Sun, H., Poor, H.V.: Energy imbalance management using a robust pricing scheme. IEEE Trans. Smart Grid pp. 1–9. (2012)
15. U.S. Department of Energy.: Benefits of demand response in electricity markets and recommendations for achieving them pursuant to section 1252 of the energy policy act of 2005. pp. 97. (2006)
16. Opryshko, V.: Regulation of power supply modes in local microgrid systems. Technical Electrodynam. **4**, 77–79 (2016)
17. Denisyuk, S., Opryshko, V.: Analysis of electricity consumption daily schedule optimizing possibilities. Bull. Kyiv Natl. Univ. Technol. Des. Tech. Sci. Ser. **128**(6), 20–28 (2019)
18. Drechsler, R.: In: Measurement and Evaluation of Power Quality Under Asymmetric and Nonlinear Loads. pp. 113. Moscow, Energoatomizdat (1985)
19. Zhuikov, V., Denisyuk, S.: In: Energy Processes in Electrical Circuits with Key Elements. Kyiv: Text. pp. 264. (2010)
20. Denisyuk, S., Opryshko, V.: Assessment of the level of uneven electricity consumption in the local power supply system. In the 'Manager Assistant' software package. The structure of the algorithm for reducing the unevenness of electricity consumption. AS №77262, 2018.21. (2018)
21. Attia, H.A.: Mathematical formulation of the demand side management (DSM) problem and its optimal solution. In: 14th International Middle East Power Systems Conference, vol. 10, pp. 953–959. (2010)
22. Dubois, G., et al.: It starts at home? climate policies targeting household consumption and behavioral decisions are key to low-carbon futures. Energy Res. Soc. Sci. **52**(February), 144–158 (2019)
23. Opryshko, V.: VP Mechanisms for implementing electricity demand management programs in world practice. Energy: Econom. Technol. Ecol. **3**, 44–51 (2018)

Short-Term Forecasting of Photovoltaic Solar Power Generation Based on Time Series: Application for Ensure the Efficient Operation of the Integrated Energy System of Ukraine

Alla Bosak , **Dmytro Matushkin** , **Liudmyla Davydenko** ,
Leonid Kulakovskyi , **and Vadym Bronytskyi**

Abstract Over the last decade, there has been a growing in the dependence of electricity production by solar power plants (SPPs) in Ukraine. Therefore, there is a need to optimize the structure of the energy balance of the state, based on the requirements of energy security and ensure the share of renewable energy at 25%. However, with the development of renewable energy sources (RESs) there is a problem of ensuring the appropriate maneuverability of the power system. This is due to the fact that the structure of generating capacity of the United Power System of Ukraine in terms of effective regulation of frequency and power in the power system is suboptimal. Among the reasons for this, the main ones are unregulated and variable operation of a SPP, which is exacerbated by the lack of tools and approaches for the power generation modes forecasting. That is why the issue of accurate forecasting of the possible electricity generation volume has become acute. However, solar energy forecasting is a rather difficult task, as it largely depends on climatic conditions that change over time. This study presents an analysis and application of the seasonal autoregressive integrated moving average (SARIMA) method to develop a model that can support and provide forecasting the amount of power produced by SPP. Data for the development of the model were obtained from the time series of electricity generation on the example of the SPP in the village of Velyka Dymerka, Kyiv region. The data consisted of more than 26 thousand samples collected from July 1, 2020, to December 31, 2020, which characterize the operating conditions of solar panels with a capacity of 9 MW. This led to the choice of the SARIMA model. The coefficient of determination (R^2) for the obtained model was 92%. This indicates the ability of the final model to accurately represent and give forecast based on data set of the SPP power generation.

A. Bosak (✉) · D. Matushkin · L. Kulakovskyi · V. Bronytskyi
National Technical University of Ukraine "Igor Sikorsky Kyiv Polytechnic Institute", Kyiv, Ukraine
e-mail: allabosak@gmail.com

L. Davydenko
Lutsk National Technical University, Lutsk, Ukraine

1 Introduction

Energy instability has led to the depletion of natural fuel and energy resources and the
devastating effects of climate change. Thus, the priority of sustainable development
of society is to ensure climate neutrality.

According to the Paris Agreement on Climate Change [1], the European Union had
set a goal of reducing greenhouse gas emissions by 40% by 2030. In [2] established
a new aim of reducing greenhouse gas emissions by at least 55% by 2030.

According to [3], more than 75% of all greenhouse gas emissions come from
energy production and use. The decarbonisation of the energy system is an important
step in meeting climate neutrality. Achieving these goals on the path to climate
(carbon) neutrality "requires an energy transition to clean energy and a much larger
share of RESs in the integrated energy system" [4]. According to [5], the share of
renewable sources in the EU energy complex should be 32% by 2030, and according
to the European Commission, this share should increase to 40% [6].

However, the decarbonisation of the economy requires coordinated planning and
operation of the energy system, taking into account the links between different energy
sources and consumption sectors [7]. This process involves the electrification of final
consumption sectors and, as a consequence, increasing demand for electricity [7].
Solar and wind energy, as well as the production of renewable energy at sea are
considered as sources of increased electricity needs [7]. At the same time, the inten-
sive construction of solar and wind power plants, which have an unstable generation,
causes a number of problems of both management and operation of the energy system
[8]. For instance, the intermittent nature of generation causes uncertainty in energy
supply and can lead to an imbalance of supply and demand [9, 10]. Therefore, in the
context of the growing share of renewable energy, the issues of efficiency of integra-
tion of RESs into the electricity grid, monitoring of renewable energy generation, the
coordination of operating modes of RESs and power systems to cover electricity load,
etc. are becoming increasingly acute. Providing the planning of renewable energy
generation and its control within the system of monitoring the modes of operation
of RESs will increase the efficiency of the energy system and its economy and reli-
ability. Creating a system for forecasting the generation of electricity from RESs is
an important means of optimizing the modes of operation of energy infrastructure,
management and ensuring the optimal functioning of the energy system.

2 Integration of Renewable Energy Sources into the Electricity System of Ukraine: Current Status, Tasks and Challenges

Ukraine has acceded to the Energy Community Treaty [11] and other European initiatives [12], in particular in the fields of energy production, transportation, supply and final consumption. By becoming a member of the Energy Community, Ukraine has committed itself to the implementation of basic acts of EU energy legislation on energy efficiency and the transition to clean energy [13–15]. Energy Strategy of Ukraine until 2035 [16] contains a number of tasks to meet Ukraine's commitments under the Energy Community Treaty, aimed at reforming the energy sector, optimizing and innovatively developing energy infrastructure, and ensuring sustainable development.

Among these tasks are the following [16]:

- further development of RES and growth of the share of renewable energy to the level of 12% of Total primary energy supply (TPES) and not less than 25%—by 2035;
- development of distributed generation and Smart Grid implementation;
- creation of a full-fledged electricity market in accordance with EU energy legislation, which provides for the introduction of a new model of electricity market operation. Launch of all market segments: the market of bilateral agreements; day-ahead market; intraday market; balancing market; ancillary services market.

Stimulating the construction of solar and wind power plants and the introduction of "green tariffs" contributes to the rapid development of renewable energy. As of August 1, 2021, the installed capacity of the renewable energy sector of Ukraine reached 8,877 MW (ed. including domestic SPPs) (Fig. 1) [17].

The reduction in the price of solar panels per unit, the cost of maintenance per installation compared to other renewable energy sources, as well as the expected service life of more than 20 years contributed to the growing share of PV-generation in the structure of RESs. The installed capacity of the industrial solar energy sector at the end of 2021 amounted to 6,351 MW [17]. At the same time, in 2021 the capacity of solar installations of private households increased by 156 MW. Thus, the cumulative installed capacity of domestic SPPs has increased to 933 MW (Fig. 2).

In 2021, the annual production of "green" electricity by all RESs power plants in Ukraine reached 10,023 million kWh, of which 230.5 million kWh accounted for wind farms in Ukraine (ed. which is 1,230 million kWh more than in 2020), and 6,053.9 million kWh were generated by national SSPs, including domestic SSPs (Fig. 3).

According to the Law of Ukraine №2019-VIII "On the Electricity Market" adopted in April 2017, in July 2019 a new wholesale electricity market was launched in Ukraine [13]. Thus, the country has moved from a pre-existing centralized single-buyer market model to a competitive liberalized model based on five distinct market
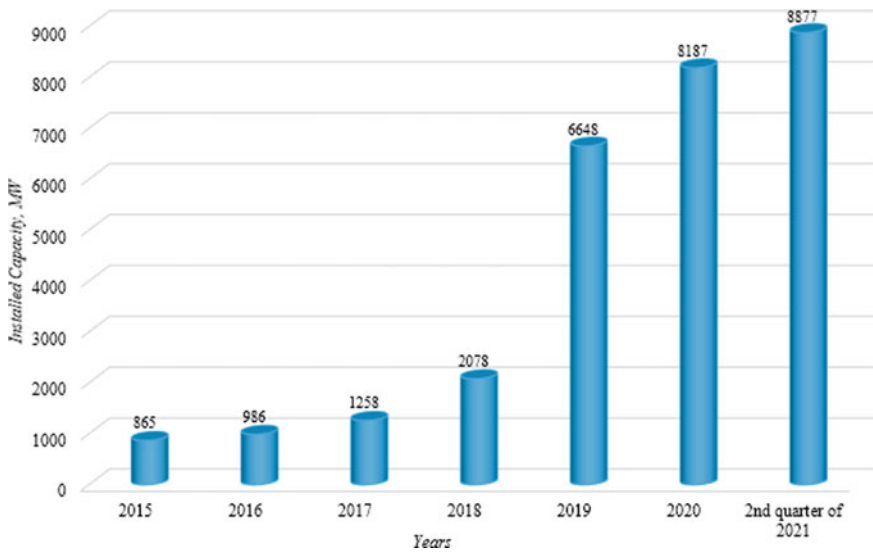
Fig. 1 Annual increase in the capacity of renewable energy sources in Ukraine
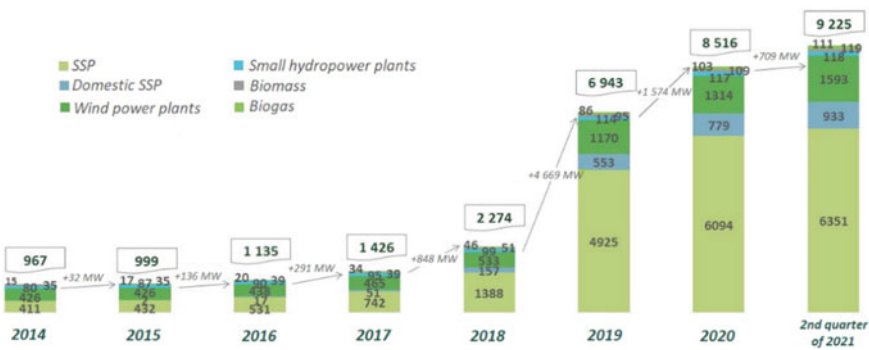
Fig. 2 Dynamics of growth of installed capacity of renewable energy facilities, MW (*Source* SAEE Ukraine, 2021)

segments: the market of bilateral agreements; day-ahead market; intraday market; balancing market; ancillary services market.

The use of RESs contributes to reducing the needs of the UES of Ukraine in the amount of balancing and regulatory capacity. The production of electricity by SPPs is quite flexible, which allows them to be adjusted to adapt to changing energy demand. At the same time, the growing share of solar energy sources, in particular solar installations of private households, causes a number of problems in terms of energy efficiency. The main reasons for the negative impact of solar generation on the electricity grid are interruptions and unpredictability due to dependence on solar
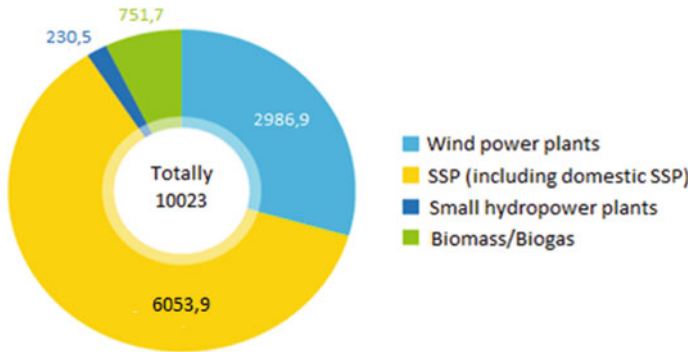
Fig. 3 Diagram of "green" electricity production in the renewable energy sector, by types, as of the end of 2021 in million kWh (source: The State Enterprise "Guaranteed Buyer")

radiation and weather conditions, as well as dispatching of generated energy [18, 19], and as a consequence of voltage fluctuations, low power quality and low stability [20]. To ensure the stable operation of the electricity system, it is necessary to plan the generation and demand of electricity, and forecasting the volume of renewable energy generation is an important step in this process. An energy production forecast, that provides information on how much energy a particular power plant will produce, can be useful for optimizing the marketing of renewable energy and, therefore, deploying system integration. Timely and accurate forecasts of solar electricity generation are necessary both for energy market participants engaged in the purchase or sale of energy, and for energy system operators who maintain the stability of the energy system [21]. The application of forecasting the volumes of photovoltaic generation at different time scales is the basis for achieving the balance of the grid [22], ensuring safe operation, efficient management and stability of the power system [9, 18]. As noted in [23], "reliable forecasting is key to several Smart Grid applications, such as optimal scheduling, demand response, grid regulation and intelligent energy management". The solar generation forecasting is an important part of the process of planning a sustainable power supply and covering the electrical load of power systems according to demand. The projected value of electricity generation volumes at the level of the SPP is necessary for coordination with the electricity network operator of the generation plan [8]. The solar generation forecast for the day ahead is an important point for placing proposals of the owner of the SPP on day-ahead market, as well as for optimizing electricity rates in day-ahead market and intraday market [8]. For small SPPs, solving the problem of generation forecasting is the cornerstone of sustainable development. As the contribution of green energy to the grid is constantly growing, the problem of building reliable models for forecasting energy production from such sources is becoming increasingly important. Accurate prediction of solar generation increases the reliability and cost-effectiveness of SPPs using.

3 Analysis of Factors Influencing Solar Generation

Solar photovoltaic energy is a function of solar radiation [25]. However, other environmental factors (temperature and relative humidity, wind speed, rainfall, length of daylight, cloudiness and amount of solar radiation) have a significant impact on the production of electricity by solar power plants. Changes in temperature and solar radiation can reduce solar energy generation by more than 20% [24]. In addition, different weather variables have different nature and significance of the impact on PV generation [19]. Moreover, the correlation of each variable with the amount of generated energy is different for different days [19]. The influence of various factors on the efficiency of solar panels and electricity generation of a SPP is considered in many studies. In particular, in [26, 27] the effect of changes in humidity on the performance of the solar panel was studied. In [28], the authors investigated the interdependence of dust accumulation, humidity and air velocity and their combined effect on photovoltaic performance. In [29] the influence of weather factors was studied, as well as fluctuations in radiation, which is strongly influenced by the shadow of the cloud. For this purpose, the spatial characteristics of clouds and the concentration of solid particles in the atmosphere moving in the wind direction were taken into account.

Factors influencing the efficiency of hourly forecast of the SSP generation include forecast horizon, local weather conditions, geographical location, data availability (e.g. volume, location, methods of obtaining and reliability of information), data quality (e.g. time consistency, accuracy, breakdown and correction of the territory coverage), etc.

Investigations of the dynamics of weather parameters (such as temperature, solar radiation, humidity, atmospheric pressure, wind direction and speed) and the SSP generation (Fig. 4) were performed to identify the relationship between them. The data set contained samples of measurements of the amount of electricity generation and weather parameters, which were recorded from July 1, 2020 to December 31, 2020. The measurements were performed for SSP in the village of Velyka Dymerka, Kyiv region.

Mainly the amount of generation is affected by *solar radiation*, W/m^2. The voltage of the solar cell depends on the light flux incident on it, namely: with increasing light, the voltage increases to a certain limit. In turn, the intensity of solar radiation depends on the *air temperature*, which directly affects the amount of heating panels. Most panels are designed to operate in temperatures from -40 to $+80\,°C$, and the lower the temperature, the higher the level of conversion. For instance, considering the 270 W panel, in hot summer at $+35\,°C$ it's power will be approximately 257 W, and in winter at $-20\,°C$ may be 298 W. This is due to the fact that as the temperature increases, the flow of electrons inside the cell increases, which causes an increase in current and voltage drop. The voltage drop is more than the increase in current. Therefore, the total power ($P = UI$) decreases, which reduces the efficiency of the panel. To numerically characterize the decrease in electricity generation with increasing solar panel temperature, manufacturers specify the value of the temperature coefficient. The temperature coefficient is a parameter that indicates how much the efficiency of
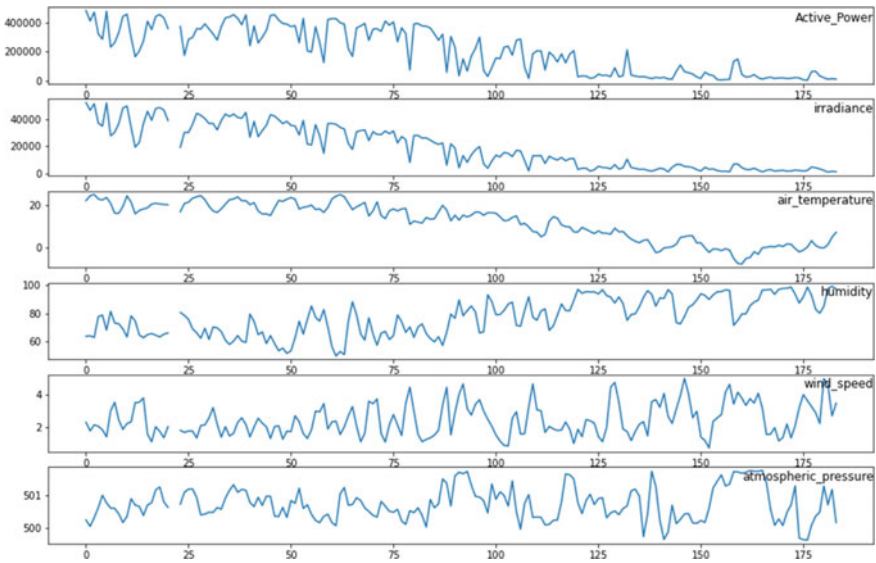
Fig. 4 Dynamics of changes in the active power of the Dymer solar power plant and influencing weather factors

the solar panel decreases with increasing air temperature by each degree. The value of this coefficient is obtained by the manufacturer experimentally and specified in the specifications. In summer, the own temperature of the panel can rise to 60−70 °C. On average, when the temperature rises by 20 °C, the power loss is about 10%.

Humidity has a great influence on the efficiency of solar panels. The generation of electricity from solar panels can be reduced to 15–30% depending on how high the humidity level is, as high humidity can form a layer of water on their surface. In this case, the probability of cloud formation, fog and scattering radiation also increases.

The next parameter that affects the amount of electricity generation is *wind speed*. By increasing the wind speed, more heat can be removed from the surface of the photocells. Also, higher air velocity reduces the relative humidity, which in turn leads to improved efficiency. Conversely, the wind raises dust and disperses it into the environment, which can lead to shading and poor performance of photovoltaic cells [30].

It is also necessary to note the possibility of the influence of *wind direction.* Depending on the angle and side of the wind blows the panels, the effect of wind speed on the efficiency of the panels may increase or decrease. The direction of the wind can also affect the shading of the panels from the deposition of dust or snow. If the wind blows in the direction of the panel, the snow will settle better on the surface than if it blows opposite to the slope of the panel.

It is a known that before bad weather (precipitation) the atmospheric pressure drops, and before clear (dry) weather—the pressure increases [10]. Short-term precipitation has small effect on efficiency. However, significant rainfall is usually character

in cloudy weather when radiation and, accordingly, generation in this situation are reduced. Atmospheric pressure by itself is not a factor that directly affects the level of electricity generation. But it has an indirect effect on the main factors. In general, depending on the increase or decrease of atmospheric pressure, the influence of temperature, wind and humidity on energy production can increase or decrease.

The study of the degree of influence of weather parameters on SSP generation was performed using correlation analysis. The cross-correlation coefficient was used to estimate the degree of relationship between the parameters [31]:

$$r_{xy} = \frac{\sum_{i=1}^{n}(x_i - \overline{x})(y_i - \overline{y})}{(n-1)s_x s_y} = \frac{\sum_{i=1}^{n}(x_i - \overline{x})(y_i - \overline{y})}{\sqrt{\sum_{i=1}^{n}(x_i - \overline{x})^2 \sum_{i=1}^{n}(y_i - \overline{y})^2}}, \qquad (1)$$

where $\overline{x}$, $\overline{y}$—the average values for the sample x and y, s_x and s_y—unbiased (adjusted) estimate of the standard deviation for x and y.

Graphs of correlations between weather factors and the active power of the solar power plant are shown in Fig. 5.

Three parameters have positive correlations with the active power generation. Such parameters are solar radiation, air temperature and wind speed. And relatively humidity has negative correlation. It should be noted that the wind direction correlates directly with atmospheric pressure. This means that the value change of one parameter almost completely depending on the value of another. In other words, these factors in the model will be duplicated. And this will increase the complexity of the model, may increase the error of the model and increase the possibility of retraining. Therefore, the "wind speed" parameter is excluded from the model.

4 Methodological Bases of Solar Generation Forecasting

4.1 Solar Photovoltaic Generation Forecasting Methods: A Review

Many solutions have been proposed to solve the problem of solar generation forecasting. According to the length of the forecast period, there are methods of short-term, medium-term and long-term forecasting of solar generation. In terms of forecasting strategies, there are three groups of methods [21, 23, 32–34]: physical; statistical and hybrid.

Physical methods for estimating the generated power include the construction of a physical model of the photovoltaic module, or PV performance model, taking into account the models of radiation and temperature of photovoltaic modules in combination with weather forecast data. The main advantage of these methods is
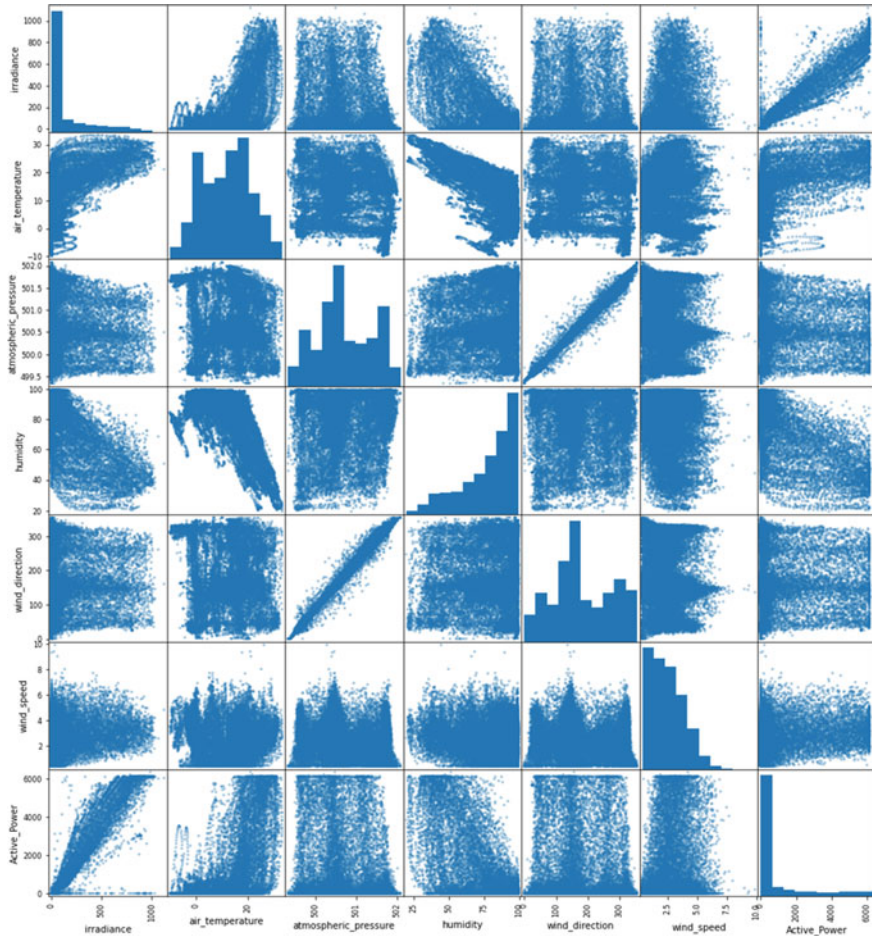
Fig. 5 Correlation of weather factors and solar generation

independence from historical data [23, 32]. However, the efficiency of the predictive model of PV performance significantly depends on the efficiency of numerical weather forecasting [32], and the process of physical modeling is complex [21].

Statistical methods are based on the use of large sets of historical data on weather factors and the generation of solar electricity to identify certain patterns and relationships in these data sets. They do not require internal information about the state of the system to build a model [33]. Statistical methodologies are better and easier to implement [23], they can have higher forecasting accuracy [32] than physical models. Statistical approaches are widely used for short-term forecasting of solar electricity generation [23].

Hybrid models involve a combination of physical and statistical modeling strategies.

Existing approaches to solar energy forecasting based on statistical methods belong to two groups [20, 21]: (1) methods based on a structural approach and (2) methods based on a time approach. The first group includes methods that apply the principle of "indirect forecasting", which is based on historical data on weather factors that affect the performance of the photovoltaic battery. These are the so-called multivariate forecasting methods. The forecast of an endogenous variable is based on exogenous variables (one or more) that have a significant impact on the endogenous variable. The second group includes methods based on the principles of "direct forecasting", which directly predicts the power of PV based on historical data from the generation of solar energy. These are the so-called one-dimensional forecasting methods. The forecast of an endogenous variable is based on previous values of the same variable (i.e. time series).

It should be noted that forecasting energy production is a dynamic process. Forecasting for the next 48 h requires constant updating of information on weather factors, pre-production of energy to ensure proper calibration of the system. However, the control of solar power plant energy production depends not only on the uncontrolled energy resource, but also on the management strategies of the power plant. The implementation of management strategies depends on technical constraints, price volatility, user demand and etc. It should be noted that all the necessary information is not always available, which makes forecasting renewable energy difficult to control. In addition, to forecast production taking into account weather conditions, it should be performed a weather forecast, the error of which affects the final result. One-dimensional methods are simpler and cheaper. For their implementation it is enough to have only the value of the time series of solar energy and do not need to perform additional measurements of weather factors that require maintenance of weather stations or other measuring instruments (except solar meters) [35]. Also, according to the authors [23, 35], one-dimensional methods of solar energy forecasting work better and are more efficient, especially in conditions of dynamic control, which requires short-term forecasting of solar energy generation [35].

4.2   Application of Time Series for Solar Generation Forecast

Time series forecasting methodology has wide practical application in the energy field [21]. There are many examples in the literature of the use of time series models for predicting solar generation [18, 21, 24, 25, 35].

The approach to time series forecasting is based on the following assumption: some knowledge can be obtained from a series that describes the initial process, and based on this knowledge to build a process model to predict future process behavior. The primary objective of time series analysis is to develop mathematical models that provide plausible descriptions from sample data.

The time series forecasting is solved using classical methods, such as autoregression and moving average methods [18, 36–38], and methods of machine learning and artificial intelligence [10, 24, 38].

Among the classical methods of time series forecasting, the moving average autoregression model (ARMA) is widely used [36, 37]. The moving average model uses current and previous white noise values for forecasting. ARMA contains two parts, autoregressive (AR) and moving average (MA). White noise is created from forecast errors or residuals when observations become available. The ARMA model requires a lot of preliminary data. The main requirement for the application of the ARMA model is the requirement of stationary time series.

However, the time series of solar electricity generation have seasonal and non-seasonal variations and are non-stationary [24, 25]. One of the most commonly used methods for predicting nonstationary time series is the Box-Jenkins model—ARIMA (integrated model of autoregression-moving average). In the ARIMA model, the predicted value is defined as a linear combination of past values (simulated by AR autoregression) and noise (simulated by the moving average (MA)), and the number of differences to convert the time series into a stationary simulated integrated (I) part [35]. The advantage of the ARIMA model is its simplicity. To apply the ARIMA model to non-stationary time series, the conversion of time series data into a stationary series is performed by taking the difference of some order from the original values of the time series. This approach was used in [24, 36] to predict the generation of solar energy.

In [39] the method of forecasting for several months ahead (one, two and three months) the average monthly time series of global solar generation and forecasting based on solar radiation data is presented. ARMA and ARIMA models are used to predict the nearest values of the global time series of solar radiation. Both models are applicable to stationary and non-stationary time series of solar radiation data.

To identify and take into account trends and seasonality that occur in the time series of solar generation, use the seasonal extension of the ARIMA model—the seasonal model of autoregressive integrated moving average (SARIMA). SARIMA models have received considerable attention for the formation of time series forecasts for RES due to their good ability to identify seasonality [21].

The SARIMA model is used to predict the production of energy from solar power plants, both small [18] and large installed capacity [38].

4.3 Methodology of Construction of Seasonal Model of Moving Average Autoregression

Time series models are data-driven models, ie, learn or obtain useful information from a set of historical data to predict the outcome [20]. The purpose of the forecasting process is to determine the amount of solar energy generation one step ahead based on a sample of historical data. Assume that there is a function that can be applied to both past and future data [35]:

$$\hat{p}(t) = f(p(t-1), \ p(t-2), \ldots),$$ (2)

where $p(t)$ is the actual power generated by the solar power plant at the time t, $\hat{p}(t)$ is a forecast of energy produced by a solar power plant at a time t, $p(t-1)$ indicates the power output for the previous time $(t-1)$.

Time series consist of four components: seasonal, trend, cyclical and random. Seasonal components are the result of systematic and calendar effects and are defined as repetitive or predictable fluctuations over a period of time that include natural conditions such as weather fluctuations. Due to components such as trend and seasonality, real time series are usually non-stationary. Non-stationary time series data cause errors and unsatisfactory forecasting results. Because seasonal components can affect some off-season characteristics of a time series and some trends in it, seasonal adjustments are applied to the process. Seasonal adjustment is the evaluation and then the removal of seasonal components.

The SARIMA model is the introduction of seasonal terms into the ARIMA model, which are denoted as SARIMA (p, d, q) (P, D, Q) s, where p, d, and q represent the parameters of the non-seasonal part of the model. P, D and Q represent the parameters of the seasonal part of the model, and s is the seasonal period. Values (p, d, q) (P, D, Q) s are used to parameterize the model. The parameters p and P characterize the autoregressive part of the model (respectively non-seasonal and seasonal components) and allow us to take into account in the model the effect of past values in our model. Parameters d and D characterize the integral part of the model and take into account the amount of differentiation (i.e. the number of moments of the past time that must be subtracted from the current value) to apply to the time series. Parameters q and Q characterize the part of the moving average model and allow to establish the error of the model as a linear combination of error values observed in previous moments in the past.

The following formula is used to build the model:

$$\begin{cases} \phi(B)\nabla^d X_t = \Theta(B)\varepsilon_t; \\ E(\varepsilon_t) = 0, \ Var(\varepsilon_t) = \sigma^2, \ E(\varepsilon_t\varepsilon_x) = 0, \ s = 24; \\ E(X, \varepsilon_t) = 0, \ \forall s < t, \end{cases} \tag{3}$$

where $\nabla^d = (1-B)^d$, B is the delay operator, $\nabla^d X_t$ is time series after the difference of the final order, ε_t is the sequence of white noise, $\Theta(B)$ is a stable and reversible polynomial of the moving smoothing coefficient of the ARMA (p, q) model, $\phi(B)$ is the polynomial of the autoregression coefficient of the stationary and reversible ARMA (p, q) model.

Preliminary observations are described by a polynomial:

$$X^t = \varepsilon_t + \psi_1\varepsilon_{t-1} + \psi_2\varepsilon_{t-2} + ... = \varphi(B)\varepsilon_t, \tag{4}$$

where ψ_1, ψ_2 are determined by the equation:

$$\phi_B(1-B)^d\psi(B) = \theta(B). \tag{5}$$

If $\phi^*(B)$ defined as a generalized autocorrelation function, we have

$$\phi^*(B) = \psi(B)(1-b)^d = 1 - \phi_1 B - \phi_2 B - \dots \quad . \tag{6}$$

Values ψ_1, ψ_2 satisfy the equation:

$$\begin{cases} \psi_1 = \phi_1 - \theta_1; \\ \psi_2 = \phi_1 \psi_1 + \phi_2 - \theta_2; \\ \dots, \\ \psi_j = \phi_1 \psi_{j-1} \dots + \phi_{p+d} \psi_{j-p+d} - \theta_j. \end{cases} \tag{7}$$

In this formula:

$$\psi_j = \begin{cases} 0, \ j < 1; \\ 1, \ j = 0, \end{cases}$$

where j is the autoregression coefficient, θ_j is the moving average coefficient.

Then the forecast value of SSP generation can be written as follows:

$$X_{i+1} = (\varepsilon_{i+1} + \psi_i \varepsilon_{i+l-1} + \dots + \psi_{l-1} \varepsilon_{t+1}) + (\psi_i \varepsilon_t + \psi_{l+1} \varepsilon_{i-1} + \dots). \tag{8}$$

Therefore, the SARIMA model is expressed by the formula:

$$\nabla^d \nabla^D_s x_t = \frac{\Theta(B)\Theta_s(B)}{\phi(B)\phi_s(B)} \varepsilon_t, \tag{9}$$

where

$$\phi_s(B) = 1 - \varphi_1 B^s - \dots - \varphi_p B^{ps}, \ \Theta(B) = 1 - \theta_1 B - \dots - \theta_q B^q$$
$$\Theta_s(B) = 1 - \theta_1 B^s - \dots - \theta_p B^{QS}$$

Choosing the optimal model is one of the problems that arise during forecasting. The choice of the optimal structure of the model is performed on the basis of analysis of the values of the information criterion Akaike (AIC), Schwartz Bayes test (VIC), the residual sum of squares (RSS) [24]. The choice is based on determining the quality of the statistical model on the data set to determine which set of model parameters provides the best performance.

The constructed model should be tested for adaptability. This step is to check the compliance of the remnants of the model with white noise. If the residuals of the model are a sequence of white noise, then the construction of the model fully reflects the information contained in the data. In this case, the seasonal model is adaptive. Otherwise, the model must be optimized and these model parameters reconfigured.

The forecasting process involves finding an estimate of p(t) that optimizes the performance criterion (or forecast error). The effectiveness of the forecast model is measured by various indicators associated with forecast error. The following key indicators are used to assess the performance of the model [21, 35]: Mean Absolute Error (MAE), Root Mean Square Error (RMSE) and R-squared. These criteria are useful for comparing the predictive power of models of different structures.

5 Results of Modeling and Verification of Forecast Accuracy

5.1 SARIMA Models for Short-Term PV Generation Forecasting

Seasonality can be determined by regularly located peaks of the curve or flatness with the same value during this period. The change in the value of the time series may also be associated with a change in the component of the time series trend. In some cases, the trend (or irregular components) may dominate over the seasonal components, and then it is impossible to detect the small seasonality that is represented in the time series (Fig. 6).

The model will be presented in the form of SARIMA (p, d, q) × (P, D, Q) s, where (p, d, q) are non-seasonal parameters, respectively, autoregressive part of the model, integral part of the model and part of the moving average model; (P, D, Q) are the same in terms of part of the model, but apply to the seasonal component of the time
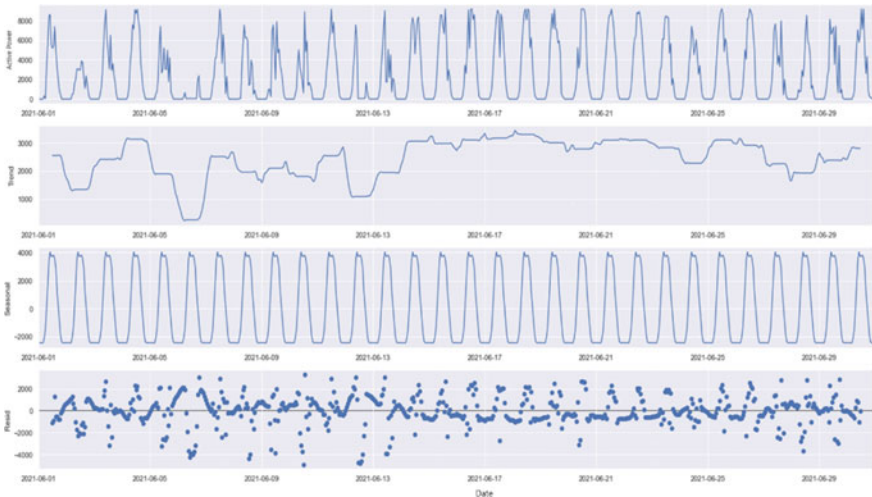
Fig. 6 Annual solar power plant generation with seasonal time series decomposition

Table 1 Seasonal ARIMA parameter combinations

ARIMA (p, d, q) combinations considered	Seasonal parameters (P, D, Q, S) considered
(0, 0, 0)	(0, 0, 0, 24)
(0, 0, 1)	(0, 0, 1, 24)
(0, 1, 0)	(0, 1, 0, 24)
(0, 1, 1)	(0, 1, 1, 24)
(1, 0, 0)	(1, 0, 0, 24)
…….	……….

series; s is the periodicity of the time series (s = 4 for quarterly periods, s = 12 for annual periods, s = 24 for daily periods).

The forecast was made for two days ahead.

The study used the "grid search" method to iteratively investigate different combinations of parameters. A new seasonal ARIMA model with SARIMA function was selected for each combination of parameters. After researching the full range of parameters, the optimal set of parameters was the one that gave the best performance for the criteria of interest. Table 1 shows the different combinations of parameters that needed to be evaluated: it was now possible to use the triplets of parameters defined above to automate the learning process and evaluate ARIMA models on different combinations.

When evaluating and comparing statistical models with different parameters, each of them can be ranked against each other based on how it corresponds to the data or its ability to accurately predict future data points. The choice of a more efficient model was based on the assessment of the quality of the model on the data set according to the information criterion Akaike (AIC) [24]. The AIC (Akaike Information Criterion) value was used, which is convenient to rotate with ARIMA models installed using the statsmodels Python 3.8 module. The AIC measures how well the model matches the data, taking into account the overall complexity of the model. A model that matched the data very well using a large number of functions was assigned a higher AIC score than a model that had fewer functions to achieve the same match. Therefore, there was interest in finding the model that gives the lowest AIC value (Table 2).

The modeling results are shown in Figs. 7 and 8. The best model with parameters SARIMA (1, 0, 1) × (2, 1, 0, 24) is presented in Fig. 8.

After selecting the model with the best parameters, the residual graphs were checked to verify the correctness of the model. The best forecasting method has a minimum of information that will remain in the residuals, if any.

At this stage, residual diagnostics, standard residue, histogram plus estimated density, normal Q−Q and correlogram were checked for model analysis (Fig. 9).

The coincidence of the residual points with the normal on the graph "Normal Q−Q" indicates the absence of systematic deviation. In addition, the Correlogram shows that there is no autocorrelation in the residues, so they are actually white noise. Therefore, these residues are uncorrelated and have a zero average. This suggests that the model is adaptive and the model's relevance to historical data is sufficient.

ARIMA (p, d, q) combinations considered	Seasonal parameters (P, D, Q, S) considered	AIC
(0, 0, 0)	(2, 1, 0, 24)	13,105.512
(2, 0, 0)	(1, 1, 0, 24)	12,954.057
(0, 0, 0)	(0, 1, 0, 24)	13,388.464
(1, 0, 1)	**(2, 1, 0, 24)**	**12,826.840**
(0, 0, 0)	(2, 1, 0, 24)	13,104.847
…….	……….	

Table 2 Seasonal ARIMA parameter combinations with AIC

Bold represents the best ARIMA model according to the AIC criterion
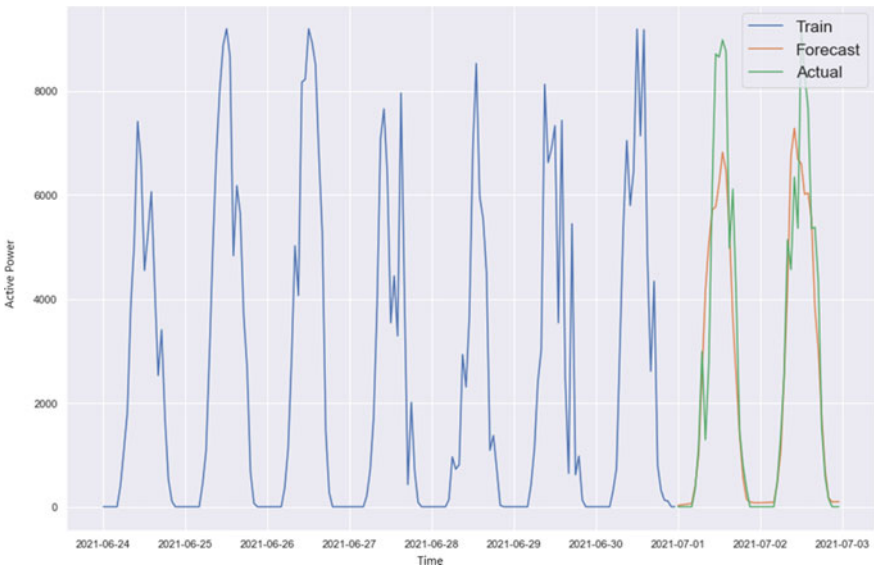
Fig. 7 Model with SARIMA parameters: $(1, 1, 2) \times (2, 1, 2, 24)$

5.2 Verification of the SARIMA Model Forecast Accuracy

The following equations were used to evaluate the effectiveness of each model:

$$MAE = \frac{1}{N} \sum_{i=1}^{N} |\hat{y}_i - y_i|; \tag{10}$$

$$RMSE = \sqrt{\frac{1}{N} \sum_{i=1}^{N} (y_i - \hat{y}_i)^2}; \tag{11}$$
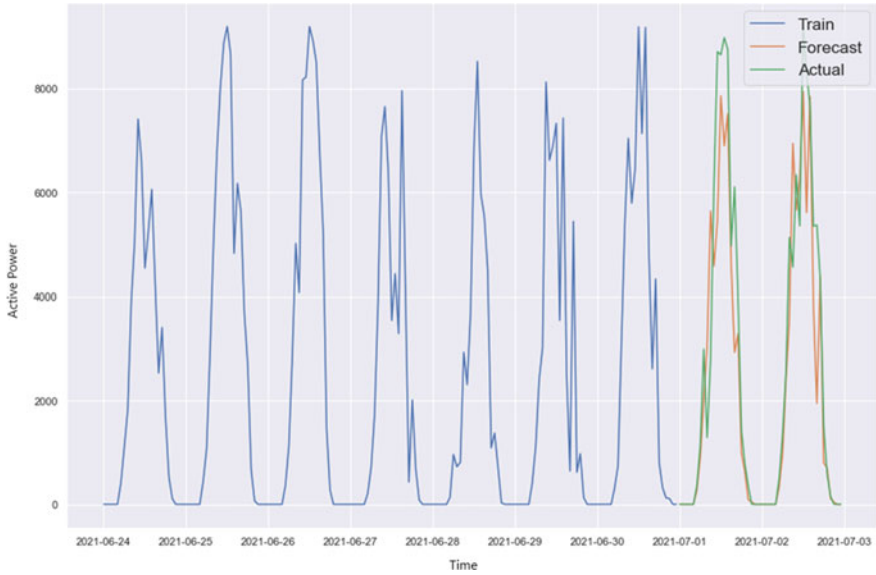
Fig. 8 Model with SARIMA parameters (1, 0, 1) × (2, 1, 0, 24)
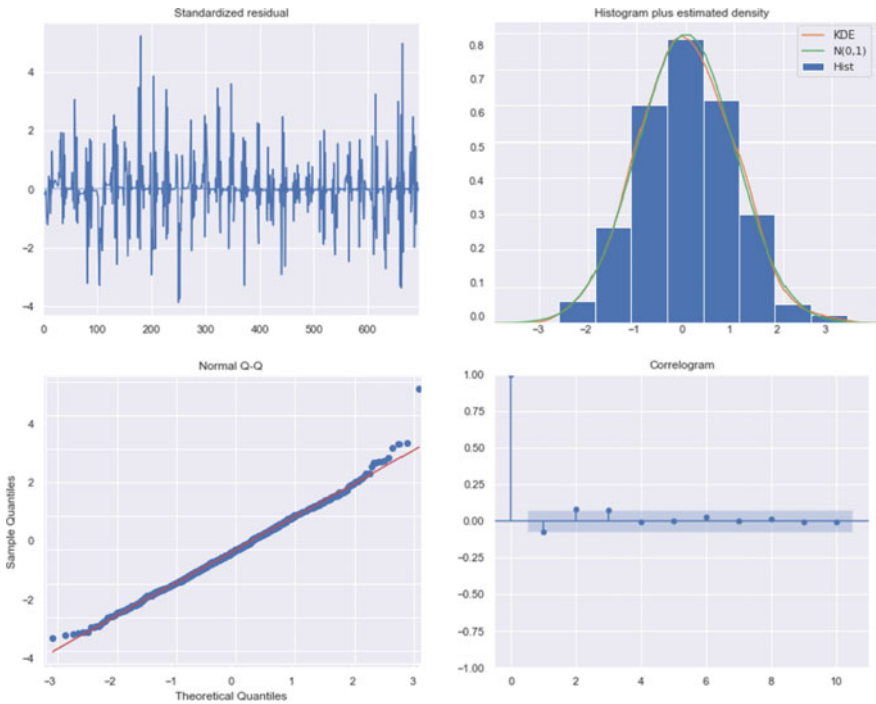
Fig. 9 Residual graphs of the SARIMA model (1, 0, 1) × (2, 1, 0, 24)

Table 3 Comparison of errors criteria for the results obtained for each of the test from the solar radiation forecast

Model	MAE, W	RMSE, W	R^2, abs. un
SARIMA (1, 1, 2) × (2, 1, 2, 24)	315.12	1245	0.87
SARIMA (1, 0, 1) × (2, 1, 0, 24)	258.57	1259	0.92

$$R^2 = 1 - \left(\sum_{i=1}^{N} \left(y_i - \hat{y}_i \right)^2 / \left(y_i - \overline{y}_i \right)^2 \right), \tag{12}$$

where N is the sample size; y_i is the actual value; $\hat{y}_i$ is the predicted value; $\overline{y}$ is the sample mean.

The results of the comparison of the best selected SARIMA models based on the values of MAE, RMSE and R^2 are shown in Table 3.

The results show that the SARIMA (1, 0, 1) × (2, 1, 0, 24) model performed better than SARIMA (1, 1, 2) × (2, 1, 2, 24) in data prediction, with the value of R^2 of 0.92, the value of MAE of 258.57 W and the value of RMSE of 1259 W. Lower the value of MAE and the value of R^2 closer to 1, indicate a correlation between observed and predicted dataset.

6 Conclusions

This chapter proposes a time series approach for forecasting the generation of solar power plants. The dynamic series of solar energy generation is characterized by rigid seasonality, so the optimal solution is to use an autoregressive model with a seasonal component—SARIMA. This model allows us to take into account trends and identify seasonal fluctuations in day-ahead generation, which perfectly meets the needs of the electricity day-ahead market.

The use of the proposed model SARIMA (1, 0, 1) × (2, 1, 0, 24) reduces the average forecast error for the day ahead to 2.58% from 3.15% and has a correlation coefficient R2 of 0.92. The developed mathematical models are implemented in the form of a computer program.

References

1. Council of the European Union: Council Decision (EU) 2016/590 of 11 April 2016 on the signing, on behalf of the European Union, of the Paris Agreement adopted under the United Nations Framework Convention on Climate Change. Official Journal of the European Union. **L 103/1**, 1–2 (2016). http://data.europa.eu/eli/dec/2016/590/oj

2. European Commission, Secretariat-General: Communication from the Commission to the European Parliament, the Council, the European Economic and Social Committee and the Committee of the Regions. 'Fit for 55': delivering the EU's 2030 Climate Target on the way to climate neutrality. European Commission Brussels. **COM(2021) 550 final** (2021)

3. European Commission, Secretariat-General: Communication from the Commission to the European Parliament, the European Council, the Council, the European Economic and Social Committee and the Committee of the Regions. The European Green Deal. European Commission. Brussels. **COM(2019) 640 final** (2019)

4. European Commission, Directorate-General for Energy: Commission Staff Working Document Impact Assessment Report. Accompanying the Proposal for a Directive of the European Parliament and the Council amending Directive (EU) 2018/2001 of the European Parliament and of the Council, Regulation (EU) 2018/1999 of the European Parliament and of the Council and Directive 98/70/EC of the European Parliament and of the Council as regards the promotion of energy from renewable sources, and repealing Council Directive (EU) 2015/652. European Commission. Brussels. **SWD(2021) 621 final** (2021)

5. European Parliament, Council of the European Union: Directive (EU) 2018/2001 of the European Parliament and of the Council of 11 December 2018 on the promotion of the use of energy from renewable sources (Text with EEA relevance). PE/48/2018/REV/1 Official Journal of the European Union. **L 328/82**, 82–209 (2018). http://data.europa.eu/eli/dir/2018/2001/oj

6. European Commission, Directorate-General for Energy: Commission Staff Working Document Impact Assessment Report. Accompanying the Proposal for a Directive of the European Parliament and of the Council on common rules for the internal markets in renewable and natural gases and in hydrogen (recast) Proposal for a Regulation of the European Parliament and of the Council on the internal markets for renewable and natural gases and for hydrogen (recast). European Commission. **SWD(2021) 455** (2021)

7. European Commission, Directorate-General for Energy: Communication from the Commission to the European Parliament, the Council, the European Economic and Social Committee and the Committee of the Regions. Powering a climate-neutral economy: An EU Strategy for Energy System Integration. European Commission. **COM(2020) 299 final** (2020)

8. Mitra, I., Heinemann, D., Ramanan, A., et al.: Short-term PV power forecasting in India: recent developments and policy analysis. Int. J. Energy Environ. Eng. (2022). https://doi.org/10.1007/s40095-021-00468-z

9. Kim T, Kim J.: A regional day-ahead rooftop photovoltaic generation forecasting model considering unauthorized photovoltaic installation. Energies. **14**(14), 4256, 1–23 (2021). https://doi.org/10.3390/en14144256

10. Miroshnyk, V., Shymaniuk, P., Sychova, V.: Short term renewable energy forecasting with deep learning neural networks. In: Power Systems Research and Operation. Studies in Systems, Decision and Control. vol. 388, Springer, Cham, (2022). https://doi.org/10.1007/978-3-030-82926-1_6

11. The Verkhovna Rada of Ukraine: the Law of Ukraine.: "On Ratification of the Protocol on Accession of Ukraine to the Treaty establishing the Energy Community" № 2787-VI. (Ukr) (2010). https://zakon.rada.gov.ua/laws/show/2787-17

12. The Verkhovna Rada of Ukraine: the Law of Ukraine.: "On Ratification of the Association Agreement between Ukraine on the one part, and the European Union and the European Atomic Energy Community and their member states on the other" № 1678-VII. (Ukr) (2014). https://zakon.rada.gov.ua/laws/show/en/1678-18

13. The Verkhovna Rada of Ukraine: the Law of Ukraine "On Electricity Market" № 1931-IX. (Ukr) (2017) https://zakon.rada.gov.ua/laws/show/2019-19

14. The Verkhovna Rada of Ukraine: the Law of Ukraine "About alternative energy sources". (Ukr) (2003). https://zakon.rada.gov.ua/laws/show/555-15

15. The Verkhovna Rada of Ukraine: the Law of Ukraine "On Energy Efficiency". (Ukr) (2022). https://zakon.rada.gov.ua/laws/show/1818-20

16. The Cabinet of Ministers of Ukraine: Energy Strategy of Ukraine for the Period Up to 2035 "Security, Energy Efficiency, Competitiveness". № 605-p. (Ukr) (2017). https://zakon.rada.gov.ua/laws/card/605-2017-%D1%80

17. State Agency for Energy Efficiency and Energy Saving of Ukraine: Statistics on the development of renewable electricity at the end of the first half of 2021. (Ukr) (2021). https://saee.gov.ua/uk/news/3930

18. Kushwaha, V., Pindoriya, N.M.: Very short-term solar PV generation forecast using SARIMA model: a case study. In: 2017 7th International Conference on Power Systems (ICPS), pp. 430–435. (2017). https://doi.org/10.1109/ICPES.2017.8387332

19. Acharya, S.K., Wi, Y.-M., Lee, J.: Day-ahead forecasting for small-scale photovoltaic power based on similar day detection with selective weather variables. Electronics 9(7), 1117 (2020). https://doi.org/10.3390/electronics9071117

20. Gupta, P., Singh, R.: PV power forecasting based on data-driven models: a review. Int. J. Sustain. Eng. 14(6), 1733–1755 (2021). https://doi.org/10.1080/19397038.2021.1986590

21. Basmadjian, R., Shaafieyoun, A., Julka, S.: Day-ahead forecasting of the percentage of renewables based on time-series statistical methods. Energies 14(21), 7443 (2021). https://doi.org/10.3390/en14217443

22. Inman, R.H., Pedro, H.T.C., Coimbra C.F.M.: Solar forecasting methods for renewable energy integration. Progress in Energy and Combustion Sci. 39(6), 535–576 (2013). https://doi.org/10.1016/j.pecs.2013.06.002

23. Massucco, S., Mosaico, G., Saviozzi, M., Silvestro, F.A.: Hybrid technique for day-ahead PV generation forecasting using clear-sky models or ensemble of artificial neural networks according to a decision tree approach. Energies 12(7), 1298 (2019). https://doi.org/10.3390/en12071298

24. Fara, L., Diaconu, A., Craciunescu, D., Fara, S.: Forecasting of energy production for photovoltaic systems based on ARIMA and ANN advanced models. Int. J. Photoenergy. (2021) https://doi.org/10.1155/2021/6777488

25. Ghofrani, M., Alolayan, M.: Time series and renewable energy forecasting. time series analysis and applications. London. United Kingdom: IntechOpen (2017). https://doi.org/10.5772/intechopen.70845

26. Panjwani, M.K., Narejo, B.G.: Effect of humidity on the efficiency of solar cell (photovoltaic). Int. J. Eng. Res. General Sci. 2(4), 499–503 (2014)

27. Park, N.C., Oh, W.W., Kim, D.H.: Effect of temperature and humidity on the degradation rate of multicrystalline silicon photovoltaic module. Int. J. Photoenergy (2013). https://doi.org/10.1155/2013/925280

28. Mekhilef, S., Saidur, R., Kamalisarvestani, M.: Effect of dust, humidity and air velocity on efficiency of photovoltaic cells. Renew. Sustain. Energy Rev. 16(5), 2920–2925 (2012). https://doi.org/10.1016/j.rser.2012.02.012

29. Kim, B., Suh, D.A.: Hybrid spatio-temporal prediction model for solar photovoltaic generation using numerical weather data and satellite images. Remote Sensing. 12(22), 3706 (2012). https://doi.org/10.3390/rs12223706

30. Matushkin, D., Bosak, A., Kulakovskyi, L.: Analysis of factors for forecasting electric power generation by solar power plants. Power Eng.: Econo. Technique Ecol. 4, 64–69 (2020)

31. Taylor, R.: Interpretation of the correlation coefficient: a basic review. J. Diagnos. Med. Sonography. 6(1), 35–39 (1990). https://doi.org/10.1177/875647939000600106

32. Sangrody, H., Zhou, N., Zhang, Z.: Similarity-based models for day-ahead solar PV generation forecasting. IEEE Access. 8, 104469–104478 (2020). https://doi.org/10.1109/ACCESS.2020.2999903

33. Al-Dahidi, S., Muhsen, H., Sari, M.S., Alrbai, M., Louzazni, M., Omran, N.: An adaptive approach-based ensemble for 1 day-ahead production prediction of solar PV systems. Adv. Mech. Eng. 14, 3 (2022). https://doi.org/10.1177/16878132221089436

34. Ying, Y., Tianyang, Y., Weiguang, Z., Xianhui, Z.: Kalman filter photovoltaic power prediction model based on forecasting experience. Front. Energy Res. **9**, 682852 (2021). https://doi.org/10.3389/fenrg.2021.682852
35. Majidpour, M., Nazaripouya, H., Chu, P., Pota, H.R., Gadh, R.: Fast univariate time series prediction of solar power for real-time control of energy storage system. Forecasting **1**(1), 107–120 (2019). https://doi.org/10.3390/forecast1010008
36. Atique, S., Noureen, S., Roy, V., Subburaj, V., Bayne, S., Macfie, J.: Forecasting of total daily solar energy generation using ARIMA: A case study. In: Proceedings of the 2019 IEEE 9th Annual Computing and Communication Workshop and Conference (CCWC). pp. 114–119. (2019). https://doi.org/10.1109/CCWC.2019.8666481
37. Alsharif, M.H., Younes, M.K., Kim, J.: Time series ARIMA model for prediction of daily and monthly average global solar radiation: the case study of Seoul. South Korea. Symmetry. **11**(2), 240 (2019). https://doi.org/10.3390/sym11020240
38. Sharadga, H., Hajimirza, S., Balog, R.S.: Time series forecasting of solar power generation for large-scale photovoltaic plants. Renew. Energy. **150**, 797–807 (2020). https://doi.org/10.1016/j.renene.2019.12.131
39. Belmahdi, B., Louzazni, M., Bouardi, A.E.: One month-ahead forecasting of mean daily global solar radiation using time series models. Optik. **219** (2020). https://doi.org/10.1016/j.ijleo.2020.165207

Research and Development of Means of Automated Monitoring of Time-Synchronization Devices of Power Systems

Olexandr Samkov ⓘ **, Valerii Koval** ⓘ **, Vitaliy Lysenko** ⓘ **, Vyacheslav Vakas** ⓘ **, and Oleksandr Osinskyi** ⓘ

Abstract The ways to increase the reliability of time-synchronization signals of power systems are considered. The features of the development, research, and implementation of a system for automated multi-channel monitoring of time-synchronization devices are presented. The necessity of simultaneous measurements of several signals of time-synchronization devices and the use of IP technologies for the transmission of digital measurement data is determined. The description of the developed schemes of the multi-channel monitoring device, which includes: LPC2378 microcontroller, programmable logic chips "ALTERA", electronic elements of the RS-232 interfaces, Ethernet, is presented. Theoretical and probabilistic studies of the stability of characteristics of multi-channel monitoring device in real operating conditions on the objects of electric power networks are carried out. The influence of changes in the ambient temperature, supply voltage, frequency-dependent parameter, and frequency of the time-synchronization signal on the variable of deviation of pulse duration of the finite signal of single vibrator from the nominal value are considered. Analytical dependencies were obtained to determine the estimation of the actual value and confidence area for the deviation of the variable of pulse duration of the finite signal of single vibrator in the real operating conditions of the device. The actual operating variable of the deviation of pulse duration of the finite signal of single vibrator and the conditions of optimal temperature stability of the device for multi-channel monitoring of time-synchronization signals of power systems are determined. Laboratory samples of functional parts and a prototype of multi-channel monitoring device were made; their adjustment and testing were performed. Experimental studies were conducted using the receivers of the GPS satellite navigation system, which confirmed technical capability of the device to carry out a reliable real-time monitoring of four time-synchronization signals

O. Samkov (✉) · O. Osinskyi
Institute of Electrodynamics of the National Academy of Sciences of Ukraine, Kyiv, Ukraine
e-mail: samkov@ied.org.ua

V. Koval · V. Lysenko
National University of Life and Environmental Sciences of Ukraine, Kyiv, Ukraine

V. Vakas
Private Joint Stock Company "Kyivstar", Kyiv, Ukraine

simultaneously. The use of the obtained digital monitoring data allows to improve the quality of time-frequency support and, as a result, to increase the reliability and energy efficiency of SMART Grid power systems.

1 Introduction

Reliability and energy efficiency of power systems depend on real-time control processes [1–7]. A time uncertainty in power grids is supposed to be solved with the help of time-synchronization devices, which generate the appropriate signals. According to the SOU NPC 20.261:2021 standard "The technical policy of the NPC "Ukrenergo" in the field of development and operation of main and interstate power networks", time synchronization should be performed both at substations with out-of-date equipment, and at new substations [8]. Also, a similar time synchronization should be performed in the automated systems of technological processes control of 220–750 kV substations of UES of Ukraine [9]. The problem of time-synchronization signals generation, and the problem of ensuring control and monitoring of their quality indicators are important [1, 8, 9].

One of the functions, which should be performed by the automated systems of technological processes control of substations, is a diagnostics of the time-synchronization devices, i.e. a set of methods and means for determining their technical condition according to the Technical policy of the private joint-stock company "National power company" "Ukrenergo" (NPC "Ukrenergo") [8, 9]. Moreover, the SOU NPC 20.261:2021 standard states that the compliance with Technical policy requirements and provisions is mandatory not only for NPC "Ukrenergo", but also "for research, design and survey, repair, construction-assembly, and adjusting organizations that provide services to ensure the functioning, operation, and development of the main and interstate power networks, as well as other business entities engaged in the distribution and production of electricity (electricity entities) in accordance with the contractual obligations" [8]. Given the above, in the process of solving the formulated problem, it is important to conduct research and develop the tools for automated monitoring of time-synchronization devices of power systems.

2 Problem Formulation

A general approach to the development of technologies for diagnosing the quality of functioning of power generation sources, systems of transmission, conversion,

distribution and consumption of electrical energy, and improving their energy efficiency, is based on the global and national experience in the development of electrical complexes, process control tools for substations of electric power networks, devices of synchronization signal transmission and generation [1–4, 10–23]. In the digital telecommunications systems, at the digital substations of SMART Grid power networks, synchronization signals must provide an appropriate frequency grid and time scale with ability to control and manage (quality of signal generation, transmission and reception, fault handling, means configuration, technical safety, etc.) [16, 24–27]. Within the maintenance and technical operation of the systems of synchronization signal transmission and generation, it is envisaged to conduct operational control by using built-in measuring instruments, which provide continuous monitoring, analysis of the performance, equipment parameters and issuance of messages, including emergency ones. In most cases, built-in measuring instruments allow to save resources, but, at the same time, the objects of measurement are the input signals in relation to these measuring instruments. The measurement results of the input signals do not provide any direct information about the quality of synchronization signal. Moreover, the results of such measurements are not entirely objective, since a reference signal in this case is just an output signal of the same measuring instrument, which means that the obtained data is limited reliable (for example, if the input signal of the measuring instrument is unstable, we will receive data on the instability of the output signal) [16, 26]. It should also be noted that some built-in synchronization devices are not controlled by the control systems of the respective networks, which also makes it difficult to identify synchronization problems in a timely manner [10, 28, 29].

Generation of synchronization signals with a given quality and increased reliability can be technically implemented through the development, research, and implementation of a system for automated multi-channel monitoring of time-synchronization devices. At the same time, this raises a problem of carrying out a significant number of measurements, which necessitates the development of measuring instruments (multi-channel monitoring devices) that allow to obtain real-time measurement results without direct human participation, that is, in automatic mode, and transmit it using the infocommunication systems [1, 24]. In turn, the development of measuring instruments is associated with a device optimization in accordance with a number of criteria and their adaptation to the action of destabilizing factors during the technical operation. It is also important to solve a number of problems related to the processing of the results of simultaneous measurements of several synchronization signals, their accumulation, archiving, storage and joint statistical processing, that is, essentially, a creation of a computer-integrated system for monitoring time-synchronization devices of power systems. On the basis of the obtained data, the operational and technological control of the technological process of providing the corresponding objects of electric power systems with time-synchronization signals with increased reliability is carried out.

These problems need to be solved by using the technical capabilities provided by new information and communication networks based on IP technologies, as

well as modern microelectronic and microprocessor elements for the implementation of complex methods of management and information processing. The main requirements that must be taken into account when developing a multi-channel monitoring device are the following: the need for simultaneous multi-channel measurements of controlled time-synchronization signals; the use of IP technologies for measurement data transmission; the algorithmic processing and visual presentation of multi-channel monitoring results in real time and in an operator-friendly format.

3 Development of a Device for Multi-channel Monitoring of Time-Synchronization Signals of Power Systems

An analysis of the tasks to be performed by the monitoring system confirms a definition of the monitoring process of time-synchronization devices as a process of checking a compliance of their parameters with the established technical characteristics. Moreover, an information on the measurement results of the parameters of controlled time-synchronization devices "should be displayed in the form of mnemonic symbols, signal information, and important quantitative indicators with mandatory provision of interactive mode of operation for operator, who, based on the control data, helps to make decisions regarding the quality indicators of time-synchronization signals and possibility of their use for solving the management problems of SMART-GRID power network" [24].

Improving the reliability of the monitoring process of time-synchronization signals is provided by using the method of multi-channel monitoring [18, 22], on the basis of which a prototype device for multi-channel monitoring of time-synchronization signals (DMCMTSS) was developed.

The device for multi-channel monitoring of time-synchronization signals (DMCMTSS) is one of the key components of the monitoring system, a block diagram of which is shown in Fig. 1, and is its primary sensor, which "provides a primary conversion of the time interval error (controlled quality indicator). The primary converter converts the input physical variable - the phase difference (time interval) - into a proportional output signal, presented in the form of a digital code combination (digital data)" [1].

The device for multi-channel monitoring of time-synchronization signals consists of: input interfaces, switchboard, periodicity control units (PCUs), primary converters, auto-tuning frequency systems of voltage-controlled quartz oscillator, microcontroller, LED indication, RS-232 interface, and Ethernet interface [1]. A block diagram of the developed device is shown in Fig. 2.

The device for multi-channel monitoring of time-synchronization signals (DMCMTSS) can "work from a state reference source by using cable IP networks as a transport medium, which are a real alternative to foreign satellite navigation systems" [1] and will increase reliability of time-synchronization signals of power systems.
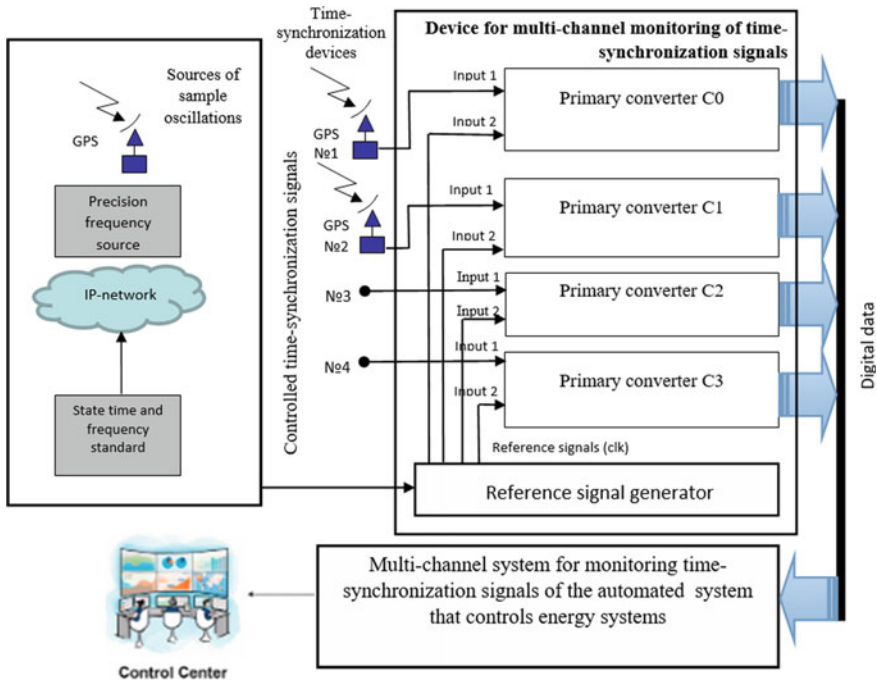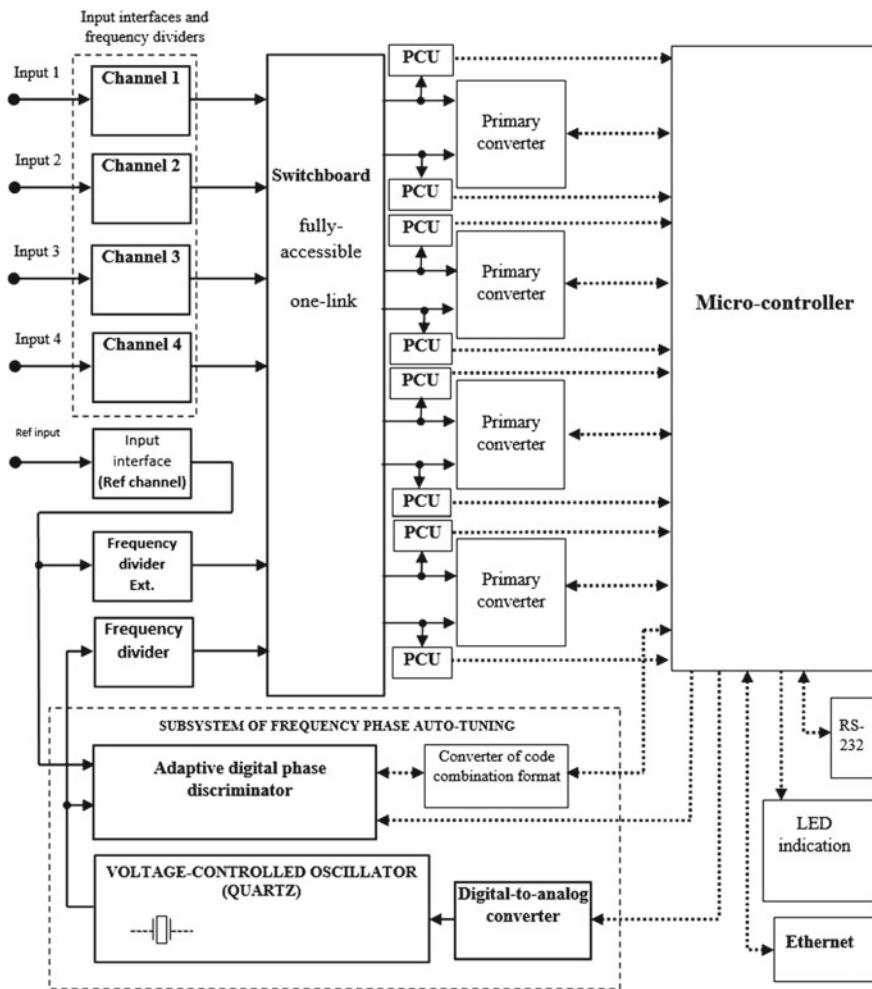
Fig. 1 A block diagram of the system for monitoring time-synchronization devices

A laboratory sample of the functional parts of the device for multi-channel monitoring of time-synchronization signals (DMCMTSS) was developed to conduct an experimental verification of the possibility of using forming signals in the device, which are measured by using a programmable logic device (PLD "ALTERA"), a precision reference signal generator with an auto-tuning system, and corresponding primary converters built on the basis of the diagrams of the adaptive digital phase discriminator (ADPD), for which a patent of Ukraine for inventions No. 113473 [30] was received, and other components. At the same time, the practical possibilities of applying the underlying principles of microprocessor system organization, the structure and functioning of the basic components (input/output controllers, real-time clock, independent EEPROM memory, Ethernet controller, RS-232 port, etc.), as well as the possibilities of its programming by appropriate hardware and software tools are tested.

A laboratory sample of functional parts of the device for multi-channel monitoring of time-synchronization signals (DMCMTSS) consists of circuit fragments, which are placed on boards, namely, on a processing unit (PU) board, signal generator board (SGB) and additional development boards.

The processing unit (PU) board provides measurements, pre-processes data and generates data for transmission and reception via RS-232 and Ethernet interfaces. The PU board contains microcontrollers of ARM TDMI family manufactured by

Fig. 2 A block diagram of the device for multi-channel monitoring of time-synchronization signals (PCU—periodicity control units)

NXP (formerly PHILIPS) LPC2378 and interface communication chips, such as chips of Ethernet module and RS232 interface. The processor board also has a fully accessible single-link switchboard that allows to connect any input signal to the input of the EPM7128SLC84-15 chip of the "ALTERA" programming logic of MAX7000 family. The integrated circuit has dividers that generate to the corresponding frequencies both the signals from the local precision generator and signals, which are coming through the input connectors.

The signal generator board (SGB) performs matching and conversion of input signals to the levels and forms that can be received and processed digitally on the processing unit board of this hardware design of DMCMTSS. Signal generator
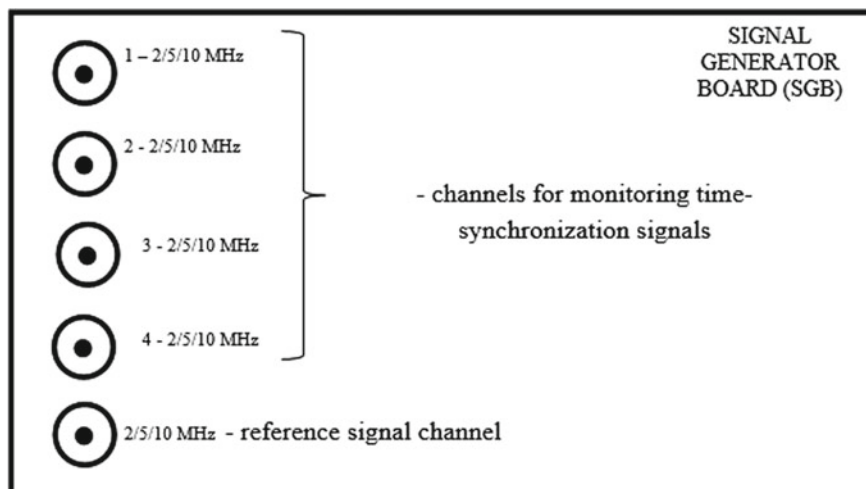
Fig. 3 Signal generator board of laboratory sample of the functional parts of DMCMTSS

board of the laboratory sample of functional parts of DMCMTSS provides multi-channel due to use of five input interfaces (Fig. 3). The PU board for measuring time-synchronization signals relative to the reference signal has four channels to which signals are applied:

- input interface 1—first channel, signal type 2048 Mbit/s, 2048 MHz, 5 MHz, 10 MHz;
- input interface 2—second channel, signal type 2048 Mbit/s, 2048 MHz, 5 MHz, 10 MHz;
- input interface 3—third channel, signal type 2048 Mbit/s, 2048 MHz, 5 MHz, 10 MHz;
- input interface 4—fourth channel, signal type 2048 Mbit/s, 2048 MHz, 5 MHz, 10 MHz;
- input interface 5—reference signal channel, signal type 2048 Mbit/s, 2048 MHz, 5 MHz, 10 MHz.

All input lines have a transformer isolation. The CMP401 comparators convert sinusoidal signals as well as the signals in NRZ and HDB3 codes into digital CMOS signals. A fragment of electrical circuit of the input interface on the CMP401 integrated circuit is shown in Fig. 4.

Figure 5 shows a fragment of the electrical circuit of the input interface built on the CMP401 integrated circuit, which provides detection of HDB3 code and formation of digital CMOS signals. A hardware design of the circuit fragment contains comparators, integrated circuits of 74HC123 single vibrator and 74AC00 digital logic, designed to detect HDB3 code and generate digital CMOS signals. At the comparator output DA1:D, a logical unit signal occurs, which corresponds to the state of the input signal in HDB3 code.
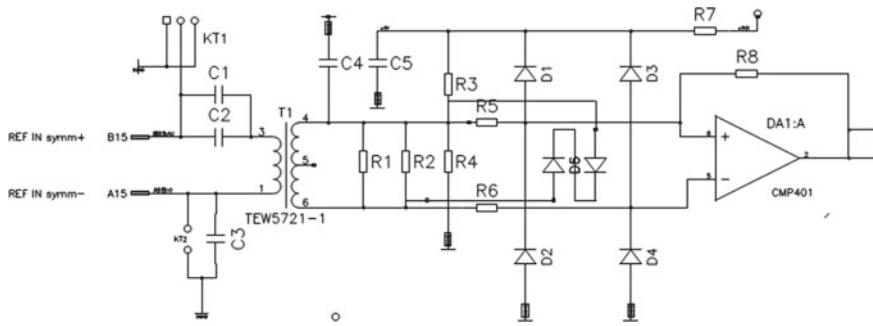
Fig. 4 A fragment of the electrical circuit of the input interface
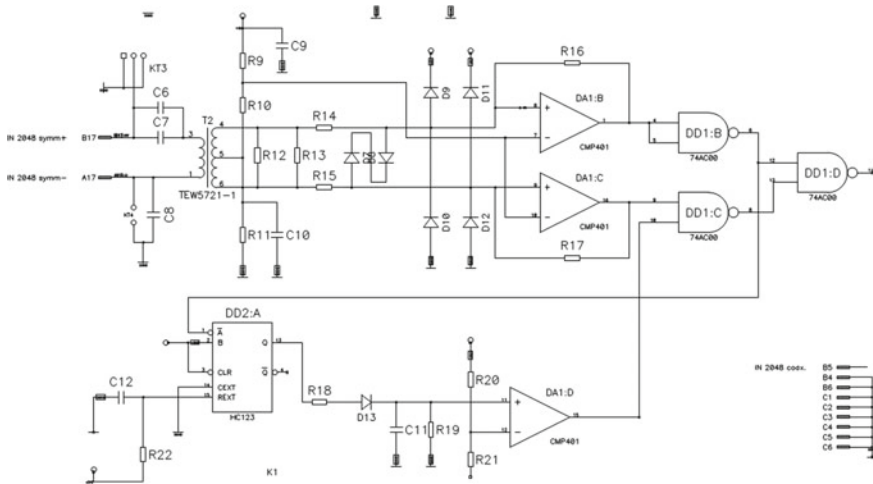
Fig. 5 A fragment of the electrical circuit of the input interface built on the CMP401 integrated circuit, which provides detection of HDB3 code and formation of digital CMOS signals

In addition to the input interface components, the signal generator board (SGB) also contains integrated circuits of voltage stabilizers that generate constant supply voltages. A 5 V voltage is generated for the operation of the signal generator board's components, and for the operation of the processing unit board, which receives power supply from signal generator board. In addition, the signal generator board (SGB) contains a DC voltage stabilizer to power quartz oscillator and an installed DAC1220 integrated circuit, which generates a signal for controlling quartz oscillator's frequency.

The PU board and signal generator board are connected to each other by connectors. A block diagram of the signal generator board and the processing unit board connection is shown in Fig. 6. The connection diagram contains a connector for
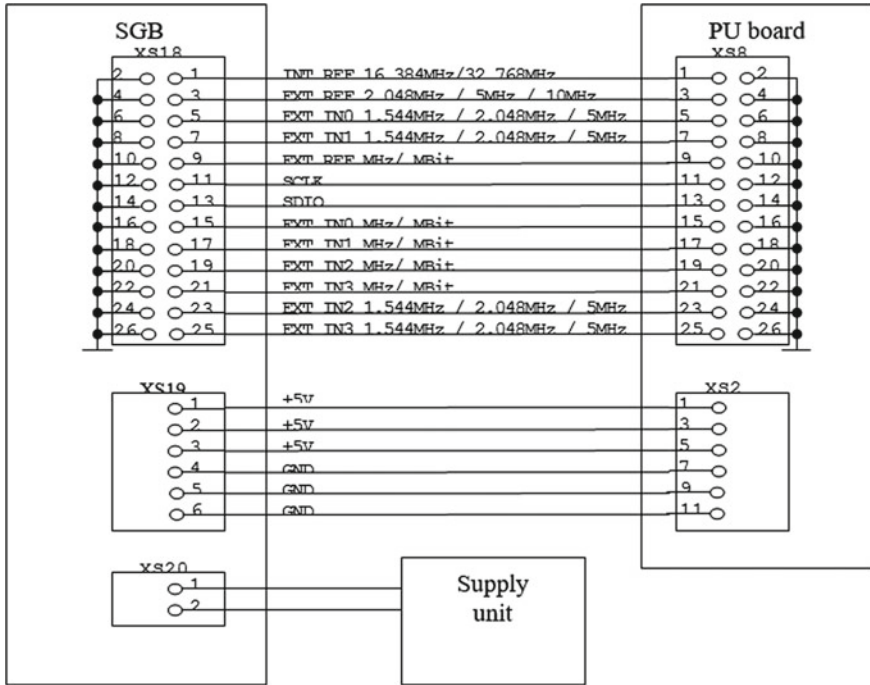
Fig. 6 A scheme of signal generator board (SGB) and PU board connection

connecting a laboratory sample of functional parts of the DMCMTSS to a power supply.

According to the electrical circuit diagrams of the signal generator board and processing unit board, the wiring diagrams were developed. Figure 7 presents a wiring diagram of marking (silk-screen printing) of a lower layer of the signal generator board of DMCMTSS.

4 Theoretical and Probability Studies of the Characteristics' Stability of the Means of Automated Monitoring of Time-Synchronization Devices in Real Operating Conditions at Power Network Facilities

The use of DMCMTSS to control time-synchronization signals of power systems with a nanosecond accuracy makes it necessary to increase the requirements for both technical characteristics of the device as a whole and its individual components. One of the functional parts of DMCMTSS is the periodicity control unit (PCU).
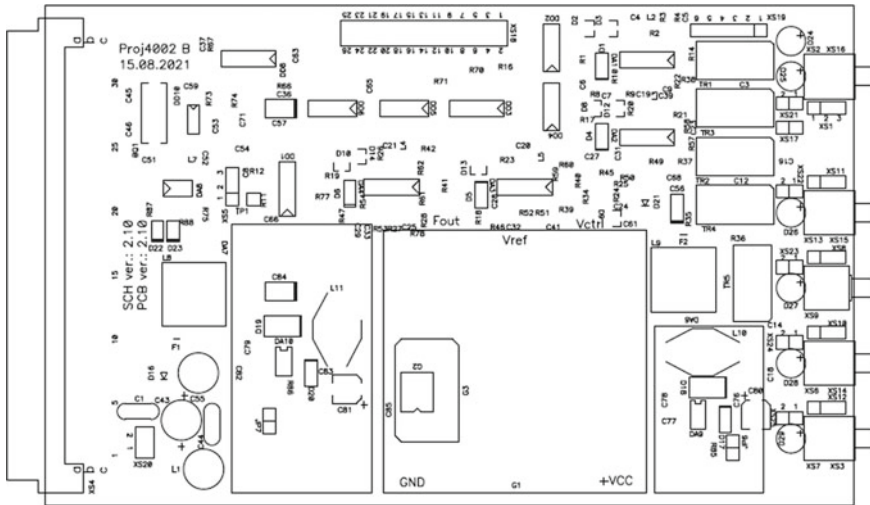
Fig. 7 A wiring diagram of marking (silk-screen printing) of an upper layer of the signal generator board (SGB)

PCU provides an ability to eliminate uncertainty about the presence or absence of controlled signals at a given clock rate. A multi-channel nature of DMCMTSS necessitates the use of a significant number of such blocks and, accordingly, their study using analytical methods. A photo of an assembled board fragment with a digital integrated circuit 74HC123 (two single vibrators with standby and restart possibility), on the basis of which the periodicity control unit (PCU) is implemented, is shown in Fig. 8.

A functional diagram of a single vibrator of periodicity control unit (SVPCU), which is implemented on the integrated circuit 74HC123, is shown in Fig. 9 [31]. An approximate time interval is a transient process of RC-link under the condition of pulse action applied to the inverted input A of 74HC123 integrated circuit of single vibrator with standby and restart possibility (Fig. 9) [31].

A pulse duration at the output Q of the integrated circuit (Fig. 10) is determined by the parameters of the integrating RC-link (resistor R and capacitor C, which are connected to the RC and C terminals of the 74HC123 integrated circuit of single vibrator).

Single vibrator is started after the pulse edge of the controlled signal is applied to the inverted input A, and, as a result, an output pulse with a logic value 1 is formed at the output Q (Fig. 10) [31]. A value of the logic 1 state at the SVPCU output corresponds to the presence of periodicity in the controlled signal, and logic 0 corresponds to its absence.

A duration of T_{SVPCU} pulse at the output Q of the integrated circuit is determined by the τ variable that is a duration of transient process in the integrating RC-link. A duration of the output pulse T_{SVPCU} continues by τ variable, due to the possibility of single vibrator restart when the next edge of controlled pulse is applied to the
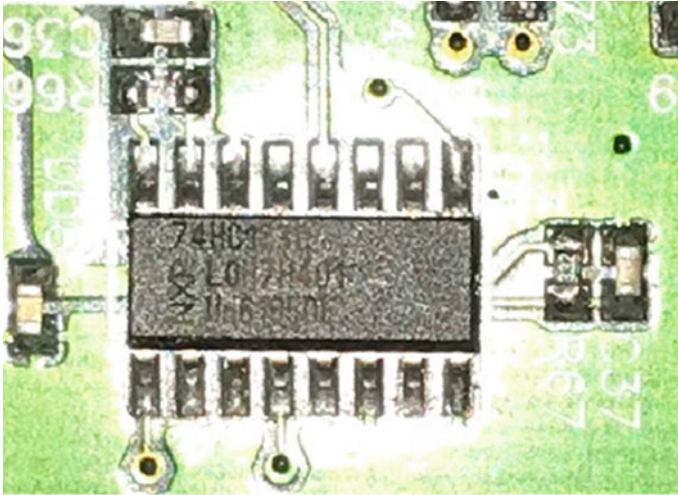
Fig. 8 A fragment of the assembled board with a digital integrated circuit, on the basis of which the periodicity control unit of DMCMTSS is implemented
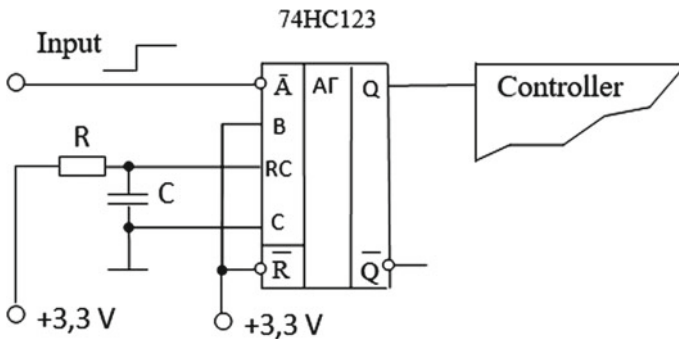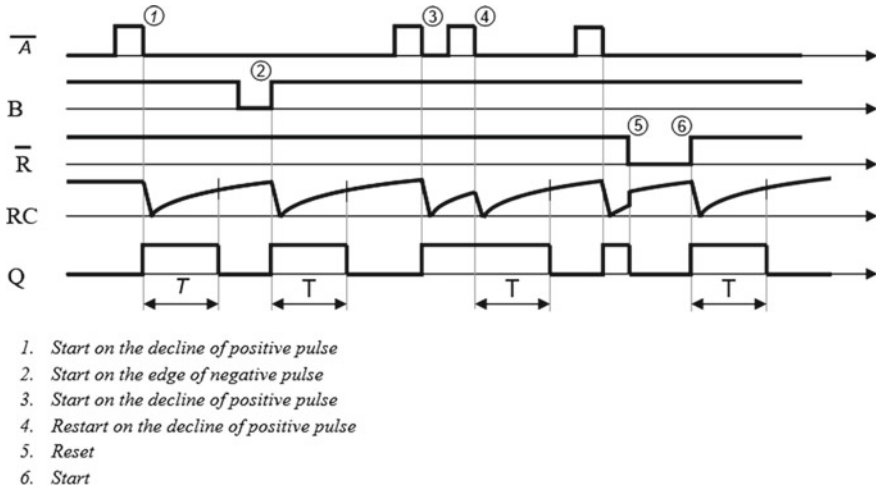

Fig. 9 Functional diagram of SVPCU

inverted input A. Therefore, a continuous value of logic 1 at the SVPCU output is maintained when the next edge of the controlled pulse is applied for a time less than τ, which corresponds to the presence of periodicity in the controlled synchronization signal.

If the restart pulse would not be applied in τ time, then the SVPCU output will generate an output pulse with a value of logic 0, which indicates an absence of periodicity in the controlled synchronization signal. Therefore, the duration of transient process in the integrating RC-link τ essentially acts as a sample time interval with which a duration of the clock interval of the controlled synchronization signal is compared. If the duration of clock interval (including the absence of the signal itself) does not exceed the duration of sample time interval τ, an output pulse with a value

1. Start on the decline of positive pulse
2. Start on the edge of negative pulse
3. Start on the decline of positive pulse
4. Restart on the decline of positive pulse
5. Reset
6. Start

Fig. 10 Timing diagrams explaining SVPCU operation

of logic 0 is generated at SVPCU output, which indicates an absence of periodicity in the controlled synchronization signal.

The timing diagrams in Fig. 10 illustrate the principle of SVPCU operation.

According to the block diagram of DMCMTSS (Fig. 2), the periodicity control unit (PCU) allows to determine in digital pulse sequence the changes in its state (from logic 1 to logic 0) over the duration of the finite signal generated by the integrating RC-link of the single vibrator of periodicity control unit (SVPCU).

The value of the logic 1 state at SVPCU output corresponds to a presence of the corresponding change in the controlled signal's state over a given time interval, and the value of the logic 0 corresponds to an absence of the specified change.

The duration of finite signal generated by the integrating RC-link of SVPCU is selected based on the possibility of the specified control of the periodic signal of a "meander" type with the frequency values specified in technical requirements: 2048, 5000, 10,000 kHz. For this group of signals, the duration of finite signal must be at least $1/2{,}048{,}000$ Hz $= 488.28125$ ns. In this case, the value of logic 1 is generated at the SVPCU output.

Specified in the technical requirements, a type of the controlled digital time-synchronization signal of 2.048 Mbit/s after being processed by the input interface will have periodic pulses with a repetition frequency of 1024 kHz, which will form at the SVPCU output a digital pulse sequence close to the "meander" type.

If there are no changes in the state of the controlled digital signal over the time interval set in SVPCU, the value of logic 0 is formed at its output.

So, the signals generated at the SVPCU output transmit the following information to the microcontroller:

- a value of logic 1 corresponds to the presence of controlled digital time-synchronization signal with 2048, 5000 and 10,000 kHz frequencies;

- a digital pulse sequence close to the "meander" type with a frequency of 1024 kHz corresponds to the presence of controlled digital time-synchronization signal of 2.048 Mb/s;
- a value of logic 0 corresponds to the absence of controlled digital time-synchronization signal with 2048, 5000, 10,000 kHz and 2.048 Mb/c frequencies.

The performed analysis of the operation of PCU of DMCMTSS shows that making a decision on the presence or absence of signals with a given clock rate depends both on time characteristics of finite signal of single vibrator of the periodicity control unit and on the characteristics of time-synchronization signals of power systems to be controlled. The need for theoretical and probabilistic study of one of the important characteristics of finite signal of single vibrator of PCU, namely the pulse duration, is caused by the nature of this error, which is associated with a statistical nature of operating conditions of geographically distributed DMCMTSS across the facilities of power systems, as well as the inevitable scatter of the equipment parameters and its constituent elements.

Monitoring of the characteristics of time-synchronization signals of power systems using DMCMTSS leads to further stringent requirements regarding the accuracy and stability of the duration of time intervals, including the pulse duration of the finite signal of single vibrator of PCU. Improving the quality of time indicators of the devices is possible through the use of more advanced circuit solutions and the use of modern electronic elements, which will provide high stability of the characteristics from power supply voltage, climatic, and other impacts.

The theoretical and probabilistic consideration of the formation mechanism of the total deviation of pulse duration of the finite signal of SVPCU from the nominal value is expedient to perform with its consistent detailing up to the impact on total instability and especially its temperature component of the parameters of each part of the unit. On the one hand, this gives a calculation apparatus to determine reasonable tolerances on the parameters of the unit elements, and, on the other hand, this allows a reasonable determination of the optimal temperature stability of the pulse duration of single vibrator of PCU of DMCMTSS, and determination of the measures, based on the use of modern electronics achievements, to increase stability of some components of the impacts. Such approach to solving the formulated problem necessitates experimental studies, statistical calculations, and optimization of the unit characteristics. At the same time, it is important to know a degree of stability caused by physical nature of the elements of RC-link and single vibrator of PCU, in order to assess, based on the measurements, a degree of stability reduction of pulse duration of the finite signal of single vibrator of the PCU from the nominal value due to the influence of elements' characteristics or imperfection of the development and production technology.

Unfortunately, despite the large amount of literature on the properties and characteristics of the elements of RC-link and single vibrator of PCU [32–46], there are few materials for such calculations. That is why, we considered the ways to improve the accuracy of pulse duration of the finite signal of the single vibrator of PCU using theoretical and probabilistic methods of research.

The experimental studies conducted on the basis of the integrated circuit 74HC123 of SVPCU, which is a functional part of the DMCMTSS, confirmed that the pulses of the finite signal of a single vibrator are random variables [24, 33, 36, 42]. Based on this, we set a task to determine, by using theoretical and probabilistic methods of calculation, an actual operating variable of deviation of pulse duration of the finite signal of single vibrator of PCU from the nominal value in the conditions of actual operation of the equipment at digital substations of electric power networks and series production of DMCMTSS.

In addition to estimating an actual value of the distribution parameter, it is necessary to determine a confidence area for the deviation parameter of pulse duration of the finite signal of single vibrator of the PCU from the nominal value. Due to the fact that this area can vary from sample to sample, we can only talk about the probability that such an area covers an actual value of the deviation parameter of pulse duration of the finite signal from the nominal value. According to this, if you set a sufficiently small number $\varepsilon > 0$, then it is possible to determine a rule according to which, with the probability $1 - \varepsilon$, the actual value of deviation parameter of pulse duration of the finite signal of single vibrator of the PCU from the nominal value will fall into a certain area of confidence in the parametric space.

To estimate the actual value and confidence area for the variable of deviation of pulse duration of the finite signal of single vibrator of the PCU from the nominal value by using theoretical provisions [46–49], we assume that there is a sequence of variables of deviation of pulse duration of the finite signal of single vibrator of the PCU from the nominal value $\{O_k, k \geq 1\}$, which are random and mutually independent and have unknown distribution functions.

$$O_k(x) = P\{O_k, < O\}. \tag{1}$$

For each random variable $O_k, k = 1, \ldots, m$, which is the deviation of pulse duration of the finite signal of single vibrator of the PCU from the nominal value, we will construct a simple sample model $y_n = (O_1, \ldots, O_n)$, which is the main statistical structure of classical mathematical statistics [48], of the volume n from the general population with P distribution, where $O_1, \ldots, O_n$ are the measurement results obtained during the execution of n independent repetitions of a random experimental study associated with a random variable $O \in O_k$. Let's define the distribution functions, evaluation, and confidence area (time interval). They are an integral part of the general task, which consists of making a decision and taking appropriate optimization measures, if it is impossible to meet the requirements for the deviation of pulse duration of the finite signal of single vibrator of the PCU from the nominal value. For example, in our case, on the basis of the conducted research, it is necessary to decide that this generator of the presence signals and the type of pulse sequence of the digital time-synchronization signal may or may not be used as a PCU of the DMCMTSS of power systems. To do this, when carrying out the theoretical calculations, it is necessary to take into account the results of experimental studies of single vibrators of the PCU based on the 74HC123 integrated circuit, which form pulses of a finite signal used to determine the changes in its state in the digital pulse sequence,

and then these data are taken into account when deciding on the presence or absence of synchronization signal.

Important condition for the probabilistic study of the deviation of pulse duration of the finite signal of single vibrator of the PCU from the nominal value is to execute Liapunov limit theorem [49] and conditions regarding the specific weight of individual components in the total sum. In addition, these random variables must satisfy Bernstein's conditions regarding the closeness of the connections between individual components [46–49]. When the indicated conditions of Liapunov and Bernstein are satisfied, the probability density of the total deviation of pulse duration of the finite signal of single vibrator of the PCU from the nominal value can be represented as:

$$F(O) = \frac{1}{\sqrt{2\pi D(O)}} \cdot exp\left\{-\frac{O[\tau - M(O)]^2}{2D(O)}\right\}, \tag{2}$$

where O is the total deviation of the pulse duration of finite signal of single vibrator of the PCU from the nominal value; $M(O)$ is the mathematical expectation of the total deviation of pulse duration of the finite signal of single vibrator of the PCU from the nominal value; $D(O)$ is the variance of total deviation of pulse duration of the finite signal of single vibrator of the PCU from the nominal value, and the distribution itself is a normal distribution with unknown parameters. Evaluation of the parameters consists of determining statistical characteristics, which are the functions of sample values of the deviation of pulse duration of the finite signal of single vibrator the PCU from the nominal value.

Taking into consideration the fact that the total variable of deviation of pulse duration of the finite signal of single vibrator of the PCU from the nominal value is determined by individual, basically independent components, it is necessary to determine the distribution law and its statistics separately for each component $O_k, k = 1, \ldots, m$. Then, according to the rules of probability theory, the necessary statistics for the obtained total variable of the deviation of pulse duration of the finite signal of single vibrator of the PCU from the nominal value, namely $M(O)$ and $D(O)$, should be calculated according to the formulas:

$$M(O) = \sum_{i=1}^{m} M(O_i); \tag{3}$$

$$D(O) = \sum_{i=1}^{m} D(O_i), \tag{4}$$

where $M(O_i)$ and $D(O_i)$ are, respectively, the average values and dispersions of the individual components of the deviation variable of pulse duration of the finite signal of single vibrator of the PCU O_i from the nominal value, which are formed by the integrating RC-link of single vibrator of the PCU.

To determine the confidence interval O_{max}, within which there can be found almost all values of the deviation of pulse duration of the finite signal of single vibrator of the

PCU from the nominal value, let's set the confidence factor $1 - \varepsilon = 0.997$. Then, for the normal distribution law, almost the limiting deviation variable of pulse duration of the finite signal of single vibrator of the PCU from the nominal value O_{max}, will be determined by mathematical equation [47]:

$$O_{max} = |M(O)| \pm 3\sqrt{D(O)}. \tag{5}$$

Based on the comparison of O_{max} value and allowance for the O_{add} variable, a decision $\wedge$ is made about the possibility $\wedge = 1$ or impossibility $\wedge = 0$ of using the studied PCU as a part of DMCMTSS. Decision rule:

$$\begin{cases} \wedge = 1, \ if \ |O_{max}| \leq O_{add} \\ \wedge = 0, \ if \ |O_{max}| > O_{add} \end{cases}. \tag{6}$$

Based on the proposed methodology, taking into account the experimentally obtained results, we determine the distribution law and its evaluation for individual components. Among the components of the total deviation variable of pulse duration of the finite signal of single vibrator of the PCU from the nominal value, there are components that are associated with the changes in environmental parameters (temperature, humidity, pressure, etc.) and power supply voltage. Among these components there is also a change in the period (frequency) of the controlled time-synchronization signal, since it is the pulse fronts of the specified signal that set the start and restart moments of single vibrator of the PCU. With respect to the approximate time interval τ, which is formed due to the transient process in the integrating RC-link of SVPCU, a comparison of the time interval formed by the pulse fronts of the controlled time-synchronization signal is performed. These pulse fronts maintain a continuous value of logic 1 at the SVPCU output, which corresponds to the presence of periodicity, provided that the next pulse front arrives in less time, which is essentially the period (frequency) of the controlled time-synchronization signal. In case the specified ratio is not fulfilled, a false formation of the value of logic 0 or, vice versa, a false formation of the value of logic 1 on the SVPCU output is possible.

Taking into account the performed calculations and assumptions, we will analyze three components of the total deviation variable of pulse duration of the finite signal of single vibrator of the PCU from the nominal value, namely, the change in power supply voltage, ambient temperature, and the change of the period (frequency) of the controlled time-synchronization signal.

Impact analysis of the changes in the ambient temperature and the temperature-dependent parameter on the variable of deviation of pulse duration of the finite signal of single vibrator of the PCU from the nominal value in real operating conditions. Geographically distributed time-synchronization devices of power systems, as well as DMCMTSS, in most cases, will be operated in different climatic conditions. Therefore, there is a need to study the characteristics of DMCMTSS, which depend on the ambient temperature. One of these characteristics is the deviation of pulse duration of the finite signal of single vibrator of the PCU from the nominal value.

The explanation of this dependence is that almost all parameters of the electronic elements, from which the DMCMTSS is developed, depend to a greater or lesser extent on temperature.

The deviation of pulse duration of the finite signal of single vibrator of the PCU from the nominal value in case of the changes in ambient temperature can be presented as an analytical dependence:

$$\Delta O_t = \Delta t° \times \Delta O_{1°}, \tag{7}$$

where $\Delta O_{1°}$ is the deviation variable of pulse duration of the finite signal of single vibrator of the PCU from the nominal value when ambient temperature changes by 1 °C; is the temperature deviation from the value, at which the unit was configured. The $\Delta O_{1°}$ is a random variable, because it is determined by the parameters that have some variation in the production process due to the different electronic components of the PCU of DMCMTSS. The temperature deviation $\Delta t°$ from the value, at which the device was configured, is also a random variable, which depends on the operating conditions. Based on this and taking into account statistical independence of $\Delta O_{1°}$ and $\Delta t°$, and the theorem on the set of two independent random variables [49], we determine the mathematical expectation and dispersion ΔO_t

$$M(\Delta O_t) = M(\Delta O_{1°}) \cdot M(\Delta t); \tag{8}$$

$$D(\Delta O_t) = \left[M^2(\Delta O_{1°}) + D(\Delta O_{1°}) \right] \cdot \left[M^2(\Delta t) + D(\Delta t) \right] - M^2(O_t). \tag{9}$$
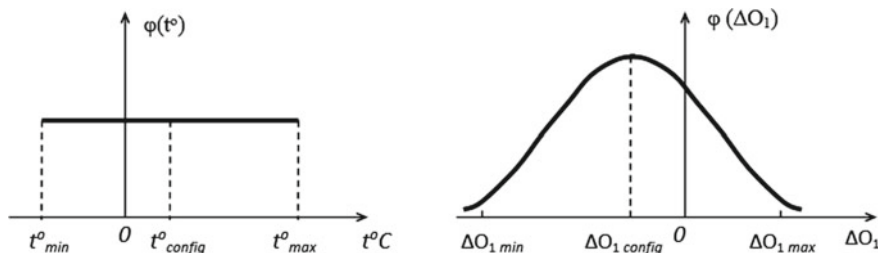
We assume that the law of temperature distribution within the limits specified during the development of the device is uniform (Fig. 11). Then we can write:

$$M(\Delta t) = \frac{t_{max} + t_{min} - 2t_{config}}{2}; \tag{10}$$

$$D(\Delta t) = \frac{(t_{max} - t_{min})^2}{12}, \tag{11}$$

where t_{min} and t_{max} are, respectively, the maximum and minimum temperature values, at which the operation of DMCMTSS of power networks is expected (specified by the technical conditions); t_{config} is the temperature at which DMCMTSS was configured.

Let us determine the statistics of the temperature-dependent parameter $\Delta O_{1°}$, which is the deviation of pulse duration of the finite signal of single vibrator of the PCU from the nominal value if the ambient temperature changes by 1 °C. The $\Delta O_{1°}$ is a random variable, which is explained, first of all, by the conditions of serial production of the device and, secondly, by the dependence of resulting deviation of pulse duration of the finite signal of single vibrator of the PCU from the nominal value when the temperature changes by 1 °C from the sum of the shift components determined by a considerable number of individual electronic components of the

Fig. 11 The law of temperature distribution and probability density of the deviation of pulse duration of the finite signal of single vibrator of the PCU

PCU of DMCMTSS. Therefore, it can be argued that the probability distribution of individual values of deviation of pulse duration of the finite signal of single vibrator of the PCU from the nominal value is subject to Gauss law (Fig. 11) [49], and the mathematical expectation of deviation of pulse duration of the finite signal of single vibrator of the PCU from the nominal value when the temperature changes by 1 °C, can be determined by the formula:

$$M(\Delta O_{1^\circ}) = (\Delta O_{1^\circ})_{nom}, \tag{12}$$

and, accordingly, the dispersion by the following formula:

$$D(\Delta O_{1^\circ}) = \frac{(\Delta O_{1^\circ})^2_{max}}{9}, \tag{13}$$

where $(\Delta O_{1^\circ})_{nom}$ and $(\Delta O_{1^\circ})_{max}$ are, respectively, the nominal and maximum value of the dispersion of the deviation of pulse duration of the finite signal of single vibrator of the PCU from the nominal value when the temperature changes by 1 °C.

By substituting (10) and (12) into Eqs. (8), and (11) and (13) into Eq. (9), respectively, we obtain the expressions for the average value and dispersion of the deviation of pulse duration of the finite signal of single vibrator of the PCU from the nominal value when the ambient temperature changes:

$$M(\Delta O_t) = (\Delta O_{1^\circ})_{nom} \cdot \frac{t_{max} + t_{min} - 2t_{config}}{2} \tag{14}$$

$$D(\Delta O_t) = \left[(\Delta O_{1^\circ})^2_{nom} + \frac{(\Delta O_{1^\circ})^2_{max}}{9} \right] \cdot \left[\frac{(t_{max} + t_{min} - 2t_{config})^2}{4} + \frac{(t_{max} - t_{min})^2}{12} \right]$$

$$- \left[\frac{t_{max} + t_{min} - 2t_{config}}{9} \cdot (\Delta O_{1^\circ})_{nom} \right]^2. \tag{15}$$

Based on the obtained analytical dependences (14) and (15), it is possible to calculate the deviation of pulse duration of the finite signal of single vibrator of the

PCU from the nominal value, due to its temperature dependence, under real operation of DMCMTSS in electric power networks taking into account their serial production.

Impact analysis of the changes of power supply voltage and voltage-dependent parameter on the deviation variable of pulse duration of the finite signal of single vibrator of the PCU from the nominal value in real operating conditions. It is known that when the power supply voltage changes, the deviation variable of pulse duration of the finite signal of single vibrator of the PCU from the nominal value changes. This is due to the fact that DMCMTSS contains a significant number of passive and active electronic elements. A number of PCU parameters of almost every electronic element depend on the power supply voltage. For example, the integrated circuits 74HST123 have a dependence of the response time on the power supply voltage [42].

To study the impact of the statistics of power supply voltage changes on the deviation variable of pulse duration of the finite signal of single vibrator of the PCU from the nominal value, it is necessary to ensure the absence of other destabilizing factors. This condition can be satisfied by keeping other destabilizing factors constant during the experimental studies. In this case, the O_U, which is the deviation variable of pulse duration of the finite signal of single vibrator of the PCU from the nominal value, can be represented as a function of two variables:

$$O_U = \Delta O_{1B} \cdot \Delta U, \tag{16}$$

where ΔO_{1B} is the design parameter of the PCU of DMCMTSS, namely the change in the deviation of pulse duration of the finite signal of single vibrator of the PCU from the nominal value when the power supply voltage changes by 1 V; ΔU is the deviation of power supply voltage from the nominal value, at which the single vibrator of the PCU of DMCMTSS was configured.

Assuming that random variables ΔO_{1B} and ΔU are independent based on the theorem of mathematical expectation and dispersion of two random variables [49], we obtain:

$$M(\Delta O_U) = M(\Delta O_{1B}) \cdot M(\Delta U); \tag{17}$$

$$D(\Delta O_U) = \left[M^2(\Delta O_{1B}) + D(\Delta O_{1B}) \right] \cdot \left[M^2(\Delta U) + D(\Delta U) \right] - M^2(O_U). \tag{18}$$

Let's determine the statistical characteristics of the changes of power supply voltage of the PCU. In this case, we will take into account that the limits of voltage change are specified in the technical requirements, as the maximum U_{max} and minimum U_{min} allowable values, at which the device must operate. It is obvious that the voltage, at which the U_{config} is configured, must be within these limits, namely:

$$U_{min} \leq U_{config} \leq U_{max}. \tag{19}$$
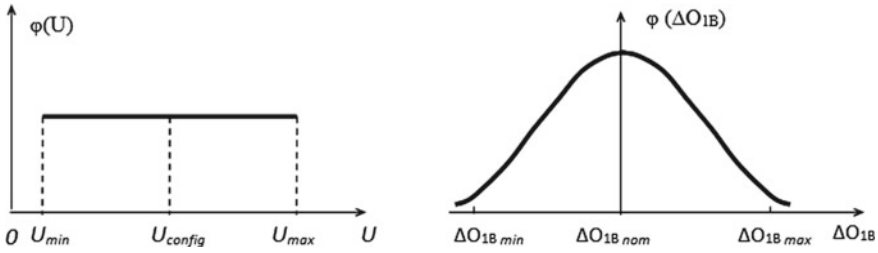
Fig. 12 The law of power supply voltage distribution and probability density of the deviation of pulse duration of the finite signal of single vibrator of the PCU

We assume that the law of power supply voltage distribution of the PCU within these limits will be uniform, since no reservations are made about a type of the distribution law within these limits, and the DMCMTSS operational guideline will most likely indicate the device operability with the declared characteristics. Therefore, we believe that in the real conditions of technical operation of the device there will be a uniform probability of any voltage from the indicated limits (Fig. 12).

Based on the above, the mathematical expectation of the power supply voltage changes of the PCU can be written as:

$$M(\Delta U) = \frac{U_{min} + U_{max} - 2U_{config}}{2}. \tag{20}$$

The dispersion of the power supply voltage change of the PCU is determined by the equation:

$$D(\Delta U) = \frac{(U_{max} - U_{min})^2}{12}. \tag{21}$$

By substituting expressions (20) and (21) in (17) and (18), respectively, we obtain the mathematical expectation for the single-type PCU of DMCMTSS:

$$M(\Delta O_U) = \frac{U_{min} + U_{max} - 2U_{config}}{2} \cdot M^2(O_U), \tag{22}$$

and dispersion of the deviation of pulse duration of the finite signal of single vibrator of the PCU from the nominal value under the action of power supply voltage change:

$$D(\Delta O_U) = \left[\frac{(U_{min} + U_{max} - 2U_{config})^2}{4} + \frac{(U_{max} - U_{min})^2}{12} \right]$$
$$\times \left[M^2(\Delta O_{1B}) + D(\Delta O_{1B}) \right] - M^2(O_U). \tag{23}$$

Let's determine the statistics of the design parameter of DMCMTSS $\Delta\Theta_{1B}$, which is the deviation of pulse duration of the finite signal of single vibrator of the PCU from the nominal value when the power supply voltage changes by 1 V.

Let's assume that the probability distribution of individual values of the deviation of pulse duration of the finite signal of single vibrator from the nominal value in case of power supply voltage change of the PCU is subject to Gauss law, since this parameter is determined by the sum of the influence of a large number of individual DMCMTSS parts (integrated circuits, resistors, diodes, capacitors, etc.). Based on this, it can be argued that the mathematical expectation of the deviation of pulse duration of the finite signal of single vibrator of the PCU from the nominal value in case of voltage change by 1 V is equal to:

$$M(\Delta O_{1B}) = (\Delta O_{1B})_{nom}, \tag{24}$$

and the dispersion for 99.73% of all possible cases will be determined by the following equation

$$D(\Delta O_{1B}) = \frac{(\Delta O_{1B})^2_{max}}{9}, \tag{25}$$

where $(\Delta O_{1B})_{max}$ is the maximum value of the deviation variance of pulse duration of the finite signal of single vibrator of the PCU from the nominal value in case of the voltage change by 1 V [49].

By substituting (24) and (25) into the (22) and (23), respectively, for the general case with asymmetric changes in the power supply voltage of the PCU we finally obtain:

$$M(\Delta O_U) = \frac{U_{min} + U_{max} - 2U_{config}}{2} \cdot (\Delta O_{1B})_{nom}; \tag{26}$$

$$D(\Delta O_U) = \left[\frac{\left(U_{min} + U_{max} - 2U_{config}\right)^2}{4} + \frac{(U_{max} - U_{min})^2}{12} \right]$$
$$\times \left[(\Delta O_{1B})^2_{nom} + \frac{(\Delta O_{1B})^2_{max}}{9} \right]$$
$$- \left[\frac{U_{min} + U_{max} - 2U_{config}}{2} \cdot (\Delta O_{1B})_{nom} \right]^2. \tag{27}$$

Based on the obtained analytical dependences (26) and (27), it is possible to calculate the deviation of pulse duration of the finite signal of single vibrator of the PCU, due to the dependence on the power supply voltage of PCU under the conditions of DMCMTSS operation on the existing electric power networks.

Analysis of the changes of the frequency-dependent parameter and period (frequency) of time-synchronization signal, taking into account the actual conditions of its transmission to the objects of electric power networks. Automated monitoring

tools and time-synchronization devices of power systems are frequency-dependent [1]. The change of the frequency of time-synchronization signal can be explained by non-ideal characteristics of the synchronization means, the presence of static phase error of the automatic control system, digital processing of the control signal in the microprocessor and other factors.

The study of the influence of statistics of the frequency change of time-synchronization signal on the deviation variable of the start and restart moments of the single vibrator of PCU will be carried out by assuming that there is no influence of other destabilizing facts, as it was done in previous cases. Then the value ΔO_f of the deviation of start and restart moments of the single vibrator of PCU can be represented as a function of two variables:

$$\Delta O_f = \Delta f \times \Delta O_{1\,\text{Hz}}, \tag{28}$$

where $\Delta O_{1\,\text{Hz}}$ is the deviation of the start and restart moments of single vibrator of the PCU when the frequency of time-synchronization signal changes by 1 Hz; Δf is the change of the frequency value of time-synchronization signal relative to the initial value of Δf_{config}, at which the device was configured.

This representation is convenient because the random variable is divided into two random variables: $\Delta O_{1\,\text{Hz}}$ is a random variable in terms of series production of the devices; Δf is a random variable under operating conditions of the devices at electric power networks. Moreover, the first term of the random variable ΔO_f is completely determined by the technical properties of the devices, and the second one is determined by the operating conditions. Based on the theorem of mathematical expectation and dispersion of two independent random variables [49], we obtain:

$$M(\Delta O_U) = \frac{U_{min} + U_{max} - 2U_{config}}{2} \cdot (\Delta O_{1B})_{nom}; \tag{29}$$

$$D(\Delta O_f) = \left[M^2(\Delta O_{1\,\text{Hz}}) + D(\Delta O_{1\,\text{Hz}})\right] \cdot \left[M^2(\Delta f) + D(\Delta f)\right] - M^2(\Delta O_f). \tag{30}$$

Let's define the statistics of the frequency change of time-synchronization signal $M(\Delta f)$ and $D(\Delta f)$. At the same time, we take into account that the limits of the frequency change of time-synchronization signal are set in the form of the maximum allowable deviations Δf_{max} relative to the nominal value. The synchronization signal for time-synchronization devices can be obtained from satellite navigation systems, such as GPS, GLONAS, from atomic frequency standards, using telecommunication systems or IP-networks with the PTP protocol as a transport medium. As an example, let's consider the case when the time-synchronization signal with a nominal value of 2048 kHz is moved from atomic frequency standards to the time-synchronization devices of power systems using the IEEE-1588v2 protocol [16, 50, 51].

The distribution of the frequency change for a sufficiently representative sample of time-synchronization devices will follow the Gauss law (see Fig. 13). The limit values of the change of 2048 kHz clock rate of the US-1588 equipment Δf_{max}
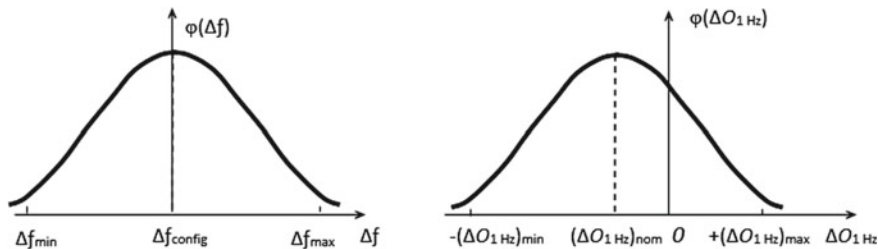
Fig. 13 The distribution law of frequency deviation of the time-synchronization signal and probability density of the deviation of the time moments of starting and restarting of the single vibrator of PCU

and Δf_{min} are determined by its technical characteristics and conditions of signal transmission by the IP-network.

So, the mathematical expectation and dispersion of the frequency value change of time-synchronization signal will be determined by the equations:

$$M(\Delta f) = 0; \tag{31}$$

$$D(\Delta f) = \frac{(\Delta f_{max})^2}{9}. \tag{32}$$

By substituting the expressions (31) and (33) in the (29) and (30), respectively, we obtain the mathematical expectation for the general case of operation of the single-type devices:

$$M(\Delta O_f) = 0, \tag{33}$$

and dispersion of the deviation variable of the start and restart moments of single vibrator of the PCU when the frequency of time-synchronization signal changes:

$$D(\Delta O_f) = \left[M^2(\Delta O_{1\,Hz}) + D(\Delta O_{1\,Hz}) \right] \frac{(\Delta f_{max})^2}{9}. \tag{34}$$

Let's determine the statistics of the frequency-dependent parameter $\Delta O_{1\,Hz}$, which is the deviation of the start and restart moments of the single vibrator of PCU in case of frequency change of time-synchronization signal by 1 Hz. The probability distribution of individual values of this parameter is subject to Gauss law (see Fig. 13). This is explained by the presence of a significant number of individual parts (quartz resonator, varicaps, inductances, capacitances, etc.), the parameters of which determine the $\Delta O_{1\,Hz}$ variable.

Taking this into account, it can be written that the mathematical expectation of the deviation of the start and restart moments of single vibrator of the PCU, when

the frequency of the time-synchronization signal changes by 1 Hz, is equal to the nominal value:

$$M(\Delta O_{1\,\text{Hz}}) = (\Delta O_{1\,\text{Hz}})_{nom}, \tag{35}$$

and the dispersion will be determined from the following equation with a probability of 0.997:

$$D(\Delta O_{1\,\text{Hz}}) = \frac{(\Delta O_{1\,\text{Hz}})^2_{max}}{9}, \tag{36}$$

where $(\Delta \Theta_{1\,\text{Hz}})_{max}$ is the maximum value of the deviation dispersion of the start and restart moments of the single vibrator of PCU when the frequency of time-synchronization signal changes by 1 Hz.

By substituting (35) and (36) in (33) and (34), respectively, we finally obtain, for the general case, the mathematical expectation and the dispersion of the deviation variable of the start and restart moments of single vibrator of the PCU during the frequency change of time-synchronization signal:

$$M(\Delta O_f) = 0; \tag{37}$$

$$D(\Delta O_f) = \left[(\Delta O_{1\,\text{Hz}})^2_{nom} + \frac{(\Delta O_{1\,\text{Hz}})^2_{max}}{9} \right] \cdot \frac{(\Delta f_{max})^2}{9}. \tag{38}$$

Based on the obtained analytical dependences (37) and (38), it is possible to calculate the deviation of the start and restart moments of the single vibrator of PCU, which are caused by the frequency (period) changes of the time-synchronization signal, taking into account the real conditions of its transmission to the facilities of electric power networks.

To obtain the necessary statistics, it is planned to manufacture a batch of PCU devices for multi-channel monitoring of time-synchronization signals, and conduct appropriate experimental studies.

The analytical dependences (14), (15), (26), (27), (37), and (38) obtained by using theoretical and probabilistic methods make it possible to determine the actual operating variable of the deviation of pulse duration of the finite signal of single vibrator from the nominal value and the deviation of the start and restart moments of the single vibrator of PCU in the conditions of actual operation of the equipment at the digital substations of electric power networks and the serial production of DMCMTSS.

5 Experimental Studies of the Device for Multi-channel Monitoring of the Time-Synchronization Signals of Power Systems
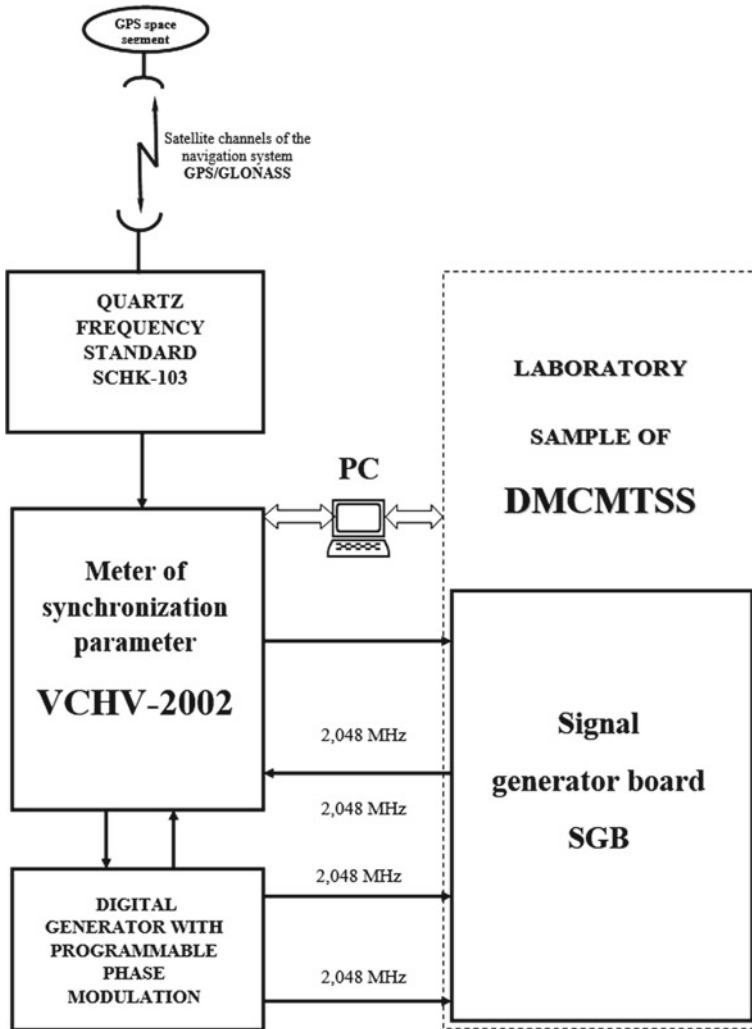
The block diagram of the laboratory stand for experimental studies of the device for multi-channel monitoring of the time-synchronization signals of power systems is shown in Fig. 14. In the process of experimental studies, the measurements of the time characteristics o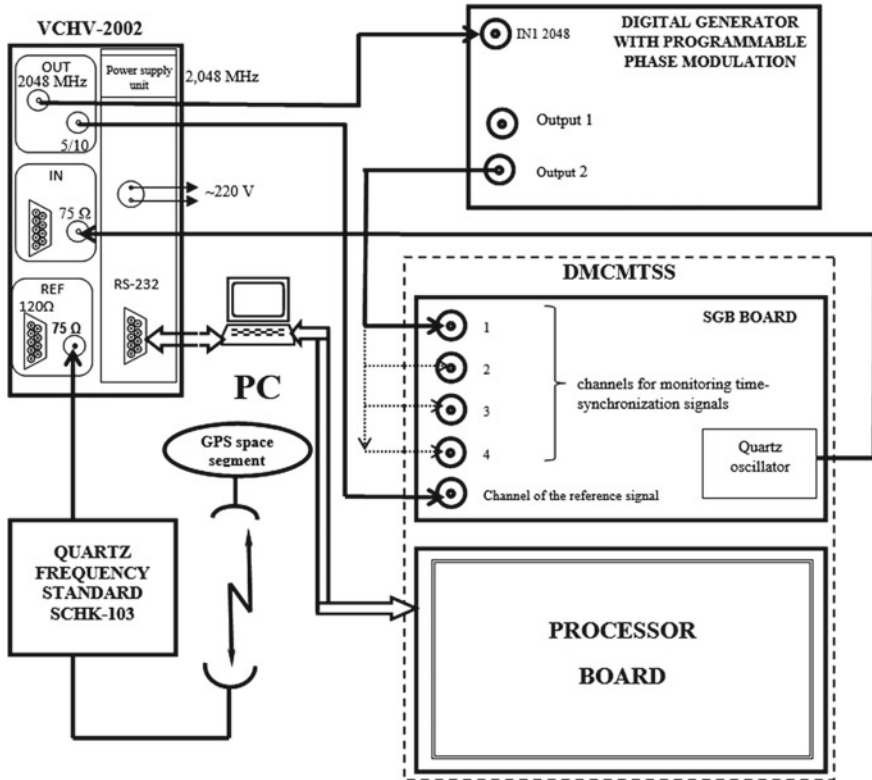f synchronization signal of the SGB quartz oscillator are made. The functional diagram of the laboratory stand for measuring time characteristics of the synchronizat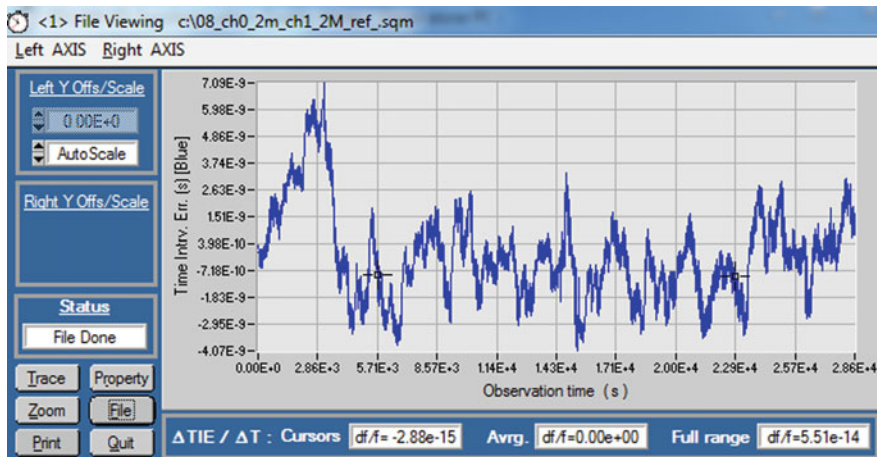ion signal of the quartz oscillator of SGB of DMCMTSS is shown in Fig. 15. The measurement is made by using the GPS satellite navigation system, frequency standard of the quartz SCHK-103 (СЧК-103), digital generator with a programmable phase modulation, personal computer, and time interval meter VCHV-2002 (ВЧВ-2002).

The measurements of time characteristics of the SGB signals are made in order to determine the phase distortion of the reference synchronization signal under the condition of simultaneous digital processing of two or more controlled time-synchronization signals. Based on the measurement results of the time interval error (TIE), a calculation of the secondary parameters of synchronization signals of MTIE, TDEV, which are defined in Recommendations ITU-T G.810 and G.8262. The comparative analysis of the calculation results with the norms is the basis for making a decision on the implementation of these norms.

The results of TIE measurements of the synchronization signal of the quartz oscillator of the SGB of DMCMTSS, which is synchronized from the time interval meter VCHV-2002 (ВЧВ-2002), are shown in Fig. 16. The values of the maximum time interval error (MTIE) and the time interval deviation (TDEV), obtained by processing the data of these measurements, are shown in Figs. 17 and 18. A comparative analysis of the results obtained according to the norms of the European standard ETS 300 462-4 indicates the implementation of these norms with a substantial margin.

The hardware structure of DMCMTSS is implemented on the basis of the multi-channel monitoring method, which allows simultaneous monitoring of up to four synchronization signals in real time (Fig. 2). In the process of experimental studies, the technical characteristics of DMCMTSS are checked if it is used to control the quality of two synchronization signals with different nominal frequencies relative to the third one, which is connected to the reference signal channel. This possibility is provided through the use of a single-link fully accessible switchboard and controlled frequency dividers. It expands the device's functionality for the manager to quickly select a pair of synchronization signals that can be connected to one of four primary converters to measure the time interval error and convert the measurement results into digital data. The functional diagram of the laboratory stand for checking the technical characteristics of DMCMTSS for simultaneous control of two synchronization signals in real time is shown in Fig. 19.

The results of experimental studies of the process of simultaneous monitoring of two synchronization signals in real time using the P4000winXP software are

Fig. 14 Block diagram of the laboratory stand for experimental studies of the SGB of DMCMTSS (PC—personal computer)

shown in Fig. 20. The graphs (Fig. 20) show fragments of a dependence of the TIE of two controlled synchronization signals (Channel C0 and Channel C1) relative to the third one (signal of the reference channel). In this case, a simultaneous connection of two controlled synchronization signals to the DMCMTSS doubles its performance compared to the single-channel devices. Examples of such devices are well-known meters of synchronization parameters, such as IPS-2002 (manufacturer LLC "IST", Ukraine), PJS2000compact (manufacturer PLLB, Italy), IVO-1M (manufacturer ALTO, Russia).

Fig. 15 Functional diagram of the laboratory stand for measuring time characteristics of synchronization signal of the quartz oscillator of the SGB of DMCMTSS (PC—personal computer)

Fig. 16 The results of TIE measurements of the synchronization signal of quartz oscillator of the SGB
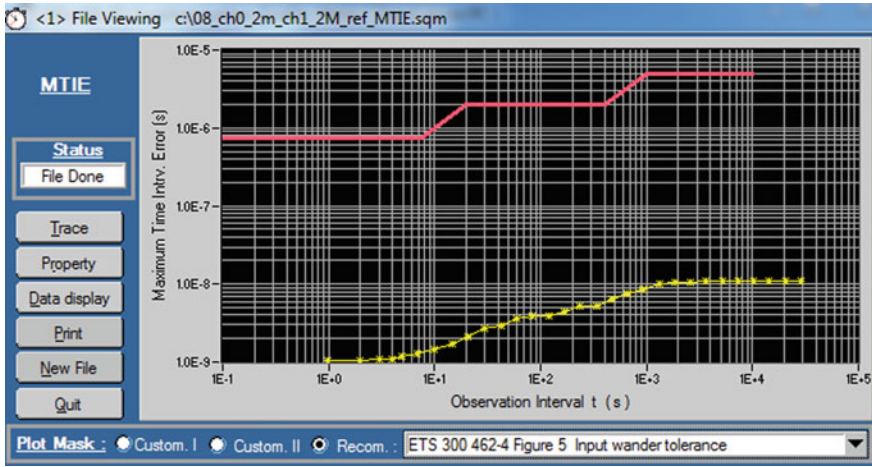
Fig. 17 Dependence on the time of maximum time interval error (MTIE) of the synchronization signal of quartz oscillator of the SGB
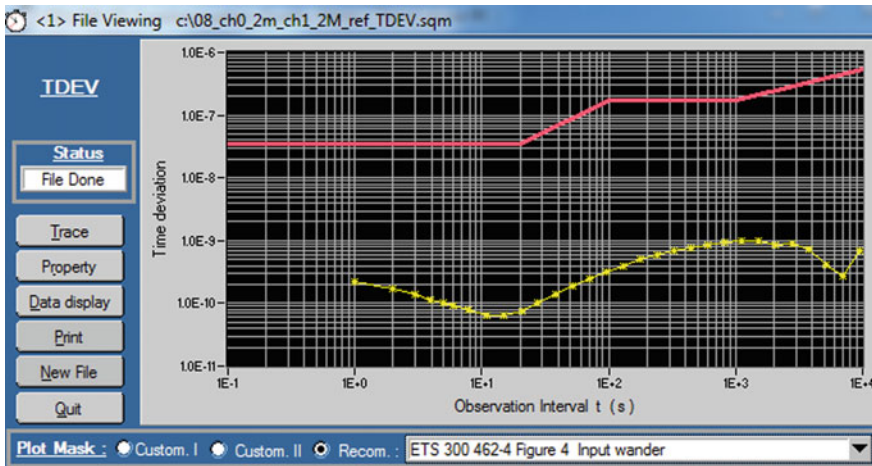

Fig. 18 Dependence on the time of time interval deviation (TDEV) of the synchronization signal of quartz oscillator of the SGB

A photo of a prototype of the device for multi-channel monitoring of synchronization signals, which was used to carry out experimental studies of the DMCMTSS of power systems, is shown in Fig. 21.
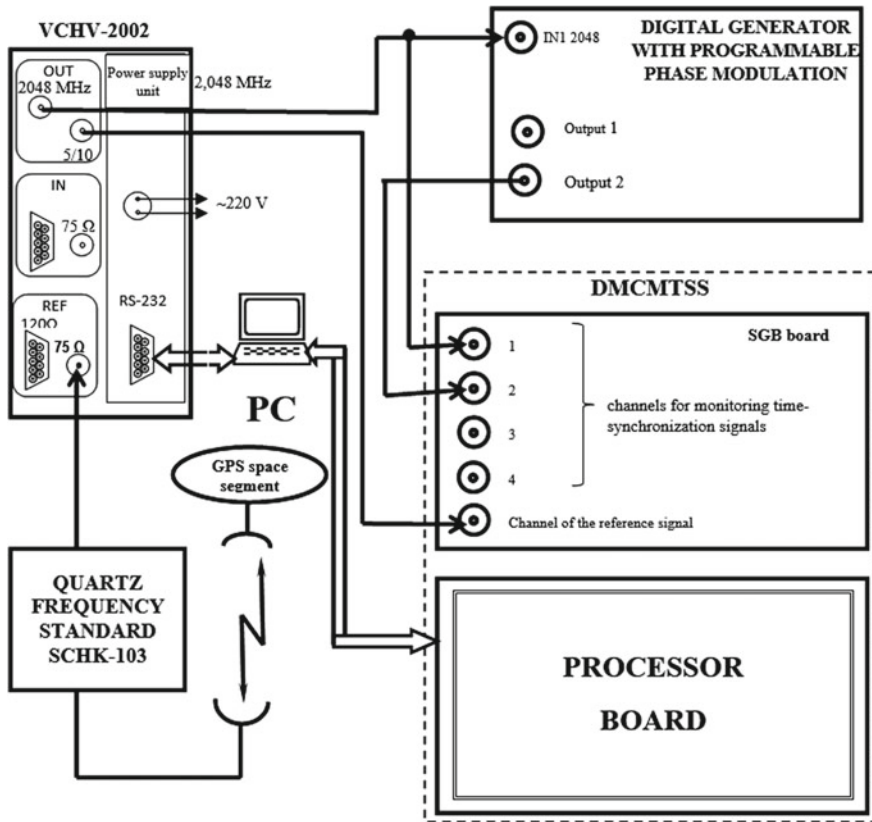
Fig. 19 Functional diagram of the laboratory stand for studying the process of simultaneous monitoring of two synchronization signals in real time (PC—personal computer)

6 Conclusions

1. The relevance of scientific research is substantiated with the subsequent introduction of a system for automated multi-channel monitoring of the parameters of time-synchronization devices, which will provide a formation of time-synchronization signals of power systems with increased reliability.
2. We identified the tasks that should to be solved using the technical capabilities provided by new information and communication networks based on IP technologies, as well as modern microelectronic and microprocessor elements for implementing complex methods of management and information processing.
3. The schemes of the system and device for multi-channel monitoring of time-synchronization signals are developed, and the description of its functional parts is given.
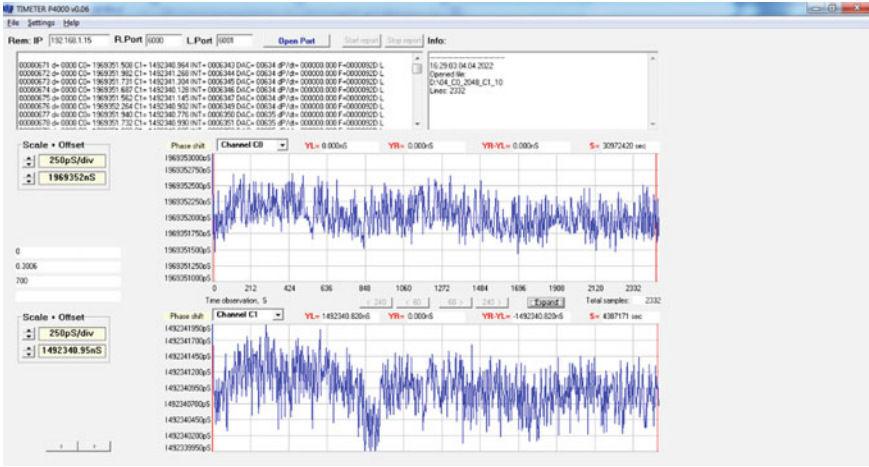
Fig. 20 Fragments of the measured parameters of TIE under the condition of simultaneous monitoring of two synchronization signals in real time
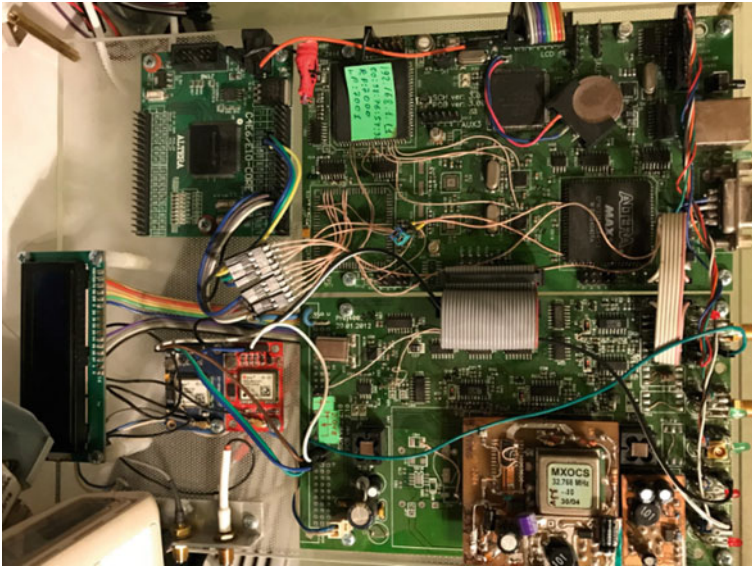

Fig. 21 A photo of DMCMTSS prototype

4. Theoretical and probabilistic studies of the stability of PCU characteristics, as a functional part of the device for multi-channel monitoring of time-synchronization signals, have been carried out in real operating conditions at the facilities of electric power networks.

5. A computational apparatus was obtained for determining reasonable tolerances on the parameters of the unit elements, which allows to approach a reasonable determination of the conditions of optimal temperature stability of the pulse duration of the single vibrator of PCU of the device for multi-channel monitoring of time-synchronization signals of power systems.

6. Analytical dependences were obtained to estimate the actual value and confidence area for the deviation variable of pulse duration of the finite signal of single vibrator of the PCU from the nominal value in real operating conditions of the DMCMTSS device.

7. Laboratory samples of functional parts and prototype of the DMCMTSS device were made; their configuration was performed; and experimental studies were carried out.

8. The results of experimental studies of the DMCMTSS prototype confirm the possibility of increasing the number of measurement channels that can be processed simultaneously up to four. The operator can also analyze the obtained monitoring results of the controlled synchronization signals presented in digital and graphical form. This improves the performance and allows comparative evaluation of the monitoring results up to four channels as opposed to a single-channel device.

The presented results of the development and research of the tools for automated monitoring of time-synchronization devices of power systems allow us to state that they can be used to control synchronization signals in power systems built in accordance with the SMART-Grid concept, and can serve as a basis for developing a technology to analyze performance of the time-and-frequency support tools in various economy sectors of the country, and can be used to improve the defense and security.

The materials of the monograph part were prepared based on the results of scientific and technical work commissioned by the state.

References

1. Koval, V.V., Samkov, O.V., Blinov, I.V., Lameko, O.L., Trach, I.V., Polischuk, S.J., Vakas, V.I., Chopyk, V.V., Osinskyi, O.L.: Automated Monitoring of Time-Synchronization Signals of Power Systems: Monograph, 380 p. NUBIPU Publishing Center (2021)

2. Denysyuk, S.P., Tarasevych, P.J., Spodynskyi, O.V., Derevyanenko, D.G.: Ensuring the reliability of operation and sustainability of intelligent energy systems. In: Proceedings of the Institute of Electrodynamics of the NAS of Ukraine, issue 27, pp. 27–33 (2010)

3. Kyrylenko, O.V., Blinov, I.V., Parus, E.V., Trach I.V.: Evaluation of efficiency of use of energy storage system in electric networks. Tech. Electrodyn. **4**, 44–54 (2021). https://doi.org/10.15407/techned2021.04.044

4. Kyrylenko, O.V., Pavlovsky, V.V., Blinov, I.V.: Scientific and technical support for organizing the work of the IPS of Ukraine in synchronous mode with the Continental European power system ENTSO-E. Technical Electrodynamics **5**, 59-66 (2022). https://doi.org/10.15407/techned2022.05.059

5. Kyrylenko, O.V., Blinov, I.V., Tankevych, S.E.: Smart grid and organization of information exchange in electric power systems. Tekhnichna Elektrodynamika **3**, 44–54 (2012)

 6. Kyrylenko, O.V., Blinov, I.V., Parus, Ye.V.: Operation evaluation of power plants in the provision of ancillary services of primary and secondary frequency control in the Ukrainian power system. Tekhnichna Elektrodynamika, **5**, 55–60 (2013)
 7. Kyrylenko, O.V., Basok, B.I., Baseyev, Ye.T., Blinov, I.V.: Power industry of Ukraine and realities of the global warming. Tekhnichna Elektrodynamika **3**, 52–61 (2020). https://doi.org/10.15407/techned2020.03.052
 8. SOU NPC 20.261:2021 Standard: The technical policy of the NPC "Ukrenergo" in the field of development and operation of main and interstate power networks
 9. SOU NPC 35.101:2018: General technical requirements for automated process control systems of 220–750 kV substations of UES of Ukraine
10. Koval, V.V., Kalian, D.O., Samkov, O.V.: Automated System for Transmitting Synchronization Signals Over IP Networks: Monograph, 182 p. NUBIPU of Ukraine (2016)
11. Koval, V.V.: Leaded Synchronization Devices with Periodic Auto-adjustment of Telecommunication Networks: Monograph, 342 p. "KOMPRINT" PC (2017)
12. Development of the concept of scientific and applied foundations for creating a unified information system for distributing national time scale using IP technologies: R&D report by state order, 172 p. NUBIPU of Ukraine; The state registration number: 0115U003376 (2016)
13. Kalian, D.O., Koval, V.V., Samkov, O.V., Shkliarevskyi, I.Y.: Improvement of the energy efficiency of integrated power supply systems of Smart-technologies through the highly reliable synchroinformation support. In: Materials of the XVIII International Scientific and Practical Conference "Renewable Energy and Energy Efficiency of the XXI Century", Kyiv, NTUU "KPI", Institute of Renewable Energy of the NASU, 27–29 Sept 2017, pp. 139–142. Printing company "CALENDAR" LLC (2017)
14. Koval, V.V., Kalian, D.O., Maksymenko, Y.A., Samkov, O.V.: Оптимальне за швидкодією фазове автопідстроювання частоти синтезатора міток точного часу інтегрованих систем електропостачання Smart-технологій. Scientific Bulletin of the National University of Bioresources and Nature Management of Ukraine. Series "Engineering and Energy of Agro-industrial Complex", issue 283, pp. 89–98 (2018)
15. Kalian, D.O., Koval, V.V., Maksymenko, Y.A., Samkov, O.V., Dubovych-Kostetskyi, V.G.: Optimizing for speed automatic frequency control of quartz crystal oscillator for synchronization signal control systems. E-ed. Energy Autom. **3**, 15–33 (2018). http://journals.nubip.edu.ua/index.php/Energiya/article/view/10897/9540
16. Koval, V.V., Samkov, O.V., Piskun, O.M., Medina, M.S., Golovnia, M.V., Shkliarevskyi, I.Y.: Information system of the time scale transmission through an integrated electric power networks of SMART-technologies. Bulletin of the University "Ukraine". Series "Informatics, Computer Engineering, Cybernetics" **1**(22), 231–239 (2019)
17. Koval, V., Lysenko, V., Osinskiy, O., Samkov, O., Khudyntsev, M.: Infocommunication technologies and networks for multichannel monitoring of synchronization signals of SMART grid and microgrid electrical systems. In: Conference Proceedings: International Scientific and Practical Conference "Problems of Infocommunications, Science and Technology" (PICS&T-2019), 8–11 Oct 2019, pp. 153–156. Borys Grinchenko Kyiv University, Kyiv, Ukraine (2019)
18. Projectowanie, badania, i eksploatacja. Tom 1. Monografia. Dmytro Kalian, Nadiia Kazakova, Boris Kravchenko, Valerii Koval. Automated system for Monitoring Synchronizing precise time signals at SMART-GRID power plants. Wydawnictwo naukowe Akademii techniczno-humanistycznej w Bielsku-Bialej, pp. 155–160. Bielsku-Bialey, Poland (2019). http://www.engineerxxi.ath.eu/book/designing-researches-and-exploitation-2019-vol-1/
19. Koval, V., Osinskiy, O., Lysenko, V., Samkov, O., Khudyntsev, M.: Infocommunication technologies and networks for multichannel monitoring of synchronization signals of SMART grid and microgrid electrical systems. In: 2019 IEEE International Scientific and Practical Conference "Problems of Infocommunications Science and Technology" (PICS&T-2019)—Proceedings, 9061443 (2019). https://ieeexplore.ieee.org/document/9061443
20. Koval, V.V., Samkov, O.V., Osinskyi, O.L., Khudyntsev, M.M., Shkliarevskyi, I.Y., Dubovych-Kostetskyi, V.G.: Transmitting the accurate time using the PTP protocol for an intellectual

SMART-grid network. Bulletin of the University "Ukraine". Series "Informatics, Computer Engineering, Cybernetics" **2**(23), 85–94 (2019)

21. Koval, V., Kalian, D., Osinskyi, O., Samkov, O., Khudyntsev, M., Lysenko, V.: Diagnostics of time synchronization means of the integrated power grid of SMART technologies by using an optimal performance system of automatic frequency adjustment. In: Proceedings of the 15th International Conference on Advanced Trends in Radioelectronics, Telecommunications and Computer Engineering (TCSET 2020), Lviv-Slavske, Ukraine, 25 Feb–29 Feb 2020, pp. 269–276 (2020). https://ieeexplore.ieee.org/document/9088587

22. Koval, V., Kazakova, N., Samkov, O., Osinskyi, O., Kalian, D., Samoilenko, V.: Multi-channel digital discriminator of automated monitoring system of smart-grid power networks time synchronization tools. Przetwarzanie, transmisja I bezpieczenstwo informacja: Monografia. Wydawnictwo naukowe Akademii techniczno-humanistycznej w Bielsku-Bialey, pp. 135–144. Bielsku-Bialey, Poland (2020)

23. Koval, V.V., Lysenko, V.P., Kalian, D.O., Osinskyi, O.L., Samkov, O.V.: Improving efficiency of the phase-locked loop for reference oscillator of the multichannel system for time-synchronization signals telemonitoring. In: Vorobiyenko, P., Ilchenko, M., Strelkovska, I. (eds.) Current Trends in Communication and Information Technologies. IPF 2020. Lecture Notes in Networks and Systems, vol. 212, pp. 60–79. Springer, Cham (2021). Print ISBN 978-3-030-76342-8. Online ISBN 978-3-030-76343-5. https://doi.org/10.1007/978-3-030-763 43-5_4

24. Koval, V.V., Samkov, O.V., Fedorova, N.V., Vakas, V.I.: Automated Quality Control of Synchronization Signals Generation Based on IP Technologies: Monograph, 424 p. NUBIPU of Ukraine (2019)

25. Velychko, O., Golovnia, M., Koval, V., Shkliarevskyi, I.: The concept of the national system for the dissemination of synchronization information. In: Proceedings of the II International Scientific and Practical Conference "Global and Regional Problems of Informatization in Society and Nature Management'2014", Kyiv, Ukraine, NUBIPU, 26–27 June 2014, pp. 22–23. Agrar Media Group (2014)

26. Bregni, S.: Synchronization of Digital Telecommunications Networks (trans. from English), 456 p. Mir (2003)

27. Kalian, D.O.: Automation of the process of monitoring quality parameters of digital signal synchronization devices of flexible manufacturing system. Dissertation for obtaining the scientific degree of the candidate of technical sciences: 05.13.07, 284 p. NUBIPU (2020)

28. Koval, V.V.: Devices of Synchronization of Infocommunication Networks with Periodic Auto-adjustment: Monograph—Koval, V.V., Kalian, D.O., 412 p. NUBIPU of Ukraine (2016)

29. Baklanov, I.G.: Measurement Technologies in Modern Telecommunications, 264 p. Echo-Trends (1998)

30. Patent for Invention No. 113473 Ukraine, IPC (2016.01) H 03 D 13/00, H 03 D 3/04 (2006.1). Adaptive digital phase discriminator. Pat. No. 113473 Ukraine, IPC (2016.01) H 03 D 13/00, H 03 D 3/04 (2006.1)/Koval, V.V., Kalian, D.O., Koval, V.V. (Ukraine) - № a 2015 11981, Statement. 03.12.2015, Publ. Application details 10/05/2016, Bul. № 9. Publ. Bul. №2, 25.01.2017. http://uapatents.com/6-113473-adaptivnijj-cifrovijj-fazovijj-diskriminator.html

31. 74HC123; 74HCT123: Dual retriggerable monostable multivibrator with reset. Product data sheet. Rev. 10—3 Dec 2015. NXP Semiconductors N.V. (2015). http://www.nxp.com

32. Borsch, V.I., Koval, V.V., Ali, S.: Experimental studies of the phase jitter of synchronization signal of the microprocessor-based TCB TSS EASS. Abstracts of the Report Republican Scientific and Technical School-Seminar "Analysis and Synthesis of Queuing Systems and Computer Networks", Part 2, Odessa, pp. 180–181 (1990)

33. Drobyk, O.V., Koval, V.V., Kostyk, B.Y.: Laboratory and full-scale experimental studies of the developed dedicated devices for synchronizing information networks and infrastructures. Bull. UBENTZ **1**, 85–92 (2004)

34. Statistical studies of the dedicated synchronization devices and development of the methods of operation of the control system of the synchronization network of the transport network of SDH of JSC "Ukrtelecom": R&D report (intermediate), State University of Information and Communication Technology (SUICT), № DR 0105U001671 (2006)

35. Borsch, V.I., Kostik, B.Y., Koval, V.V., Drobyk, O.V.: Field measurements and statistical processing of characteristics of network synchronization signals of telecommunications. Electron. Commun. Part 3, 106–110 (2007)
36. Yanitskyi, I.Y.: Statistical optimization of the accuracy of generators of periodic time readings with a phase-locked loop VPSTSS of telecommunication networks. Sci. Notes Ukrainian Res. Inst. Commun. **1**(9), 27–38 (2009)
37. Koval, V.V., Petrusenko, K.A., Sukach, G.O., Chernova, K.S., Yanitskyi, I.Y.: Statistical parameters of the accuracy of forming periodic time readings by dedicated devices for synchronizing information networks. In: Collection of Scientific Works of the Institute of Modeling Problems in the Energy. G. E. Pukhov of the NAS of Ukraine, issue 54, pp. 171–177 (2009)
38. Bohutska, O.A.: Probabilistic theoretical calculation of the accuracy of forming periodic time readings of a dedicated device for synchronizing telecommunication networks. In: Bohutska, O.A., Vilchynskyi, M.A., Koval, V.V., Petrusenko, K.A., Yanitskyi, I.Y. (eds.) The World of Information and Telecommunications—2009: The VI International Scientific and Technical Conference of Students and Young Scientists, 28–29 Apr 2009: Abstracts of Reports, pp. 40–42 (2009)
39. Yanitskyi, I.Y.: Optimization of the generator of periodic time readings with a phase-locked loop of a dedicated device for synchronizing telecommunication networks. Dissertation for obtaining the scientific degree of the candidate of technical sciences: 05.12.02, 165 p, State University of Information and Communication Technology (2009)
40. Shytikov, G.T.: Stabilized Band Oscillators (Theory and Calculation). Sovetskoe Radio (1965)
41. Borodachev, N.A.: Basic Questions of the Theory of Production Accuracy. Publishing House of the Academy of Sciences of the USSR (1970)
42. Designing with the SN74AHC123A and SN74AHCT123A. Texas Instruments Incorporated. SCLA014 Oct 1999. http://www.ti.com/lit/an/scla014/scla014.pdf
43. Koval, V.V., Osinov, S.M.: Methodical recommendations for educational and technological practice in computer technology, tasks and instructions for performing laboratory and practical work in the field of training—6.050202. In: Automation and Computer-Integrated Technologies, 118 p. NUBIPU of Ukraine (2016)
44. Gridchin, V.A., Dragunov, V.P.: Physics of Microsystems: Tutorial. In Part 2, Part 1, 416 p. NGTU Publishing, Novosibirsk (2004)
45. Arbuzov, V.P.: Temperature error correction for capacitive measuring circuits. Sens. Syst. **4**, 39–42 (2007)
46. Turchyn, V.M.: Mathematical Statistics. Publishing Center "Akademia" (1999)
47. Bronstein, I.N., Semendiaev, K.A.: Handbook of Mathematics for Engineers and University Students, 608 p. Nauka (1965)
48. Koroliuk, V.S., Portenko, N.I., Skorokhod, A.V., Turbin, A.F.: Handbook of Probability Theory and Mathematical Statistics, 640 p. Nauka (1985)
49. Gorban, I.I.: Probability Theory and Mathematical Statistics for Scientists and Engineers, 244 p. NAS of Ukraine, Institute of Problems of Machines and Systems (2003)
50. Velychko, O.M., Koval, V.V., Samkov, O.V., Shkliarevskyi, I.Y.: Time-scale distribution modern protocols for smart grid power systems with low accident rate. Scientific Bulletin of the National University of Life and Environmental Sciences of Ukraine. Series "Engineering and Energy of Agro-industrial Complex", issue 242, pp. 41–50 (2016)
51. Golovnya, M., Shkliarevskyi, I., Velychko, O., Koval, V., Nikitenko, O.: IEEE 1588 based national time-scale distribution project in Ukraine. In: International IEEE Symposium on Precision Clock Synchronization for Measurement Control and Communication (ISPCS), 04–09 Sept 2016, Stockholm, Sweden, pp. 78–82 (2016). https://ieeexplore.ieee.org/document/7579513

Power Quality Monitoring System for Electrical Networks

Tetyana Dzheria [ID] **, Vitaly Shevchuk** [ID] **, and Anatolii Voloshko** [ID]

Abstract   Ensuring the quality of electricity is one of the ways to increase the efficiency of the entire energy complex of Ukraine and its individual energy systems. At the same time, it is necessary to note the following. Analysis of the current state of Ukraine's electricity industry shows that its current integration with the electricity sector of the EU requires compliance with the necessary conditions for compliance with strict requirements for electricity quality parameters, which must be within acceptable levels set in a number of regulations. It should be noted the following. The development of measures to ensure the required quality of electricity is possible only after assessing its actual state in all nodes of the country's electricity system. Therefore, the system of real-time monitoring of electricity quality should be based on real-time monitoring system. This study considers the model of information flow in the electrical network, which is a hierarchical structure of comparative, frequency calculation of local maxima of wavelet transform coefficients with time shift, adaptive to the singular behavior of the signal. This model allows from a single mathematical standpoint based on the analysis of frequency-time and spectral characteristics of comparative wavelet coefficients to conduct the full range of data processing on power consumption modes, definition, identification and classification of distortions of electricity quality. Based on the analysis of the detailed coefficients of the wavelet composition, a generalized identifier of the distortion of the quality of electric energy is presented, which serves as a basis for the express analysis of the quality of electric energy in real time. Its application allows, regardless of the type of distortion, its direct detection, beginning and/or end. Further identification of the type of distortion and its classification is carried out using the developed modified vector of features of the classification of distortions of electricity quality. Whereas, as a result of wavelet decomposition of the information signal and analysis of the obtained wavelet coefficients, time-localized information on its distortion (deviation from the nominal values of its parameters) from the high- and low-frequency ranges is obtained, therefore, the frequency-energy properties of these coefficients are the basis of the method of classification of distortions in the quality of electrical energy. The presented approach

T. Dzheria (✉) · V. Shevchuk · A. Voloshko
Institute of Energy Management and Energy Saving, National Technical University of Ukraine "Igor Sikorsky Kyiv Polytechnic Institute", Kyiv, Ukraine
e-mail: avolosko820@gmail.com; tatyanakurus0202@gmail.com

to the formation of the system of monitoring the quality of electricity, in contrast to the existing approaches in which sequential processing of the measurement signal to determine individual indicators of quality of electricity, allows building a system of monitoring the quality of electricity in real time.

Keywords Signal processing · Quality of electric energy · Distortion · Electricity quality indicator · Wavelet transform

1 Introduction

Ensuring the quality of electricity is one of the ways to improve the efficiency of the entire energy complex of the country and its individual energy systems. Today in Ukraine, the electricity quality indicators (EQI) are almost not controlled.

Electricity transmission organizations when issuing technical conditions for the connection of electricity consumers and when concluding contracts for the supply of electricity do not include in them the requirements for indicators of electricity quality, do not determine the conditions for control EQI. If the control is carried out, then only formal, without the application of any measures to bring the quality of electricity to the level specified by the State Standard.

Monitoring of EQIs would allow to form a statistical database of measurements, which, in turn, would improve the forecasting processes in the electricity network, determine the expected levels of reliability of electricity supply and electricity quality in the future, plan necessary measures to ensure reliability of electricity supply and electricity quality. At present, the monitoring of electricity quality indicators is carried out only by analyzing the accumulated statistical information for a certain period of time. This is because the processes in the power grid are instantaneous. They can only be recorded, and in the future can be processed and analyzed, that are indicators of electricity quality are not measured directly, but by processing statistical information.

In order to increase the reliability and informativeness of the obtained results of electricity quality monitoring, as well as to increase the efficiency of electricity quality management, control over its indicators should be carried out continuously. The creation of a real-time system for monitoring the quality of electricity will allow for timely control of its indicators and their deviations and take appropriate measures to bring the quality of electricity in accordance with the requirements of the State Standard.

Wavelet transform has been introduced rather recently in Energetics, even though the essential ideas that lead to this development have been around for a longer period of time.

In contrast to the Fourier transform, wavelet analysis allows you to simultaneously detect fluctuations in the frequency and time domain, evaluate the frequency features of the time series, which presuppose in time unexpected and lonely bursts. In the mainstream literature, wavelets were first applied to power system in 1994 by
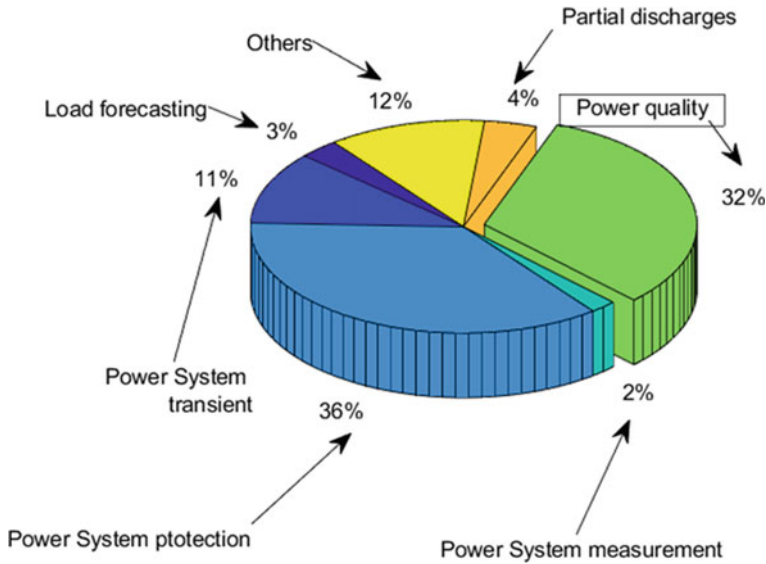
Fig. 1 Percentage of wavelet publications in different power system areas [1]

Roberson and Riberio. From this year the number of publications in this area has increased.

Figure 1 shows the percentage of publications in each technical area. Areas where more work has been developed are electricity quality and protection. The following section provides a general description of the use of wavelets in the field of electricity quality. In the area of power quality several studies have been carried out to detect and locate disturbances using the wavelet transform as an useful tool to analyze interferences, impulses, notches, glitches, interruptions, harmonics, flicker, enc. of non stationary signals. And the following section provides a general description of the use of wavelets in the field of electricity quality.

2 Information Model for Determining the Presence of Distortion of Electricity Quality and Its Type

The analysis of existing research results proved the possibility of creating an information model for detecting and identifying distortions of electricity quality, which is a hierarchical structure of comparative, frequency calculation $Wf(u, 2^j)$ of local maxima of wavelet transformation $\left(\left|Wf(u, 2^j)\right|\right)$ with an offset, adaptive to the studied signal. This model is presented in Fig. 2.

The model of information flows, created on the basis of sequential comparative wavelet decomposition, allows from a single mathematical position based on the
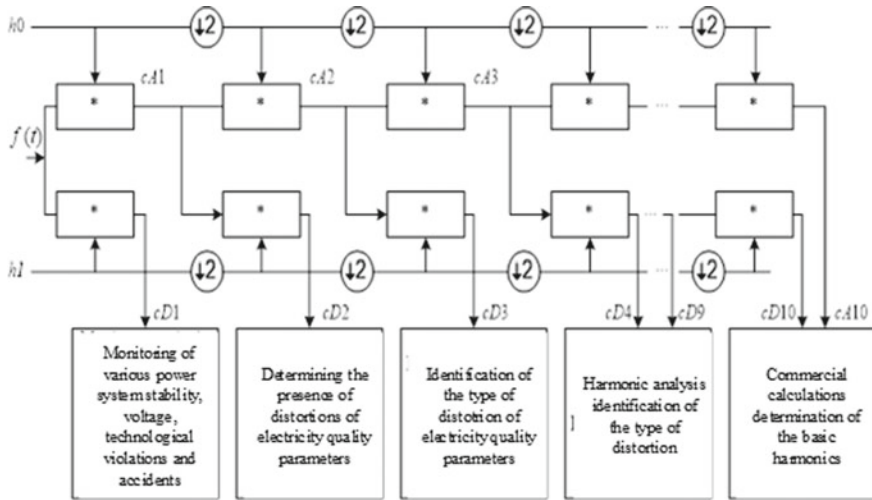
Fig. 2 Consistent information model for detection and identification of distortions of electricity quality

analysis of frequency-time and spectral characteristics of comparative wavelet coefficients to conduct the full range of data processing on power consumption modes, determination and identification not only of the type of distortions in the quality of electricity, but also the place of their detection and the culprit of distortions throughout the chain from the generation of electricity to its consumption.

So from Fig. 2 it follows that the analysis and processing of the first level of the model—the coefficient *cD1* (frequency range from 25 to 50 kHz) based on information about P—active power, U and I—voltage and current, accordingly, df/dt—frequency fluctuations to monitor power system regimes, technological disturbances and accidents. Analysis and processing of information of the second level of the model—the coefficient *cD2* (frequency range from 12.5 to 25 kHz) serves to determine the presence of distortions in the quality of electricity and their duration [2–4]. The information of the third level of the model is the coefficient *cD3* (frequency range from 6.25 to 12.5 kHz) used to identify the type of distortion of electricity quality.

Processing information that corresponds to the fourth-ninth levels of the model—coefficients *cD4–cD9* (frequency range from 0.1 to 6.25 kHz) used for rapid monitoring of electricity quality and harmonic analysis, and tenth level—coefficients *cA10*, *cD10*—for commercial settlements.

That is, the created model allows, depending on the task, to analyze and process information at individual levels, which provides:

- real-time monitoring of quantitative and qualitative characteristics of electricity consumption;

- conducting rapid monitoring of electricity quality for timely introduction of preventive control influences and identification of the culprit of the existing distortion;
- carrying out balance calculations for the consumed electric energy in accordance with its quality.

3 Generalized Identifier of the Presence of Distortions in the Quality of Electricity

As you know, there are two main groups of distortions in the quality of electricity: stationary (or quasi-stationary) and distortions that change over time. Harmonics and interharmonics, voltage fluctuations and voltage imbalances belong to the first group, and transients of voltage, voltage reduction/excess, voltage interruption and other high-frequency distortions are the second group.

A large number of methods for processing information signals are used to determine the quality of electricity. All of them have both advantages and disadvantages for their application in electricity quality monitoring systems.

The analysis of literature sources allowed to outline the main existing methods of identifying the presence and type of distortions in the quality of electricity:

- artificial neural networks (hidden Markov's models);
- based on expert systems;
- expert systems with fuzzy logic;
- SVM—precedent-based teaching methodology;
- combined methods—artificial neural networks and SVM;
- wavelets and Markov's models, fuzzy logic expert systems, and Fourier analysis.

Analysis of the application of these methods allowed to outline the most important problems in detecting and identifying distortions of electricity, which are not sufficiently resolved at present. Based on the above, to build a system for monitoring the parameters of electricity quality, it is necessary to develop such methods and algorithms that implement them, which will:

- determine and identify the presence of voltage and current distortion in the electrical network;
- to ensure the definition of certain types of distortion that are simultaneously present in the electrical network;
- develop a generalized identifier for the distortion of electricity quality, which would allow real-time monitoring of electricity quality.

This article considers the approach to building a system for monitoring the quality of electricity in terms of developing a generalized identifier to determine the presence of distortions in the quality of electricity, the time of its occurrence and duration in real time.

4 Method for Unambiguous Identification of the Presence of Distortions in the Quality of Electricity

According to scientific publications, real-time monitoring of electricity quality (EQ) parameters is currently impossible, as their determination requires time for data collection and statistical processing. Also, in most cases, each EQ parameter requires a separate algorithm and mathematical apparatus to determine. Currently, there is no generalized identifier for determining the presence of an arbitrary type of distortion. Therefore, it is important from a scientific and practical point of view to develop a method for unambiguous identification of deterioration of EQ in real time.

As the results of many studies show, frequency-time atoms with different time carriers are needed to analyze the structure of signals of different durations. In orthogonal transformations, the wavelet function is used as a family of such frequency-time atoms $\psi_{u,s}(t)$ as a result of its scaling by the value s and offset by the value u

$$\psi_{u,s}(t) = \frac{1}{\sqrt{s}} \psi \left(\frac{t-u}{s} \right). \tag{1}$$

In this case, the orthogonal transformation from the time of u and scale s is as follows

$$Wf(u, s) = \langle f, \psi_{u,s} \rangle = \int\limits_{-\infty}^{+\infty} f(t) \frac{1}{\sqrt{s}} \psi \left(\frac{t-u}{s} \right) dt, \tag{2}$$

where $\langle f, \psi_{u,s} \rangle$—scalar multiplication.

As follows from expression (2), wavelet transform can focus on local signal structures using the object zoom procedure, which gradually decreases/increases the scale parameter. Features and smooth surfaces of the signal often contain basic information about its characteristics. Since the local signal smoothness is characterized by a decrease in the amplitude of the wavelet transform with decreasing scale, the paper examines the features and differences of the signal by analyzing the local maxima of wavelet transform at small scales, which allowed to detail the "anomalies" in the signal [5].

As noted in the scientific literature, the decrease in the amplitude of the wavelet coefficients depending on the scale is due to the uniform and point smoothness of the Lipschitz's signal better. Measurement of this asymptotic decrease is equivalent to the approximation of signal structures at a scale that goes to zero. That is, if $f \in L^2(R)$ satisfies the condition Lipschitz α, $\alpha \leq n$, on $[a, b]$, it exists $A > 0$ such that

$$\forall (u, s) \in [a, b] \times R^+, \quad |Wf(u, s)| \leq As^{\alpha+1/2}. \tag{3}$$
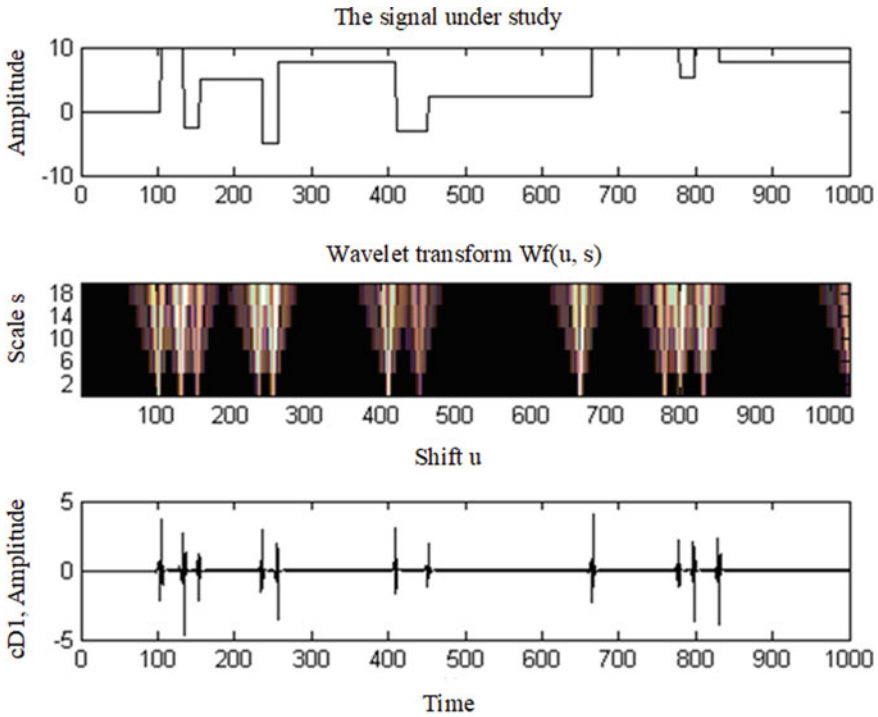
Fig. 3 Wavelet transform $|Wf(u, s)|$ calculated for the signal $f(t)$

Inequality (3) is a condition of asymptotic decline $|Wf(u, s)|$, if s goes to zero (Fig. 3).

At the same time, when reducing the scale s function $|Wf(u, s)|$ characterizes small-scale changes in the environment u. The scale s must be more than 2, otherwise, the sampling step may be larger than the wavelet carrier. Therefore, when calculating the smallest scale of wavelet transform is limited to the separation of discrete data. As is well known, discrete wavelet transform is calculated on a scale $2^j \geq s \geq \mu N^{-1}$, where μ may be large enough to eliminate the effect of inaccurate sampling on the smallest scale wavelets. Therefore, the largest scale 2^j should be chosen so that it is less than the distance between two consecutive features in time, in order to prevent the influence of other features on $|Wf(u, s)|$.

At each scale 2^j the representation of the maxima gives value $Wf(u, 2^j)$, where $Wf(u, 2^j)$—local maximum. In this case, when the value of the function $f(t)$ offset on τ, each $Wf(u, 2^j)$ also shifted to τ, as well as their maxima.

5 Approbation of Research Results

To verify the adequacy of the theoretical solution and its practical significance, we will conduct a comparative analysis of the results of signal processing using Fourier and wavelet analysis. The following are selected as information signals: the presence of breaks of the first kind (amplitude differences) and the presence of the third and fifth harmonics (Figs. 4 and 5).

The results of the Fourier analysis indicate the presence of anomalies in the signal (Fig. 4a) and the presence of the third and fifth harmonics (Fig. 4b), but without identifying the time of their occurrence and duration.

The results of the wavelet analysis, which are presented in Fig. 5a, show the following. Values of wavelet coefficients of the first level of wavelet analysis $Wf(u, 2^j) - cD1$ indicate the presence of anomalies in the signal, characterize the time of their occurrence and duration. The results of the wavelet analysis (Fig. 5b) show the following. Reducing the scale of wavelet transform allows you to detail anomalies $cD5 - cD6$. The level of decomposition depends on the sampling frequency, which is chosen according to Kotelnikov's theorem. In our case, at a sampling frequency of 12.8 kHz, we have 1024 discrete values. This corresponds to the level of wavelet decomposition $j = \log(1024) = 7$. That is, the analysis of Fig. 5b shows not only the presence in the signal of the third and fifth harmonics (frequency range $cD5$ corresponds to 200–400 Hz, and $cD6$ corresponds to 100–200 Hz), but also their duration.

(a)   (b)
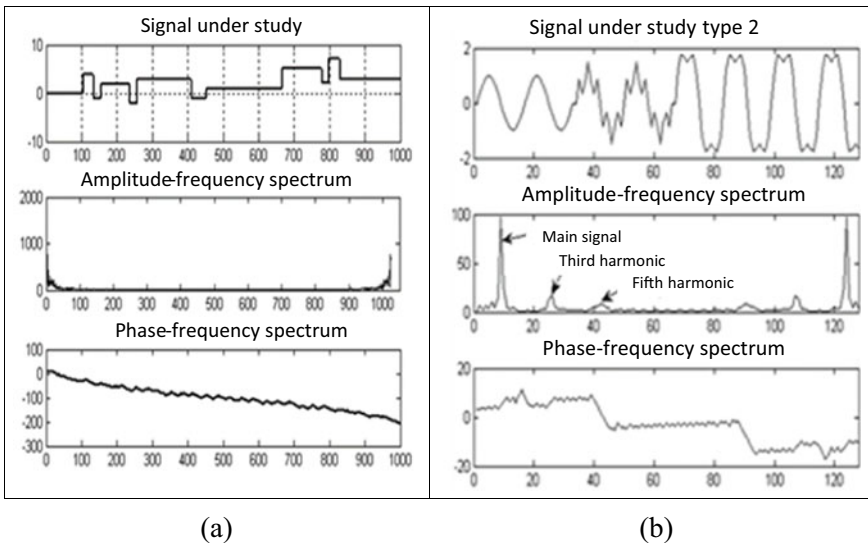
Fig. 4 The results of Fourier analysis of signals with the presence of **a** breaks of the first kind (amplitude differences) and **b** the third and fifth harmonics

(a)   (b)
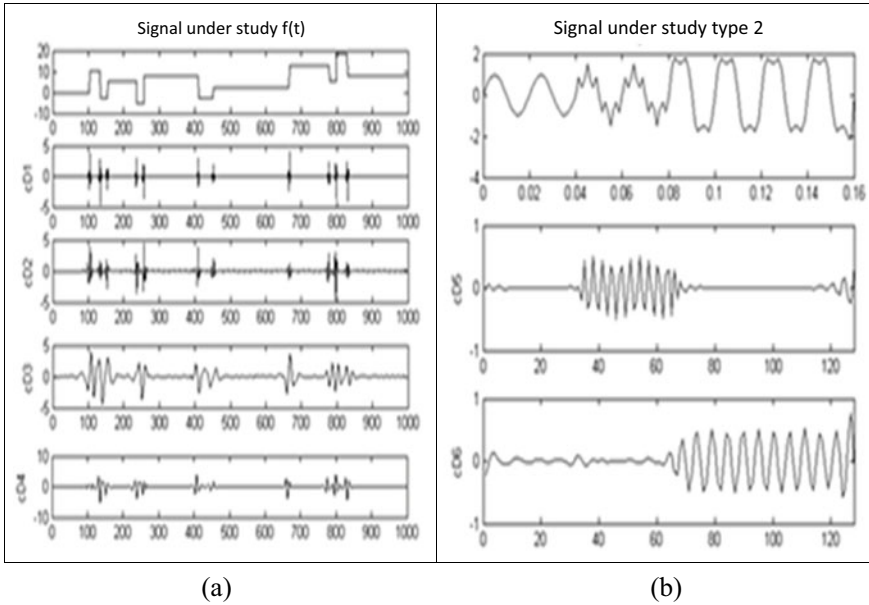
Fig. 5 The results of wavelet analysis of signals with the presence of **a** breaks of the first kind (amplitude differences) and **b** the third and fifth harmonics

Let's analyze the influence of the presence of distortions that are present in the information signal on the results of its orthogonal transformation (Figs. 6, 7, 8 and 9).

The results of the wavelet analysis (Fig. 6) show the following. Distortion of the type of voltage interruption leads to the value of the coefficient $cD1$ (in contrast to the exclusively sinusoidal signal). You can also set the start and end of the distortion value by the value of $cD1$.

Distortion of the type of undervoltage and overvoltage also leads to the value of the coefficient $cD1$ indicating the beginning and end of distortion. The maximum values of wavelet coefficients are observed at the seventh ($cD7$) and eighth (cD) levels of wavelet decomposition.

The presence of harmonic components in the signal is clearly manifested at the first level of wavelet decomposition of the signal (a). Short-term distortions lead to the appearance of $cD1$ (b)—(short-term changes in its values). Repetitive high-frequency distortions (output voltage of the six-pulse converter) lead to the appearance of the coefficient $cD1$ in the form of a sequence of short values.

The wavelet coefficients of the first level $cD1$ show the presence of distortion and its duration. The wavelet coefficient of the fourth level of wavelet decomposition is of the greatest importance. Oscillatory high-frequency distortions are characterized by the highest value of the wavelet coefficient at the third level of wavelet decomposition.
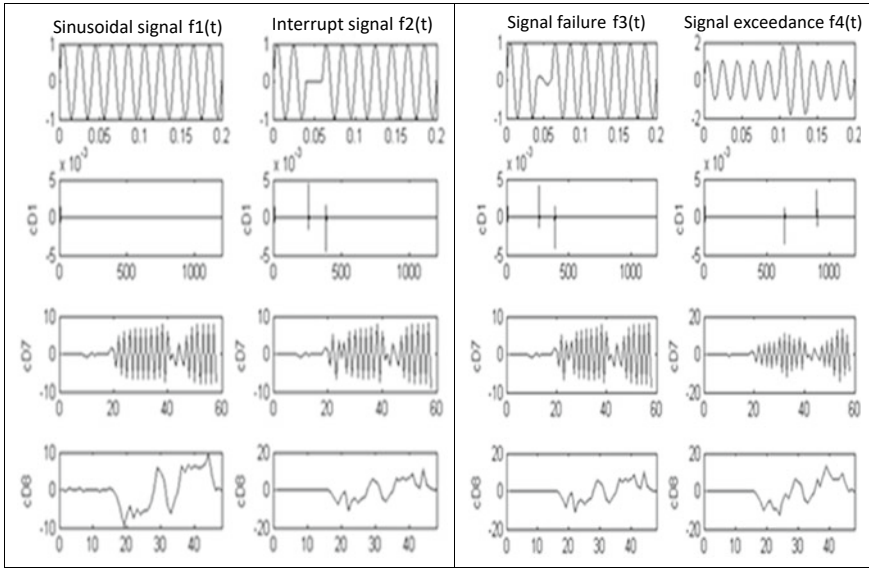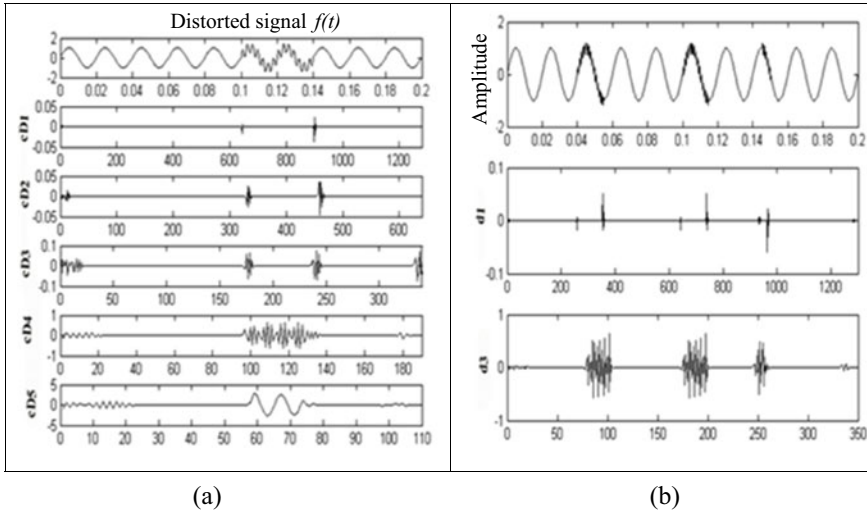
Fig. 6 Wavelet-conversion of information signals: **a** sinusoidal signal and the presence of voltage interruption, **b** lowering and exceeding the voltage
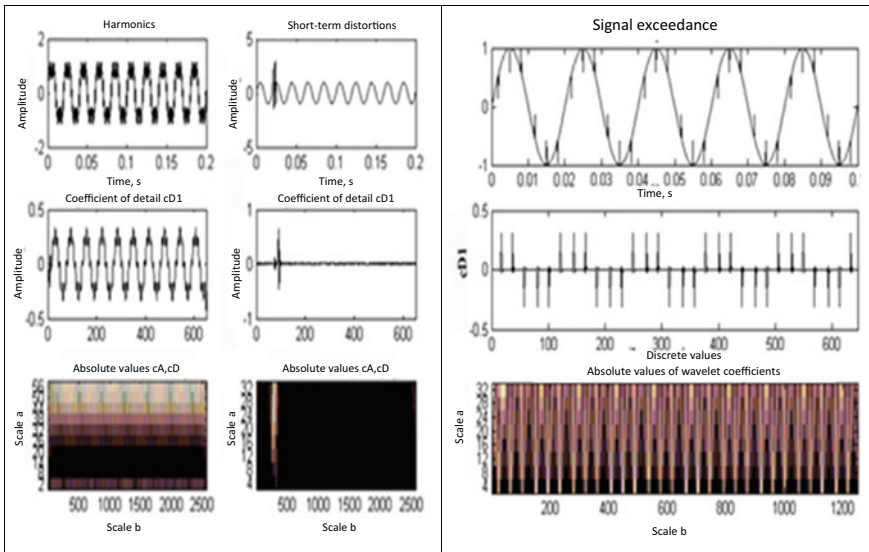
Fig. 7 Wavelet decomposition of distorted signals (**a** harmonics), **b** short term and periodic distortions) and their scalograms

(a)   (b)

Fig. 8 Wavelet decomposition of distorted signals (presence of the seventh harmonic (**a**), oscillating high-frequency distortion (**b**))

(a)   (b)
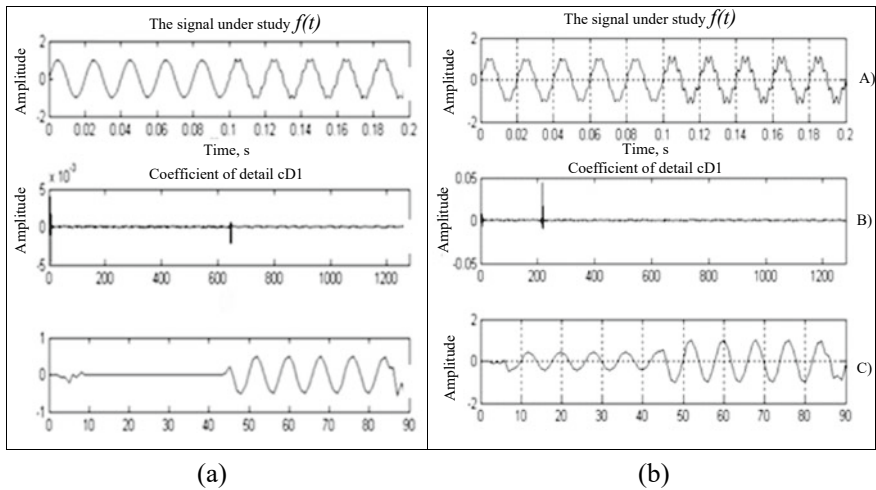
Fig. 9 Wavelet decomposition of distorted signals (presence of harmonics from a certain period (**a**) and with a change in amplitude (**b**))

Where—(a)—the presence of the seventh harmonic in the signal, starting from the sixth period, the wavelet coefficient of the first level and—the detailed coefficient of the fifth level of the wavelet decomposition; (b)—the presence in the signal of the seventh harmonic from the 1st to the 5th period 30% and from the 6th to the 10th

period—60% of the amplitude of the fundamental harmonic, detailing the coefficient of the first level and the fifth level of wavelet decomposition.

6 Development of Method for Detecting and Identifying Distortions of Electricity Quality

The study is based on computer model calculations, which reproduce the most characteristic distortions of signals (transients, short-term distortions, distortions of the waveform, deviations from the nominal value), followed by a series of multi-level determination of distortions that occur. The result of the analysis in the future is the basis of the algorithm for identifying the type of distortion. In [5] the generalized results of the analysis and characteristic signs on which it is possible to identify distortions are resulted.

The analysis of the obtained results in [6] wavelet transform of sinusoidal signal and distortions of electric energy quality (values of detailing coefficients of the first level of decomposition and scalogram) shows the possibility of only detecting distortions and determining the beginning and/or the end of the corresponding distortion by the value of the detail coefficient of the first level of wavelet decomposition. This detail wavelength repetition rate has zero values at most points except those where the violation occurs. The amplitude changes in a very short time and drops rapidly to zero, it can also be used to determine the duration of distortion (its *beginning* and *end*).

As noted earlier, the wavelet transform allows you to divide the input signal into frequency subbands depending on the level of decomposition, according to Table 1.

As shown earlier, by analyzing the values of the detail coefficient of the first level of wavelet decomposition, it is only possible to determine the presence of distortion

Table 1 Wavelet transform frequency bands (signal sampling frequency 12.8 kHz)*

Decomposition levels	Frequency ranges	
	Coefficients of approximation, cA_j	Coefficients of detail, cD_j
1	0…3.2 kHz	3.2… 6.4 kHz
2	0…1.6 kHz	1.6…3.2 kHz
3	0…800 Hz	800 Hz…1.6 kHz
4	0…400 Hz	400…800 Hz
5	0…200 Hz	200…400 Hz
6	0…100 Hz	100…200 Hz
7	0…50 Hz	50…100 Hz

* Based on the requirements of the methodology [5] of MRA properties, harmonic analysis should be performed up to 50 harmonics, which led to the choice of sampling rate 12.8 kHz

and its duration. Determination of the type of distortion should be carried out by further analysis of the results of wavelet decomposition (in accordance with the frequency ranges—Table 1). That is, the level of detail will depend on the type of distortion and its frequency range.

Analysis of the results of wavelet transform, allows us to make the following generalizations. The presence of values of the detail factor at the first level of wavelet transform *cD1* indicates signal distortion and its duration. Further detail on the levels of wavelet decomposition (analysis of the detail coefficients of the second—fifth level) shows that the greatest energy of the wavelet coefficient is at the fourth level (*cD4*), which clearly indicates the presence in the signal of harmonics in the range 400–800 Hz (according to the data given in Table 1). It also follows that the detailing coefficient *cD1* (frequency ranges 3.2–6.4 kHz) insensitive to steady signals, but shows large fluctuations in amplitude, which are associated with high-frequency short-term distortion of the waveform. If these coefficients have sharp and short amplitude peaks, then there are distortions of short duration, such as voltage drop (failure), excess or short signal interruptions. Otherwise, if they are represented by long series of peaks, then they are correlated with repeated high-frequency distortions.

In the Table 2 presents a systematization of the results. It is shown that for the so-called express analysis of electricity quality it is advisable to use a two-level wavelet transform (Fig. 2). This allows you to quickly determine the presence of distortion, its duration and assign it to a separate group (Table 2).

Summarizing the above, it is necessary to note the following. The developed information model for determining and identifying the type of distortion of electricity quality parameters is a hierarchical structure of comparative calculation of local maxima of wavelet transform with a bias adaptive to the studied signal (Fig. 10).

Table 2 The original frequency ranges of the decomposition tree and the corresponding types of distortion

Decomposition level	Frequency range (kHz)	Distortion type
Level 1 (detailed coefficient $cD1(n)$)	3.2–6.4	• Presence of distortion, its duration
Level 2 (detailed coefficient $cD2(n)$)	1.6–3.2	• High frequency distortion; • Harmonics (>30 times); • Short-term periodic; • Non-stationary low-frequency
Level 2 (approximation coefficient $cA2(n)$)	0–1.6	• Base frequency and harmonic components up to 30 harmonics; • Transitional processes; • Oscillating high-frequency; • Short-term voltage reductions and increases; • Interruption, lowering and exceeding the nominal value of voltage
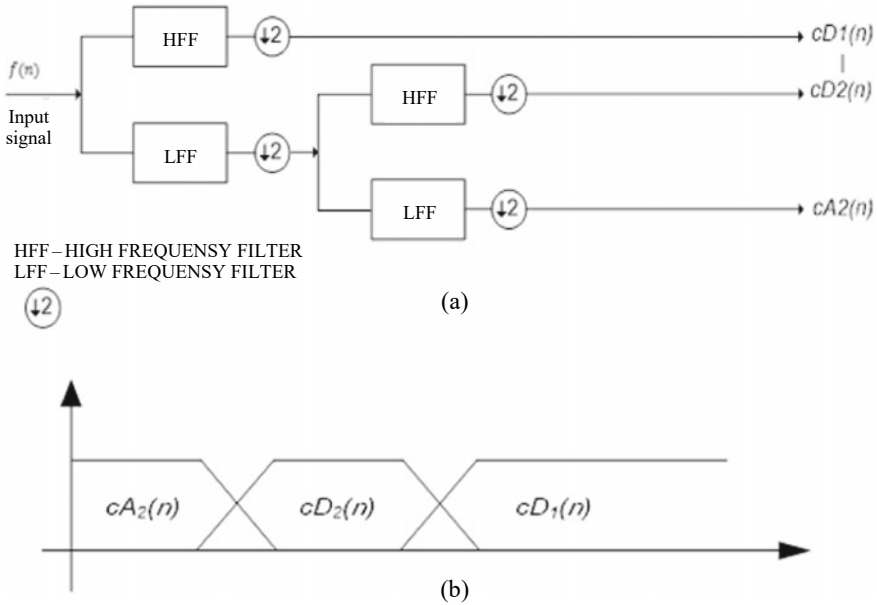
Fig. 10 Two-level wavelet decomposition tree for express analysis of identification of distortions of quality of electric energy (**a**), frequency half-axes of two-level wavelet decomposition (**b**)

Analysis of the value of the detailing coefficient of the first level of wavelet decomposition allows to detect the presence of distortion, and then, depending on the frequency range, analyze the values of the detailed coefficients of wavelet decomposition levels 2–8 with fixing not only the presence of the type of distortion, but also its location in time space.

Wherein, superficial analysis of the presented model allows us to draw some conclusions, namely:

Firstly, the presence of transient distortion or non-stationary low-frequency in the signal is determined by the value of the detailed wavelet coefficient of the first level as follows. Value *cD1* compared with the threshold value μ. The initial value of the threshold value is determined on the basis of regulatory documents and is calculated as follows: $\mu = \delta * \max|cA_J(n)|$, where δ is from 0.1 to 1% the maximum value of the approximating wavelet coefficient of the last level of wavelet decomposition $(cA_J(n))$. Comparison with value μ is performed at each point of the coefficient *cD1(n)*. If an arbitrary meaning *cD1(n)* more than μ—there is a transient distortion, otherwise—non-stationary low-frequency distortion.

Second, distortions of transients usually consist of frequency components from hundreds of Hz to several MHz and their duration does not exceed half of the period of the fundamental frequency.

Third, in accordance to the standard [7], low-frequency distortions should be analyzed on the basis of 10/12 (harmonics) or 5/6 cycles (harmonics of the 40th

or 50th order, above 9 kHz). That is, information about low-frequency components should be stored for about 100 or 200 ms. This requires both a significant amount of memory to store them and an increase in computing resources in the case of high sampling rate, which is necessary to analyze the distortion data by processing the sampled values of the input signal stored in memory.

7 The Formation of the Vector of Classification Features of Electric Power Quality Distortions

When classifying distortions of electric power quality parameters, it is essential to highlight the features that, firstly, have to be resistant towards different cases of distortions in electricity network, and secondly, will allow identifying and highlighting quality changes in voltage signals and in the current of many network. The majority of distortions are identified and classified in terms of such parameters as amplitude, duration, frequency range, or wave shape. As a result, separate distortions of electric power quality may not be interpreted explicitly in the process of classification. Namely, there is a need in development of a vector of classification features, with help of which it will be possible to identify both the occurrence of distortion of electric power quality and its moment and place of the occurrence.

The contrastive analysis of methods of identification features formation and informative signals classification has been conducted in this research. The methods have been conditionally divided into two general groups: statistical methods and methods based on division of input realization into several systems of orthogonal functions. The analysis has showed that methods of the first group are traditionally used in power industry [8–10]. However, the second group of methods of identification features formation and classification provides more general and independent algorithms, which allow to provide identification of bigger number of input realizations based on one unified approach [11].

Thus, it becomes necessary to develop a method of identification features formation and classification of electric load graphs. Such method could be based on division of input realization in the system of orthogonal functions, and which could provide the possibility of information signals features identification—the gaps of type I with increased promptness, accuracy and unification of processing algorithm in comparison with existing methods.

According to previous researches, typical features of a signal are represented at different levels during wavelet decomposition. The statement from Parseval's theorem is chosen for the basis of the identification and classification of electric power quality distortions method developed in this research: "The signal power in the time space equals the sum of powers, concentrated at different levels of decomposition of appropriate wavelet transformation of the signal given" [12]. Mathematically it is formulated as following: $\|\varepsilon\|_2^2 = \sum_i |< \varepsilon, \psi_i >|^2$, where $\varepsilon \in L^2$ and ψ_i are the orthonormal basis L^2 (the complete power function). At the same time, it is accepted

that the power, identified as its L^2 norm squared, remains during orthonormal wavelet transformation as well.

Paying attention to the features of wavelet transformation of a signal, Parseval's theorem is to be written as following:

$$\sum_{k=1}^{N} |f(k)|^2 = \sum_{k=1}^{N} |cA_J(k)|^2 + \sum_{j=0}^{J} \sum_{k=1}^{N} |cD_j(k)|^2, \tag{4}$$

where $\sum_{k=1}^{N} |f(k)|^2$ is the overall power of a discredited signal, N—the number of discrete units in a period; $\sum_{k=1}^{N} |cA_J(k)|^2$ is a power, which is contained in approximating coefficients of the last (J) wavelet decomposition level (in a case of wavelet transformation according to Mallat algorithm); $\sum_{j=0}^{J} \sum_{k=1}^{N} |cD_j(k)|^2$ is a power, which is contained in detailing coefficients of all wavelet decomposition levels—from level 0 to level J.

As a result of wavelet decomposition of a signal with the help of wavelet coefficients analysis, time localized information about its distortion obtained (the deviation from the nominal values of its parameters). Such a distortion is identified within high- and low-frequency ranges. The values of the given coefficients (their frequency and power features) are also defined and used for the basis for deviation classification of electric power quality [13–15]. Individual information regarding electric power quality distortions (the time of the deviation, its duration and power distribution) is contained in detailing coefficients. That is why analysis of these parameters is to be concerned in the developed method.

As previous researches showed, the identification and further classification of deviations of electric power quality parameters distortions through identification of the values of wavelet coefficients not always give clear results. This is caused by fundamental frequency harmonic in the studied signal. Moreover, the given method is used only for the quick express analysis. In order to avoid that, a modified vector of classification features of distortions of electric power quality parameters.

The analysis of the results of research on distorted signal power distribution according to decomposition levels, provided there are simultaneous frequency and amplitude distortions, showed the following. As known, the signal of limited duration added by a distortion is presented as $f(t) = p(t) + s(t)$, where $p(t)$ is a sinusoidal signal, $s(t)$—a distorted signal. In a wavelet sphere, such a signal will be presented as following:

$$V_{f(t)} = [cA_J, cD_1, cD_2, ..., cD_J], \tag{5}$$

while the signal power

$$E_{f(t)} = [\|cA_J\|, \|cD_1\|, \|cD_2\|, ..., \|cD_J\|]. \tag{6}$$

Appropriately, sinusoidal signal will be presented as:

$$V_{p(t)} = \left[cA_{J(p(t))}, cD_{1(p(t))}, cD_{2(p(t))}, ..., cD_{J(p(t))} \right],$$ (7)

while sinusoidal signal power will be the following:

$$E_{p(t)} = \left[\left\| cA_{J(p(t))} \right\|, \left\| cD_{1(p(t))} \right\|, \left\| cD_{2(p(t))} \right\|, ..., \left\| cD_{J(p(t))} \right\| \right].$$ (8)

The vector of classification features of electric power quality distortions $V_{features}$ is represented by the difference between powers according to wavelet decomposition levels $\Delta E_{j=1}^{J} = E_{j=1(f(t))}^{J} - E_{j=1(p(t))}^{J}$ and mathematically represented as following (Fig. 11):

$$V_{features} = \left[\Delta E_{cA_J}, \Delta E_{cD_1}, \Delta E_{cD_2}, ..., \Delta E_{cD_J} \right].$$ (9)

Let's analyze the needed frequency of information signal discretization and, respectively, necessary level of signals processing while maintaining sufficient characteristics of precision and quality of classification of electric power quality distortions types. As known, the filters of high and low frequency, which are used for wavelet transformation, have half frequency line in relation to the analyzed signal. Let's mark the discretization frequency of information signal as *Fs*. Figure 12
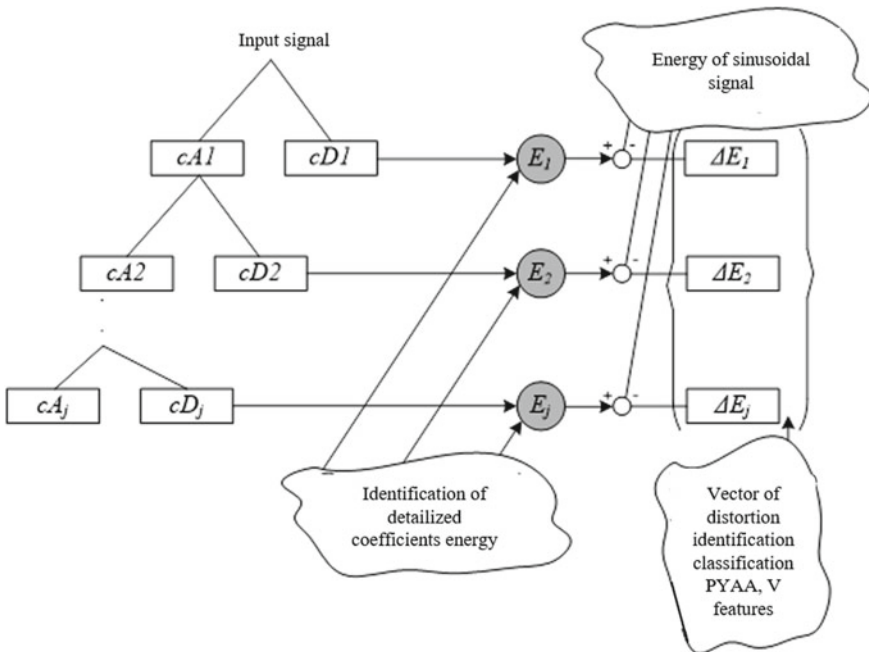

Fig. 11 The algorithm of vector of identification and classification formation of electric power distortions according to the difference between powers of wavelets coefficients according to wavelet decomposition levels

and Table 3 show the frequency ranges of wavelet transformation depending on decomposition level.

As known, wavelet decomposition breaks signal into frequency subranges (according to wavelet decomposition levels) depending on discretization frequency. In Table 3 such a frequency break is shown in general.

Fundamental frequency of the signal is $f_{r.s.} = 50$ Hz, the highest level of wavelet decomposition is J. Then a frequency range needed for the study of the signal will match frequency range of the detailing coefficient of the last wavelet decomposition level, in particular $F_s/2^{J+1} \leq F_{f(t)} \leq F_s/2^J$. Having the logarithm problem, a range of the necessary value of decomposition level J is obtained i.e.,
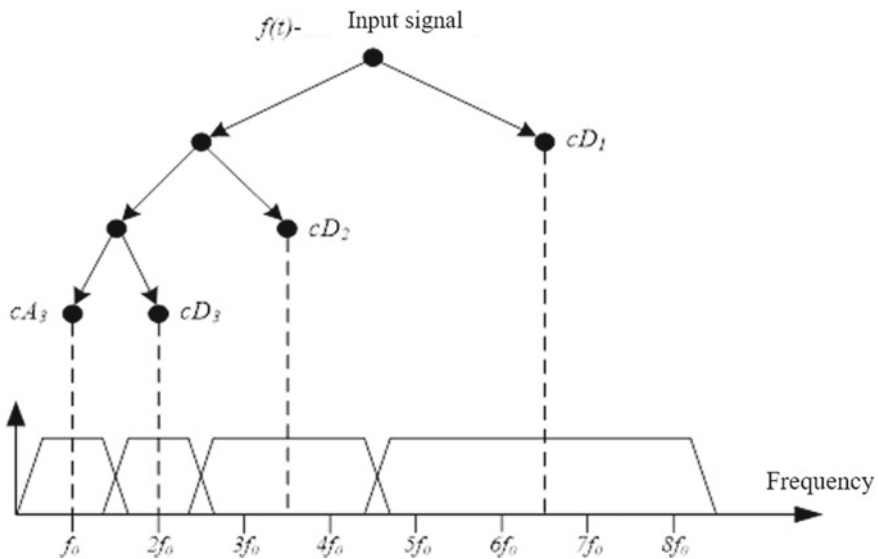
Fig. 12 Frequency ranges of wavelet transformation according to Mallat algorithm (multiresolution analysis)

Table 3 Frequency ranges of wavelet decomposition according to Mallat

Decomposition level (j)	Frequency range	
	Approximation coefficient (cA_j)	Detailing coefficient (cD_j)
1	From 0 to $F_s/2^2$ Hz	From $F_s/2^2$ to $F_s/2^1$ Hz
2	From 0 to $F_s/2^3$ Hz	From $F_s/2^3$ to $F_s/2^2$
…	…	…
J	From 0 to $F_s/2^{j+1}$	From $F_s/2^{2\,J+1}$ to $F_s/2^J$

$$\log_2\big(F_s\big/F_{f(t)}\big) - 1 \le J \le \log_2\big(F_s\big/F_{f(t)}\big). \tag{10}$$

For the studied case (discretization frequency is 3 200,00 Hz) we have the following. So, according to the Eq. (6), we have $3 \le J \le 4$. In this research, $J = 4$ is accepted. Owing to the fact that for the accuracy of the electric power distortion classification, the fundamental frequency $F_f(t)$ is the object of the research, the minimal analyzed decomposition level is $N_{min} = 2*J = 8$.

In this research, the influence of various wavelet types (Haar, Daubechies, Coiflets, Symlets, Morlet, Meyer) on the efficiency of such a method of vector formation of classification features of electric power quality distortion is also studied [16, 17]. The analysis of the results showed the following.

The choice of optimal accepted maternal wavelet without consideration of distortion type is a difficult procedure. At the same time, firstly, short-term and fleeting distortions are best marked with the help of Daubechies wavelet *db4* and *db6*, whereas slow distortions—*db8* and *db10*. Secondly, Haar wavelets use causes distortion energy shift and lowering of voltage into decomposition levels sphere 3–4, as well as to more expressed values of low-frequency distortions. Authors suggest making choice of maternal wavelet the following way. As wavelet is more localized in time at the upper levels, and its oscillations are of high speed and with low period, those levels are more useful for identification of short-term and fleeting distortions. While at lower decomposition levels, it is better to choose wavelets with the bigger oscillation periods. With regard to this, it is recommended to use the following types of wavelets—*Db2, Sym2, Coif.*

References

1. Baleanu, D.: Advances in Wavelet Theory and Their Application in Engineering, Physics and Technology/Croatia. (2012). www.intechopen.com.
2. Girgis, A., Chang, B., Makram, E.: A digital recursive measurement for on line tracking of power systems harmonics. IEEE Trans. On Power Deliv. **6**(3), 1153–1160 (1991)
3. Dash, P., Pradham, A., Panda, G.: Frecuency estimation of distorted power system signals using extended complex Kalman filters. IEEE Trans. Power Deliv. **14**(3), 761–766 (1999)
4. Hart, D., Uy, D., Novosel, D., Kunsman, S., Laplace, C., Tallarini, M.: Improving power quality. ABB Rev. **4**(1), 12–19 (2000)
5. Mallat, S.A.: A theory for multiresolution signal decomposition: The wavelet representation. IEEE Trans. Pattern Anal. Mach. Intell. **11**, 674–693 (1989)
6. Volodarsky, E.T.: Electricity quality monitoring system in decentralized power supply systems /E.T. Volodarsky, A.V. Voloshko. East. Euro. J. Adv. Technol. **3/8**(69), 10–17 (2014)
7. GOST P 51317.4.7: Compatibility of technical means is electromagnetic. General guide to measuring instruments and measurements of harmonics and interharmonics for power supply systems and technical means connected to them (2008)
8. Razumnyi, I.T.: Klassifikatsiia grafikov elektricheskoi nagruzki pogruppam elektropriy-omnikov ugolnukh shakht. In: Razumnyi, I.T., Rukhlov, A.V. (eds.) Naukovyi visnyk NHU, vol 12, pp. 63–65 (2009)
9. Prakhovnik, A.V.: Kompleksnaia optimizatsyia rezhymov elektropotrebleniia promyshlennykh obiiektov. In: Kn (ed.) Sovremennyie problemy energetiki, pp. 82–85. Kiev (1980)

10. Fukunaga, K.: Vvedeniie v statisticheskuiu teoriiu raspoznavaniia obrazov. Per. s anl. – M.: Nauka, Glavnaia redaktsyia fiziko-matematicheskoi literatury, pp. 386 (1979)
11. Voloshko, A.V.: Sravnytelnyi analiz metodov klasterizatsyi grafikov elektricheskikh nagruzok. In: Voloshko, A.V., Lutchyn, T.N. (eds.) Enerhetyka: ekonomika, tekhnolohii, vol. 2, pp. 111–115 (2009)
12. Osowski, S.: SVD technique for estimation of harmonic components in a power system: a statistical approach. Gen. Trans. Distrib. IEE Proc. **141**(5), 473–479 (1994)
13. Stoica, P.: List of references on spectral line analysis. Sig. Proc. **31**(3), 329–340 (1993)
14. Pham, V.J., Wong, K.P.: Antidistortion method for wavelet transform filter banks and non-stationary power system waveform. IEE Proc. Gen. Trans. Distrib. **148**(2), 117–122 (2001)
15. Huang, S.-J., Hsich, C.-T.: Visualizing time-varying power system harmonics using a Morlet wavelet transform approach. Electric Power-Syst. Res. **58**(2), 81–88 (2001)
16. Zhen, R., Qungu, H., Lin, G., Wenying, H.: A new method for power systems frequency tracking based on trapezoid wavelet transform. Int. Conf. Adv. Power Syst. Control, Oper. Manag. **2**, 364–369 (2000)
17. Diego, R.J., Barros, J.: Global method for time-frequency analysis of harmonic distortion in power systems using the wavelet packet transform. Electric Power Syst. Res. **79**(8), 1226–1239 (2009)

Faults Indicators Applying for Smart Monitoring System for Improving Reliability Electric Power Distribution

Ihor Blinov , **Ievgen Zaitsev** , **Euvgen Parus** ,
and Victoriia Bereznychenko

Abstract The development of the digital technology industry, the growing dependence of industry and household consumers on electricity, and the world's entry into the fourth industrial revolution (Industry 4.0) are factors in the growing need for smart, efficient and reliable next-generation energy systems. Building a new generation of smart grids ("Smart grid") involves the use of advanced information, communication and computing technologies to ensure the flexibility and efficiency of the grid at all stages of electricity from its production to consumption. It should also be borne in mind that the main purpose of electrical systems in general and electrical networks in particular is to meet the needs of consumers to ensure a sufficiently stable and reliable supply of electricity. Stable and reliable supply of electricity caused by power outages is generally undesirable, and in some cases can lead to very unpleasant consequences—disruption of communication systems, shutdown of technological processes of industrial enterprises, the impossibility of normal living conditions and activities of the population. To prevent this, special measures using for during the design and operation of electrical networks and systems to improve the operation of all their elements and increase the reliability of electricity supply to consumers. One of the key measures is the construction of backup systems, the use of special protection devices and automation, more careful supervision of electrical installations during their operation, etc. All this requires significant of biggest capital investment for energy industry. In many cases, in existing electrical networks, it is advisable to use factual monitoring tools that allow obtaining telemetry data and control and diagnostic parameters from a sufficient number of grid points to ensure automatic power recovery or damage detection to minimize the consequences of failures, localization of damage. Therefore, damage to any element in the electrical network or the system as a whole, there are transients that occur quickly. The mode parameters are significantly different from the allowable ones. Faults indicators for overhead and cable power lines are an effective means of monitoring that increase the efficiency of locating damage to electrical networks. Faults indicators its tools that allow automatic indication of the damaged section of the line, and used to determine interphase short circuits and SPGFs, detection of stable and unstable damage,

---

I. Blinov (✉) · I. Zaitsev · E. Parus · V. Bereznychenko
Institute of Electrodynamics of the National Academy of Sciences of Ukraine, Kyiv, Ukraine
e-mail: blinovihor@gmail.com

235

depending on the type of neutral in low and medium voltage distribution networks. Therefore, this section of the monograph is devoted to issues related to ensuring the use of faults indicators for LV and MV distribution networks, and was contains:

- review of faults indicators application in the distribution power network;
- calculation of parameters for the selection of the optimal number of faults indicators conditions in the structure of monitoring system of radial electrical networks depending on the cost of maintenance of distribution power network;
- taking into account the components of losses of the energy supply company related to power outages to consumers (shortage of electricity);
- analysis of emergency current zones in LV and MV grid to calculate ranges of measurement of faults indicators.

Consideration and solution of the above issues allowed forming within these work requirements for the use of faults indicators as part smart monitoring system of distribution power network of IPS of Ukraine. Moreover, need to use faults indicators for LV and MV power grid to ensure recovery power supply associated with unplanned interruptions in the operation of electrical networks.

Keywords Faults indicators · Distribution power network · Energy supply · Emergency current zones · Smart grid

1 Introduction

One of the important directions of development of the electric power industry both in the world and in Ukraine is the improvement and construction of electric power networks and systems in accordance with the Smart Grid concept. The main idea of such systems is reliable, energy efficient and high-quality energy supply, which based on the growing role of management as a leading factor in the innovative development of electricity and building high-performance information and computing infrastructure.

The introduction of modern Smart Grid technologies in the grid allows increasing the reliability of electricity supply to electricity consumers and increasing the efficiency of distribution system operators in market conditions of electricity. The development of modern electrical networks according to the Smart Grid concept allows increasing the flexibility in the operation of power systems in the conditions of increasing the number of distributed energy sources and renewable energy sources. This allows providing favorable conditions for the decarbonization of electric power.

Ensuring the flexibility of power grids and the efficiency of management of power grids and systems directly depends on the availability and quality of data provided, which allow obtaining telemetry data and control and diagnostic parameters from a sufficient number of grid points. Such data allow to provide flexible management of the power grid and to estimate the current technical condition of the electric power equipment on-line [1–3]. In this case, the various sensors and control devices

built in accordance with the Smart Grid concept using obtain telemetry data and control and diagnostic parameters [3–6]. The use of sensors and control devices in combination with the prompt processing of data obtained from sensors can minimize the occurrence of emergencies caused by poor connections, faulty sensors, ensuring inadequate communication between components of the power grid. Such defects can lead to inefficient operation of control systems and thus lead to serious interruptions in the power supply to consumers. However, in the event of emergencies and abnormal regimes, it is necessary to have technologies for rapid detection and elimination of these regimes, which allows providing the necessary conditions to improve the reliability and safety of energy systems and networks. It is also important to use modern methods of managing electrical networks together with real-time forecasting tools [7–12] based on the use of computer modeling and decision-making methods [13].

Achieving this in accordance with the concept of Smart Grid involves the implementation of automation systems and diagnostic maintenance of distribution networks, determining the location of damage to the network, followed by automatic restoration of power supply [4, 5]. One of the main components of systems built on the concept of Smart Grid is the diagnosis of emergency modes and fault monitoring [2]. This is due to the fact that fault to power lines leads to disruptions in electricity networks, which affects the quality and reliability of electricity supply to consumers. Therefore, it is important for quickly and accurately determine the location of fault to power lines [14]. Effective solution of this problem gives a significant economic effect due to the reduction of power outages, reducing transport costs to bypass power lines, minimizing the total time of organization of repair and restoration work [15, 16].

One of the ways to increase the efficiency of locating fault and the level of monitoring of electrical networks in general is the installation faults indicators for control faults of overhead and cable power lines. One of the ways to increase the efficiency of fault finding and monitoring the level of electrical networks in general is to install indicators of emergency conditions of overhead and cable transmission lines—tools that are becoming more common in European networks and allow automatic indication of damaged sections of the line [16–19]. Such devices using to detect interphase short circuits and SPGFs, detection of stable and unstable damage, depending on the type of neutral in the distribution networks of 6–10, 35 and 110–150 kV.

In Fig. 1 shows, a typical structure of the system for determining the location of damage in the distribution network implemented in accordance with the concept of Smart Grid. The application of the structure allows ensuring the provision of the required quality and reliability of electricity supply to the consumer.

Given the progressive trends in the development of electrical networks for more effectively solve the problem of finding the location of damage to power lines using indicators of emergency conditions, it is advisable to build an automatic system for monitoring the state of electrical networks and locating damage. Moreover, will manage electric network switching devices, using existing information exchange networks according to GSM or UMTS communication standards and integration with SCADA-systems used in electric power networks.
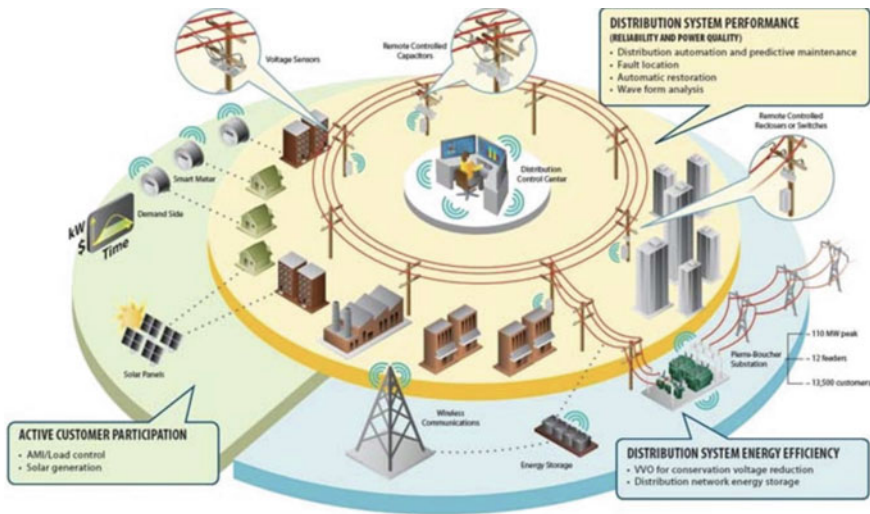
Fig. 1 Structure of Smart Grid with indicators of emergency conditions (natural resources Canada)

In this case, it is necessary to provide such systems with an intellectual component through the construction of expert systems for determining the location of damage based on the analysis of the obtained control and diagnostic parameters of the monitoring of the state of the transmission line. This will allow the formation based on the received information of control actions on localization of places of damages or reduction of loading for avoidance of occurrence of damages at the expense of use of recloses or switches with remote control.

2 Faults Indicators as Part of Smart Grid Distribution Networks

A significant number of damages that occur on power lines and lead to disruption of electricity networks affect the reliability of electricity supply to consumers. Therefore, quick and accurate determination of the location of the overhead line damage will reduce the interruption in the power supply to end users, reduce transport costs for inspection of the line and minimize the total time of repair and restoration work.

Emergency locking devices (ELD) in the areas of radial electrical networks help to reduce the time of finding the location of damage [20–22]. This makes it easier to find the emergency area and reduces the total downtime of the line. Such devices can detect interphase short circuits (short circuits) and single-phase earth faults, detect stable and unstable damage, regardless of the type of neutral in the distribution networks of 6–35 and 110–150 kV. The most effective use of ELD is to install them

on the most important sections of the line to quickly determine the location of damage in the event of an accident [24, 25].

According to the principle of operation, these devices are those that measure the parameters of the emergency mode, carrying out continuous monitoring of the magnetic field below the wire of the transmission line. The value measured by the damage detection indicator consists of horizontal (zero sequence current) and vertical (zero sequence voltage) components of the electromagnetic region. Thus, the indicator responds to a change in the value of the current that exceeds the programmed threshold value and signals the occurrence of damage in the area entrusted to it. A description of the principle of operation of such indicators is given, for example, in [15, 24, 26–29].

When installing indicators, there are two types: resistance and transmission line wires. Each of these types responds to different damages, so it is planned to install them to work with the joint suspension on power lines of different voltage classes. There are features of the ELD depending on the location. Thus, ELD, which are installed on the support of the transmission line (see Fig. 2a), allow to distinguish between phase-to-phase short-circuits and single-phase damage, including earth faults, regardless of the type of neutral. In addition, the advantage of this type of indicator is the ability to determine the direction of the damage location relative to the installation site.

The principle of the direct vindication of the fluctuation of the field affects the pore-nanny of the vector values of the measured voltage (and itself—the intensity of the electromagnetic field) and the transient stream (the flow of the electromagnetic field). If the vector of the transient current is near the phase and the stress vector,
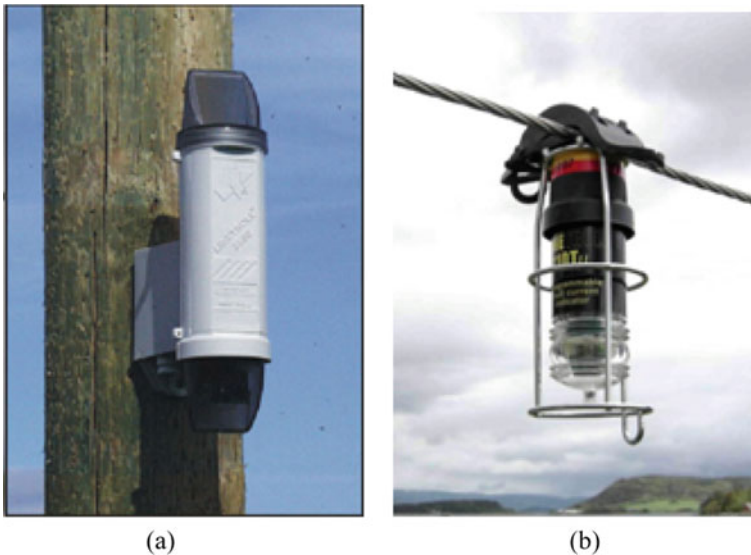

(a)   (b)

Fig. 2 ELD appearance

the indicator will show "short before ELD", and if the vector and current are at the opposite phase, then the indicator will show "shock behind ELD". The presence of such ELDs on all phase wires allows you to designate the type of short circuit: one, two–three-phase short circuits. Such annexes are completely autonomous and do not require a connection to the outside living quarters. The stench can be mounted without interruption on the wires of the power transmission line without streak lines in quiet weather, if it is necessary for the minds to save the power supply, it is allowed by the regulations for the operation of the power transmission line.

Installed on the wires of the ELD power transmission line (div. Fig. 2b)—single-phase attachments, which show single-phase faults, and for the presence of sufficient struma power—single-phase earth faults.

Let's take a look at the main principles of the functioning of the system for monitoring accidents of the stations with ELD victories. In the event of faulty faults on the wires (wires) of the damaged phase of all ELD, located between the place, and the revitalizing substation, fix the fact of the presence of emergency plumes. Installed in other areas of the ELD and should be changed to the so-called "sleep" mode (Fig. 3).

As can be seen from Fig. 3, ELD help to change the hour of the request for the emergency line of the power transmission line for the time of seeing the path through the emergency streams. In this way, ELD is added to the change of the route by looking around the LEP for an hour, looking for an emergency car. Therefore, the task of choosing the optimal configuration of the system and monitoring the emergency stations of the distributive line without intermediary interfering with the task of choosing the optimal route for looking around the power transmission line.

Thus, on the one hand, the presence or absence of emergency currents in sections of the line should reduce the time of inspection of transmission lines by refusing to inspect certain branches or areas with difficult access, where ELD did not record an
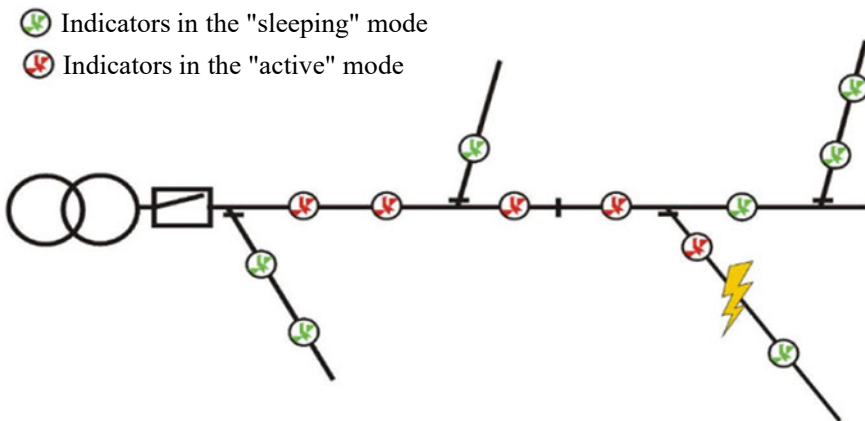

Indicators in the "sleeping" mode
Indicators in the "active" mode

Fig. 3 Operation scheme

emergency. On the other hand, the decision to install ELDs should be made only if there is an appropriate effect from their use.

3 Selection of the Optimal Configuration of the Monitoring System for Radial Electric Networks

Consider the indicators of the economic effect of the installation of fault indicators for one transmission line, reduced to one year of operation.

According to market conditions, the main criterion for the economic efficiency of using the monitoring system is to obtain the maximum possible additional profit for electricity distribution system operators, i.e.:

$$C^{(w)} - C^{(wo)} \to \max, \tag{1}$$

where: $C^{(w)}$—costs of electricity distribution system operators in the implementation of the monitoring system based on ELD; $C^{(wo)}$—costs of electricity distribution system operators in the operation of the transmission line without monitoring system.

The costs of electricity distribution system operators in the operation of the transmission line without a monitoring system consist of losses incurred as a result of interruptions in the power supply to consumers:

$$C^{(wo)} = L_{un}^{(wo)} + L_{fs}^{(wo)} + L_{fr}^{(wo)} + F_c^{(wo)}, \tag{2}$$

where: $L_{un}^{(wo)}$—losses of electricity distribution system operators due to undersupply of electricity to consumers; $L_{fs}^{(wo)}$—losses of electricity distribution systems operators due to fines stipulated by bilateral agreements; $L_{fr}^{(wo)}$—losses of electricity distribution systems operators due to fines for non-compliance with the reliability of electricity supply; $F_c^{(wo)}$—fuel consumption to search a place of fault in the electrical network.

Nowday, it is almost impossible to estimate the values of $L_{fs}^{(wo)}$ and $L_{fr}^{(wo)}$. Thus losses of electricity distribution systems operators due to fines stipulated by bilateral agreements may depend both on the number of interruptions in the power supply and the duration of such interruptions. For a detailed account of these factors, should be followed the terms of bilateral agreements between the electricity distribution systems operators and the consumers receiving electricity from this transmission line.

The introduction of a fault monitoring system in the distribution electrical network helps to reduce the search time for a damaged section of a power transmission line. This will reduce the power interruptions time. Thus the use of fault indicators will help improve the reliability of SAIDI and ENS. Obviously, if the power supply reliability indicators are observed within the normative values, there are no losses from fines: $L_{fr}^{(wo)} = 0$. In case of non-compliance with standard reliability indicators,

the electricity distribution systems operators must take a set of measures to reduce the number of interruptions and reduce their duration for the entire electrical network. Therefore, the numerical values of fines for non-compliance with standard reliability indicators for one distribution line should be calculated as a component in solving the problem of complex optimization of the operation of the all electrical network.

In the absence of rules for calculating fines for non-compliance with reliability indicators, it is impossible to develop formal procedures for calculating the value of $L_{fr}^{(wo)}$ when optimizing the objective function (2) in relation to one distribution line. Accordingly, the calculated values of the SAIDI and ENS indices for one distribution line today should not be considered either as a component of the objective function, or as a restriction on the decision to install fault indicators.

Considering the above factors, when developing formal algorithms for solving the problem of determining the number and places of establishing fault indicators, we take $L_{fs}^{(wo)} = 0$ and $L_{fr}^{(wo)} = 0$. Calculated indicators of power supply reliability will be calculated only to assess the effectiveness of the decision made in accordance with the standard values and values of reliability indices for a distribution line that operates without fault indicators installed on it.

The fuel consumption that occurs when searching for a fault section of a power transmission line depends, first of all, on the strategy for searching site of emergency. Therefore, the value of fuel consumption should be calculated with reduction to a significant period of time (for example, with reduction to one year), taking into account emergency at different sections of the transmission line in relation to the chosen general strategy for searching for an emergency on the transmission line.

The introduction of a fault monitoring system is accompanied by additional costs for the purchase, installation (C_i) and scheduled maintenance of these devices. Thus, the costs of electricity distribution systems operators in the implementation of the project to install fault indicators will have the following main components:

$$
\begin{aligned}
C^{(w)} &= \left(\frac{C_i}{P_s} + C_{as} \right) + L_{un}^{(w)} + L_{fs}^{(w)} + L_{fr}^{(w)} \\
&= C_{i(y)} + L_{un}^{(w)} + L_{fs}^{(w)} + L_{fr}^{(w)} + F_c^{(w)},
\end{aligned}
\tag{3}
$$

where: C_i—costs of purchase and installation of ELD; P_s—planned service life of ELD; C_{as}—annual cost of servicing the ELD; $C_{i(y)}$—reduced to one year of operation costs for ELD, installed on the distribution line; $L_{un}^{(w)}$—losses of electricity distribution systems operators due to undersupply of electricity to consumers during the operation of the emergency monitoring system; $L_{fs}^{(w)}$—losses of electricity distribution systems operators due to fines stipulated by bilateral agreements during the operation of the emergency monitoring system; $L_{fr}^{(w)}$—losses of electricity distribution systems operators due to fines for non-compliance with the reliability indicators of electricity supply during the operation of the emergency monitoring system; $F_c^{(w)}$—fuel consumption for the search of the emergency section of the transmission line operation of the fault monitoring system.

According to the above factors, we accept in the future $L_{fs}^{(w)} = 0$ and $L_{fr}^{(w)} = 0$.

Equation (3) takes into account the total cost of all ELD installed in the distribution line. However, when solving the problem of choosing the optimal configuration of an fault monitoring system in a distribution electrical network, the number of these devices should be taken into account. There are several ways to account for this factor. In the simplest case, the costs of installing and maintaining ELD are assumed to be the same regardless of the location of their installation. Then reduced to one year of operation costs for ELD, installed on the distribution line, as a function of the number of these devices $C_{i(y)}(N_i)$ will look like:

$$C_{i(y)}(N_i) = \left(\frac{C_i^{(1i)}}{P_s} + C_{as}^{(1i)} \right) \cdot N_i, \qquad (4)$$

where: $C_i^{(1i)}$—cost of purchasing and installing one ELD; $C_{as}^{(1i)}$—annual maintenance costs of one ELD; N_i—number of ELD installed on the line.

If necessary, (4) can be expanded to specify the cost of installation and maintenance depending on the location of each ELD.

When developing and making a decision on the implementation of a monitoring system for emergency conditions of a distribution electrical network, one should take into account the level of automation of emergency situations diagnostics. In a simpler case, a direct view of the distribution line is carried out, guided by the light indication of the ELD. Then the value of $C_{in}^{(1i)}$ in (4) will be calculated from the cost of ELD, as well as the resources that will be spent on the installation of one ELD. The value of $C_{as}^{(1i)}$ in this case will be calculated based on the resources spent on maintenance of the ELD during the year (for example, the cost of maintain energy supply).

Another option for using ELD is the formation of a centralized system for diagnosing emergencies on the distribution line. In this case, the cost of the SCADA system supplied by the manufacturer of fault indicators is added to (4). In addition, the component $C_{in}^{(1i)}$ in (4) will additionally contain the cost of the GSM-communication module, and $C_{as}^{(1i)}$ will additionally include reduced to one indicator cost of annual maintenance of the SCADA system by the GSM-communication operator.

4 Accounting for the Components of Losses of the Electricity Distribution System Operators from Undersupply of Electricity

Consider in more detail the components of losses of the electricity distribution systems operators from the deficit of electricity due to unplanned interruptions in the power supply (emergency). Let consider the simplest line with a length of 1 km without branches with one consumer of electricity, the calculated power of which is P kW. Let the statistical emergency rate of the line be ϑ emergencies per year, and t_{int}

is the average value of the interruption time for such emergencies. Then the annual losses of the electricity distribution system operators from undersupply of electricity due to unplanned interruptions caused by emergency on this line are estimated by Eq. 5:

$$3_{pl} = \vartheta \cdot t_{int} \cdot P \cdot T_V \ (₴/year), \tag{5}$$

where: ϑ—emergency of the line (emergencies/year); t_{int}—the average value of the interruption time for each emergency (h); P—the calculated power of the consumer (kW); T_V—electricity distribution tariff (₴/kWh).

The duration of the unplanned interruption in the power supply t_{int} consists of the duration of the search for the place of fault t_f and the duration of repair and restoration work t_r. Since ELD helps to reduce the search time of the fault location t_f, this parameter is the optimization variable for the objective function (1).

Ratio between the cost indicators of the ELD and point of emergency depends on the tasks assigned to the ELD and the configuration of the distribution network. There are two main tasks:

- the task of reducing the search time of the emergency section of the transmission line by monitoring emergencies on hard-to-reach sections of the line (in this case, the minimization of the search time is achieved due to the fact that to assess the state of the hard-to-reach area, it is enough to check the state of the ELD on both sides of this area);
- the task of reducing the search time for the emergency section of the transmission line by installing ELD on the branches of the line (in this case, the minimization of the search time is achieved due to the fact that the verification of a number of branches of the transmission line is not carried out based on ELD signals).

Let generalize the function of losses from interruptions in the power supply (5) for a distribution transmission line of arbitrary structure. Suppose that the distribution line is given by the set of sections of the transmission line $S_s = \{S_1, S_2, \ldots, S_N\}$. Then, according to (5), the annual fault from emergency on any i-th section of the transmission line will be calculated by the formula [4]:

$$S^{(i)} = \vartheta^{(i)} \cdot t_{int}^{(i)} \cdot \sum_{j=1}^{N} \left(P_j^{(i)} \cdot T_{e(j)} \right) (₴/year), \tag{6}$$

where: $\vartheta^{(i)}$—emergency rate of the i-th section of the transmission line (emergencies/year); $t_{int}^{(i)}$—the average duration of the interruption for emergency on the i-th section of the transmission line (h); $P_j^{(i)}$—estimated power of the j-th consumer, de-energized due to an emergency on the i-th section of the transmission line (kW); $T_{e(j)}$—tariff for distribution of electricity for the j-th consumer, de-energized due to an emergency on the i-th section of the transmission line (₴/kW · h).

We introduce additional definitions for the calculation model. Let the linear emergency rate of the i-th section of the transmission line reflect the total number of emergency during the year along the 1st kilometer of the section:

$$\tau^{(i)} = \frac{\vartheta^{(i)}}{l^{(i)}},$$

where: $l^{(i)}$ is the length of the i-th section of the transmission line (km).

Then the emergency rate of the i-th section can be submitted as:

$$\vartheta^{(i)} = \tau^{(i)} \cdot l^{(i)}.$$

The average duration of a interruptions in the power supply for emergencies on the i-th section of the transmission line consists of the duration of the search for an emergency on the i-th section and the recovery time of the i-th section: $t_{\text{int}}^{(i)} = t_f^{(i)} + t_r^{(i)}$.

Accordingly, (6) can be submitted in the form of:

$$S^{(i)} = \tau^{(i)} \cdot l^{(i)} \cdot \left(t_f^{(i)} + t_r^{(i)}\right) \cdot \sum_{j=1}^{N} \left(P_j^{(i)} \cdot T_{e(j)}\right) \ (\text{₴/year}).$$

Then the annual losses from electricity shortages due to emergencies on the distribution line, consisting of N sections, will be calculated by the formula:

$$S^{\text{TL}} = \sum_{i=1}^{N} S^{(i)} = \sum_{i=1}^{N} \left(\tau^{(i)} \cdot l^{(i)} \cdot \left(t_f^{(i)} + t_r^{(i)}\right) \cdot \sum_{j=1}^{N} \left(P_j^{(i)} \cdot T_{e(j)}\right) \right) (\text{₴/year}) . \quad (7)$$

Formula (7) is universal and can be used for transmission lines of any configuration. To simplify the analysis of the connection between the tasks of calculating losses in the maintenance of transmission lines without an emergency monitoring system and with this system, we introduce some simplifications in the problem statement. In the absence of partitioning on the distribution line, as a result of an emergency at any site, all consumers are turned off. Accordingly (7) it is possible to simplify to the form:

$$S^{TL} = P_{\Sigma} \cdot T_{\text{av}} \cdot \sum_{i=1}^{N} \left(\tau^{(i)} \cdot l^{(i)} \cdot \left(t_f^{(i)} + t_r^{(i)}\right) \right) (\text{₴/year}) , \quad (8)$$

where: P_{Σ}—total calculation load of the transmission line; T_{av}—average value of the tariff for the distribution of electricity to consumers.

In the absence of systematic accumulation statistics of emergencies in the distribution electrical networks, it is impossible to adequately assess the emergency rate of individual sections of transmission lines. Therefore, when solving design problems,

it is expedient to use in (8) the average values of emergencies in electrical networks of individual voltage classes. Similarly, when solving design problems, it is enough to use the standard time of repair and restoration work in the electrical networks of certain voltage classes. Then (8) takes the form:

$$S^{\text{TL}}(t_{\text{f}}) = S_{\text{f}}^{\text{TL}}(t_{\text{f}}) + S_r^{\text{TL}}$$

$$= P_\Sigma \cdot T_{\text{av}} \cdot \tau_{\text{av}} \cdot \sum_{i=1}^{N}\left(l^{(i)} \cdot t_{\text{f}}^{(i)}\right) + P_\Sigma \cdot T_{\text{av}} \cdot \tau_{\text{av}} \cdot t_{\text{f}}^{(i)} \cdot l_\Sigma$$

where: $S_{\text{f}}^{\text{TL}}(t_{\text{f}})$—annual losses of the distribution system operator during the search for the emergency site in the transmission line; S_r^{TL}—annual losses of the distribution system operator during emergency and recovery works in the transmission line; τ_{av}—average emergency rate in electrical networks; l_Σ—total length of transmission line, $l_\Sigma = \sum_{i=1}^{N} l^{(i)}$.

Then the objective function of the problem of choosing the optimal configuration of the emergency monitoring system of radial distribution networks takes the form:

$$C^{(\text{w})} - C^{(\text{wo})} = P_\Sigma \cdot T_{\text{av}} \cdot \tau_{av} \cdot \sum_{i=1}^{N}\left(l^{(i)} \cdot t_{\text{f}}^{(\text{wo})(i)}\right)$$

$$- P_\Sigma \cdot C_{\text{av}} \cdot \tau_{\text{av}} \cdot \sum_{i=1}^{N}\left(l^{(i)} \cdot t_{\text{f}}^{(\text{w})(i)}\right)$$

$$- \left(\frac{C_i^{(1\text{i})}}{P_s} + B_{as}^{(1\text{i})}\right) \cdot N_i \to \max.$$

where: $t_f^{(\text{wo})(i)}$—the duration of the search for the place of fault in the event of an emergency on the i-th section of the line during the operation of the transmission line without emergency monitoring system; $t_{\text{f}}^{(\text{w})(i)}$—the duration of the search for fault in the event of an emergency on the i-th section of the line during the operation of the transmission line with emergency monitoring system.

Finally, the objective function will look like:

$$P_\Sigma \cdot T_{\text{av}} \cdot \tau_{\text{av}} \cdot \sum_{i=1}^{N}\left(l^{(i)} \cdot \left(t_{\text{f}}^{(\text{wo})(i)} - t_{\text{f}}^{(\text{w})(i)}\right)\right) - C_{i(y)}(N_i)$$

$$= \text{VG}_{i(\text{p})}(N_i, \text{mz}_i) - C_{i(y)}(N_i) \to \max, \tag{9}$$

where: $\text{VG}_{i(\text{p})}(K_i, \text{mz}_i)$—reduced to one year the benefit from the introduction of an emergency monitoring system, as a function of the number of ELD and the places of their installation.

It should be noted that the component of costs for the purchase, installation and maintenance of ELD $C_{i(y)}(N_i)$ in (9) is given only as a function of the number of

installed on the ELD line, ie regardless of the location of these devices. If is needed a more accurate calculation (for example, to account for fuel costs), the cost function can be extended with additional cost components. However, in the vast majority of cases it is enough to limit the average values of costs for the installation and maintenance of ELD. At the same time, the value of the benefit function from the use of ELD $VG_{i(p)}(K_i, mz_i)$ largely depends not only on the number of these tools, but also on the place of their installation. Therefore, for this component (9), the ELD installation sites are mandatory optimization variables.

The given consumption function does not take into account the losses of electricity suppliers due to faulty electrical networks.

It is obvious that the ELD installation and operation cost function has a step graph. In this case, each option of installing K ELD on the transmission line will correspond to the scalar value of losses from interruptions in the power supply. Thus, the objective function (9) will have a step graph. Variables such as the number of ELD and their location has discrete character. In addition, the duration of the search for the emergency site depends primarily on the sequence of inspection of the line. The choice of the optimal route, as one of the classical problems of graph theory [5], has exclusively algorithmic solutions [6]. Thus, the objective function (9) should be solved by discrete optimization methods [7]. Thus, to solve (9), it is necessary to formalize the problem of optimizing the time to search for the location of fault to power transmission lines as a combinatorial problem of choosing the optimal route for a graph of arbitrary configuration. Accordingly, the problem of determining the optimal configuration of the emergency monitoring system on transmission lines will have combinatorial solutions [8].

If necessary, the payback period of the investment is calculated by the general formula:

$$P_p = \frac{C_{i(y)}(N_i) \cdot P_s}{VG_{i(p)}(K_i, mz_i)}.$$

Obviously, the introduction of an emergency monitoring system is considered profitable provided:

$$P_p \ll P_s. \tag{10}$$

It should be noted that the analysis of payback period (10) and cost-effectiveness (9) is used primarily to compare the configuration options of the emergency monitoring system and choose the most optimal. When making the final decision on the introduction of emergency monitoring tools, it should be further taken into account that with the introduction of a system of fines for non-compliance with the reliability of electricity supply, losses from long interruptions will increase significantly. Therefore, it is possible to decide on the implementation of an emergency monitoring system solely to bring the calculated reliability indicators within the specified limits, even if such a decision is currently not economically viable, or the economic effect of implementing such a system is insufficient to obtain an acceptable payback period.

The problem of choosing the optimal configuration of the emergency monitoring system of radial electrical networks with the objective function (9) has two additive components:

- losses from undersupply of electricity as a function of the duration of the search for a fault section of the line (an elementary fragment of a distribution line, consisting of one or more runs between supports and is considered as a whole in the analysis);
- costs of purchase, installation and maintenance of ELD.

Changing the number and location of ELD affects the change in the duration of the search for the fault section of the distribution line. When changing the configuration of the emergency monitoring system, the duration of the search for the damaged area also changes. In this case, in the General case, the optimal route of the line inspection may change. Thus, both components of the objective function (9) are algorithmically related and cannot be analyzed separately from each other. As a result, the search for the extremum of function (9) should be performed by solving several combinatorial problems recursively. The structure of recursive solution of these problems is given below:

- the first level of optimization: the task of determining the number of ELD and places of their installation, where the maximum of the target function is achieved;
- the second level of optimization: for the given number and places of ELD installation is determined the ELDtest route of inspection of the transmission line;
- the third level of optimization: for the current route of the transmission line inspection, emergency situations are simulated on all sections of the distribution line;
- the fourth level of optimization: for the current emergency, the passage along the current route of the power line survey is simulated to calculate the time of passage to the accident site.

The third and fourth levels of optimization together have a factorial combinatorial complexity of the number of sections of the transmission line. At the same time, it is impossible to reduce the amount of computational actions at these levels, because it is at these levels that the components of losses from electricity shortages are calculated.

The second level of optimization—finding the optimal route for the review of transmission lines—NP-difficult problem of combinatorial optimization, which does not have a deterministic solution algorithm. Effective solutions to such problems are carried out using heuristic algorithms that provide only an approximate solution. Moreover, as mentioned above, it is necessary to clarify the problem in general, taking into account the availability of access roads to sections of the line.

The first level of optimization is the task of determining the optimal configuration of the emergency monitoring system. Since the efficiency of each of the configuration options is calculated algorithmically based on the results of internal levels of optimization, it is almost impossible to determine the direction of the search for the optimal solution based on the results of calculations of other options. Thus, in

the general case, the problem of determining the optimal configuration of the emergency monitoring system should be solved by combinatorial search of all possible solutions with NP-heavy combinatorial search. In this case, each option is evaluated by the results of solving the NP-difficult problem (search for the shortest route of inspection of the transmission line) at the second level of optimization. For each of the options for solving the problem of the second level of optimization, the components of the objective function are calculated it's problem with factorial complexity of computational operations.

According to preliminary estimates, the solution of the problem by lexical search of options in a reasonable time for design decisions is possible only for the line with 6–7 sections. To analyze a larger number of sites, there is a need to use heuristic algorithms.

Based on the results of previous studies, the possibility of a significant reduction in the level of combinatoriality of the problem of the first level of optimization (choosing the optimal configuration of the monitoring system for emergency conditions of a distribution line) has been established by taking into account the topological features of the line. In the further work it is planned to carry out the analysis of various configurations of distribution lines for definition of rules of cutting off a priori of unfavorable variants, that is to develop expert system of the decision of the set task.

5 Analysis of Zones of Sensitivity of Emergency Locks to Emergency Currents in LV and MV Electrical Networks 10 kV

Let's consider the restrictions related to the features of operating and emergency modes, which should be taken into account when choosing the installation and configuration sites for the ELD in the sections of distribution electrical networks. The main types of fault to overhead transmission lines are:

- three-phase short circuit;
- two-phase short circuit;
- two-phase short circuits with earth fault;
- single-phase ground fault.

Single-phase ground fault (SPGF) in 10 kV electrical distribution networks have features due to the mode of isolated neutral and will be considered separately. For other types of fault at this stage of the analysis we distinguish the range of values of emergency currents from the largest (three-phase short circuit) to the smallest (two-phase short circuit). For the power transmission line section, there are three main areas of ELD sensitivity to different types of fault (Fig. 4):

- area of reliable monitoring, where the lower limit of the range of values of emergency currents I_{sc} is more than twice the value of the ELD operation setting I_{os}: $2 \cdot I_{os} \leq I_{sc}$;
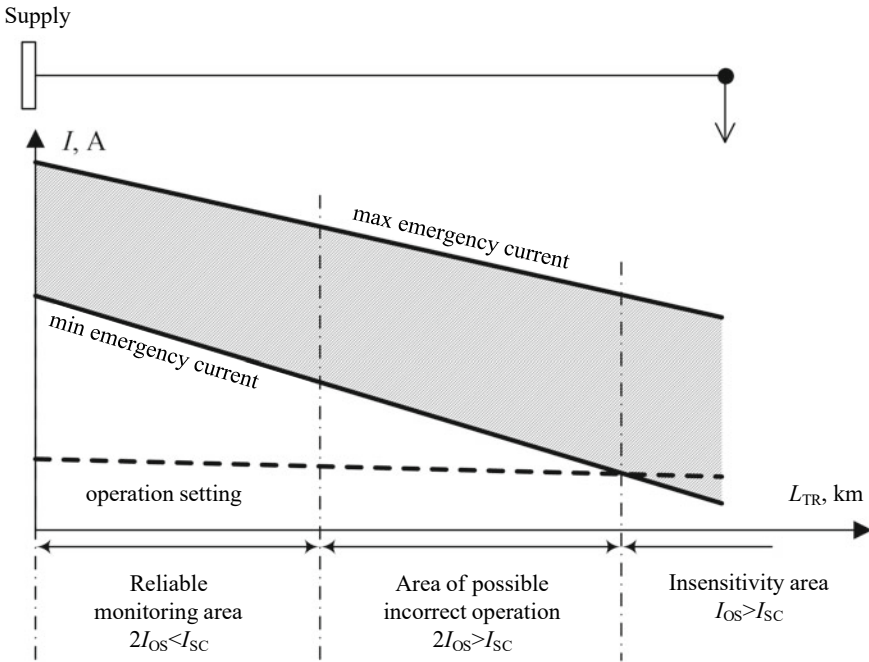
Fig. 4 Areas of sensitivity of the ELD to fault to transmission lines

- area of unreliable monitoring, where the lower limit of the range of values of emergency currents exceeds the value of the set point of ELD operation not more than twice: $I_{os} < I_{sc} \leq 2 \cdot I_{os}$; area of insensitivity to fault, where the lower limit of the range of values of emergency currents is less than the value of the set point ELD $I_{os} > I_{sc}$.

The area of unreliable monitoring is characterized by an increased probability of false alarms and/or non-operation of the ELD in case of fault transmission line. In the areas of transmission lines in the area of unreliable monitoring, the installation of ELD is not recommended, since in general such monitoring tools will not provide reliable information about the presence of fault in the area of insensitivity to fault to the transmission line, the installation of ELD is generally impractical.

For distribution electrical networks of 10 kV of significant length, it is necessary to determine the characteristic sections of the line with areas of reliable monitoring separately for each ELD operation setting (Fig. 5).

At the same time, for distant sections of the line (more than 5 km from the power center), there is a need for additional verification of the detuning of the ELD from the operating load currents of the power transmission line I_l, the calculated values of which should be two times less than the value of the setting for triggering the means of fixing emergency conditions: $I_{os} \leq 2 \cdot I_l$.
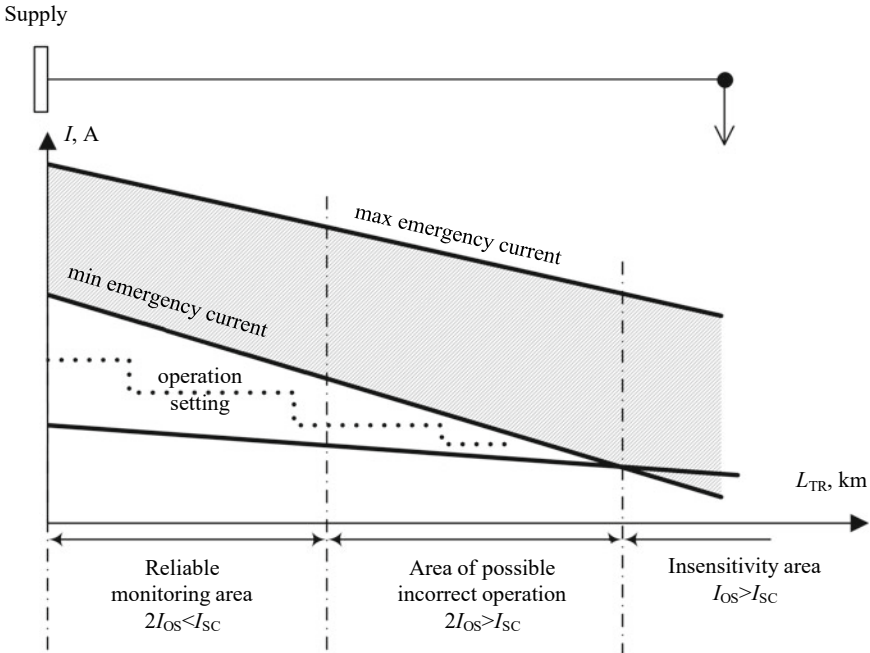
Supply

Fig. 5 Regime restrictions on ELD installation sites

As can be seen from the above reasoning, when determining the ELD actuation, it is necessary to focus on the value of the lower limit of the range of emergency current values in individual sections of the transmission line. Thus, in order to determine the ELD actuation for 10 kV distribution electrical networks, it is necessary to preliminarily calculate the graphs of the two-phase short circuit current values in different sections of the line.

For 10 kV overhead electrical networks, the SPGF currents are determined by the capacitance between the phases of the transmission line and the ground. At the theoretical level, there are two components of the currents of the SPGF (Fig. 6):

- capacitive current fed from the power supply center;
- capacitive discharge current due to the charging power of the transmission line.

The recharged capacitive current of the SPGFs is directed from the power center to the fault site. The value of this current is directly proportional to the distance from the power center to the fault part of the distribution line: with increasing distance, the value of the current increases. In case of damage at the far end of the distribution line, the SPGFs current will have the maximum possible value, which will correspond to the charging power of the transmission line route from the power supply center to the place of fault.
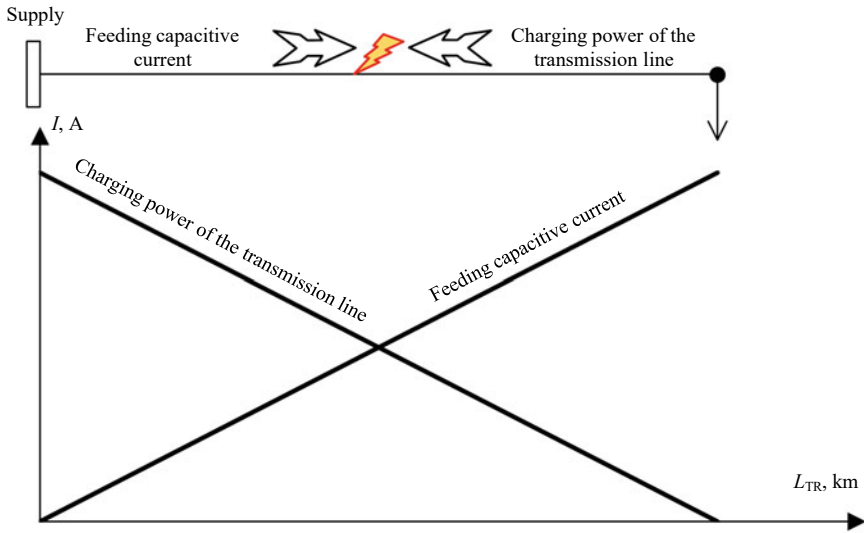
Fig. 6 Components of SPGF currents

The component of the current of the SPGFs, due to the charging power of the part of the distribution line, de-energization by fault, has similar causes. The numerical value of this component of the SPGFs current is inversely proportional to the distance from the power supply center to the fault section of the distribution line, i.e. increases with increasing proportion of the line de-energization due to fault.

Analysis of the sensitivity of the ELD to the currents of the SPGFs.

To simulate the SPGFs along the unbranched route of a 10 kV distribution transmission line, were calculations of capacitive currents made using the formula:

$$I_{\text{SPGF}} = 3 \cdot U_f \cdot \omega \cdot C_f \cdot L (\text{A}),$$

where: U_f—rated voltage of the transmission line phase; ω—cyclic frequency, for current frequency of 50 Hz $\omega = 314$ (rad/s); C_f—transmission line phase linear capacity, the research used the average statistical value of the capacity of overhead transmission lines 10 kV $C_f = 0.0256$ (µF/km); L—distance between the power center and the place of fault to the transmission line.

The linear value of the capacitance of 10 kV overhead electric lines is approximately 0.0256 (µF/km). Since the values of differences in the diameters of wires of different brands are insignificant compared to the values of the geometric distances between the phases, then for overhead power transmission lines of 10 kV, in practical calculations of the SPGFs currents, it is permissible not to take into account the type of wire and analyze the use of the above average value of linear capacitance.
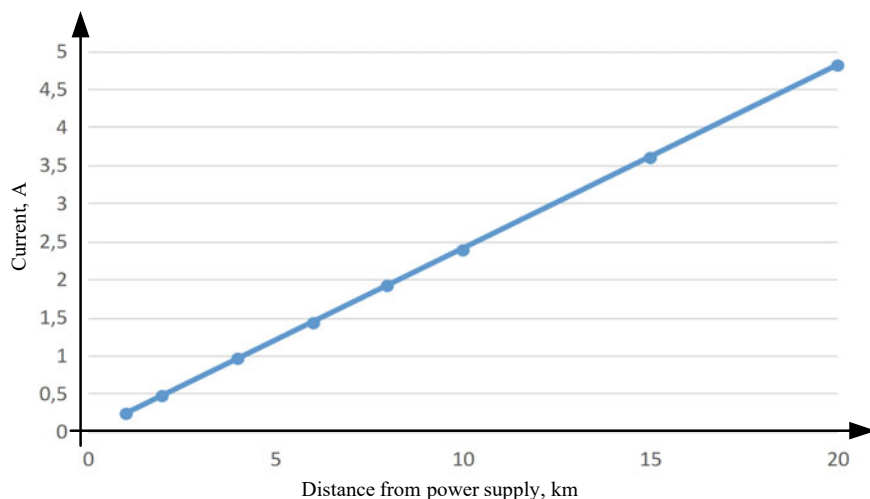
Fig. 7 Dependence of the value of the current of the SPGFs from the distance to the power center

In Fig. 7 shown the value of the fed capacitive current of the SPGFs in the event of fault to the 10 kV overhead power line at a distance of 20 km from the power center will be 4.8 A.

For branched electrical networks, the value of SPGFs current will increase slightly due to the charging power of the branches, but in practice, SPGFs currents in 10 kV electrical distribution networks do not exceed 20–25 A. Such low values of emergency current make it almost impossible to adjust the ELD to fix the SPGFs with the adjustment of the working load of the line. Therefore, monitoring and recording of SPGFs currents in 10 kV distribution networks based on verification of emergency current values is in principle possible only at the far edges of overhead electrical networks with cable inserts (the presence of which increases the charging capacity of the line).

Therefore, in order to detect SPGFs in 10 kV electrical distribution networks, the emergency monitoring system in addition to the control of currents in the phases of the transmission line should involve other means of monitoring the regime. Such means include, first of all, sensors for monitoring zero-sequence currents and sensors for monitoring voltage levels in the phases of transmission lines. Sensors for monitoring zero-sequence currents in the phases of transmission lines allow you to record the presence of a ground fault. However, taking into account the need for detuning from the operating modes of the 10 kV electrical network for a distribution transmission line, there will be a dead zone at the beginning of the line.

Voltage level monitoring sensors allow to record the fact of fault to the transmission line phase at the place of wire breakage. Therefore, the emergency monitoring system in 10 kV distribution networks, equipped with phase voltage sensors, should

contain analysis functions that take into account the probability of operation of individual voltage level sensors on the way from the power center before and after fault site.

The width of the sensitivity range of voltage level sensors in the phases of 10 kV transmission lines is determined by the design features of the distribution network. Therefore, the settings of the settings and the analysis of the operation of the voltage level sensors of the FAS are unique for each distribution line. Within the scope of this work, we note only the requirements for the means of analyzing emergency conditions, taking into account the signaling of the voltage level when a SPGF appears on the line:

- analysis functions of emergency signals should take into account the appearance of voltage drop signals before and after the place of the wire break;
- analysis functions of emergency signals should take into account that the width of the voltage drop fixation zones during SPGF is determined by the design features of the distribution network and the fault location.

The second requirement predetermines the need for a detailed analysis of the electrical distribution network and a unique setting of voltage level sensors installed at different sections of the power transmission line. Accordingly, there is a need for the introduction of tools for automatic analysis of the operation of ELD funds in SPGF on the line.

6 Conclusions

Ensuring the increase of reliability of electricity supply to consumers and efficiency of restoration of electricity supply by distribution system operators in the conditions of martial law and post-war time depends on the availability of means of control of the actual technical condition of distribution systems of IPS of Ukraine. To ensure control, it is proposed to use emergency identification tools built on the concept of SmartGrid systems. An important aspect of the practical implementation of emergency indicators is to provide such systems with an intellectual component and ensure long-term autonomous operation after the loss of power at the control point. The main advantage of using emergency indicators in the IPS of Ukraine is the ability to locate damage or reduce the load to avoid damage due to the use of reclosers or switches with remote control by analyzing data obtained from damage indicators.

References

1. Henriques, H.O., Correa, M.R.L.S.: Use of smart grids to monitor technical losses to improve non-technical losses estimation. In: Proceedings of the 7th Brazilian Electrical Systems Symposium, pp. 1–6 (2018). https://doi.org/10.1109/sbse.2018.8395924

2. Zaitsev, I., Levytskyi, A., Bereznychenko, V.: Hybrid diagnostics systems for power generators faults: systems design principle and shaft run-out sensors. In: Kyrylenko, O., Zharkin, A., et al. (eds.) Power Systems Research and Operation: Selected problems, pp. 71–98. Springer (2021). https://doi.org/10.1007/978-3-030-82926-1_4

3. Zaitsev, I., Levytskyi, A., Kromplyas, B, Rybachok, P.: Optical fiber in nuclear power plants: applications to improve the reliability, safety and work stability of fault control instrumentation. In: Zaporozhets, A. (eds.) Systems, Decision and Control in Energy III, pp. 123–138. Springer (2021). https://doi.org/10.1007/978-3-030-87675-3_7

4. Kyrylenko, O.V., Blinov, I.V., Tankevych, S.E.: Smart grid and organization of information exchange in electric power systems. Tekhnichna elektrodynamika **3**, 44–54 (2012)

5. Baranov, G., Komisarenko O., Zaitsev, I.O., Chernytska, I.: SMART technologies for transport tests networks, exploitation and repair tools. In: Proceedings of the International Conference Artificial Intelligence and Smart Systems (ICAIS), 25–27 March 2021, Pichanur (India), pp. 621–625 (2021). https://doi.org/10.1109/ICAIS50930.2021.9396055

6. Postranecky, M., Svitek, M.: Smart city near to 4.0—an adoption of industry 4.0 conceptual model. In: Proceedings in Smart City Symposium Prague (SCSP), Prague (2017)

7. Chin-Ying, H., Tsung-En, L., Chia-Hung, L.: Optimal placement of fault indicators using the immune algorithm. IEEE Trans. Power Syst. **26**(1), 38–45 (2011). https://doi.org/10.1109/TPWRS.2010.2048725

8. Worighi, I. Maach, A., Hafid, A.: Modeling a smart grid using objects interaction. In: Proceedings of the 3rd International Renewable and Sustainable Energy Conference (IRSEC), pp. 1–6 (2015). https://doi.org/10.1109/IRSEC.2015.7454968

9. Zaitsev, I., Shpylka, A., Shpylka, N.: Output signal processing method for fiber bragg grating sensing system. In: Proceedings of the 15th International Conference on Advanced Trends in Radioelectronics, Telecommunications and Computer Engineering (TCSET-2020), pp. 152–155 (2020). https://doi.org/10.1109/TCSET49122.2020.235412

10. Nguyen, C.P., Flueck, A.J.: Modeling of communication latency in smart grid. In: Proceedings of the IEEE Power and Energy Society General Meeting (2011)

11. Lopes, A.J., Lezama, R., Pineda, R.: Model based systems engineering for smart grids as systems of systems. Procedia Comput. Sci. **6**, 441–450 (2011)

12. Nutaro, J.: Designing power system simulators for the smart grid: combining controls communications and electro-mechanical dynamics. In: Proceedings of the 2011 IEEE Power Engineering Society General Meeting, pp. 1–5 (2011)

13. Li, W., Zhang, X.: Simulation of the smart grid communications: challenges techniques and future trends. Comput. Electr. Eng. **40**(1), 270–288 (2014)

14. Blinov, I., Zaitsev, I.O., Kuchanskyy, V.V.: Problems, methods and means of monitoring power losses in overhead transmission lines. In: Babak, V., Isaienko, V., Zaporozhets, A. (eds.) Systems, Decision and Control in Energy I, pp. 123–136. Springer (2020). https://doi.org/10.1007/978-3-030-48583-2_8

15. Blinov, I.V., Parus, E.V., Polishchuk, O.Y., Zhuravlyov, I.V.: Monitoring of overhead power lines using damage indicators. Energ. Electr. **9**, 7–11 (2013)

16. Applegate, D.L., Bixby, R.M., Chvátal, V., Cook, W.J.: The traveling salesman problem. In: Combinatorial Optimization Algorithms and Combinatorics, vol. 21, pp. 527–562 (2008)

17. Parus, Y.V., Blinov, I.V., Bets, O.Y.: Fault indicators location and quantity selection on distribution line as a problem of combinatorial optimization. Tech. Electrodyn. 58–60 (2016). https://doi.org/10.15407/techned2016.05.058

18. Shahsavari, A., Mazhari, S.M., Fereidunian, A., Lesani, H.A.: Fault indicator deployment in distribution systems considering available control and protection devices: a multi-objective formulation approach. IEEE Trans. Power Syst. **5**(29), 2359–2369 (2014)

19. Rezinkina, M.M., Sokol, Y.I., Zaporozhets, A.O., Gryb, O.G., Karpaliuk, I.T., Shvets, S.V.: Monitoring of energy objects parameters with using UAV. In: Control of Overhead Power Lines with Unmanned Aerial Vehicles, vol. 359, pp. 1–8. (2021) https://doi.org/10.1007/978-3-030-69752-5_1

20. Senderovich, G.A., Zaporozhets, A.O., Gryb, O.G., Karpaliuk, I.T., Shvets, S.V., Samoilenko, I.A.: Automation of determining the location of damage of overhead power lines. In: Control of Overhead Power Lines with Unmanned Aerial Vehicles, vol. 359, pp. 35–53 (2021). https://doi.org/10.1007/978-3-030-69752-5_3
21. Bjerkan, E., Venseth, T.: Locating earth-faults in compensated distribution networks by means of fault indicators. In: Proceedings of the International Conference on Power Systems Transients (IPST'05), 107 (2005)
22. Jahedi, A., Javidan, J., Nasiraghdam, H.: Multi-objective modeling for fault indicators placement using of NSGA II to reduce off time and costs in distribution network. Tech. Phys. Prob. Eng. **6**(21), 106–111 (2014)
23. Ho, C.-Y., Lee, T.-E., Lin, C.-H.: Optimal placement of fault indicators using the immune algorithm. IEEE Trans. Power Syst. **26**(1), 38–45. (2011)
24. Akbari, M., Ghaffarzadeh, N.: Optimal fault indicator placement in distribution networks using SFLA algorithm. World Appl. Programm. **4**(8), 181–192 (2014)
25. Senderovich, G.A., Zaporozhets, A.O., Gryb, O.G., Karpaliuk, I.T., Shvets, S.V., Samoilenko, I.A.: Experimental studies of the method for determining location of damage of overhead power lines in the operation mode. In: Control of Overhead Power Lines with Unmanned Aerial Vehicles, vol. 359, pp. 55–77 (2021). https://doi.org/10.1007/978-3-030-69752-5_4
26. Babak, V.P., Babak, S.V., Eremenko, V.S., Kuts, Y.V., Myslovych, M.V., Scherbak, L.M., Zaporozhets, A.O.: Models and measures for the diagnosis of electric power equipment. In: Models and Measures in Measurements and Monitoring, vol. 360, pp. 99–126 (2021). https://doi.org/10.1007/978-3-030-70783-5_4
27. Lee, C., Ho, T., Lin, C.: Optimal placement of fault indicators using the immune algorithm. IEEE Trans. Power Syst. **26**(1), 38–45 (2011)
28. Kyrylenko, O.V., Pavlovsky, V.V., Blinov, I.V.: Scientific and technical support for organizing the work of the IPS of Ukraine in synchronous mode with the Continental European power system ENTSO-E. Tech. Electrodyn 5, 55–66 (2022). https://doi.org/10.15407/techned2022.05.059
29. Parus, Y.V., Blinov, I.V., Bets, O.Y.: Fault indicators location and quantity selection on distribution line as a problem of combinatorial optimization. Tech. Electrodyn. **5**, 58–60 (2016). https://doi.org/10.15407/techned2016.05.058.

Information Technology Platform for Automation of Decision-Making Processes by the Organizational Management System

Zelim Borukaiev ⬛, **Konstantin Ostapchenko** ⬛, **Olexandr Chemerys** ⬛, and **Volodymyr Evdokimov** ⬛

Abstract The chapter examines the development problems of specialized tools for mathematical and computer modeling, information technology support for automation of the preparation and decision-making process by appropriate organizational management systems (OMS) with advanced tools for meaningful data processing and user interface of competitive electricity market participants operating in complex relationships and potential risks. The peculiarities of the electricity market functioning are determined, which require advanced computer simulation tools that provide market participants with the opportunity to formulate and accept strategies for their own behavior in different segments of the competitive market. Existing solutions and research in the field of creating modern software tools for modeling, forecasting and optimizing the functioning of energy markets in the world are analyzed. The development direction of such tools is determined and the structural-functional composition of the information technology platform for OMS is proposed, that is represented by the functional components of the preparation and decision-making process to develop a strategy for market participant's own behavior on its segments. The basics of creating an information technology platform for building decision support systems (DSS) for energy companies as entities/subjects of the electric energy market, a feature of which is a new formalization of the components of the DDM (Data-Dialog-Model) paradigm, are considered. In particular, typical operations of the decision maker interaction in the performance of functional tasks that are interrelated with data processing methods are classified. A unified model of the DSS data structures is proposed, which defines common approaches to representing market entities at all management levels through the selection of their properties and relationships and creation of a unified system of classifiers, reference catalogs that ensure the operation of the entire set of mathematical models of computational and analytical problems that are logically and informationally interconnected between

Z. Borukaiev · O. Chemerys (✉) · V. Evdokimov
Pukhov Institute for Modelling in Energy Engineering of National Academy of Sciences of Ukraine, Kyiv, Ukraine
e-mail: a.a.chemeris@gmail.com

K. Ostapchenko
National Technical University of Ukraine "Igor Sikorsky Kyiv Polytechnic Institute", Kyiv, Ukraine

257

itself according to its intended purpose, input and output data parameters of energy companies on the market, optimization and forecasting algorithms.

Keywords Information technology platform · Decision support system · Organizational management system · Electricity market

1 Introduction

Among the main tasks of energy companies at the current stage of the electricity market development are to determine the main directions of strategies formation and conditions for their implementation in different segments of the electricity market, methods and tools for modeling decision-making processes in optimizing the structure of sales/purchases of electricity and ancillary services by the criteria of profitability and opportunities to level the risk of decisions. However, effective work in these market segments requires not only experience but also software tools that will allow market segment participants to perform the necessary modeling and forecasting calculations to identify risks and find effective strategies for their behavior in these segments.

Solving only these problems, necessitates the creation of specialized tools for mathematical and computer modeling, information technology support for the automation of the process of preparation and decision-making by the appropriate OMS of market participants at all stages.

Thus, a problem of improving information technology tools for the development of DSS with advanced tools for meaningful data processing and user interface through the use of modern information technology, developing and formation of the necessary databases that characterize the performance indicators state of the management object and changes in its external environment, including changes in energy markets, continues to be relevant. A separate and very important task is to develop a simulation models database of the functioning of electricity market segments to solve the computational problems of analysis and forecasting of the changes in indicators for the segments functioning and their management.

2 Automation of Decision-Making Processes by the Organizational Management System

2.1 Problem Formulation of Creating the Organizational Management System of the Electricity Market

Complicated organizational-technical systems (COTS), which certainly include the electricity market, usually combine many interdependent human-machine objects—subsystems that interact with each other and with other technical systems in various

fields' vital activity of society, and differ in the purpose of production and products. Many of them have common characteristic features of management tools, such as OMS as structural subsystems of COTS. The main of these features are the following [1]:

- hierarchical multilevel nature of organizational, technological and information interaction of subsystems;
- changes in time of own structure and functions;
- incomplete compliance of the structure with the development goals of COTS due to changes in the management and functioning mechanisms over time, etc.

To implement the functions and tasks of interconnected organizational, production, technological and information management in the management structures of the COTS, it is necessary to create computer modeling systems that are designed to solve the problems of decision-making support in their OMS. The application and development of such systems, which actually function as COTS, requires continuous improvement of mathematical and information technology. And this in turn encourages finding solutions related to unification in the processes and technologies of design and improvement of such modeling systems.

Obviously, the main purpose of building modeling systems to solve decision-making support problems is to significantly increase the productivity of organizational management, namely:

1. Efficiency–as a result of reducing the number of service personnel;
2. Operativeness—due to the reduction of processing time of large amounts of information;
3. Validity of the adopted decisions—as a result of carrying out a multivariate analysis of the proposed options for making changes to the OMS functioning mechanisms (rules) to achieve the management goals and assess the consequences of the adopted decisions.

Many experts associate the increase in productivity of organizational management with the development of research on improving the methods and tools of mathematical and computer modeling of decision-making processes and the creation of qualitatively new computer OMS based on them. Computer OMS are usually used to adequately represent the research processes of the OMS functioning mechanisms, monitoring, analysis and forecasting of key informative indicators that reproduce the components of the COTS entities state vector, taking into account the subsystems interaction included in them.

In the OMS theory, the functioning mechanisms are understood as a set of rules and procedures that determine the sequence of actions of elements (subjects included in systems) in decision-making processes for managing organizational, technological and information activities [2]. The decision-making process to improve the OMS functioning mechanisms for a wide range of COTS for industrial and technical purposes, whose products are sold in competitive markets, includes the formulation and comprehensive solution of a large number of interdependent tasks.

It is natural to assume that the construction of a modeling system, which is actually designed to implement interactive, intelligent functions of DSS, is possible only with a computer modeling system, which provides the ability to design and build simulation computer models of OMS functioning processes. Such a system should include:

- tools of formal mathematical description of OMS complex subjects and processes of their organizational interaction between themselves and the external environment;
- a single information space that combines the means of object-oriented conceptual and information modeling of the interaction processes of OMS complex subjects between themselves and the external environment;
- unified system of classifiers and reference catalogs, data storage structure, unified system of protocols and interfaces;
- single tools of programming computer models.

This paper proposes an original approach to solving the problem of building DSS with advanced tools for object-oriented modeling (OOM) of the COTS subjects functioning processes to form a single database structure of a unified user modeling environment.

The main purpose of the proposed approach is to create an information technology platform (ITP) for building an integrated adaptive DSS to increase information support of DSS users by reducing the time to automate decision-making processes, accelerate the provision of user interaction interfaces with integrated information DSS resource—data base, model base, knowledge base, and creating a single unified software environment for automation object.

Achieving the stated goal determines the following areas of development work of ITP construction of DSS for electricity market OMS:

- building an organizational model of information technology platform for DSS design;
- conceptual representation formation of the organizational structure for the integrated adaptive subject-independent DSS;
- object modeling of the subject area data for automation object in order to form a single unified database structure for the organizational management entities;
- functional modeling of the data processing and presentation technological processes for the purpose of unification (standardization) of the system software interface by the classification of user interaction operations with objects from subject area in the software system;
- information protocols/interfaces development for data exchange with the different purposes models which are connected to a database of the organizational management subjects.

2.2 Analysis State of the Modern Research on the Creation of Organizational Management Systems for Energy Markets

Among the arising problems of OMS creating are the high cost of implementing a market model, the complex structure of market division into its segments, the inevitable volatility and manipulation of spot prices, manipulation of individual players by market authorities, the difficulty of reducing generation costs, unpredictability of market prices energy resources, unpaid cost of electricity production by part of generating capacity, unequal distribution of revenues from the sale of jointly produced and supplied to consumers [3]. Therefore, in many countries around the world are simulating models of market functioning to conduct research to find the most rational and optimal mechanisms for balanced revenue distribution between market segments and their participants—market subjects/entities.

Paper [4] qualitatively describes the analysis of various methodologies and modeling methods, computer tools and information technologies used to create such simulation models and systems. The methodological basis for the energy markets OMS creation is formed by economic, macroeconomic, simulation, retropolation, multicriteria models. Therefore, the core in the form of a module/subsystem of the problem "solver", which is presented as a library of mathematical methods, is one of the most widely used OMS in the world. In the simplest OMS in terms of size and amount of data used can be utilizes "solvers" that are publicly available. But in more advanced systems, it is advisable to use libraries of methods which are developed and improved by leading research institutions and specialized commercial companies.

Currently, almost all well-known major global manufacturers of software and hardware platforms, such as SAP, ORACLE, IBM, Siemens and others, provide comprehensive solutions and tools for building computer systems, as well as, the most ready-made systems, including for organizational management of energy markets. But in addition to these platforms, specialized computer systems have been built and are in operation in the world today, which provide modeling of the energy markets functioning. The most famous of them are NEMS, GEMS, GEMINI (USA), PRIMES, PLEXOS, AURORA (EU), NEMSIM (Australia) [5–7].

All these software packages are mostly focused on modeling energy in general and are used by national regulators to analyze strategies for the development of energy complexes. However, the structure analysis of the producers and suppliers of electricity markets shows that energy markets of this scale in the world are formed not only from large players, but also from a large number of participants with small working capital. And such participants do not have economic incentives and opportunities to use complicated software packages as an "assistant" in shaping the strategy of their own behavior in the market. In addition, these packages usually do not provide an opportunity to assess the mutual influence of strategy and tactics of many market participants, which may in the future become objects of "distributed generation" in the energy system and influence pricing processes in the market. This fact adds a

significant share of uncertainty in shaping the strategy for the development of the electricity market as a whole.

Therefore, the urgent task is to create a user-friendly information modeling system in the competitive electricity market as part of the OMS energy markets, which aggregates all available information about the processes of their operation and focuses on reproducing stages in the development and decision-making on the formation of the own behavior strategy of market participants in its segments.

2.3 Directions for Improving the Organizational Management Systems of the Electricity Market

At present, in the theory and practice of OMS based on DSS, new trends have emerged both in approaches to the classification of such systems and in determining their place in the organizational management cycle. Thus, the analysis of a wide variety of papers [8–12] on the creation of DSS or systems with elements of automation of decision support processes allowed formulating the following conclusions about the conceptual development of DSS theory and practice for organizational management:

1. Developed only a general concept and general approaches to building information systems, which should be classified as DSS. Each variant of DSS implementation can be considered as a specialized system that solves specific problems and implements calculation methods specific to a given applied subject area of the automation object. That is, in terms of unification in the approach to the DSS construction, they should be attributed to problem-oriented systems with their own approaches;

2. All modern areas of information systems development—OLTP, OLAP, Data Mining, Data Warehouse, Business Intelligence, focused on methods and mechanisms of data collection, processing and presentation and are not related to the mechanisms of development, analysis and decision-making. That is, they are secondary to the subject of research—the process of DSS building.

3. Functionally, DSS should implement the following main stages in working with data—data collection, situation analysis, development (selection) of solutions, solution implementation. Thus by performing these tasks one differs from other classes of automated information systems.

Structures of complex management systems, which should include OMS, are usually built using hierarchical and functional principles of subsystems allocation for situational management—management based on established facts and circumstances, which can be represented as a functioning indicators set of the management object [13]. As a result, the management systems of each level actually become subsystems in the overall management system on the higher level. Thus each level is characterized by the own features of the management purposes and operations which are connected with data processing [14]. It is known that management operations implement the information function of the control object, which is to perform in the

automated mode the information collection, processing, interpretation and presentation for production function realization of this object, namely the implementation of management tasks [15].

As a result, several levels of subsystems can be identified in the OMS structure due to different degrees of the information function automation, among which especially should be noted the information-analytical monitoring system (IAMS) and the information-modeling system (IMS) for preparation and analysis of development options based on object management models.

The main directions of works on the development of a unified approach to the DSS construction for a OMS wide class with advanced tools of semantic data processing and user interface, computer models construction and computational algorithms development for analysis and synthesis of OMS functioning mechanisms, forecasting the consequences of decision-making on the implementation of new functioning mechanisms at all levels of organizational management was formulated in [16].

In order to OMS develop and improve, it is proposed to expand its functionality as a DSS not only through IAMS [17], but also through IMS, which will act as a tools implementing the problem analysis functions and be represented by such unified data processing methods:

- calculation-modeling, which according to the known functional dependence to form the calculation result and are presented in the form of a formula and are used to calculate the state of market indicators;
- calculation-search, which according to the cyclically repeated procedure to form the calculation result and are presented in the form of a procedure consisting of a list of formulas and are used for simulation of changes in market indicators;
- calculation-optimization, which by organizing the option search (selection and comparison) to form the calculation result and are presented in the form of a set consisting algorithm and criterion for evaluating options and are used to optimize market indicators;
- calculation-forecasting, which by purposeful option synthesis and solution analysis of their calculation to form a calculation result and are presented in the form of a predictive procedure and are used to forecast market indicators.

In general, the basic set of object-oriented integrated adaptive DSS can be built on the decomposition principles and structured with subsystems (modules) that implement tasks that reflect the stages of preparation and decision-making process for organizational market management.

3 Conceptual Representation of the Information Technology Platform for Automation of Decision-Making Processes by the Organizational Management System
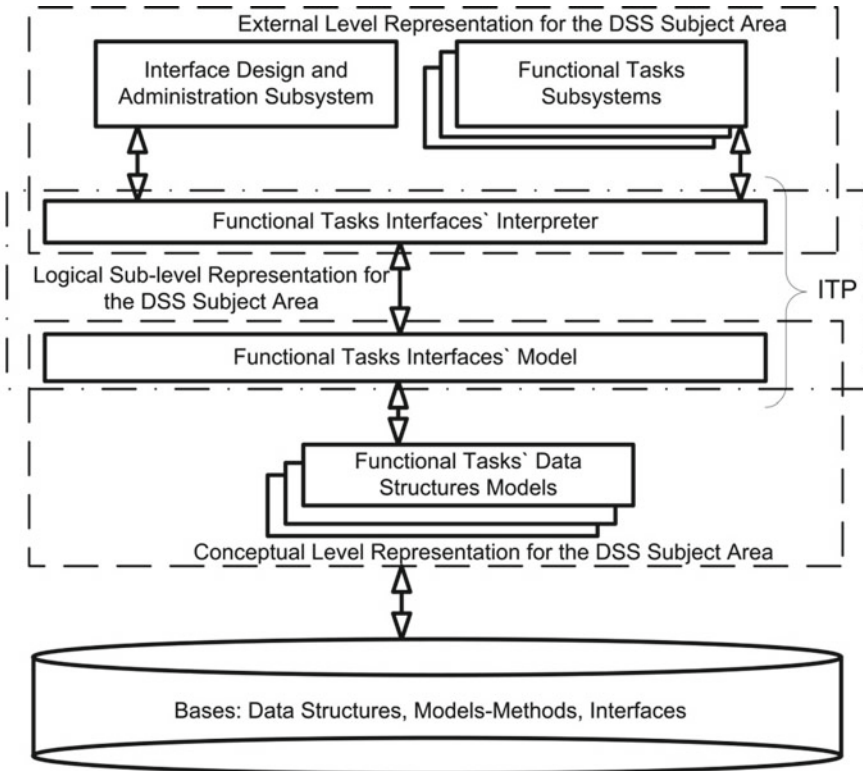
3.1 Organizational Schema of Information Technology Platform for Decision-Making Process Automation

The basis of the adaptive organizational scheme of ITP for the construction of object-oriented integrated DSS should be based on typical features that can be used to distinguish one data object from another. The expediency of such analysis and allocation of subject area object classes in the development of models for external (reflecting the system software application interface) and conceptual (reflecting the data representation of functional tasks in the system software application) levels in the ITP organizational schema is due to the fact that for different functional tasks of the software application often uses the same visualization and transformation operations over information data sets. In addition, the functions and processes of data processing in the phased implementation of subsystems in the integrated hierarchical system are rapidly modified, reproducing the variable user requirements to the subject area.

All this requires such an organization of the system structure through which objects in the subject area and the relationships between them would be defined regardless of the implementation of specific functional tasks for data processing in software procedures and interfaces and represented a single structure. As a result, the object of design and description in the organizational schema of the system should be not only data structures in the subject area but also the procedures for implementing functional tasks [18]. The introduction of an additional intermediate logical sublevel for representation of procedural and interface parts of the ITP software environment between the conceptual and external levels in the organizational schema for subject area will provide the necessary independence and DSS adaptability to possible changes and extensions in the models and data structures (Fig. 1).

As a result, the visualization logic of functional tasks in the subject area also becomes data presented in the form of its own interface model, which is included to the conceptual model. The ITP technological part becomes as instrumental software package of adaptive information system, whose function is the interpretation and reproduction by the subsystems tasks the interdependent data from the models of the functional tasks interfaces and data structures in the conceptual level of the subject area.

However, the simple availability of separate functional subsystems in DSS does not provide a solution to the whole set of tasks related to reliable and efficient operation during the longest possible life cycle, which will occur both at the stage of practical software development and operation. Therefore, the required functionalities of modern DSS should be the system property as open structure, the availability of a flexible interface (mechanism) for the inclusion of new objects and algorithms to

Fig. 1 The ITP organizational schema for DSS construction of organizational management

solve applied tasks and the ability to adapt around changes in both objects structure and parameters values in subject area.

Thus, the information part as the database and the technological part as the ITP software will consist of functional and information components. Functional will reflect the features and processes, and information will reflect the unified ways of interacting with objects from the subject area.

A distinctive feature of the proposed conceptual approach to creating an information technology platform for building and implementing DSS functions is to formalize the components of DDM-paradigm (Data-Dialog-Model) as problem-independent components in the DSS conceptual model for OMS [19, 20]:

1. The component Data is a block of object-oriented modeling of the subjects participating in structure-forming communications in the organizational management defining rules of the energy market functioning and indicators (parameters) of its functioning.
2. The component Dialog is an adaptive model of interaction (interface) and data presentation to the user, which implements a dynamic binding method organized
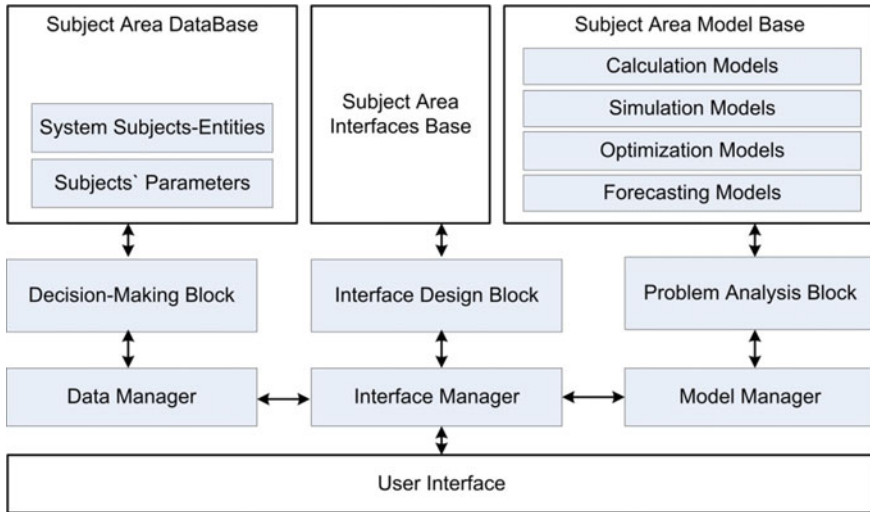
Fig. 2 The ITP conceptual model for DSS construction of organizational management

by the creating a mappings dictionary the data structures and attributes of the energy market functional tasks with the data visualization operations.

3. The component Model is a ITP tools for generating models that provide the problem analysis function, which are presented as unified methods—modeling algorithms to define the rules for formation and change the values of energy market functioning indicators when implementing the data management main stages in DSS.

In papers [16, 18, 21] the DDM-paradigm improvement is offered and the following problem-independent components of representation are substantiated to include in DSS structure for automated management of COTS subjects (Fig. 2):

- models of entities/subjects involved in the structure-forming relations of organizational management to determine the rules of COTS functioning;
- models of indicators/parameters for state definition of COTS functioning;
- modeling algorithms/models with various calculation purposes, which determine the rules for formation and change of indicators values of COTS functioning;
- interfaces model for interaction definition and data presentation to the COTS user;
- managers of data, interfaces, models for the organization of COTS functioning.

An important component of the ITP conceptual model for the DSS construction is the data manager, which provides a user interface to the data structures of the OMS subject area with the ability to further monitor and evaluate the COTS functioning indicators. Therefore, when using the object-oriented approach to the adaptive DSS creation, it is necessary to provide for the object analysis stage of the applied subject area (ASA) and then based on it the implementation next stage of the object-oriented ASA modeling for this management object.

3.2 Analysis of the Functioning Processes Representation for the Organizational Management System

One of the main conditions for creating adaptive information systems is the data unification. The development of a single unification system is a complex and time-consuming task, to solve which it is advisable to use international experience and standards [22, 23]. The basis for building a single classification system and a single data space should be a generalized information model, which in the same way according to IEC standards describes the whole set of typical physical OMS subjects based on the principles of object-oriented modeling (OOM) [24–26]. Adhering to the OOM principles, such a generalized information model supports the description of OMS physical subjects at all levels of COTS, which allows to simultaneously representing in the information system their properties, relationships and behavior, creating the opportunity to apply a single system of classifiers, reference catalogs and unify data access system.

Object-oriented approach to the adaptive DSS creation involves primarily the stage of ASA object analysis. But the essence of this analysis is to identify the entities—OMS ASA subjects and processes in the form of a set of information objects that interact with each other based on the OOM principles and develop on their basis a single representation specification for the subject area of OMS functioning.

It is known that the basic concepts of OOM are objects, classes, properties, events, methods, and the principles are encapsulation, inheritance and polymorphism. Object model describes the structure of objects that make up the formal system $Object = (Attribute, Condition, Behavior)$, which consists of the object attributes *Attributes*, the current functioning state *Condition*, the methods of behavioral operations *Behavior*. Therefore, in such an object model should be reflected those concepts and objects of the already real environment of the COTS ASA, which are important for the OMS being developed. And the created classes of ASA objects must be organized into a hierarchical structure built on the subordination relations, which are based on the principles of encapsulation, inheritance and polymorphism.

The physical OMS subjects and their functioning processes serve as objects of the COTS ASA, which are provided by the OOM means with all its principles. The subjects include organizational structures that carry out activities within the framework of ASA. In the general case, the OMS subject, depending on the management functions may be represented by a hierarchical structure in the composition of other subjects of activity. Therefore, any subject should be characterized by individuality, condition state, structure and certain behavior.

The individuality of OMS subjects is described by a set of qualitative and quantitative characteristics such as attributes that distinguish each subject from another and characterize changes in its state as a result of interaction with other subjects. As a rule, the subject individuality is represented by constant (technical) characteristics namely functioning properties of the subject and dynamic characteristics namely functioning parameters. The functional state of each subject is determined by a list

of parameters and their values, which reproduce the various quantitative indicators of its activities over a time period.

The activity (behavior) of the subject is regulated by the calculation-technological processes that are carried out on the states of all ASA subjects in the OMS. These processes are identified by regulatory documents and implemented using modeling algorithms/scenarios for the formation of parameters values—indicators of the management state for subjects. After completion of all regulated procedures and relevant calculation-technological processes in the ASA, will be obtained data on changes in the COTS functioning state as a whole.

Thus, the composition of the basic elements-ASA entities, which become the objects of the information model are include subjects, subject types, property types of subjects, subordination/relationship types of subjects, parameters, parameter types, types of functional interlink between parameters and subjects. And the mechanisms of change in the functioning states of the subjects are presented by the established schemes of algorithms/scenarios for modeling, forecasting and other calculations, the results of which are reflected in the quantitative values of the calculated indicators.

Therefore, in general the information model of the OMS functioning processes should use the principle of presenting ASA information objects by the metadata as a reproducing means for OOM concepts.

3.3 Information Model for Subject Area of the Organizational Management System

The selection of a set of information objects with these characteristics and the relationship between them, makes it possible to build an object information model of a particular ASA and on this basis to further develop a unified system of classifiers, reference catalogs, storage structure and single system of protocols, interfaces, tools for programming computer models of technological processes in the COTS also [27].

Therefore, the ASA specification of adaptive DSS can be presented in the form of a semantic net of classes in the information model (Fig. 3), which consists of declarative and procedural parts:

$$SP = \left(E, SN, f^{SN}\right),$$

where $E = E^{DECL} \cup E^{PROC} = \{e_i | e_i \in SA\}$, $E^{DECL} \cap E^{PROC} = \emptyset$ is a set of entities in subject area SA, which is determined by the aggregate of its information classes e_i; $f^{SN} : E \times E \to SN$ is a semantic net of classes in the ASA specification, which is defined by a set of semantics (assignments) SN.

Semantics' set SN establish the information objects' typical relationships—"classification", "belonging", "composition", "characterization", which are associated
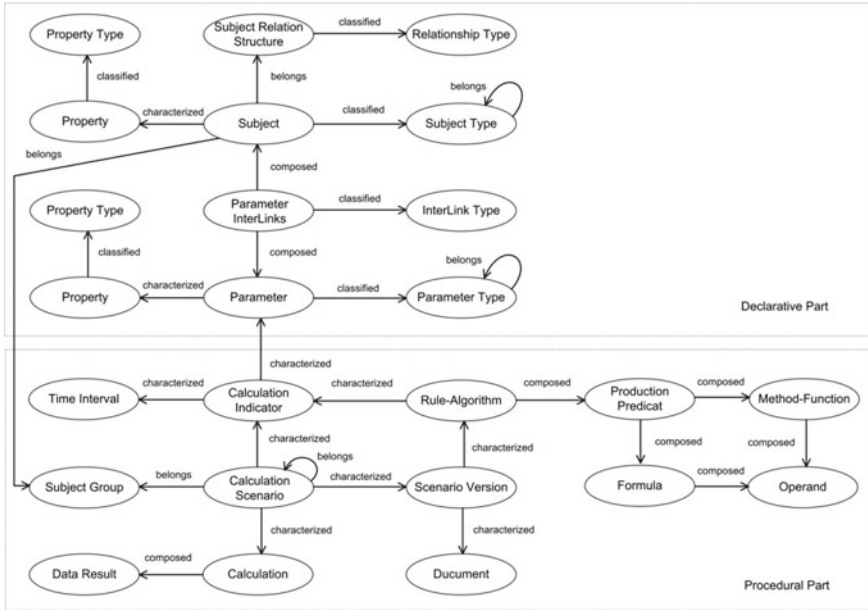
Fig. 3 Semantic net of classes for ASA specification

with the corresponding ways of reproducing information in data structures (relationships between elements, sets and parts of OOM objects [25])—association "IS-A", generalization "PART-OF", aggregation "HAS-PART", dependencies "IN-OTHER".

Object analysis of ASA for the organizational management leads to the following construction of the components in ASA dictionary:

$$SA = \left(S, C, P, ST, PT, f^S, SC\right),$$

where $S \subseteq ST \times C$ is a ASA subject; C is a static property that identifies the subject in its class (subject type) ST; $P \subseteq PT \times S$ is a dynamic parameter that belongs to one of the established classes (parameter types) PT and characterizes the component of the current state vector of the subject $S = (C, P)$; $f^S : S \times S \to LT$ is a ASA subject structure, which is determined by the set of relationship classes (relationship types) LT that are established between subjects within ASA; $SC = \left(O, f^O, V, M, f^V\right)$ are functioning scenarios of subjects in the ASA; O are the calculation-technological operations (operation groups); $f^O : O \times O \to \{0, 1\}$ is a scheme of operations calculation scenario; $V \subseteq P \times D$ are the calculation indicators for subjects parameters in a certain estimated time interval D; $M = \left(R_i | i = \overline{1, n}\right)$ are the rules (algorithms, procedures) for the implementation of calculation-technological operations, built on the basis of product rules predicate R_i; $f^V : O \to V \times M$ is a result of the calculation-technological operation.

The model classes of the declarative part E^{DECL} allow describing the composition, connections and properties of the ASA subjects, but the classes of the procedural (technological) part E^{PROC} allow describing the structure and relationships for technological processes of subject functioning in the ASA.

Based on the given specification the subjects in the semantic net includes objects of organizational management, structures in their technological equipment, legal entities and other organizational structures, the state vector of which changes due to calculation-technological operations of optimization, forecasting and other purposes. Each subject in the description has its own type, a list of its own properties and a list of subjects with whom the relations is established. The functional state of the subject is determined by a list of parameters—components of the state vector, which reproduce various indicators of its activities. Each parameter in the description has its own type, a list of its own properties and a list of subjects to which it relates.

Modeling algorithms of the calculation-technological operations are used to establish relationships between the parameters of different subjects. Algorithms are implemented using scenarios of calculation schemes based on the production rules of their representation, calculation indicators of parameter's values, calculation methods-functions, production predicates, formulas and their operands.

Therefore, the information model, which is formalized in the form of an ASA specification of DSS, will be presented as a whole as a set of the following components:

- models of organizational management objects that participate in the structure-forming relations of the ASA subjects;
- models of parameters that determine the functioning state of the ASA subjects;
- modeling algorithms (algorithms for implementing methods) that determine the rules to formation and change the values of the subjects functioning parameters;
- results' arrays of optimization, forecasting calculations, which determine the prospects of the ASA subjects.

Thus, the application of OOM to the design of the adaptive DSS specification will provide a number of advantages:

- the system description in the form of information objects corresponds to the semantics (content) of the ASA subjects;
- the behavior of the ASA subjects is presented by the objects of certain classes, which contributes to the easy change of their behavior;
- combining information objects into a net with the certain semantic relations allows to unify the structure of data storage and interfaces of their relationship;
- ensuring the possibility of parallel calculations of the subjects' states, each of which has its own properties and behavior.

The use of OOM as the basis for constructing an information model of OMS functioning processes made it possible to present the information space in the form of a unified data system. The developed specification of the OMS subject area for building computer models of organizational management provides adaptation to changes in

existing or the emergence of new mechanisms for the COTS functioning and its effective support at different stages of the OMS life cycle when building an integrated adaptive DSS.

3.4 Functional Model of Information Technology Platform for Decision-Making Processes Automation

Functional organization is a structured representation of the OMS functions, data flows and entities of the information model, which link these functions into a single whole. It is built by the decomposition method from complex functions to simpler ones. Elements of each decomposition level are actions on transformation of information flows with use of certain OMS functioning processes under their management. Thus, the functional organization is formed by subsystems that are characterized by input and output data flows, as well as data management mechanisms and implemented functions of their processing.

Consider the functional organization of ITP for the construction of object-oriented integrated adaptive DSS (Fig. 4). The DSS structure for the management of market participants includes the following structural-functional elements for certain components of the ITP conceptual representation.

1. The component Data are:

   - the base of subjects involved in the structure-forming relations of organizational management in the market;
   - the base of parameters—indicators of subjects functioning in the market;
   - the data warehouse on the state of functioning indicators for market subjects.

2. The component Model are:

   - the modeling algorithms—models of calculation, simulation, optimization, forecasting on the basis of unified data processing methods, which determine the rules of formation and change of indicators values about functioning of market subjects.

3. The component Dialog are:

   - the model of interfaces about data interaction and presentation to the user;
   - the managers for data, models and interfaces;
   - the functional subsystems—modules of stages in the preparation and decision-making process on the organizational management of market functioning (tuning, preparation, modeling-calculation, analysis-estimation, reporting, monitoring).

The component Data form the IASM information model and the component Model form the IMS functional model in the DSS for organizational management of market functioning.
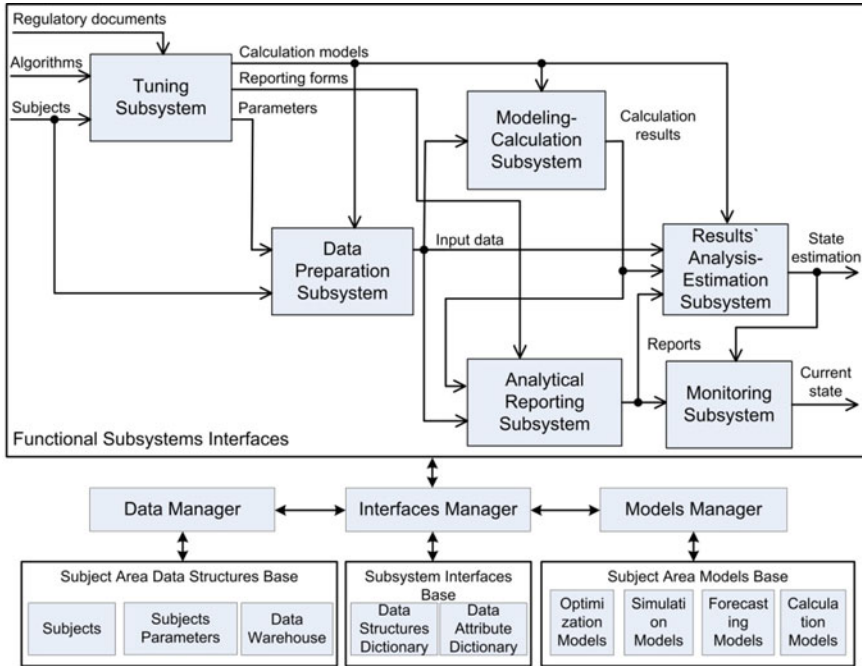
Fig. 4 The ITP functional model for DSS construction of organizational management

The manager of data in the ITP functional model provides manipulation of the state in the information model for the market subject area through the organization of input and output data flows in DSS. As a result, all input and output data in the information model are presented in the form of information blocks of data about the subjects, the parameters of the subjects, calculation algorithms, calculation results, the formation of reporting documents and more.

The manager of models in the ITP functional model acts as a means of generating models in DSS, which implement the functions of problem analysis and are presented as unified data processing methods, which include such as formula (used to calculate the state of indicators), procedure (used to simulate changes in indicators), search for alternatives (used to optimize indicators), predictions (used to forecast indicators).

The manager of interface in the ITP functional model acts as a link between data and model managers, which implements the function of presenting and interpreting information generated from data and models.

As a result, managers of data, models and interfaces form the technological part, and databases—the information part of the ITP construction and implementation of functional subsystems in the DSS for market organizational management. In general, the basic software package of object-oriented integrated adaptive DSS built on the principles of decomposition and structured with subsystems, implements

tasks that reflect the stages of preparation, analysis and decision-making in the functioning process of the information model for the subject area of market organizational management [17].

4 Organization of the User Interface in the Information Technology Platform for Decision Support System Construction

4.1 Classification of User Interaction Operations with Subject Area Objects of the Organizational Management System

In the organizational structure, the software of object-oriented integrated adaptive DSS consists of functional subsystems and software interpreter of functional tasks interfaces. And its information support is presented in the form of subject area objects conceptual representation and metadata of the user interaction interfaces with DSS functional tasks.

The organization of the DSS functioning technological process provides the functions of preparation, implementation and data processing of calculation results and consists of sequential tasks implementation by the functional subsystems which purposes are corresponds to basic typical interaction operations for end user with DSS.

The manager of interfaces, as a link between data and model managers in the DSS conceptual model, acts as a tool of presenting and interpreting information generated from data and models. As a result, the DSS software built on the basis of object-oriented adaptive ITP should consist of subsystems focused on solving functional tasks in providing user information needs from the OMS subject area.

The adaptive object-oriented organizational model of the interfaces manager should be based on standard features that allow classifying and reflecting the differences between the ASA objects from each other. The expediency of such analysis and selection of object classes in the information models development is due to the fact that for different functional tasks often use the same operations of visualization and transformation over information data flows. In addition, the functions and processes of data processing during the phased DSS implementation are rapidly modified, reflecting the changing user requirements to the subject area. All this requires such an organization of the ITP structure, in which the subject area objects and the relationship between them would be defined in the software procedures and interfaces, regardless of the implementation of specific functional tasks for data processing and represent a single structure. Such a mechanism is a dynamic binding method, which is implemented in the form of its own model by creating a mappings dictionary of functional tasks data structures on visualization operations [18].

Thus, the following conceptual scheme of ITP construction in the form of a three-level organizational structure is proposed, namely this "functional environment of the

subject area—functional task—instrumental (operation) processing function". As a result, the software (technological) part of the system will be structured with subsystems, which are distinguished not by problem-oriented features, but only functional (object) ones. Because are focused on typical interaction operations with objects in the subject environment when interpreting and presenting data to the DSS user.

4.2 Information Model for Representing User Interfaces of the Decision Support System

Consider the mechanism of data representation in object-oriented integrated adaptive DSS, built using metadata technology.

The effectiveness of complicated information systems largely depends on the ways of semantic matching of the software application interface with the data of its business logic, which are processed at the conceptual and physical representation levels [18, 28]. It is very important in what way provides a degree of data independence (consistency) from the programs logic. There are several ways of semantic matching through the binding mechanism of data structures with the program application, which can be carried out both at the stages of program compilation (design) and execution (translation).

Embedding data structures in programs and binding them to the business logic, which is carried out before the program start, namely at the design stage, provides static semantic matching. In the case of the conceptual data model modification to successfully perform the functional task of the software application with this binding option, it is necessary to recompile and build a new program image, suitable for use with modified data structures.

Implementation of the binding mechanism for data structures at the stage of program execution, by simultaneous sampling of application data and interface from the database, allows ensuring dynamic data independence from possible changes in their conceptual representation. This mechanism provides maximum flexibility in the software application implementation.

Such dynamic binding is realized by creating a mappings dictionary of data structures for functional tasks in the subject area conceptual level to the software application interfaces and is presented in the form of own model of interfaces for functional tasks. In this case, the conceptual data model modification does not destroy the initial state of the software application, because changes in it will be reproduced by modifying the data in its own representation model, but the structure of which remains unchanged.

Thus, the main structures of one's own model of dynamic binding are models of relations and attributes. The principle of mapping information objects in the subject area to the elements of the ITP interface model is shown in Fig. 5.

Each relationship model record contains general information about the data structure of a particular DSS functional task, the primary key of which is the relationship
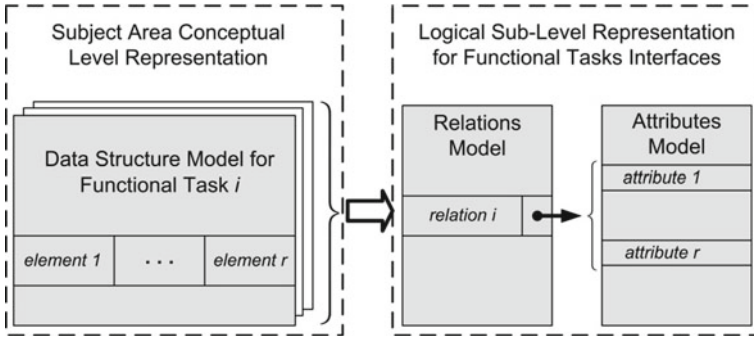
Fig. 5 The principle of mapping the information objects in the subject area

identifier. This identifier uniquely determines the mapping of the data structure from the subject area conceptual level to the functional task interface.

The attributes model determines the characteristics (properties) of the data structure elements of the functional task, the affiliation of which is determined by the identifiers of the relationship and attribute. Implementation of new data structures to the subject area is carried out by adding new records to the relationship model and the formation of new data about the attributes of this relationship. The operations of the ITP software application is automatically modified depending on the data entered into its own interface model.

Thus, the adaptive ITP software environment will be declared as a set of the following:

$$P = (T, U, G, f_G, f_T),$$

where $T = \{t_i | i \in I\}$ is a set of the functional tasks for software application, $U = \{u_j | j \in J\}$ is a set of the software application users, $G = \{g_k | k \in K\}$ is a set of the user groups, $f_G : U \times G \to \{0, 1\}$ is a user affiliation function by the group, $f_T : (U \cup G) \times T \to \{0, 1\}$ is a access function by the functional tasks.

Software application functional tasks are defined by the following sets:

$$t_i = \left(R, A, f_R^T, f_A^T, D, f_D, M, f_M\right),$$

where $R = \{r_i | i \in I\}$ is a set of the data structures for functional tasks, represented in the relationship model $f_R^T : T \to R$, $A = \{a_y | y \in Y\}$ is a set of the data structure elements for functional tasks, represented in the attribute model $f_A^T : A \times T \to R$, $D = \{d_h | h \in H\}$ is a set of the methods that processing elements of data structures for functional tasks in the form $f_D : D \to T$, $M = \{m_l | l \in L\}$ is a set of the binding types for data structures that define the interface model for functional task in the forn $f_M : T \to M = \{\text{Table,Tree,Card,Report}\}$.

Methods that processing elements of data structures are defined as sets:

$$d_h = \left(S, f_S, f_R^D, f_A^D \right),$$

where $S = \{s_v | v \in V\}$ is a set of the data processing ways in the form—view, edit, create, delete, search (filter), generate aggregated data, call the related data structure, $f_S : D \rightarrow S$ is a affiliation function of the data processing ways, $f_R^D : D \rightarrow R$ is affiliation function for the related data structures to the data processing ways, $f_A^D : A \times D \rightarrow R$ is affiliation function for the related data structure elements to the data processing ways.

4.3 Functional Modules of the Decision Support System User Interfaces

The application of the vertical and horizontal decomposition principles allows distinguishing three interaction levels of the interfaces to the data for DSS functional tasks in the organizational structure of the ITP software package:

- the level of problem-oriented user environment of the OMS subject area;
- the level of tools for solving the functional task selected by the user;
- the level of implementation of the data processing tool for the functional task.

The first level organizes the user's work in solving the applied problem for the OMS subject area and reproduces a set of functional tasks due to the external level of OMS representation. This level is represented by the module "Interface Manager", which reproduces the available set and sequence of tasks in the form of a hierarchical menu or a tree of subsystems.

The second level reproduces the realization procedure of the functional task defined at the first level, the type of which is established depending on the information binding of data structure elements with interfaces of the functional task presented at the OMS subject area conceptual level. Each functional task can use the following types of information links between elements of data structures:

- simple relations of the list type "to each other";
- structured relations of hierarchical type "one to many";
- functional relations of join for several data structures with formation of new data elements by means of aggregative functions also.

Depending on the relations type between the data structures elements that form a functional task in the ITP software package, the following modules are used: module "Table" for simple relations, module "Tree" for structured relations, modules "Report", "Card" for functional relations.

In addition to the above modules, to ensure the proper functioning of the information system, the second level also includes the following service module "Registration", which identifies users and determines their access rights to functional tasks and functions.

The third level provides the typical functions implementation of the processing procedures for data structures of the functional task, such as view, edit, create, delete, search (filter), generate aggregated data and call the related data structure.

As a result, the system basis for formation of the uniform information and software environment for DSS construction is created on the basis of the presented specification of the ITP software package that include:

- a single system of classifiers and catalogues;
- a single system of protocols and interfaces for user interaction;
- unified data storage structure;
- unified system of real-time data collection and commercial accounting of functioning indicators for the market subjects.

Therefore, the development and application of such a software environment on the proposed ITP will provide a single software product for the deployment and DSS maintenance, which will reduce the risk, complexity and costs in the transition to new organizational management tasks for market participants.

5 Conclusions

Based on the analysis of the mechanisms peculiarities of the organizational management in the energy market, it can be concluded that DSS should be considered as an object-oriented integrated adaptive system to automate the organizational management processes in the electricity market. As a result, the functional modeling of technological processes, both in data processing and in the formation of a model for solving applied control problem, plays a significant role in solving the object modeling problem of the organizational management subject area in the electricity market. The functional modeling purpose is the unification of the software interface for a single integrated system through the classification for user interaction operations with the data structures of the OMS subject area.

A distinctive feature of the developed ITP for the DSS construction which implements the organizational management of energy companies in the electricity market is a new formalization of the DDM-paradigm components, namely:

- the conceptual bases for construction of the DSS organizational model are defined, which include bases of data structures, bases of models, bases of user interaction interfaces, and carry it to a information system class of operative short-term decision-making on management;
- the unified model of DSS data structure is defined, which forms unified approaches to the market participants representation at all management levels based on determining their properties and relationships by creating a single system of classifiers, reference books to use in models of parameter calculations, algorithms of parameter optimization and their forecasting;

- the organizational model of ITP as an environment of interaction and data presentation to the OMS user is offered, that provides improvement the technological processes of OMS subjects information interaction in the electricity market due to the flexible mechanism of creation and use the mathematical models for various calculation-analytical tasks, interconnected by purpose, input and output data.

References

1. Solovyov, I.V.: Problems of researching a complicated organizational-technical system. Vestn. MGTU MIREA **1**(1), 20–40 (2013) (Rus)
2. Novikov, D.A.: Organizational Systems Management Theory, Publishing House of Physics-Mathematics Literature, Moscow, p. 604 (2012) (Rus)
3. Mokhor, V.V., Evdokimov, V.A.: About creating a multi-agent simulations model of processes pricing in the electricity market. Electron. Model. **42**(6), 3–17 (2020) (Ukr). https://doi.org/10.15407/emodel.42.06.003
4. Saukh, S.Y.: Methodology and methods of mathematical modeling of energy engineering in market conditions. Electron. Model. **40**(3), 3–32 (2018) (Ukr). https://doi.org/10.15407/emodel.40.03.003
5. The national energy modeling system: an overview 2018. https://www.eia.gov/outlooks/aeo/nems/documentation/
6. Plexos market simulation software. https://energyexemplar.com/solutions/plexos/
7. Aurora electric modeling, forecsting and analysis software. https://energyexemplar.com/solutions/aurora/
8. Eom, S.B.: Decision support systems research: current state and trends. Ind. Manage. Data Syst. **99**(5), 213–221 (1999). https://doi.org/10.1108/02635579910253751
9. Eom, S.B.: DSS, BI, and data analytics research: current state and emerging trends (2015–2019). In: Moreno-Jiménez, J., Linden, I., Dargam, F., Jayawickrama, U. (eds.) Decision Support Systems X: Cognitive Decision Support Systems and Technologies. ICDSST 2020. Lecture Notes in Business Information Processing, vol. 384. Springer, Cham (2020). https://doi.org/10.1007/978-3-030-46224-6_13
10. Larichev, O.I., Petrovskiy, A.B.: Decision support systems: current state and development prospects. Itogy nauki i tehniki: Tehnicheskaya kibernetika, VINITI, Moscow, Russia, vol. 21, pp. 131–164 (1987) (Rus)
11. Trakhtengerts, E.A.: Computer systems for support of management decisions. Inf. Technol. Manage.: Manage. Probl. **1**, 13–28(2003) (Rus)
12. Tikhanychev, O.V.: Theory and practice of automating decision support. Edithus, Moscow, Russia, p. 76 (2018) (Rus)
13. Pospelov, D.A.: Situational Management: Theory and Practice. Nauka, Moscow, USSR, p. 288 (1986) (Rus)
14. Makarov, I.M., Evtikhiev, N.M., Dmitrieva, N.D. and etc.: Fundamentals of Manufacturing Control Automation. Vyshaiya shkola, Moscow, USSR, p. 504 (1983) (Rus)
15. Yampolsky, L.S., Melnichuk, P.P., Ostapchenko, K.B., Lisovychenko, O.I.: Flexible computer-integrated systems: planning, modeling, verification, management. ZhDTU, Zhytomyr, Ukraine, p. 786 (2010) (Ukr)
16. Borukaiev, Z.K., Ostapchenko, K.B., Lisovychenko, O.I.: Concept of building an information technology platform for the design of decision support systems for organizational management of the energy market. Adapt. Syst. Autom. Control **1**(32), 3–14 (2018). https://doi.org/10.20535/1560-8956.32.2018.145538

17. Ostapchenko, K., Lisovychenko, O., Evdokimov, V.: Functional organization of system of support of decision-making of organizational management. Adapt. Syst. Autom. Control **1**(36), 17–31 (2020). https://doi.org/10.20535/1560-8956.36.2020.209753

18. Evdokimov, V.F., Borukaiev, Z.K., Ostapchenko, K.B., Lisovychenko, O.I.: Theoretical-game and object-oriented modeling of organizational management systems. IPME, Kiev, Ukraine, p. 283 (2019) (Ukr)

19. Sprague, R.H., Carlson, E.D.: Building Effective Decision Support Systems. Prentice-Hall, Englewood Cliffs, NJ (1982)

20. Sprague, R.H., Watson, H.J.: Decision Support for Management. Prentice-Hall, Englewood Cliffs, NJ (1996)

21. Borukaiev, Z.K., Ostapchenko, K.B., Lisovychenko, O.I.: An approach to building decision support systems for automating organizational management processes in the energy sector. Adapt. Syst. Autom. Control **1**(30), 36–48 (2017) (Rus)

22. IEC 62325-301.: Framework for energy market communications. Part 301: Common information model (CIM) extensions for markets. https://webstore.iec.ch/publication/31487 (2018)

23. IEC 62325-351.: Framework for energy market communications. Part 351: CIM European market model exchange profile. https://webstore.iec.ch/publication/25128. (2016)

24. Kolesov, Y.B.: Object-oriented modeling of complex dynamic systems. SPbGPU, Saint Petersburg, Russia, p. 240 (2004) (Rus)

25. Graham, I.: Object-Oriented Methods: Principles & Practice, 3rd edn, Williams, Moscow, Russia, p. 880 (2004) (Rus)

26. Buch, G.: Object-Oriented Analysis and Design with Sample C++ Applications. Williams, Moscow, Russia, p. 720 (2008) (Rus)

27. Borukaiev, Z.K., Ostapchenko, K.B., Lisovychenko, O.I.: Object-oriented modeling of the processes of functioning of the subjects of organizational and technical systems. Electron. Model. **40**(6), 37–52 (2018) (Rus). https://doi.org/10.15407/emodel.40.06.037

28. Trofimova, L.A., Trofimov, V.V.: Management decisions (methods of adoption and implementation). SPbGUEF, Saint Petersburg, Russia, p. 190 (2011) (Rus)

Increasing the Reliability of Lightning Protection of Electric Power Facilities

Marina Rezinkina , **Vitalii Babak** , **Oleg Gryb** , **Artur Zaporozhets** , **and Oleg Rezinkin**

Abstract The lightning protection system can become a factor in super-powerful electric fields, which is very dangerous for technical means that are located in such field, as example, unmanned aerial vehicles. But it is difficult to predict the cases when lightning strikes the current-carrying parts of electrical equipment. Therefore, it is necessary to have calculations on the distribution of fields during a lightning strike. This chapter presents models of the electric field in the vicinity of long thin wire rods and a model of the distribution of electric fields in the presence of an ionized streamer zone near the lightning top. The processes of corona at the tops of grounded rods, which imitate protected objects and lightning rods, are analyzed. The physical modeling of electromagnetic processes during the development of the corona on rod electrodes with different vertices has been performed.

Keywords Electric field · Lightning · Corona discharge · Corona current

1 Introduction

During choosing lightning protection means, data on the level of electromagnetic field (EF) strength in the "lightning leader—lightning rod" systems are needed. Studies aimed at solving the problem of calculating the EF in the vicinity of long thin conductive objects such as wires or rods, the length of which is on order of magnitude or more greater than their diameter, located in an external EF, are described in [1–5].

Direct measurement of the electrical parameters of such objects as the lightning leader channel presents significant difficulties. Therefore, their mathematical modeling has become widespread. During modeling the EF in systems containing long thin rods, a number of problems arise due to the large difference between their diameter and length. More often, long discharge channels are presented in the form

M. Rezinkina · O. Gryb · O. Rezinkin
National Technical University "Kharkiv Polytechnic Institute", Kharkiv, Ukraine

V. Babak · A. Zaporozhets (✉)
Institute of General Energy of NAS of Ukraine, Kyiv, Ukraine
e-mail: a.o.zaporozhets@nas.gov.ua

of a charged filament [6]. It is also possible to use as a model of such objects an electrically conductive ellipsoid on which a charge located, as well as an electrically conductive ellipsoid located in a uniform external EF [7]. The closest model to real objects is the "cylinder in an external EF" model. It should be assessed how the choice of the rod model affects the distribution of potentials and strengths of the EF. When solving practical problems of lightning protection, analytical methods are mainly used, however, the use of numerical methods of calculation [8–10] makes it possible to take into account the real shape of lightning and lightning rods, the nature of the distribution of charges on them, the presence of ionized zones near them, as well as the influence of the earth on the magnitude and nature of the intensity distribution.

2   EF Simulation in the Vicinity of Thin Conductive Rods of Great Length

To assess the electrical parameters of a thin conductive channel in solving practical problems of lightning protection, as a rule, it is replaced by a filament with a charge uniformly distributed along its length. Then the distribution of potentials in the vicinity of an infinitely thin charged filament of length $2a$ located parallel to the Oz axis with center coordinates x_0, y_0, z_0 can be found using the well-known analytical expression [11]. However, in real systems, along the length of the leading rod, as a rule, not a charge, but a potential is given. It is known that the conductivity of the leader channel of lightning is quite large: for example, in [12] it is noted that the level of EF intensity in the leader channel is close to $E_L = 10^4$ V/m. Thus, in some approximation, the leader lightning channel can be considered the main and, during describing its EF, the analytical solution for the potential of free charges on the leading ellipsoid can be used [13, 14]. The performed calculations showed that the values of the potentials and strengths of the EF in the vicinity of sufficiently long and thin conductive rods, obtained by representing them in the form of a thin charged filament or a conducting ellipsoid, practically coincide, except that in the 2nd case there is an increase in the charge density and tension of the EF at the tops of the rods.

During calculating the parameters of the lightning leader channel, it should be taken into account that a real EF in a thunderstorm environment corresponds to a system that is a lightning leader channel located in a close to uniform external EF with strength E_0 (Fig. 1a). In this case, the well-known analytical solution for the leading prolate ellipsoid in the external EF can be used.

We assume that the ellipsoid is in a homogeneous EF with intensity E_0, directed along its major semi-axis a, parallel to the Oz axis, and its minor semi-axes are equal to each other: $b = c$. By transforming the expression for the potential outside the ellipsoid [14] for the case when its center has coordinates x_0, y_0, z_0, and taking the corresponding integrals, we finally obtain:

$$\varphi(x, y, z) = E_0 \cdot [z \cdot (1 - a_1/a_2) + z_0 \cdot a_1/a_2], \tag{1}$$
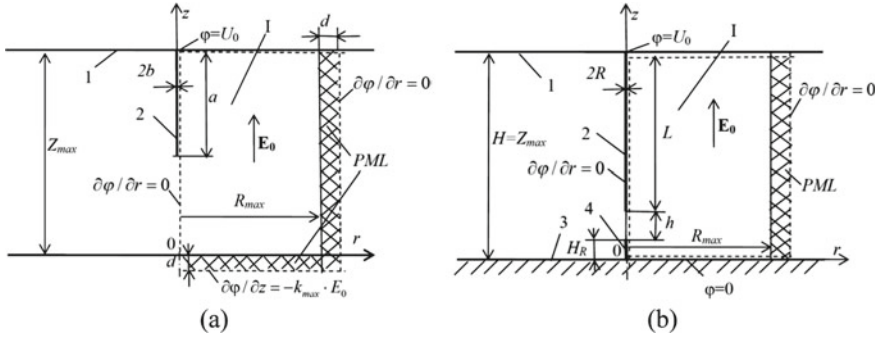
Fig. 1 Calculation system: **a** leader channel is located far from the ground in a EF with intensity E_0; **b** leader channel approaches to the ground and the lightning rod (1—upper limit of the considered area, 2—leader channel of the lightning, 3—ground, 4—lightning rod, – – – calculation area)

where $a_1 = -\dfrac{1}{(a^2-b^2)^{\frac{3}{2}}} \cdot \ln\dfrac{\sqrt{\xi+a^2}+\sqrt{a^2-b^2}}{\sqrt{\xi+a^2}-\sqrt{a^2-b^2}} + \dfrac{2}{(a^2-b^2)\cdot\sqrt{\xi+a^2}};\ a_2 = -\dfrac{1}{(a^2-b^2)^{3/2}} \cdot \ln\dfrac{a+\sqrt{a^2-b^2}}{a-\sqrt{a^2-b^2}} + \dfrac{2}{(a^2-b^2)\cdot a};\ \xi = -f_1 \pm \sqrt{f_1^2 - f_2};\ f_1 = -\dfrac{(a^2+b^2)-[(x-x_0)^2+(y-y_0)^2+(z-z_0)^2]}{2};\ f_2 = a^2b^2 - a^2 \cdot [(x - x_0)^2 + (y - y_0)^2] - b^2 \cdot (z - z_0)^2.$

2.1 Statement of the Problem of Calculating the EF in the Vicinity of Conductive Rods of Great Length

In some cases, to calculate the EF in the vicinity of conductive rods, it is necessary to use numerous methods. In [15] the numerical calculation of the EF distribution in such systems is described. Let us consider the application of the finite volume method (FVM) for such calculations [16, 17]. In this case, the computational area is divided by a grid, in the nodes of which unknown quantities are determined that characterize the parameters of the EF. The difference between FVM and conventional finite-difference methods lies in the fact that to obtain the solving system, the integration of the initial equations over the volumes of elementary cells, into which the computational area is divided, is used. One of the advantages of this approach is that the conditions at the media interfaces are fulfilled automatically, which simplifies the calculation of electromagnetic fields in inhomogeneous media.

Let us calculate the EF distribution in the vicinity of the lightning leader channel and lightning rods in a pre-thunderstorm situation. Since the leader channel moves relatively slowly towards the ground, such a calculation can be performed in a quasi-stationary approximation.

The equation to be solved is obtained by applying to the Maxwell equation

$$\mathrm{div}\,\vec{D} = \rho,$$

where $\vec{D}$—electrical induction, expressed through the strength of the EF $\vec{E}$ and electric potential φ:

$$\vec{D} = \varepsilon_0 \varepsilon\, \vec{E} = -\varepsilon_0 \varepsilon\, grad\, \varphi,$$

the operation of integration over V volumes of elementary cells into which the computational area is divided, and using the Gauss theorem. Let's finally write:

$$\int\limits_{S} -\varepsilon \cdot \frac{\partial \phi}{\partial n} \mathrm{d}s = \frac{q_S}{\varepsilon_0}, \tag{2}$$

where S—surface enclosing the volume V; n—normal to the surface S; q_S—elementary charge placed on the surface S.

The system of equations obtained as a result of writing in the difference form equations of the form (2) for all nodes of the computational grid was solved by the iterative method of alternating directions using sweep.

To assess the accuracy of the numerical calculation, the following test system was used: an electrically conductive ellipsoid with a ratio of the major and minor semiaxes $a/b = 50$ and located in a homogeneous EF with a strength $E_0 = 1$ V/m and that its potential $U_0 = 1$ V. EF in such system can be described analytically by [18].

Since the rod has axial symmetry, a cylindrical coordinate system [19, 20] was used for the numerical calculation. Half of the original system was considered, such that its left boundary coincides with the axis of symmetry of the rod, the right boundary is located at a distance $R_{\max} = a$ from the axis, the upper boundary divides the major axis of the ellipsoid in half and coincides with its horizontal axis of symmetry, the lower boundary is removed from the upper one by a distance $Z_{\max} = 2a$. To take into account the ellipsoidal shape of the rod, the number of splits in the radial direction in the zone of the computational area $0 \le r \le b$ was chosen 10. It was assumed that the electrically conductive ellipsoid includes cells of the computational grid that lie completely inside its surface.

To reduce the dimensions of the computational domain when finding the EF distribution, the so-called uniaxially perfectly matched layer (PML) [21–23] are used on its right and lower boundaries. In such layers of thickness d, the permittivity is considered like a tensor that varies with the depth of the layers in accordance with the polynomial law, and its components in the directions of the coordinate axes Oz and Or are different.

So, for PML perpendicular to the Oz axis, in the range $z < 0$, the dependences of the z-th $\varepsilon_z^{PML}(z)$ and r-th $\varepsilon_r^{PML}(z)$ components of the tensor $\varepsilon(z)$ are written as [22, 23]:

$$\varepsilon_z^{PML}(z) = \varepsilon|_{z=0} \cdot k(z); \quad \varepsilon_r^{PML}(z) = \varepsilon|_{z=0}/k(z),$$

where $k(z) = 1 + (k_{max} - 1) \cdot [|z|/d]^m$; m—index; k_{max}—the maximum k value at the outer boundary of the PML; $\varepsilon|_{z=0}$—the ε value of the medium adjacent to the inner boundary of the PML.

Expressions for the tensor components in the PML perpendicular to the Or axis are written in a similar way. The values of the tensor components in the intersection zones of the PMLs are multiplied. According to the recommendations [21–23], 10 PMLs with parameters $m = 3$, $k_{max} = 300 \cdot \varepsilon|_{z=0}$ were used in the calculations.

The limiting conditions are shown in Fig. 2. The calculated distributions of lines of equal potential when the rod is represented as an elongated ellipsoid are shown in Fig. 2a: the solid curves correspond to the numerical calculation, the dotted curves correspond to the analytical calculation. Comparison of the results of numerical and analytical calculations of the values of potentials and strength modules of the EF showed that the relative differences between the levels φ and $\vec{E}$ depend on the step size of the computational grid and at $\Delta = b$ (except for the step in the range $0 \le r \le b$, where $\Delta l = b/10$) do not exceed 4.6%. The difference between the numerical and analytical results is related to the stepwise approximation of the ellipsoid in the numerical solution. However, the discharge channels and lightning rods are closer in shape not to an ellipsoid, but to a cylinder. It can be seen that even at large ratios a/b, a decrease in several times the cross section of the ellipse at approaching its tops significantly affects the distribution of the EF. A comparison was made of the distributions of EF strengths in the above-described calculation system using these two representations in order to assess how much they differ from each other.

Figure 2b shows the numerical solution for the lines of uniform strength of the EF $\vec{E} = const$ in the same system as for Fig. 2a, but for a cylindrical rather than
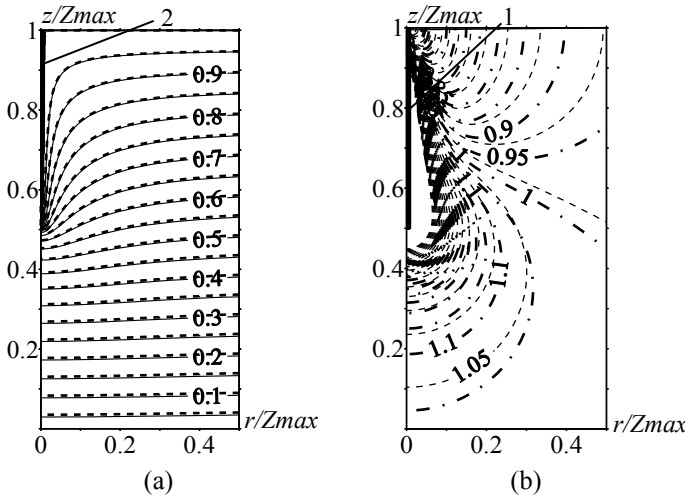
Fig. 2 Calculated distributions of lines of equal potential (**a**) and equal EF strength (**b**) at $H/R = 50$ (1—rod in the form of a cylinder, 2—rod in the form of an ellipsoid, — numerical solution for ellipsoid, – – – analytical solution for ellipsoid, –·–·– numerical solution for cylinder)

ellipsoidal rod shape. Dashed lines with dots correspond to the numerical solution for a cylindrical rod, and the dashed lines correspond to the analytical solution for an ellipsoid. It was believed that the radius of the cylinder $R = b$, and its height $H = a$. Calculations have shown that when the rod is represented as a cylinder, one step in space in the zone $0 \leq r \leq R$ is sufficient, equal to the radius of the cylinder $\Delta l = R$. For the considered parameters of the rods, when $H/R \geq 50$, the additional partition of the area $0 \leq r \leq R$ affects only the distribution of φ and $\vec{E}$ in a small area near the edge of the cylinder.

As can be seen from Fig. 2b, the distributions corresponding to the representation of the rod in the form of an ellipsoid and in the form of a cylinder differ significantly at $H/R \sim 50$.

For sufficiently long thin conducting rods, when the H/R ratio exceeds 10^2–10^3, the use of the usual representation of derivatives for finite difference methods in the form of differences in the values of the desired function at the nodes of the computational grid (piecewise linear approximation) leads to a complication of the problem. This is due to the fact that to provide an adequate description of the EF, the use of a computational grid is required, the step of which is of the same order as the radius of the rod, and for large values of H/R, the fulfillment of such condition is associated with a significant increase in the number of unknowns, as well as the number of iterations at their finding. To solve this problem, an approach similar to that described in [24] can be used, when it is considered that for a thin infinitely long rod, the change in the EF strength between the node of the computational grid located on its surface and the node adjacent to it in the radial direction does not occur along linear law, but inversely proportional to the distance of the nodes to the rod's axis. In [5], this approach was extended with respect to rods of finite length. The use of this approach makes it possible to calculate the EF with a significantly larger step of partitioning of the computational area, which is determined not by the radius of the rod, but by its length.

As an illustration, Fig. 3 shows the calculated distributions of lines of equal strength $\vec{E} = const$ in a system similar to that described above, but for the case when there is no PML at the lower boundary of the computational area ($z = 0$), and the potentials, which located on its nodes, equal to zero ("rod over a grounded plane" system) (Fig. 2b). Other system parameters and limit conditions are the same as described above.

Let's consider a cylindrical rod with a ratio of length to radius $H/R = 1000$. Such system simulates the presence of an electrically conductive discharge channel moving toward the ground. Solid curves in Fig. 3 correspond to the calculation performed taking into account the logarithmic decrease in potentials near the axis of the rod depending on the distance to it in the radial direction [5], the step of the computational grid is $\Delta = H/25$. The same figure shows the distributions $\vec{E} = const$, calculated using the usual for finite-difference methods representation of derivatives in the form of the difference of the desired functions at the nodes of the computational grid: dashed lines with dots obtained with the same step of the computational grid; dotted lines—with the step of the computational grid $\Delta = H/250$. As shown by the numerical experiments, a further decrease does not lead to a change in the potential

Fig. 3 Calculated distributions of lines of equal intensity of EF when the rod is represented as a cylinder ($H/R = 1000$) (— numerical solution according to the method [5] with a step in space $\Delta =$ $H/25$; – – – numerical solution by the usual finite difference method at $\Delta = H/250$; –·–·– numerical solution by the usual finite difference method at $\Delta = H/25$)
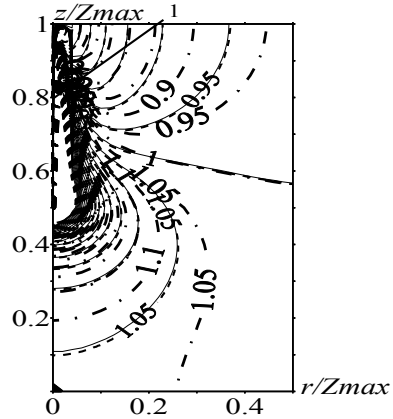
values in the zone around the rod. In all calculations, the step along the coordinate in the direction of the *Or* axis in the area $0 \leq r \leq R$ was equal to $\Delta_1 = R$.

The numerical solution with a computational grid step having the same order as the rod radius can be considered basic in assessing the accuracy of the calculation using information about the logarithmic law of decreasing potential along the radius in the vicinity of the rod with a step Δ having the same order as the rod length.

As can be seen from a comparison of the solid and dotted curves, the distribution calculated using the usual finite-difference representation of derivatives with a sufficiently small step of computational grid practically coincides with the distribution obtained using a grid with step in 10 times larger, in the case of finite-difference representation of the equations takes into account information about the logarithmic nature of the decrease in the potentials of the EF in the zone, which is removed from the axis of the rod by one step of the computational grid. As can be seen from Fig. 3, the calculation at the same step of the computational grid ($\Delta = H/25$) using the usual finite difference method differs significantly from the basic solution of this problem.

As shown by numerical experiments [5, 23], at $H/R \geq 2 \cdot 10^4$ and $\Delta/R \geq 800$, the calculation results, when the rod is represented as a cylinder and using information about the nonlinear decrease in the potential in the direction perpendicular to its axis, coincide within 3% with the results analytical calculations of potentials in the vicinity of electrically conductive rods—ellipsoids. With such parameters, the step of the spatial grid, which depends on the length of the rod, is so much larger than its radius that the differences in the levels of potentials and intensities near the axis of the rod fall out of the scope of consideration. At the same time, as shown by numerical experiments, in the zone more distant from the axis, the distributions of EFs calculated when the rod is represented as an ellipse and a cylinder with the indicated *H/R* practically coincide. This means that if the zone directly adjacent to the surface of the rod is not interesting in the study, they can be modeled both with the help of a cylinder and with the help of an ellipsoid, with the considered ratios of the parameters of the electrically conductive rods.

2.2 EF Distribution in the Presence of Ionized Streamer Zone Near the Top of the Lightning Leader Channel

According to the sources [25, 26], the movement of the leader lightning with negative polarity forms by steps, and in the vicinity of the top of the leader there is an ionized (so-called streamer) zone, in which the space charge is concentrated. Numerical calculation methods make it possible to take into account the presence of such a zone, as well as to evaluate its effect on the increase in the EF strength in the vicinity of grounded objects when the lightning leader approaches the ground.

It is known that an increase in the EF strength at the top of the lightning leader channel can cause the development of a counter leader from ground objects [27]. To determine under what conditions this is possible, we calculate the distribution of the EF in systems simulating the movement of the leader lightning to the ground.

For the development of the leader channels, a minimum (let's call it E_{cr}) strength of the EF is required. According to the available data, the leaders of negative polarity develop at EF strength $E_{cr-} = 10^6$ V/m, and positive polarity—$E_{cr+} = 5 \cdot 10^5$ V/m [27].

As noted in [27], the development of numerous streamers from the top of the leader lightning, when it moves to the ground, leads to the fact that the streamer zone is filled with a space charge. It was also suggested there that the EF strength in this zone is close to homogeneous, since, as follows from the measurement results, the streamer velocity is about 10^5 m/s and practically does not change along the length of the streamer zone, and this is possible in a homogeneous EF, the strength of which is close to the minimum strength at which the development of streamer channels (E_{cr}) occurs.

Representing the streamer zone as an inhomogeneously charged sphere with a uniform EF, using the Gauss theorem, we can write the expression for the charge density in it in the form:

$$\rho(r) = 2\varepsilon_0 E_{cr}/r, \tag{3}$$

where r—distance to the top of the leader channel.

The streamer zone radius R_{str} is determined from the equation

$$U_L = \frac{1}{4\pi\varepsilon_0\varepsilon} \int\limits_0^{R_{str}} \frac{4\pi r^2 \rho(r)}{r}\,\mathrm{d}r = 2E_{cr}\cdot R_{str},$$

where U_L—potential of the top of the leader channel.

Then, for a negatively charged leader channel, R_{str} has the form:

$$R_{str} = 0.5 \cdot U_L/E_{cr}. \tag{4}$$

It is known that during a thunderstorm, the EF strength near the ground is about $E_0 = 2 \cdot 10^4$ V/m. We will consider lightning of negative polarity, the most typical for all latitudes, except for equatorial ones. The condition under which it is possible to develop an ascending leader of positive polarity from lightning rods is the achievement of the critical strength E_{cr+} in the movement zone of the lightning leader channel.

It is known that in local zones, adjacent to the tops of long thin conductive rods, the EF strength significantly (by 1–2 orders of magnitude) exceeds the applied voltage E_0. Therefore, the condition for reaching the strength at the top of the lightning rod, which is necessary to start the discharge ($E_{br} = 3 \cdot 10^6$ V/m), for lightning rods with $H/R \geq 300$–500 in thunderstorm conditions is certainly fulfilled. Then we can assume that the development of an ascending leader from a lightning rod with such parameters is possible if in the zone between its top and the head of the descending leader channel there is a continuous area (path for the streamer) in which the EF strength levels exceed E_{cr+}:

$$\left|\vec{E}_z\right|/E_{cr+} \geq 1, \tag{5}$$

where $\left|\vec{E}_z\right|$—EF intensity modules in the zone connecting the tops of the lightning rod and the lightning channel.

Consider an example of using the described EF calculations to assess the possibility of developing a counter leader from lightning rods. Radius of the leader lightning channel R_L is about several millimeters, and its length H_L has order of the average cloud height in thunderstorm conditions ($H_L \sim 3$–5 km). Since H_L/R_L exceeds 10^6, we will use the method for long leading rods described in [28] for calculation.

Let's consider a system with average parameters of lightning and lightning rods: $E_0 = 2 \cdot 104$ V/m, $H_L = 4000$ m, leader channel potential in the cloud area $U_0 = 80$ MV, leader channel top potential, taking into account the voltage decrease in it due to the presence of a gradient E_L in the channel: $U_L = U_0 - E_L \cdot H_L = 40$ MV, distance from the top of the leader channel to the top of the lightning rod $h = 40$ m, lightning height $H_R = 30$ m, charged streamer zone radius $R_{str} = 20$ m. For simplicity, we will assume that the leader channel is direct. The limiting conditions used in the calculation are shown in Fig. 4b, the dimensions of the computational area: $R_{max} = 0.5 \cdot H$, $Z_{max} = H$, computational grid step $\Delta = 1.25$ m. The results of calculating the lines of equal potential and equal strength of the EF in the vicinity of the top of the leader channel and the lightning rod are shown in Fig. 4.

To simplify the calculations, it was assumed that the radii of the leader channel and the lightning rod are the same: $R = 0.01$ m. As the numerical experiments have shown, for the described calculation system, in the presence of a charged streamer zone, variation of R in the range 0.01–0.1 m does not lead to a significant change in the values of φ and $\vec{E}$ in the vicinity of the top of the lightning rod.

The performed calculations showed that with the above-described parameters of the "leader—lightning rod" system, condition (5) is satisfied when the distance
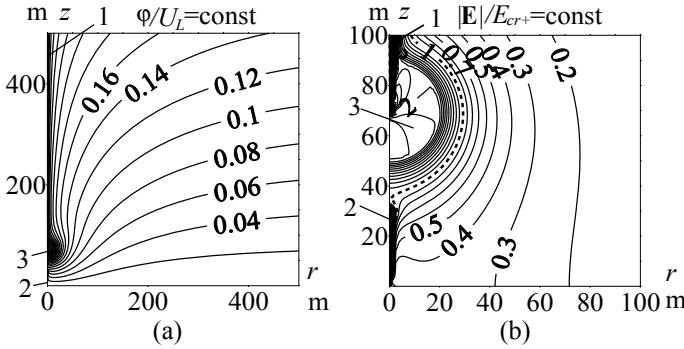
Fig. 4 Calculated distributions of lines of equal potential (**a**) and equal strength of EF (**b**) in the system simulating the approach of the lightning leader channel (1) to the lightning rod (2) in the presence of a charged streamer zone (3) ($H/R = 4 \cdot 10^5$, $R_{str} = 0.5 \cdot U_L/E_{cr} = 20$ m, $h = 2 \cdot R_{str+} = 40$ m, $E_0 = 2 \cdot 10^4$ V/m)

between the top of the lightning leader channel and the top of the lightning rod is less than

$$h \leq U_L/E_{cr-}. \tag{6}$$

In Fig. 4b, the thick dotted line shows the level $\left|\vec{E}\right|/E_{cr+} = 1$. As can be seen from this figure, $\left|\vec{E}\right|$ over the entire gap between the tops of the lightning rod and the lightning channel is greater than or equal to E_{cr+}. To determine, if condition (5) is always performed, numerical experiments were carried out for other values of the parameters of the lightning leader channel. Thus, the case of a relatively high EF intensity in a pre-thunderstorm situation was considered: $U_0 = 200$ MV, $U_L = 150$ MV, $R_{str} = 75$ m. EF calculations were also carried out at relatively low EF strength values: $U_0 = 60$ MV, $U_L = 30$ MV, $R_{str} = 15$ m. These calculations showed that the fulfillment of condition (5) is sufficient for the presence of an area between the tops of the leader channel and the lightning rod from $\left|\vec{E}\right|/E_{cr+} \geq 1$. Moreover, in this area, the EF levels do not change significantly during varying the height of the lightning rod H_R in the range 20–50 m.

3 Statistical Model of Electrophysical Processes During a Lightning Strike into Ground Objects

At present time the protection zones of lightning rods are determined in accordance with regulatory documents. However, the practical application of such standards for the choice of lightning protection means for extended objects is difficult. Damage

from a lightning strike to some facilities, such as launch complexes or storage tanks for petroleum products, can lead to significant material costs and even technological disasters [29–33]. Physical modeling of electromagnetic processes accompanying a lightning strike is quite expensive and, moreover, does not provide a complete representation of the phenomena occurring during a lightning strike. This necessitates the development of mathematical models of the processes accompanying the movement of the lightning leader channel and makes it possible to evaluate the reliability of the chosen lightning protection means.

One of the most common methods for assessing protected areas is the so-called electrogeometric method [34–36]. In this case, it is considered that the lightning rod zone lies inside the area, the outer boundary of which is formed by a "rolling sphere" with a radius $R_{last\ stroke} = 30$ m (last stroke is the average distance from which the "selection" of the strike place by lightning begins). Despite the clarity, this approach is a simplified representation of the lightning protection process, which does not take into account such important characteristics as, for example, the scattering of $R_{last\ stroke}$ values. At the same time, more complex models for predicting the processes of lightning movement to the ground [27], as a rule, are very far from solving the problems of practical lightning protection.

To simulate the statistical process of movement of the lightning leader channel in relation to the evaluation of the effectiveness of the developed lightning protection systems, the approach described in [37] can be used.

The model described in [37] is based on a generalization of experimental studies of pulsed high-voltage discharges in long gaps "rod-plane" and lightning [38–40]. At developing model, it was taken into account that the last stage of the movement of the lightning leader channel when it is oriented to a ground object (the so-called "last stroke" stage) begins when the streamed zone of the descending lightning leader channel reaches it. It is believed that the last hit is the process of moving the leader channel through the streamer zone. At the same time, it was taken into account that the magnitudes of the speed and acceleration of lightning depend on its potential, as well as on the angle between the velocity vectors of its movement and the EF strength in the surrounding space.

The model took into account that the corresponding grounded area can be struck by lightning in the considered numerical experiment if at least one of the two conditions described below is carried out. The first condition is to reduce the resistivity of one of the streamer channels to a level close to the resistivity of the lightning leader channel. The second condition assumes that one of the competing spark channels moving in the streamer zone of the lightning leader channel reaches the considered grounded area.

To describe the process of "selection" by the lightning leader of the strike place on the ground, a principle similar to the "Least Time—Maximum Probability" was used. It is believed that the probability of a lightning strike into a grounded area is inversely proportional to the time it takes the lightning leader channel to reach it at the final stage of its movement.

A rectangular computational grid (let's call it "grid 1") is overlapped on the area of the studied object. A rectangular computational grid (let's call it "grid 2") is also

overlapped on the area above the object, from where the development of leader lightning can occur. Moreover, the area of grid 2 significantly exceeds the area of the studied object, since it corresponds to the zone from which lightning can strike this object. When the model is running, the probabilities of a lightning strike into each cell of grid 1 from each cell of grid 2 are calculated. This takes into account the probability of occurrence of lightning carrying various potentials into the ground.

Comparison of the calculated and normalized ratios between the predicted number of lightning breakthroughs to the lightning rod and protected objects showed their coincidence within 10%.

Let's consider the use of this model to select a lightning protection system for a storage tank for petroleum products, which is a cylinder with a radius of 39 m and a height of 34 m. Using the developed model, several options for lightning protection systems for this object were considered.

At determining the probability of being struck by lightning, the N-predicted number of direct lightning strikes per year into an object with an area S_0 was used for a given geographical area:

$$N \approx N_m \cdot S_0, \tag{7}$$

where N_m—average number of lightning strikes per year per 1 km^2 in a given geographical area; S_0—object area.

Calculations were made for the case when annual average density of lightning strikes per square kilometer was equal to $N_m = 1$.

Figure 5 shows the calculated distribution of the predicted number of lightning strikes per year in a storage tank for petroleum products for the case of the absence of lightning protection facilities. At the same time, the total predicted number of lightning strikes on this object is such that lightning can hit it once every 6 years. The uneven distribution of the number of breakdowns along the outer tops of the tank is caused by the discreteness of the problem of nodes into which lightning strikes are calculated, and also due to the use of a rectangular computational grid relative to a cylindrical object.

Figures 6 and 7 show the calculated distributions of the predicted number of lightning strikes per year into the studied object in the presence of 1, 2 and 4 lightning rods, respectively, with 90 m height. In this case, the total predicted number of lightning strikes into this object is such that lightning can get into it once in 8, 11 and 19 years, respectively.

If, for safety reasons, it is still necessary to reduce the total predicted number of lightning strikes into the studied object, wire lightning rods can be used. The calculated distribution of the lightning strike probability in this case is shown in Fig. 7b (the height of the cables is 50 m). With such an arrangement of wire lightning rods, the predicted number of lightning breakthroughs to a given object is not higher than one per 100 years. Moreover, as shown by the computer simulation (Fig. 8), the use of 14 lightning rods with 90 m height, located in the same way as for the case shown in Fig. 7b, gives the predicted number of lightning breakthroughs to this object once every 43 years.
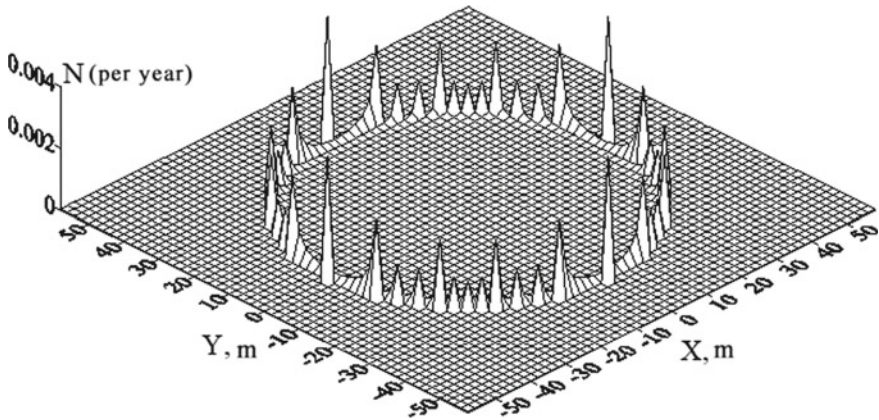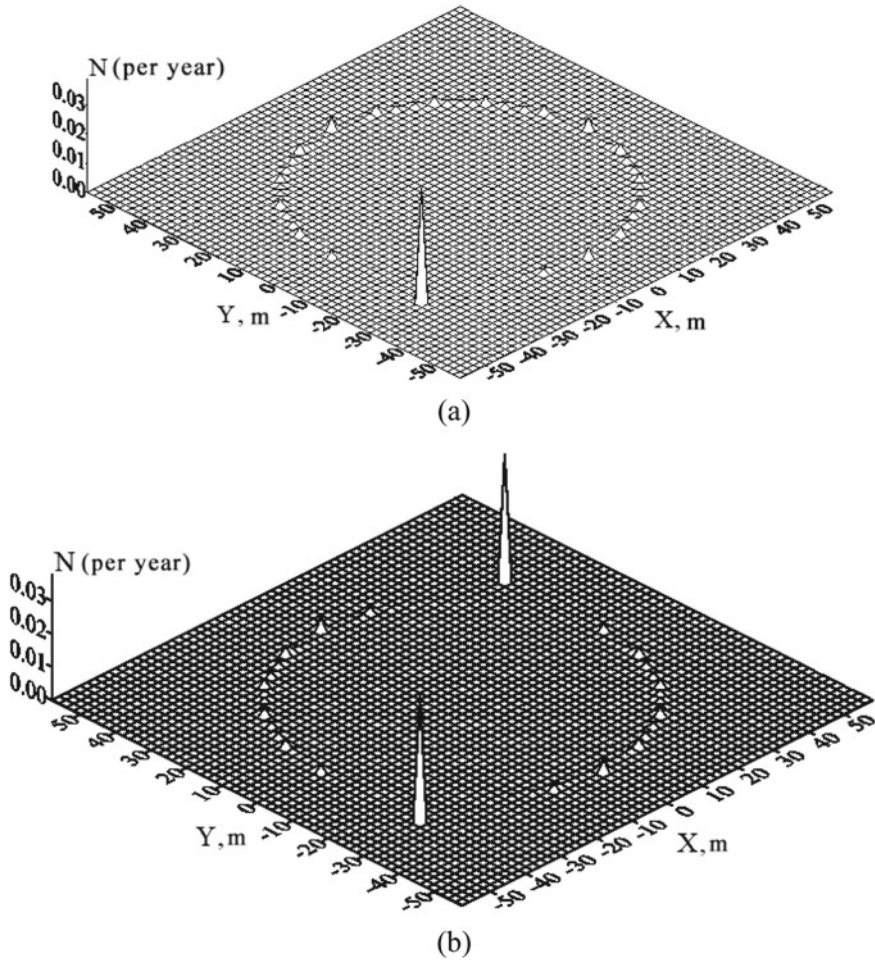
Fig. 5 Calculated distribution of the number of lightning strikes into the considered petroleum tank

The computer simulation of the processes accompanying the movement of the lightning leader channel at the last stage before the "selection" of the impact place of a grounded object made it possible to determine the predicted number of strikes of lightning rods and a non-standard protected object (tanks with oil products), to assess the degree of impact of the used lightning rods, and also to show that the use of wire lightning rods of the selected configuration makes it possible to practically eliminating lightning strikes into the studied object during the entire period of its operation.

As noted above, due to the complexity of the experimental study of the processes associated with the "choice" of the lightning leader channel of the strike place on the ground, a large number of mathematical models have been developed that describe these processes [41–43].

The most famous of them, quite simple and illustrative (the so-called electrogeometric method and the rolling sphere model) form the basis for the normalization of lightning rod zones, for example, in the USA [44]. These methods indirectly imply the presence of an ascending leader channel from ground objects.

However, targeted research related to the physical and mathematical modeling of ascending discharges from objects on the ground is not enough. As shown in a number of publications [4, 27, 45, 46], the discharge channels that develop from grounded objects in a thunderstorm situation play a significant role in orienting the lightning leader channel to ground objects. Thus, in France and Spain, there are regulatory documents that provide for testing the so-called active lightning rods, the principle of operation of which is supposedly based on the generation of counter leaders. However, the tests specified in these documents do not allow to fully take into account the electrophysical processes that accompany the emergence and movement of ascending leaders, and to evaluate the advantages and disadvantages of various lightning rods in a thunderstorm environment.
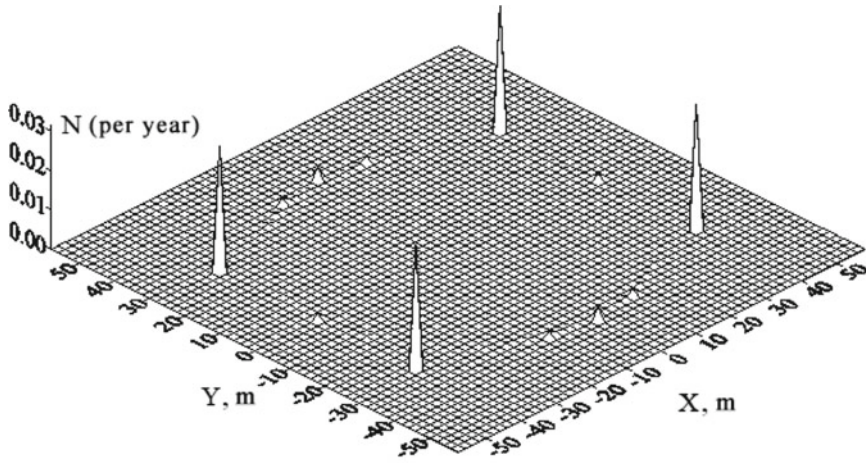
Fig. 6 Calculated distribution of the number of lightning strikes in the system: **a** tank—lightning rod with height 90 m; **b** tank—2 lightning rods with 90 m height

3.1 Statistical Modeling of the "Selection" of the Strike Place by Lightning

During statistically modeling the place of a lightning strike, it is necessary to carry out a number of mathematical experiments and vary all possible zones from which lightning leader channels can develop. In this case, one should take into account the distribution of lightning current values, determined by the levels of its potential, and the height at which its orientation to ground objects begins.
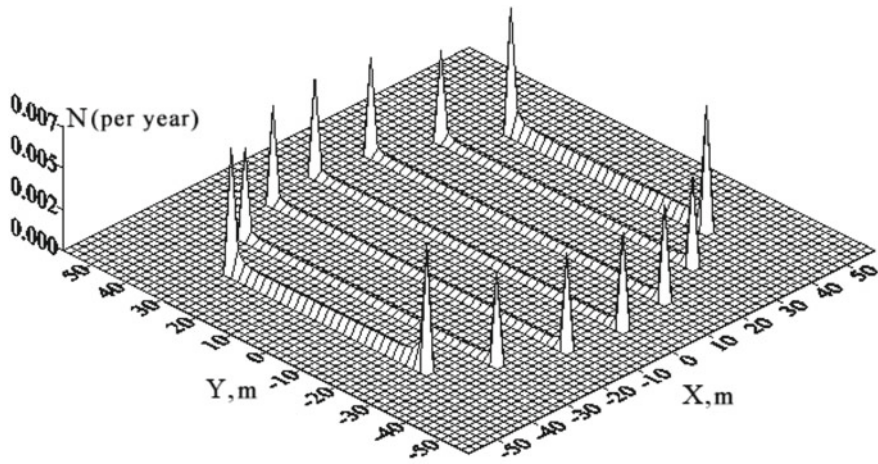
Fig. 7 Calculated distribution of the number of lightning strikes in the system: **a** tank—4 lightning rods with height 90 m; **b** tank—7 wire lightning rods

The value of the maximum reverse stroke current at the main stage of lightning I_m can be measured, and therefore there are systematic experimental data on the probability distribution of the lightning occurrence with a certain value of the discharge current [47–49].

In [50], it is indicated that the height of lightning orientation to ground objects (l_s) is determined based on the condition for reaching the "critical EF" E_{cr}, which is necessary for the breakdown of the gap. It is also noted there that E_{cr} must be greater than or equal to $0.5 \cdot 10^6$ V/m for negative leaders and $0.3 \cdot 10^6$ V/m for positive ones.
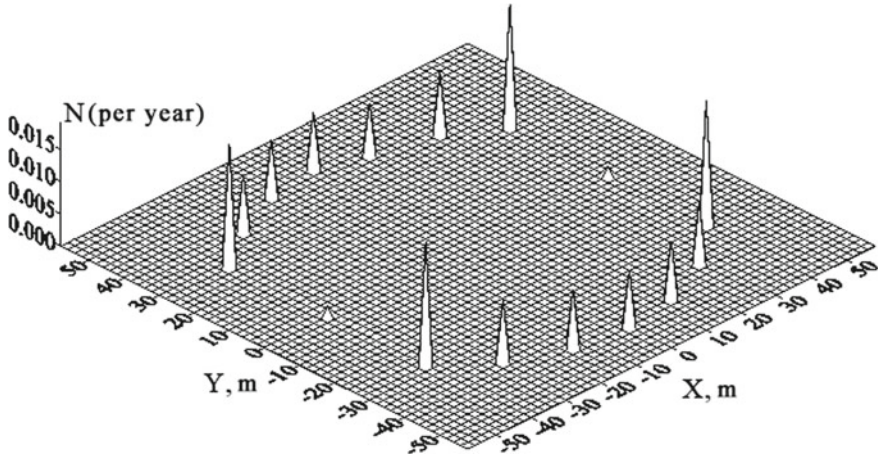
Fig. 8 Calculated distribution of the number of lightning strikes in the system "tank—14 lightning rods with height 90 m"

The value of E_{cr} is defined as being between the intensity of the EF required for the development of negative streamers E_{st-} and positive streamers E_{st+}. However, the EF intensity required for the development of a negative streamer is considered to be equal to E_{st-}.

The relationship between I_m and l_s is presented as:

$$l_S = a \cdot I_m^b, \tag{8}$$

where a, b—coefficients; l_s value measured in [m]; I_m value measured in [kA].

The values of the coefficients in Eq. (8) in different sources are considered equal: a—from 1.9 to 10, b—from 0.65 to 0.9.

At modeling the process of choosing the strike place by the lightning leader channel, its potential U_m is an important parameter. The U_m value is proportional to I_m, and there is a connection between I_m and U_m: $U_m \approx k_U \cdot I_m \cdot Z$ ($k_U \sim 1.7$, $Z \sim 500\ \Omega$). Then, assuming that $l_S = U_m/E_{st-}$, we get:

$$l_S \sim 0.8 \cdot I_m. \tag{9}$$

A similar approach for determining distances, from which the orientation of negative lightning leaders begins, describes as:

$$l_S = 1.9\, I_m^{0.9}, \tag{10}$$

although the intensity of the EF in the interval "leader—ground" is considered equal to E_{st+}.
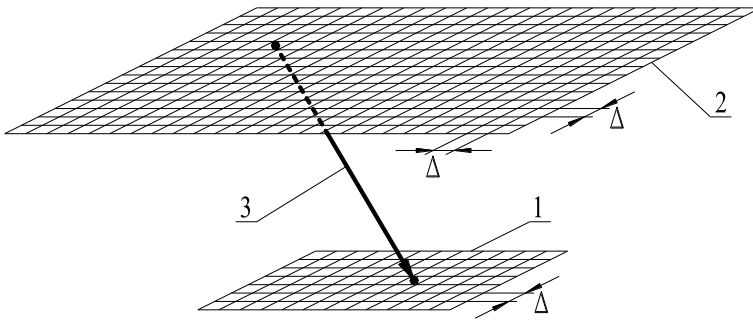
Fig. 9 Calculation system: 1—"area on the ground", 2— "thundercloud", 3—leader channel of lightning

For taking into account all possible options for a lightning strike into the study area ("area on the ground", Fig. 9), we divide its area (S_G) with a square grid with a step Δ. As a result, we get K_G cells with area $S_{Gk} = S_G/K_G = \Delta^2$.

We will assume that the probability of cell destruction is inversely proportional to the time of movement of the lightning leader channel to the corresponding node. Since lightning can strike the "area on the ground" from a larger area above it ("thundercloud", Fig. 9), to simulate all possible starting points for descending lightning leaders, we increase S_G by M cells, resulting in K_S cells and the corresponding them nodes ($K_S > K_G$). We assume that the probability of a lightning strike is the same within the k-th cell of the computational grid and is proportional to its area S_{Gk}.

In [51], based on the analysis of experimental data, it was shown that the root mean square (RMS) deviation of the breakdown voltage dispersion for discharge gaps 2–30 m long weakly depends on their length (6–7%). It is also noted there that the factors influencing the occurrence of the scattering can be variations in the moment of the emergence of the leader, the rate of its development, the length of the streamers, and the intensity in the leader and streamer zones. Based on these data, it is assumed that the relative dispersion of the discharge development times is $\varepsilon_S = 0.07$. We assume that a lightning discharge of a given potential U_i from the j-th node of the "thundercloud" can occur only in those nodes of the "area on the ground", the duration of the movement of the leader channel to which does not exceed more than ($1 + \varepsilon_S$) times the minimum time of movement of competing discharge channels to all cells of the "area on the ground" in this numerical experiment: $t_{k,j}^i \leq (1 + \varepsilon_S) \cdot t_{j\min}^i$, where $t_j^i = \min\{t_{k,j}^i\}$. The defeat of all other cells in this numerical experiment will be considered impossible, and the probability of these events for these cells is considered equal to zero. Here, the nodes of the "area on the ground" into which a lightning breakthrough can occur have the k index; the total number of such nodes for a given numerical experiment which simulating a lightning strike with potential U_i from node j can be K_j^i.

Considering that in this numerical experiment there can be only one lightning strike, we will consider under $P_{k,j}^i$ probability density of a lightning breakthrough

into the k-th node of the "area on the ground" part of the lightning strikes into it from all possible cells "thundercloud" in this numerical experiment. We will proceed from the assumption that the value $P_{k,j}^i$ is inversely proportional to the propagation time to the k-th node on the ground of the lightning leader $P_{k,j}^i \sim 1/t_{k,j}^i$ and depends on the number and area of cells, the defeat probability of which in this numerical experiment is different from zero. For example, if the calculation indicated that the periods of movement of the leader lightning to each of the K_j^i nodes are the same, then the probability densities of the defeat of each of these nodes are the same.

Let us normalize the coefficient proportional to the probability of a lightning breakthrough into a node ($K P_{k,j}^i$) so that it is equal to 1 for the nodes, the movement time to which is minimal ($t_{j\min}^i$), in this numerical experiment, and for nodes, the time of movement to which is more than $(1 + \varepsilon_S)$ times greater than $t_{j\min}^i$ it was equal to zero:

$$K P_{k,j}^i = 1 - \frac{1/t_{j\min}^i - 1/t_{k,j}^i}{1/t_{j\min}^i - 1/[t_{j\min}^i \cdot (1+\varepsilon_S)]} = 1 - \frac{1+\varepsilon_S}{\varepsilon_S} \cdot \frac{1/t_{j\min}^i - 1/t_{k,j}^i}{1/t_{j\min}^i}. \tag{11}$$

In order to take into account the dependence of the probability of a lightning strike on the "area on the ground" node on the total number and area of cells that can be struck in this numerical experiment, we write $P_{k,j}^i$ as:

$$P_{k,j}^i = K P_{k,j}^i \cdot K_j. \tag{12}$$

The coefficient K_j is obtained from the condition of equality of the hitting probability one of the K_G nodes of the "area on the ground" in this numerical experiment:

$$\sum_{k=1}^{K_G} P_{k,j}^i = K_j \cdot \sum_{k=1}^{K_G} K P_{k,j}^i = 1.$$

Then

$$K_j = 1/\sum_{k=1}^{K_G} K P_{k,j}^i. \tag{13}$$

Let, for example, calculations show that when lightning moves from the j-th node of the "thundercloud", the duration of movement to two nodes of the "area on the ground" is significantly (by an order of magnitude or more) less than for all other nodes (for example, the coordinates of these nodes) correspond to the coordinates of the lightning rods), and,

$$t_{k1,j}^i = t_{j\min}^i,$$

$$t^i_{k2,j} = (1/0.95) \cdot t^i_{k1,j} = 1.0526 \cdot t^i_{k1,j}.$$

Then from (11) we get: $KP^i_{k1,j} = 1$, $KP^i_{k2,j} = 0.236$. Substituting these values into (13), we get:

$$K_j = 1/\sum_{k=1}^{2} KP^i_{kjj} \approx 0.81$$

Let's finally calculate the probability of being struck by lightning for each lightning rod in this numerical experiment, substituting the obtained values into (12):

$$P^i_{k1,j} = KP^i_{k1,j} \cdot K_j \approx 0.81 \cdot P^i_{k2,j} \approx 0.19.$$

Thus, the total probability of this event is 1:

$$P^i_{k1,j} + P^i_{k2,j} = 0.81 + 0.19.$$

Knowing P_i the probability of occurrence of lightning with a current less than I_i, summing up all $P^i_{k,j}$ from lightning strikes with amplitudes I_i, whose leaders beginning from the j-th cells of the "thundercloud", we obtain an expression for the predicted number of lightning strikes in k-th node of the "area on the ground" in the form:

$$N_k = 10^{-6} \cdot N_m \cdot \sum_{i=1}^{M} \left\{ (P_{i+1} - P_i) \cdot \sum_{j=1}^{J} \left[\Delta^2 \cdot P^i_{k,j} \right] \right\}, \qquad (14)$$

where M—number of intervals into which the range of lightning current variation is divided, and $\sum_{i=1}^{M} (P_{i+1} - P_i) = 1$; N_m—average annual number of lightning strikes per 1 km^2 of the earth's surface in a given geographical area; Δ^2—cell square, [m^2].

The time of movement of the descending leader channel from the j-th node of the "thundercloud" to the k-th node of the "area on the ground" is calculated as follows:

$$t^i_{k,j} = \left(L_{k,j} - l^i_S \right)/v^i_{0L\downarrow} + l^i_S/\left(v^i_{L\downarrow} + v^i_{L\uparrow} \right), \qquad (15)$$

where $L_{k,j}$—distance between the k-th node of the "area on the ground" and the j-th node of the "thundercloud" at the beginning of the process of movement of the lightning leader channel from it; l^i_S—lightning orientation height with potential U_i, the leader channel of which moves from the j-th node of the "thundercloud"; $v^i_{0L\downarrow}$, $v^i_{L\downarrow}$—respectively, the speed of the descending leader channels of lightning with the potential U_i before and after the beginning of the through phase; $v^i_{S\uparrow}$—speed of the rising spark from ground objects for lightning with the potential U_i.

In the case when the conditions for the emergence and development of an ascending leader are not fulfilled, the value $v_{S\uparrow}^{i}$ in (14) is considered equal to zero.

## 3.2 Comparison of Experimental and Calculated Data on the Place of Discharge in Long Air Gaps

To compare the results of calculating the probabilistic places of damage by a high-voltage discharge in the presence and absence of a counter spark from grounded objects, let's consider the systems described in [27]. Despite the part these were carried out based on data obtained more than 70 years ago, they still have influence, if only because they form the basis of the regulatory document [52], which still regulates lightning rod zones. Almost all experiments, the results of which are given in [27], were carried out with a positive polarity voltage applied to a high-voltage electrode simulating the lightning leader channel. To substantiate this approach, [27] provides comparative data on breakdown points when a pulsed voltage of positive and negative polarity is applied to a high-voltage electrode for the same system parameters. In these experiments (the scheme is shown in Fig. 10a), a high-voltage rod electrode (1) was located above a grounded plane (2) at a distance $L = 1.6$ m from it and from grounded objects simulating a lightning rod (3), and protected object (4).

As follows from the experiments, when a voltage of positive polarity is applied to high-voltage electrode 1, approximately $N_2 = 0.80$ of all discharges hits the plane: $\sum N_2 \approx \approx 0.80$, for electrode 3—$N_3 \approx 0.08$ and for electrode 4—$N_4 \approx 0.12$ (where N_2, $\sum N_2$—particles of high-voltage discharges entering a separate cell on a grounded plane and all cells on a grounded plane, respectively; N_3, N_4—particles of high-voltage discharges entering the 3rd and 4th grounded electrodes. At determining $\sum N_2$, all probable breakdowns in all cells of the plane were summed up, therefore, despite the fact that N in Fig. 10a for individual cells of the plane is less than for rod lightning rods, the total share of predicted breakdowns in the plane is much larger ($\sum N_2 > N_3$, $\sum N_2 > N_4$). Mathematical modeling with using the method described above gave the following results: for the plane—$\sum N_2 = 0.76$, for electrode 3—$N_3 = 0.10$, for electrode 4—$N_4 = 0.14$ (Fig. 10a).

With this simulation, it was assumed that a counter spark from grounded objects would not develop, since the development of a spark of negative polarity requires an EF intensity that significantly (up to 2 times) exceeds the intensity in the streamer channel of the positive polarity descending leader.

It follows from the experiments that when a voltage of negative polarity is applied to the high-voltage electrode, when a counter spark can develop from object 3, approximately $N_3 \approx 0.85$ discharges strike electrode 3 and $\sum N_2 \approx 0.15$—the plane. Mathematical modeling using the technique described above gave the following results: for electrode 3—$N_3 = 0.84$, for the grounded plane (2)—$\sum N_2 = 0.16$ (Fig. 10b).

Fig. 10 Calculated distributions of the predicted distribution of the number of hits of downward discharges into objects (3, 4) located on the ground (2) when voltage is applied to the high-voltage electrode (1): **a** positive polarity; **b** negative polarity
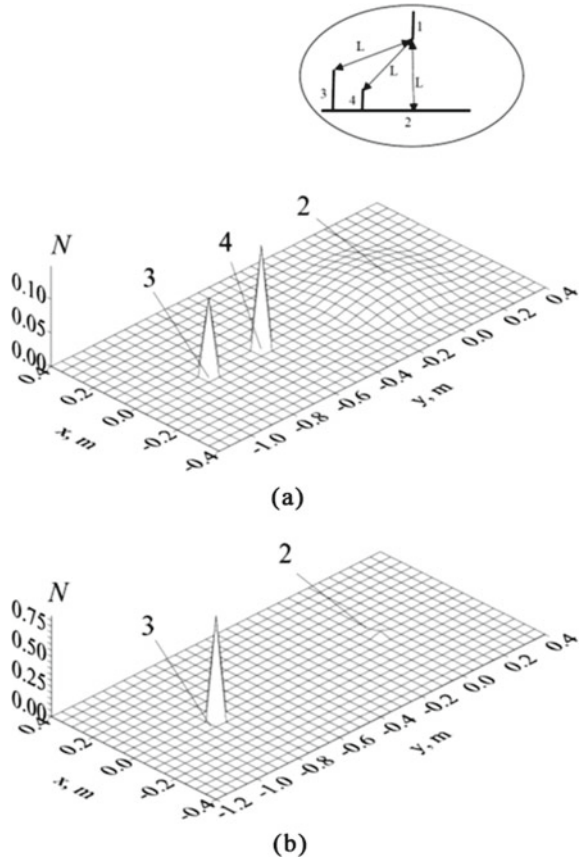
During modeling, it was considered that a positive voltage $U = +0.7$ MV or a negative voltage $U = -1.4$ MV was applied to electrode 1. The speed of the streamers was set equal to 10^6 m/s, the capacitance per unit length of the leader in the through phase was 10 pF/m. The speed of positive descending leaders by the beginning of the through phase was considered equal to $v^i_{0L\downarrow} = 10^6$ m/s, the speed of negative descending leaders $v^i_{0L\downarrow} = 1.5 \cdot 10^5$ m/s, the speed of positive ascending leaders $v^i_{S\uparrow} = 0.3 \cdot 10^5$ m/s. In this case, the current in the through phase in the calculations was equal to 7 A when a voltage of positive polarity was applied, and 14 A when a voltage of negative polarity was applied.

Thus, the use of the described model made it possible to calculate the probability of a breakdown place when pulses of positive and negative polarity are applied to the gap "high-voltage rod—two rods on a grounded plane". Simulation and experiment data [27] coincide within 5–25%.

4 Study of Corona Processes at the Tops of Grounded Rods Simulating Protected Objects and Lightning Rods

The occurrence of corona discharges on the elements of electrical systems leads to a number of negative consequences. The most significant of these consequences is the loss of electricity. Another consequence is the appearance of high-frequency electromagnetic interference. High-frequency components of current, voltage and electromagnetic field, appearing through a corona discharge, have a negative impact on the operation of sensitive digital and electronic equipment, including automation and control systems. The most common corona processes are on the overhead power lines, so many works are devoted to this problem, for example, [22, 23, 53–55]. There are technical means to solve it, for example, [56–58]. At the same time, corona processes on sharp tops (systems of the "plane-point" type) are studied mainly with respect to an ozonizer [59–61]. Experimental studies of corona discharges were carried out mainly in systems with a "point-plane" geometry, with electrode-needles, to which EF of constant voltage of both polarities is applied. Usually, the EF intensity around electric power facilities is sufficient to create corona discharges around the most geometrically pointed elements of structures and equipment, for example, insulators, fittings, switches, high-voltage bushings, etc. The corona that develops around such elements may be caused by EF of direct current (DC) (positive or negative), such as resulting from a thunderstorm, or may be due to high alternating current (AC) voltage in the power system. The theory of corona processes is quite complex and has been repeatedly described in the literature, for example [62–66]. Thus, a corona discharge can be considered as consisting of two components:

- diffuse form of a gas discharge, which is often called a "luminous corona" (stationary component);
- incomplete plasma channels, which is often called "streamer corona" (impulse corona).

The first component can be easily measured with a microammeter, while the second component is measured with an oscilloscope and an impulse counter. Experimental studies of the dependence of the corona current on the applied EF and the geometry of the rod electrodes are described, for example, in [22, 64]. However, the conditions for corona initiation were not considered in these works.

5 Physical Modeling of Electromagnetic Processes During the Development of the Corona on Rod Electrodes with Different Vertices

5.1 Method for Measuring Corona Current

For physical modeling of the corona formation processes at the tops of grounded rod electrodes, a stand was used, the scheme and photographs of which are shown in Fig. 11. The experiments were carried out under conditions of normal temperature and atmospheric pressure (temperature $T = 20...23$ °C, atmospheric pressure $p = 1$ atm).

This stand contains potential 1 and grounded surfaces 2 with dimensions 4 m × 4 m and located at a distance $d = 2.1$ m from each other, as well as a rod 3 installed on a grounded surface with height h and a vertex in the form of a sphere with radius R (Fig. 11). A high voltage U_0 was applied to potential surface 1, as a result of which an EF appeared in the zone between surfaces 1 and 2, which had an average intensity $E_0 \approx U_0/d$. To measure the corona current, a circuit was used that makes it possible to measure the number of pulses of the corona current in a time of 10 ms, equal to the duration of the half-cycle of the power frequency voltage.

A voltage proportional to the corona current flowing into the ground was taken from a low-inductance resistor $R_S = 75$ Ω. This voltage was applied with the help of measuring cable 4 to a high-frequency amplifier (HFA) 5 and a Rigol DS 1204B four-channel oscilloscope (Fig. 11b). At the opposite end, a low-inductance resistor $R_T = 25$ Ω was used to prevent reflection of pulses from the end of the cable. The equivalent input impedance of the measuring system was 37.5 Ω. The amplified signal triggered the generator of rectangular pulses 6. As a result, a sequence of rectangular pulses was formed, each of which corresponded to its own impulse of the corona current, and which was fed to the output of the pulse counter 9. Starting pulses of the beginning and end of the countdown of the counter were formed using a rectangular pulse generator 8 connected to 220 V (50 Hz) network through a phase shifter 7. Thus, by changing the phase of the mains voltage, the positions of the beginning and end of the pulse count were measured.

To ensure broadband registration of corona discharge pulses, the base of the ground electrode consisted of a short metal tube with a coaxial cable inside, as shown in Fig. 11b.

To provide a total resistance of 75 Ω, equal to the characteristic impedance of the cable, 6 low inductance resistors were connected in parallel at the top of the cable. The average corona current pulses were integrated and the resulting values were multiplied by the average pulse repetition frequency.

The DC component of the corona current was measured using an electromagnetic system microammeter (M266M) connected in series between the electrode rod and the grounded surface.
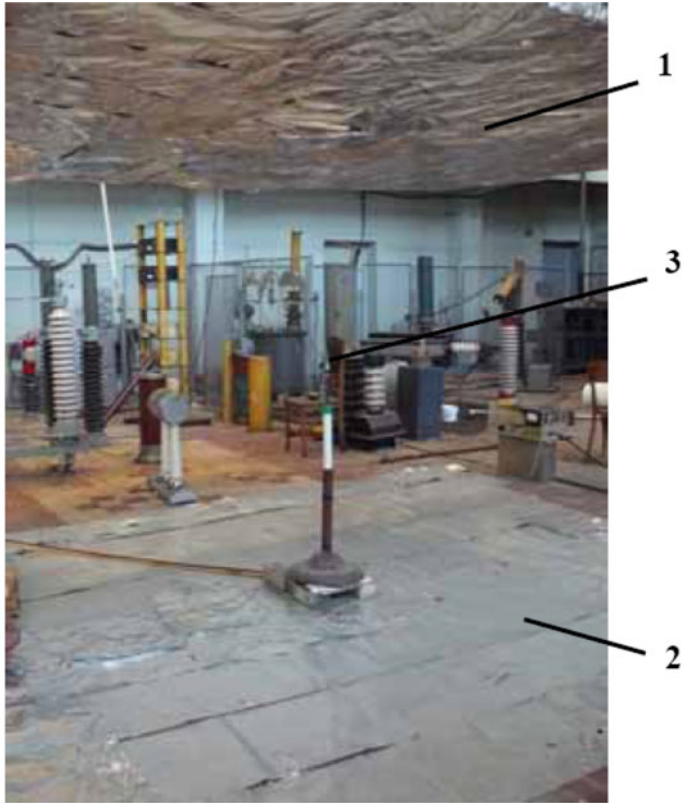
(a)
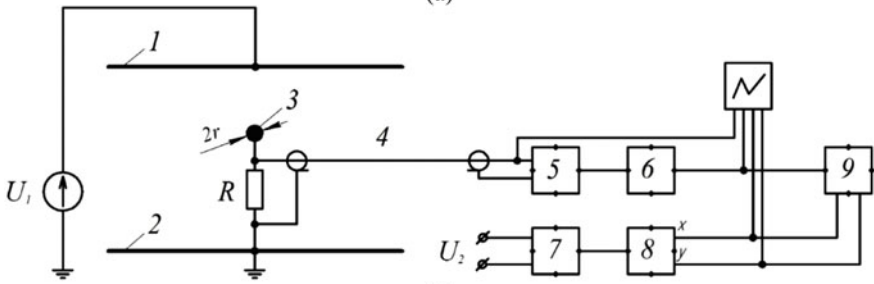
(b)

Fig. 11 Experimental stand for registration of corona current pulses: **a** appearance, **b** scheme of the stand (U_1—high voltage source (HV); 1, 2—potential and grounded electrodes-planes; 3—grounded rod electrode; R_S—shunt resistor ($R_S = 75\ \Omega$); 4—measuring cable; 5—high-frequency amplifier (U3-33); 6, 8—pulse generators (G5-54); 7—phase shifter; 9—frequency meter (F5034) in pulse counting mode)

5.2 Dependence of the Corona Current on the EF Nature

Corona current measurements were made for three cases, namely:

- I—a constant voltage of positive polarity was applied to the potential surface (maximum value—170 kV);
- II—a constant voltage of negative polarity was applied to the potential surface (the maximum value—170 kV);
- III—an alternating voltage of industrial frequency with an effective value of up to 100 kV was applied to the potential surface.

Figure 12 shows corona current oscillograms obtained from the ground electrode tip for three cases. The height of the grounded electrode *h* for all cases was equal to 1.2 m. The rod used in these tests had a conical top 0.14 m long, a base diameter of 0.04 m, and a radius of curvature at the end of the order of 0.1 mm.

For the first case (Fig. 12a), aperiodic corona current pulses were obtained, the average amplitude and duration at half height of which were practically independent of the applied voltage and amounted to about 2.27 mA and 28 ns, respectively.

(a)   (b)

(c)   (d)
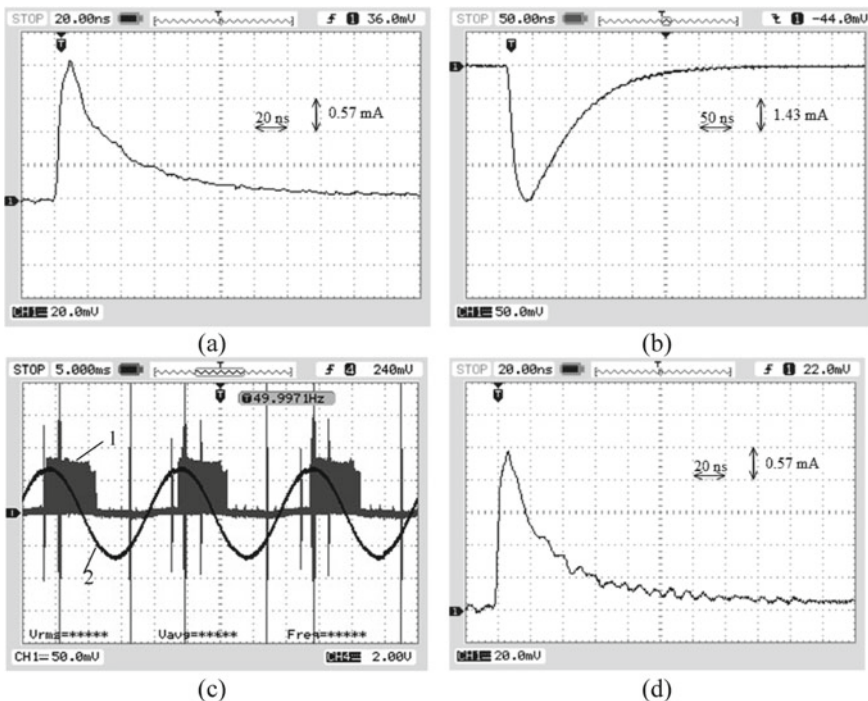
Fig. 12 Oscillograms of the corona current when a voltage of positive **a** and negative **b** polarity is applied to the potential surface, as well as an alternating voltage with frequency of 50 Hz **c**, **d** (on the oscillogram c: 1—corona current, 2—voltage applied between potential and grounded surfaces)

The average charge carried by the pulse was about 0.1 nC. The pulse transmission frequency increased in proportion to the applied voltage and, when a voltage of 50 kV was applied to the potential plane, was 3.18 kHz. The average corona current pulse was 0.3 mA. The constant component of the corona current, measured with a microammeter, was about 2.6 mA. Therefore, the corona current impulse was about 10% of the average DC current.

In case II (Fig. 12b), corona current pulses were observed only in a narrow range of applied voltages, i.e. from 30 to 40 kV. However, the average amplitude and duration at half height of these pulses were significantly higher than in case I (5.72 mA and 85 ns, respectively) On the other hand, the pulse repetition frequency was much lower—about 100 Hz. The average charge carried by the pulse was about 2 nC. The average pulsed corona current was approximately 0.2 mA, which is about 20% of the corona stationary current measured with a microammeter.

In case III (Fig. 12c, d), groups of corona current pulses appeared near the peaks of the positive half-cycle of the applied sinusoidal voltage, but they are almost absent at negative peak cycles. The positive half-cycle of the corona current pulse is very similar to that obtained in case I (application of a positive DC high voltage). When a high AC voltage of 50 kV RMS was applied to the potential area, the measured corona current was 2.85 mA with with a half-height duration of 30 ns It has been established that averaged charge, transported with pulse, was 0.1 nC. The pulse passing frequency at an RMS voltage level of 50 kV was significantly higher than in the previous two cases and was about 28.7 kHz. The average component of the corona current in this case was about 2.7 mA.

5.3 Dependence of the Corona Current on the Rod Geometry

The dependence of the corona current on the geometry of the rod was estimated using grounded rods with 6 different end radii R of rounding of spherical tops, namely: 0.0055, 0.00775, 0.009, and 0.0125 m, 0.01 at 4 values of their height h, namely: 1.2, 1.15, 1.05, and 0.93 m. A DC voltage U_0 of negative polarity up to 170 kV was applied to the potential surface, and the DC component of the corona current I_{cor} was measured. Table 1 presents the measurement results.

Figure 13 shows the dependence of the measured average value of the DC component of the corona current I_{cor} on the level of the applied DC voltage of negative polarity U_0 at the height of the grounded electrodes $h = 1.2$ m. Figure 14 shows the measured I_{cor} values at the same voltage as before, but with a fixed support radius $R = 0.009$ m and different rod heights. Measurements were also made for the case of the top of a grounded electrode with a height $h = 1.2$ m, made in the form of a cone with a height 0.14 m, a base diameter 0.04 m, and a top rounding radius of about 0.1 mm. However, all three voltage options (I, II and III) mentioned earlier were used for this configuration.

Figure 15 shows the measured dependences of I_{cor} on U_0—the module of the applied DC voltage of positive and negative polarity, for the case of a grounded

Table 1 Measured average values of the DC component of the corona current I_{cor} [mA] when a voltage of negative polarity is applied to the potential surface

U_0, kV	R, m	h, m			
		1.2	1.15	1.05	0.93
90	0.0055	2.5	2	–	–
100		4	4	2	–
110		8	7	4	2
120		13	11	7	4
130		20	17	12	8
140		30	26	18	14
150		42	38	27	20
160		61	54	40	30
170		85	74	56	42
110	0.00775	4	3	–	–
120		9	7	4	–
130		14	13	8	4
140		24	21	15	9
150		36	33	25	16
160		54	49	37	25
170		84	70	54	37
120	0.009	6	4	3	1.7
130		10	9	5	2
140		20	17	10	5
150		32.5	27	19	10
160		49	44	31	18
170		80	66	48	29
120	0.0125	2	1.3	–	–
130		5.5	3.5	–	–
140		13.5	11	5	–
150		24	20.5	13	5
160		36	33	22	12
170		55	50	36	21
140	0.015	8	4.5	–	–
150		19	14	6	–
160		33	27	15	7.5
170		53	40	30	16
150	0.019	5	–	–	–
160		21	13	2	–
170		43	33	15	0.3

Fig. 13 Experimentally obtained dependences of the corona current (I_{cor}) on the modulus of the applied constant voltage of negative polarity (U_0) at different R radii of tops' curvature (electrode height $h = 1.2$ m): 1—0.0055 m; 2—0.00775 m; 3—0.009 m; 4—0.0125 m; 5—0.015 m; 6—0.019 m
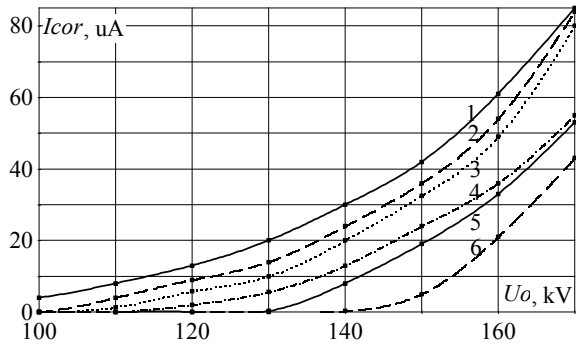
Fig. 14 Experimentally obtained dependences of the corona current (I_{cor}) on the module of the applied constant voltage of negative polarity (U_0) at different electrode heights (top rounding radius $R = 0.009$ m): 1—1.2 m; 2—1.15 m; 3—1.05 m; 4—0.93 m
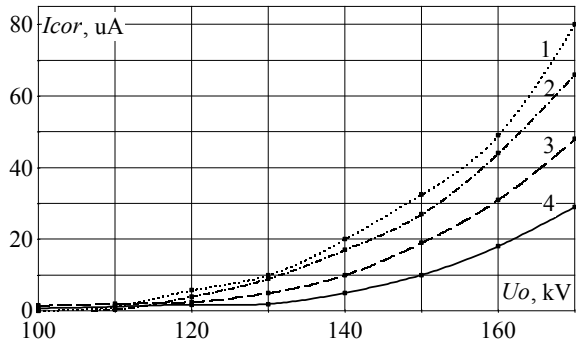
electrode with a height $h = 1.2$ m and a cone-shaped apex. Curve 1 corresponds to the case of applying a constant positive voltage to the potential plane, curve 2 corresponds to the negative polarity. As can be seen from Fig. 15, when a positive polarity EF is applied, the corona current is greater than when a negative polarity EF is used. However, the relative differences between the measured I_{cor} levels for these two cases do not exceed 20%.

Fig. 15 Experimentally obtained dependences of I_{cor} on the level U_0—the module of the applied direct voltage of positive (curve 1) and negative (curve 2) polarity
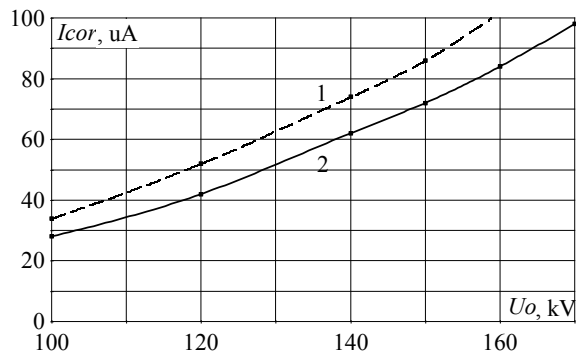
Fig. 16 The experimentally obtained dependences of I_{cor} on the level U_0—the applied DC voltage of positive polarity (curve 1) and the effective value of the power frequency AC voltage (curve 2) (the top of the grounded electrode has the shape of a cone with a height $h = 1.2$ m)
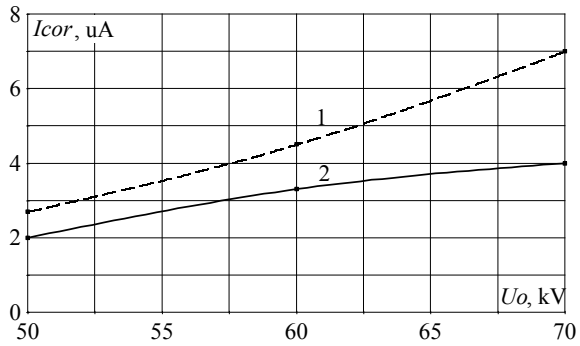
Figure 16 shows the measured values of the corona current when a DC voltage of positive polarity (curve 1) and an AC voltage with a frequency of 50 Hz (curve 2) are applied. The measurements were made for the case of a grounded electrode of height h = 1.2 m with a cone-shaped apex.

As can be seen from Fig. 16, the levels of corona current, when an AC voltage is applied, is less than when a DC voltage of positive polarity is applied. Perhaps this is due to the fact that when the intensity levels of the applied EF are relatively small, corona occurs only on the positive half-waves of the sinusoidal voltage.

5.4 Experimental Results

From the experimental results, it can be concluded that corona processes on electrodes, consisting of a grounded rod located in an external EF, can be most typical for the case of a negative DC voltage of EF. This case represents the "average dependence" of I_{cor} on U_0 (or EF). The results obtained are average between those obtained with the application of a positive voltage and an alternating voltage with a frequency of 50 Hz.

6 Mathematical Modeling of Corona Discharges from Rod Electrodes

6.1 Comparison of Calculated and Experimental Results

In [67], the results of calculations of the strength of the EF at the tops of the rods with height h, curvature radius R, in relation to the strength of the applied average EF E_0 are given. The dependence $E_{\max}/E_0 = f(h/R)$ (where $E_{\max}$ is the maximum

strength at the top of the rod) is calculated, approximated by a polynomial. For the $h/R > 60$ range, the dependence can also be represented as a linear function:

$$K_{max} = E_{max}/E_0 \approx 0.6 \times h/R + 12.5. \tag{16}$$

To achieve conditions at the top of a grounded rod electrode under which breakdown develops in air under normal conditions in the zone of a weakly inhomogeneous EF [68], an applied EF with a strength $E_{ap} \geq 30$ kV/cm is required. Then from (16) it is possible to obtain a relation between the curvature radius R of the sharp top of a grounded object and its height h, upon fulfillment of which, for an object located in the zone of action of an EF of strength E_0 [V/m], suppression or a significant decrease in the corona intensity at a given object performed:

$$R/h > 0.6/\left(3 \cdot 10^6/E_0 - 12.5\right). \tag{17}$$

The last expression can be used to estimate the radius with which sharp tops should be rounded on objects of height h, which are located in the zone of action of the EF with strength E_0, so that corona discharges do not occur on them.

It can also be used to obtain an expression for the critical strength of the EF E_{cr}, which will lead to the appearance of a crown at the end of the rod electrode with a height h and a curvature radius R of the top, namely:

$$E_{cr}(h/R) \geq 3 \cdot 10^6/(0.6 \times h/R + 12.5). \tag{18}$$

Predictions for the appearance or absence of a corona on grounded rods of different heights with different tops rounding radii using formula (16) coincide with the results of physical modeling (Fig. 13). Thus, according to formula (16), the maximum excess of the EF strength on a rod electrode with a height of 1.2 m and a curvature radius of the top $R = 0.019$ m is about $K_{max} = E_{max}/E_0 \approx 50$. That is, corona discharges at the top of such an electrode should appear at an EF strength $E_0 \geq 30$ kV/cm/50 $= 0.6$ kV/cm. For the configuration considered earlier with $d = 2.1$ m, this EF corresponds to the applied minimum voltage. Comparison with experimental results under the assumption that the beginning of a corona occurs when the current exceeds $I_{min} = 1$ mA (curve 6 in Fig. 13) shows that for this current level $U_0 = 150$ kV. This test voltage is slightly higher than U_0^{min}, but they are not too different. All configurations for which the beginning of coronation was measured (Table 1) can be estimated in a similar way.

6.2 Dependence of the Corona Current on E_{max}

It is also important to evaluate the dependence of I_{cor} on E_{max}, calculated in accordance with Eq. (16) for the corresponding values of h, R and E_0.
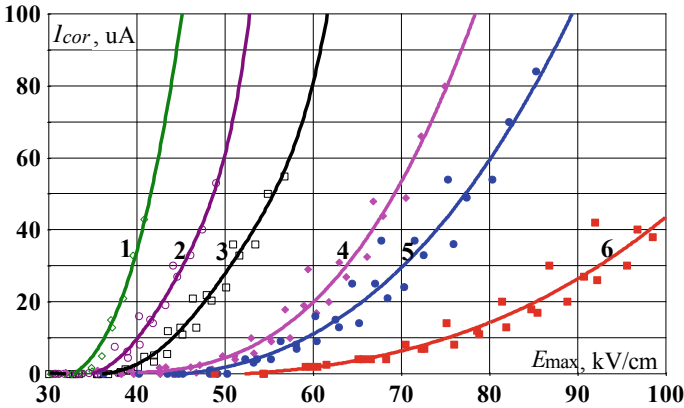
Fig. 17 Dependences of the corona current (I_{cor}) on the value of the maximum intensity at the tops of grounded rods (E_{max}) at different radii R of their curvature (1—0.019 m; 2—0.015 m; 3—0.0125 m; 4—0.009 m; 5—0.00775 m; 6—0.0055 m). Electrode height h and applied voltage levels U_0 varied. The dots show the measured values of I_{cor} at E_{max} calculated for the corresponding geometry and U_0, the curves show their approximation by polynomials

Figure 17 shows the dependences of the corona current on the level of the maximum intensity of the EF at the top of the grounded rod electrode, calculated in accordance with (16). The experimental data used in the construction of these dependences are given in Table 1. Each of curves 1–6 corresponds to electrodes with the same curvature radius R, 4 values of their height h (1.2 m, 1.015 m, 1.05 m, 0.93 m) and different levels of applied voltage of negative polarity U_0. With this U_0 variation, E_0 also changes, since d in all experiments was unchanged and equal to 2.1 m.

As can be seen from Fig. 17, the level of the EF maximum strength $E_{max} = K_{max}(h/R) \times E_0$ affects on the corona current value, and, therefore, the corona intensity. In this case, the lines corresponding to each curvature radius of the top of the grounded electrode have different curvature (see Fig. 1.2, curves 1–6). Based on the data shown in Fig. 17, it follows that the level of the EF maximum strength at the tops of the grounded electrodes cannot fully characterize the intensity of the corona processes, since this process, in addition to this parameter, is clearly affected by the value of the electrode curvature R. Moreover, the larger R, the lower levels of E_{max} achieve the same values of I_{cor}. Obviously, this is due to the fact that the volumes of the zones in which coronation occurs at the tops of the rods are proportional to R. In order to test this hypothesis, the calculations of the EF strength distributions in the considered systems were carried out.

Fig. 18 Calculation system for mathematical modeling of the EF distribution on the tops of grounded rods (3) located in the system of potential (1) and grounded (2) planes, 4—PMLs, 5—electrode rounded top with radius R
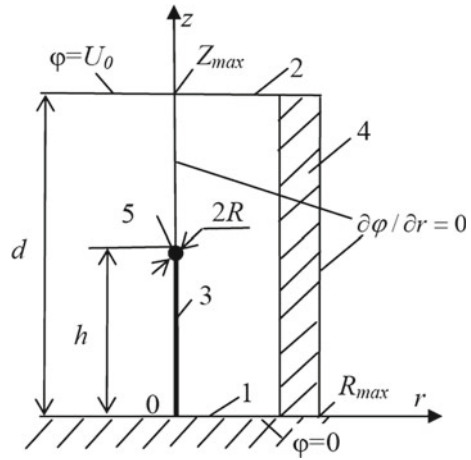
6.3 Dependence of the Initial Value of the Corona on the Volume of the Zone Due to the Critical EF

To study the above effect, the EF spatial distribution in each of the considered configurations is calculated. Numerical calculations were performed using the system configuration with limiting conditions, as shown in Fig. 18. The use of axial symmetry of the system means that a cylindrical coordinate system can be used for calculations. Details of the calculation method are described in [69, 70]. Efficient calculations in the considered systems with different heights and curvature radii of the grounded electrode rods show that the spatial distribution can be represented as generalized variables, as shown in Fig. 19:

$$E^*(r^*, z^*) = E/E_{\max}, \tag{19}$$

where $r^* = r/R$; $z^* = [z - (h - R)]/R$; $E_{\max}$—maximum EF force at the end of the rod, calculated with the equation coefficient (16); and E—EF value at any point in space. As the comparison of the distributions $E^*(r^*, z^*)$, which made at different R and h, showed, they coincide in the vicinity of the tops of the grounded electrodes within 10–20%.

The volumes located within equal levels of the EF at $E^* = $ const (Fig. 19) were calculated using numerical integration. Dependency can be expressed as
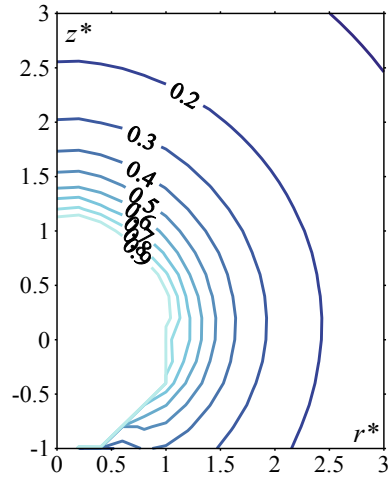
$$V_{cor}^* = f(E^*), \tag{20}$$

where $V_{cor}^* = V_{cor}/V_0$; V_{cor}—volume of the zone in which the EF force exceeds a certain level E^*; and $V_0 = 4/3\pi R^3$—volume of the tip of the spherical rod.

Equation (20) can be replaced by a more convenient form by substituting $E^* = E/E_{\max}$ from Eq. (19) into Eq. (20):

Fig. 19 Calculated distributions of lines of the same level of EF relative intensity E^* in coordinates $(r^*; z^*)$ at $R = 0.0125$ m and $h = 1.2$ m

$$V_{cor}^* = f(E_{max}), \tag{21}$$

Equation (21) was used to obtain a volume in which the beginning of breakdown and corona discharges depends on E_{max}. Figure 20 shows the dependence $V_{cor}^*(E_{max})$, where E_{max} measured in [kV/cm]. This dependence can be approximated by a fourth-order polynomial for small values of E_{max} (dashed line in Fig. 20):

$$V_{cor}^*(E_{max}) = -1.62 \cdot 10^{-7} \cdot E_{max}^4 + 4.07 \cdot 10^{-5} \cdot E_{max}^3$$
$$+ 8.2 \cdot 10^{-4} \cdot E_{max}^2 - 0.19 \cdot E_{max} + 4.31. \tag{22}$$

For large values of E_{max} ($E_{max} > 150$ kV/cm), such a curve can be approximated by a second-order polynomial (solid line in Fig. 20):

$$V_{cor}^*(E_{max}) = 0.0034 \times E_{max}^2 - 0.19 \times E_{max} + 2.34. \tag{23}$$

Thus, the maximum EF strength at the end of the rod (E_{max}) can be obtained by calculating K_{max} from condition (16) for a grounded rod with a given coefficient h/R and obtaining the multiplication of this value and the applied strength E_0, and then using Eq. (22) or (23) for obtaining V_{cor}^*.

Using this procedure, $V_{cor} = V_{cor}^* \times V_0$ was calculated.
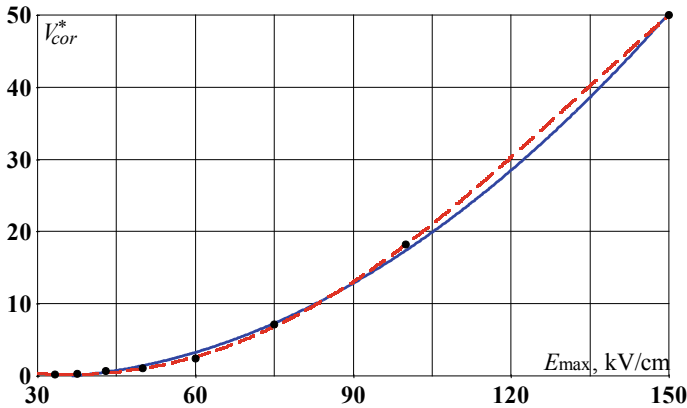
Fig. 20 Dependence of V_{cor}^* on the E_{max} value (points correspond to the calculated values, the solid line is the approximation by the 2nd order polynomial, the dotted line is the approximation by the 4th order polynomial)

References

1. Bonnell, J.W., Mozer, F.S., Delory, G.T., Hull, A.J., Ergun, R.E., Cully, C.M., Harvey, P.R.: The electric field instrument (EFI) for THEMIS. In: The THEMIS Mission, pp. 303–341. Springer, New York, NY (2009). https://doi.org/10.1007/978-0-387-89820-9_14

2. Lindqvist, P.A., Olsson, G., Torbert, R.B., King, B., Granoff, M., Rau, D., Tucker, S.: The spin-plane double probe electric field instrument for MMS. Space Sci. Rev. **199**(1), 137–165 (2016). https://doi.org/10.1007/s11214-014-0116-9

3. Ezawa, M.: A topological insulator and helical zero mode in silicene under an inhomogeneous electric field. New J. Phys. **14**(3), 033003 (2012)

4. Rezinkina, M.M.: Calculation of three-dimensional electric fields in systems with thin wires. Elektrichestvo **1**, 44–49 (2005). ISSN 00135380

5. Rezinkina, M.M.: Simulation of electric fields in the presence of rods with rounded upper ends. Tech. Phys. **60**(3), 337–343 (2015). https://doi.org/10.1134/S1063784215030238

6. Theberge, F., Daigle, J.F., Kieffer, J.C., Vidal, F., Chateauneuf, M.: Laser-guided energetic discharges over large air gaps by electric-field enhanced plasma filaments. Sci. Rep. **7**(1), 1–8 (2017). https://doi.org/10.1038/srep40063

7. Jiang, Z., Zeng, Z., Li, J., Liu, F., Li, W.: Simulation and analysis of GPR signal based on stochastic media model with an ellipsoidal autocorrelation function. J. Appl. Geophys. **99**, 91–97 (2013). https://doi.org/10.1016/j.jappgeo.2013.08.005

8. Rakov, V.A., Rachidi, F.: Overview of recent progress in lightning research and lightning protection. IEEE Trans. Electromagn. Compat. **51**(3), 428–442 (2009). https://doi.org/10.1109/TEMC.2009.2019267

9. Zeng, R., Zhuang, C., Zhou, X., Chen, S., Wang, Z., Yu, Z., He, J.: Survey of recent progress on lightning and lightning protection research. High Voltage **1**(1), 2–10 (2016). https://doi.org/10.1049/hve.2016.0004

10. Rezinkina, M.M., Knyazyev, V.V., Kravchenko, V.I.: Mathematical description of leader channel propagation for selection of model experiment parameters and lightning guard system. Tech. Phys. **52**(8), 1006–1010 (2007). https://doi.org/10.1134/S1063784207080075

11. Yu, A., Chabot, V., Zhang, J.: Electrochemical Supercapacitors for Energy Storage and Delivery: Fundamentals and Applications, p. 383. Taylor & Francis (2013)

12. Zhang, N., Yuan, P., ting An, T., Zhang, M., rong Chen, R.: The conductivity and propagation property of lightning leader tip. Atmos. Res. **245**, 105099 (2020). https://doi.org/10.1016/j.atmosres.2020.105099

13. Green, N.G., Jones, T.B.: Numerical determination of the effective moments of non-spherical particles. J. Phys. D Appl. Phys. **40**(1), 78 (2006)

14. Balanis, C.A.: Advanced Engineering Electromagnetics. Wiley (2012)

15. Rezinkina, M.M.: Growth of dendrite branches in polyethylene insulation under a high voltage versus the branch conductivity. Tech. Phys. **50**(6), 758–765 (2005). https://doi.org/10.1134/1.1947354

16. Wu, J., Traoré, P., Louste, C.: An efficient finite volume method for electric field–space charge coupled problems. J. Electrostat. **71**(3), 319–325 (2013). https://doi.org/10.1016/j.elstat.2012.12.004

17. Neimarlija, N., Demirdžić, I., Muzaferija, S.: Finite volume method for calculation of electrostatic fields in electrostatic precipitators. J. Electrostat. **67**(1), 37–47 (2009). https://doi.org/10.1016/j.elstat.2008.10.007

18. Masouri, Z., Hatamzadeh-Varmazyar, S.: Evaluation of current distribution induced on perfect electrically conducting scatterers. Int. J. Ind. Math. **5**(2), 167–173 (2013)

19. Babak, V.P., Babak, S.V., Eremenko, V.S., Kuts, Y.V., Myslovych, M.V., Scherbak, L.M., Zaporozhets, A.O.: Examples of using models and measures on the circle. In: Models and Measures in Measurements and Monitoring, pp. 127–156. Springer, Cham (2021). https://doi.org/10.1007/978-3-030-70783-5_5

20. Munir, A.: Computational approach for resonant frequency calculation of coaxial cavity resonator using cylindrical coordinate system-based FDTD method. In: 2015 International Conference on Quality in Research (QiR), pp. 73–76. IEEE. https://doi.org/10.1109/QiR.2015.7374898

21. Bérenger, J. P. (2007). Perfectly matched layer (PML) for computational electromagnetics. In: Synthesis Lectures on Computational Electromagnetics, vol. 2(1), pp. 1–117.https://doi.org/10.2200/S00030ED1V01Y200605CEM008

22. Rezinkina, M.M., Rezinkin, O.L.: Modeling of the electromagnetic wavefront sharpening in a nonlinear dielectric. Tech. Phys. **56**(3), 406–412 (2011). https://doi.org/10.1134/S1063784211030169

23. Rezinkina, M.M., Sokol, Y.I., Zaporozhets, A.O., Gryb, O.G., Karpaliuk, I.T., Shvets, S.V.: Mathematical modeling of the electromagnetic processes of the corona's formation during the operation of electric power facilities. In: Control of Overhead Power Lines with Unmanned Aerial Vehicles (UAVs), pp. 99–118. Springer, Cham (2021). https://doi.org/10.1007/978-3-030-69752-5_7

24. Taflove, A., Hagness, S.C., Piket-May, M.: Computational electromagnetics: the finite-difference time-domain method. In: The Electrical Engineering Handbook, vol. 3 (2005)

25. Gamerota, W.R., Idone, V.P., Uman, M.A., Ngin, T., Pilkey, J.T., Jordan, D.M.: Dart-stepped-leader step formation in triggered lightning. Geophys. Res. Lett. **41**(6), 2204–2211 (2014). https://doi.org/10.1002/2014GL059627

26. Sima, W., Li, Y., Rakov, V.A., Yang, Q., Yuan, T., Yang, M.: An analytical method for estimation of lightning performance of transmission lines based on a leader progression model. IEEE Trans. Electromagn. Compat. **56**(6), 1530–1539 (2014). https://doi.org/10.1109/TEMC.2014.2314772

27. Rezinkina, M.M., Knyazyev, V.V., Kravchenko, V.I.: Computation of the probability of lightning damage to ground objects. Tech. Phys. **52**(1), 59–64 (2007). https://doi.org/10.1134/S1063784207010100

28. Van Bladel, J.G.: Electromagnetic fields, vol. 19. Wiley (2007)

29. Kyrylenko, O.V., Blinov, I.V., Tankevych, S.E.: Smart Grid and organization of information exchange in electric power systems. Tekhnichna elektrodynamika **3**, 47–48 (2012)

30. Kyrylenko, O.V., Blinov, I.V., Parus, E.V., Trach, I.V.: Evaluation of efficiency of use of energy storadge system in electric networks. Tech. Electrodyn. **5**, 44–54 (2021). https://doi.org/10.15407/techned2021.04.044

31. Kyrylenko, O.V., Basok, B.I., Baseyev, Y., Blinov, I.V.: Power industry of Ukraine and realities of the global warming. Tech. Electrodyn. **3**, 52–61 (2020). https://doi.org/10.15407/techne d2020.03.052

32. Baranov, G., Komisarenko, O., Zaitsev, I.O., Chernytska, I.: SMART technologies for transport tests networks, exploitation and repair tools. In: 2021 International Conference on Artificial Intelligence and Smart Systems (ICAIS), pp. 621–625. IEEE (2021, March). https://doi.org/10.1109/ICAIS50930.2021.9396055

33. Zaitsev, I., Levytskyi, A., Bogdan, K., Pavlo, R.: Optical fiber in nuclear power plants: applications to improve the reliability, safety and work stability of fault control instrumentation. In: Systems, Decision and Control in Energy III, pp. 123–138. Springer, Cham (2022). https://doi.org/10.1007/978-3-030-87675-3_7

34. Sreedhar, S., Srinivasan, V., Arulmozhivarman, P., Selvaraj, T.: Reliability assessment of lightning protection of renaissance architecture based heritage church in india using electrogeometric methods. In: 2021 Innovations in Power and Advanced Computing Technologies (i-PACT), pp. 1–7. IEEE (2021, November). https://doi.org/10.1109/i-PACT52855.2021.9696880

35. Martínez, J.M., Angarita, E.M.N., Alvarez, J.R.N., Crespo, M.H., Pertuz, P.J.F.: Lightning rod system: mathematical analysis using the rolling sphere method. Int. J. Power Electron. Drive Syst. (IJPEDS) **13**(1), 2829–2838 (2022)

36. Zhang, L., Wang, G., Zhang, W., Ma, Y., Guo, Z., Li, Q.: An electro-geometric model for lightning shielding of multiple wind turbines. Energies **10**(9), 1272 (2017). https://doi.org/10.3390/en10091272

37. Rezinkina, M.M.: Technique for predicting the number of lightning strokes to extended objects. Tech. Phys. **53**(5), 533–539 (2008). https://doi.org/10.1134/S1063784208050010

38. Meyer, H.K., Mauseth, F., Pedersen, A., Ekeberg, J.: Breakdown mechanisms of rod-plane air gaps with a dielectric barrier subject to lightning impulse stress. IEEE Trans. Dielectr. Electr. Insul. **25**(3), 1121–1127 (2018). https://doi.org/10.1109/TDEI.2018.007023

39. Aleksandrov, N.L., Bazelyan, E.M., D'Alessandro, F., Raizer, Y.P.: Dependence of lightning rod efficacy on its geometric dimensions—a computer simulation. J. Phys. D Appl. Phys. **38**(8), 1225 (2005)

40. Diaz, O., Hettiarachchi, P., Rahman, M., Cooray, V., Vayanganie, S.P.A.: Experimental study of leader tortuosity and velocity in long rod-plane air discharges. IEEE Trans. Dielectr. Electr. Insul. **23**(2), 806–812 (2016). https://doi.org/10.1109/TDEI.2015.005421

41. Vargas, M., Torres, H.: On the development of a lightning leader model for tortuous or branched channels–Part II: model results. J. Electrostat. **66**(9–10), 489–495 (2008). https://doi.org/10.1016/j.elstat.2008.04.011

42. He, J., Tu, Y., Zeng, R., Lee, J.B., Chang, S.H., Guan, Z.: Numeral analysis model for shielding failure of transmission line under lightning stroke. IEEE Trans. Power Deliv. **20**(2), 815–822 (2005). https://doi.org/10.1109/TPWRD.2004.839189

43. Cooray, V., Rakov, V., Theethayi, N.: The lightning striking distance—Revisited. J. Electrostat. **65**(5–6), 296–306 (2007). https://doi.org/10.1016/j.elstat.2006.09.008

44. National Fire Protection Association: Standard for the Installation Of Lightning Protection Systems. National Fire Protection Association (2011)

45. Bazelyan, E.M., Raizer, Y.P., Aleksandrov, N.L.: Corona initiated from grounded objects under thunderstorm conditions and its influence on lightning attachment. Plasma Sour. Sci. Technol. **17**(2), 024015 (2008)

46. Aleksandrov, N.L., Bazelyan, E.M., Raizer, Y.P.: The effect of a corona discharge on a lightning attachment. Plasma Phys. Rep. **31**(1), 75–91 (2005). https://doi.org/10.1134/1.1856709

47. Borghetti, A., Nucci, C.A., Paolone, M.: An improved procedure for the assessment of overhead line indirect lightning performance and its comparison with the IEEE Std. 1410 method. IEEE Trans. Power Deliv. **22**(1), 684–692 (2006). https://doi.org/10.1109/TPWRD.2006.881463

48. Martinez, J.A., Castro-Aranda, F.: Lightning performance analysis of overhead transmission lines using the EMTP. IEEE Trans. Power Deliv. **20**(3), 2200–2210 (2005). https://doi.org/10.1109/TPWRD.2005.848454

49. Mata, C.T., Bonilla, T.: Lightning risk assessment tool, implementation of the IEC 62305-2 standard on lightning protection. In: 2012 International Conference on Lightning Protection (ICLP), pp. 1–8. IEEE (2012, September). https://doi.org/10.1109/ICLP.2012.6344320
50. Uman, M.A.: The Art and Science of Lightning Protection. Cambridge Univ Pr. (2008)
51. Rakotonandrasana, J.H., Beroual, A., Fofana, I.: Modelling of the negative discharge in long air gaps under impulse voltages. J. Phys. D Appl. Phys. **41**(10), 105210 (2008)
52. IEC 62305-1: Protection against Lightning Part 1: General Principles (IEC 62305-1: 2010) (2011)
53. Rezinkina, M.M., Sokol, Y.I., Zaporozhets, A.O., Gryb, O.G., Karpaliuk, I.T., Shvets, S.V.: Physical modeling of discharges in long air gaps with the presence of the corona at the tops of grounded objects. In: Control Of Overhead Power Lines with Unmanned Aerial Vehicles (UAVs), pp. 85–98. Springer, Cham (2021). https://doi.org/10.1007/978-3-030-69752-5_6
54. Zaitsev, I.O., Kuchanskyy, V.V.: Corona discharge problem in extra high voltage transmission line. In: Systems, Decision and Control in Energy II, pp. 3–30. Springer, Cham (2021). https://doi.org/10.1007/978-3-030-69189-9_1
55. Zhang, Z., Zeng, R., Yu, Z.: Measurement of corona characteristics and electromagnetic environment of ±800 kV HVDC transmission lines under high altitude condition. In: Progress in Electromagnetics Research Symposium: PIERS Proceedings, pp. 18–21 (2009, August)
56. Simmelvuo, M.K.: Electric power system suppressing corona discharge from viewpoint of environment, European Patent Office. International publication number: WO, 43708(12.05) (2005)
57. Rezinkina, M., Rezinkin, O., D'Alessandro, F., Danyliuk, A., Lisachuk, G., Sosina, E., Svetlichnaya, E.: Influence of corona on strike probability of grounded electrodes by high voltage discharges. J. Electrostat. **83**, 42–51 (2016). https://doi.org/10.1016/j.elstat.2016.07.005
58. Khaddour, B., Atten, P., Coulomb, J.L.: Numerical solution and experimental test for corona discharge between blade and plate. IEEE Trans. Magn. **43**(4), 1193–1196 (2007). https://doi.org/10.1109/TMAG.2006.890954
59. Chang, J.S., Lawless, P.A., Yamamoto, T.: Corona discharge processes. IEEE Trans. Plasma Sci. **19**(6), 1152–1166 (1991). https://doi.org/10.1109/27.125038
60. Tendero, C., Tixier, C., Tristant, P., Desmaison, J., Leprince, P.: Atmospheric pressure plasmas: a review. Spectrochim. Acta Part B **61**(1), 2–30 (2006). https://doi.org/10.1016/j.sab.2005.10.003
61. Patil, J.G., Vijayan, T.: Characteristics of high-tension-induced corona-discharge plasma in ozone generator diode. IEEE Trans. Plasma Sci. **38**(9), 2422–2427 (2010). https://doi.org/10.1109/TPS.2010.2057447
62. Bazelyan, E.M., Raizer, Y.P., Aleksandrov, N.L., D'Alessandro, F.: Corona processes and lightning attachment: the effect of wind during thunderstorms. Atmos. Res. **94**(3), 436–447 (2009). https://doi.org/10.1016/j.atmosres.2009.07.002
63. Sekimoto, K., Takayama, M.: Fundamental processes of corona discharge. J. Inst. Electrostat. Jpn **33**, 38–42 (2009)
64. Rezinkina, M.M.: Modeling of the dendrite shape variation with applied electric field strength in poly(ethylene). Tech. Phys. Lett. **26**(3), 196–198 (2000). https://doi.org/10.1134/1.1262789
65. Pinnangudi, B., Gorur, R.S., Kroese, A.J.: Quantification of corona discharges on nonceramic insulators. IEEE Trans. Dielectr. Electr. Insul. **12**(3), 513–523 (2005). https://doi.org/10.1109/TDEI.2005.1453456
66. Antao, D.S., Staack, D.A., Fridman, A., Farouk, B.: Atmospheric pressure dc corona discharges: operating regimes and potential applications. Plasma Sour. Sci. Technol. **18**(3), 035016 (2009)
67. Meng, X., Zhang, H., Zhu, J.J.: A general empirical formula of current–voltage characteristics for point-to-plane geometry corona discharges. J. Phys. D Appl. Phys. **41**(6), 065209 (2008)
68. Bazelyan, E.M., Raizer, Y.P.: Spark Discharge. Routledge (2017)
69. Tamm, I.E.: Fundamentals of the Theory of Electricity (1979)
70. Protection, L., Cooray, V.: The institution of engineering and technology. Published by The Institution of Engineering and Technology, London, United Kingdom

Actual Trends of Electrical Distribution Systems Automation

Vladimir Popov [ID], **Vadim Tkachenko** [ID], **Olena Yarmoliuk** [ID], and **Dmytro Yatsenko** [ID]

Abstract Increasingly widespread integration of local sources of energy generation and accumulation in electrical distribution systems sharply reduces the efficiency of the traditionally used methods and technical means of their modes of operation control. First of all, this concerns such a popular task as choosing the optimal places of the normally open points in the circuits of distribution networks with objective to minimize loss of electrical energy. In this regard, this paper discusses the possibility, feasibility and efficiency of selective use of remotely controlled switching devices in the distribution networks with an open loop topology. The conditions for the expediency of such switching devices implantation are determined. An algorithm of economically optimal operation of remotely controlled switches is proposed, taking into account their limited switching resource. It is shown that in many cases, in order to achieve the required effect, it is advisable to focus on the so-called «soft open points» technologies, which allow independent optimal control of active and reactive power flows and to coordinate the requirements for ensuring high reliability and for minimization of electrical energy losses. A general approach to the control of the corresponding power electronic equipment is proposed to ensure optimal load flow in the distribution feeder in real time.

Keywords Distribution systems · Energy loss · Remotely controlled switch · Soft open points · Power electronics

1 Introduction

In almost all countries, electrical distribution networks were designed and operated as open circuits, which made it possible to use less expensive systems of their relay protection and automation. Such solutions provide quick isolation of damaged elements and restoration of power supply, simplified the control of the network modes. Therefore, for many decades, the choice of optimal location of normally

V. Popov (✉) · V. Tkachenko · O. Yarmoliuk · D. Yatsenko
National Technical University of Ukraine "Igor Sikorsky Kyiv Polytechnic Institute", Kyiv, Ukraine
e-mail: tig@ukr.net

open points has been considered as one of the most popular and effective problems of optimizing the modes of distribution networks, mainly built according to the loop scheme [1–6].

Both power losses, in particular, in the period of peak demand, and energy losses were considered as the objective function. The problem was solved as a single-criteria [7–9] as well as multi-criteria [10–13], where reliability and voltage levels were additionally taken into account. In several publications the influence of the adjacent networks of a higher voltage on total energy (power) losses was studied [14, 15].

Taking into account the dimension and complexity of this problem formalization, dozens of different mathematical methods were used for its solution, which was reflected in hundreds of publications on this topic. All these methods may be conditionally classified into mathematical optimization based approaches [16–18], heuristic (meta heuristic) [19–24] and hybrid methods [25–27]. However, these studies were united by the fact that in all cases the choice of the optimal place for normally open points of distribution networks was considered as a medium-term planning problem.

Thus, it was assumed that the decision made (selected open points of the distribution network circuits) would not change for a sufficiently long time. Usually, a certain season of the year was taken as such a period of time, which corresponded to relatively permanent load curves of individual network nodes.

Under the conditions prevailing at that time for the operation of most distribution networks, such an approach to problem formulation was largely justified. However, even then attention was paid to the fact that during the increases the heterogeneity of the loads of the network nodes, the efficiency of solving this problem, in particular in terms of optimizing such an integral indicator as the loss of electrical energy, decreases.

In addition, it should be noted that manually operated load break switches or disconnectors used in distribution networks did not make it possible to implement (from the standpoint of technical and economic feasibility) an another strategy of their using.

One more factor in support of such an operation strategy was the information available in distribution networks. The lack of the information obtaining in real time and even the systematic measurements of loads in the network nodes did not allow convincing modeling of network modes with a higher frequency. In this case, one focused on periodic load measurements that corresponded to the certain seasons of the year.

However, in the last two decades, the situation has begun to change dramatically. Among the main reasons, the following should be noted.

Emergence of technical capabilities and economic incentives for more active load management. As can be seen from the experience of many countries, load management is becoming more and more widespread practice not only for industrial or agro-industrial consumers, but also in the domestic sector. This results a possible increase of the heterogeneity of the loads of the network nodes.

Integration into the distribution networks of local generating sources (distributed generation). If at the initial stage diesel generators (primarily designed for backup power supply) with controllable output power were considered as such sources in many cases, recently their place has been occupied by renewable sources with uncontrolled, depending on various meteorological factors, and extremely unstable output power.

The growing number of electric vehicles and, accordingly, the appearance of charging stations in the electric power distribution systems, which last time have been considered not only as an additional load, but also in a certain sense as a means of electrical energy accumulating.

In addition, in the future, obviously, we should expect the appearance in distribution networks of different storage devices, hybrid energy sources, new technical solutions, in particular, focused on the production and use of hydrogen.

All this can cause serious changes in the traditional structure of distribution networks and their modes of operation, which will become less stable and more unpredictable. As a result, under the influence of random factors, load flows of various durations are appeared in the networks, which in many cases will differ significantly from the mode (load flow) for which the optimal normally open points were determined. As a result, this leads to an increase of electrical energy losses, and potentially to a violation of the permissible voltage levels and a decrease of reliability.

Simultaneously, a process of equipping distribution networks with modern measuring devices and systems for storing, primary processing and transmitting data is taking place. In many cases it makes possible to simulate modes of distribution lines almost in real time. This creates certain difficulties due to the need for rapid processing very large amounts of data, but at the same time opens the way to the implementation of a fundamentally different mode control strategy.

All listed factors additionally are reinforced by the appearance on the power equipment market of new switches with a large switching resource and the possibility of remote control, as well as significantly more expensive switching equipment, based on power electronics.

2   Remotely Controlled Switching Devices

The circumstances mentioned above, force to change the existing strategy for choosing the optimal configuration of distribution networks in modern conditions. On the other hand, all conditions necessary for the implementation of new technical solutions related to increasing the level of automation of electrical distribution networks are formed.

At the same time, most likely that the features of the modern distribution networks underlined above will be most pronounced only in its individual circuits. No doubt, that, the most obvious factor affecting the mode of operation of such circuits is the presence of renewable energy sources, in which the output power can quickly change

over a wide range (in some cases, from the rated value to almost zero) depending on a change in meteorological conditions and the presence of energy storage facilities.

In such cases, one of the most effective steps to improve the efficiency of choosing the optimal network configuration is the selective use of remotely controlled or automatic (for example, reclosers) switching devices instead of manually operated ones. Obviously, this technical solution will provide the greatest effect if the corresponding changes of the network mode (requiring a change of its topology to minimize power losses) occur relatively regularly and during a sufficiently long time. In fact, the effectiveness of changing the location of the normally open points will be determined by the amount of additional reduction of electrical energy losses, which can be achieved thanks to this action.

However, when making such a decision, it is necessary to take into account a number of additional factors, in particular, such as:

- the cost of not only new switching equipment, but also the cost of creating an appropriate information environment and corresponding remote control channels;
- commutation resource of switches;
- the nature of transient processes accompanying switching operations, which may create certain restrictions.

Mentioned above factors are difficult to formally take into account in a generalized form. This implies the need to evaluate them on a case-by-case basis. In particular, a situation is possible when the switching devices operated in the network have almost exhausted their switching resource and in any case require replacement. In these situations, the installation of remotely controlled switching devices in separate circuits of the distribution network requires a relatively small investment, without including the cost of the circuit breaker itself.

A very important place in assessing the technical and economic efficiency of using remotely controlled switching devices is associated with the presence of an adequate information environment, since we are talking about the possibility of controlling modes almost in real time. Accordingly, in this case, the information about the parameters of the current mode has to be received and updated in an adequate way.

Therefore, capital expenditures, which in the most cases are incurred within one year, may include only an additional cost of equipment to provide remote control of individual circuit breakers (which distinguishes this project from a traditional solution oriented to the use of manually operated switching devices), or full cost of switches with remote control, taking into account, in the general case, the return cost of the equipment being replaced. The costs to obtain adequate information and remote control channels are also taken into account to a different extent.

Formally, the any innovative technical solution requires an appropriate feasibility study. In our case, it is quite difficult to solve such a problem especially taking into account the time factor. When applying almost any of the economic indicators, it is difficult to preliminarily determine the life cycle of the project, which depends on the commutation resource of the circuit breakers and, thus, will be determined by the intensity of their use.

In addition, in the process of conducting an appropriate economic analysis and assuming a sufficiently long life cycle of the project, the decision will be greatly influenced by the uncertainty of the information used, primarily regarding the dynamics of changes in the cost of electricity, and, accordingly, its losses, level of load increasing/decreasing and its heterogeneity, operational cost, etc.

Here, the following approach can be proposed for the economic evaluation of the project, which in the future will allow one to form a strategy for the use of remotely controlled switching devices.

The maximum allowable number of daily commutations (n_c) or the desired life cycle of the project (T) can be determined by expert way. These characteristics, make it possible to estimate either the life time of the switching device ($T = \frac{N_c}{n_c}$, where N_c is rated number of commutations during the life time of the circuit breaker), or conditionally admissible number of daily commutations ($n_c = \frac{N_c}{T}$).

One more characteristic is the desired payback period of the project (T_o) from the point of view of the decision maker. This indicator makes it possible to approximately estimate the minimum effect from an additional reduction in electrical energy losses, at which it is advisable to carry out switching operation, taking into account the mentioned above conditions.

In general, the payback period is defined as $T_o = \frac{K}{C}$, where K—total investment, C—income received after the project implementation. If the time factor is taken into account, the discounted payback period is defined considering the following condition [28]

$$T_o = -K_o + \sum_{t=1}^{T} \frac{C_t}{(1+i)^t} \geq 0, \tag{1}$$

where K_o is in this case a one-time capital investment, C_t is the cash flow in the time t, i is the discount rate.

The given above expression makes it possible to form a condition on the basis of which, for a predetermined payback period of an investment project and the intensity of use of the commutation resource of circuit breakers, it is possible to estimate the lower level of additional reduction of electrical energy losses that economically justifies the feasibility of implementing the corresponding switching operation.

Based on (1), we can write

$$T_o = -K_o - \sum_{t=1}^{T_o} \frac{C_{ot}}{(1+i)^t} + \sum_{t=1}^{T_o} \frac{C_{At}}{(1+i)^t}, \tag{2}$$

where C_{ot}—operating costs in the year t; C_{At}—benefit from additional reduction of energy losses in year t.

In this case, the value of C_A can be determined as follows

$$C_A = c_{\Delta A} \sum_{j=1}^{J} \delta(\Delta P)_j \, \Delta t_j, \tag{3}$$

where $\delta(\Delta P)_j$—additional reduction of power losses on the jth time interval with a duration of Δt_j; J—is the number of time intervals in one cycle of changing the state of switching devices; $c_{\Delta A}$—the cost of electrical energy losses.

Thus, we can write that, in the general case,

$$C_A = c_{\Delta A} \delta(\Delta A) = c_{\Delta A} \delta(\Delta P) \, \Delta t.$$

If we assume that C_A corresponds to the conditional profit received by additional reducing electrical energy losses for one cycle of changing the network topology, allowable number of daily network topology changes (operations of remotely controlled switching devices) is n_k and such operations are planned to be carried out daily, then the annual profit (for the year t) will be

$$C_{At} = 365 n_k c_{\Delta A} \delta(\Delta A). \tag{4}$$

Having accepted that the project has a predefined payback period T_o, , on the basis of (1)–(4) we will obtain

$$\sum_{t=1}^{T_o} \frac{k_\Sigma c_{\Delta A} \delta(\Delta A)}{(1+i)^t} = \frac{K_o + \sum_{t=1}^{T_o} \frac{C_{ot}}{(1+i)^t}}{T_o}, \tag{5}$$

where $k_\Sigma = 365 n_k$.

Using this result, by simple transformations, it is possible to determine the minimum level of additional reduction in energy losses for each cycle of changing the location of the open point, at which the implementation of the corresponding switching operation is economically justified

$$\delta(\Delta A) = \frac{K_o + \sum_{t=1}^{T_o} \frac{C_{ot}}{(1+i)^t}}{T_o k_\Sigma \sum_{t=1}^{T_o} \frac{c_{\Delta A}}{(1+i)^t}}. \tag{6}$$

Thus, initially the problem arises of finding the conditions under which it is expedient to change the topology of a certain circuit of the distribution network in order to minimize power losses in accordance with the current mode. To simplify and speed up the solution of this problem (considering that it must be implemented almost in real time), it is proposed to use for this purpose a certain indicator.

Consider the following example (Fig. 1). Let us determine the total power losses for each part of the distribution network circuit, taking into account the existing place of normally open point.
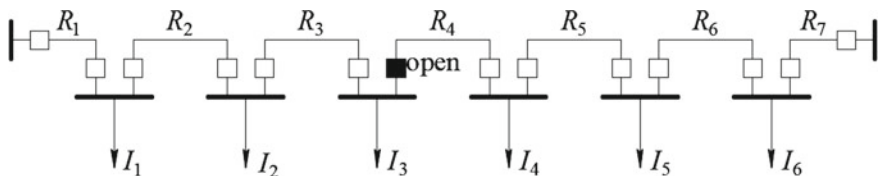
Fig. 1 Circuit of the distribution feeder

$$\Delta P_I = 3I_3^2 R_3 + 3(I_3 + I_2)^2 R_2 + 3(I_3 + I_2 + I_1)^2 R_1 = 3I_3^2 R_3 + 3I_3^2 R_2 +$$
$$+ 6I_3 I_2 R_2 + 3I_2^2 R_2 + 3I_3^2 R_1 + 6I_3 I_2 R_1 + 3I_2^2 R_1$$
$$+ 6I_3 I_1 R_1 + 6I_2 I_1 R_1 + 3I_1^2 R_1. \tag{7}$$

Similarly, for the second (right) part of the circuit (Fig. 1)

$$\Delta P_{II} = 3I_{ch}^2 R_5 + 3(I_{ch} + I_5)^2 R_6 + 3(I_{ch} + I_5 + I_6)^2 R_7 = 3I_{ch}^2 R_5 + 3I_{ch}^2 R_6 +$$
$$+ 6I_{ch} I_5 R_6 + 3I_5^2 R_6 + 3I_{ch}^2 R_7 + 6I_{ch} I_5 R_7 + 3I_5^2 R_7 + 6I_{ch} I_6 R_7$$
$$+ 6I_5 I_6 R_7 + 3I_6^2 R_7. \tag{8}$$

Let us assume that a source of distributed generation is connected to one of the nodes on the left side of the circuit. It provides current injection I_s into the network (Fig. 2). Obviously, in this case, in the right part of the circuit, the total power losses will not change

$$\Delta P_{II}^{/} = \Delta P_{II}. \tag{9}$$

For the left side of the circuit, we will have

$$\Delta P_I^{/} = 3I_3^2 R_3 + 3(I_3 + I_2 - I_s)^2 R_2 + 3(I_3 + I_2 + I_1 - I_s)^2 R_1 = 3I_3^2 R_3$$
$$+ 3I_3^2 R_2 + 6I_3 I_2 R_2 - 6I_3 I_s R_2 - 6I_2 I_s R_2 + 3I_2^2 R_2$$
$$+ 3I_s^2 R_2 + 3I_3^2 R_1 + 6I_3 I_2 R_1 + 6I_3 I_1 R_1 + 6I_2 I_1 R_1$$
$$+ 3I_2^2 R_1 - 6I_3 I_s R_1 - 6I_2 I_s R_1 - 6I_1 I_s R_1 + 3I_1^2 R_1 + 3I_s^2 R_1. \tag{10}$$
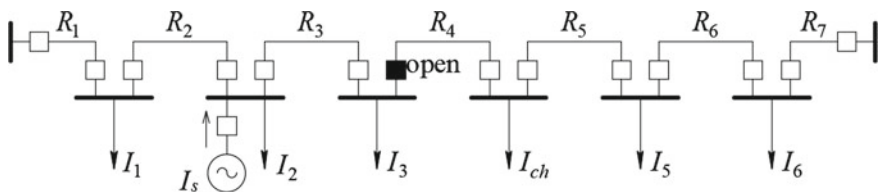

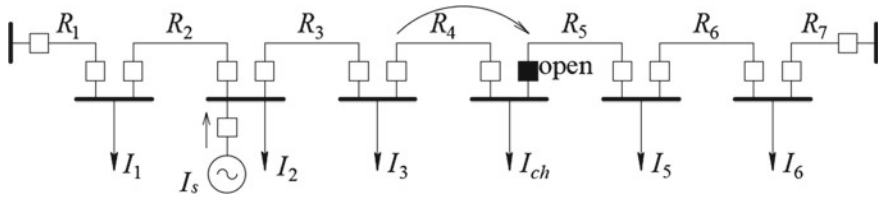**Fig. 2** Distribution network circuit with distributed generation source

Fig. 3 Change of normally open point of the distribution circuit (moving to the right)

It is logical to assume that after connecting a source of distributed generation to the network and, accordingly, partial redaction of loads in the left part of the circuit, it may be expedient to transfer the place of normally open point to the right (Fig. 3), in order to form an optimal mode to minimize power losses.

In this case, the total power losses in the right and left parts of the circuit will be

$$
\begin{aligned}
\Delta P_I^{//} =\ & 3I_{ch}^2 R_4 + 3I_{ch}^2 R_3 + 3I_3^2 R_3 + 6I_{ch}I_3 R_3 + 3I_{ch}^2 R_2 + 3I_3^2 R_2 + 3I_2^2 R_2 + \\
& + 3I_s^2 R_2 + 6I_{ch}I_3 R_2 + 6I_{ch}I_2 R_2 + 6I_3 I_2 R_2 - 6I_{ch}I_s R_2 - 6I_3 I_s R_2 \\
& - 6I_2 I_s R_2 + 3I_{ch}^2 R_1 + 3I_3^2 R_1 + 3I_2^2 R_1 + 3I_1^2 R_1 + 3I_s^2 R_1 + \\
& + 6I_{ch}I_3 R_1 + 6I_{ch}I_2 R_1 + 6I_{ch}I_1 R_1 + 6I_3 I_2 R_1 + 6I_3 I_1 R_1 + \\
& + 6I_2 I_1 R_1 - 6I_{ch}I_s R_1 - 6I_3 I_s R_1 - 6I_2 I_s R_1 - 6I_2 I_1 R_1,
\end{aligned}
\tag{11}
$$

$$
\Delta P_{II}^{//} = 3I_5^2 R_6 + 3I_5^2 R_7 + 6I_5 I_6 R_7 + 3I_6^2 R_7.
\tag{12}
$$

It is possible to make conclusion that change the location of the open point in the circuit in this case will be appropriate if the following condition is met

$$
\Delta P_{II}^{//} + \Delta P_I^{//} < \Delta P_{II}^{/} + \Delta P_I^{/}.
\tag{13}
$$

Using expressions (7)–(12) by simple transformations, it can be shown that condition (13) will be satisfied if

$$
\begin{aligned}
& 3I_{ch}^2 R_4 + 3I_{ch}^2 R_3 + 3I_{ch}^2 R_2 + 3I_{ch}^2 R_1 + 6I_{ch}I_3 R_3 + 6I_{ch}I_3 R_2 + 6I_{ch}I_3 R_1 + \\
& + 6I_{ch}I_2 R_2 + 6I_{ch}I_2 R_1 + 6I_{ch}I_1 R_1 - 6I_{ch}I_s R_2 - 6I_{ch}I_s R_1 < 3I_{ch}^2 R_5 + 3I_{ch}^2 R_6 + \\
& + 3I_{ch}^2 R_7 + 6I_{ch}I_5 R_6 + 6I_{ch}I_5 R_7 + 6I_{ch}I_6 R_7
\end{aligned}
$$

or

$$
\begin{aligned}
& I_{ch}(R_1 + R_2 + R_3 + R_4) + 2I_3(R_1 + R_2 + R_3) \\
& + 2I_2(R_1 + R_2) + 2I_1 R_1 - 2I_s(R_1 + R_2) < \\
& < I_{ch}(R_5 + R_6 + R_7) + 2I_5(R_6 + R_7) + 2I_6 R_7.
\end{aligned}
$$

Adding to the right and left parts of the inequality the value of $I_{ch}(R_5 + R_6 + R_7)$, we obtain

$$I_{ch}(R_1 + R_2 + R_3 + R_4 + R_5 + R_6 + R_7)$$
$$+ 2I_3(R_1 + R_2 + R_3) + 2I_2(R_1 + R_2) + 2I_1 R_1 -$$
$$- 2I_s(R_1 + R_2) < 2I_{ch}(R_5 + R_6 + R_7) + 2I_5(R_6 + R_7) + 2I_6 R_7.$$

Let us introduce the following notation:

$$I_{ch}(R_1 + R_2 + R_3 + R_4 + R_5 + R_6 + R_7) = I_{ch} R_{\sum},$$
$$I_3(R_1 + R_2 + R_3) = M_3,$$
$$I_2(R_1 + R_2) = M_2,$$
$$I_1 R_1 = M_1,$$
$$I_s(R_1 + R_2) = M_s,$$
$$I_{ch}(R_5 + R_6 + R_7) = M_{ch},$$
$$I_5(R_6 + R_7) = M_5,$$
$$I_6 R_7 = M_6.$$

After that we get

$$2(M_1 + M_2 + M_3) + I_{ch} R_{\sum} - 2M_s < 2(M_{ch} + M_5 + M_6).$$

Assuming that for the original network (Fig. 1)

$$M_1 + M_2 + M_3 = M_I, \quad M_{ch} + M_5 + M_6 = M_{II},$$

we will define a condition that determines the expediency of transferring the location of the open point of the circuit to the right

$$M_{II} - M_I + M_s > \frac{I_{ch} R_{\sum}}{2}. \tag{14}$$

In a similar way, it can be shown that moving the open point in the opposite direction (in this case, to the left—Fig. 4) will be justified if

$$M_I - M_{II} + M_s > \frac{I_{ch} R_{\sum}}{2}, \tag{15}$$

where in the case (Fig. 4) $M_I = M_1 + M_2 + M_{ch}$, $M_{II} = M_4 + M_5 + M_6$.

The obtained results can be extended to the case when local energy sources are integrated into both parts of the circuit (Fig. 5). Note, that as such sources, in the general case, the energy storage devices can also be considered. In last case, the current injection into the network will have a negative value.
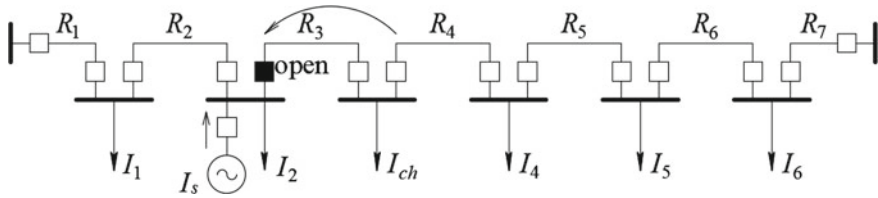
Fig. 4 Change of the open point location (moving to the left)
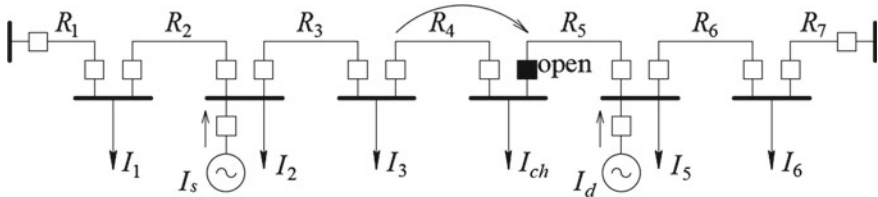

Fig. 5 Distribution circuit with several local energy sources

In such situations, the most obvious, from the point of view of the expediency of changing the location of the circuit open point, is the situation when the operating modes of the local sources integrated into its left and right parts do not coincide. For example, one of the sources increases the level of energy generation into the network, the power of the second decreases in the same period of time, or even it operates in mode of electricity consumption.

In this case, by analogy with (14) and (15) we have:

- moving the open point of the circuit to the right (Fig. 5) is advisable if

$$M_{II} - M_I + M_s - M_d > \frac{I_{ch} R_\sum}{2};$$ (16)

- moving the open point of the circuit to the left (Fig. 4) is advisable if

$$M_I - M_{II} - M_s + M_d > \frac{I_{ch} R_\sum}{2},$$ (17)

where the indices "*s*" and "*d*" refer to local sources integrated, respectively, into the left and right parts of the circuit.

In many cases, distribution networks have a more complex topology. In particular, they may contain branches, including those with local generation sources (Fig. 6). By analogy with the example considered above, it can be proved that in this case expressions (14)–(17) will also be valid to assess the feasibility of changing the location of the open point in accordance with the current mode. However, in the corresponding expressions, the total resistance $R_\sum$ does not include the resistances of the branches. Thus, the presence of branches in the distribution circuit does not affect

the decision-making procedure regarding the advisability of changing the location of the open point. Therefore, in order to simplify the calculations regarding the assessment of the feasibility of changing the location of open point in the circuit, it is advisable to construct preliminary certain equivalent of such a circuit (Fig. 7).

The advantage of this approach will be especially clear in situations where a network fragment transferred from one part of the circuit to another includes not only branches, but also local energy sources (Figs. 8 and 9). The presence of such a situation significantly complicates the structure of the equations like (14)–(17), which are used for carrying out the corresponding analysis.
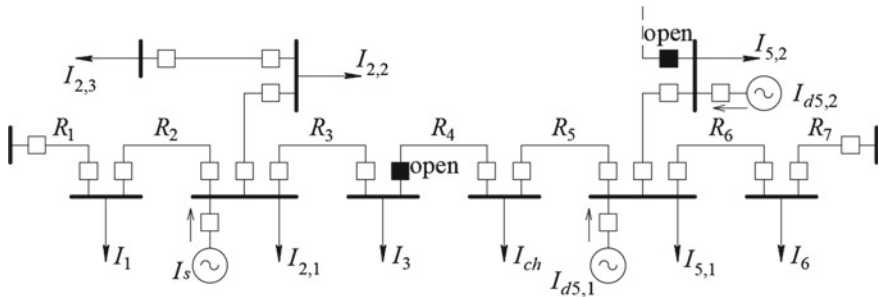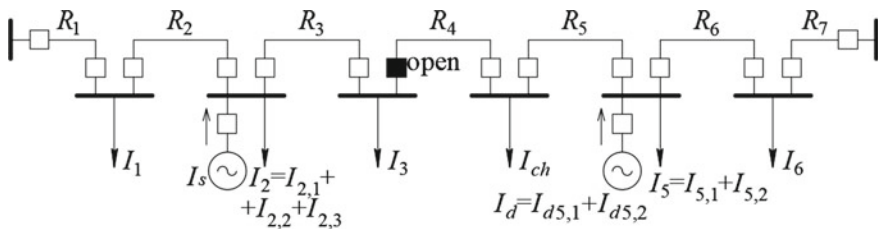

Fig. 6 Distribution circuit with branches

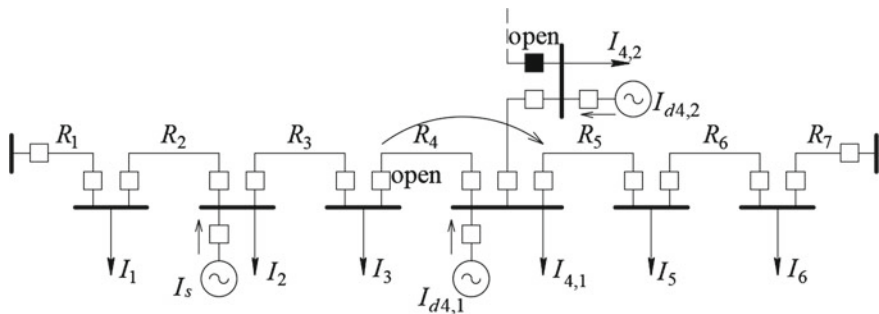**Fig. 7** Equivalent of the distribution circuit with branches

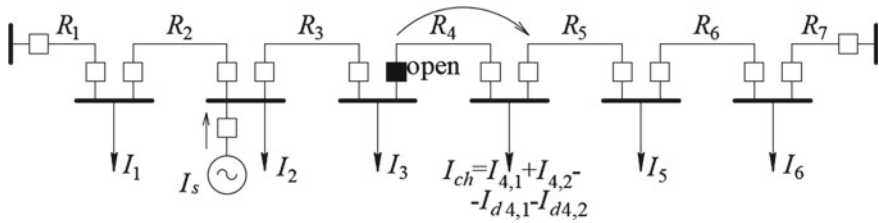**Fig. 8** Distribution circuit with multiple local energy sources

Fig. 9 Equivalent of a distribution circuit with several local energy sources

Obviously, it is of practical interest to generalize the obtained analytical equations for the distribution circuit of any topology, with an arbitrary number of load nodes, local energy sources placed at any network node.

Let us consider (Fig. 10) a generalized distribution line (circuit) and its equivalent (Fig. 11). Supposing the corresponding power sources of the considered circuit have numbers "k" and "m", respectively.

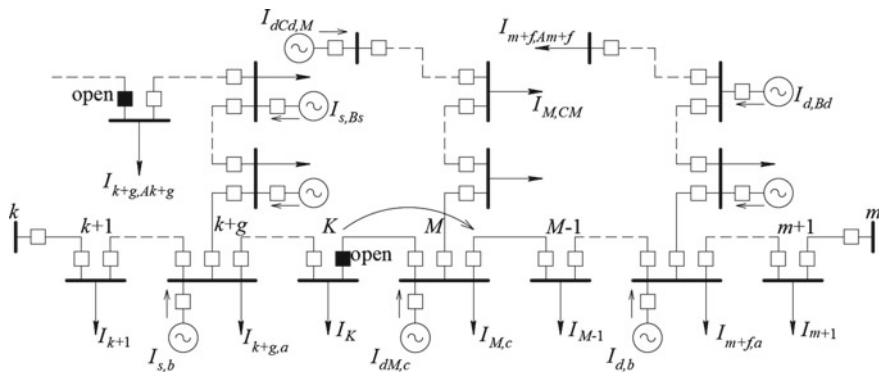In the process of formation of equivalent, we determine

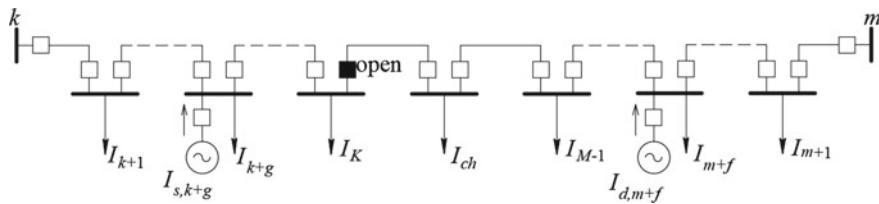

Fig. 10 Generalized distribution circuit

Fig. 11 Equivalent of the generalized circuit of the distribution network

$$I_{k+g} = \sum_{a=1}^{A_{k+g}} I_{k+g,a}, \quad g = 0, \ldots, G, \quad I_{m+f} = \sum_{a=1}^{A_{m+f}} I_{m+f,a}, \quad f = 0, \ldots, F, \quad (18)$$

where G, F are the number of branches, respectively, in the left and right parts of the circuit; A_{k+g}, A_{m+f}—the number of load nodes in the branches, connected, respectively, to $k + g$th and $m + f$th nodes of the circuit;

$$I_{s,k+g} = \sum_{b=1}^{B_s} I_{s,b}, \quad s = 1, \ldots, S, \quad I_{d,m+f} = \sum_{b=1}^{B_d} I_{d,b}, \quad d = 1, \ldots, D, \quad (19)$$

where S, D are the number of nodes with connected directly or through branches local energy sources in the left and right parts of the circuit, respectively; B_s, B_d—the number of local energy sources connected directly or through branches to the sth and dth nodes of the circuit.

$$I_{ch} = \sum_{c=1}^{C_M} I_{M,c} - \sum_{c=1}^{C_{d,M}} I_{d,c}, \quad (20)$$

where C_M—the number of load nodes that are transferred from the right side of the circuit to the left side in the process of changing the location of open point; $C_{d,M}$—the number of nodes with local energy sources that are transferred from one part of the circuit to another in the process of changing the location of open point.

Then, considering the equivalent circuit (Fig. 11), we can give expressions (14)–(17) in the following form

$$M_I = \sum_{i=k}^{K} I_i \left(\sum_{j \in \Pi i} R_j \right), \quad (21)$$

where I_i is the load of the ith network node; K is the number of nodes in the right side of the circuit; R_j—resistance of the jth section of the network; $j \in \Pi i$ means that the summation takes into account the resistances of all sections j that lie on the path of power supply to the ith load node.

$$M_s = \sum_{g=1}^{G} I_{s\,g} \left(\sum_{j \in \Pi g} R_j \right), \quad M_d = \sum_{f=1}^{F} I_{d\,f} \left(\sum_{j \in \Pi f} R_j \right), \quad (22)$$

where $I_{s\,g}$ is the current injection from the gth source of distributed generation connected to the left side of the circuit; G is the total number of local energy sources in the left side of the circuit; $I_{d\,f}$—current injection from the fth local source of energy connected to the right side of the circuit; F—the number of local energy sources connected to the right side of the circuit; R_j—resistance of the jth section of

network; $j \in \Pi g$—means that the summation takes into account the resistance of all sections j that lie on the path of power supply to the gth load node with a local energy source in the left side of the circuit; $j \in \Pi f$—means that the summation takes into account the resistance of all sections j that lie on the path of power supply to the fth load node with a local energy source on the right side of the circuit; R_{Σ}—total resistance of the equivalent circuit.

Obviously, expressions similar to (18)–(22) can also be obtained when normally open point moves in the opposite direction. It is important to note that all mode parameters involved in these calculations are determined in real time in the process of permanent monitoring the loads and the output power of local energy sources.

At the same time, as already mentioned above, in order to make a decision on changing the location of the open point, it is also necessary to evaluate the potential economic effect in the form of the cost savings due to additional reduction of energy losses, which can be obtained in this case.

This stage of analysis includes the need to solve at least the following questions. First of all, it is required to quantify the amount of additional reduction in power losses that can be obtained after changing the location of open point of the circuit in accordance with the parameters of the actual mode. Simultaneously, forecast of the mode parameters should be carried out with different intervals of prediction in order, firstly, to confirm the stability of the corresponding mode change and to determine the time during which it will take place, and, secondly, to calculate the predictive value of additional power losses reduction that can be achieved. The data obtained will allow one to evaluate the potential effect, in terms of further reducing the energy losses by changing the location of the open point of the distribution circuit, which can be obtained as a result of the implementation of such a solution. The final decision regarding change of the location of the circuit open point is made in the process of comparing the obtained (forecasted) value of the additional reduction in electrical energy losses with the threshold value determined on the basis of Eqs. (5) and (6), which are founded on technical and economic considerations.

The power losses reducing in the case of a successful change of the location of open point will be the following

$$\delta(\Delta P) = \Delta P_I^{/} + \Delta P_{II}^{/} - \Delta P_I^{//} - \Delta P_{II}^{//}.$$

In particular, in the presence of local energy sources in left, as well as in right parts of the circuit, when the open point is moved to the right, the reduction in power losses will be equal to

$$\delta(\Delta P) = (2M_{II} - 2M_I - 2M_d + 2M_s - I_{ch}R_{\Sigma})3I_{ch}. \tag{23}$$

Accordingly, if it is expedient to move the location of open point to the left, we will have

$$\delta(\Delta P) = (2M_I - 2M_{II} - 2M_s + 2M_d - I_{ch}R_{\Sigma})3I_{ch}. \tag{24}$$

Thus, the results obtained make it possible to theoretically substantiate the expediency of changing the circuit open point in accordance with the current mode. At the same time, as noted above, the practical implementation of such a solution should be justified by economic considerations.

Here the problem arises of predicting the mode parameters in order to estimate its duration and simultaneously calculate the value of the potential additional reduction in energy losses, which can be achieved in this case. Only after this the implementation of physical change of the location of open point, which is associated with the operation of the corresponding remotely controlled switching devices, can be made.

In this sense, the prediction of the node loads and the output power of the local energy sources, play an important role for the economic justification of the decision regarding change of the circuit open point location.

In order to increase the argumentation of the forecasting solutions, it is proposed to use the so-called adaptive forecasting method. Its essence is as follows. The process of short-term forecasting of the required parameters is carried out constantly on the basis of the parallel application of a number of different methods. At the same time, the methods used to predict electrical loads and output power of different local energy sources (for example, wind and photovoltaic stations) can be different.

The choice of algorithms (methods) for short-term forecasting used for these purposes is based on the analysis and generalization of recommendations formulated in extensive studies in this field (for example such as [29–33]).

In the process of forecasting, after obtaining the actual values of the predicted parameters, the error is estimated for each of the applied methods. On the basis of the method that provides the minimum error, at the next step of forecasting it is estimated (for example, on the basis of (16), (17), (21) and (22)) the expediency of changing the location of open point of the circuit both in one and in the other directions.

If calculations show that there is no such expediency, then the forecasting procedure using the entire range of selected methods continues. If the obtained predictive values of the mode parameters indicate the feasibility of changing the location of the circuit open point, then the so-called "time scanning" of the mode is carried out in order to assess its stability and duration. Here, for forecasting, a method that currently provides the minimum forecast error is used. This procedure, in fact, is a sequential prediction of the mode parameters (loads and output power of local sources) with a gradually increasing forecasting interval (Fig. 12). If the changes of corresponding parameters are unstable, then the decision regarding the change of the open point location is not implemented.

If the "time scanning" demonstrates the stability of changing the mode parameters, then at the same time, in accordance with (23) or (24), the value of the additional reduction in electrical energy losses is calculated step by step. This procedure, assuming that the area enclosed between the corresponding predictive characteristics, on a certain scale (23), (24) corresponds to the value of the additional reduction of energy losses, is shown in Fig. 12.
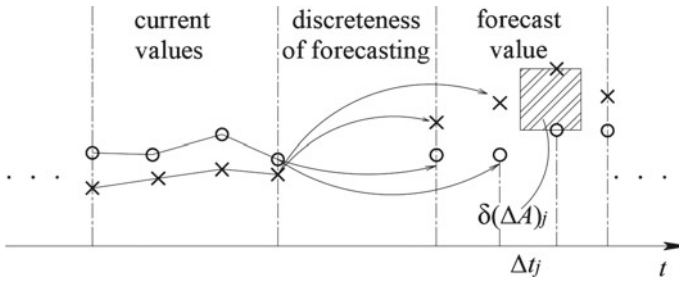
Fig. 12 «Time scanning» procedure: ○ ○ ○—corresponds to the value of parameter $\frac{I_{ch}R_\Sigma}{2}$; × × ×—corresponds to the value of parameter $M_{II} - M_I - M_d + M_s$ (when moving the open point to the right) or $M_I - M_{II} - M_s + M_d$ (when moving the open point to the left); Δt_j—step of forecasting)

When the predicted value of the additional reduction in energy losses exceeds a predetermined threshold value (determined based on the previously accepted allowable intensity of use of the circuit breakers), the location of open point of the circuit is changed.

Otherwise, the decision regarding the change the open point of the circuit (under previously formulated conditions (4)–(6)) is not implemented due to the lack of economic feasibility.
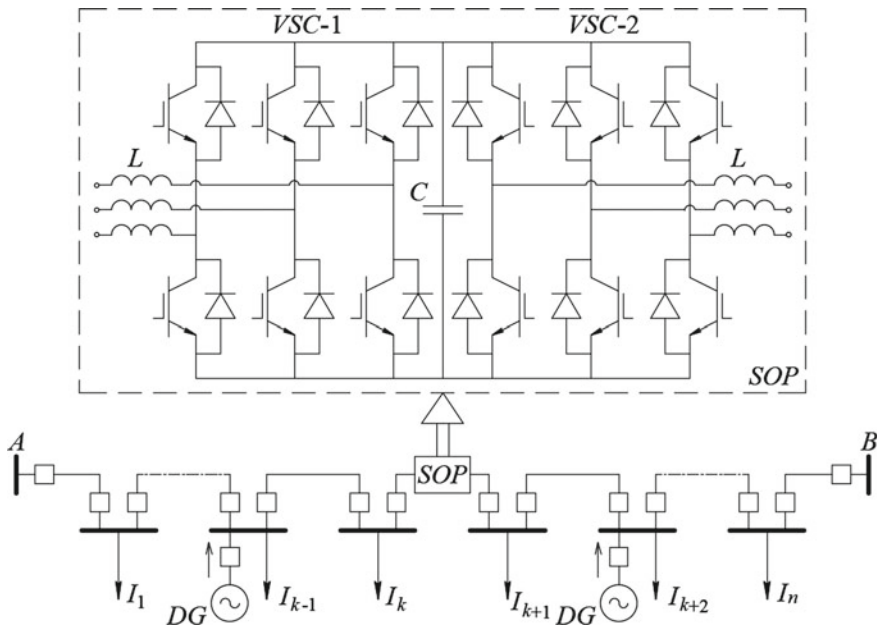
3 Soft Open Points

A more effective and universal approach to managing the modes of electrical networks (in terms of increasing their flexibility) in modern conditions is associated with the use of power electronic devices. In particular, in relation to distribution networks, built according to a loop scheme, the so-called "soft open points" (SOP) technology can be used [34–36].

This technology involves placing at the normal open point of the circuit, a certain analogue of the DC link. This solution provides a compromise between the continued use of a distribution network with formally open topology and its operation in a closed mode. In this case, the efficiency of the result is achieved by obtaining the load flow that provides at any particular time a minimum of power losses corresponding to the network operation in a closed mode.

The most common approach to the formation of SOPs is the use of voltage source converters (VSC), what is justified by the following considerations.

The possibility of flexible and independent control of active and reactive power flows. Connected in series through a capacitor on the DC side (Fig. 13), both VSC devices generate voltages with the desired amplitude and phase angle. As a result, instead of the usual commutation operation (on/off) at the open point of the circuit, it becomes possible to smoothly and continuously change the active power flows

Fig. 13 Using a "soft open points" in distribution networks

through the DC link and, regardless of this, absorb or generate reactive power from each of the terminals.

In addition, it is possible to almost instantly change the voltage generated by the VSC, that allows damping voltage fluctuations, which is an urgent problem in networks with integrated renewable energy sources.

The connection of inductivity in series with each terminal forms a filter that allows one to compensate harmonics, to limit short-circuit currents, which thanks this practically do not change. This circumstance makes it possible to eliminate the need to replace installed equipment in the network, fundamental reconstruction of relay protection and technical means of automation.

And, finally, a very important result of such a technical solution is the complete absence of restrictions on the number of switching operations.

Although the use of devices similar to SOPs has been fairly well studied from the experience of their operation in power systems, in the distribution systems the strategy and principles of their use will be significantly different.

In this regard, the problem arises of determining the basic principles of managing the operation of the SOP in order to form the optimal modes in the distribution network, in particular, to minimize power losses at any particular period of time, and, as a result, to reduce the total electrical energy losses.

In contrast to the situation with remotely controlled switching devices, the use of SOPs will be appropriate in those circuits of the distribution network where frequent, but relatively short-term changes in modes take place. It is obvious that it is not

expedient either from a technical or economic point of view to respond to such mode changes due to conventional breakers with a limited switching resource.

In this case, the main idea of using SOP in distribution networks can be defined as constant maintenance of the load flow (in the general case, separately in active and reactive power) as close as possible to that which would be formed in the same circuit in the case of its operation in closed mode.

Thus, the amount of active power that must be transmitted through the SOP from one part of the circuit to another, as well as the value of the generated or absorbed reactive power from the SOP, should be determined depending on the current values of node loads and the output power (generated or consumed) by local energy sources that are subject for permanent monitoring.

Here the problem arises of the quick modeling the mode of distribution feeder with two-way power supply. The classical approach to its solution is the application of the, so called, method of power moments [37]. According to this method, for an arbitrary line with two-way power supply (Fig. 14), in the general case, taking into account the inequality of voltages on the primary substations, the power flows in the head section, for example, assuming their direction from node "A" to node "B", are determined as follows

$$\underline{S}_{A,1} = \frac{\sum_{i=1}^{n} \underline{S}_i \, Z_{i,B}^*}{Z_\Sigma^*} + \frac{U_A^* - U_B^*}{Z_\Sigma^*} U_n m, \tag{25}$$

where $Z_{i,B}^*$ is the complex conjugate value of the resistance of the sections from node i to substation B; Z_Σ^* is the complex conjugate values of the resistance of the entire feeder; $\frac{U_A^* - U_B^*}{Z_\Sigma^*} U_n$ is an additional power flow caused by the difference in voltages in buses of substations; U_n is the rated voltage.

When the power flow through the head section of the feeder is known, the load flow in the remaining sections is determined in accordance with the Kirchhoff law, taking into account their predetermined direction. Accordingly, the negative value of the load flows on certain sections indicates that their actual direction has to be opposite.

To power flow control in a distribution feeder equipped with a SOP, this approach is not convenient enough, since there is no connection between load flows in sections and alterations of nodes loads and/or of output power of local energy sources. In this
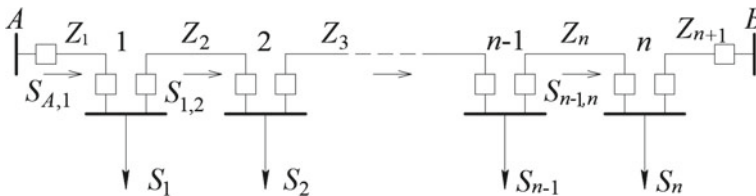

Fig. 14 Feeder with two-way power supply

regard, to determine the load flow, it is proposed approach based on the principle of superposition.

In this case, the resulting load flow is determined in several stages. Initially, we find the load flow without taking into account the difference in voltages in the primary substations. Moreover, this result is also formed using the superposition principle for pre-calculated partial power flows from each of the primary substations to any of the network nodes.

At the final stage, to this power flow is added the power flow caused by the difference of voltages on the busses of primary substations (25).

Let us consider how partial power flows from primary substations to individual network nodes can be determined. For this purpose, we use a simplified feeder with two-way power supply (Fig. 15).

For following analysis, we represent this original feeder as two equivalent ones (Fig. 16).

The voltages at nodes 2 and 3 can be calculated both from the voltage U_1 and from the voltage U_4. Without taking into account power losses, for each of the above equivalents (Fig. 16) we can write

$$\underline{U}_3 = \underline{U}_1 - \Delta\underline{U}_{1,3} = \underline{U}_4 - \Delta\underline{U}_{3,4}, \tag{26}$$
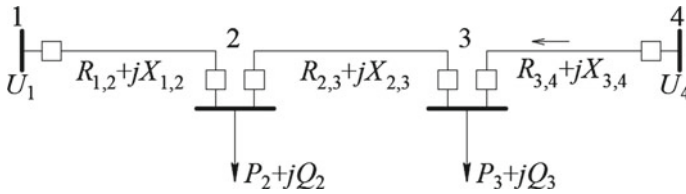

Fig. 15 Simplified two-way power supply closed ring network
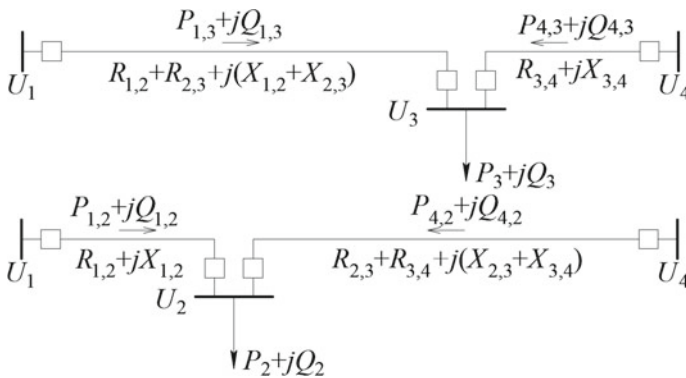

Fig. 16 Equivalents of two-way power supply closed ring network

$$\underline{U}_2 = \underline{U}_1 - \Delta\underline{U}_{1,2} = \underline{U}_4 - \Delta\underline{U}_{2,4}. \tag{27}$$

For the real part of (26) we have

$$U_1 - \frac{P_{1,3}(R_{1,2} + R_{2,3}) + Q_{1,3}(X_{1,2} + X_{2,3})}{U_{e1}} = U_4 - \frac{P_{4,3}R_{3,4} + Q_{4,3}X_{3,4}}{U_{e4}}. \tag{28}$$

For the imaginary part

$$U_1 - \frac{P_{1,3}(X_{1,2} + X_{2,3}) - Q_{1,3}(R_{1,2} + R_{2,3})}{U_{e1}} = U_4 - \frac{P_{4,3}X_{3,4} - Q_{4,3}R_{3,4}}{U_{e4}}. \tag{29}$$

Similarly, for (27) we obtain

$$U_1 - \frac{P_{1,2}R_{1,2} + Q_{1,2}X_{1,2}}{U_{e1}} = U_4 - \frac{P_{4,2}(R_{2,3} + R_{3,4}) + Q_{4,2}(X_{2,3} + X_{3,4})}{U_{e4}}, \tag{30}$$

$$U_1 - \frac{P_{1,2}X_{1,2} - Q_{1,2}R_{1,2}}{U_{e1}} = U_4 - \frac{P_{4,2}(X_{2,3} + X_{3,4}) - Q_{4,2}(R_{2,3} + R_{3,4})}{U_{e4}}. \tag{31}$$

where $P_{1,3}$, $Q_{1,3}$, $P_{1,2}$, $Q_{1,2}$ are the partial powers coming from the substation 1 to nodes 3 and 2, respectively; $P_{4,3}$, $Q_{4,3}$, $P_{4,2}$, $Q_{4,2}$ are the partial powers coming from the substation 4 to nodes 3 and 2, respectively; U_{e1}, U_{e4} are the equivalent voltages that for distribution networks may be defined as $U_{e1} = U_1$ and $U_{e4} = U_4$ or $U_{e1} = \frac{U_1 + U_n}{2}$ and $U_{e4} = \frac{U_4 + U_n}{2}$, U_n—is the rated voltage.

Additionally, taking into account that

$$S_3 = S_{1,3} + S_{4,3} \text{ and } S_2 = S_{1,2} + S_{4,2},$$

after some transformations, for the real part (28) and (30) we obtain, respectively

$$U_1 - \frac{P_{1,3}R_{1,3}}{U_{e1}} - \frac{Q_{1,3}X_{1,3}}{U_{e1}} = U_4 - \frac{P_{4,3}R_{3,4}}{U_{e4}} - \frac{Q_{4,3}X_{3,4}}{U_{e4}}$$

and

$$U_1 - \frac{P_{1,2}R_{1,2}}{U_{e1}} - \frac{Q_{1,2}X_{1,2}}{U_{e1}} = U_4 - \frac{P_{4,2}R_{2,4}}{U_{e4}} - \frac{Q_{4,2}X_{2,4}}{U_{e4}},$$

where $R_{1,2}$, $X_{1,2}$, $R_{1,3}$, $X_{1,3}$ are the resistances from substation 1 to load nodes 2 and 3, respectively; $R_{2,4}$, $X_{2,4}$, $R_{3,4}$, $X_{3,4}$ are the resistances from the substation 4 to load nodes 2 and 3, respectively.

By implementation of the superposition principle and taking into account that in this case, in fact, $P_{1,3} = P_3$, $Q_{1,3} = Q_3$, $P_{4,3} = P_3$, $Q_{4,3} = Q_3$, $P_{1,2} = P_2$, $Q_{1,2} = Q_2$, $P_{4,2} = P_2$, $Q_{4,2} = Q_2$ we will obtain.

- for the real part

$$U_1 - \frac{P_3 R_{1,2} + P_3 R_{2,3} + Q_3 X_{1,2} + Q_3 X_{2,3}}{U_{e1}} - \frac{P_2 R_{1,2} + Q_2 X_{1,2}}{U_{e1}} =$$

$$= U_4 - \frac{P_3 R_{3,4} + Q_3 X_{3,4}}{U_{e4}} - \frac{P_2 R_{2,3} + P_2 R_{3,4} + Q_2 X_{2,3} + Q_2 X_{3,4}}{U_{e4}}$$

or

$$U_1 - \frac{(P_3 + P_2) R_{1,2} + P_3 R_{2,3} + (Q_3 + Q_2) X_{1,2} + Q_3 X_{2,3}}{U_{e1}} =$$

$$= U_4 - \frac{(P_2 + P_3) R_{3,4} + P_2 R_{2,3} + (Q_2 + Q_3) X_{3,4} + Q_2 X_{2,3}}{U_{e4}}.$$

It is easy to verify that the obtained result fully corresponds to the mode of the original distribution feeder (Fig. 15).

Similar analysis can be made for the imaginary part of expressions (29) and (31). This allows for the circuits (Fig. 15) to obtain the following conditions for finding partial power flows, assuming at this stage that the voltages on the substations are the same ($U_1 = U_4$)

$$-\frac{P_{1,3} R_{1,3}}{U_{e1}} - \frac{Q_{1,3} X_{1,3}}{U_{e1}} + \frac{P_{4,3} R_{3,4}}{U_{e4}} + \frac{Q_{4,3} X_{3,4}}{U_{e4}} = 0,$$

$$-\frac{P_{1,3} X_{1,3}}{U_{e1}} + \frac{Q_{1,3} R_{1,3}}{U_{e1}} + \frac{P_{4,3} X_{3,4}}{U_{e4}} - \frac{Q_{4,3} R_{3,4}}{U_{e4}} = 0,$$

$$P_{1,3} + P_{4,3} = P_3, \quad Q_{1,3} + Q_{4,3} = Q_3,$$

and

$$-\frac{P_{1,2} R_{1,2}}{U_{e1}} - \frac{Q_{1,2} X_{1,2}}{U_{e1}} + \frac{P_{4,2} R_{2,4}}{U_{e4}} + \frac{Q_{4,2} X_{2,4}}{U_{e4}} = 0,$$

$$-\frac{P_{1,2} X_{1,2}}{U_{e1}} + \frac{Q_{1,2} R_{1,2}}{U_{e1}} + \frac{P_{4,2} X_{2,4}}{U_{e4}} - \frac{Q_{4,2} R_{2,4}}{U_{e4}} = 0,$$

$$P_{1,2} + P_{4,2} = P_2, \quad Q_{1,2} + Q_{4,2} = Q_2.$$

Obviously, in the process of solving the above systems of equations, partial power flows from the substations to each of the network nodes are determined: $P_{1,2}$, $Q_{1,2}$, $P_{4,2}$, $Q_{4,2}$, $P_{1,3}$, $Q_{1,3}$, $P_{4,3}$, $Q_{4,3}$.

Summarizing the results obtained, for example, for the network given in Fig. 14 and introducing the notation

$$\alpha_{A,k} = \frac{\sum_{i=1}^{k} R_i}{U_{eA}}, \quad \beta_{A,k} = \frac{\sum_{i=1}^{k} X_i}{U_{eA}}, \quad \alpha_{B,k} = \frac{\sum_{i=k}^{n+1} R_i}{U_{eB}}, \quad \beta_{B,k} = \frac{\sum_{i=k}^{n+1} X_i}{U_{eB}},$$

we obtain the following systems of equations

$$-\alpha_{A,k} P_{A,k} - \beta_{A,k} Q_{A,k} + \alpha_{B,k} P_{B,k} + \beta_{B,k} Q_{B,k} = 0,$$

$$-\beta_{A,k} P_{A,k} + \alpha_{A,k} Q_{A,k} + \beta_{B,k} P_{B,k} - \alpha_{B,k} Q_{B,k} = 0,$$

$$P_{A,k} + P_{B,k} = P_k, \quad Q_{A,k} + Q_{B,k} = Q_k, \quad k = 1, \ldots, n-1,$$

where k—is the number of load node, n—quantity of feeder sections.

In the process of solving these systems of equations, partial flows of power to each network nodes are determined. The resulting load flow in each section of the feeder (Fig. 17) is calculated using the principle of superposition, however at this stage without taking into account different voltages on substations.

$$P_i' = \sum_{j=i}^{n-1} P_{A,j} - \sum_{j=1}^{i-1} P_{B,j}, \quad Q_i' = \sum_{j=i}^{n-1} Q_{A,j} - \sum_{j=1}^{i-1} Q_{B,j}. \tag{32}$$

A similar approach to modeling the mode of a feeder with two-way power supply can also be implemented based on the following considerations.

Regarding the networks shown in Figs. 15 and 16, without taking into account power losses, on the basis of (25) can be obtain

$$\underline{S}_{1,3} = \frac{\underline{S}_3 \overset{*}{Z}_{3,4}}{\overset{*}{Z}_\Sigma}, \quad \underline{S}_{1,3} - \underline{S}_3 = -\frac{\underline{S}_3 \left(\overset{*}{Z}_{1,2} + \overset{*}{Z}_{2,3} \right)}{\overset{*}{Z}_\Sigma}, \quad \underline{S}_{1,2} = \frac{\underline{S}_2 \left(\overset{*}{Z}_{2,3} + \overset{*}{Z}_{3,4} \right)}{\overset{*}{Z}_\Sigma},$$
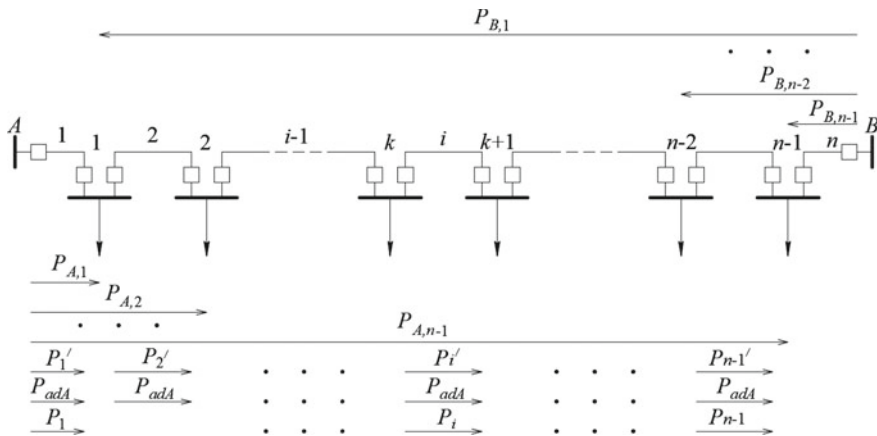

Fig. 17 Determination of the load flow in the feeder on the basis of superposition method

$$\underline{S}_{1,2} - \underline{S}_2 = -\frac{\underline{S}_2 \overset{*}{\underline{Z}}_{1,2}}{\overset{*}{\underline{Z}}_\Sigma}, \quad \underline{S}_{4,3} = \frac{\underline{S}_3\left(\overset{*}{\underline{Z}}_{1,2} + \overset{*}{\underline{Z}}_{2,3}\right)}{\overset{*}{\underline{Z}}_\Sigma}, \quad \underline{S}_{4,3} - \underline{S}_3 = -\frac{\underline{S}_3 \overset{*}{\underline{Z}}_{3,4}}{\overset{*}{\underline{Z}}_\Sigma},$$

$$\underline{S}_{4,2} = \frac{\underline{S}_2 \overset{*}{\underline{Z}}_{1,2}}{\overset{*}{\underline{Z}}_\Sigma}, \quad \underline{S}_{4,2} - \underline{S}_2 = -\frac{\underline{S}_2\left(\overset{*}{\underline{Z}}_{2,3} + \overset{*}{\underline{Z}}_{3,4}\right)}{\overset{*}{\underline{Z}}_\Sigma}.$$

In this case we have the following

$$P_{1,2} + jQ_{1,2} = \left(1 - \frac{R_{1,2} - jX_{1,2}}{R_\Sigma - jX_\Sigma}\right)(P_2 + jQ_2),$$

$$P_{1,3} + jQ_{1,3} = \left(1 - \frac{(R_{1,2} + R_{2,3}) - j(X_{1,2} + X_{2,3})}{R_\Sigma - jX_\Sigma}\right)(P_3 + jQ_3),$$

$$P_{4,2} + jQ_{4,2} = \left(1 - \frac{(R_{2,3} + R_{3,4}) - j(X_{2,3} + X_{3,4})}{R_\Sigma - jX_\Sigma}\right)(P_2 + jQ_2),$$

$$P_{4,3} + jQ_{4,3} = \left(1 - \frac{R_{3,4} - jX_{3,4}}{R_\Sigma - jX_\Sigma}\right)(P_3 + jQ_3). \tag{33}$$

Taking into account that

$$\frac{R_{ij} - jX_{ij}}{R_\Sigma - jX_\Sigma} = \frac{R_{ij}R_\Sigma + X_{ij}X_\Sigma}{R_\Sigma^2 + X_\Sigma^2} + j\frac{R_{ij}X_\Sigma - X_{ij}R_\Sigma}{R_\Sigma^2 + X_\Sigma^2}$$

and introducing the following notations

$$\alpha_{ij} = \frac{R_{ij}R_\Sigma + X_{ij}X_\Sigma}{R_\Sigma^2 + X_\Sigma^2}, \quad \beta_{ij} = \frac{R_{ij}X_\Sigma - X_{ij}R_\Sigma}{R_\Sigma^2 + X_\Sigma^2},$$

we will obtain

$$P_{1,2} + jQ_{1,2} = (1 - \alpha_{1,2} - j\beta_{1,2})(P_2 + jQ_2) =$$
$$= \left[(1 - \alpha_{1,2})P_2 + \beta_{1,2}Q_2\right] + j\left[(1 - \alpha_{1,2})Q_2 - \beta_{1,2}P_2\right],$$

$$P_{1,3} + jQ_{1,3} = (1 - \alpha_{1,3} - j\beta_{1,3})(P_3 + jQ_3) =$$
$$= \left[(1 - \alpha_{1,3})P_3 + \beta_{1,3}Q_3\right] + j\left[(1 - \alpha_{1,3})Q_3 - \beta_{1,3}P_3\right],$$

$$P_{4,2} + jQ_{4,2} = (1 - \alpha_{4,2} - j\beta_{4,2})(P_2 + jQ_2) =$$

$$= \left[(1 - \alpha_{4,2})P_2 + \beta_{4,2}Q_2\right] + j\left[(1 - \alpha_{4,2})Q_2 - \beta_{4,2}P_2\right],$$

$$P_{4,3} + jQ_{4,3} = (1 - \alpha_{4,3} - j\beta_{4,3})(P_3 + jQ_3) =$$
$$= \left[(1 - \alpha_{4,3})P_3 + \beta_{4,3}Q_3\right] + j\left[(1 - \alpha_{4,3})Q_3 - \beta_{4,3}P_3\right].$$

By generalizing the given above results, in particular for the network shown in Fig. 14, we get

$$P_{Ak} = (1 - \alpha_{Ak})P_k + \beta_{Ak}Q_k, \tag{34}$$

$$Q_{Ak} = (1 - \alpha_{Ak})Q_k - \beta_{Ak}P_k, \tag{35}$$

$$P_{Bk} = (1 - \alpha_{Bk})P_k + \beta_{Bk}Q_k, \tag{36}$$

$$Q_{Bk} = (1 - \alpha_{Bk})Q_k - \beta_{Bk}P_k, \quad k = 1, \ldots, n - 1, \tag{37}$$

where

$$\alpha_{Aj} = \frac{R_\Sigma \sum_{j=1}^{k} R_j + X_\Sigma \sum_{j=1}^{k} X_j}{R_\Sigma^2 + X_\Sigma^2}, \quad \beta_{Aj} = \frac{R_\Sigma \sum_{j=1}^{k} X_j - X_\Sigma \sum_{j=1}^{k} R_j}{R_\Sigma^2 + X_\Sigma^2}, \tag{38}$$

$$\alpha_{Bj} = \frac{R_\Sigma \sum_{j=k+1}^{n+1} R_j + X_\Sigma \sum_{j=k+1}^{n+1} X_j}{R_\Sigma^2 + X_\Sigma^2}, \quad \beta_{Bj} = \frac{R_\Sigma \sum_{j=k+1}^{n+1} X_j - X_\Sigma \sum_{j=k+1}^{n+1} R_j}{R_\Sigma^2 + X_\Sigma^2}. \tag{39}$$

Applying the superposition principle, after the calculated partial power flows (34)–(37) we determine the load flow ($P_i^{/}$, $i = 1, \ldots, n{-}1$) for the original network circuit (Fig. 17) similar to (32).

The final step in modeling the feeder mode, if it is necessary and expedient to take into account the difference in voltages on primary substations, is the adding on the obtained load flow (32) of the additional power ($\underline{S}_{ad}$), which, using the actual values of the substations voltages, is determined as follows

$$\underline{S}_{ad} = \frac{U_A - U_B}{\overset{*}{Z}_\Sigma} U_n.$$

Based on this, one can write

$$P_{adA} + jQ_{adA} = \frac{U_A - U_B}{R_\Sigma - jX_\Sigma} U_n = \frac{(U_A - U_B)R_\Sigma U_n}{R_\Sigma^2 + X_\Sigma^2} + j\frac{(U_A - U_B)X_\Sigma U_n}{R_\Sigma^2 + X_\Sigma^2}.$$

In this case, the final load flow will be defined as follows (Fig. 17)

$$P_j = P_j^/ + P_{adA}sign\left(P_j^/\right), \quad Q_j = Q_j^/ + Q_{adA}sign\left(Q_j^/\right).$$

An important advantage of the proposed above approaches to calculating the power flow in two-way power supplied distribution feeder is the ability to quickly determine the degree of change in the active and reactive power flows in a certain section of the feeder as a result of a change in load at any of the nodes or the output power of local energy sources, in particular, during the transition of the battery from charge mode to discharge mode or vice versa.

It should also be underlined that parameters (38), (39) can be calculated in advance and, as can be seen from the structure of these expressions, they remain unchanged in the process of modeling the feeder mode regardless of the values of loads and of local energy sources parameters.

If the distribution feeder has a more complex structure, in particular, includes branches, then the original circuit is transformed in equivalent one like shown in Figs. 6 and 7.

Here we consider a single-objective optimization problem, where the only goal is managing the operation of the SOP to minimize the total loss of electrical energy in the radial feeders with fixed normally open point. At the same time, it is assumed that for most distribution networks optimal result (from the standpoint of loss minimization) will be obtained when they operate in a close mode.

That is why in the process of ongoing monitoring of the mode parameters of the feeder section adjacent to the SOP, the existing load flow is compared with that which would be during the operation of this feeder in close mode, taking into account the current values of node loads and of distributed generation sources output power.

The resulting imbalance is compensated by changing the direction and magnitude of active power flows through the SOP, as well as by the volume of additional generation (or absorption) of reactive power, which is achieved by appropriate VSC control.

In the process of implementing this control strategy, certain restrictions must be taken into account, in particular, on the permissible voltage levels at the network nodes and the loads in its sections, as well as constraints on the SOP capability and voltages on it terminals.

So, in the mathematical model of the SOP, active and reactive power injections at it terminals have to be integrated into proposed load flow algorithm, at this stage of research, without considering the details of the convertor controller operation. The results elaborated, that SOP is an effective tool to improve the network operation for energy loss reduction.

4 Conclusions

The benefits of using remotely controlled commutation equipment and power electronics for distribution networks operation of modes in real time were considered focusing on electrical energy loss reduction.

Compared to the traditional distribution network reconfiguration approach, a novel dynamic reconfiguration is proposed for a system with a high penetration of renewable energy sources or high level of load heterogeneity. The decision to change the location of the open point of the network is made when the positive effect of the additional reduction in energy losses exceeds the damage from the increased use of the switching resource of the circuit breakers and reduction in their life cycle. Special algorithm is proposed to make such a decision, taking into consideration technical as well as economical aspects of the problem. In this case assumed electrical energy loss reduction is estimated using the proposed adaptive forecasting method. Technical solution regarding dynamic network reconfiguration using remotely controlled breakers is valid if changes of the network mode occur relatively regularly and during a sufficiently long time.

Power electronic devices as a "soft open points" have been proposed to combine the benefit of distribution networks operations both radial and closed modes. This solution is especially useful in the case of frequent and short-term changes in network modes. A new algorithm to speed up of independent modeling the active power and reactive power flows in feeders with to-way power supply is discussed. A general model of typical SOP device (consists on two back to back voltage source converters) operation was developed in order to constantly maintain the load flow in the radial feeder as close as possible to that which would take place during its operation in a mash mode.

In the following research, it seems appropriate to develop a more detailed algorithm for controlling the operation of the SOP, in particular, taking into account its multifunctionality (at least, such as load balancing, influence on the voltage regime and power supply reliability indicators), as well as additional power losses that occur with different rated power and operating modes of the corresponding power electronics equipment.

References

1. Civanlar, S., Grainger, J.J., Yin, H., Lee, S.S.H.: Distribution feeder reconfiguration for loss reduction. Proc. IEEE Trans. Power Deliv. **3**(1), 1217–1223 (1988)
2. Baran, M., Wu, F.: Network reconfiguration in distribution systems for loss reduction and load balancing. Proc. IEEE Trans. Power Deliv. **4**(3), 1401–1407 (1989)
3. Chiang, H.D., Jumeau, R.J.: Optimal network reconfiguration in distribution systems. Part 1: a new formulation and solution methodology. Proc. IEEE Trans. Power Deliv. **5**(3), 1902–1909 (1990)

4. Gomes, F.V., Carneiro, S., Pereira, J.L.R., Vinagre, M.P., Garcia, P.A.N., Araujo, L.R.: A new distribution system network reconfiguration approach using optimal power flow and sensitivity analysis for loss reduction. Proc. IEEE Trans. Power Syst. **21**(4), 1616–1623 (2006)

5. Raju, G., Bijwe, P.: Efficient reconfiguration of balanced and unbalanced distribution systems for loss minimization. IET Gener. Transm. Distrib. **2**(1), 7–12 (2008)

6. Sivkumar, M., Debapriya, D., Subrata, P.: A comprehensive review on power distribution network reconfiguration. Energy Syst. **8**(2), 227–284 (2017). https://doi.org/10.1007/s12667-016-0195-7

7. Sarfi, R.J., Salama, M.M.A., Chikhani, A.Y.: A survey of the state of the art in distribution system reconfiguration. Electric Power Syst. Res. **4**(1), 61–70 (1994)

8. Schmidt, P.H., Ida, M., Kagan, N., Guaraldo, J.C.: Fast reconfiguration of distribution systems considering loss minimization. Proc. IEEE Trans. Power Syst. **20**(3), 1311–1319 (2005)

9. Martin, J.A., Gil, A.J.: A new heuristics approach for distribution systems loss reduction. Electric Power Syst. Res. **78**(11), 1953–1958 (2008)

10. Mendoza, J.E., Lopez, M.E., Lopez, E.A.: Multiobjective reconfiguration considering power losses and reliability index for distribution networks. IET Gener. Trans. Distrib. **3**, 825–840 (2009)

11. Amanulla, B., Chakrabarti, S., Singh, S.N.: Reconfiguration of power distribution systems considering reliability and power loss. Proc. IEEE Trans. Power Deliv. **27**(2), 918–926 (2012)

12. Narimani, M., Vahed, A., Azizipanah, R., Javidsharifi, M.: Enhanced gravitational search algorithm for multiobjective distribution feeder reconfiguration considering reliability, loss and operational cost. IET Gener. Transm. Distrib. **8**(1), 55–69 (2014)

13. Nguyen, T.T., Truong, A.V.: Distribution network reconfiguration for power loss minimization and voltage profile improvement using cuckoo search algorithm. Electric. Power Energy Syst. **68**, 233–242 (2015). https://doi.org/10.1016/j.ijepes.2014.12.075

14. Ekel, P.Y., Terra, L.D.B., Fontes, C.C., Souza, J.P., Popov, V.A.: Taking into account power systems reaction in problems of multicriteria optimizing network configuration in distribution systems. Proc. Int. Conf. Electric Power Eng., Power Tech. **826498**, 67–70 (1999). https://doi.org/10.1109/PTC.1999.826498

15. Bernardon, D., Garcia, V., Ferreira, A., Canha, L.: Multicriteria distribution network reconfiguration considering subtransmission analysis. Proc. IEEE Trans. Power Deliv. **25**(4), 2684–2691 (2010)

16. Augugliaro, A., Dusonchet, L., Mangione, S.: Optimal reconfiguration of distribution networks for loss reduction using non linear programming. Euro. Trans. Electric. Power **1**(6), 317–324 (1991)

17. Abur, A.A.: Modified linear programming method for distribution system reconfiguration. Electric. Power Energy Syst. **18**(7), 469–474 (1996)

18. Borghetti, A.: A mixed integer linear programming approach for the computation of the minimum power losses radial configuration of electrical distribution networks. Proc. IEEE Trans. Power Syst. **27**(3), 1264–1273 (2012)

19. Vulasala, G., Sirigiri, S., Thiruveedula, R.: Feeder reconfiguration for loss reduction in unbalanced distribution system using genetic algorithm. Electr. Power Energy Syst. **2**(4), 240–248 (2009)

20. Parada, V., Ferland, J.A., Arias, M., Daniels, K.: Optimization of electrical distribution feeders using simulated annealing. Proc. IEEE Trans. Power Deliv. **19**(3), 1135–1141 (2004)

21. Abdelaziz, A.Y., Mohamed, F.M., Mekhamer, S.F., Badr, M.A.L.: Distribution system reconfiguration using a modified Tabu Search algorithm. Electric Power Syst. Res. **80**(8), 943–953 (2010)

22. Su, C.-T., Chang, C.-F., Chiou, J.-P.: Distribution network reconfiguration for loss reduction by ant colony search algorithm. Electric Power Syst. Res. **75**(2–3), 190–199 (2005)

23. Falaghi, H., Haghifam, M.R., Singh, C.: Ant colony optimization-based method for placement of sectionalizing switches in distribution networks using a fuzzy multi objective approach. Proc. IEEE Trans. Power Deliv. **24**(1), 268–276 (2009)

24. Kim, K.K., Hung, K.H.: Artificial neural network based feeder reconfiguration for loss reduction in distribution systems. Proc. IEEE Trans. Power Deliv. **8**(3), 1356–1366 (1997)
25. Su, C.T., Lee, C.S.: Network reconfiguration of distribution system using improved mixed integer hybrid differential evolution. Proc. IEEE Trans. Power Deliv. **18**(3), 1022–1027 (2003)
26. Queiroz, L.M.O., Lyra, C.: Adaptive hybrid genetic algorithm for technical loss reduction in distribution networks under variable demands. Proc. IEEE Trans. Power Syst. **24**(1), 445–453 (2009)
27. Niknam, T., Zare, M., Aghaei, J., Farsani, E.A.: A new hybrid evolutionary algorithm for distribution feeder reconfiguration. Appl. Artif. Intell. **25**(3), 951–971 (2011)
28. DeFusco, R.A., McLeavey, D.W., Pinto, J.E., Runkle, D.E.: Quantitative investment analysis 944 p (2020)
29. Charytoniuk, W., Chen, M.S.: Very short-term load forecasting using artificial neural networks. Proc. IEEE Trans. Power Syst. **15**, 263–268 (2000)
30. Jacob, M., Neves, C., Greetham, D.V.: Short term load forecasting in book: forecasting and assessing risk of individual electricity peaks pp. 15–37 (2020)
31. Jiang, H., Ding, F., Zhang, Y.: Short-term load forecasting based automatic distribution network reconfiguration. In: Proceeding IEEE Power and Energy Society General Meeting (PES GM), p. 9. USA, Chicago
32. Foley, A.M., Leahy, P.G., Marvuglia, A., McKeogh, E.J.: Current methods and advances in forecasting of wind power generation. Renew. Energy **37**, 1–8 (2012). https://doi.org/10.1016/j.renene.2011.05.033
33. Mitra, I., Heinemann, D., Ramanan, A.: Short-term PV power forecasting in India: recent developments and policy analysis. Energy Environ. Eng. **27**, 26 (2022). https://doi.org/10.1007/s40095-021-00468-z
34. Cao, W., Wu, J., Jenkins, N., Wang, C., Green, T.: Operating principle of soft open points for electrical distribution network. Appl. Energy **164**, 245–257 (2016)
35. Cao, W., Wu, J., Jenkins, N., Wang, Ch., Green, T.: Benefits analysis of soft open points for electrical distribution network operation. Appl. Energy **165**, 36–47 (2016)
36. Fuad, K.S., Hafezi, H., Kauhananiemi, K., Laaksonen, H.: Soft open point in distribution networks. IEEE Access **2020**, 16 (2020)
37. Segeda, M.S.: Electric. Netw. Syst. **Lviv**, 540 p (2015) (Ukr)
38. Zharkin, A.F., Novskiy, V.O., Popov, V.A., Yarmoliuk, O.S.: Improving the efficiency of distribution network control under the conditions of application of distributed sources generation of electrical energy and means of its accumulation. Tech. Electrodynamic **3**, 37–43 (2021). https://doi.org/10.15407/techned2021.03.037